[redacted]

[redacted]

NASA TECHNICAL MEMORANDUM

NASA TM X-2212

NASA TM X-2212

[redacted]

EFFECTS OF GROUND PROXIMITY ON THE AERODYNAMIC CHARACTERISTICS OF A SIX-JET V/STOL CONFIGURATION WITH FOUR SWING-OUT LIFT JETS

by Arthur W. Carter

Langley Research Center
Hampton, Va. 23365

NATIONAL AERONAUTICS AND SPACE ADMINISTRATION • WASHINGTON, D. C. • MAY 1971

[redacted]

[redacted]

1. Report No.	2. Government Accession No.	3. Recipient's Catalog No.
NASA TM X-2212		

4. Title and Subtitle	5. Report Date
EFFECTS OF GROUND PROXIMITY ON THE AERODYNAMIC CHARACTERISTICS OF A SIX-JET V/STOL CONFIGURATION WITH FOUR SWING-OUT LIFT JETS (U)	May 1971
	6. Performing Organization Code
7. Author(s)	8. Performing Organization Report No.
Arthur W. Carter	L-7555
	10. Work Unit No.
9. Performing Organization Name and Address	721-01-11-01
NASA Langley Research Center Hampton, Va. 23365	11. Contract or Grant No.
	13. Type of Report and Period Covered
12. Sponsoring Agency Name and Address	Technical Memorandum
National Aeronautics and Space Administration Washington, D.C 20546	14. Sponsoring Agency Code

15. Supplementary Notes

16. Abstract

A wind-tunnel investigation has been made of the effects of ground proximity on the longitudinal and lateral-directional aerodynamic characteristics and jet-interference effects of a model of a jet V/STOL variable-sweep fighter airplane that employs four direct-lift engines which swing out from the fuselage ahead of the wing and two lift-cruise engines located in the rear part of the fuselage. Data were obtained through a range of angles of attack and sideslip at simulated speeds from hover through transition at various heights of the model above a moving-belt ground plane. Power-off data and power-on data at several power conditions are presented. The data are presented without analysis or discussion.

17. Key Words (Suggested by Author(s))	18. Distribution Statement
Jet V/STOL Jet interference Aerodynamic characteristics Ground effect	[redacted]

19.	20.	21. No. of Pages	22. Price
[redacted]	[redacted]	225	

[redacted]

EFFECTS OF GROUND PROXIMITY ON THE AERODYNAMIC CHARACTERISTICS OF A SIX-JET V/STOL CONFIGURATION WITH FOUR SWING-OUT LIFT JETS*

By Arthur W. Carter
Langley Research Center

SUMMARY

A wind-tunnel investigation has been made of the effects of ground proximity on the longitudinal and lateral-directional aerodynamic characteristics and jet-interference effects of a model of a jet V/STOL variable-sweep fighter airplane that employs four direct-lift engines which swing out from the fuselage ahead of the wing and two lift-cruise engines located in the rear part of the fuselage. Data were obtained through a range of angles of attack and sideslip at simulated speeds from hover through transition at various heights of the model above a moving-belt ground plane. Power-off data and power-on data at several power conditions are presented. The data are presented without analysis or discussion.

INTRODUCTION

The out-of-ground-effect longitudinal aerodynamic characteristics of a model of a jet V/STOL variable-sweep fighter airplane which employs two lift-cruise engines located in the rear part of the fuselage and four direct-lift engines which swing out from the fuselage ahead of the wing have been presented in reference 1. An additional investigation has been made over the moving-belt ground plane in the 5.18-meter (17-foot) test section of the Langley 300-MPH 7- by 10-foot tunnel to determine the effects of ground proximity on the aerodynamic characteristics of this model. The longitudinal and lateral-directional aerodynamic characteristics and the jet-interference effects were investigated for several power conditions. The model was tested through a range of angles of attack and sideslip at simulated speeds from hover through transition at various heights of the model above the moving-belt ground plane. The data from the investigation are presented without analysis or discussion.

*Title, Unclassified.

SYMBOLS

The aerodynamic data in this paper are referred to the stability-axis system. All of the data are referred to a moment center located on the fuselage reference line at the 15-percent point of the mean aerodynamic chord of the reference wing as shown in figure 1. The forces and moments were nondimensionalized by using the geometry of the reference wing.

The physical quantities in this paper are given both in the International System of Units (SI) and in the U.S. Customary Units. The measurements and calculations were made in the U.S. Customary Units. Factors relating these two systems of units are presented in reference 2.

A_j total area of operating jet exit nozzles, square meters (square feet)

b wing span, meters (feet)

C_D drag coefficient, $\frac{D}{q_\infty S}$

C_L lift coefficient, $\frac{L}{q_\infty S}$

C_l rolling-moment coefficient, $\frac{\text{Rolling moment}}{q_\infty Sb}$

C_{l_β} effective dihedral parameter, $\frac{\partial C_l}{\partial \beta}$

C_m pitching-moment coefficient, $\frac{M}{q_\infty S\bar{c}}$

C_n yawing-moment coefficient, $\frac{\text{Yawing moment}}{q_\infty Sb}$

C_{n_β} directional-stability parameter, $\frac{\partial C_n}{\partial \beta}$

C_T thrust coefficient, $\frac{T}{q_\infty S}$

C_Y side-force coefficient, $\frac{\text{Side force}}{q_\infty S}$

C_{Y_β} side-force parameter, $\frac{\partial C_Y}{\partial \beta}$

$\bar{c}$ reference wing mean aerodynamic chord, meters (feet)

c wing chord, meters (feet)

D drag, newtons (pounds force)

D_e effective diameter of thrust nozzles (diameter of circle having same area as sum of operating nozzles), meters (feet)

h height of lowest point on fuselage above ground plane with model at $\alpha = 0^o$, meters (feet)

i_t tail incidence, degrees

L measured lift, newtons (pounds force)

M pitching moment, meter-newtons (foot-pounds force)

q_∞ free-stream dynamic pressure, newtons/meter^2 (pounds force/foot^2)

S wing reference area (area of theoretical wing excluding wing stub), meters^2 (feet^2)

T thrust, newtons (pounds force)

V_j velocity at jet exhaust, meters/second (feet/second)

V_∞ free-stream velocity, meters/second (feet/second)

α angle of attack of wing, degrees

β angle of sideslip, degrees

$\delta_{LE,IB}$ deflection of wing inboard leading-edge slat (positive when leading edge is deflected down), degrees

$\delta_{LE,OB}$ deflection of wing outboard leading-edge slat (positive when leading edge is deflected down), degrees

$\delta_{LE,ST}$ deflection of leading-edge Krueger flap on wing stub (positive when leading edge is deflected down), degrees

$\delta_{TE,ST}$ deflection of trailing-edge flap on wing stub (positive when trailing edge is deflected down), degrees

$\delta_{TE,W,P}$ deflection of partial-span trailing-edge wing flap (positive when trailing edge is deflected down), degrees (see fig. 2)

ρ_j mass density of jet exhaust, kilograms/meter^3 (slugs/foot^3)

ρ_∞ mass density of free-stream air, kilograms/meter^3 (slugs/foot^3)

∞ infinity (with reference to altitude, high enough to be out of the region of ground effect)

MODEL AND APPARATUS

The model used in this investigation was a 1/10-scale model of a jet V/STOL variable-sweep fighter airplane powered by two lift-cruise and four direct-lift engines. Geometric characteristics of the configuration are shown in figure 1. The fixed stub part of the wing has a leading-edge sweep of 65° and the movable part in the fully extended position has a leading-edge sweep of 25°. The movable part of the wing has a 10-percent chord extension at the leading edge over the outboard 23 percent of the span. Details of the wing high-lift devices are shown in figure 2. The fixed stub part of the wing has a constant-chord split trailing-edge flap and a leading-edge Krueger flap. The movable wing section has a 30-percent-chord single-slotted trailing-edge Fowler flap and a 17.5-percent-chord leading-edge slat.

The two lift-cruise engines which make up the main propulsion system for normal flight are mounted horizontally in the rear part of the fuselage with individual side and top inlets and with individual exhaust nozzles. The exhaust nozzles of these engines are capable of being rotated about the Y-axis to any position from horizontal to vertical. The four direct-lift engines are mounted forward of the wing, in pairs, on arms which swing

out from the fuselage. The engines and arms are stowed completely within the fuselage for normal forward flight. The direct-lift engines may be rotated about the Y-axis to any desired deflection. This engine arrangement eliminates the need for a separate reaction-control system for hovering and low speeds, inasmuch as adequate control can be provided by differential deflection of the direct-lift engines for yaw control and by selective throttling of all three pairs of engines for pitch and roll control.

In the hovering and transition speed range of the investigation, the airplane would operate with the wing fully extended; therefore, the model was constructed with the wing fixed in this position as shown in figure 1. The model was mounted on a sting-supported six-component strain-gage balance for direct measurement of the forces and moments on the model. The balance was located on the model reference line with the moment center of the balance located at the 20-percent mean-aerodynamic-chord station of the wing. The pitching-moment data have been transferred horizontally to a moment center located at the 15-percent mean-aerodynamic-chord station of the wing. An electronic clinometer was located in the fuselage for use in determining the geometric angle of attack of the wing during the investigation.

The principal model configurations investigated are identified in the following table:

Configuration	$\delta_{LE,OB}$	$\delta_{LE,IB}$	$\delta_{TE,W,P}$	$\delta_{LE,ST}$	$\delta_{TE,ST}$
A	30^o	30^o	40^o	Retracted	40^o
B	Retracted	Retracted	Retracted	Retracted	Retracted

Photographs of the sting-supported model above the moving-belt ground plane in the 5.18-meter (17-foot) test section of the Langley 300-MPH 7- by 10-foot tunnel are shown as figure 3. The photographs show configuration A with the direct-lift engines deflected to 90^o for vertical take-off and landing, and deflected to 45^o for short take-off and landing.

A description of the 5.18-meter (17-foot) test section of the Langley 300-MPH 7- by 10-foot tunnel is given in reference 3. Details of the moving-belt ground-plane system and drawings of the model-support system are presented in reference 4.

THRUST SIMULATION

The thrust for the model was provided by six ejector-type jet-engine simulators. A description of the ejectors and their use for jet-engine simulation in wind-tunnel models is presented in reference 5. The pair of lift-cruise engines has an effective diameter of 9.7028 centimeters (3.82 inches). One set of inlets for these engines is located on top of the rear part of the fuselage. The other set of inlets is located on the

sides of the fuselage and simulated on the model but was blocked for the investigation inasmuch as these inlets are in the region of the direct-lift engine exhaust and are normally closed during take-off and transition flight. The four direct-lift engines have an effective diameter of 10.16 centimeters (4.00 inches). These engines are positioned outside the model during operation and are equipped with simple individual bellmouth inlets. The six engines have an effective diameter of 14.05 centimeters (5.53 inches).

The six ejectors were powered by cold, dry compressed air which was brought onboard the model with thin-wall metal tubing bent to follow the sting support and to form a limber spring across the strain-gage balance so that the balance sensitivity was not changed. A sheet-metal fairing was used to shield these air lines from the airstream as shown in figure 3.

For simulation of the jet exhaust for short take-off and landing, the direct-lift engines were rotated to 25° from the horizontal; the 25° nozzles of the lift-cruise engines were used with turning vanes in the ducts ahead of the nozzles to deflect the jet exhaust. For simulation of the jet exhaust for vertical take-off and landing, the direct-lift engines were rotated to 90° from the horizontal; the 90° nozzles of the lift-cruise engines were used with turning vanes installed in the ducts ahead of the nozzles to deflect the jet exhaust. The three pairs of ejectors were calibrated statically and the thrust was determined as the resultant force of the normal and axial forces on the strain-gage balance. The deflection of the jet exhaust relative to the horizontal plane of the model fuselage was determined from the normal and axial forces on the balance. The deflection of the jet exhaust from the 25° nozzles was determined to be only about 20°, whereas the deflection of the jet exhaust from the 90° nozzles was determined to be approximately 93°. Turning vanes were not incorporated in the two pairs of direct-lift engines, inasmuch as each pair of engines was rotated on the extended arm supports. The jet exhaust, therefore, was deflected at virtually the same angle as the rotated engines.

During the wind-tunnel investigation, the thrust from each of the three pairs of ejectors was determined from the difference between the total-pressure and static-pressure measurements in each of the jet exits in a manner similar to that used in reference 5. Thrust coefficients and effective velocity ratios were determined from the total thrust measurements by use of the following equations:

$$C_T = \frac{T}{q_\infty S} \tag{1}$$

$$\sqrt{\frac{\rho_\infty V_\infty^2}{\rho_j V_j^2}} = \sqrt{\frac{q_\infty}{T/2A_j}} \tag{2}$$

$$C_T = \frac{2A_j/S}{\left(\frac{\rho_\infty V_\infty^2}{\rho_j V_j^2}\right)} \qquad (3)$$

TEST CONDITIONS

For this investigation the Reynolds number based on the free-stream dynamic pressure of 527 newtons/meter^2 (11 pounds force/foot^2) and the reference wing mean aerodynamic chord of 27.813 centimeters (10.95 inches) was 0.56×10^6.

The heights of the model above the moving-belt ground plane ranged from $\frac{h}{D_e} = 0.524$ to $\frac{h}{D_e} = 13.9$. The lower height represented the height at which the landing gear would touch down on the runway. For the upper height, the model was near the center line of the test section, and at this height the model was considered to be essentially out of ground effect. The heights of the model above the ground plane were measured relative to the lowest point on the fuselage at $\alpha = 0^o$ for the wind-off condition.

Aerodynamic force and moment data were obtained during hovering at zero wind velocity for three angles of attack. The longitudinal aerodynamic characteristics of the model were obtained for sideslip angles of 0^o and 5^o through a range of angles of attack from approximately -5^o to 25^o. Data were obtained through a range of effective velocity ratios at an angle of attack of approximately 12^o except at the height of the model representing touchdown when the angle of attack was approximately 0^o. The free-stream dynamic pressure and the jet thrust were varied in order to simulate effective velocity ratios from 0 to approximately 0.23 with the engines deflected 90^o and up to approximately 0.33 with the engines deflected 25^o. The lateral-directional aerodynamic characteristics were obtained at an angle of attack of approximately 0^o for the lowest height (touchdown) and at an angle of attack of approximately 12^o for several other heights of the model above the ground plane through a range of angles of sideslip from -5^o to 25^o. Data were also obtained for differential deflection of the direct-lift engines. In general, the aerodynamic data were obtained at four thrust coefficients which ranged from 0 to 8.

A suction slot at the leading edge of the moving-belt ground plane was utilized to remove the boundary layer at that location, and the boundary layer was prevented from building up over the belt by the use of a belt linear speed equal to that of the tunnel airstream. The moving belt was used at all heights of the model above the belt which were less than an h/D_e of 9. At h/D_e ratios of 9 or greater, the data did not appear to be influenced by the boundary layer on the belt, and at these heights of the model above the ground plane the ground belt was stationary.

No corrections have been made to the data for model blockage or jet boundary effects inasmuch as these corrections are not considered significant for this size of model in the 5.18-meter (17-foot) section of the tunnel.

PRESENTATION OF RESULTS

In order to hasten the availability of these data on this six-jet V/STOL configuration with four swing-out direct-lift jets, the effects of ground proximity on the aerodynamic characteristics of the model are being presented without analysis or discussion. These data are intended to supplement the data on this configuration out of ground effect which are presented in reference 1.

The effects of ground proximity on the longitudinal aerodynamic characteristics (lift, drag, and pitching-moment coefficients in the stability-axis system) are presented through a range of angles of attack. Thrust data are presented where applicable. The variations of the ratios of lift and drag to thrust and of pitching moment to the product of the thrust and the effective diameter of the operating jets with angle of attack, effective velocity ratio, and h/D_e ratio are presented for jet deflections of 90^o (VTOL) and 25^o (STOL).

The effects of ground proximity on the lateral aerodynamic characteristics are presented through a range of angles of sideslip for jet deflections of 90^o and 25^o and for differential deflection of the direct-lift engines. Thrust data are presented where applicable.

Thrust for the model was provided by the six ejectors which were supplied cold dry air from a high-pressure air line. An examination of the thrust data obtained in this investigation indicated some variations from the prescribed values. Some of the data indicated a decrease in thrust during the test run which apparently resulted from a drop in air-line pressure. Some of the data show a constant level of thrust which was greater or less than the prescribed value for that test run. Because of these variations in thrust, caution should be exercised in the use of the data and the thrust data should be considered in any analysis of the aerodynamic data. On the other hand, the decrease in thrust at the higher angles of attack for the data at an h/D_e of 0.524 (touchdown), in general, resulted from the back pressure on the exhausts of the lift-cruise engines caused by the close proximity of these exhausts to the ground plane and did not result from a decrease in air pressure to the ejectors.

Results of the investigation are presented in the following figures:

Figure

Longitudinal aerodynamic characteristics:

Langley Research Center,
National Aeronautics and Space Administration,
Hampton, Va., February 13, 1971.

REFERENCES

1. Carter, Arthur W.: Aerodynamic Characteristics of a Six-Jet V/STOL Configuration With Four Swing-Out Lift Jets in the Transition Speed Range. NASA TM X-2060, 1970.

2. Mechtly, E. A.: The International System of Units – Physical Constants and Conversion Factors (Revised). NASA SP-7012, 1969.

3. Kuhn, Richard E.; and Hayes, William C., Jr.: Wind-Tunnel Investigation of Longitudinal Aerodynamic Characteristics of Three Propeller-Driven VTOL Configurations in the Transition Speed Range, Including Effects of Ground Proximity. NASA TN D-55, 1960.

4. Turner, Thomas R.: A Moving-Belt Ground Plane for Wind-Tunnel Ground Simulation and Results for Two Jet-Flap Configurations. NASA TN D-4228, 1967.

5. Margason, Richard J.; and Gentry, Garl L.: Static Calibration of an Ejector Unit for Simulation of Jet Engines in Small-Scale Wind-Tunnel Models. NASA TN D-3867, 1967.

Wing (reference wing)	
Aspect ratio	6.024
Span	155.45 (61.2)
Area	.4012 meter^2 (4.318 ft^2)
Root chord	38.23 (15.05)
Tip chord	13.39 (5.27)
Mean aerodynamic chord, $\bar{c}$	27.813 (10.95)
Sweep of leading edge	25°
Dihedral	3°
Taper ratio	0.35
Horizontal tail (exposed)	
Span	73.66 (29.0)
Area	.0966 meter^2 (1.04 ft^2)

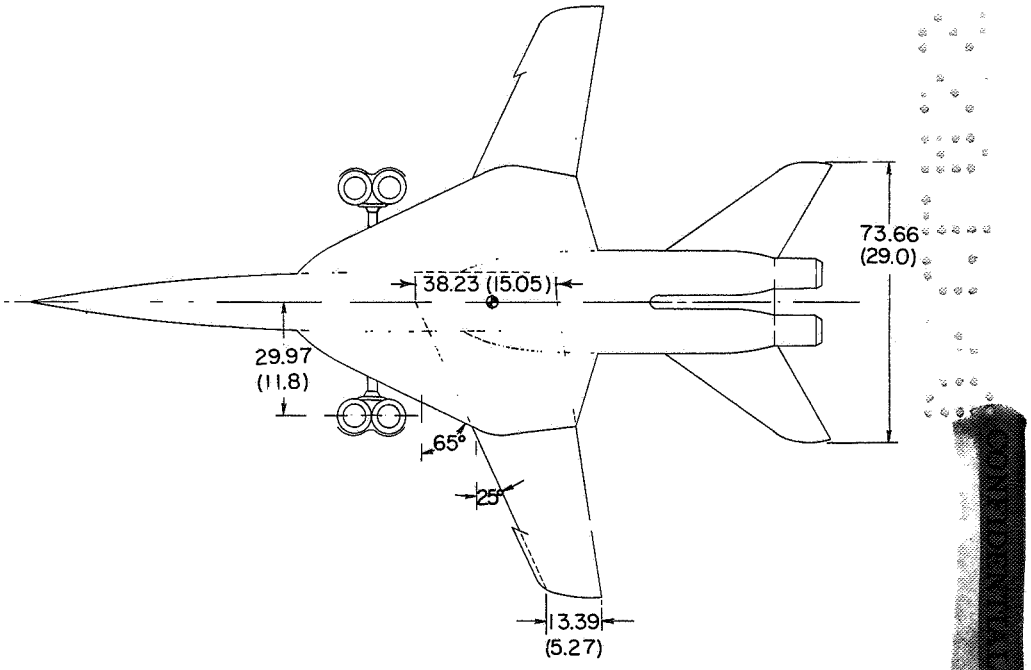

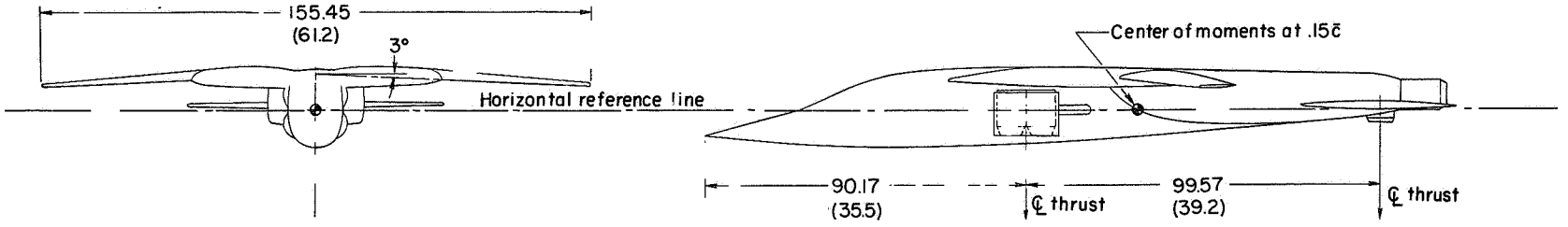

Figure 1.- Three-view drawing and geometric characteristics of model. Dimensions are given in centimeters and parenthetically in inches unless otherwise noted.

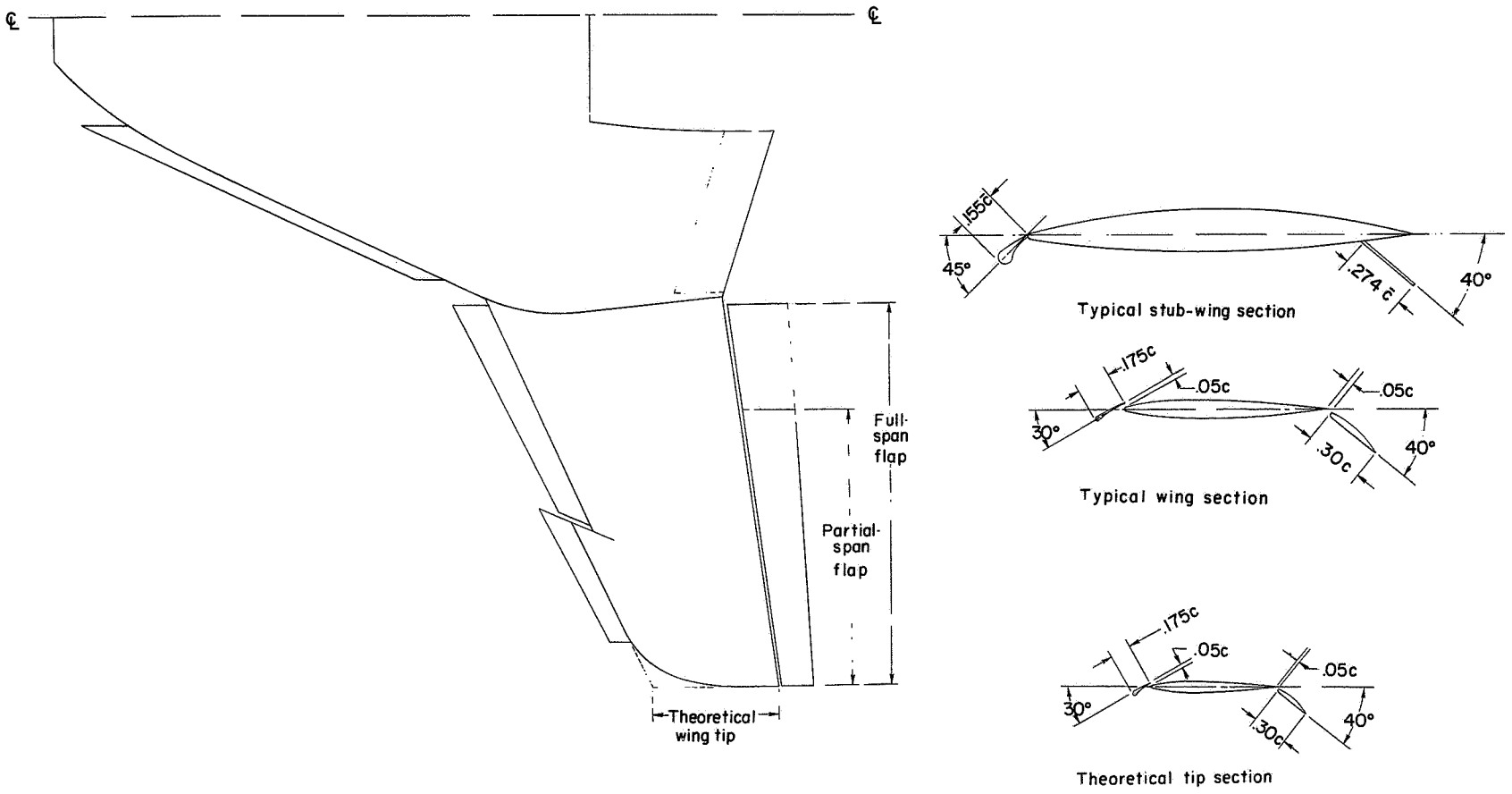

Figure 2.- Details of wing high-lift devices.

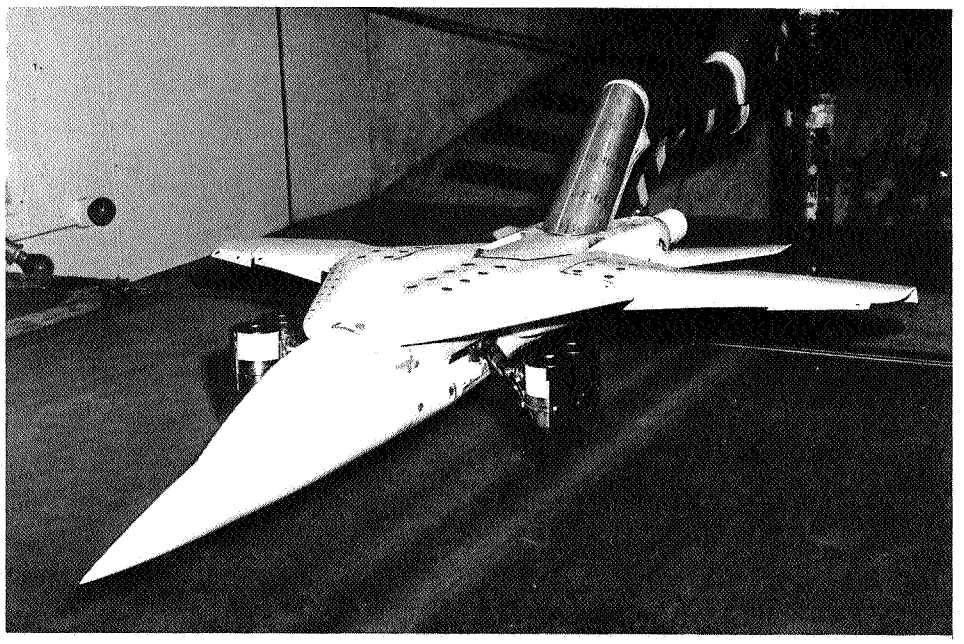

(a) View showing the direct-lift engines deflected 90° for VTOL. L-66-4928

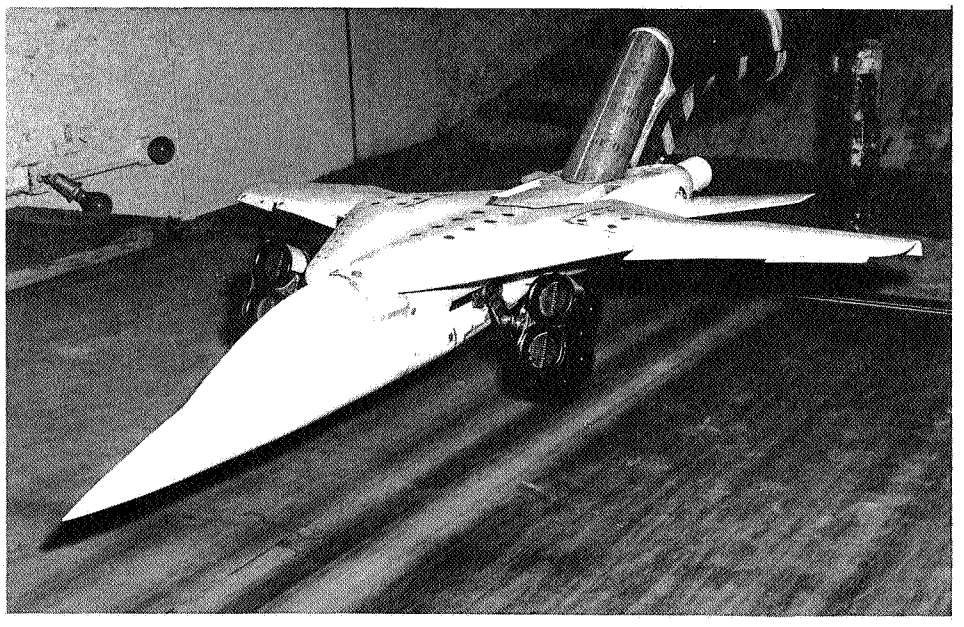

(b) View showing the direct-lift engines deflected 45° for STOL. L-66-4927

Figure 3. Photographs of configuration A above the moving-belt ground plane in the 5.18-meter (17-foot) test section of the Langley 300-MPH 7- by 10-foot tunnel.

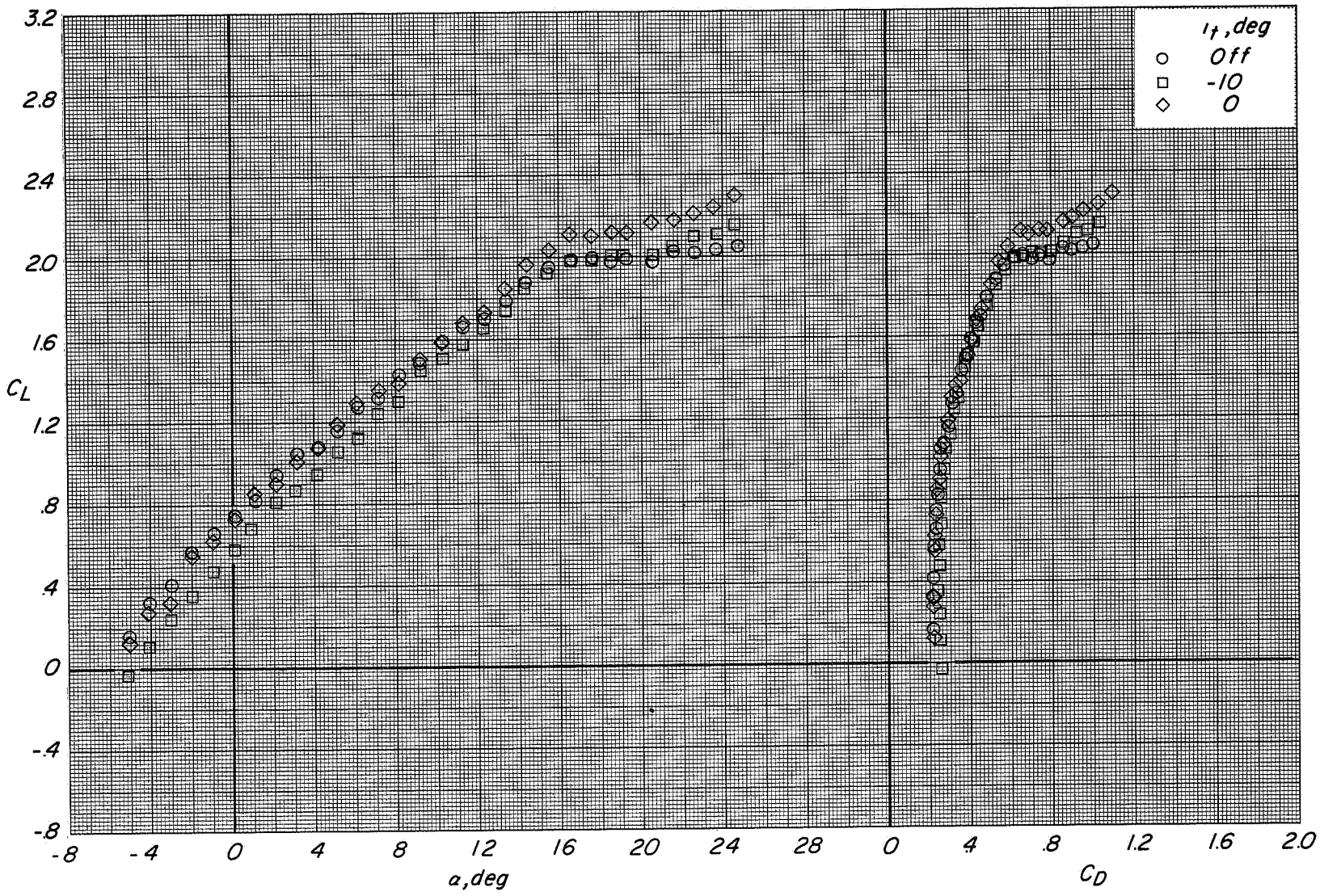

(a) Variation of C_L with α and C_D with C_L

Figure 4.- Effect of tail incidence on the longitudinal aerodynamic characteristics of configuration A with direct-lift and lift-cruise engines deflected 90°. $h/D_e = \infty$; $\beta = 0°$; $C_T = 0$.

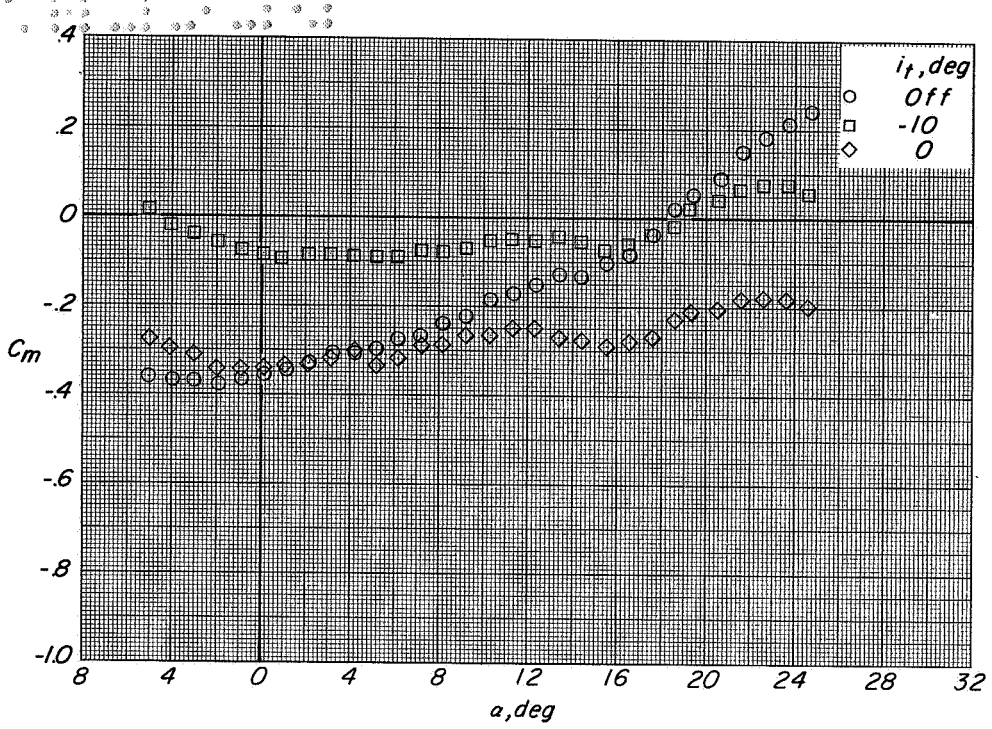

(b) Variation of C_m with α.

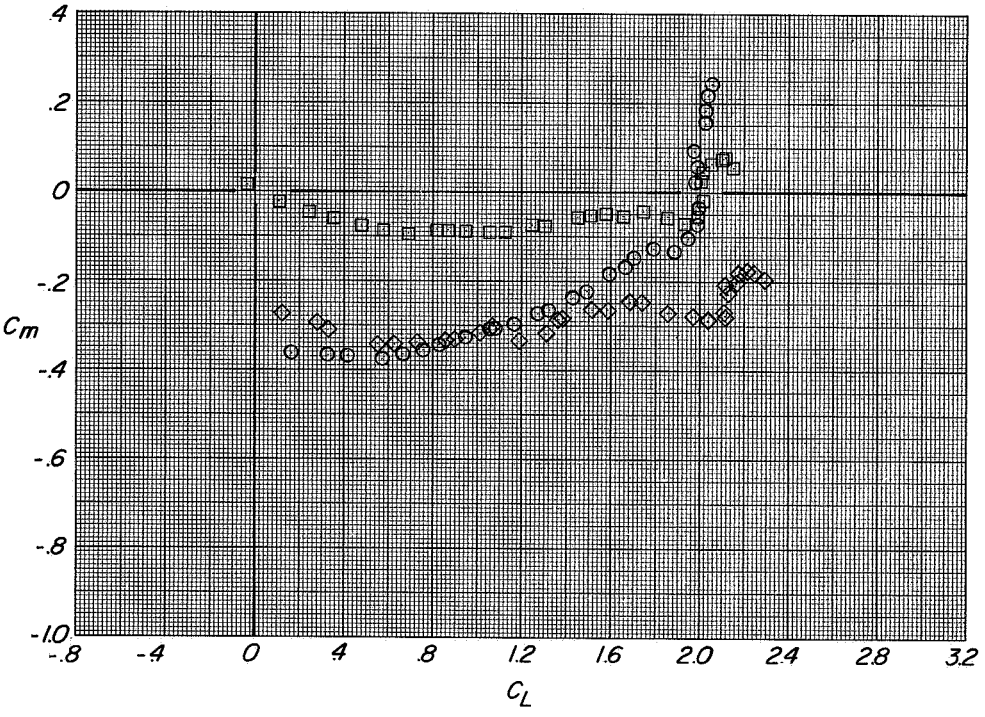

(c) Variation of C_m with C_L.

Figure 4.- Concluded.

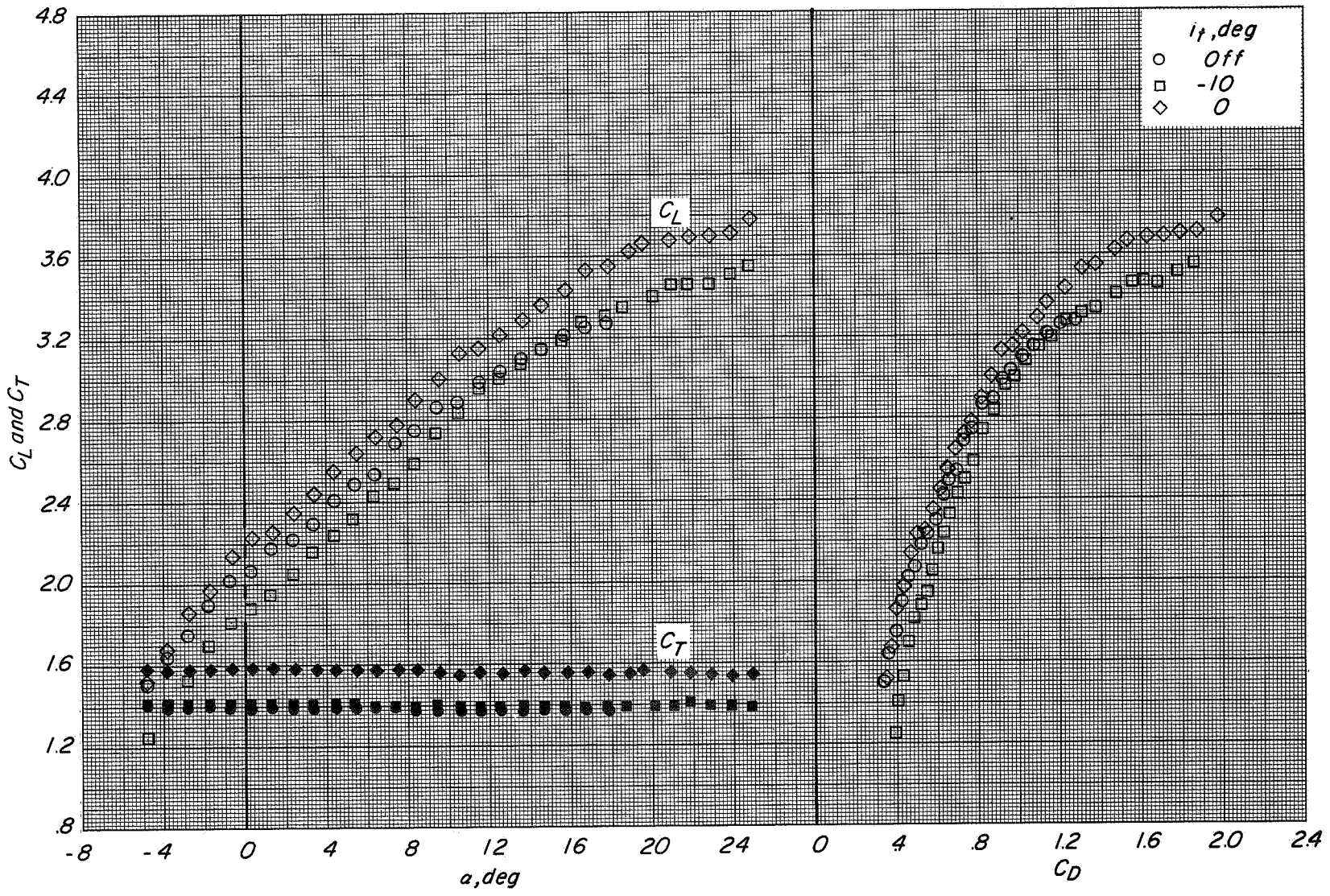

(a) Variation of C_L and C_T with α and C_D with C_L.

Figure 5.- Effect of tail incidence on the longitudinal aerodynamic characteristics of configuration A with direct-lift and lift-cruise engines deflected 90°. $h/D_e = \infty$; $\beta = 0°$; $C_T \approx 1.45$.

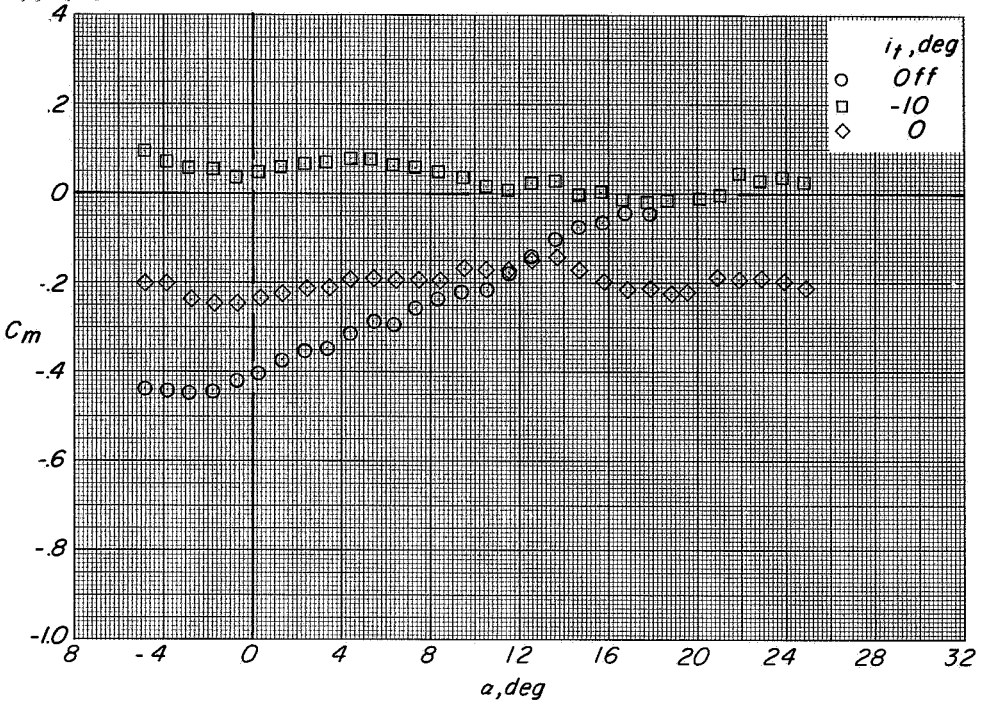

(b) Variation of C_m with α.

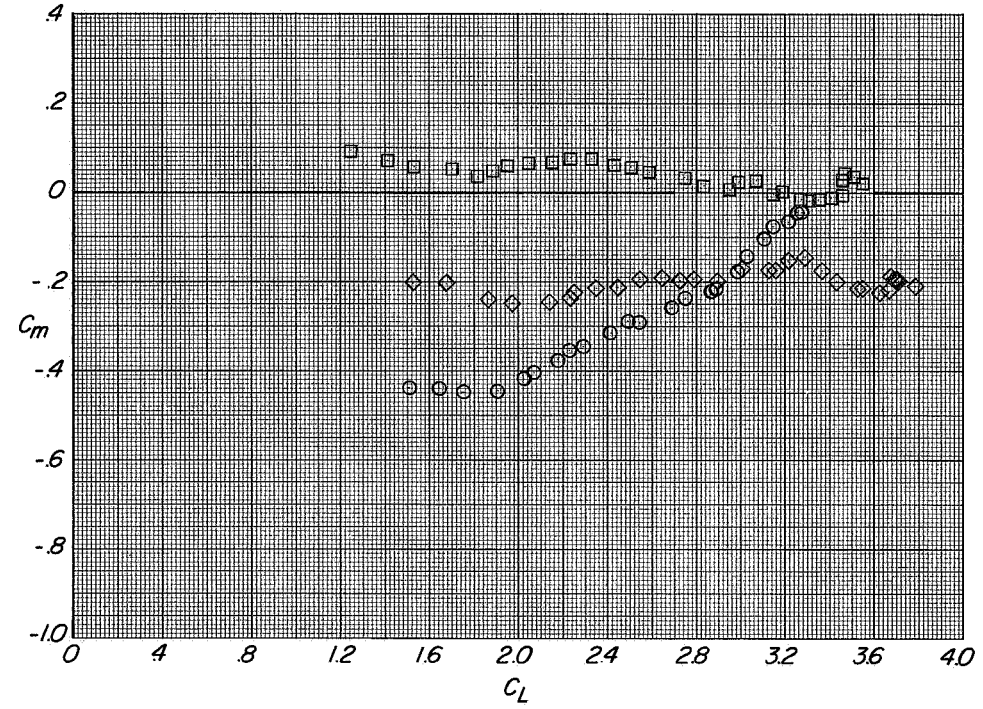

(c) Variation of C_m with C_L.

Figure 5.- Continued.

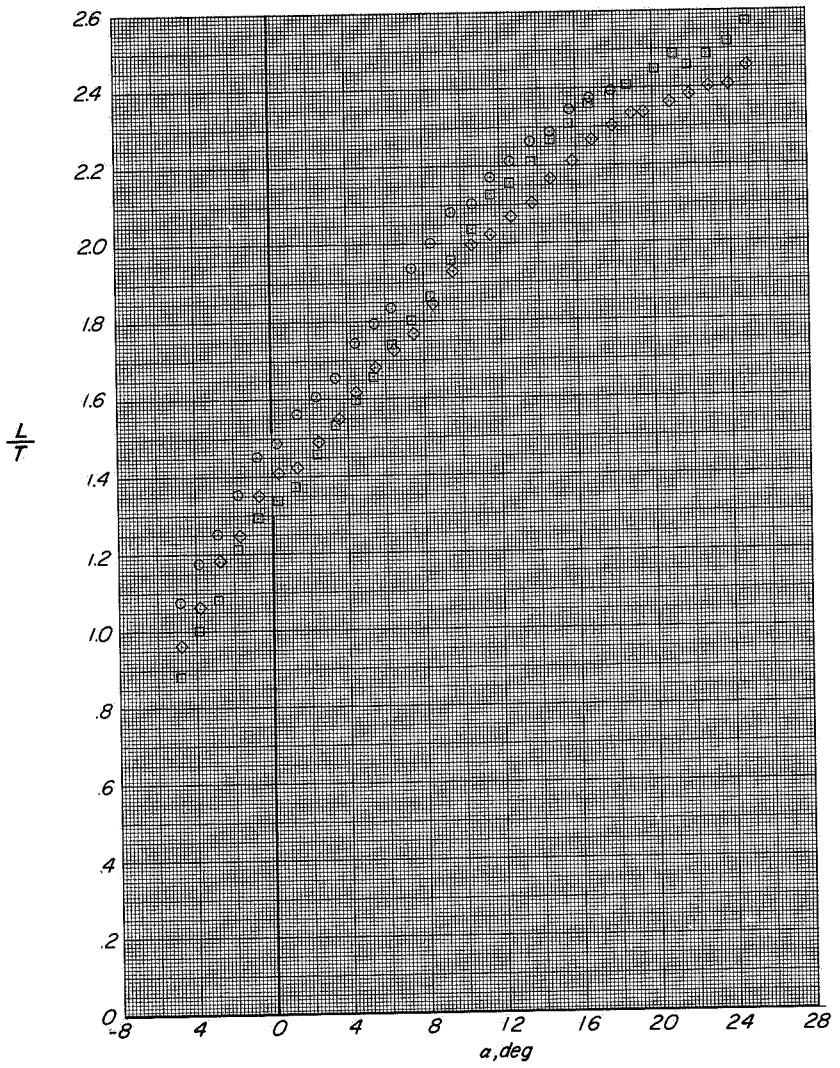

(d) Variation of L/T with α.

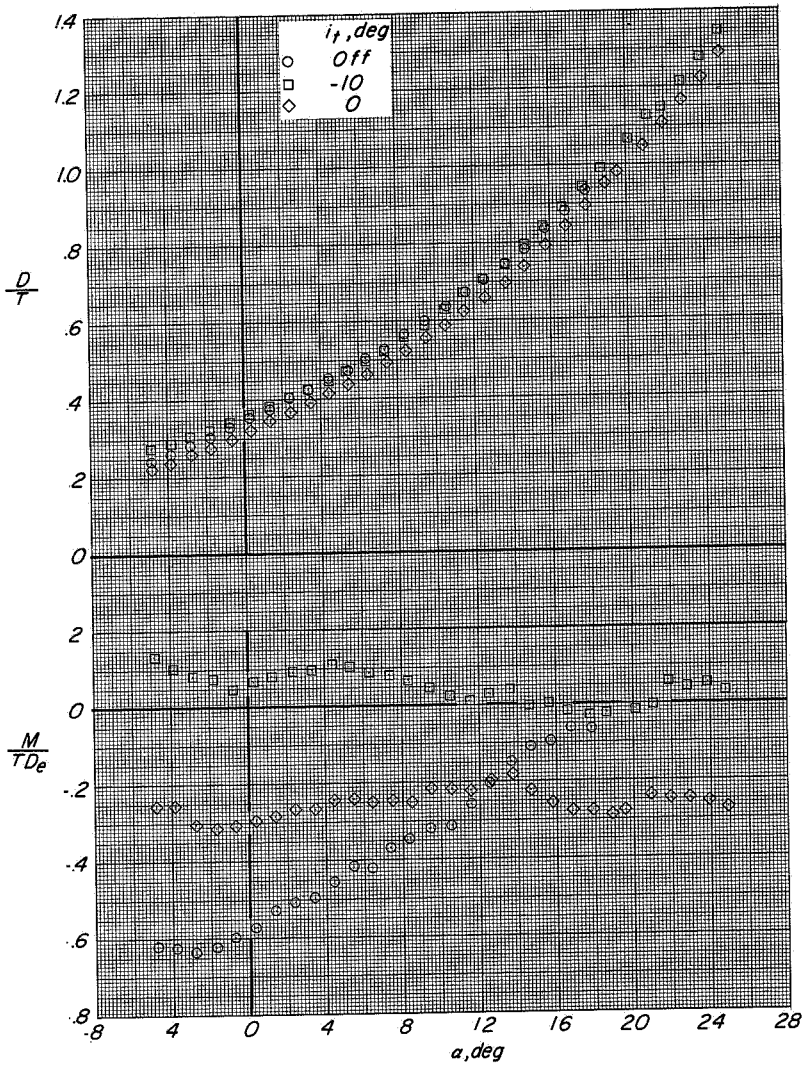

(e) Variation of D/T and M/TD$_e$ with α.

Figure 5. Concluded.

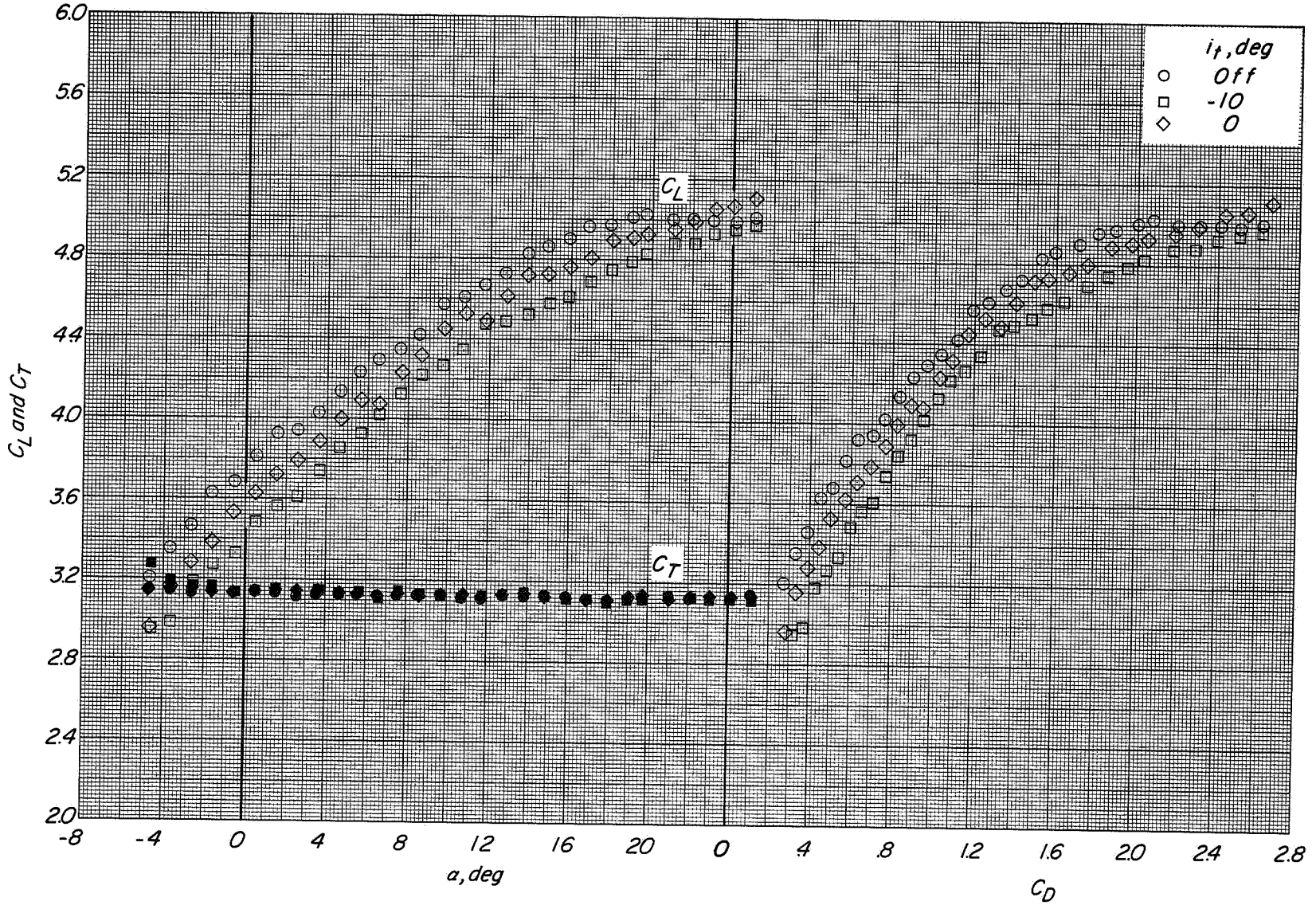

(a) Variation of C_L and C_T with α and C_D with C_L

Figure 6.- Effect of tail incidence on the longitudinal aerodynamic characteristics of configuration A with direct-lift and lift-cruise engines deflected 90°. $h/D_e = \infty$; $\beta = 0°$; $C_T \approx 3.3$.

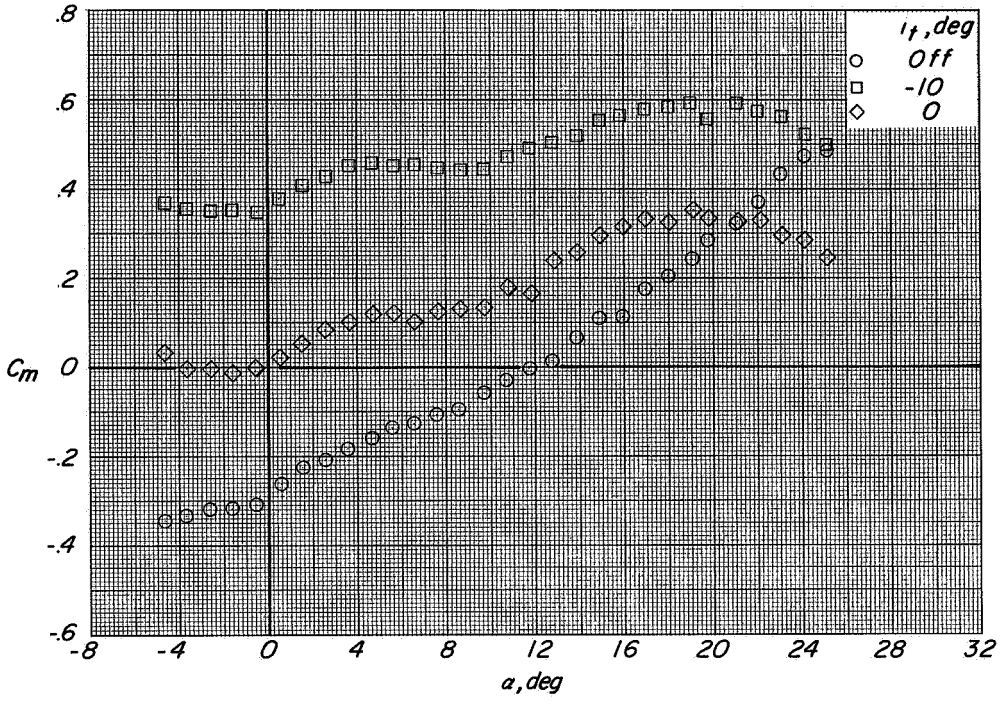

(b) Variation of C_m with α.

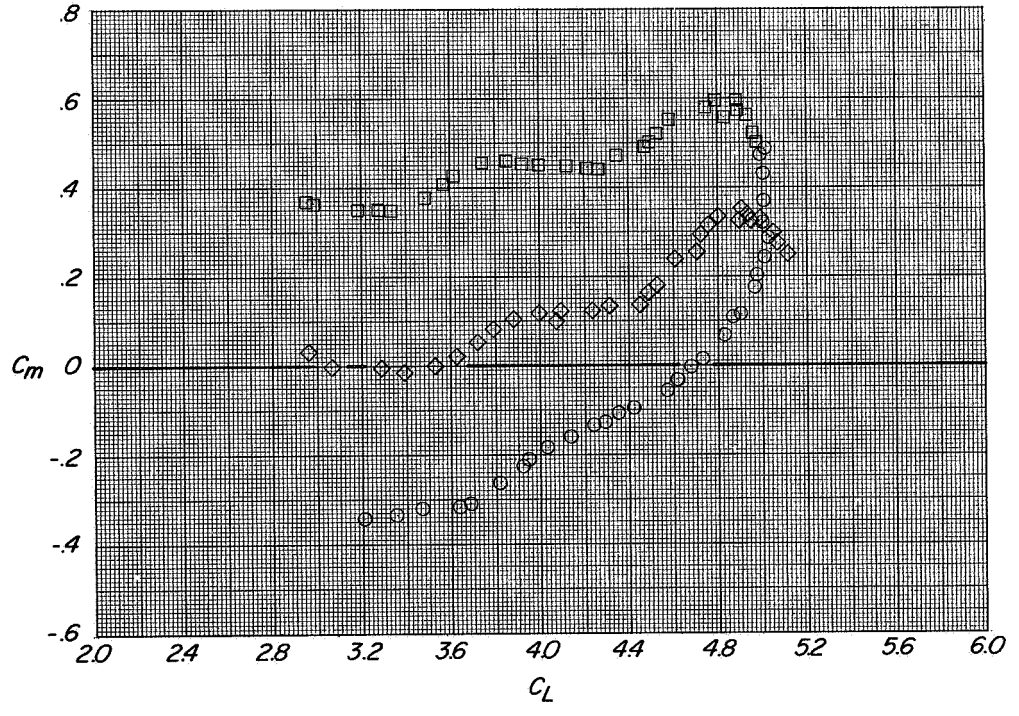

(c) Variation of C_m with C_L.

Figure 6.- Continued.

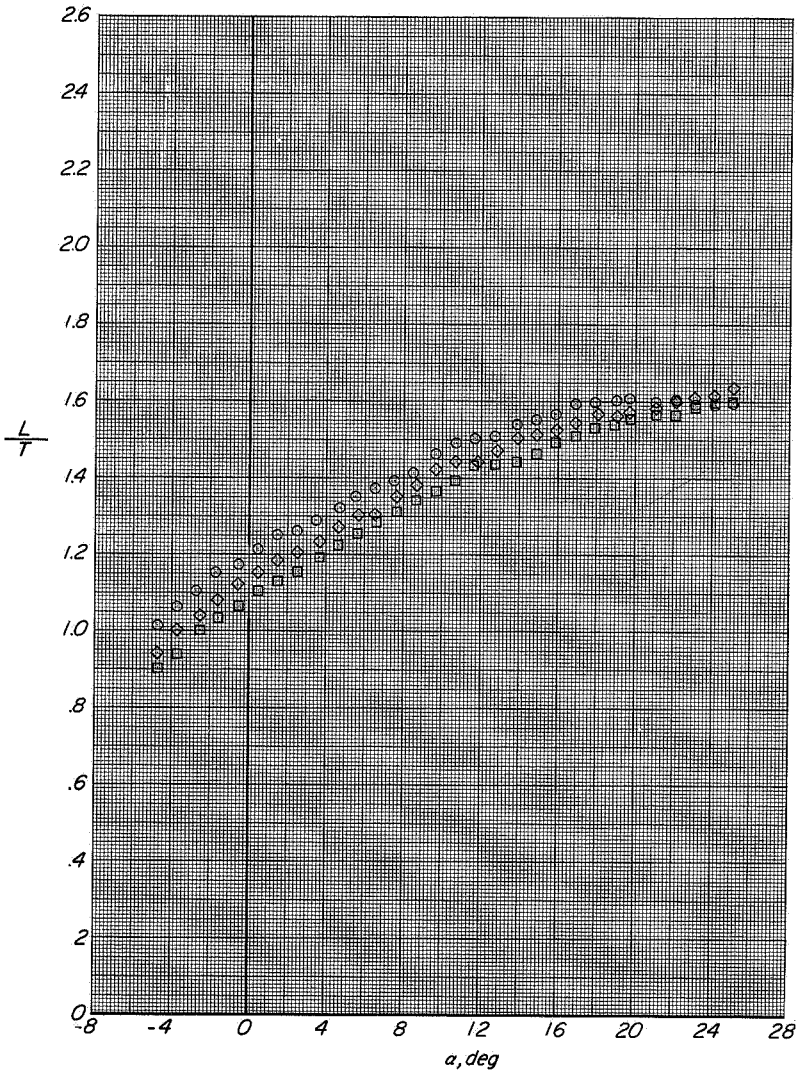

(d) Variation of L/T with α.

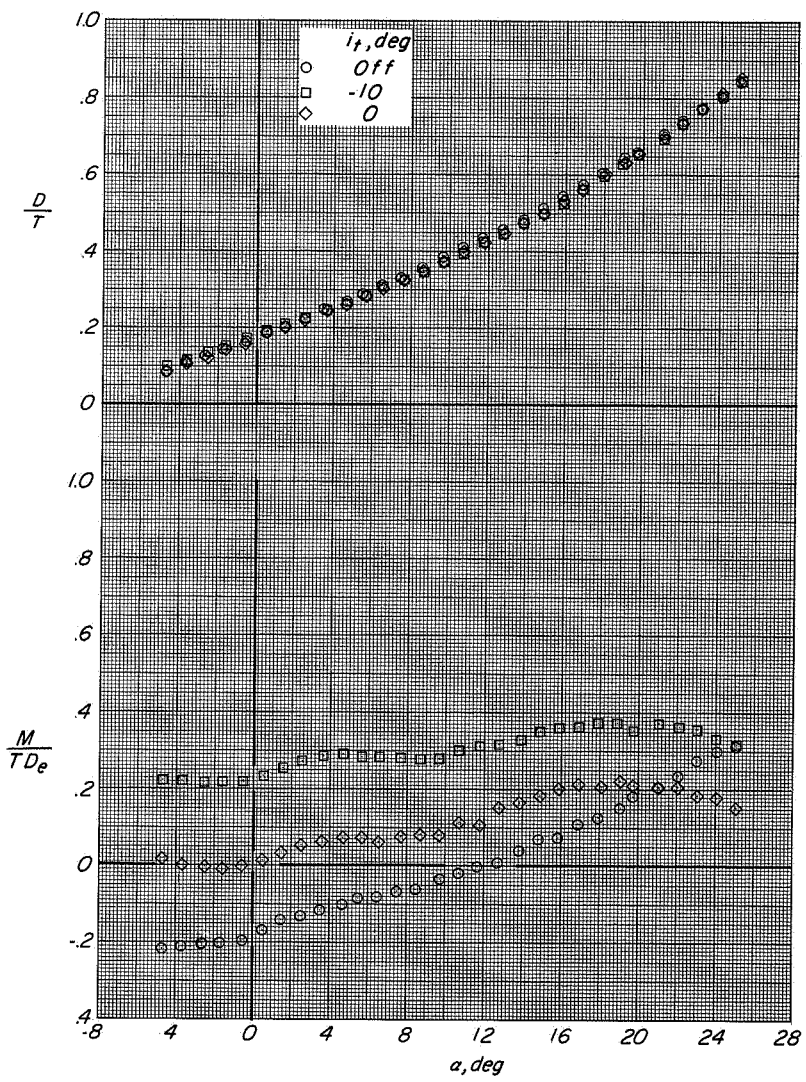

(e) Variation of D/T and M/TD$_e$ with α.

Figure 6.- Concluded.

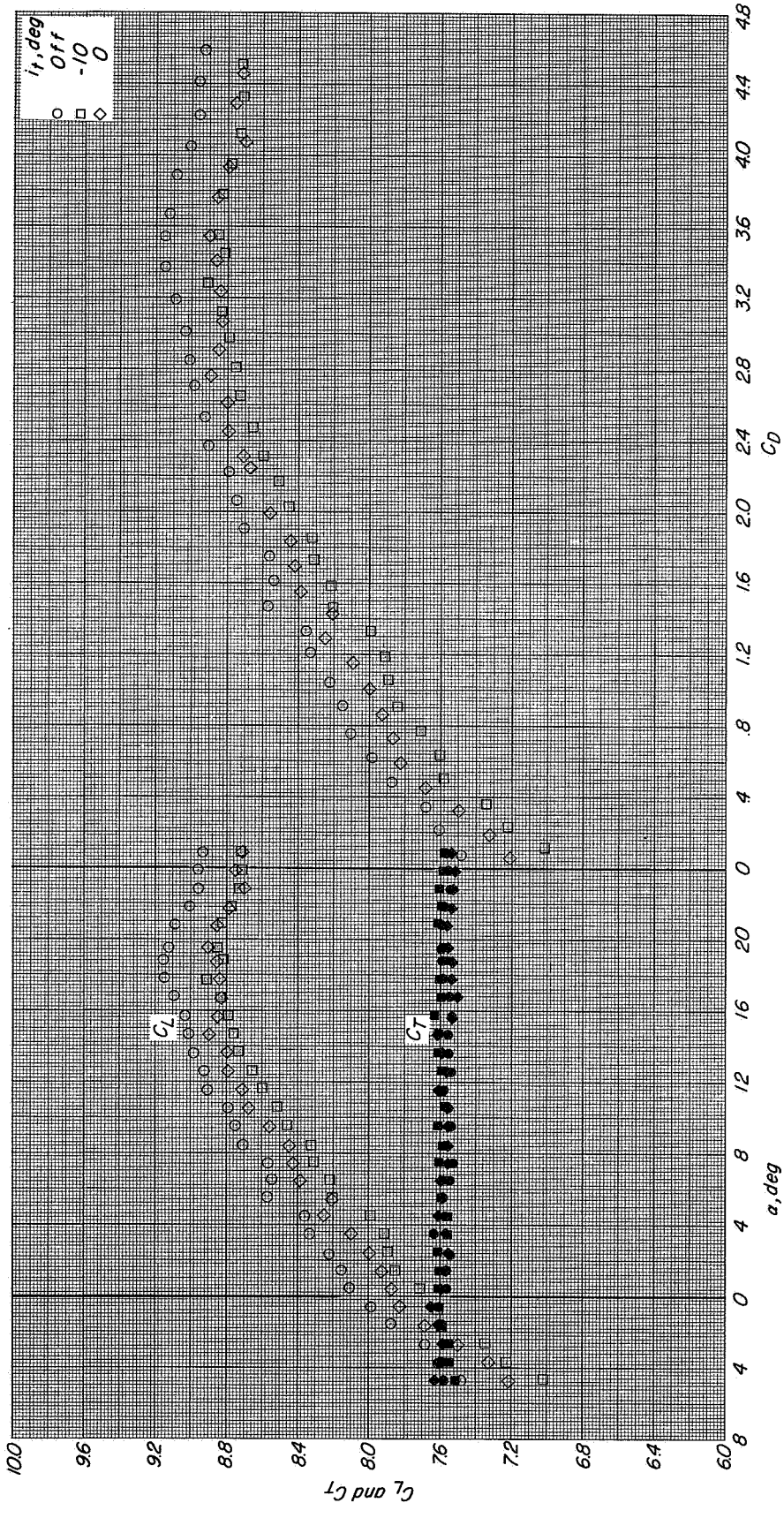

(a) Variation of C_L and C_T with α and C_D with C_L

Figure 7.- Effect of tail incidence on the longitudinal aerodynamic characteristics of configuration A with direct-lift and lift-cruise engines deflected 90°.
$h/D_e = \infty$; $\beta = 0°$; $C_T \approx 8$.

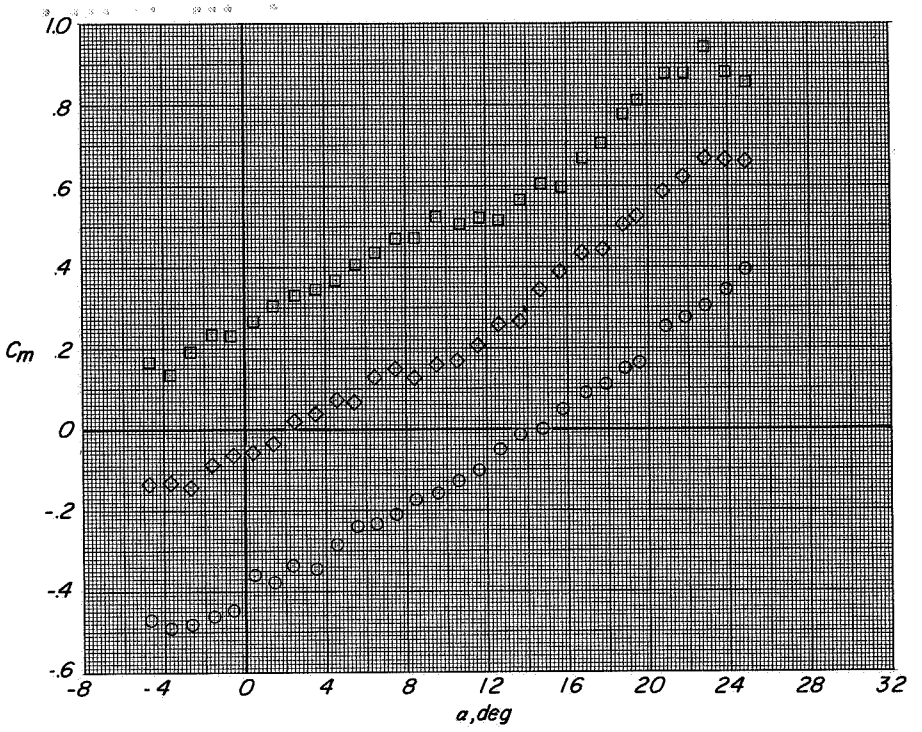

(b) Variation of C_m with α.

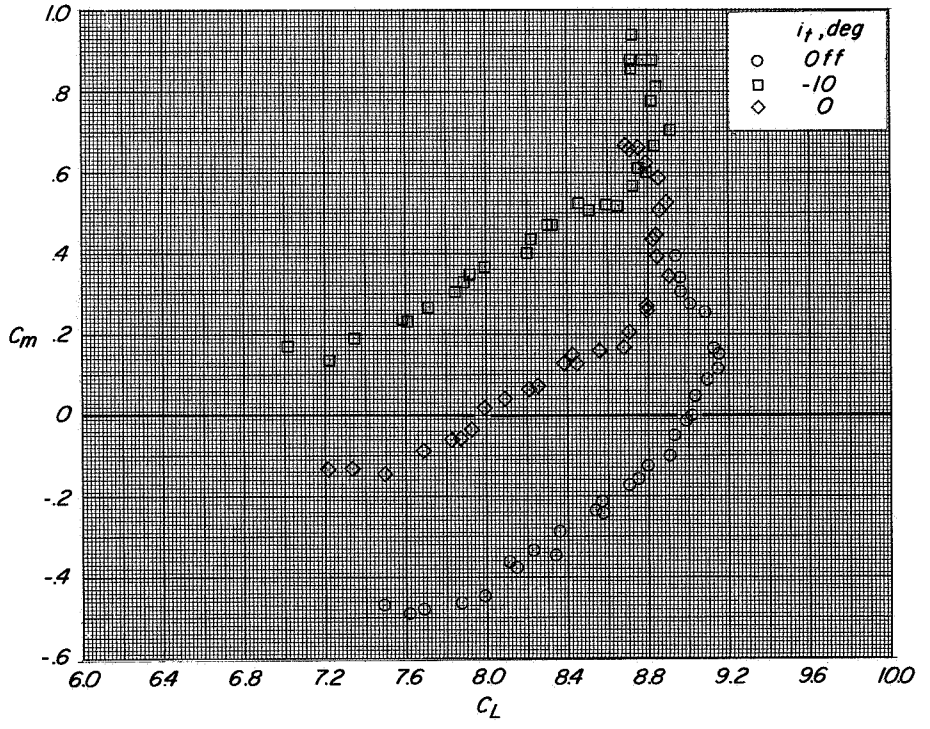

(c) Variation of C_m with C_L

Figure 7.- Continued.

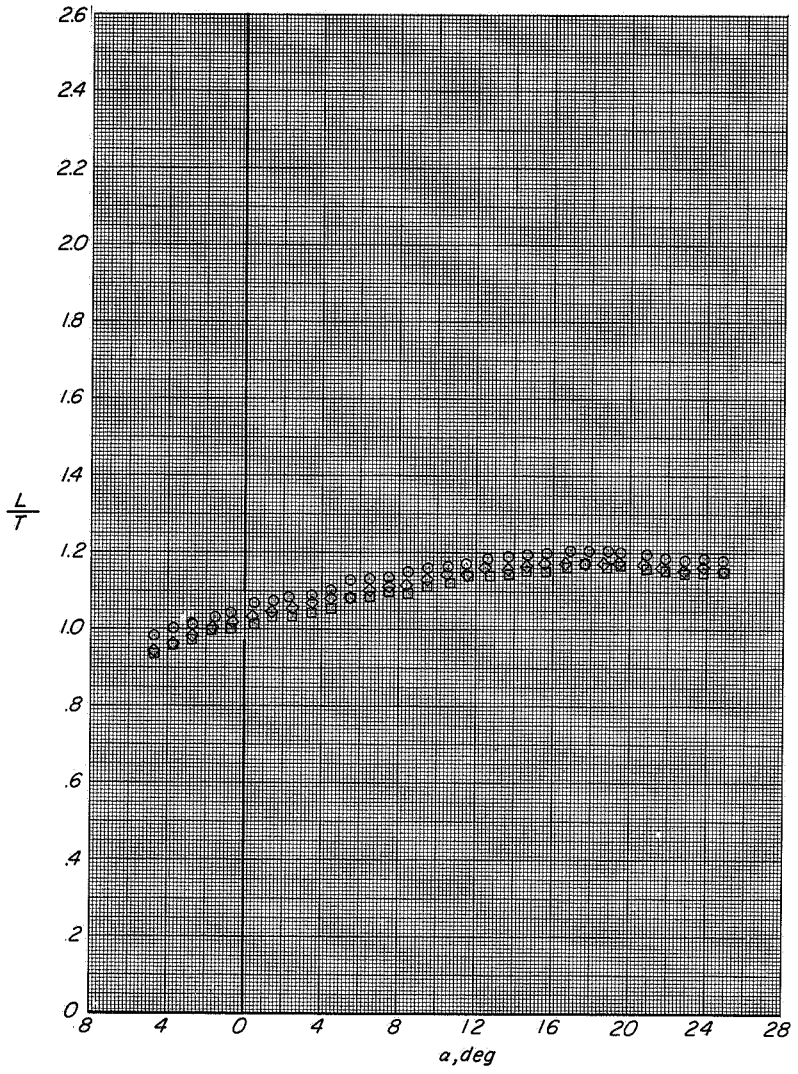

(d) Variation of L/T with α.

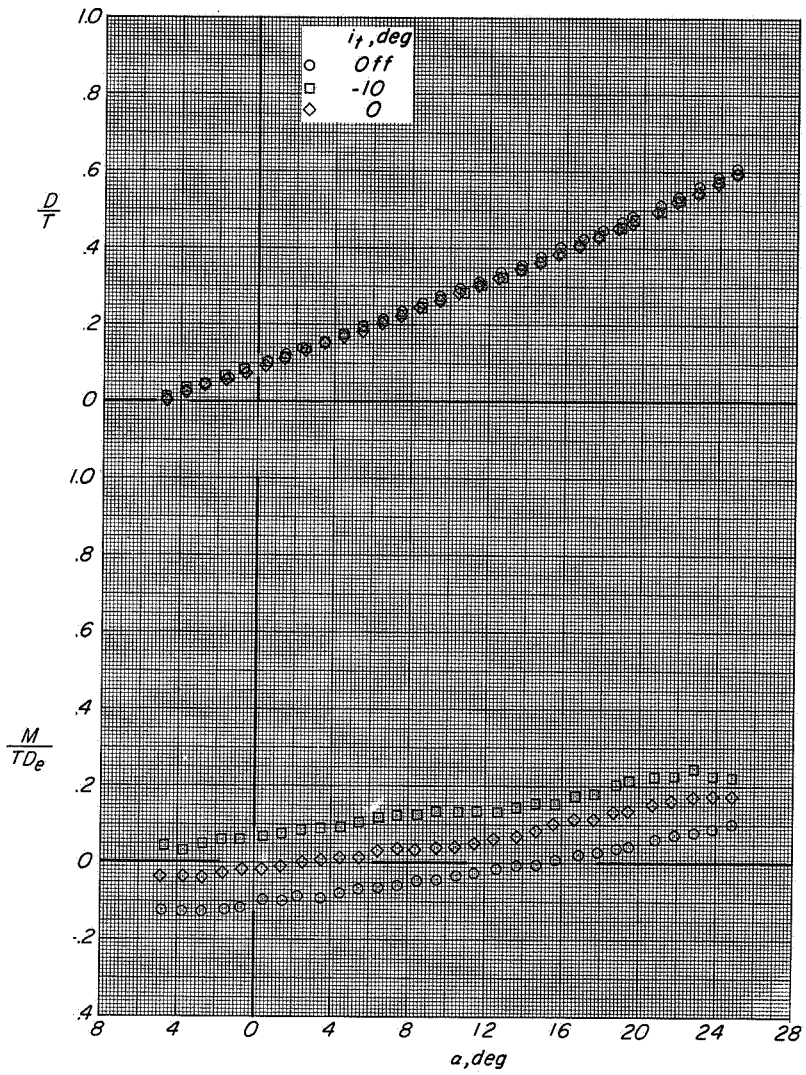

(e) Variation of D/T and M/TD_e with α.

Figure 7.- Concluded.

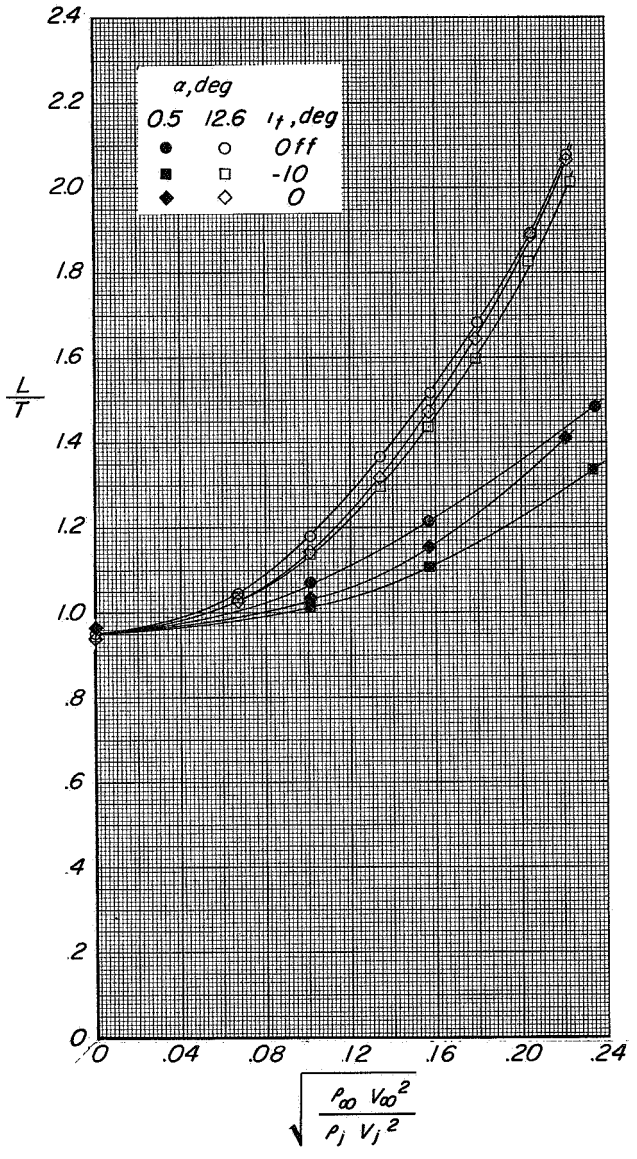

(a) Variation of L/T with effective velocity ratio.

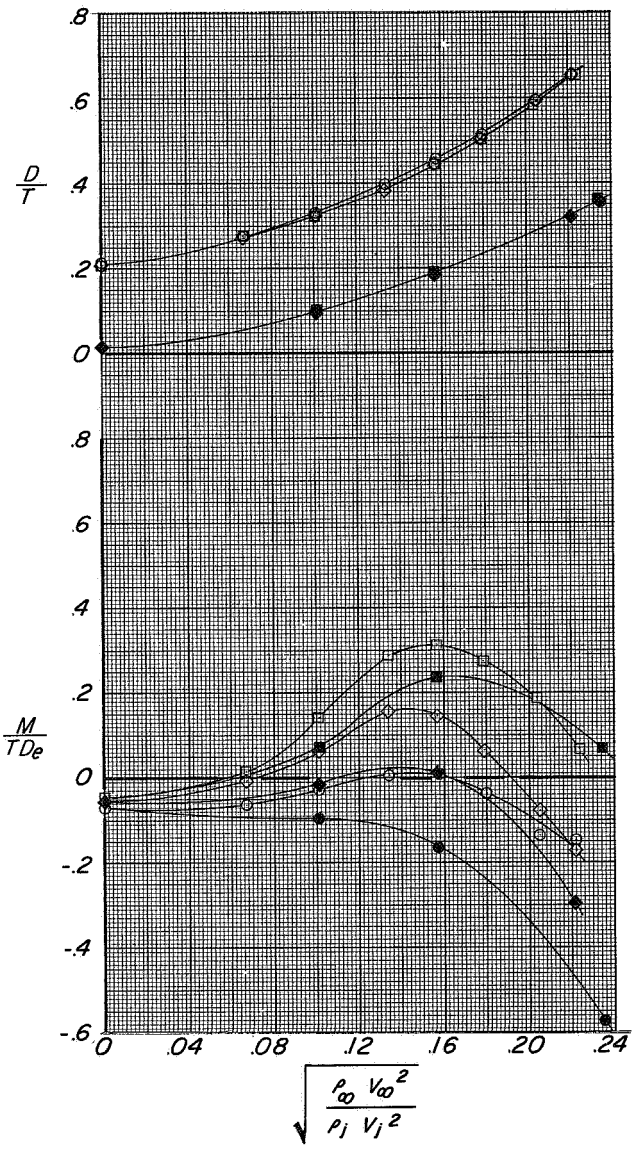

(b) Variation of D/T and M/TD_e with effective velocity ratio.

Figure 8.- Effect of effective velocity ratio on the longitudinal aerodynamic characteristics of configuration A with direct-lift and lift-cruise engines deflected 90° at several tail settings. $h/D_e = \infty$; $\beta = 0^0$

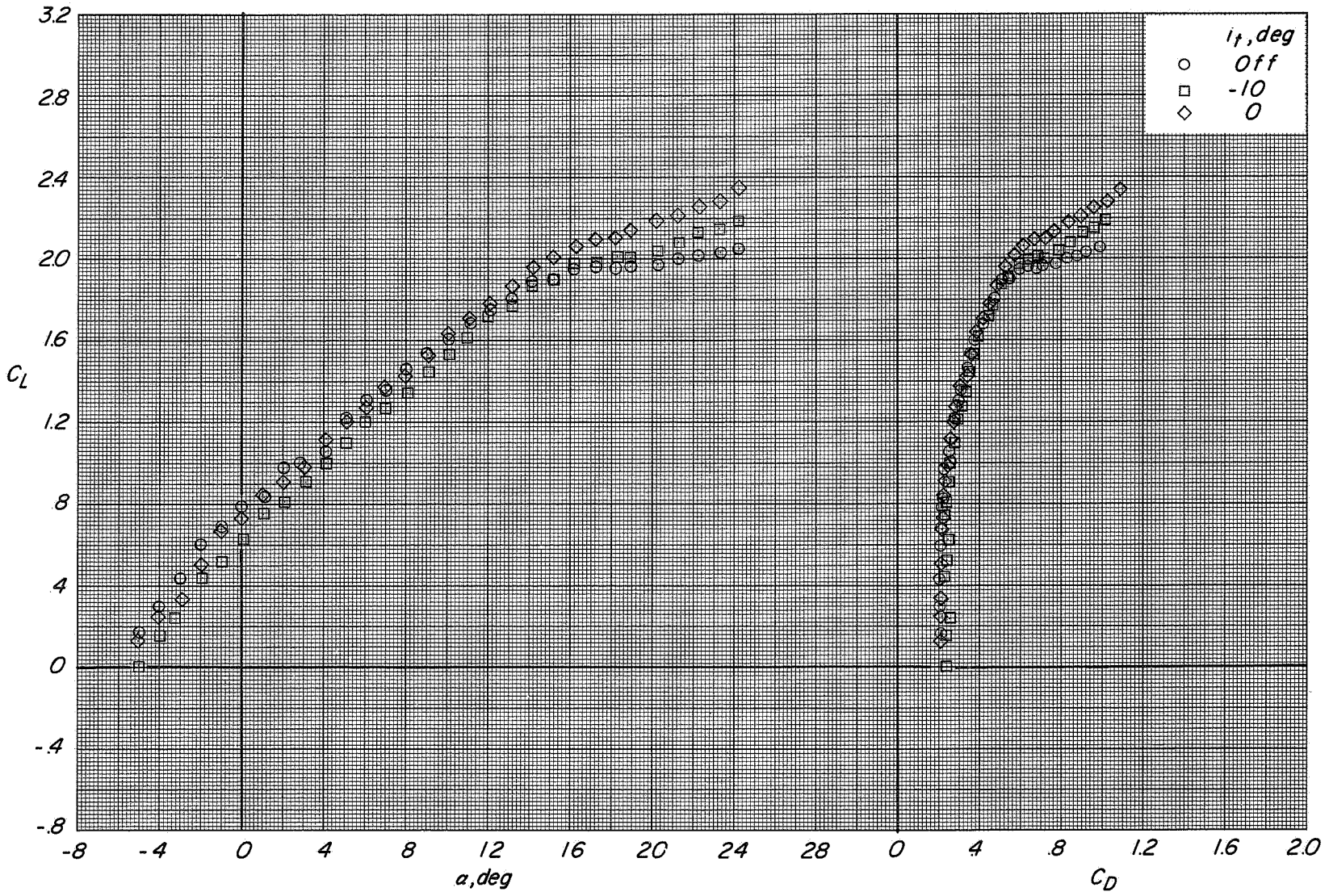

(a) Variation of C_L with α and C_D with C_L.

Figure 9.- Effect of tail incidence on the longitudinal aerodynamic characteristics of configuration A with direct-lift and lift-cruise engines deflected 90^0 $h/D_e = 3.0$; $\beta = 0^0$; $C_T = 0$.

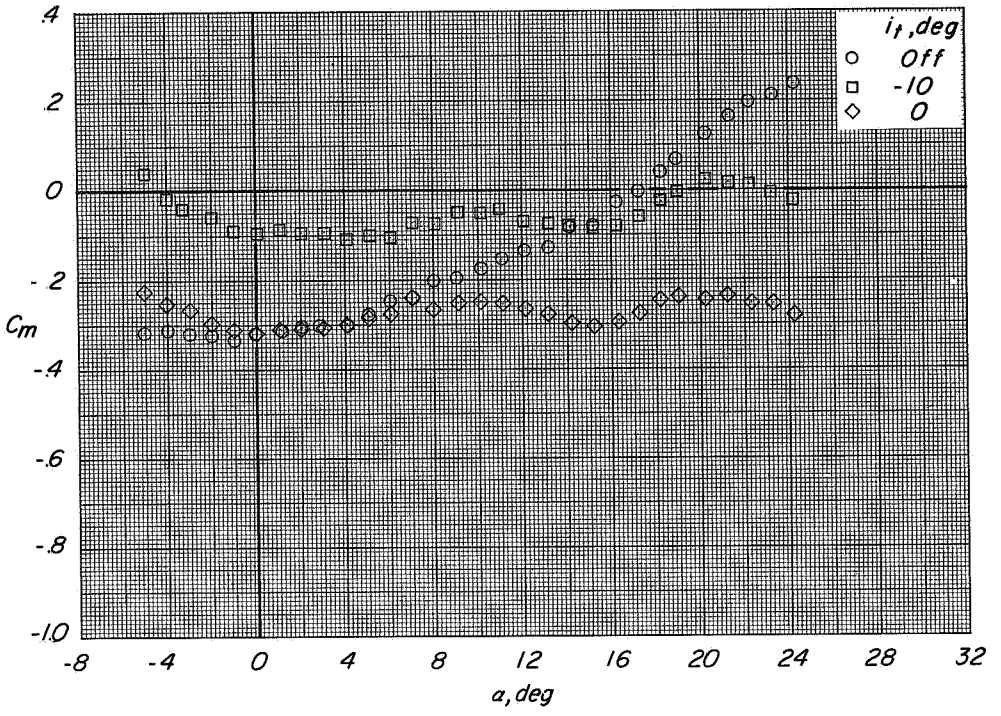

(b) Variation of C_m with α.

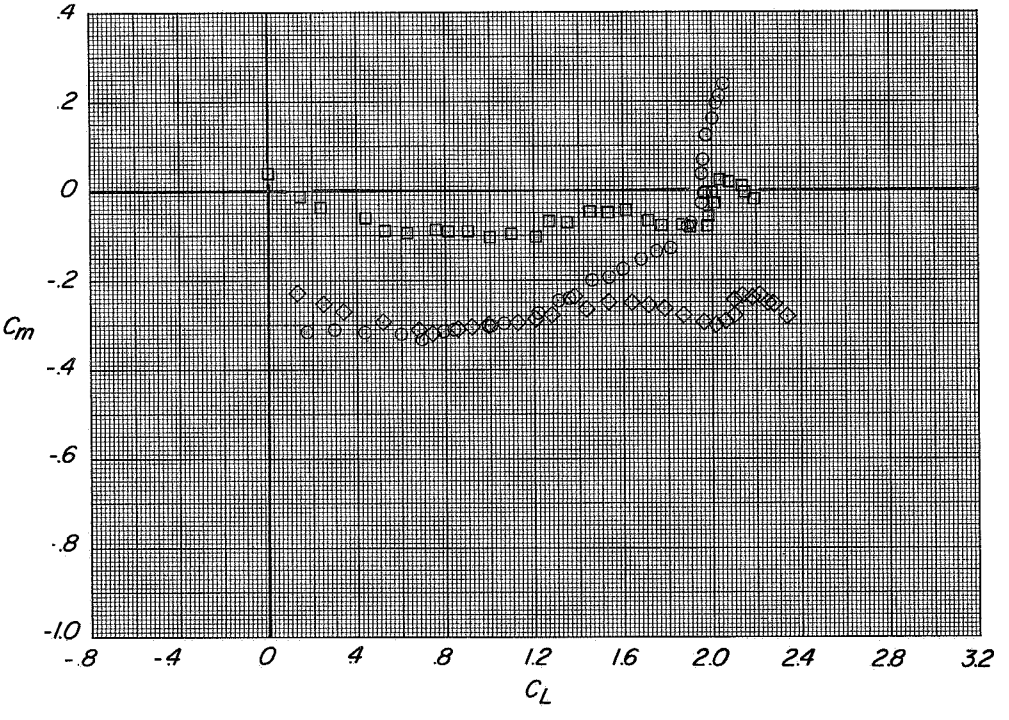

(c) Variation of C_m with C_L

Figure 9.- Concluded.

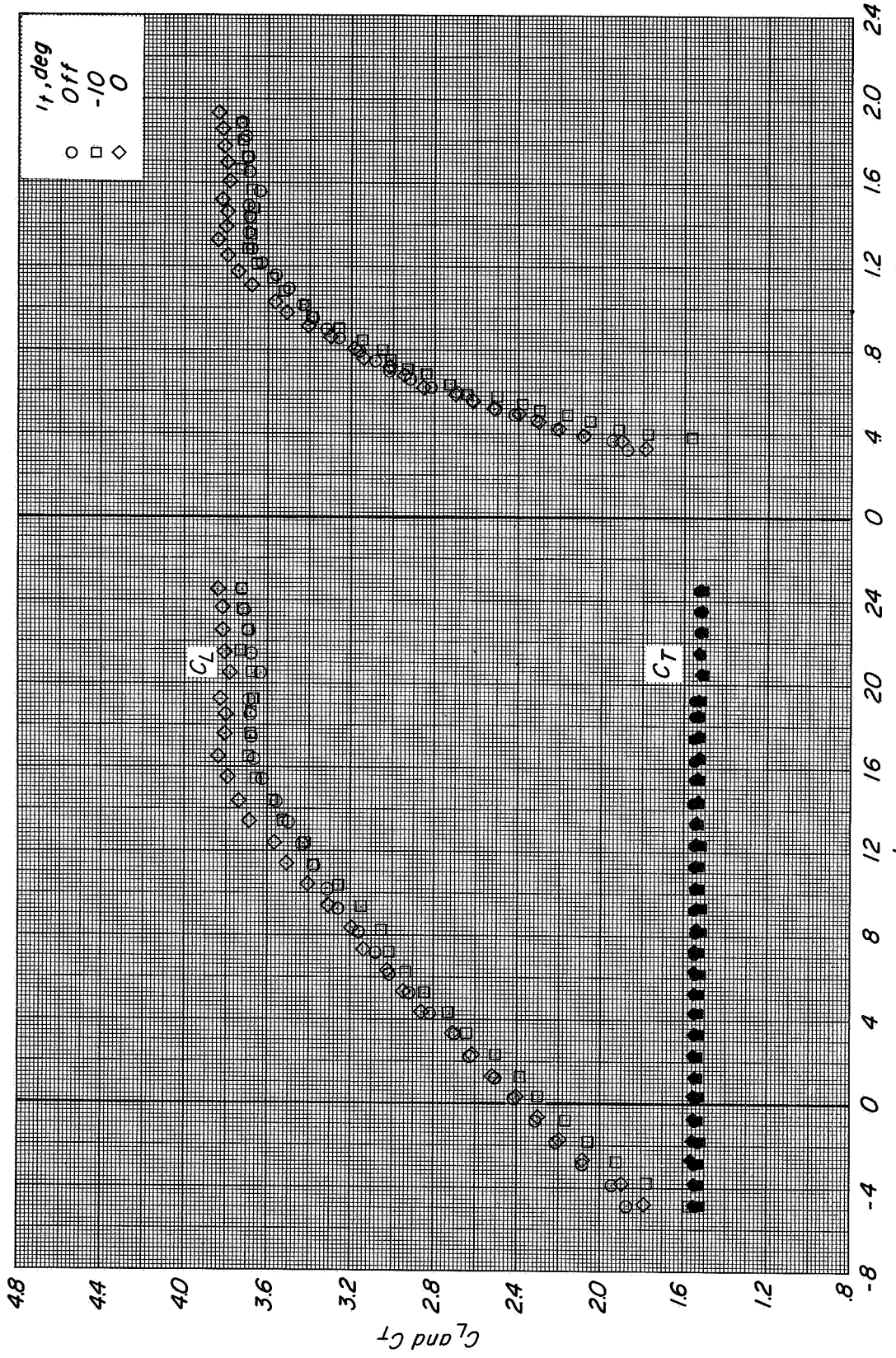

(a) Variation of C_L and C_T with α and C_D with C_L

Figure 10.- Effect of tail incidence on the longitudinal aerodynamic characteristics of configuration A with direct-lift and lift-cruise engines deflected 90°. $h/D_e = 3.0$; $\beta = 0^0$; $C_T \approx 1.45$.

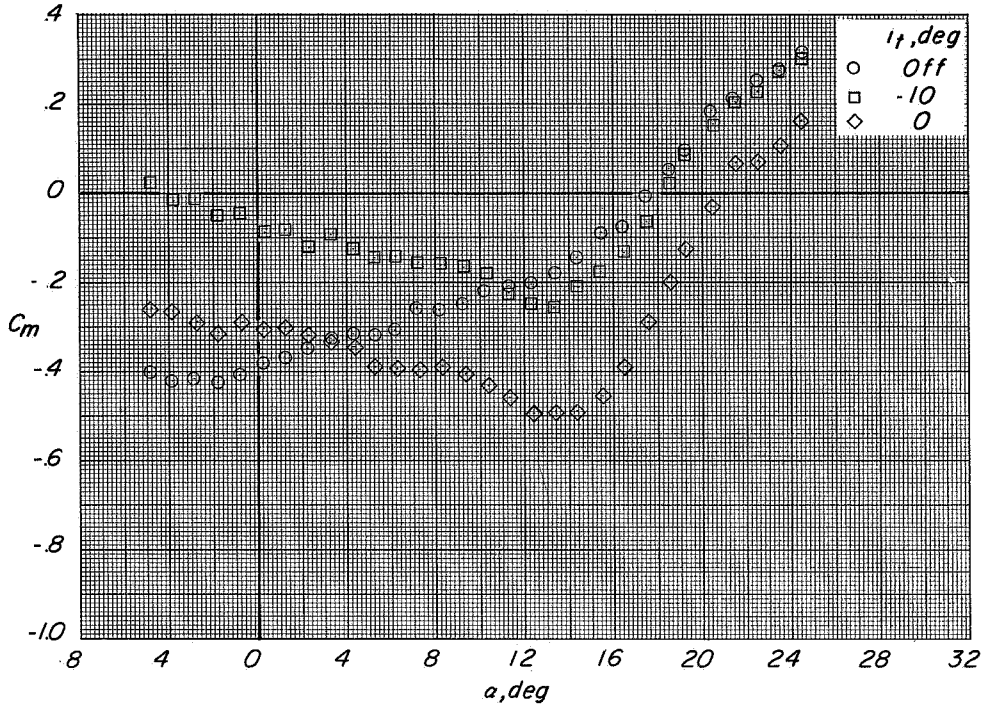

(b) Variation of C_m with α.

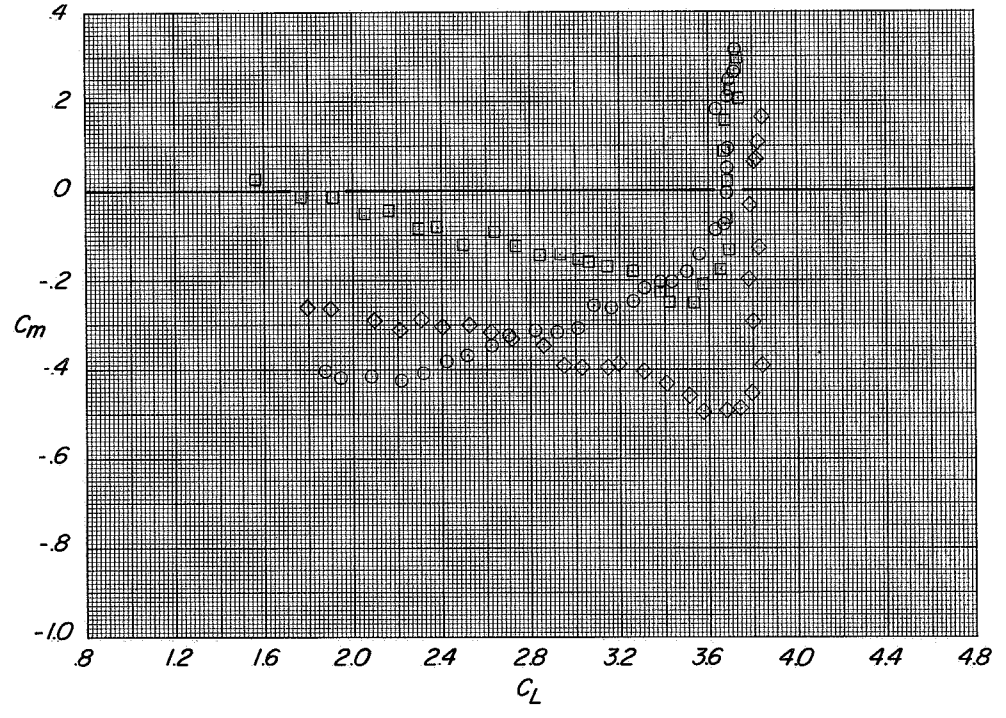

(c) Variation of C_m with C_L.

Figure 10. Continued.

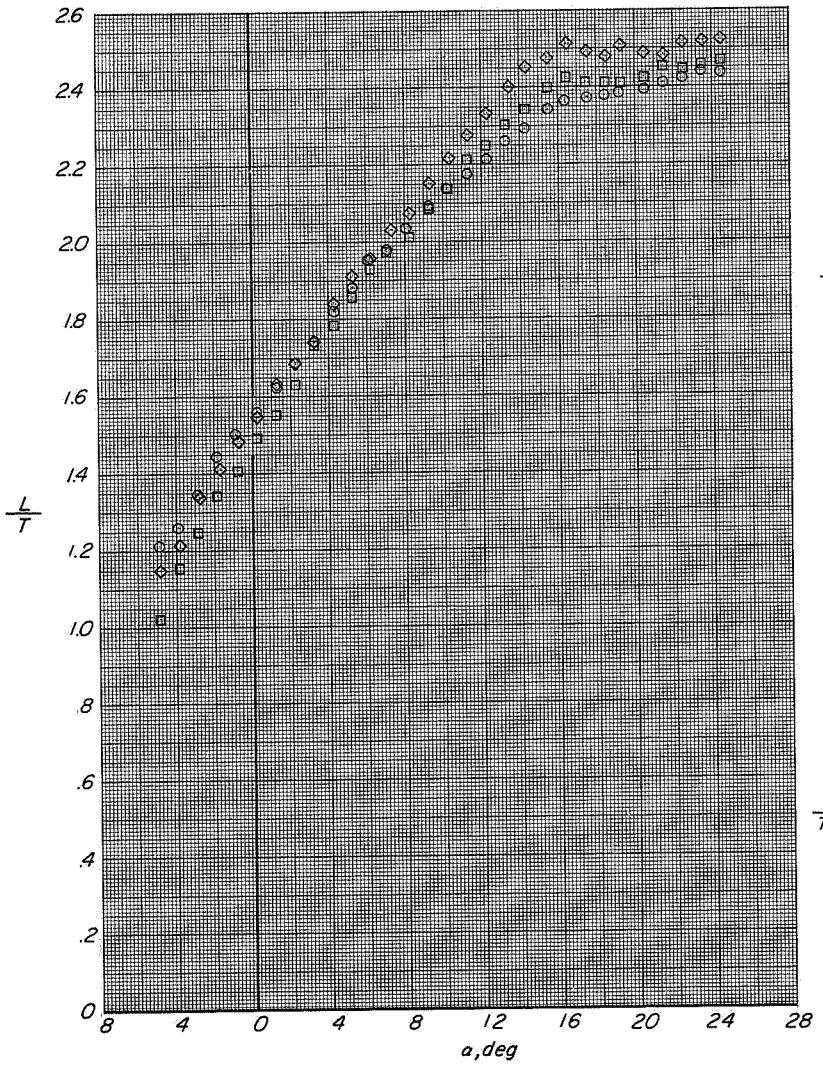

(d) Variation of L/T with α.

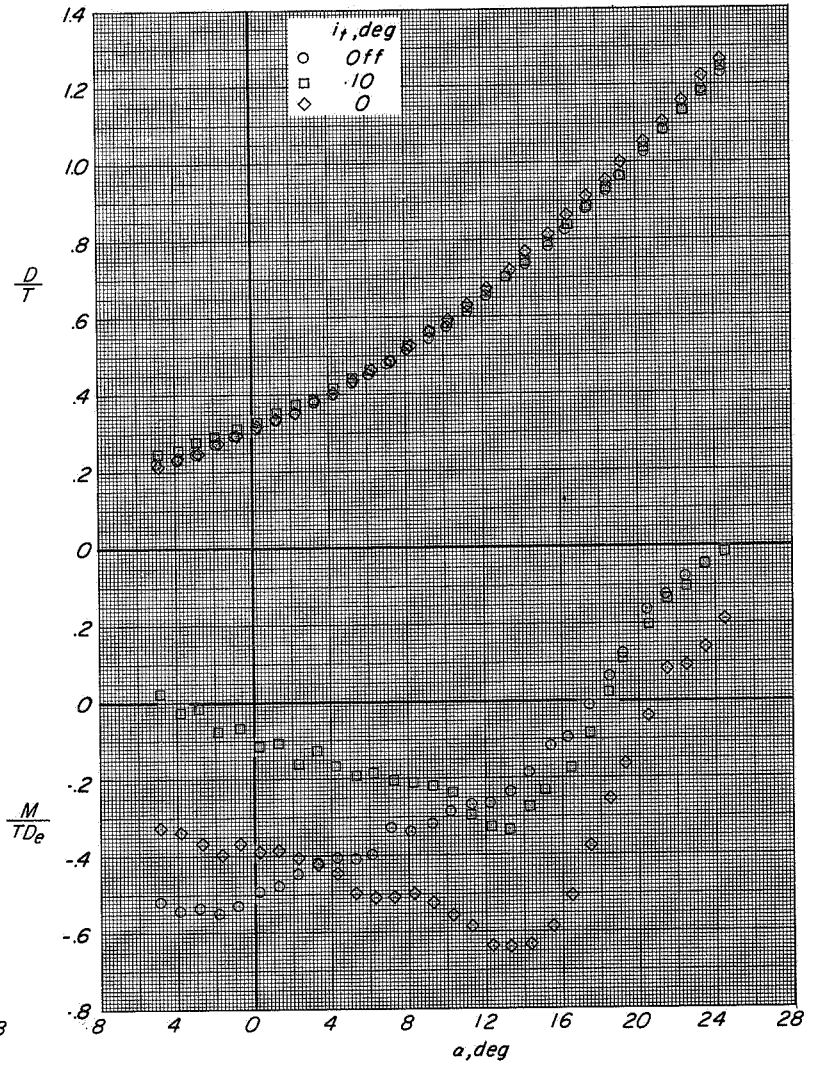

(e) Variation of D/T and M/TD_e with α.

Figure 10.- Concluded.

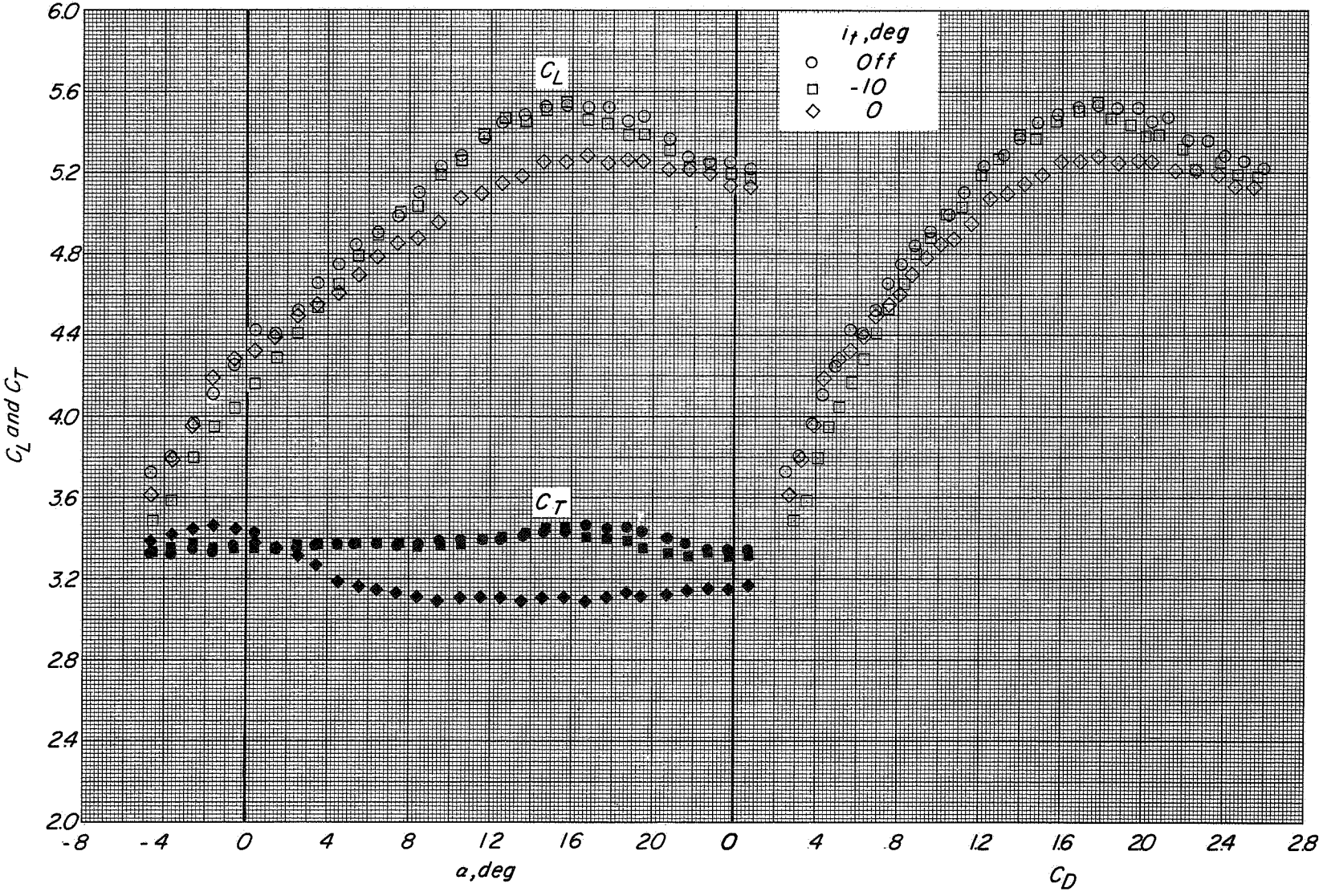

(a) Variation of C_L and C_T with α and C_D with C_L

Figure 11.- Effect of tail incidence on the longitudinal aerodynamic characteristics of configuration A with direct-lift and lift-cruise engines deflected 90°. $h/D_e = 3.0$; $\beta = 0°$; $C_T \approx 3.3$.

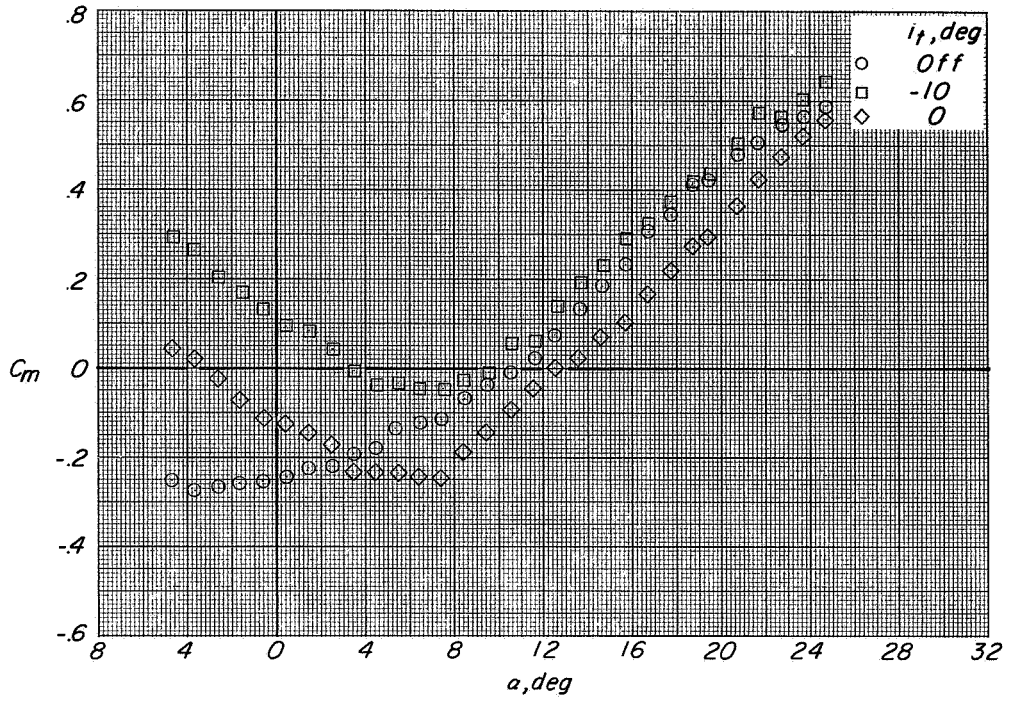

(b) Variation of C_m with α.

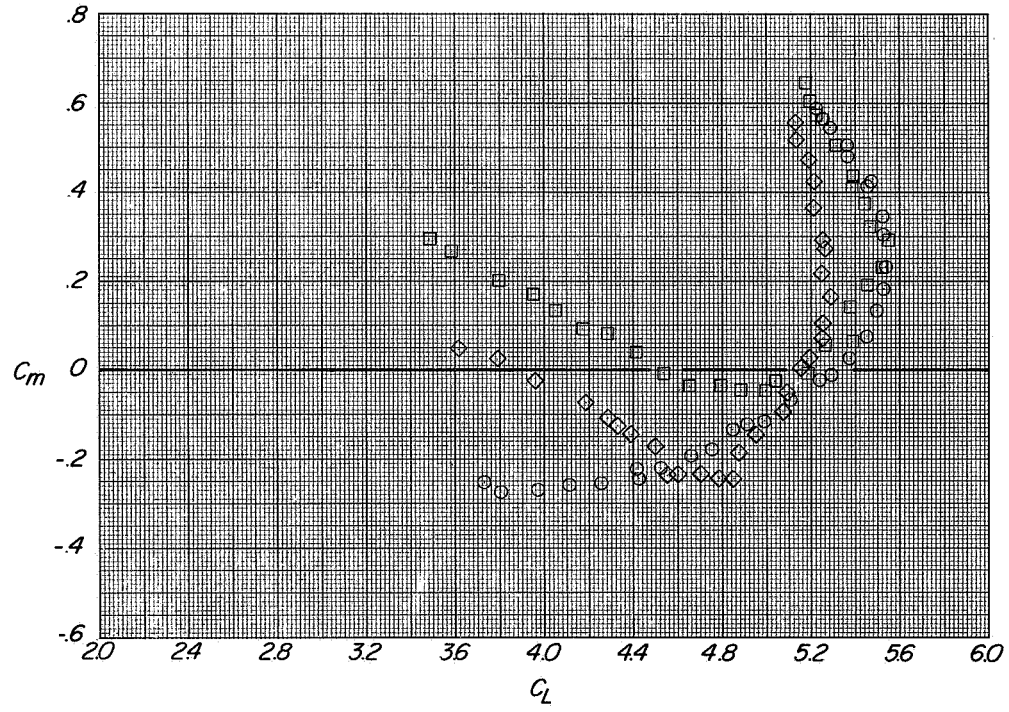

(c) Variation of C_m with C_L.

Figure 11.- Continued.

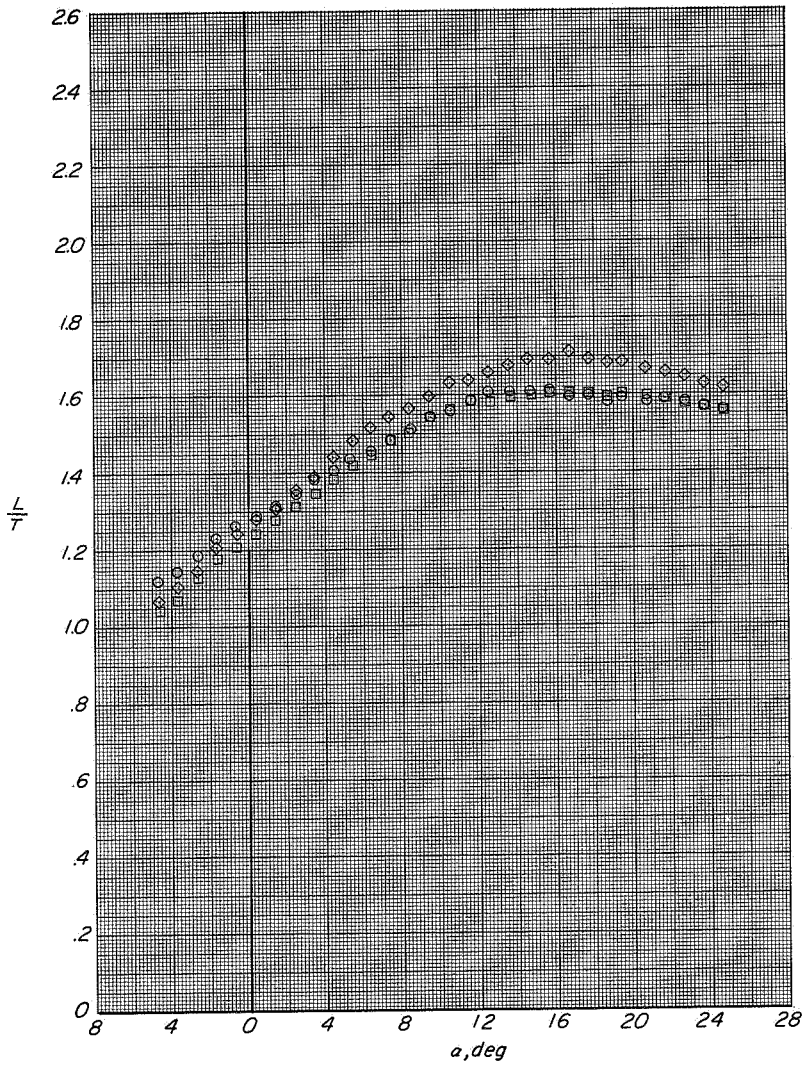

(d) Variation of L/T with α.

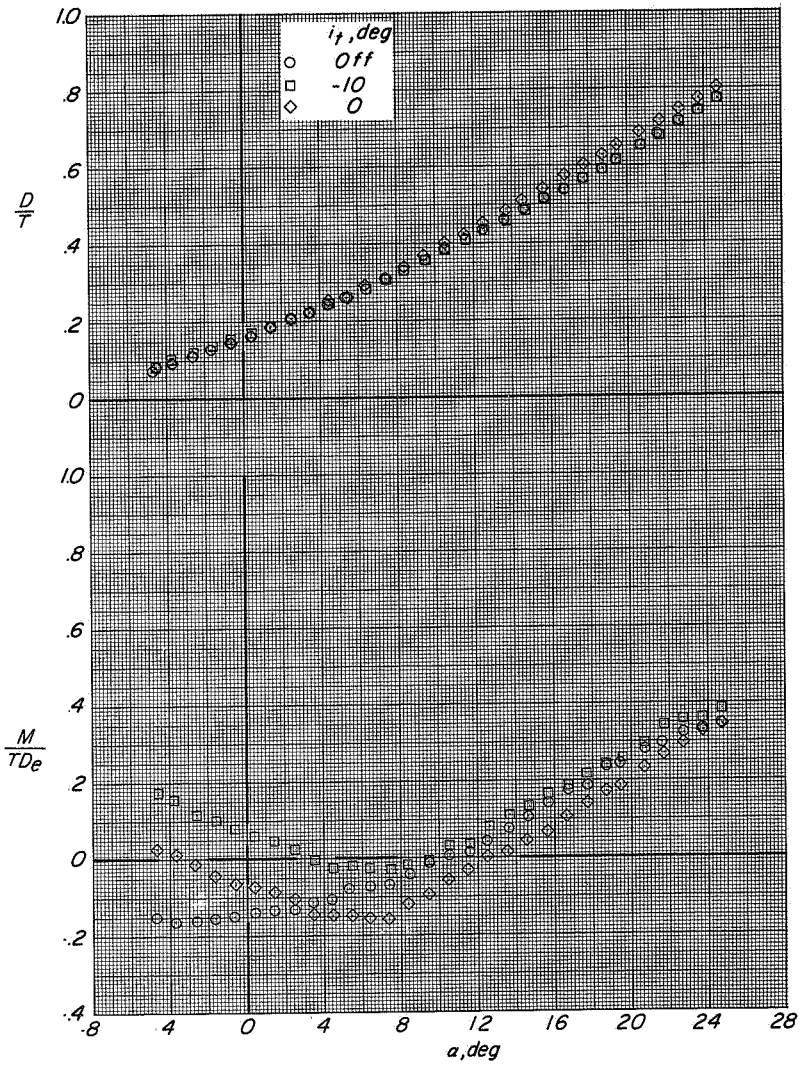

(e) Variation of D/T and M/TD_e with α.

Figure 11.- Concluded.

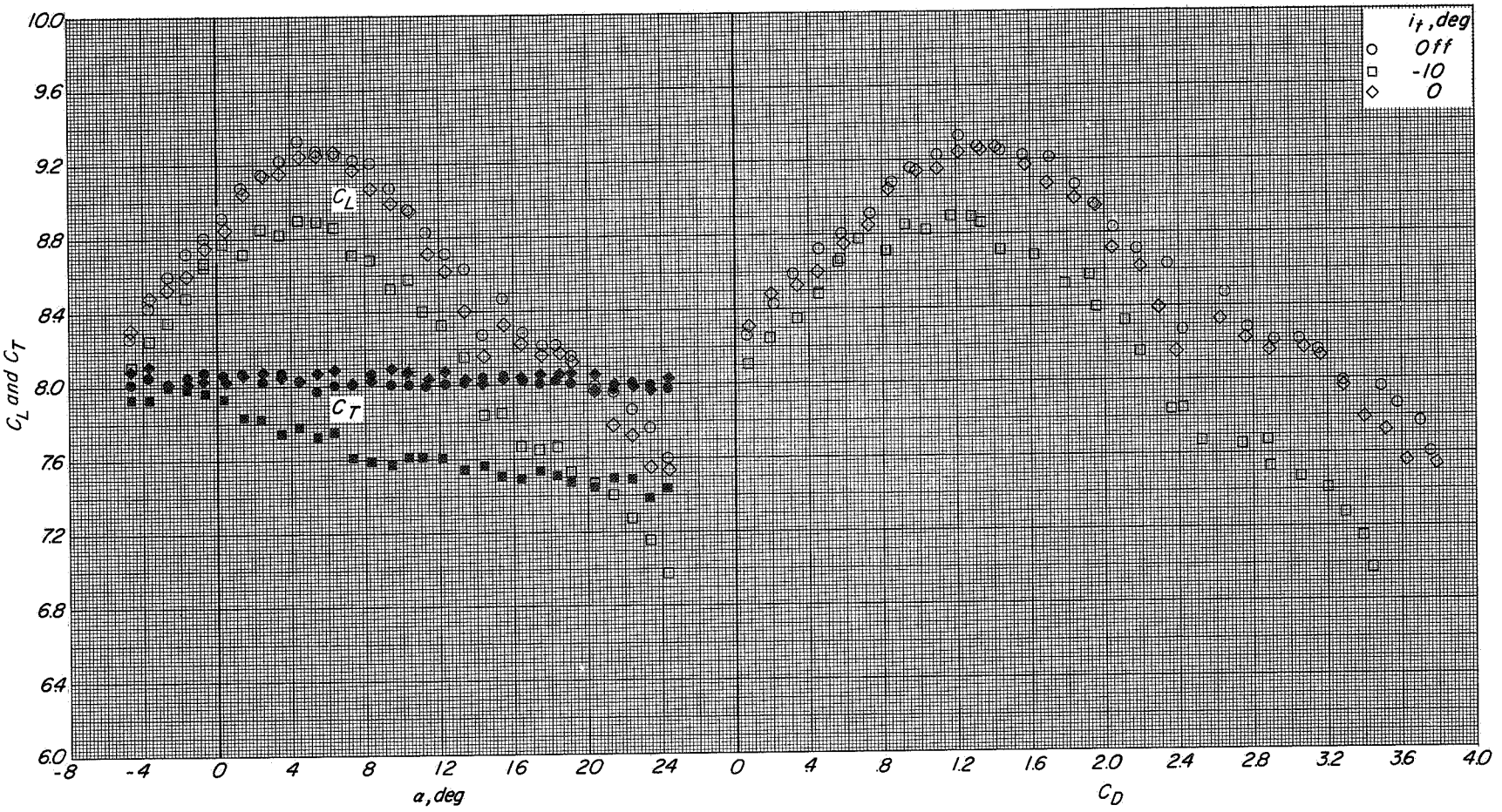

(a) Variation of C_L and C_T with α and C_D with C_L

Figure 12.- Effect of tail incidence on the longitudinal aerodynamic characteristics of configuration A with direct-lift and lift-cruise engines deflected 90^0. $h/D_e = 3.0$; $\beta = 0^0$; $C_T \approx 8$.

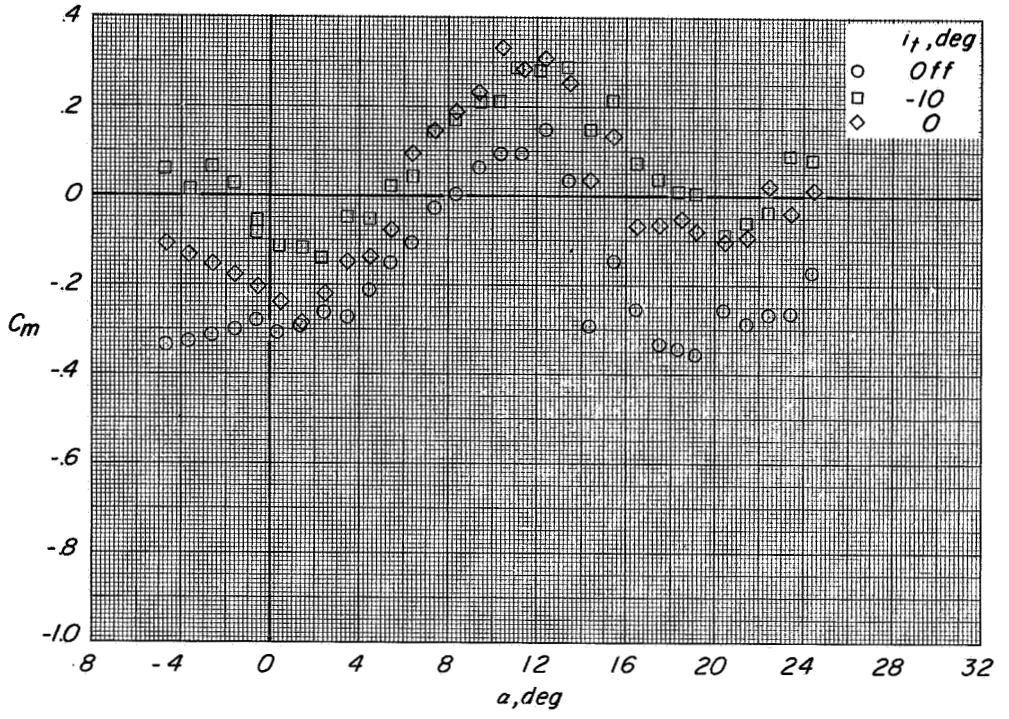

(b) Variation of C_m with α.

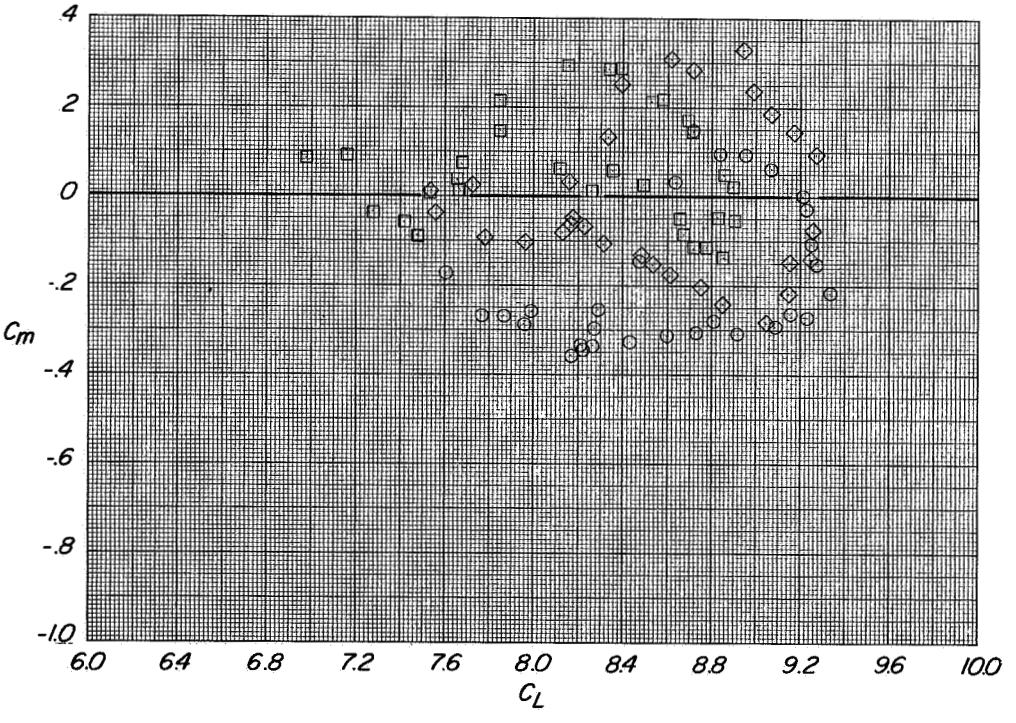

(c) Variation of C_m with C_L.

Figure 12.- Continued.

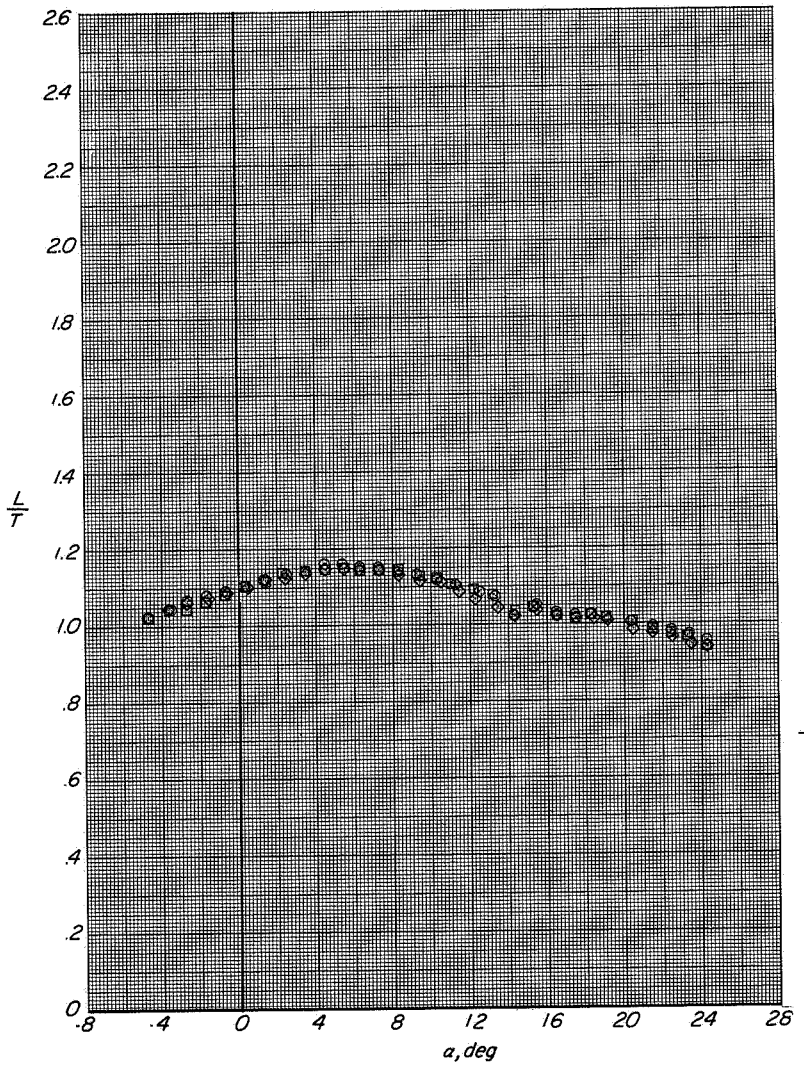

(d) Variation of L/T with α.

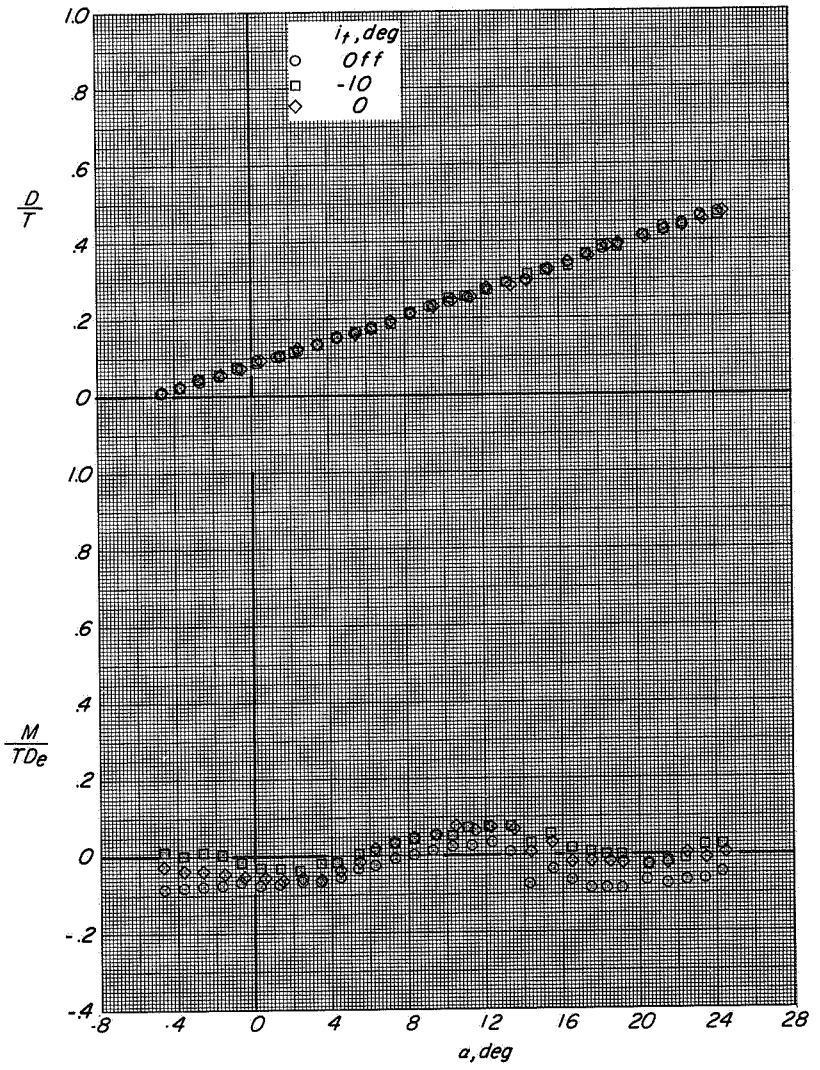

(e) Variation of D/T and M/TD_e with α.

Figure 12.- Concluded.

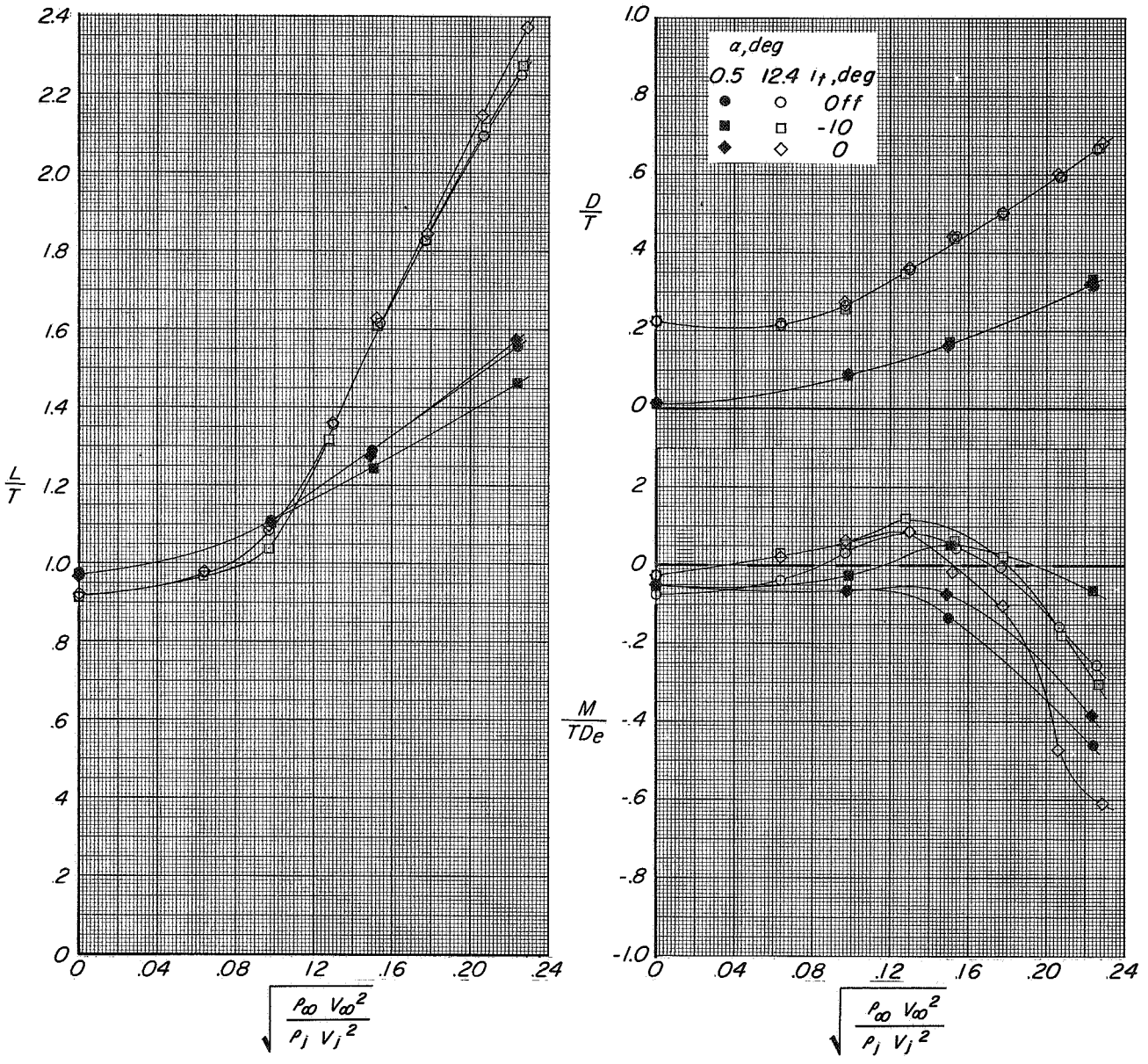

(a) Variation of L/T with effective velocity ratio.

(b) Variation of D/T and M/TD_e with effective velocity ratio.

Figure 13.- Effect of effective velocity ratio on the longitudinal aerodynamic characteristics of configuration A with direct-lift and lift-cruise engines deflected 90° at several tail settings. $h/D_e = 3.0$; $\beta = 0°$.

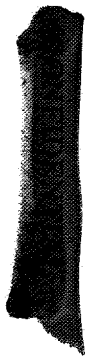

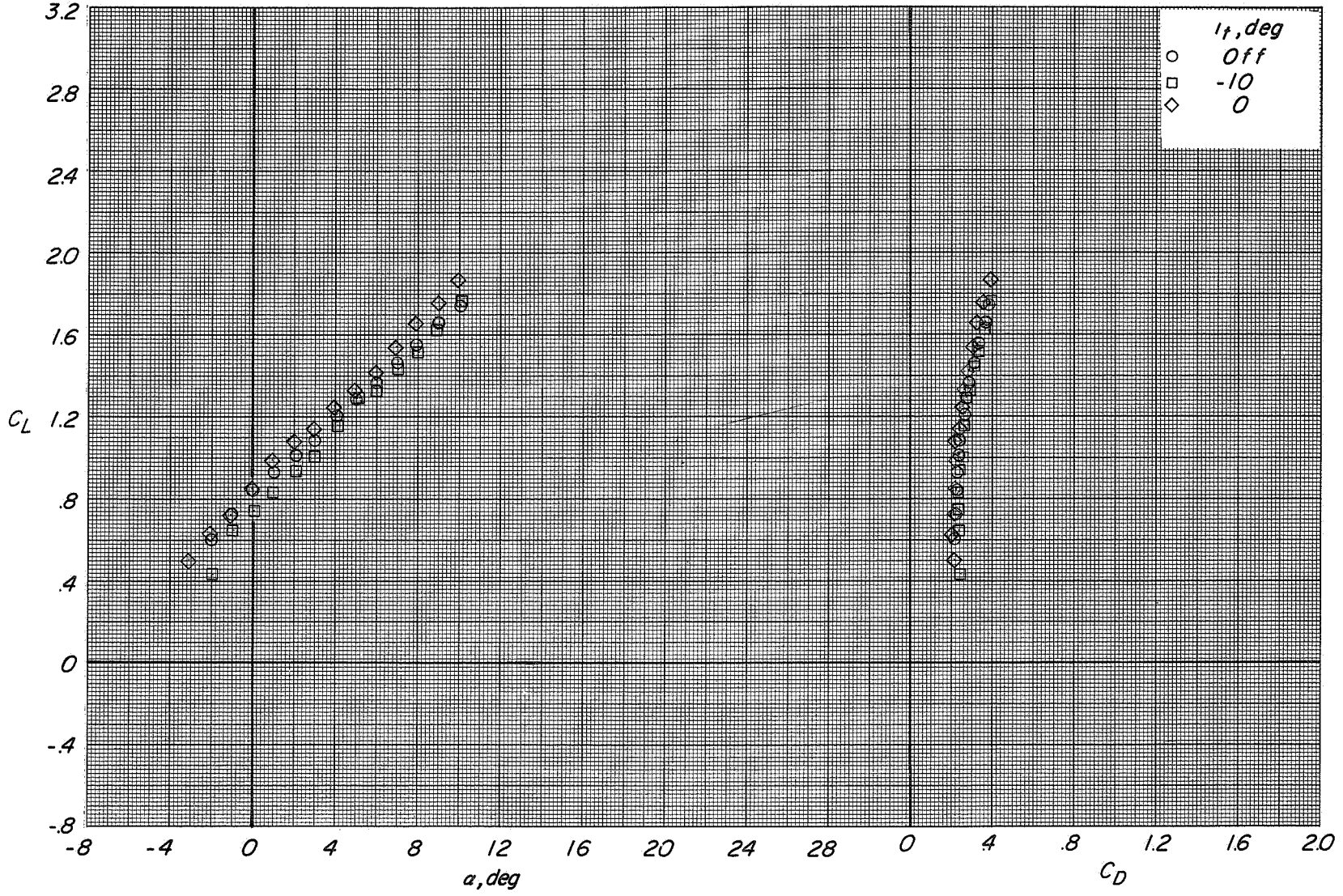

(a) Variation of C_L with α and C_D with C_L.

Figure 14.- Effect of tail incidence on the longitudinal aerodynamic characteristics of configuration A with direct-lift and lift-cruise engines deflected 90°. $h/D_e = 0.524$; $\beta = 0°$; $C_T = 0$.

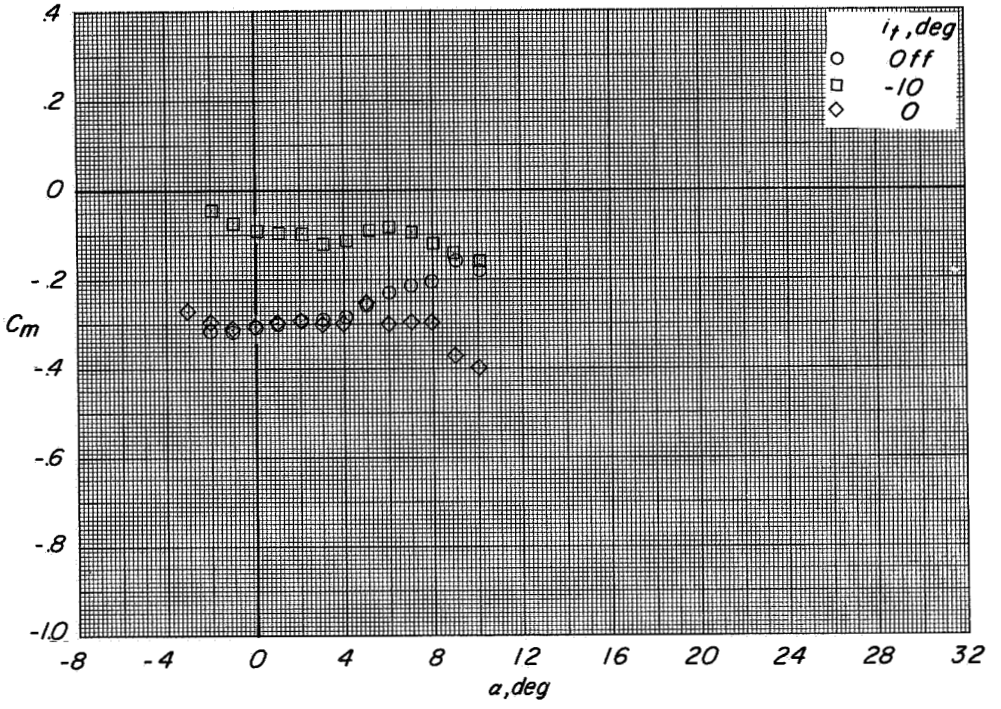

(b) Variation of C_m with α.

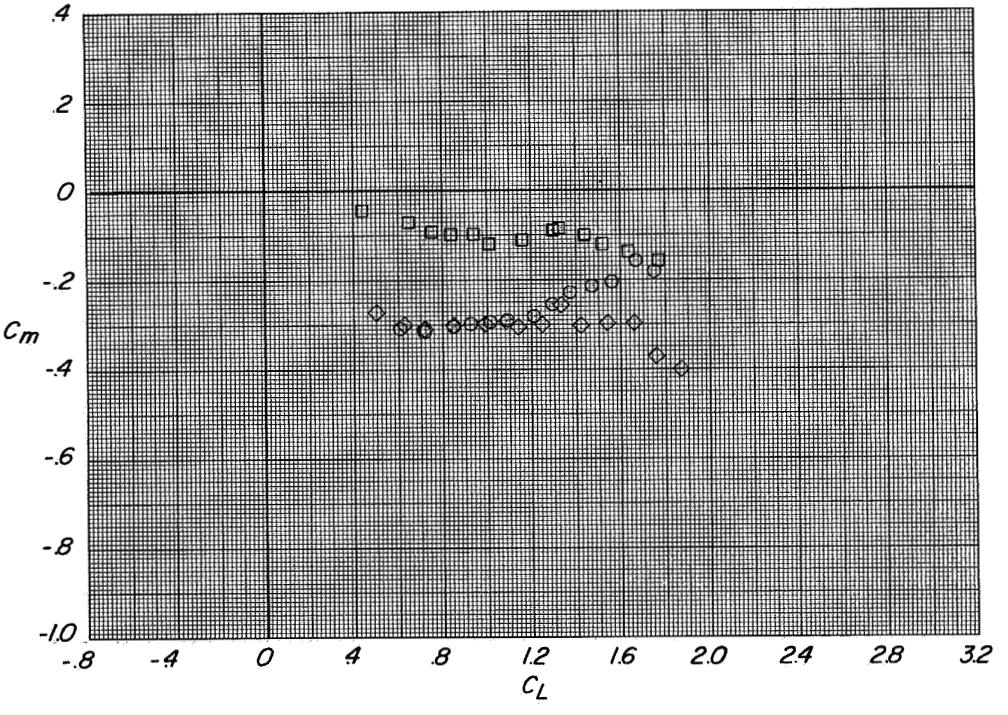

(c) Variation of C_m with C_L.

Figure 14.- Concluded.

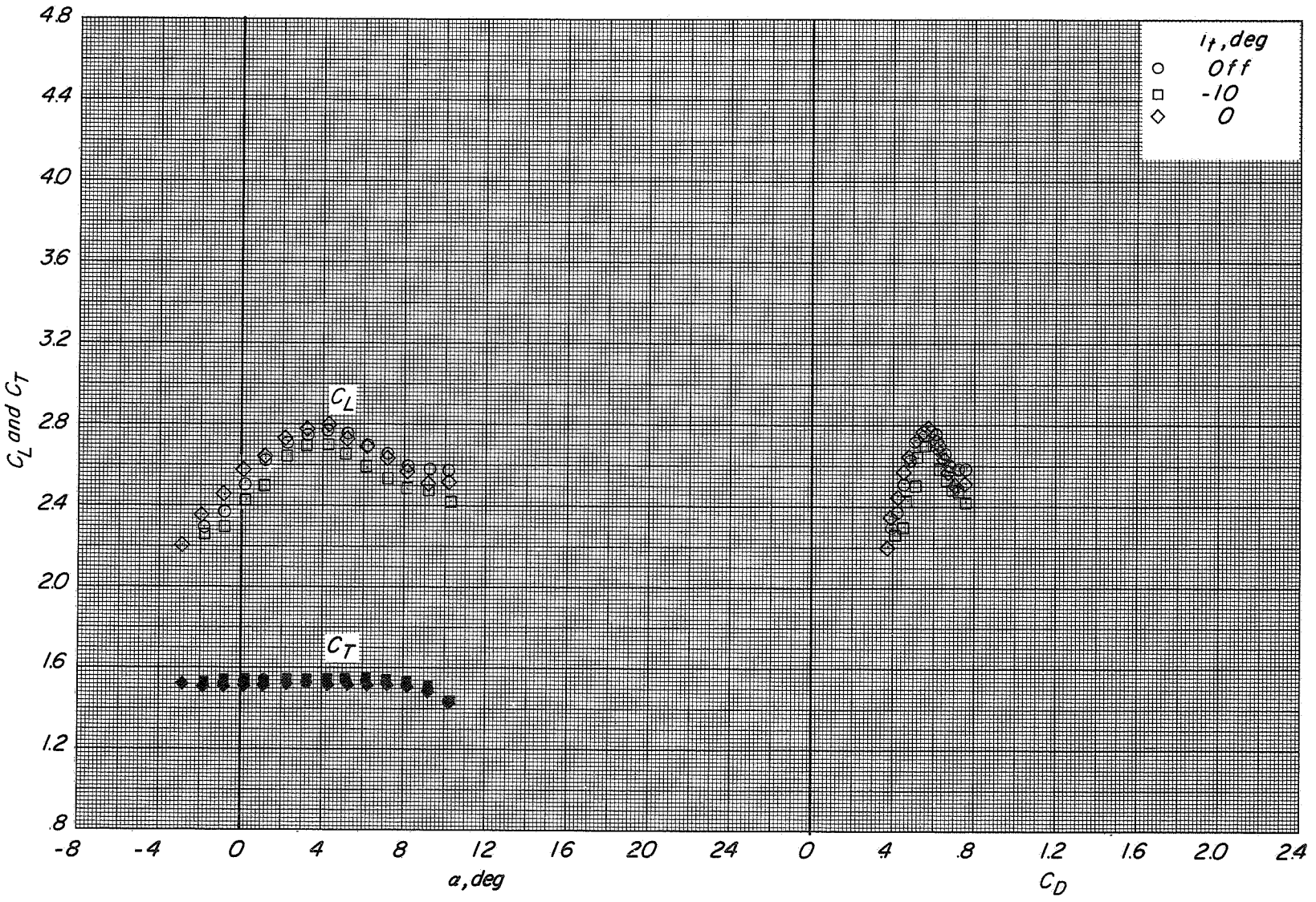

(a) Variation of C_L and C_T with α and C_D with C_L

Figure 15.- Effect of tail incidence on the longitudinal aerodynamic characteristics of configuration A with direct-lift and lift-cruise engines deflected 90°. $h/D_e = 0.524$; $\beta = 0^0$; $C_T \approx 1.45$.

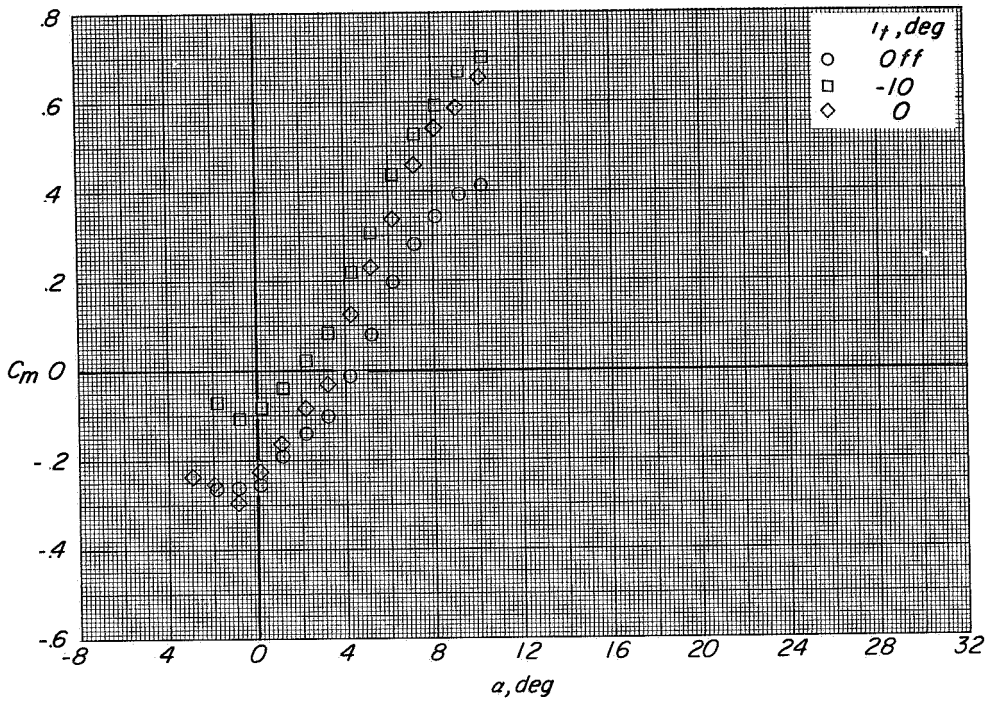

(b) Variation of C_m with α.

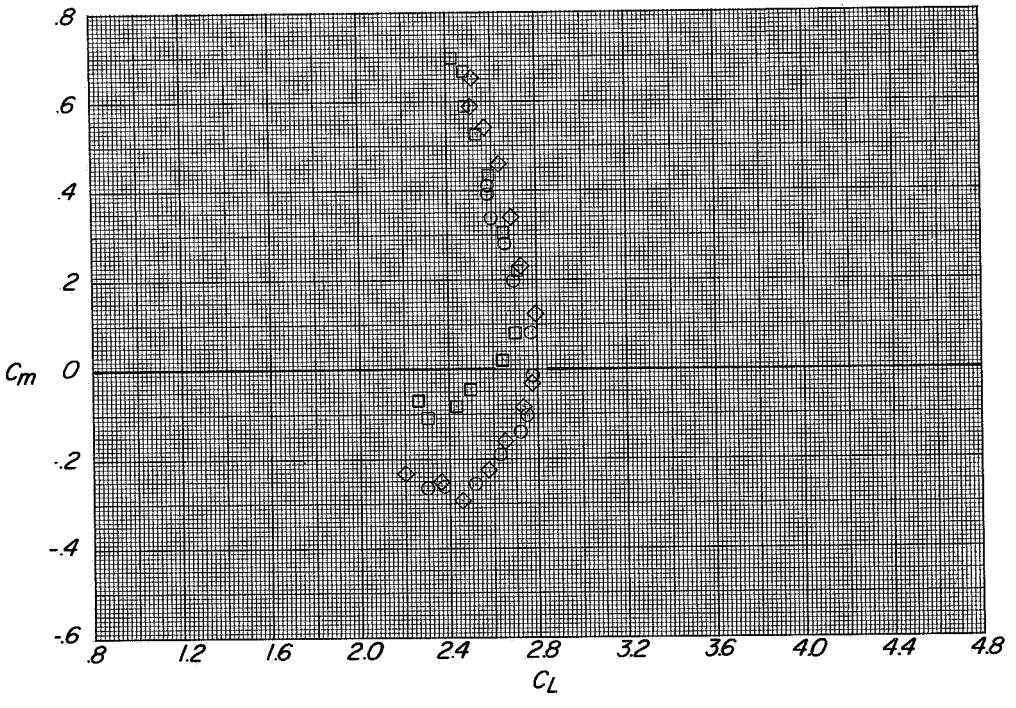

(c) Variation of C_m with C_L.

Figure 15.- Continued.

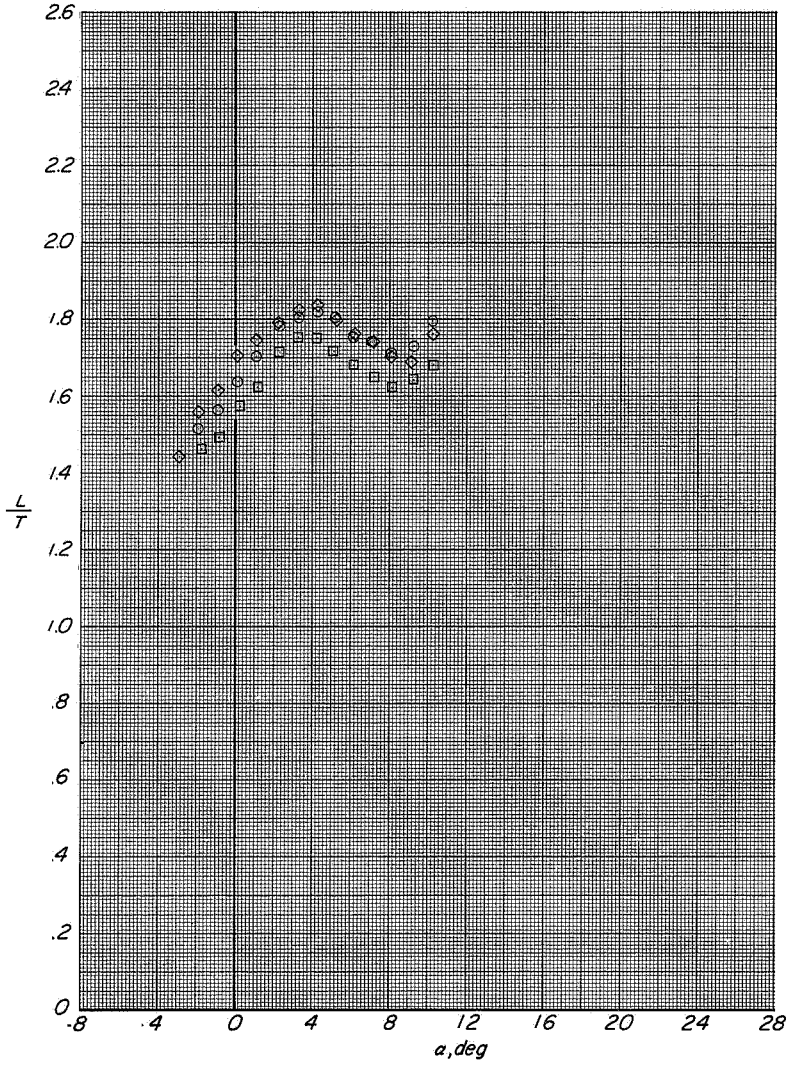

(d) Variation of L/T with α.

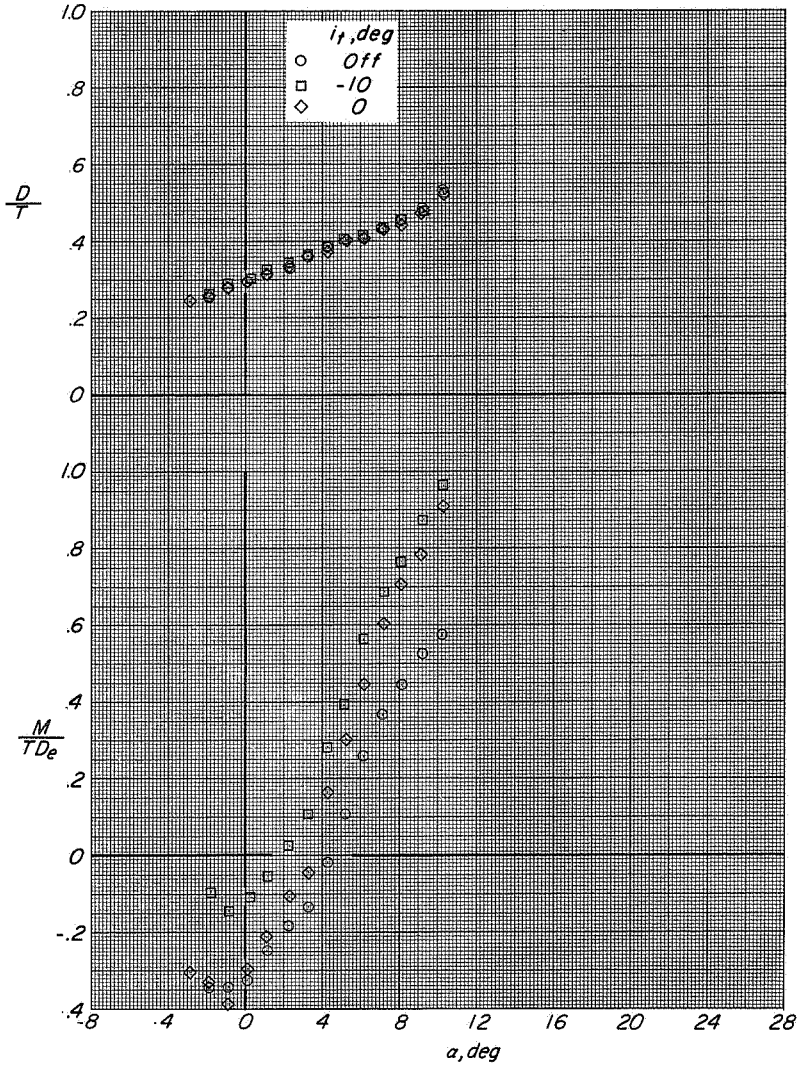

(e) Variation of D/T and M/TD$_e$ with α.

Figure 15.- Concluded.

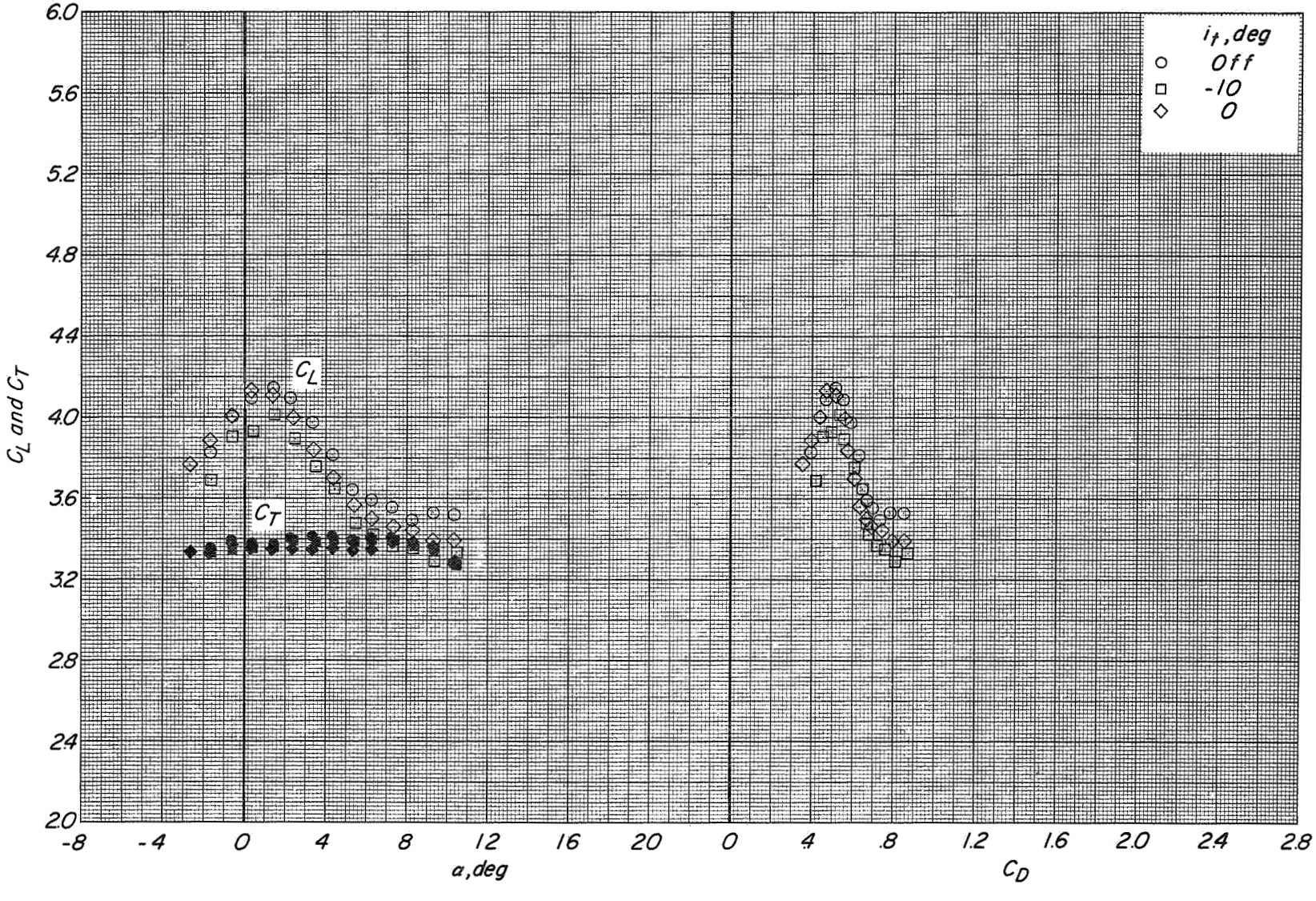

(a) Variation of C_L and C_T with α and C_D with C_L

Figure 16.- Effect of tail incidence on the longitudinal aerodynamic characteristics of configuration A with direct-lift and lift-cruise engines deflected 90°. $h/D_e = 0.524$; $\beta = 0°$; $C_T \approx 3.3$.

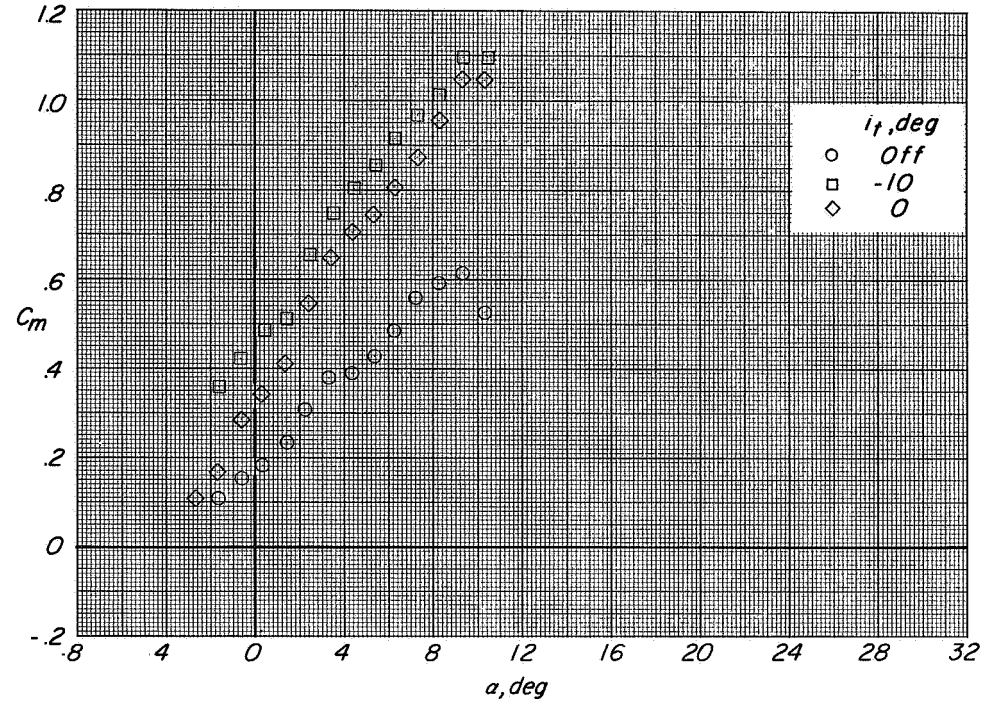

(b) Variation of C_m with α.

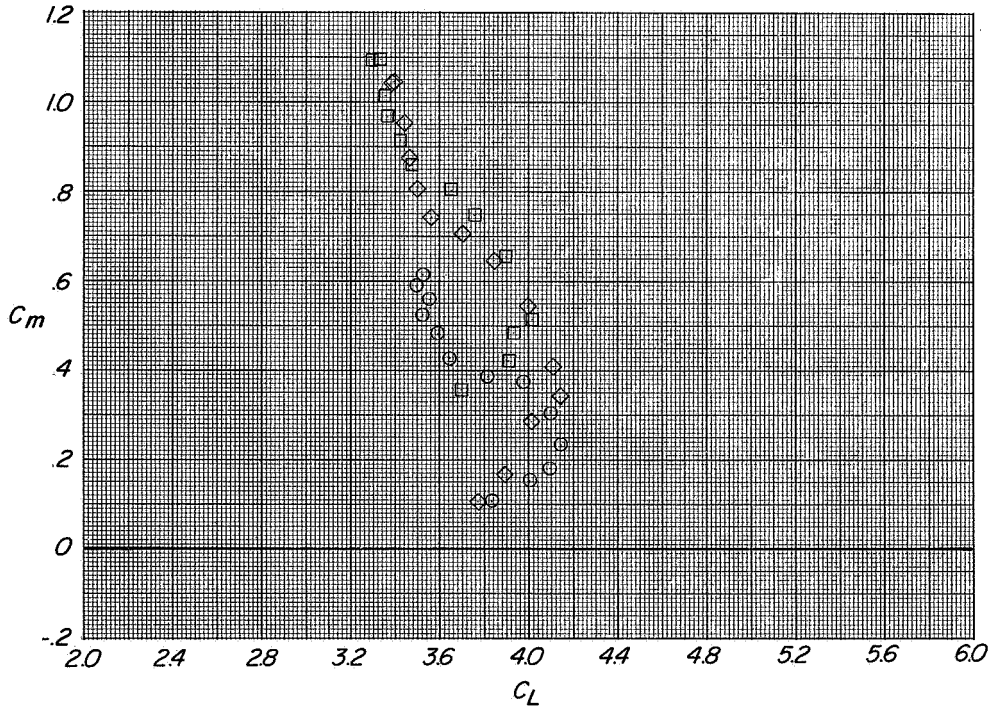

(c) Variation of C_m with C_L

Figure 16.- Continued.

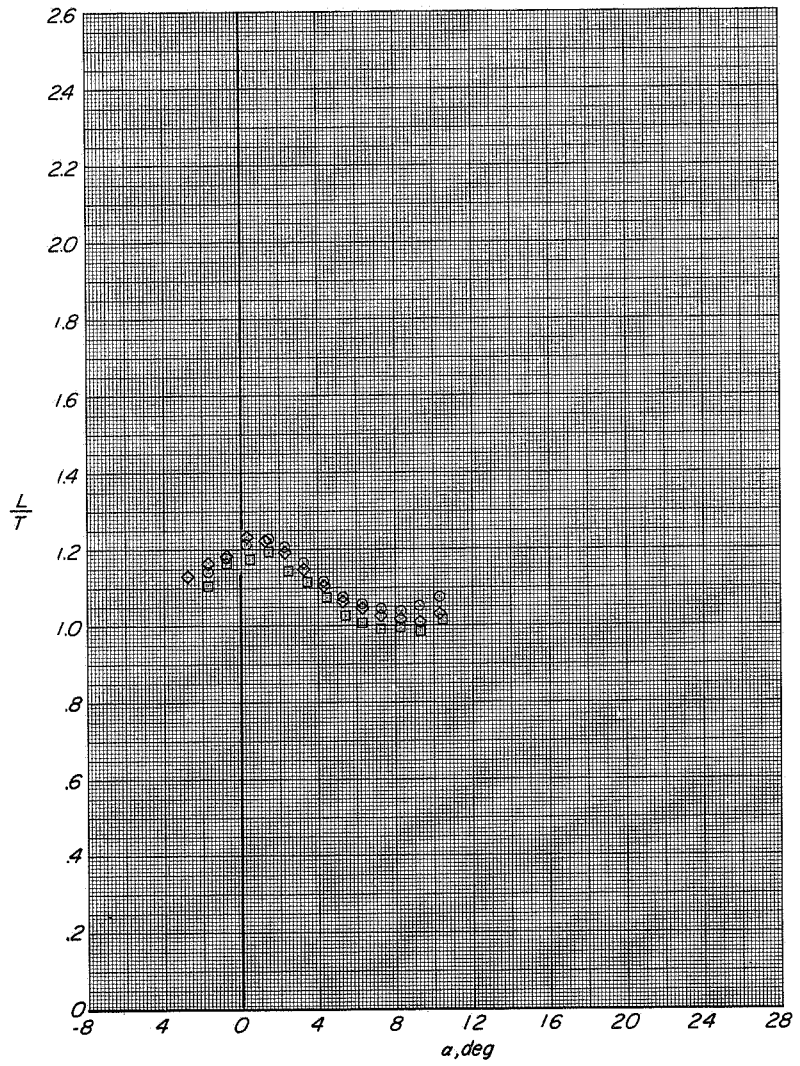

(d) Variation of L/T with α.

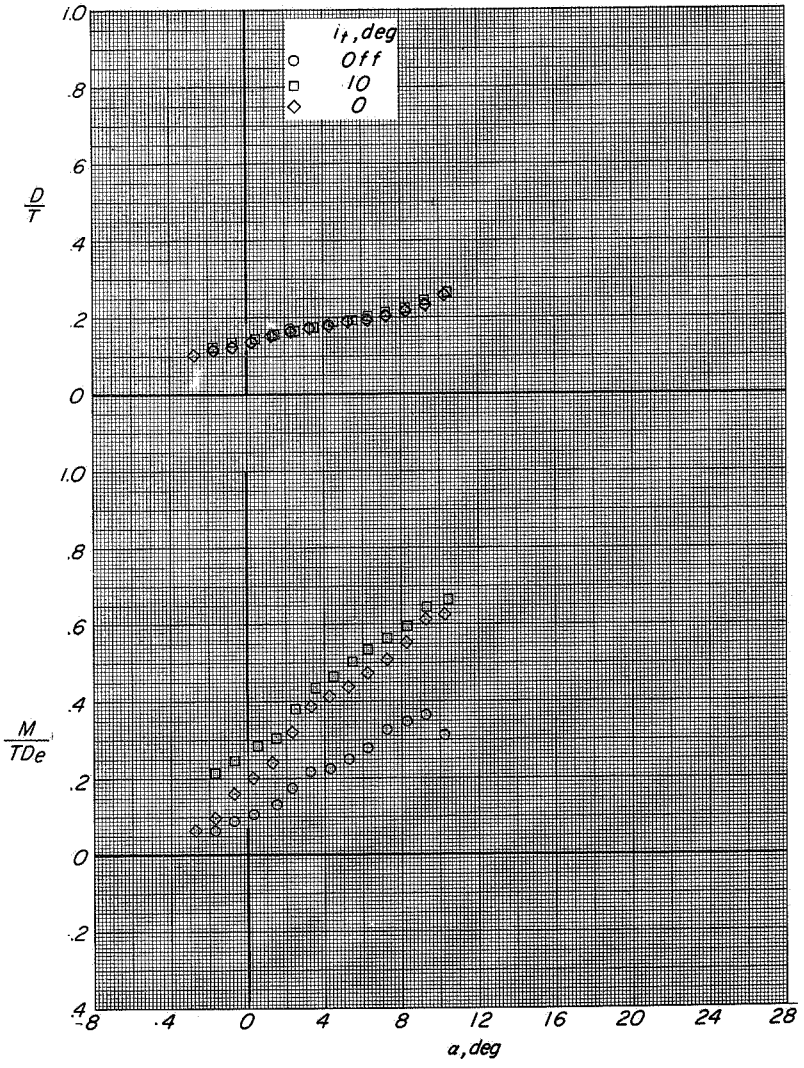

(e) Variation of D/T and M/TD_e with α.

Figure 16.· Concluded.

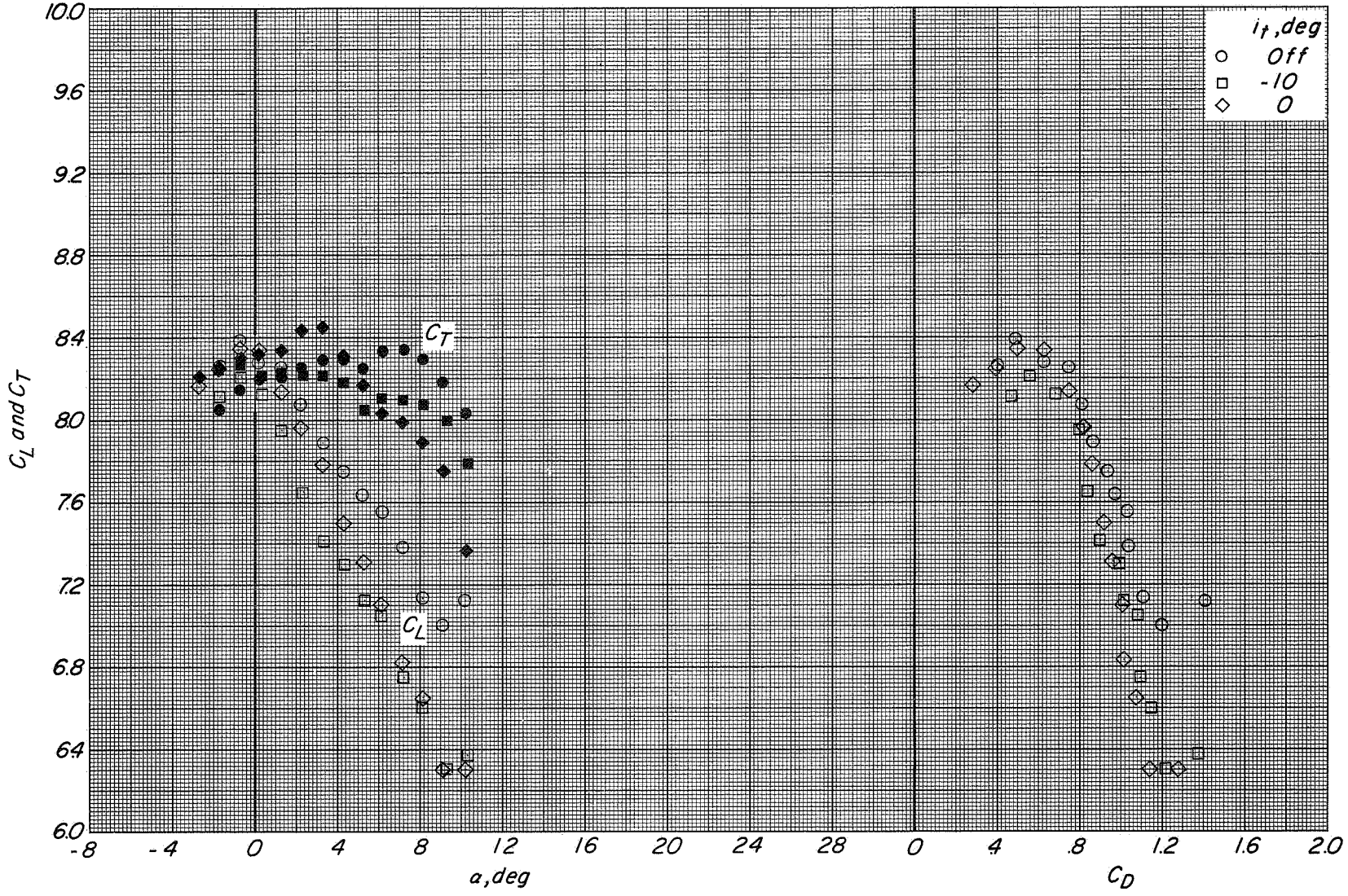

(a) Variation of C_L and C_T with α and C_D with C_L

Figure 17.- Effect of tail incidence on the longitudinal aerodynamic characteristics of configuration A with direct-lift and lift-cruise engines deflected 90^0. $h/D_e = 0.524$; $\beta = 0^0$; $C_T \approx 8$.

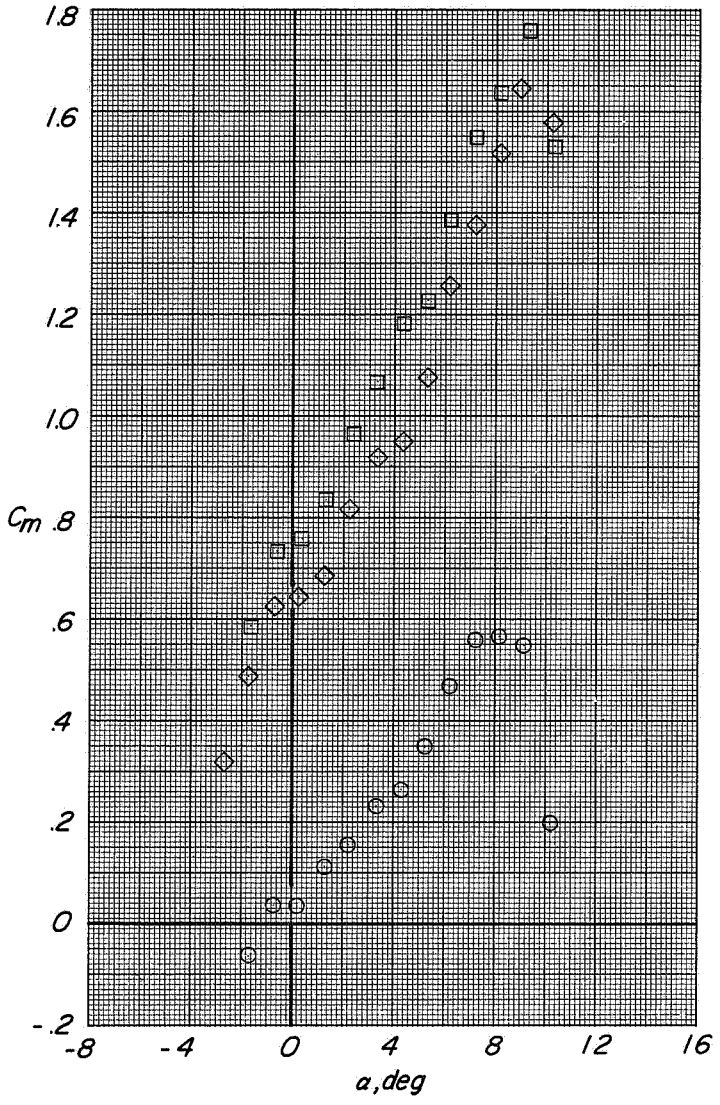

(b) Variation of C_m with α.

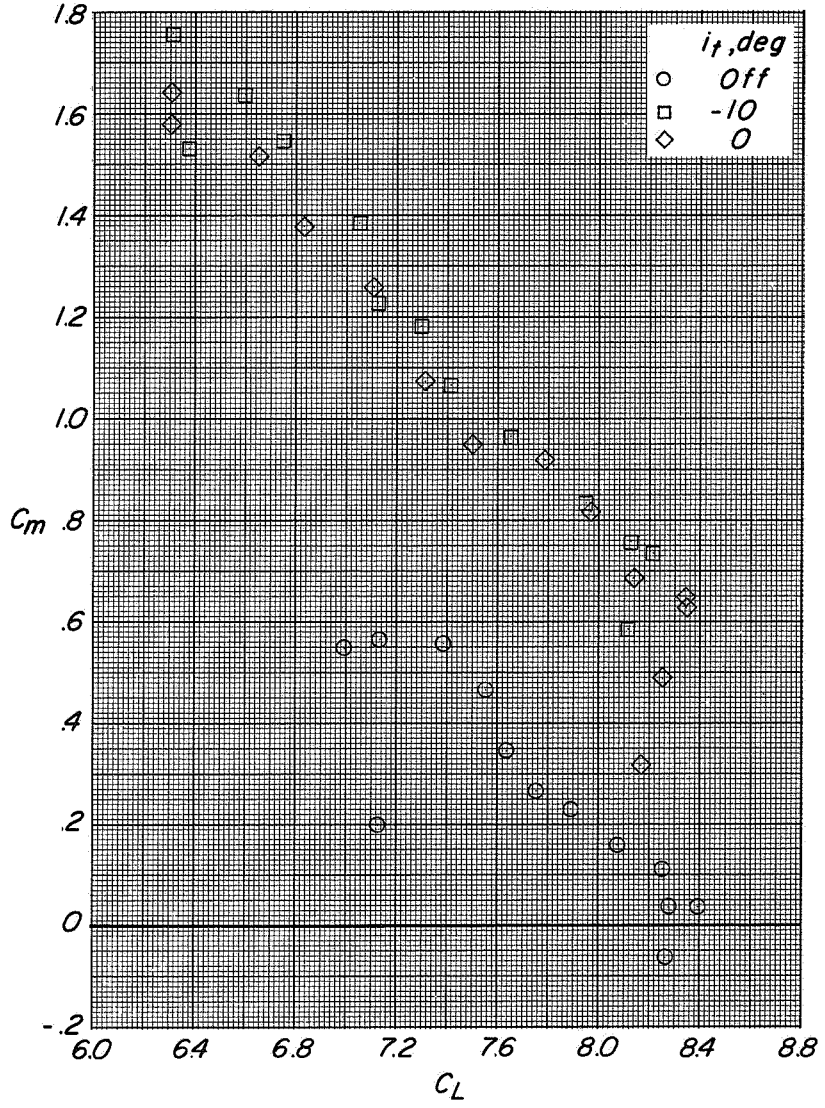

(c) Variation of C_m with C_L.

Figure 17 - Continued.

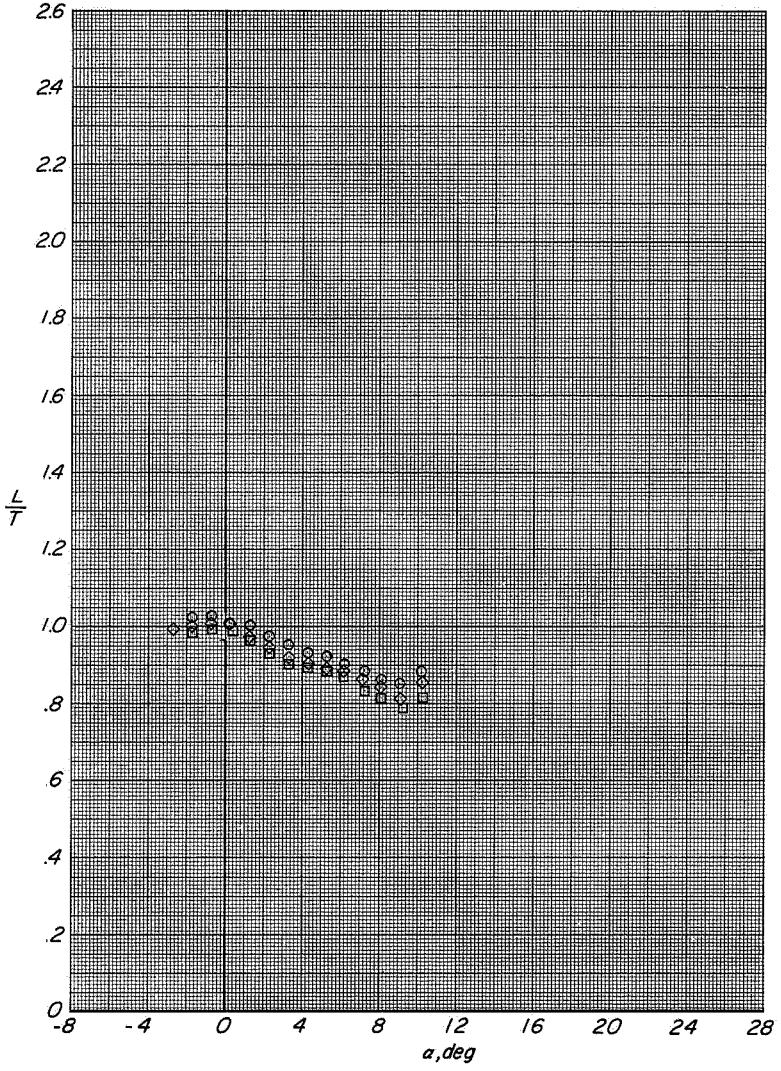

(d) Variation of L/T with α.

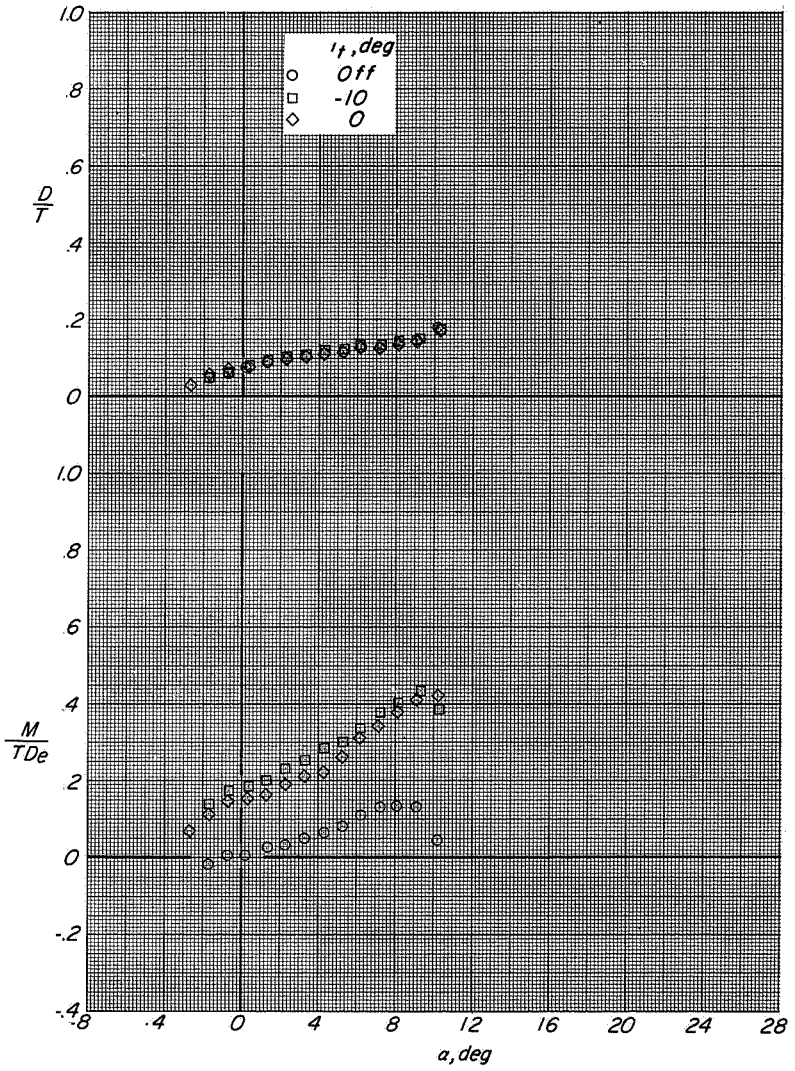

(e) Variation of D/T and M/TD_e with α.

Figure 17 - Concluded.

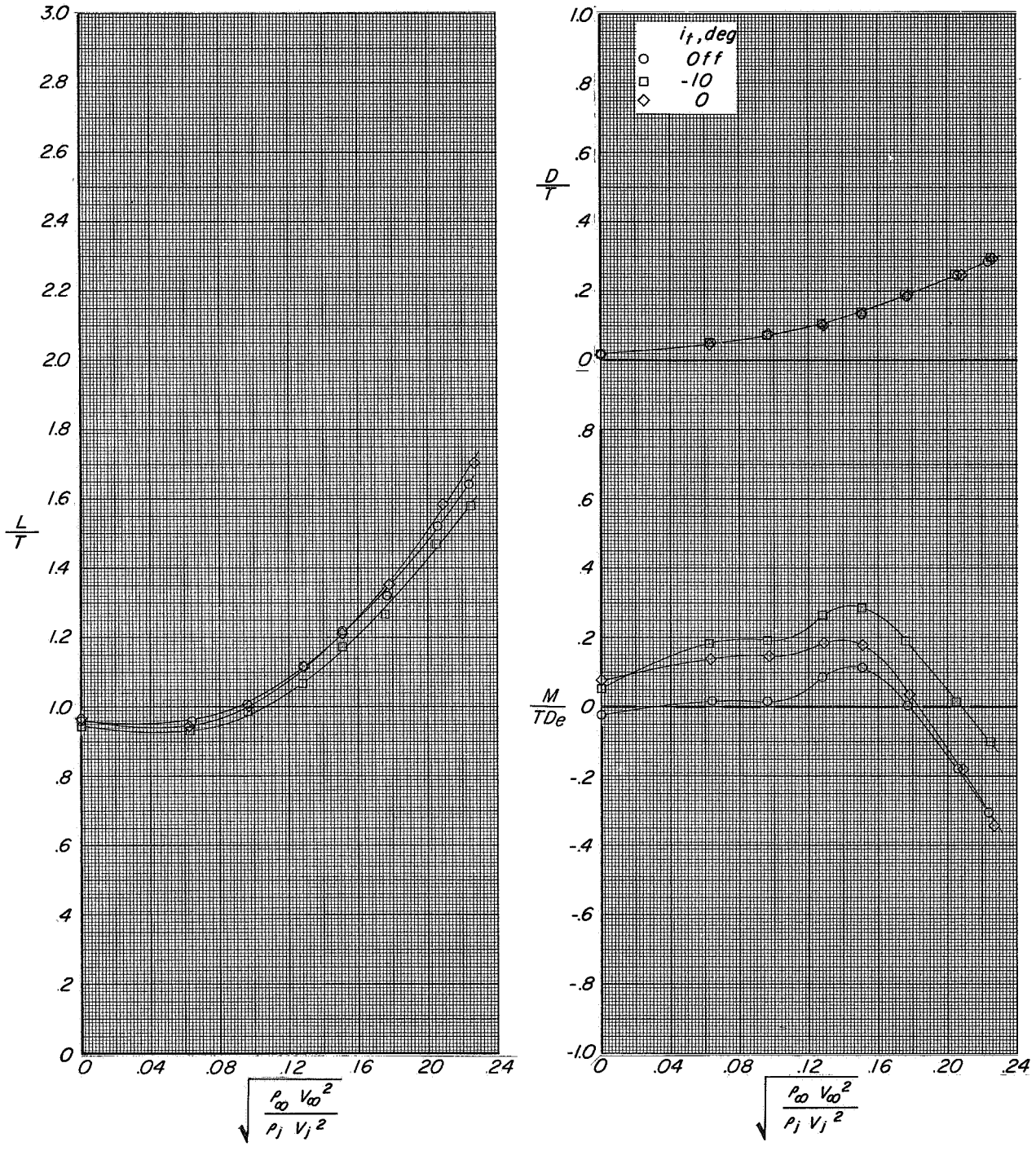

(a) Variation of L/T with effective velocity ratio.

(b) Variation of D/T and M/TD_e with effective velocity ratio.

Figure 18.- Effect of effective velocity ratio on the longitudinal aerodynamic characteristics of configuration A with direct-lift and lift-cruise engines deflected 90° at several tail settings. $h/D_e = 0.524$; $\beta = 0^\circ$; $\alpha = 0.3^\circ$.

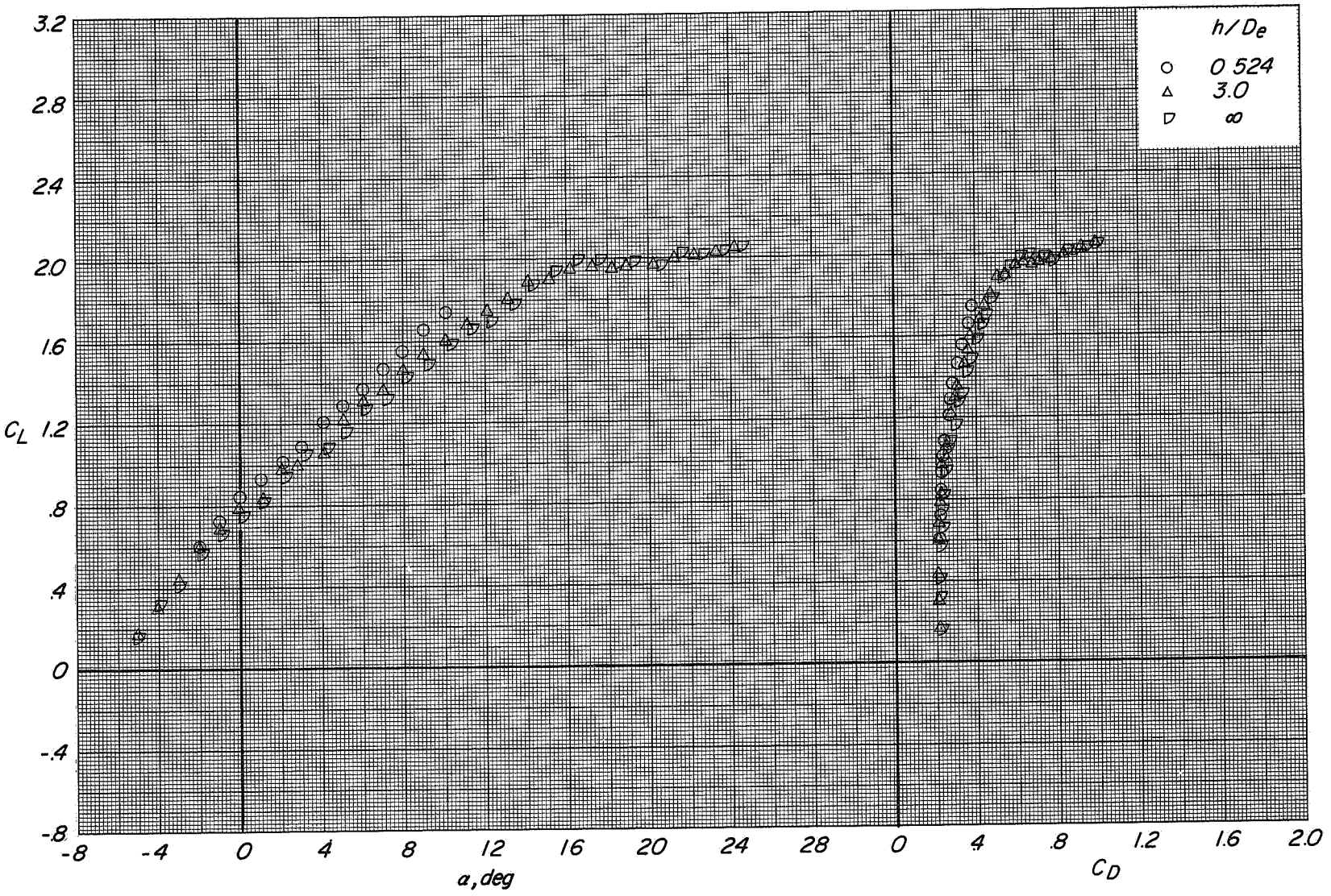

(a) Variation of C_L with α and C_D with C_L

Figure 19.- Longitudinal aerodynamic characteristics of configuration A with direct-lift and lift-cruise engines deflected 90°. Tail off: $\beta = 0°$; $C_T = 0$.

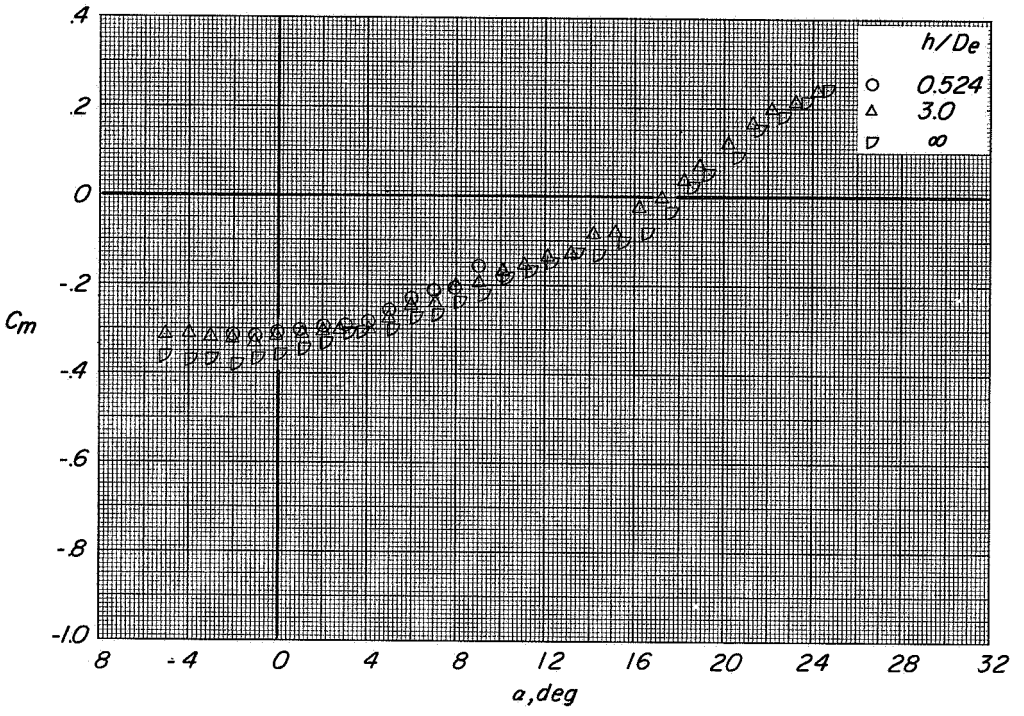

(b) Variation of C_m with α.

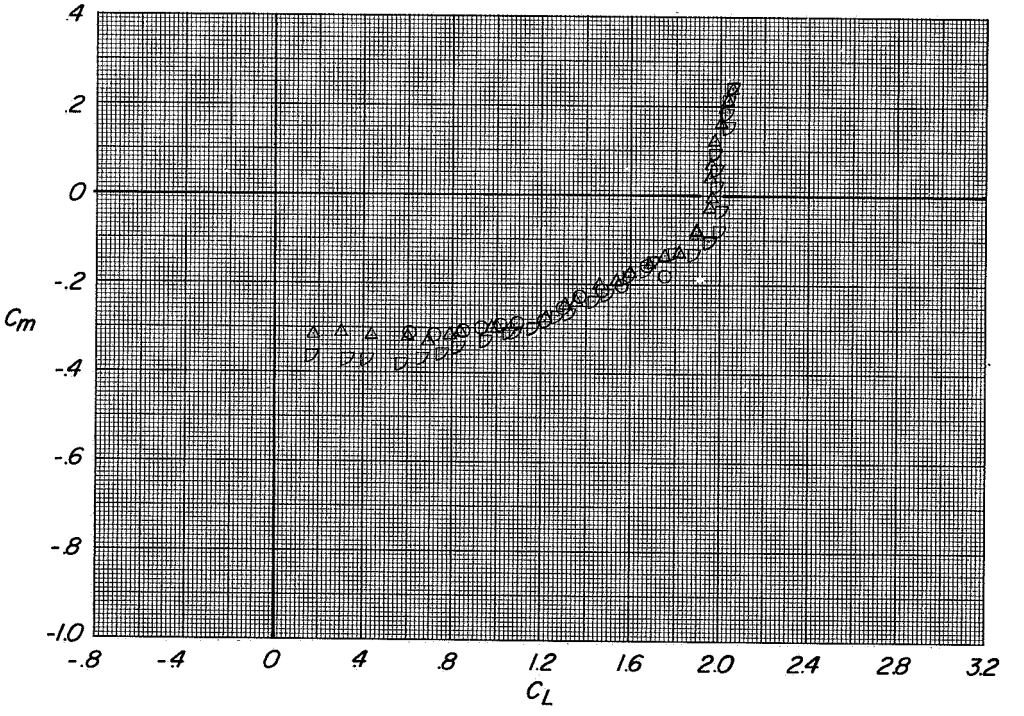

(c) Variation of C_m with C_L.

Figure 19.- Concluded.

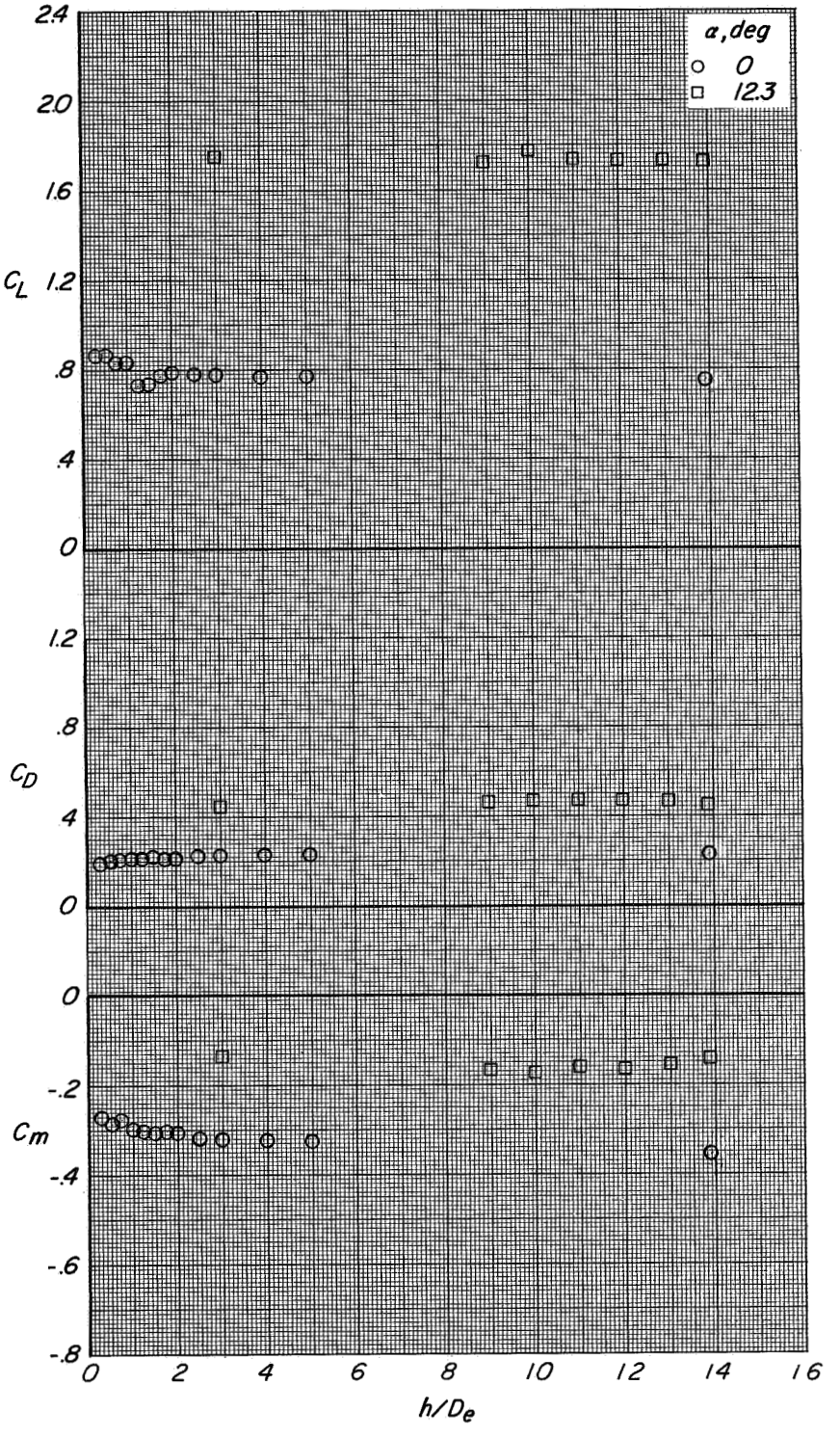

Figure 20.- Effect of height above the moving-belt ground plane on the longitudinal aerodynamic characteristics of configuration A with direct-lift and lift-cruise engines deflected 90° Tail off; $\beta = 0^0$; $C_T = 0$.

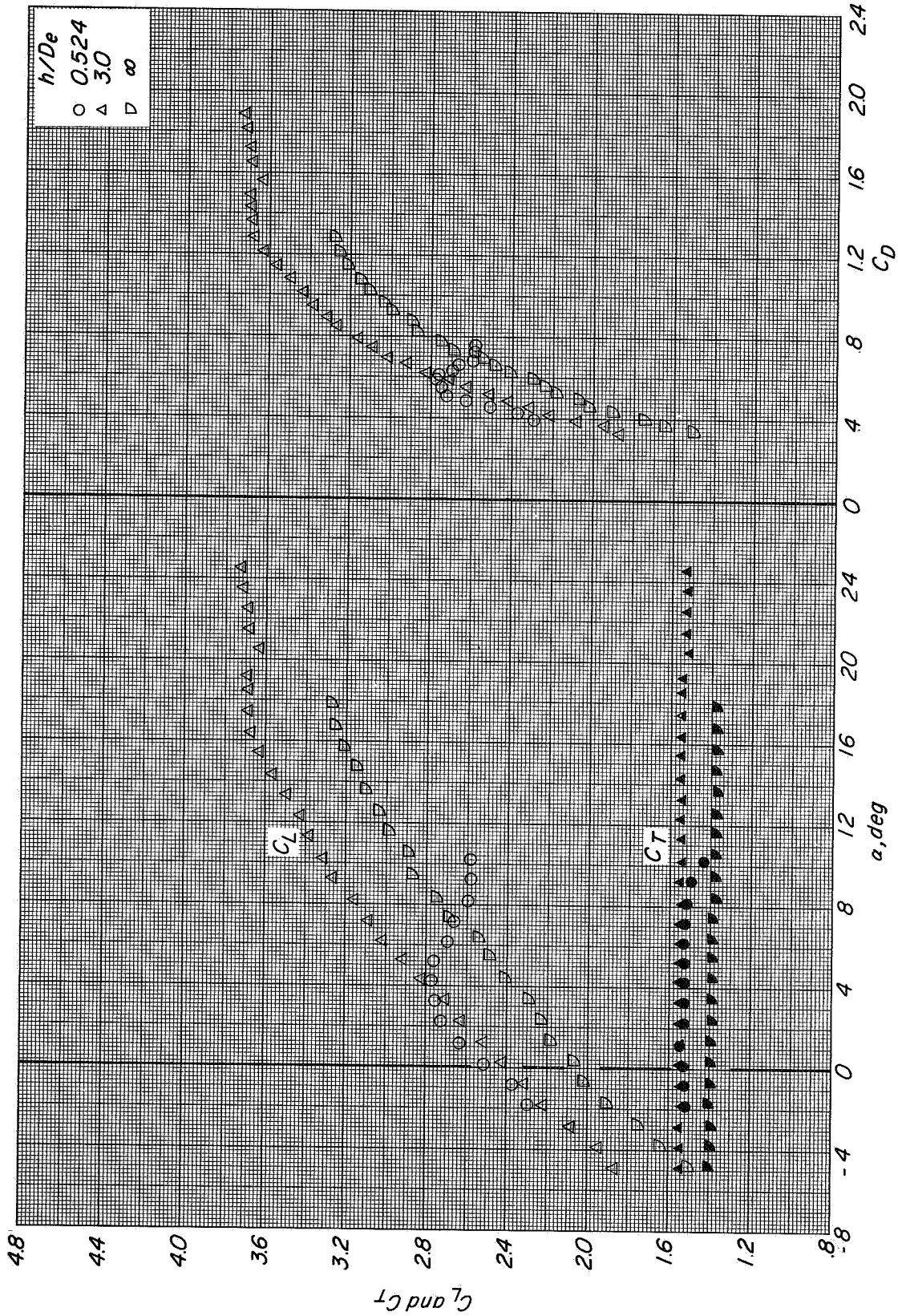

(a) Variation of C_L and C_T with α and C_D with C_L.

Figure 21.- Longitudinal aerodynamic characteristics of configuration A with direct-lift and lift-cruise engines deflected 90°. Tail off: β = 0°; $C_T \approx 1.45$.

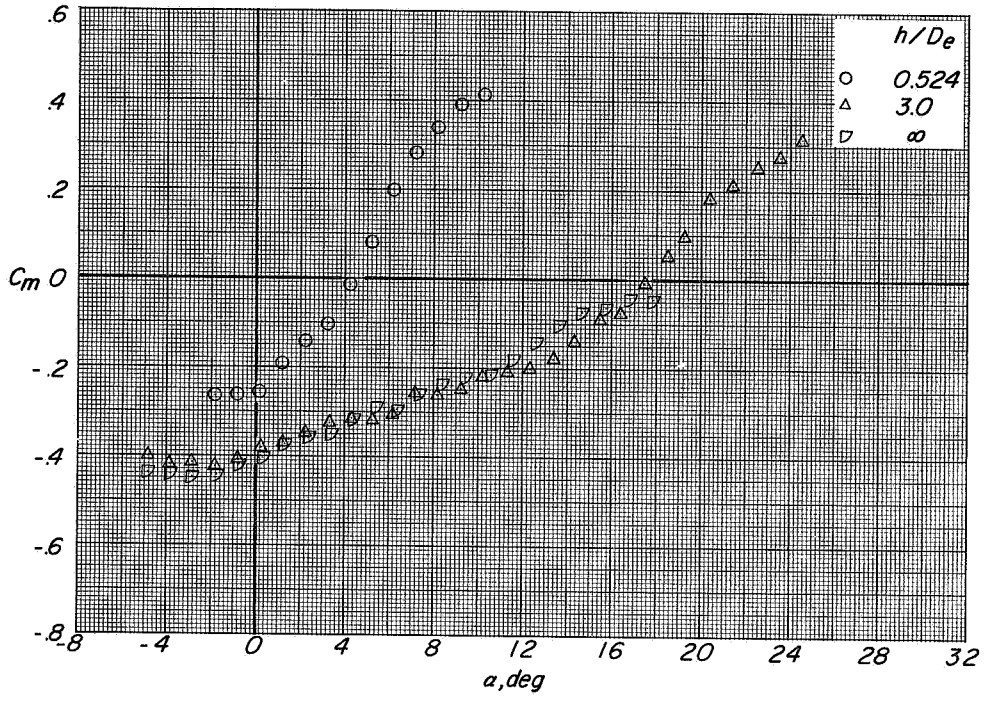

(b) Variation of C_m with α.

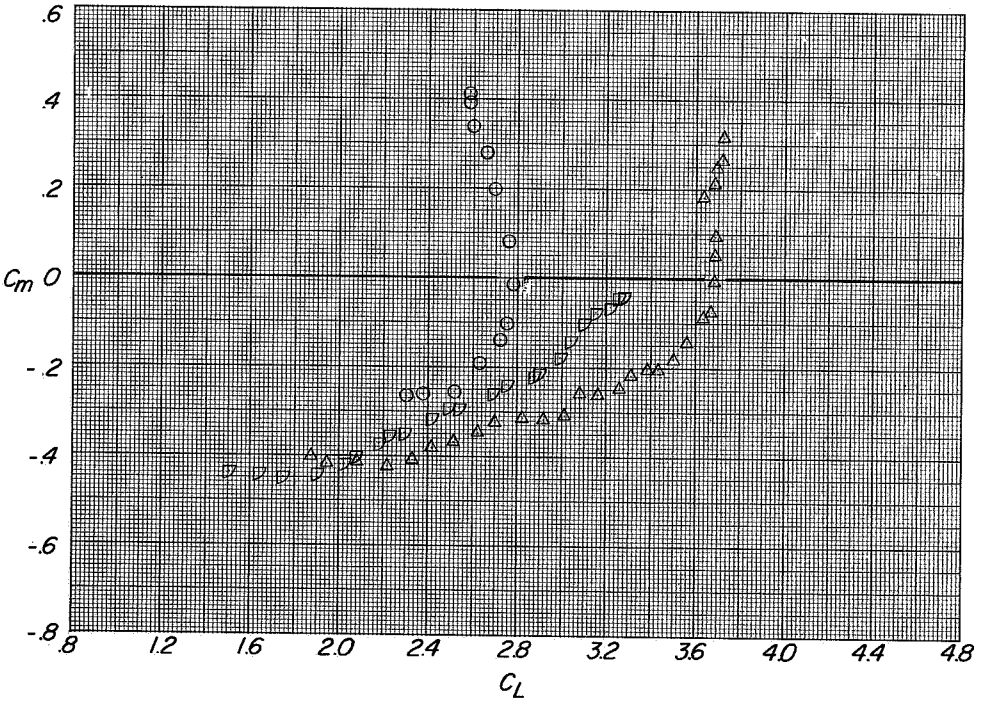

(c) Variation of C_m with C_L

Figure 21.- Continued.

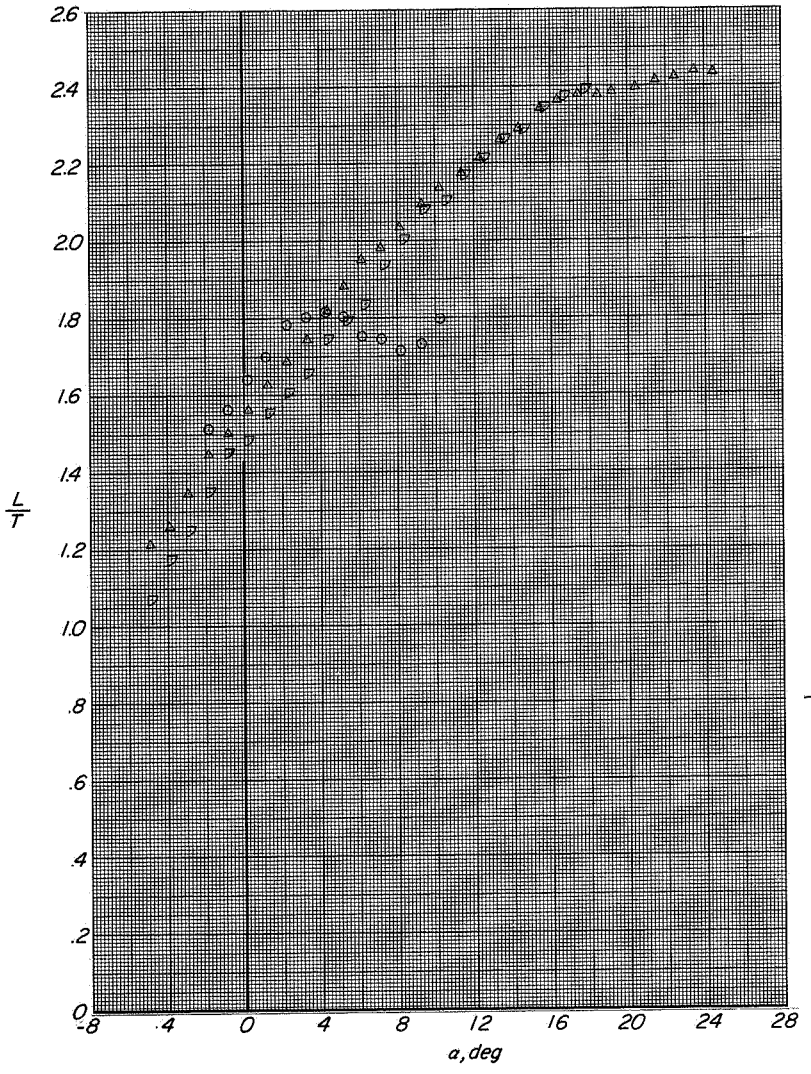

(d) Variation of L/T with α.

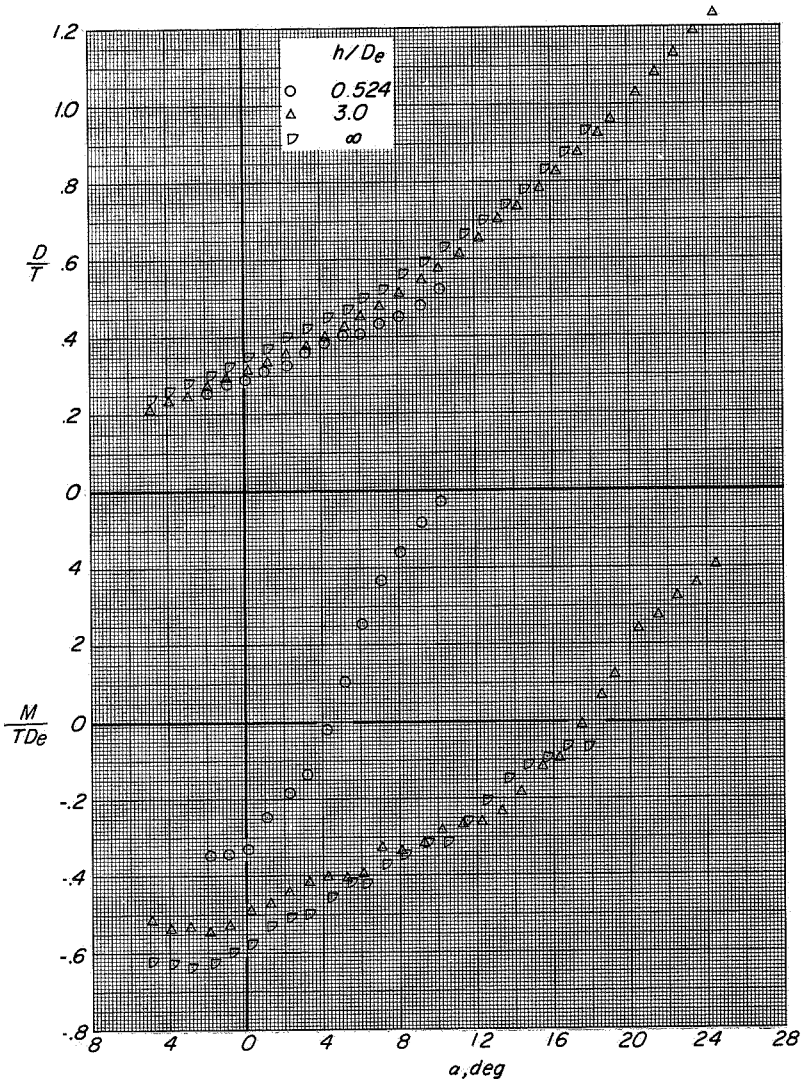

(e) Variation of D/T and M/TDe with α.

Figure 21.· Concluded.

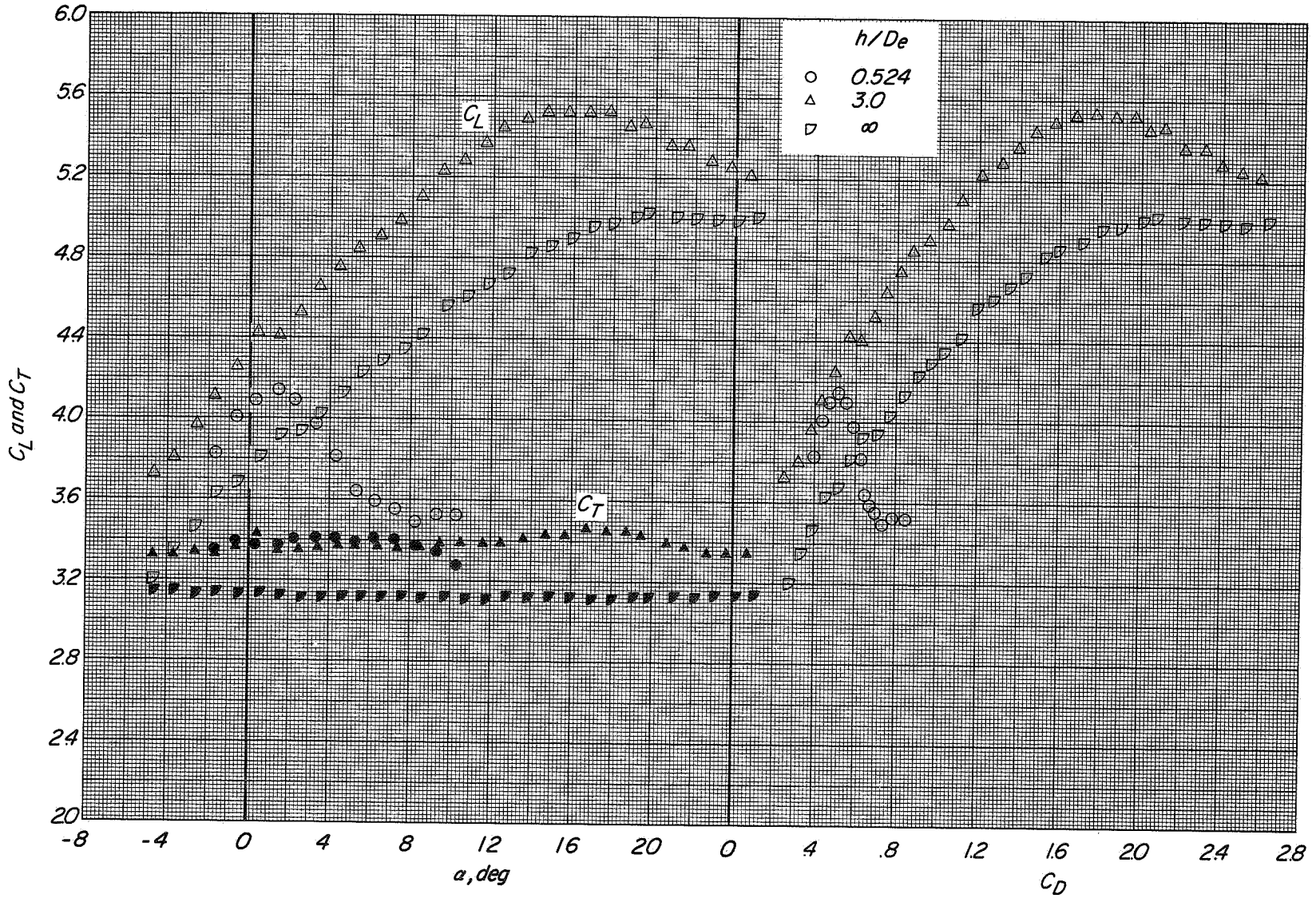

(a) Variation of C_L and C_T with α and C_D with C_L

Figure 22.- Longitudinal aerodynamic characteristics of configuration A with direct-lift and lift-cruise engines deflected 90°. Tail off: β = 0°; $C_T \approx 3.3$.

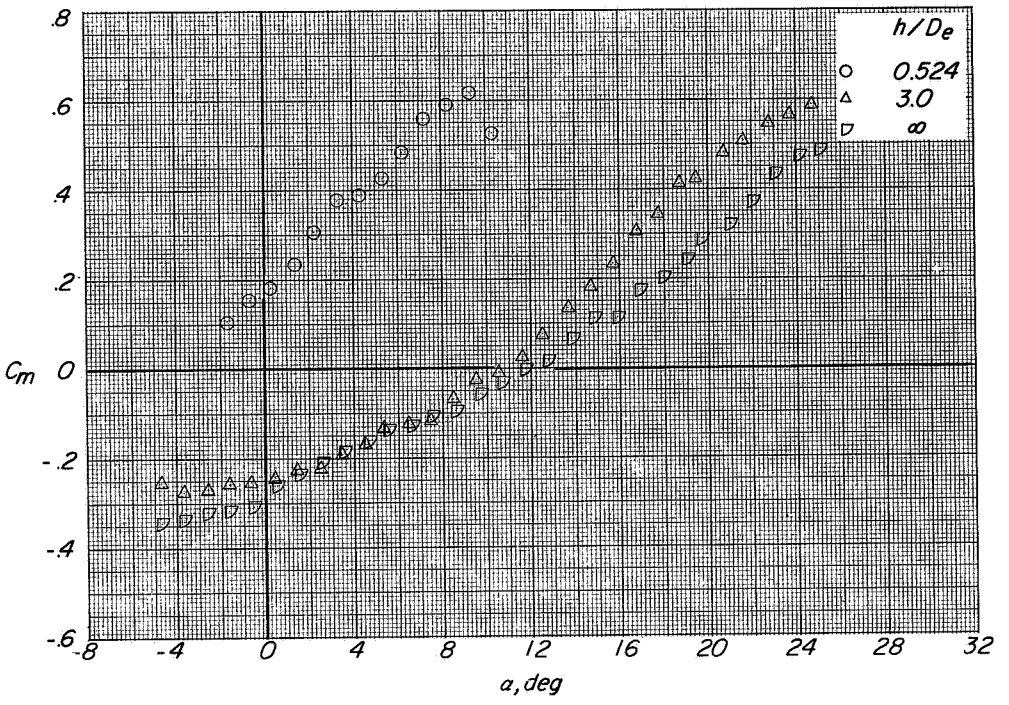

(b) Variation of C_m with α.

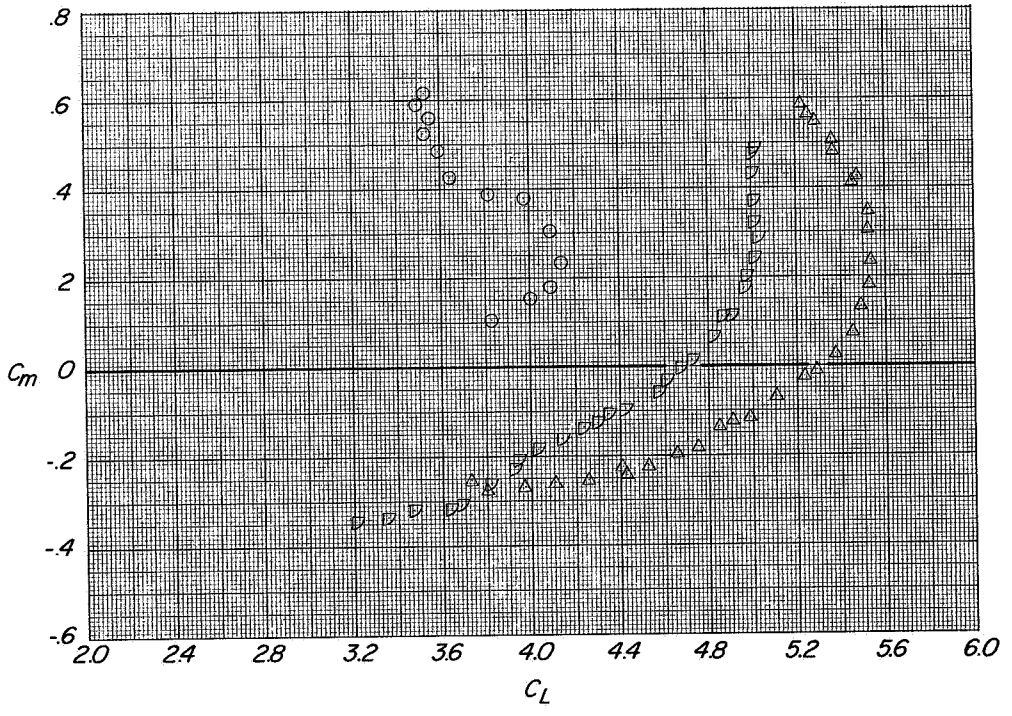

(c) Variation of C_m with C_L.

Figure 22.- Continued.

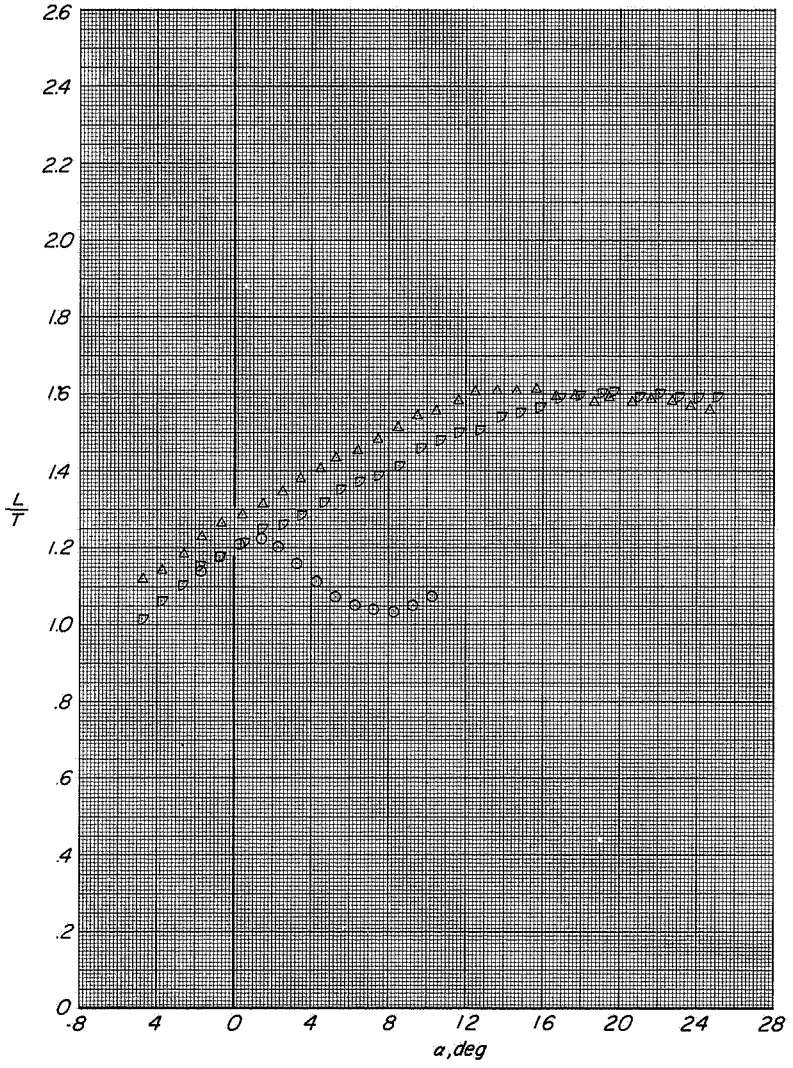

(d) Variation of L/T with α.

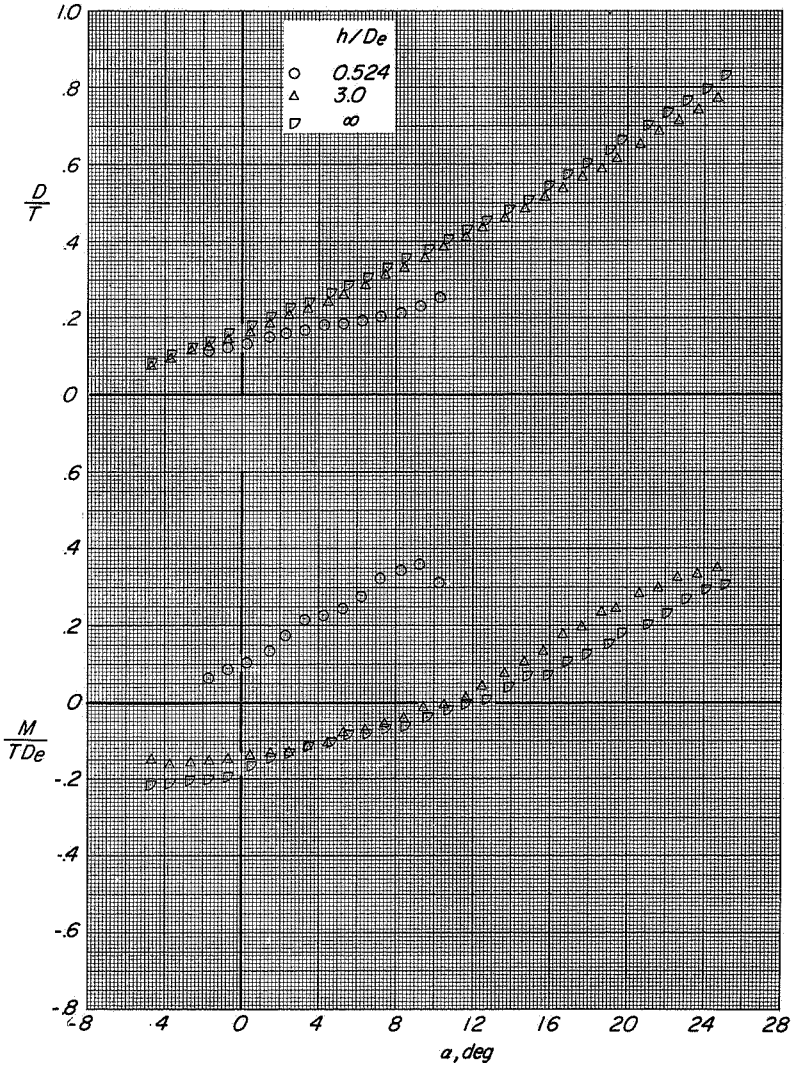

(e) Variation of D/T and M/TDe with α.

Figure 22. Concluded.

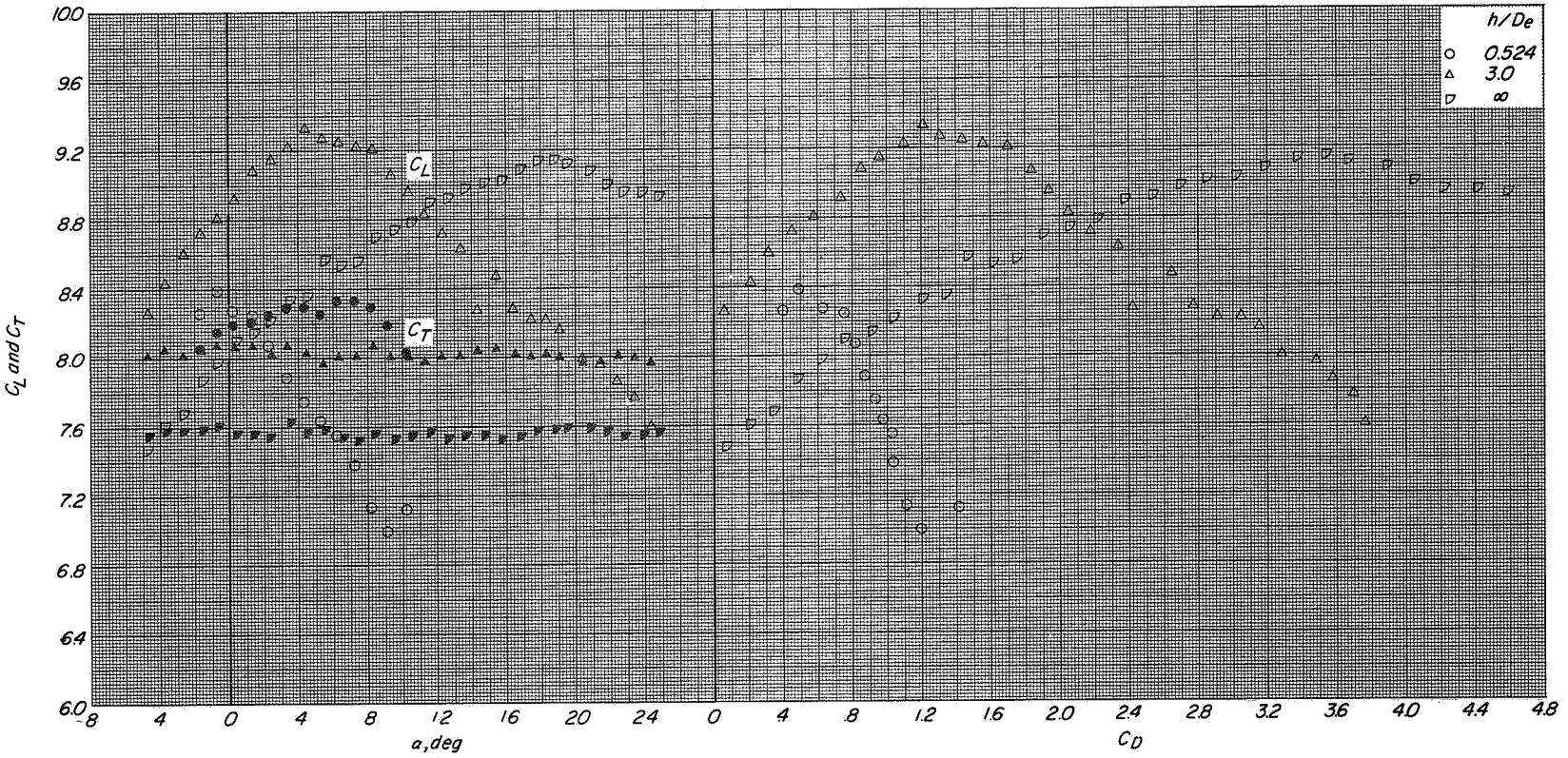

(a) Variation of C_L and C_T with α and C_D with C_L.

Figure 23.- Longitudinal aerodynamic characteristics of configuration A with direct-lift and lift-cruise engines deflected 90°. Tail off: β = 0°; $C_T \approx 8$.

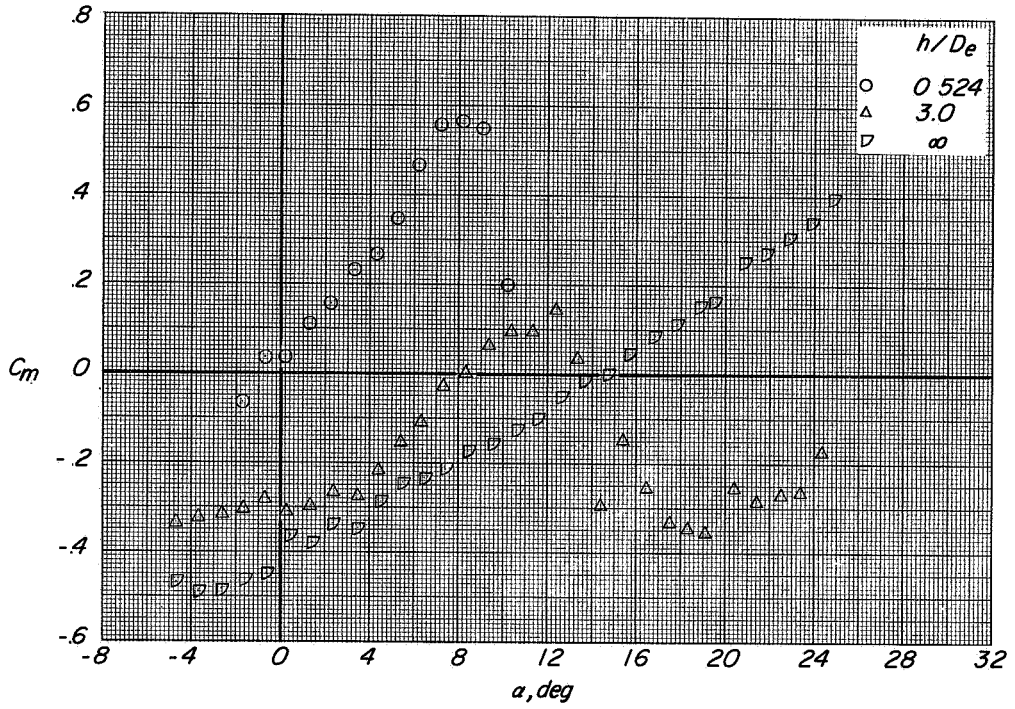

(b) Variation of C_m with α.

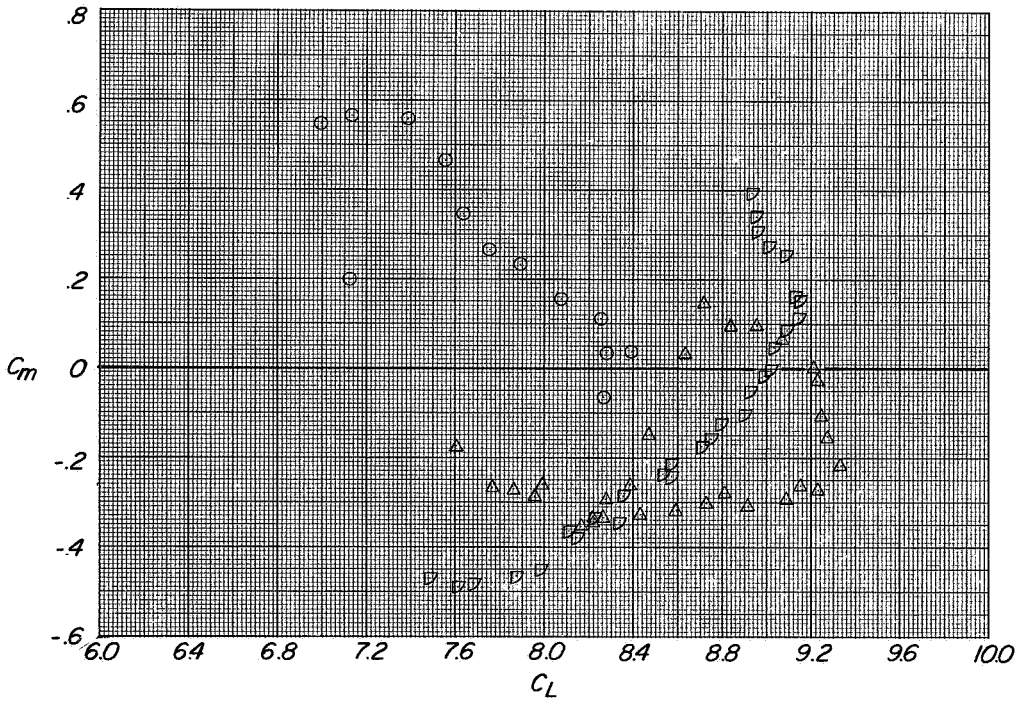

(c) Variation of C_m with C_L.

Figure 23.· Continued.

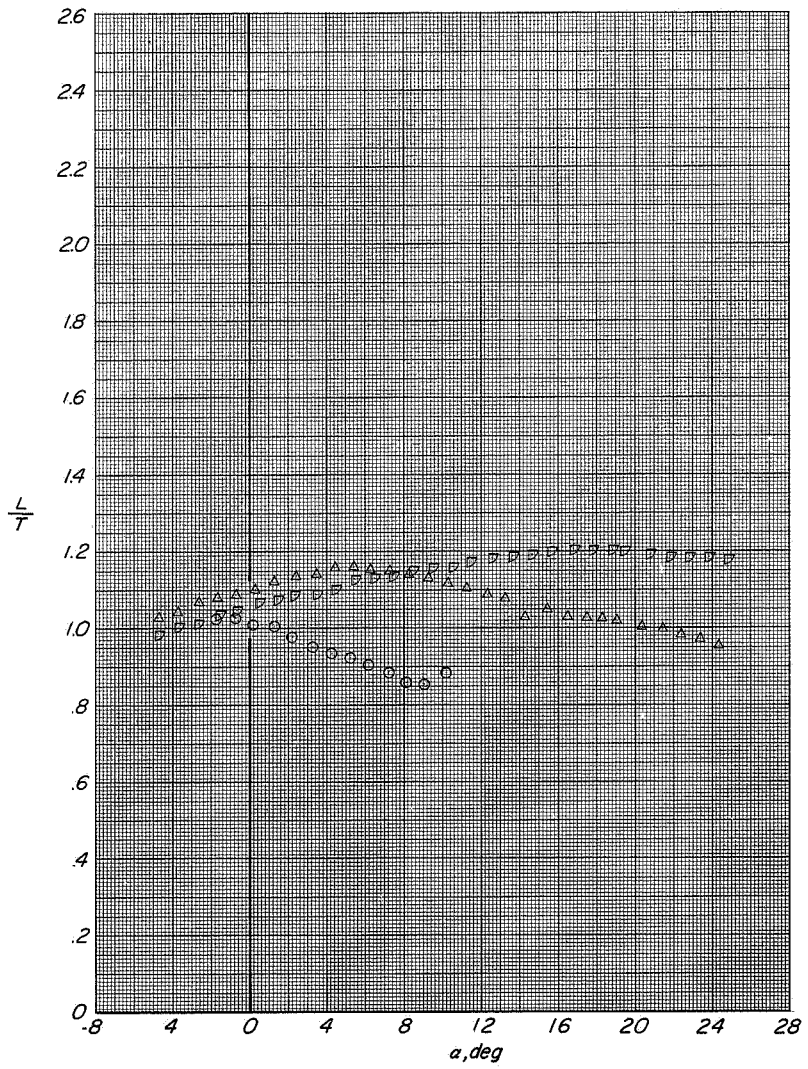

(d) Variation of L/T with α.

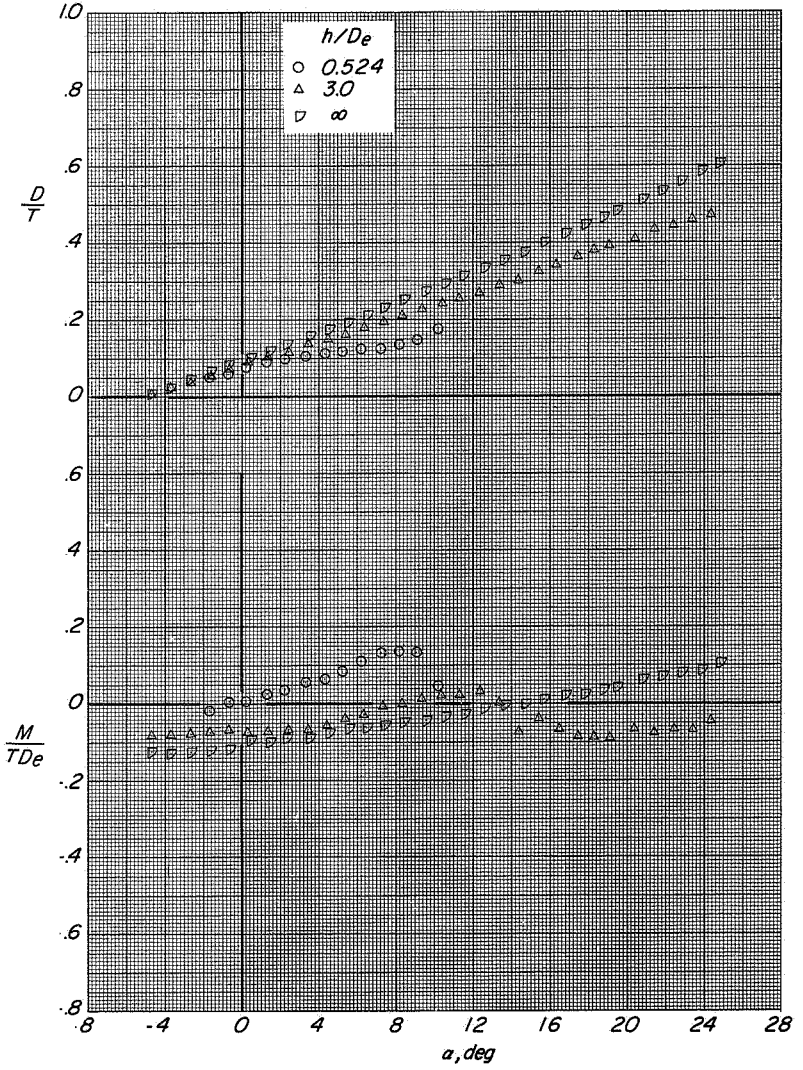

(e) Variation of D/T and M/TD_e with α.

Figure 23.- Concluded.

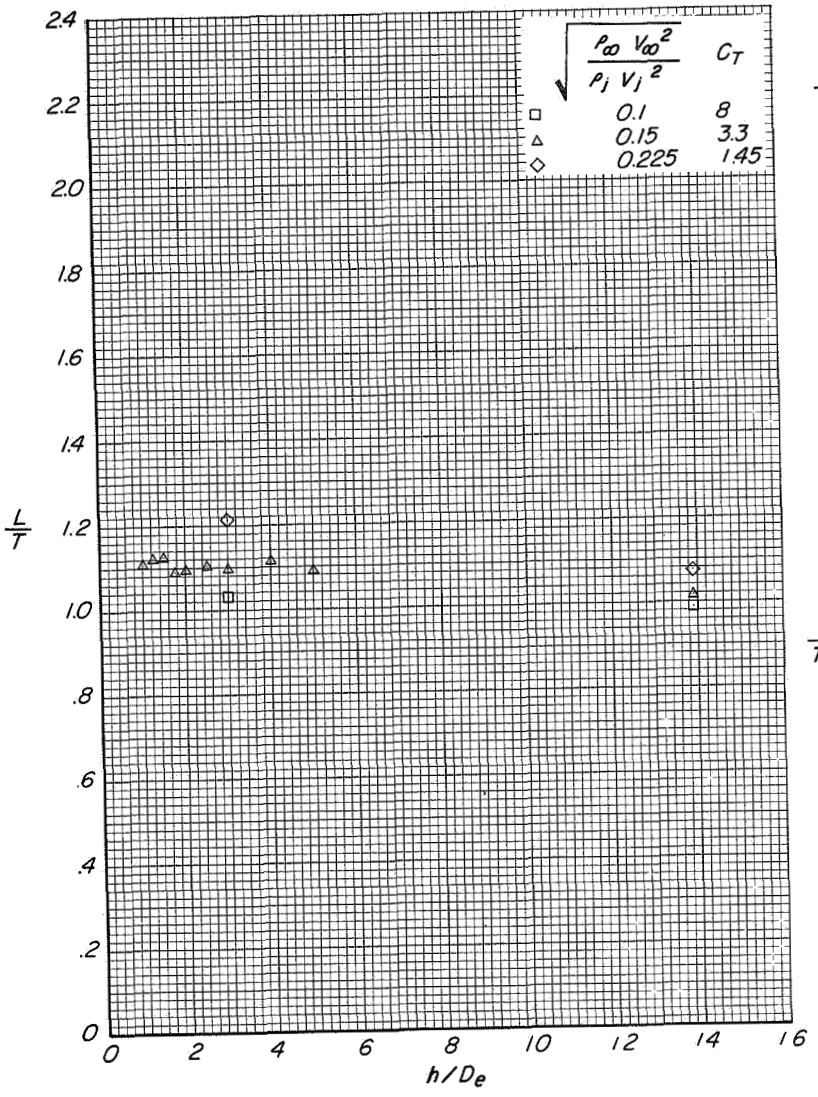

(a) Variation of L/T with h/D_e.

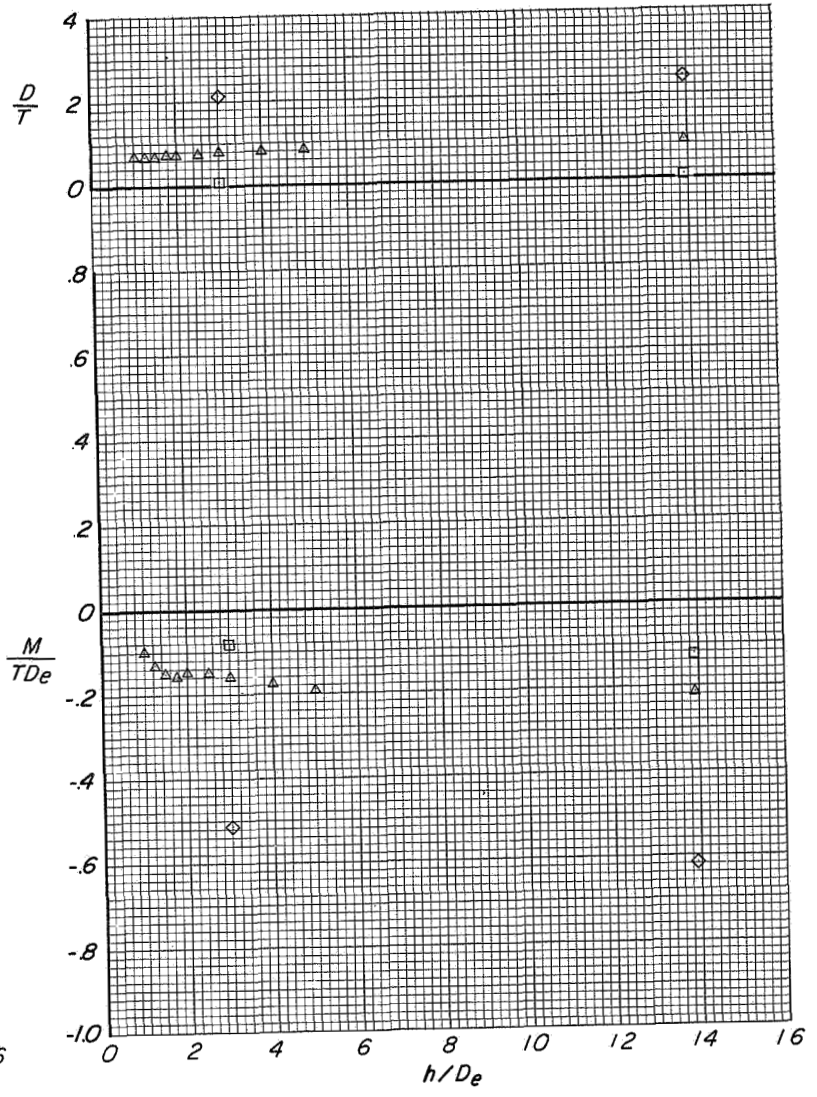

(b) Variation of D/T and M/TD_e with h/D_e.

Figure 24.- Effect of height above the moving-belt ground plane on the longitudinal aerodynamic characteristics of configuration A with direct-lift and lift-cruise engines deflected 90°. Tail off; $\beta = 0^\circ$; $\alpha = -4.7^\circ$.

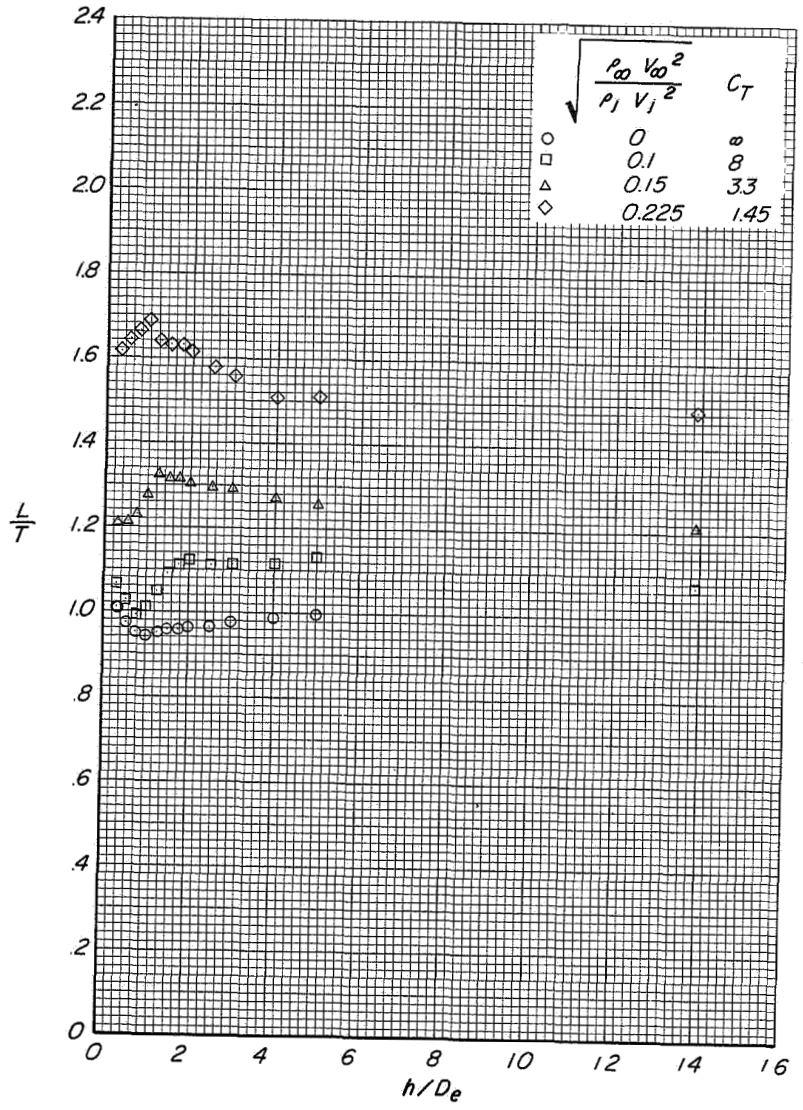

(a) Variation of L/T with h/D_e.

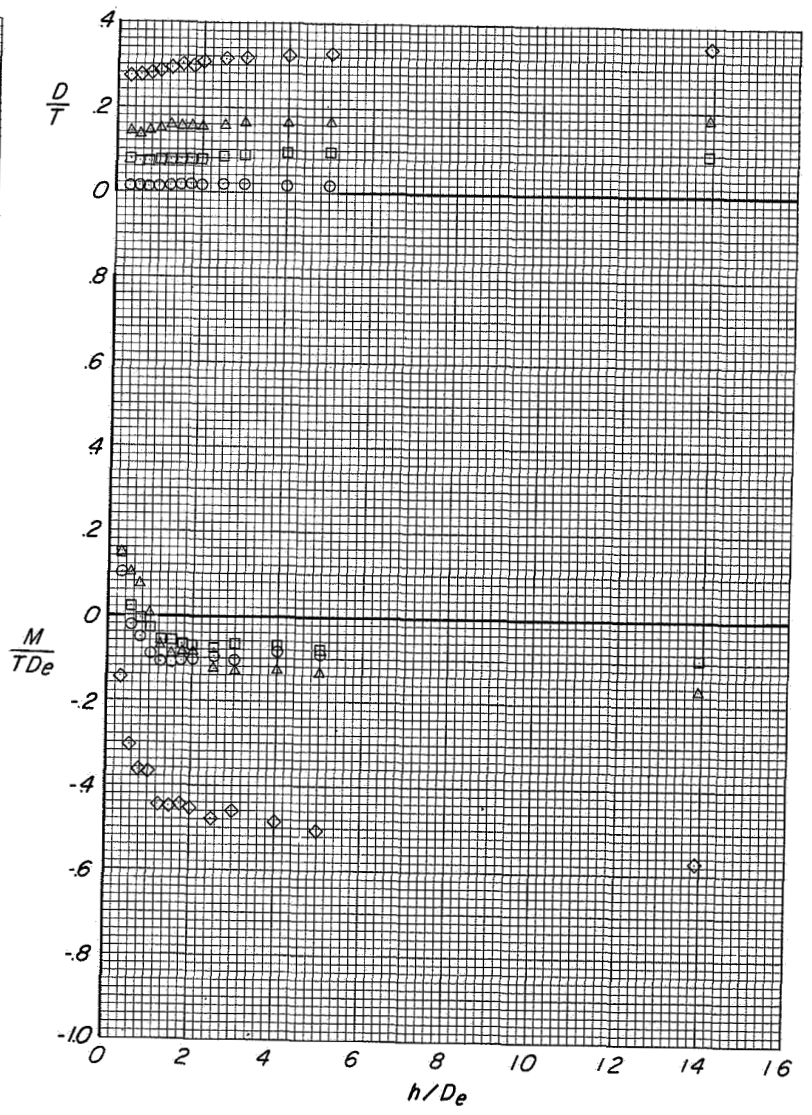

(b) Variation of D/T and M/TD_e with h/D_e.

Figure 25.- Effect of height above the moving-belt ground plane on the longitudinal aerodynamic characteristics of configuration A with direct-lift and lift-cruise engines deflected 90°. Tail off: $\beta = 0°$; $\alpha = 0.3°$.

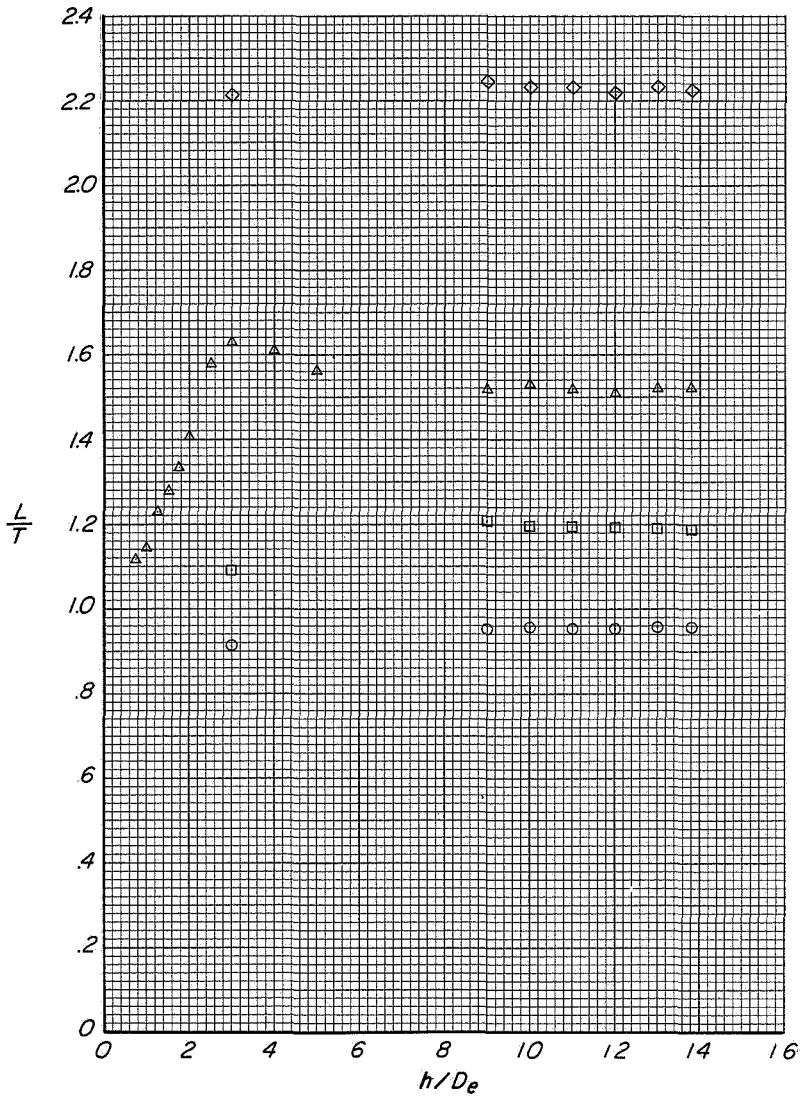

(a) Variation of L/T with h/D_e.

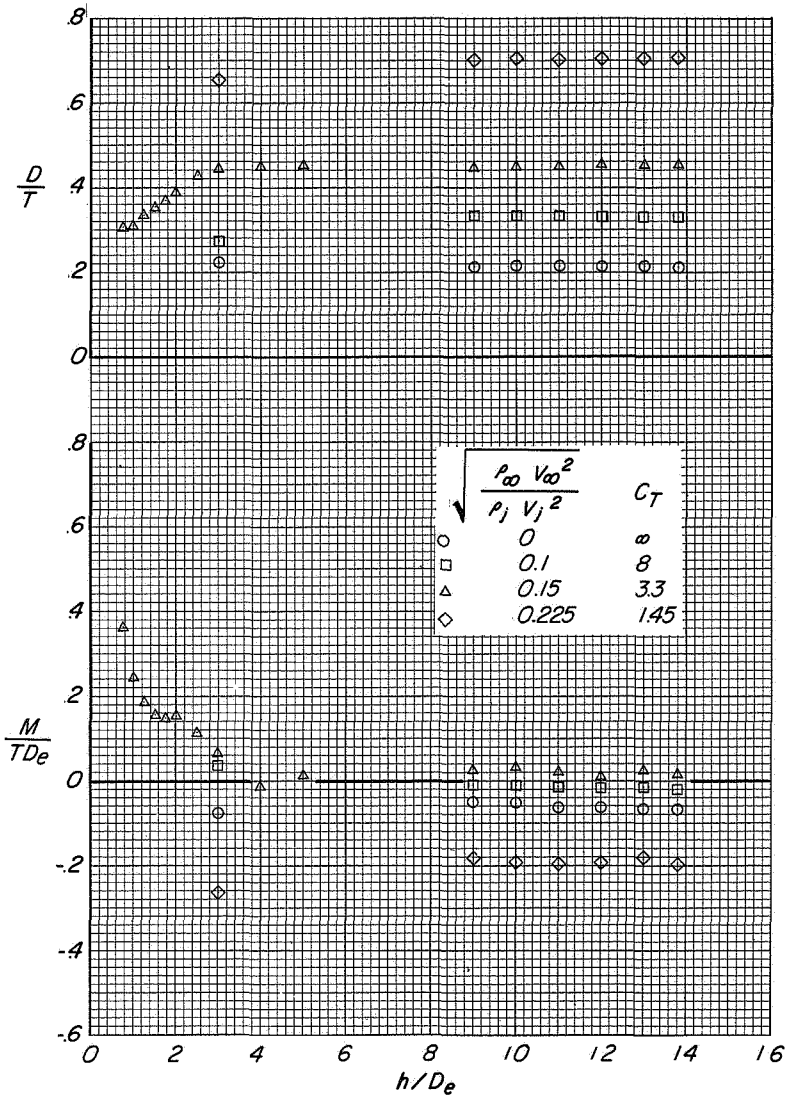

(b) Variation of D/T and M/TD_e with h/D_e.

Figure 26.- Effect of height above the moving-belt ground plane on the longitudinal aerodynamic characteristics of configuration A with direct-lift and lift-cruise engines deflected 90°. Tail off; $\beta = 0^0$; $\alpha = 12.6^0$.

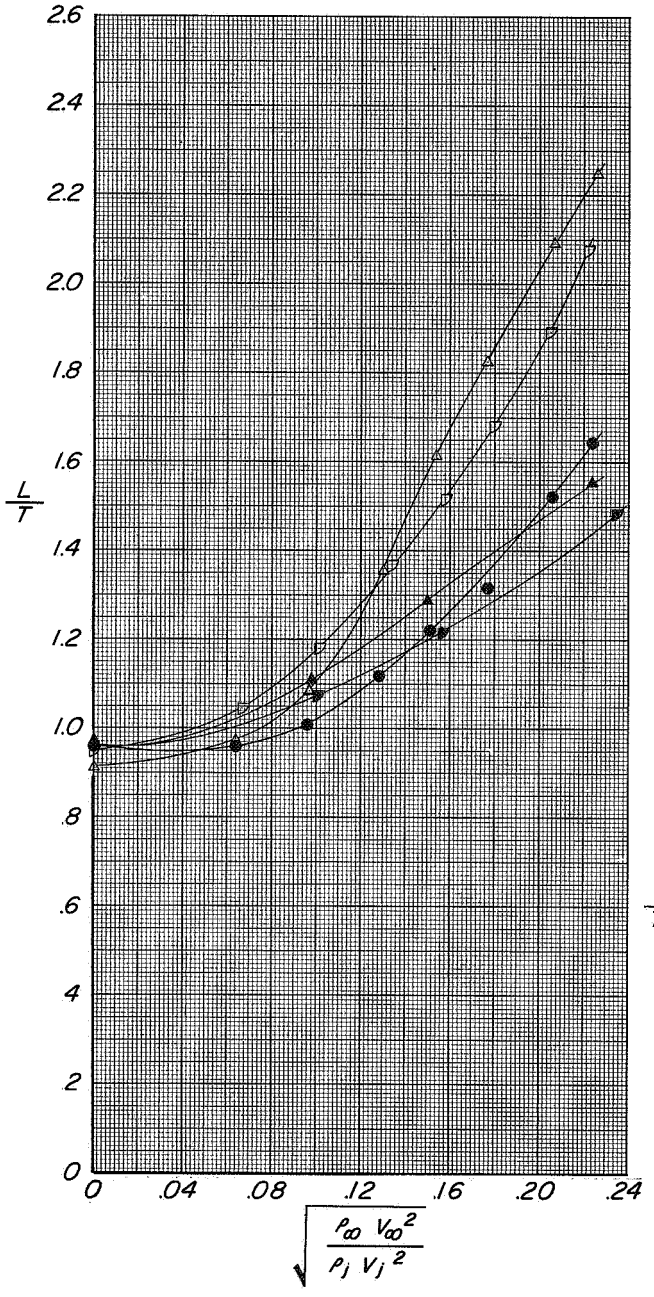

(a) Variation of L/T with effective velocity ratio.

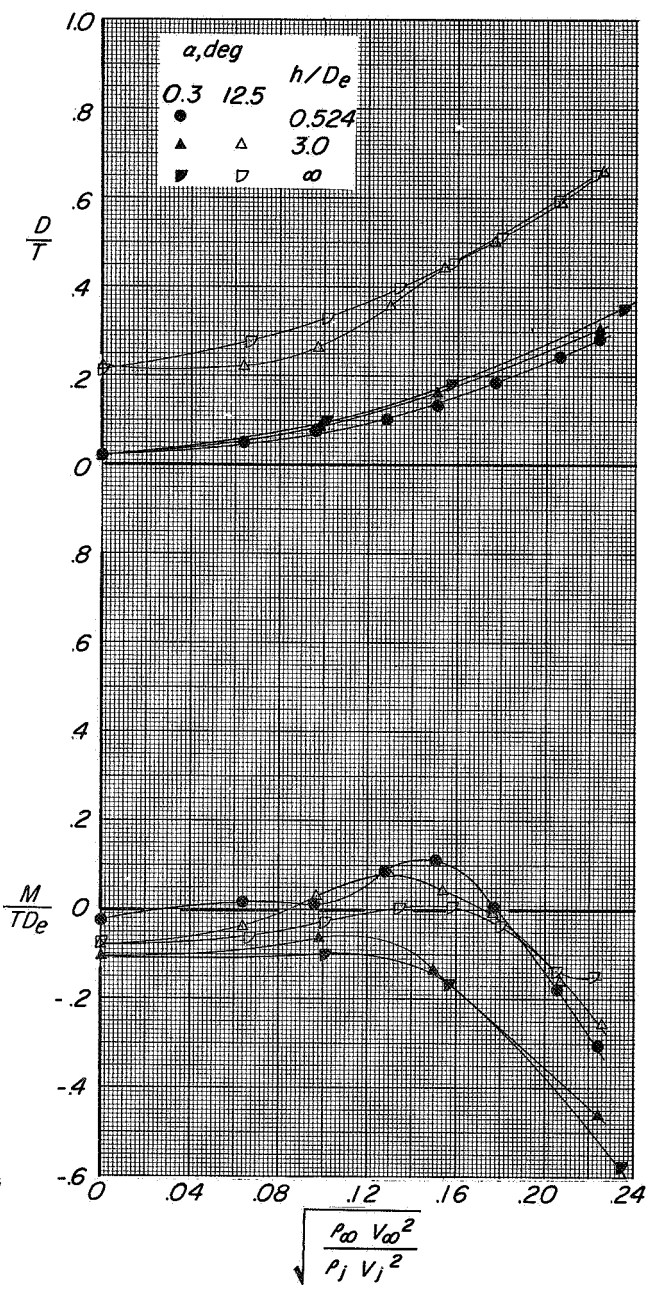

(b) Variation of D/T and M/TD_e with effective velocity ratio.

Figure 27.- Effect of effective velocity ratio on the longitudinal aerodynamic characteristics of configuration A with direct-lift and lift-cruise engines deflected 90°. Tail off: $\beta = 0^0$.

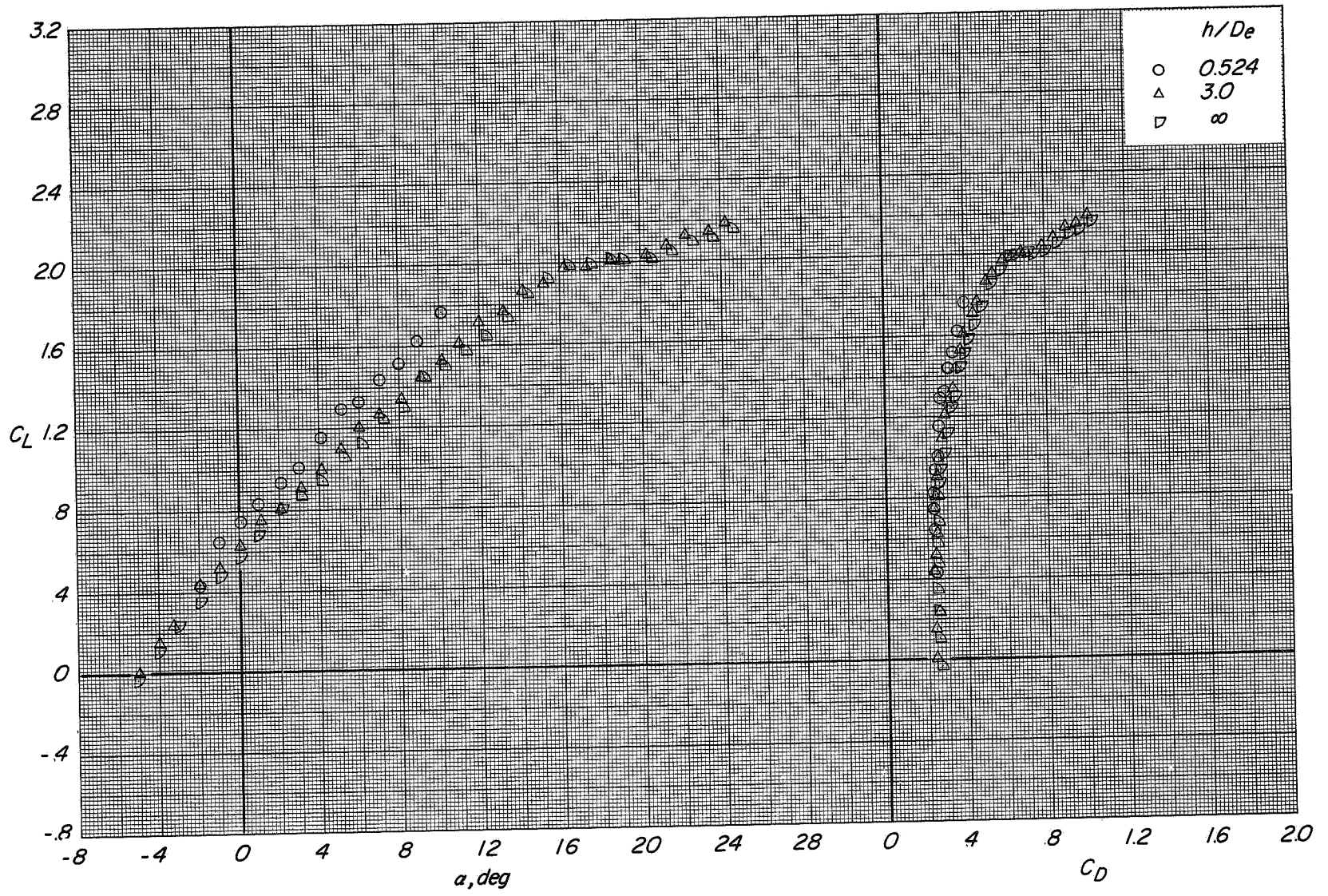

(a) Variation of C_L with α and C_D with C_L

Figure 28.- Longitudinal aerodynamic characteristics of configuration A with direct-lift and lift-cruise engines deflected 90°. $i_t = -10°$; $\beta = 0°$; $C_T = 0$.

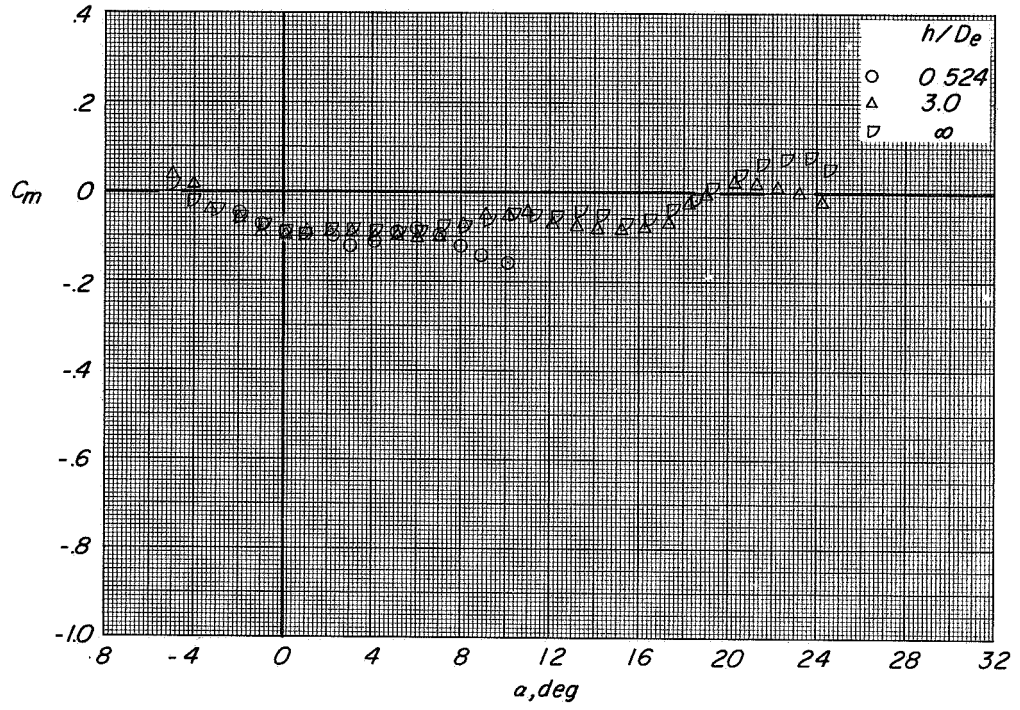

(b) Variation of C_m with α.

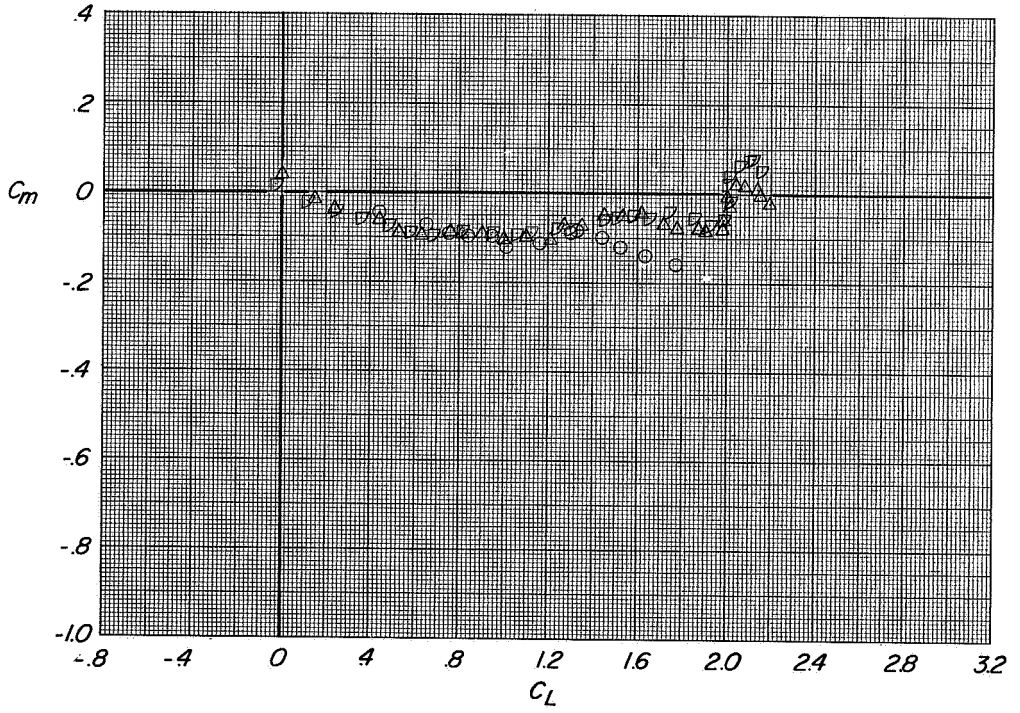

(c) Variation of C_m with C_L.

Figure 28.- Concluded.

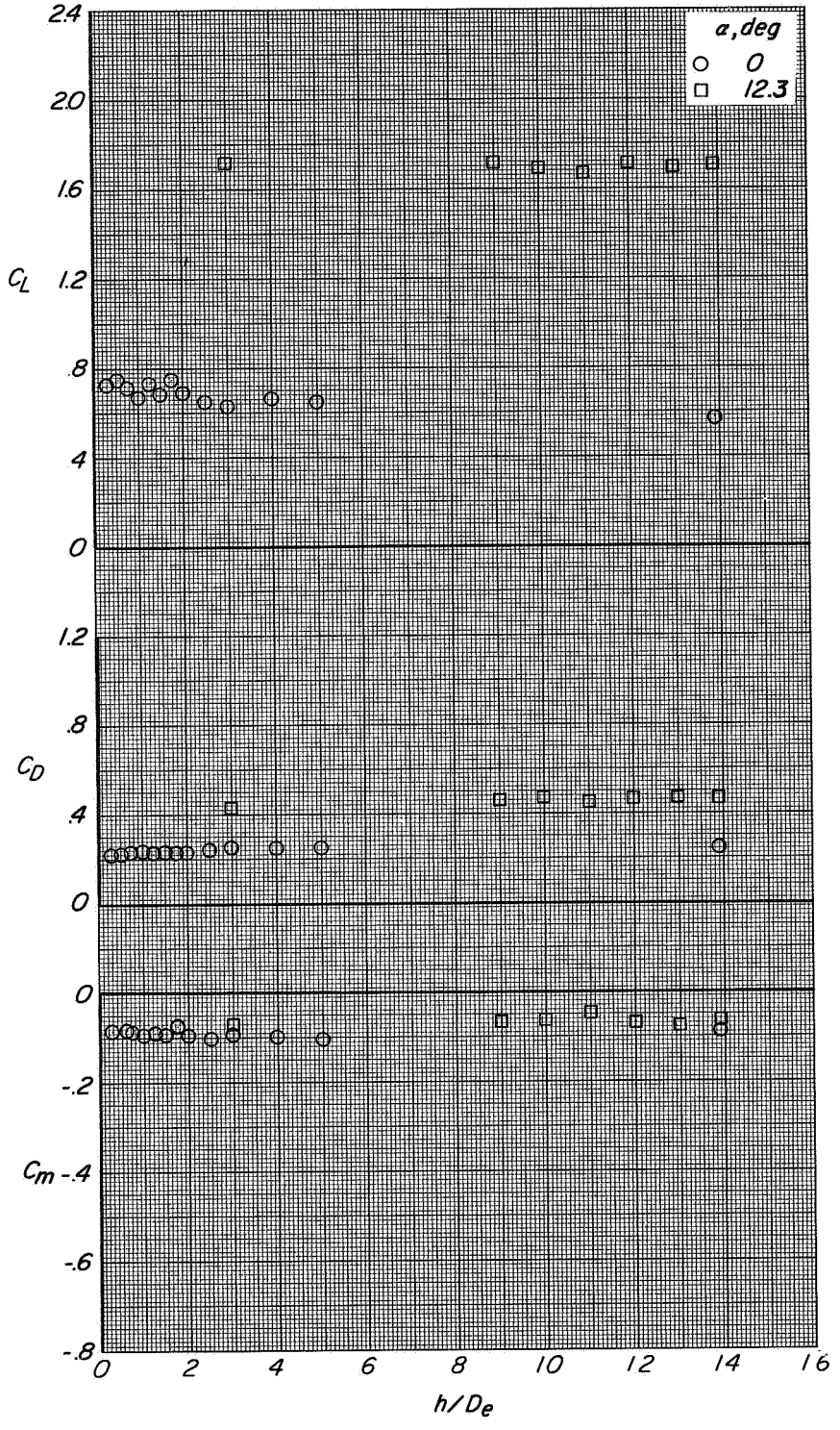

Figure 29.- Effect of height above the moving-belt ground plane on the longitudinal aerodynamic characteristics of configuration A with direct-lift and lift-cruise engines deflected 90°. $i_t = -10°$; $\beta = 0°$; $C_T = 0$.

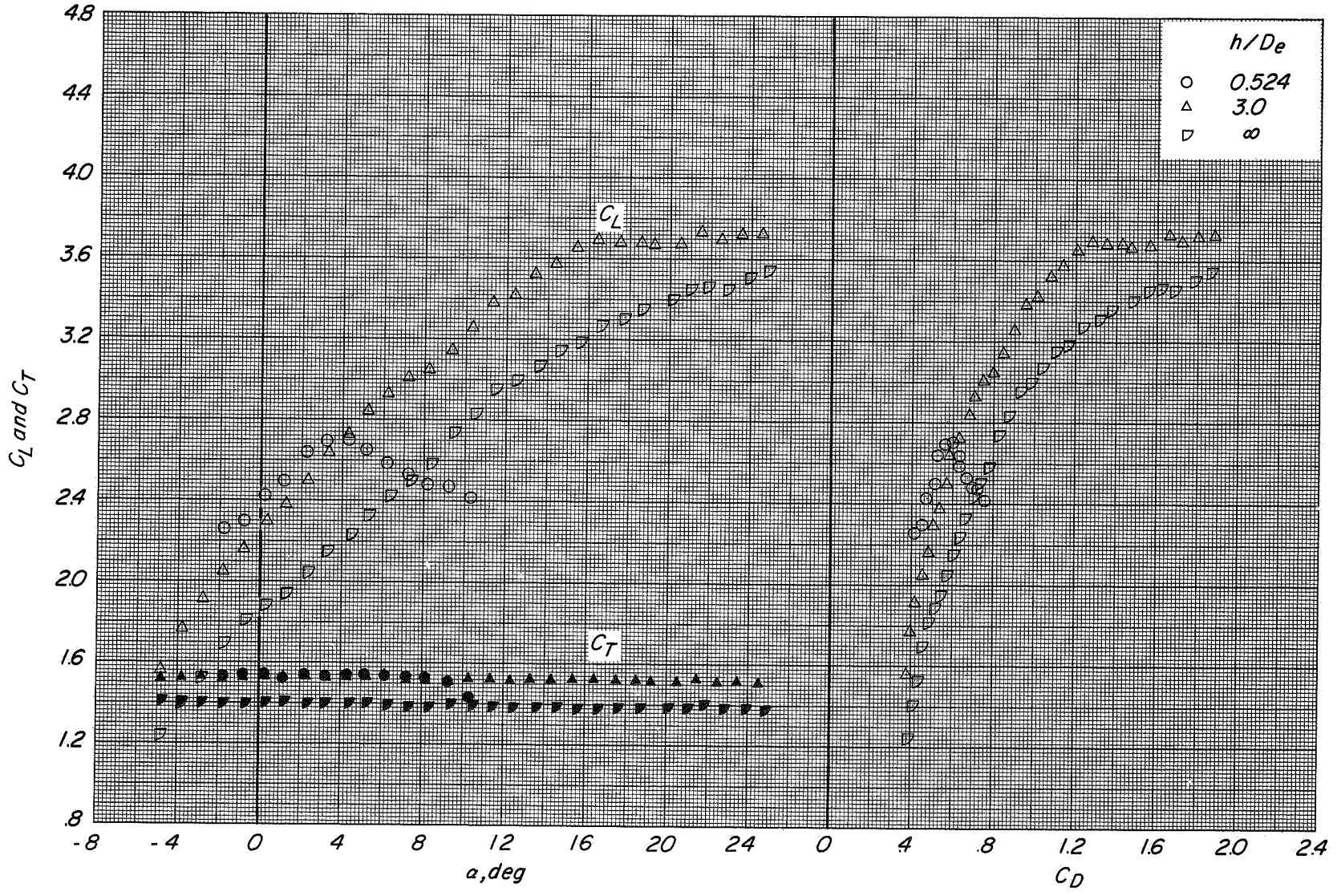

(a) Variation of C_L and C_T with α and C_D with C_L

Figure 30.- Longitudinal aerodynamic characteristics of configuration A with direct-lift and lift-cruise engines deflected 90°. $i_t = -10°$; $\beta = 0°$; $C_T \approx 1.45$.

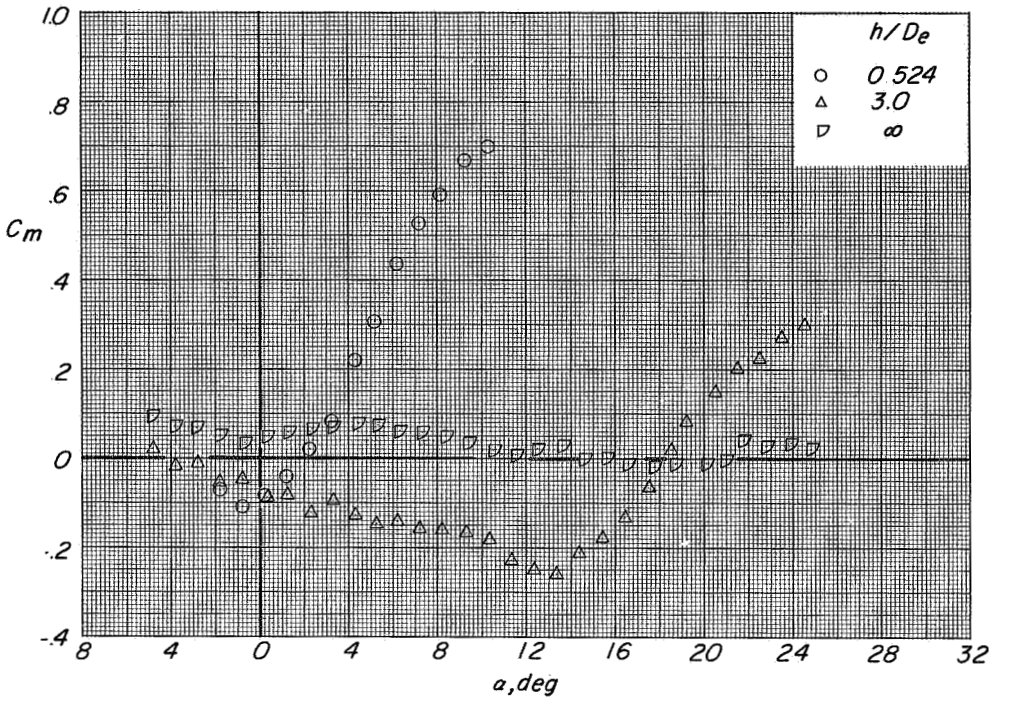

(b) Variation of C_m with α.

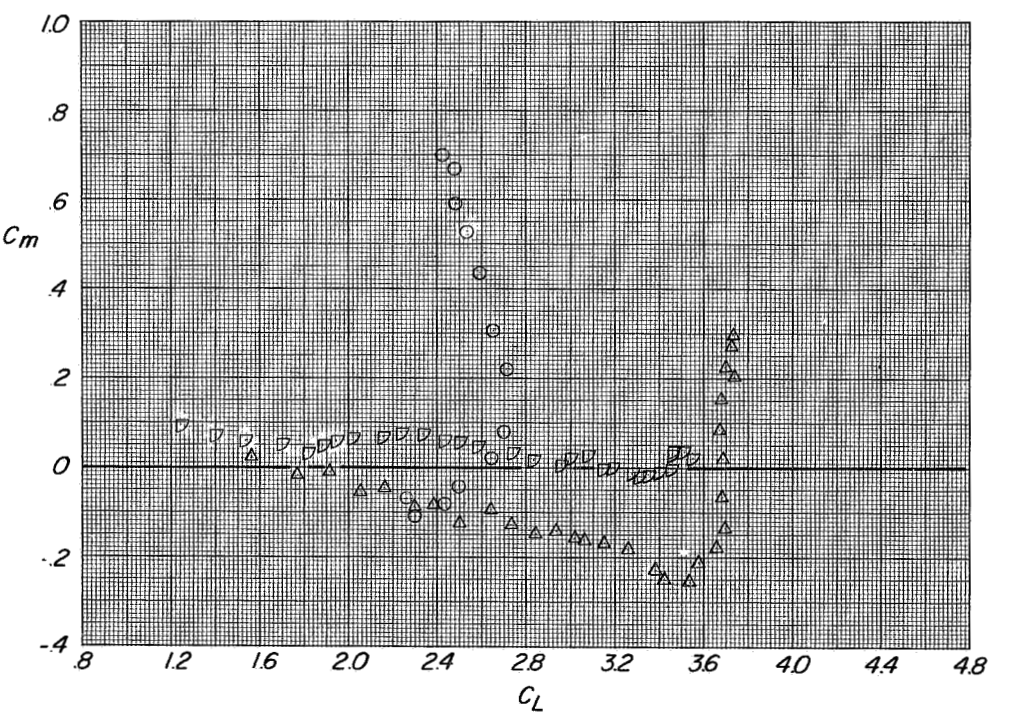

(c) Variation of C_m with C_L.

Figure 30.- Continued.

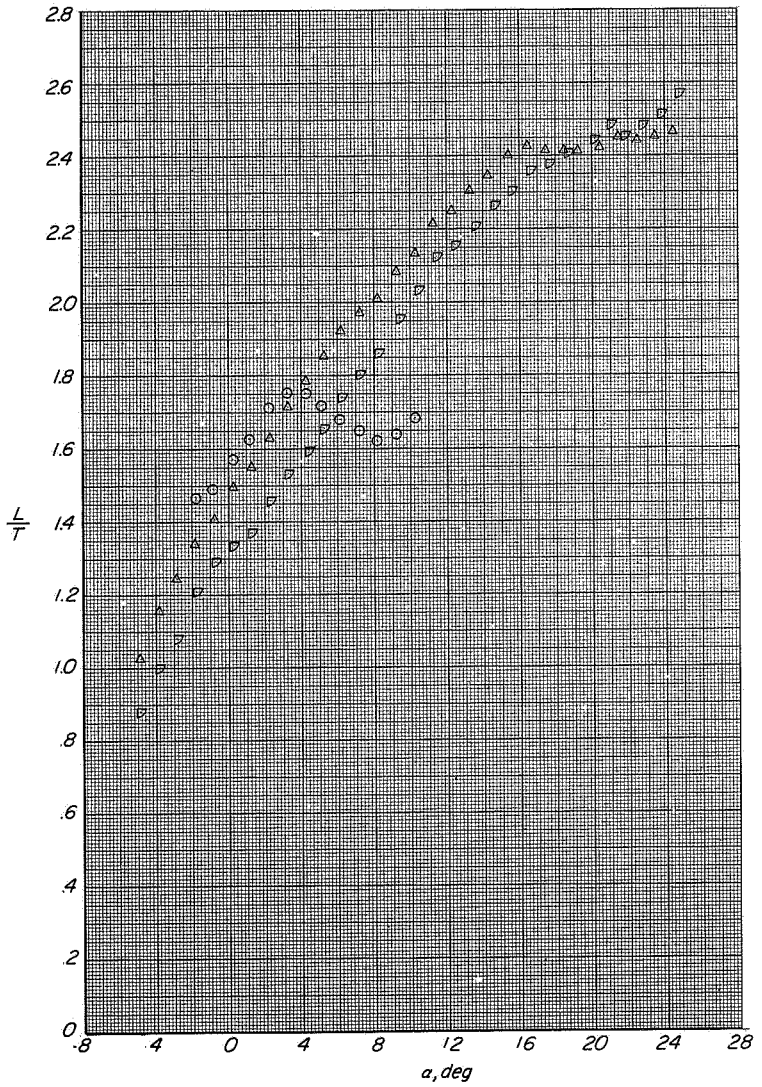

(d) Variation of L/T with α.

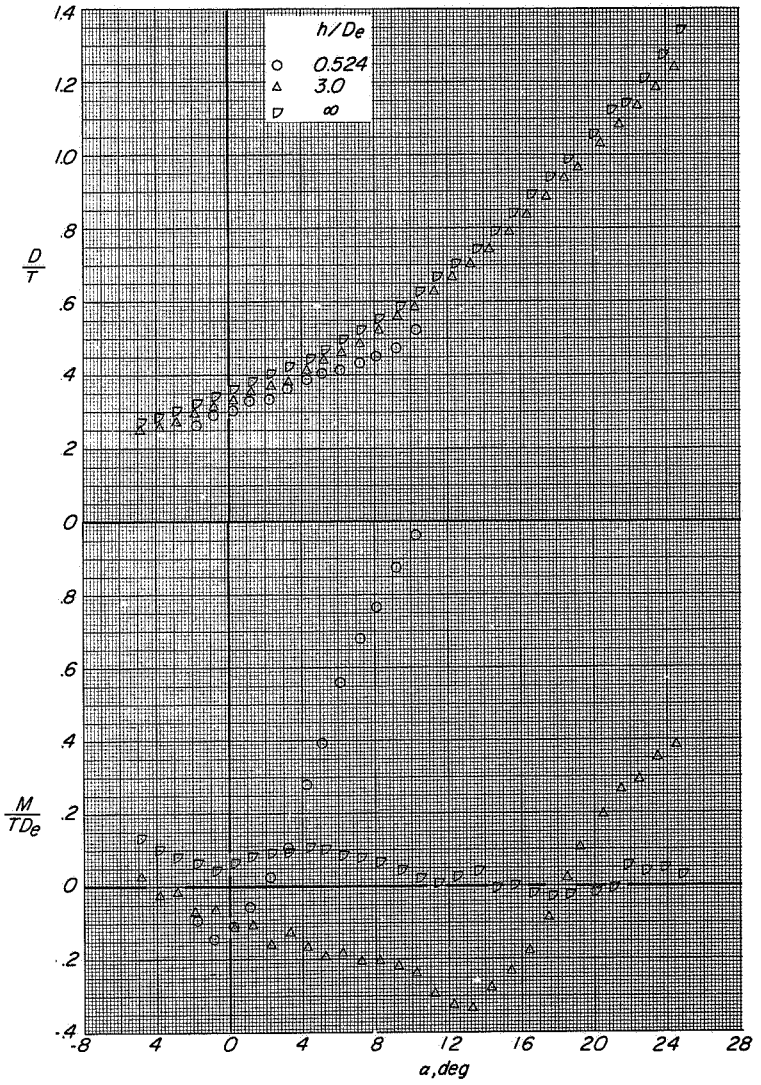

(e) Variation of D/T and M/TD_e with α.

Figure 30.- Concluded.

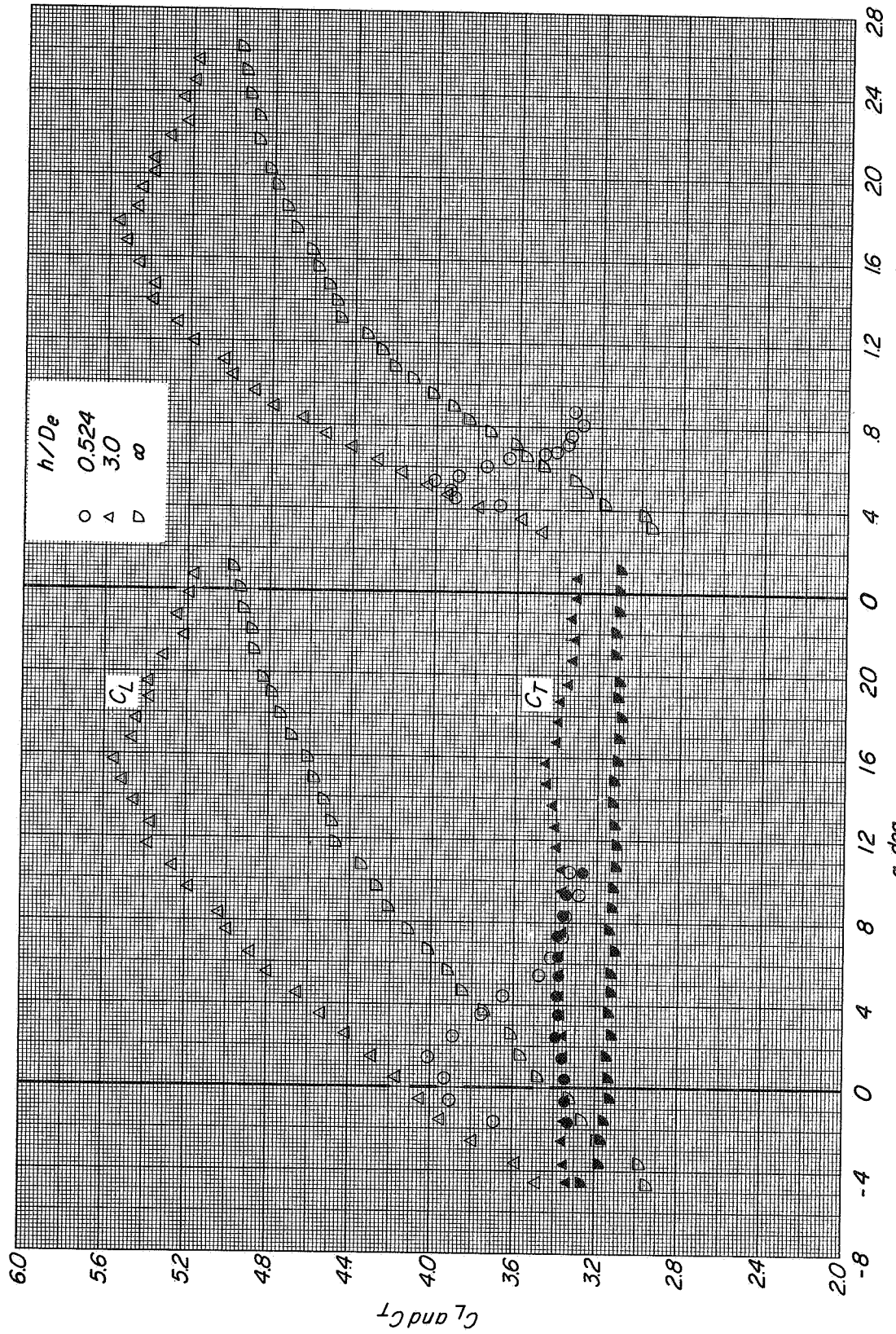

(a) Variation of C_L and C_T with α and C_D with C_L

Figure 31.- Longitudinal aerodynamic characteristics of configuration A with direct-lift and lift-cruise engines deflected 90°. $i_t = -10°$; $\beta = 0°$; $C_T \approx 3.3$.

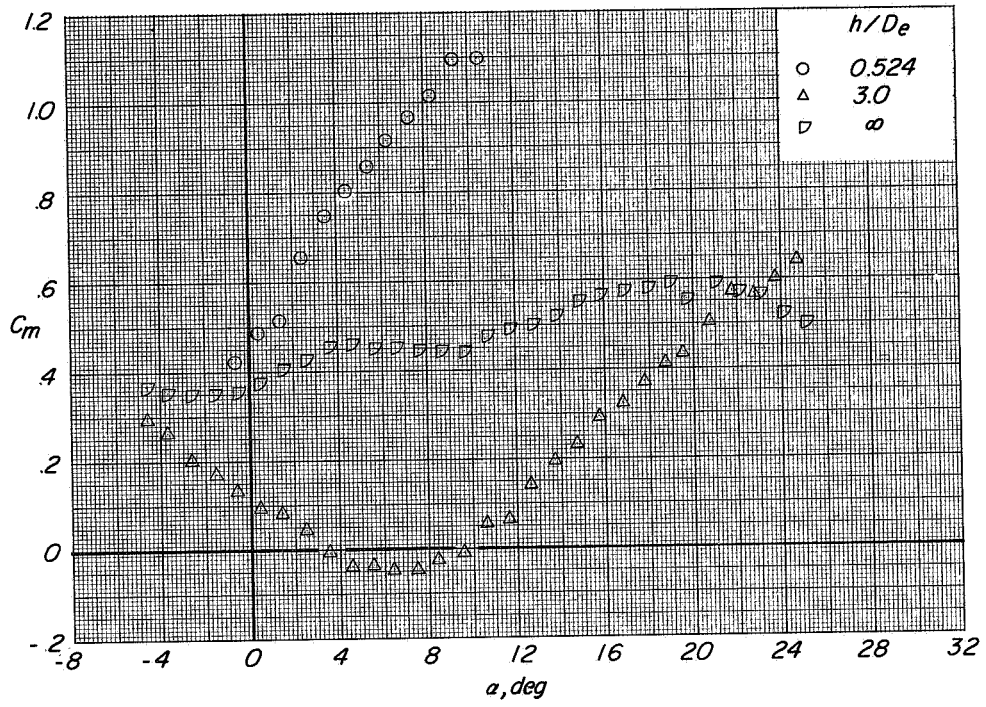

(b) Variation of C_m with α.

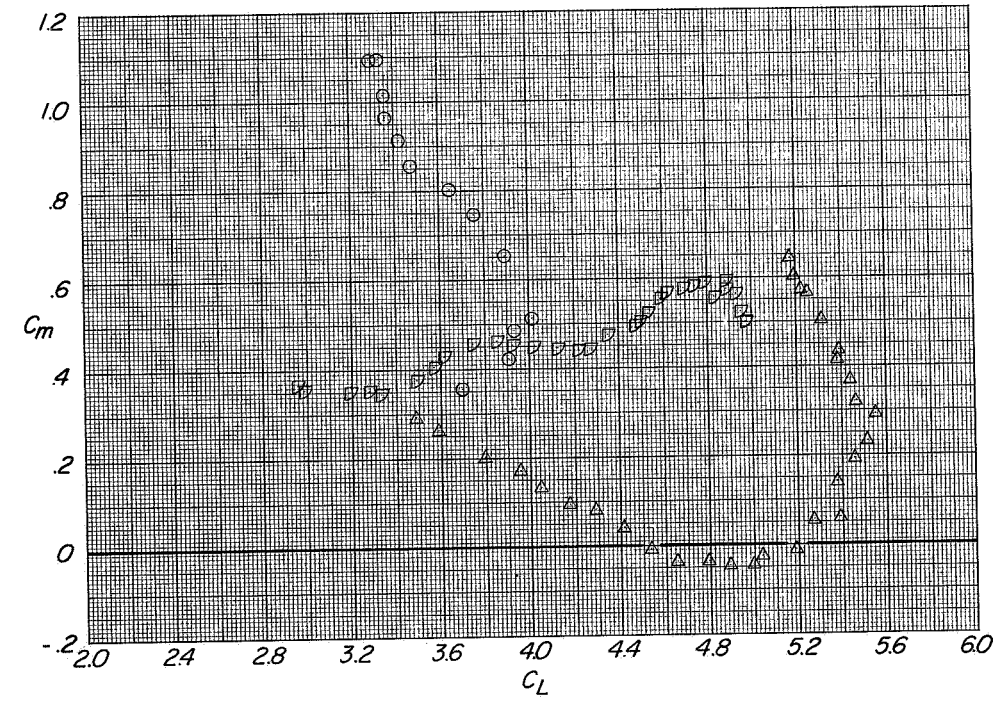

(c) Variation of C_m with C_L.

Figure 31.- Continued.

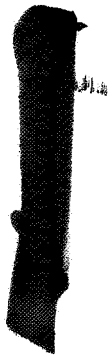

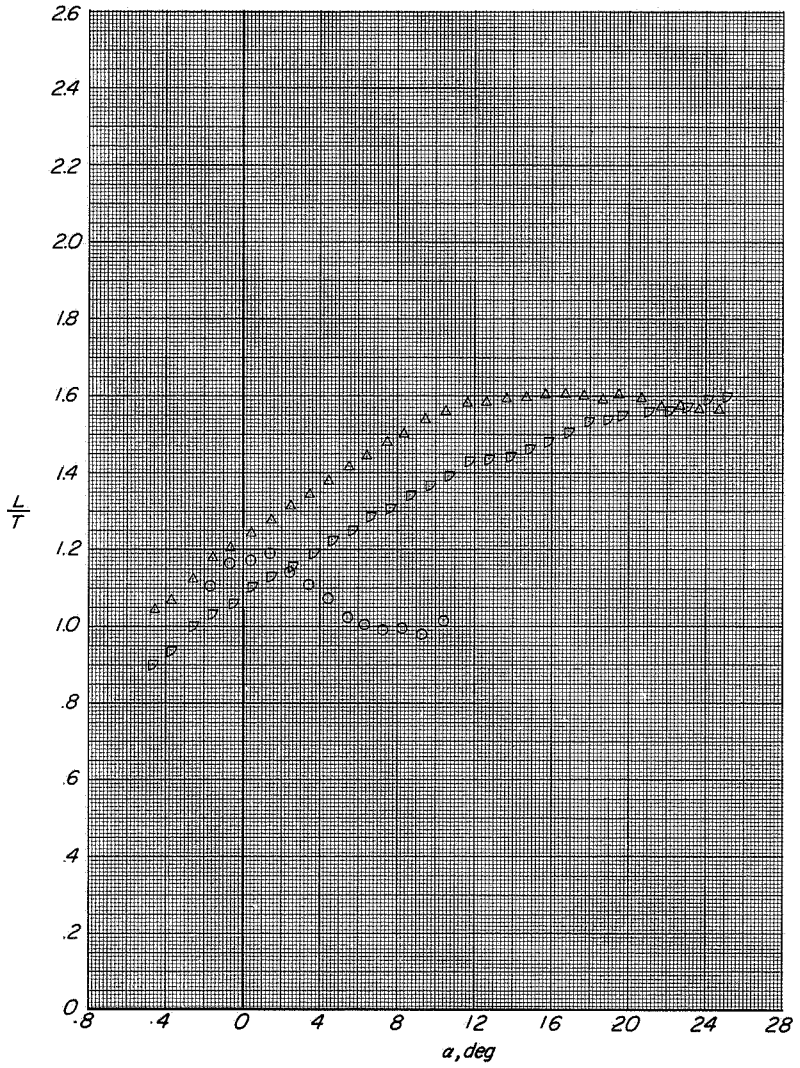

(d) Variation of L/T with α.

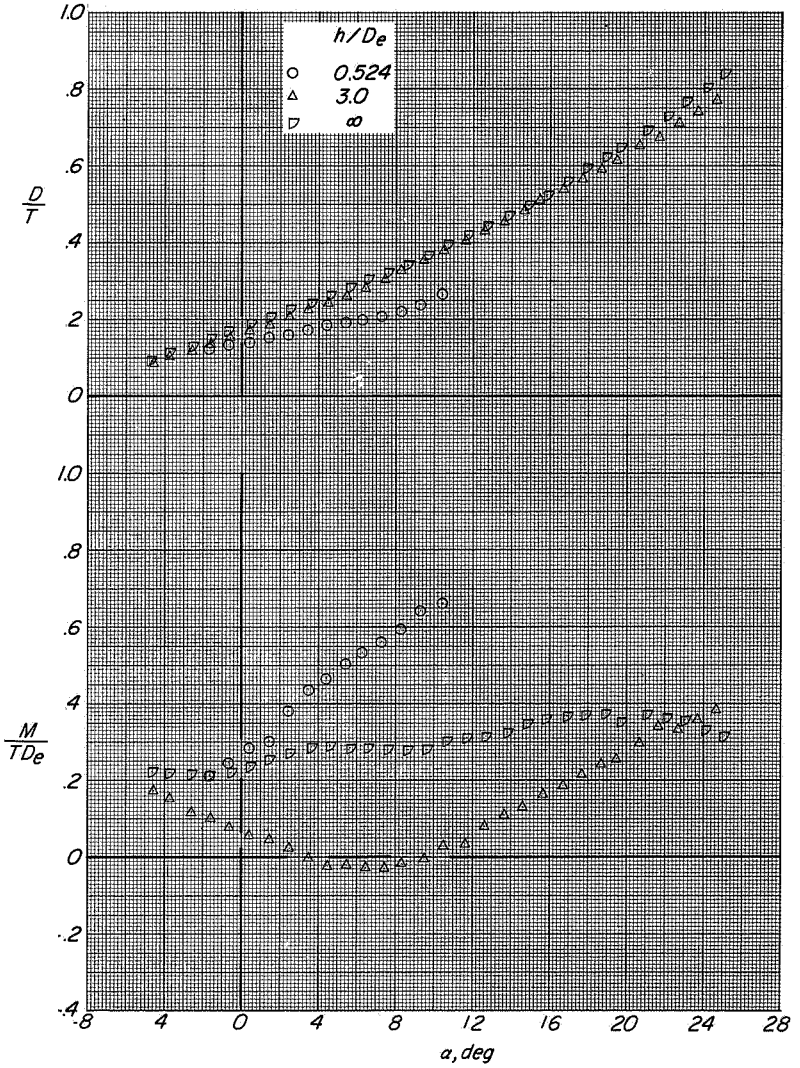

(e) Variation of D/T and M/TD_e with α.

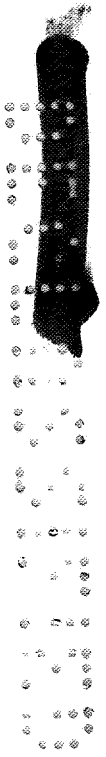

Figure 31.- Concluded.

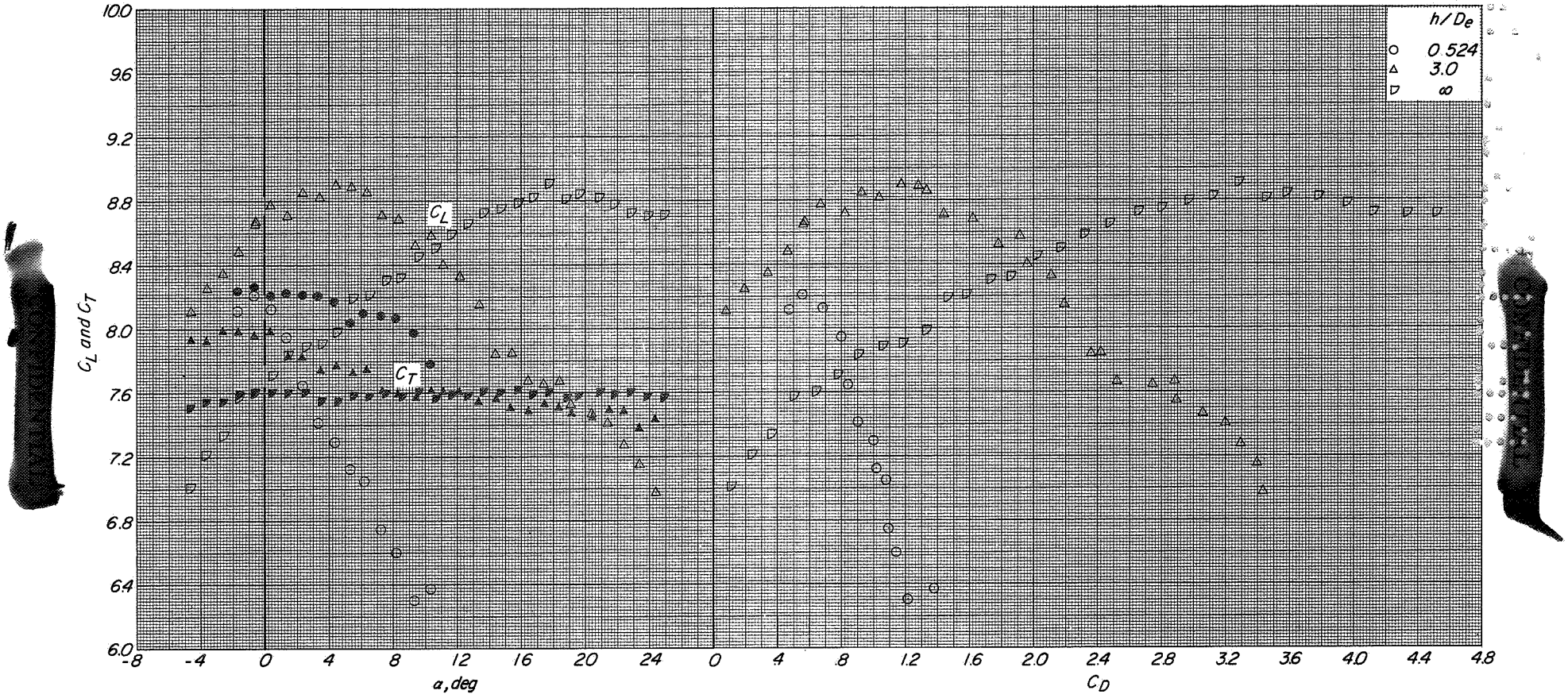

(a) Variation of C_L and C_T with α and C_D with C_L

Figure 32.- Longitudinal aerodynamic characteristics of configuration A with direct-lift and lift-cruise engines deflected 90°. $i_t = -10°$; $\beta = 0°$; $C_T \approx 8$.

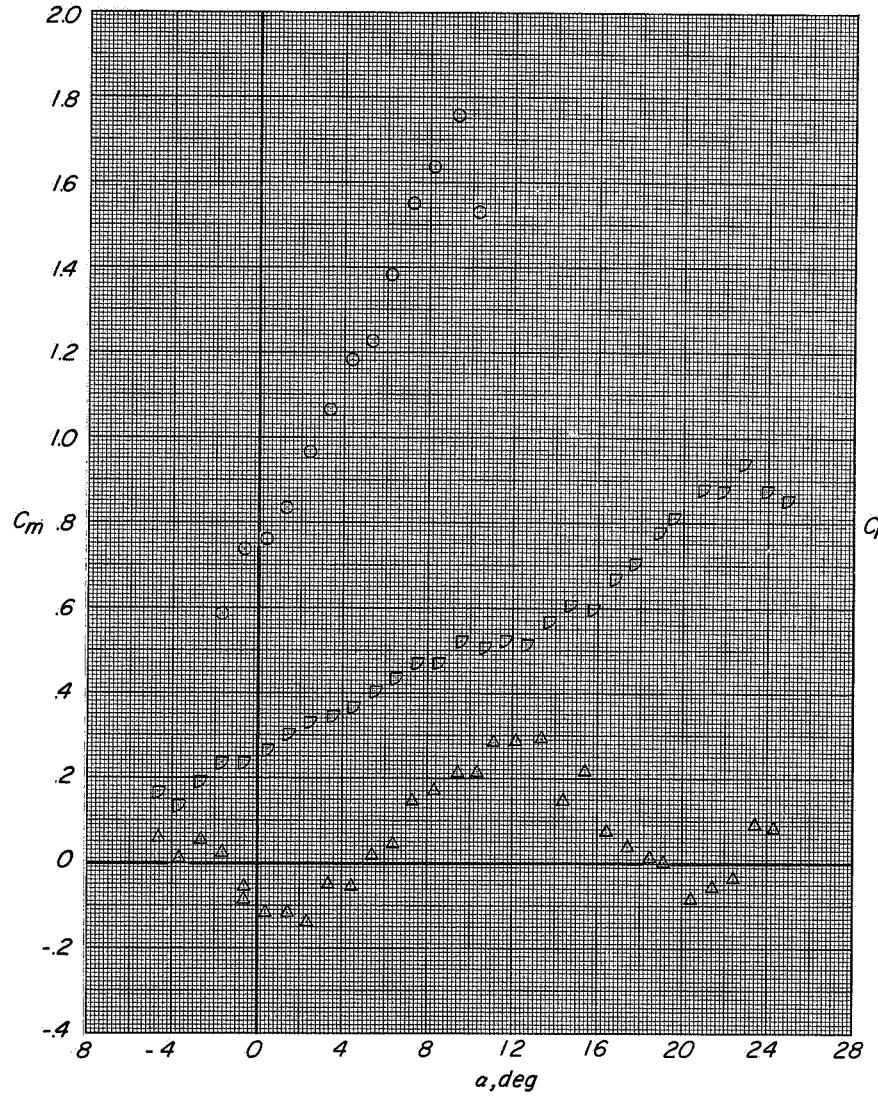

(b) Variation of C_m with α.

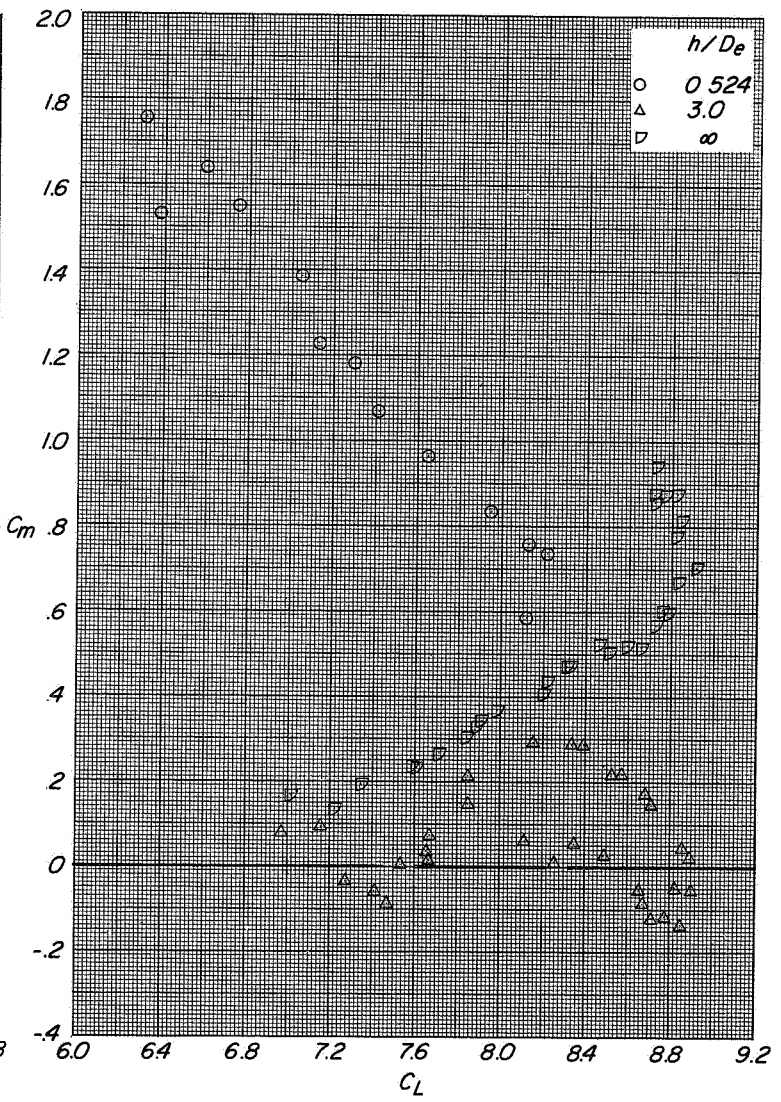

(c) Variation of C_m with C_L.

Figure 32.- Continued.

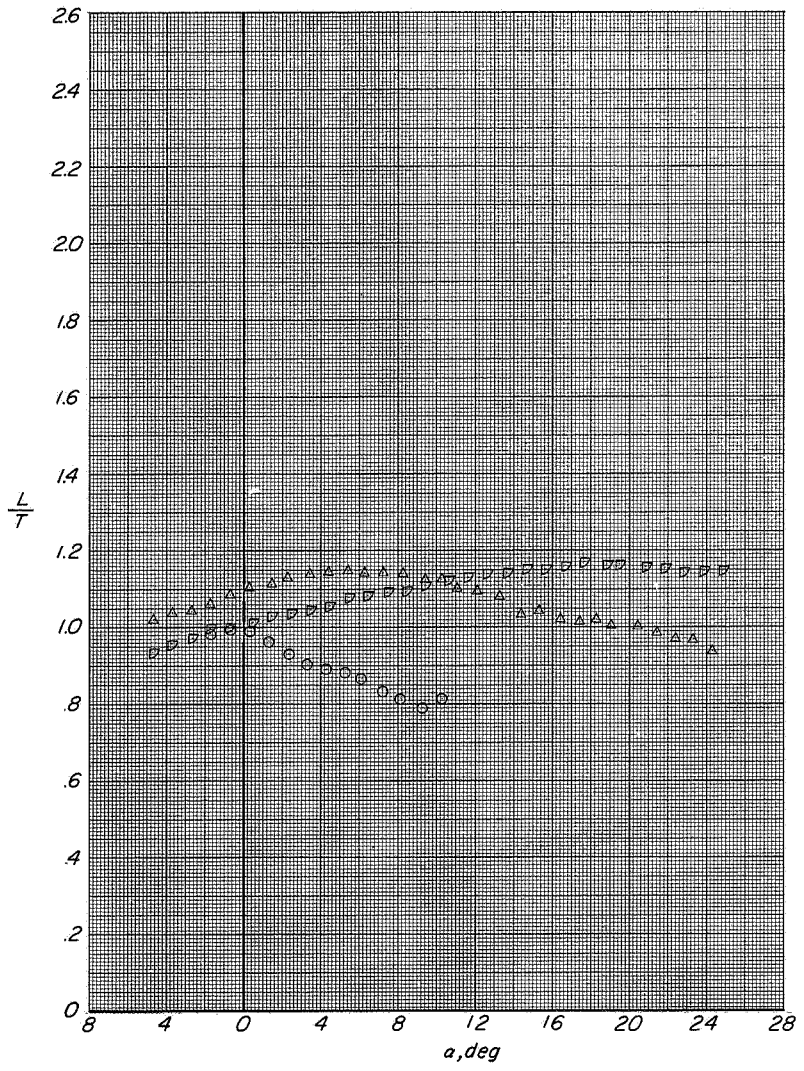

(d) Variation of L/T with α.

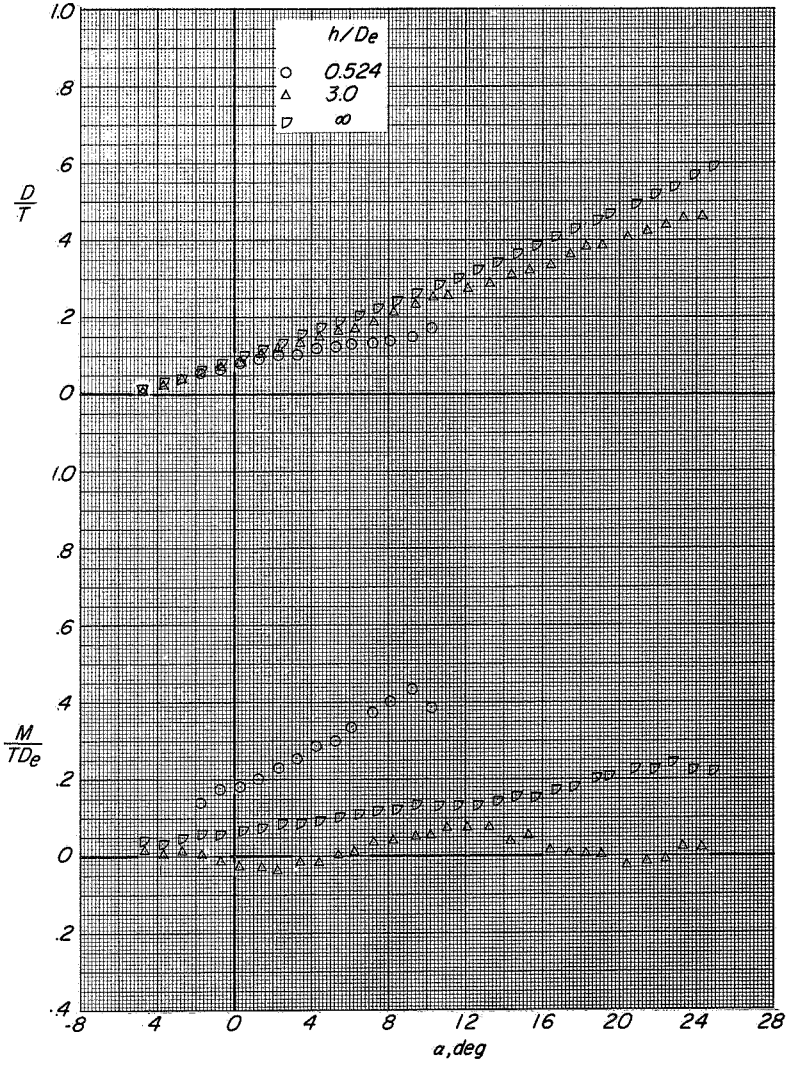

(e) Variation of D/T and M/TDe with α.

Figure 32.- Concluded.

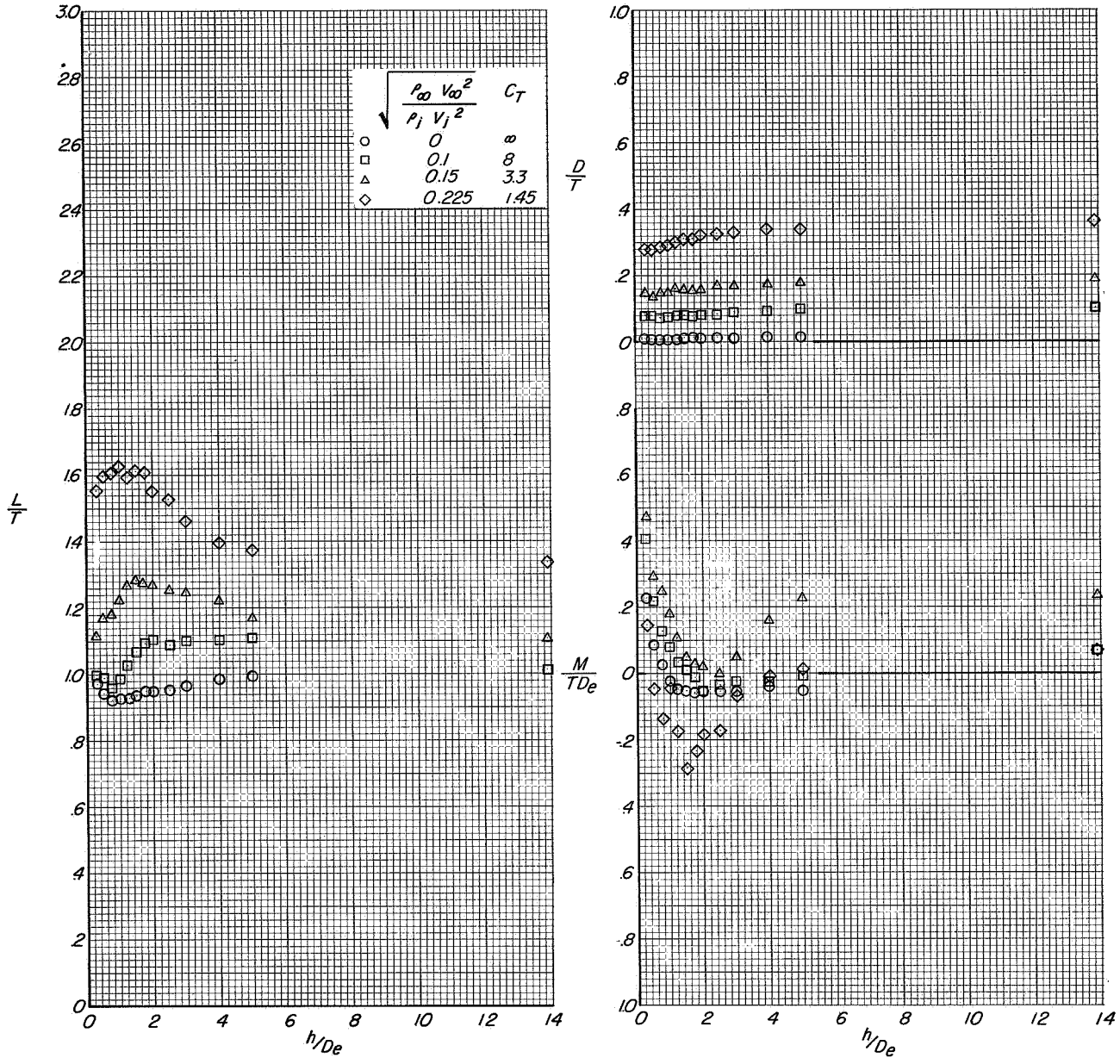

(a) Variation of L/T with h/D_e.

(b) Variation of D/T and M/TD_e with h/D_e.

Figure 33.- Effect of height above the moving-belt ground plane on the longitudinal aerodynamic characteristics of configuration A with direct-lift and lift-cruise engines deflected 90^0. $i_t = 10^0$; $\beta = 0^0$; $\alpha = 0^0$.

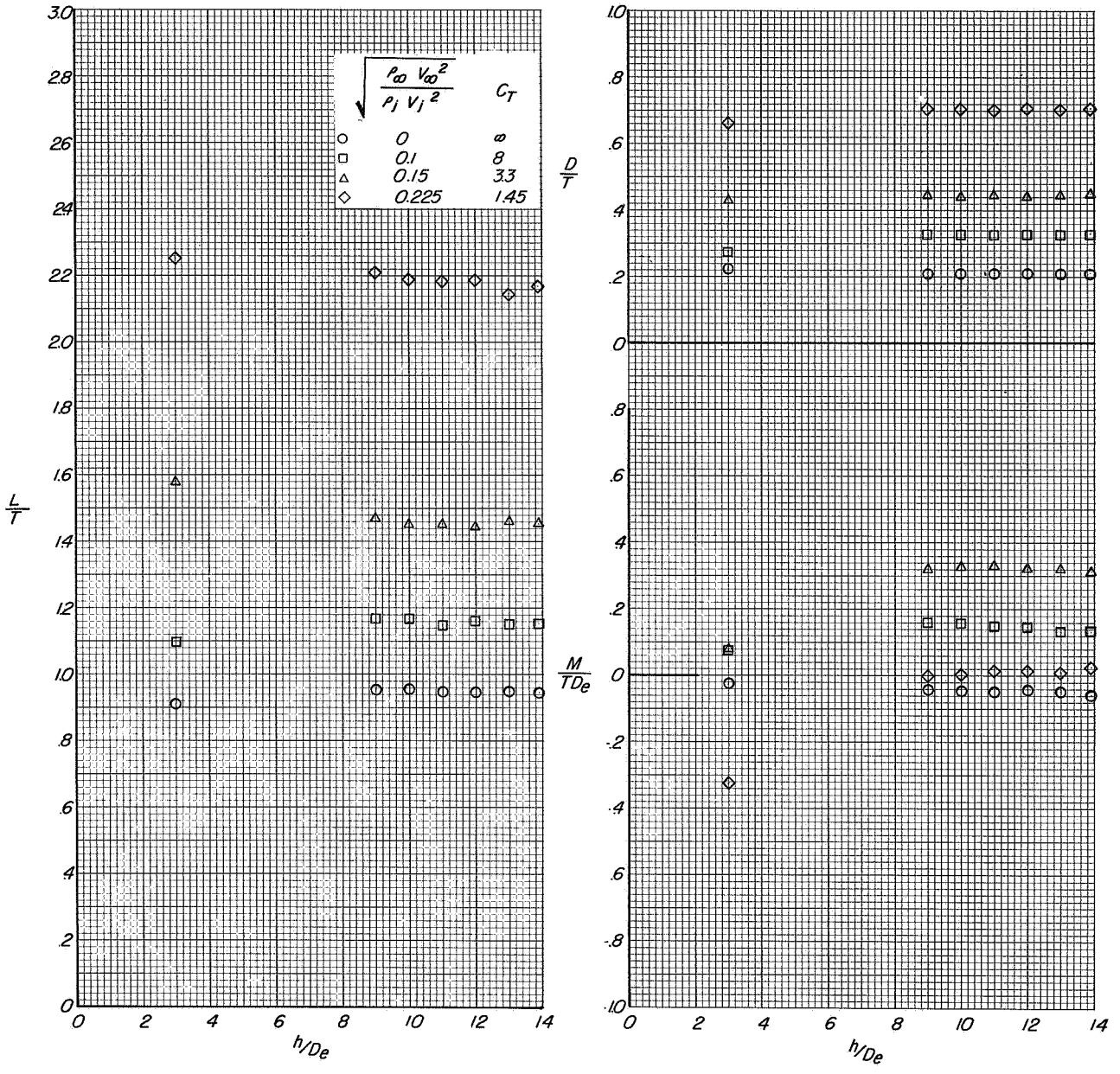

(a) Variation of L/T with h/D_e.

(b) Variation of D/T and M/TD_e with h/D_e.

Figure 34.- Effect of height above the moving-belt ground plane on the longitudinal aerodynamic characteristics of configuration A with direct-lift and lift-cruise engines deflected 90°. $i_t = -10°$; $\beta = 0°$; $\alpha = 12°$.

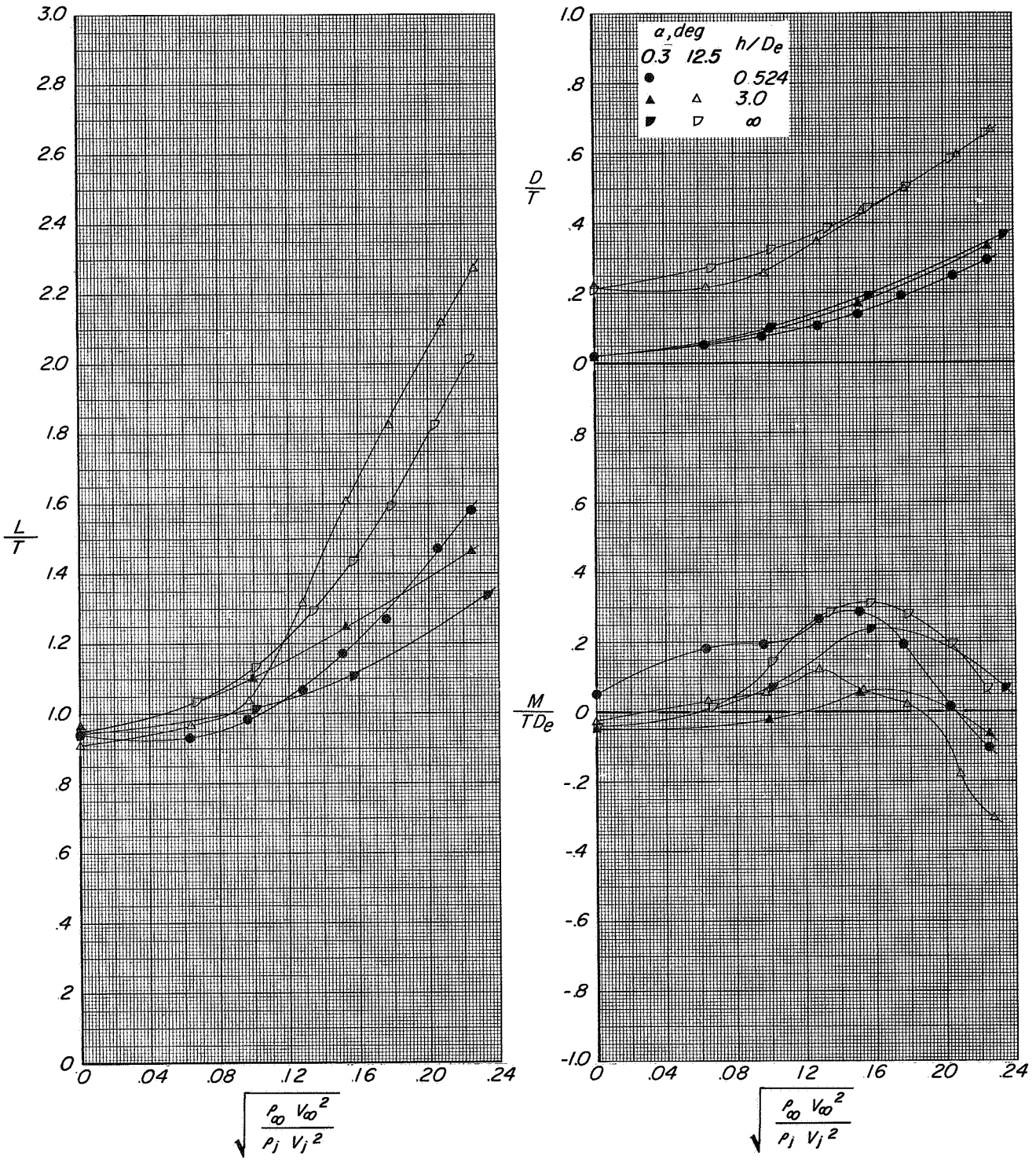

(a) Variation of L/T with effective velocity ratio.

(b) Variation of D/T and M/TD_e with effective velocity ratio.

Figure 35.- Effect of effective velocity ratio on the longitudinal aerodynamic characteristics of configuration A with direct-lift and lift-cruise engines deflected 90^0. $i_t = -10^0$; $\beta = 0^0$

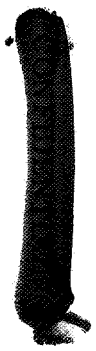

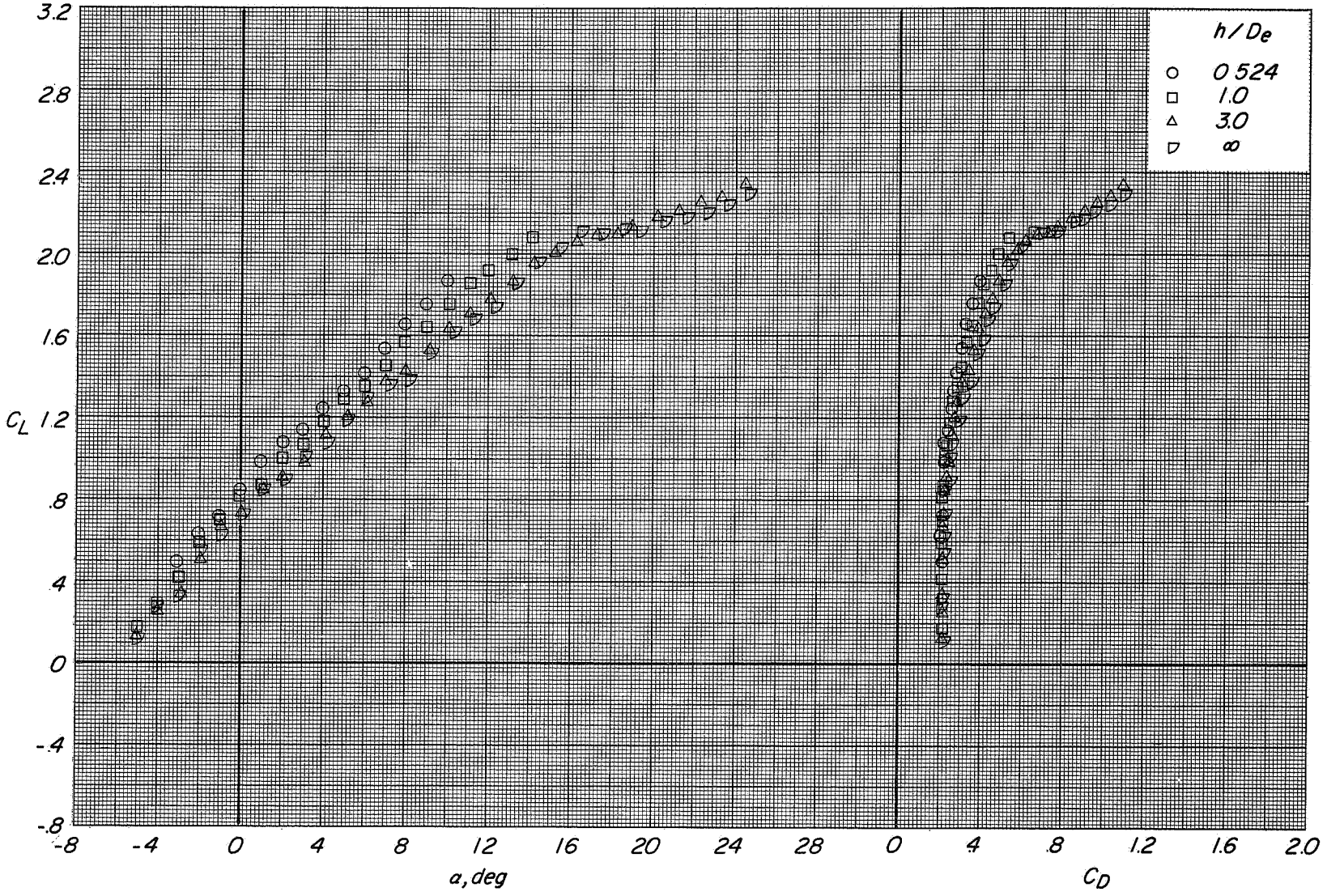

(a) Variation of C_L with α and C_D with C_L

Figure 36.- Longitudinal aerodynamic characteristics of configuration A with direct-lift and lift-cruise engines deflected 90°. $i_t = 0°$; $\beta = 0°$; $C_T = 0$.

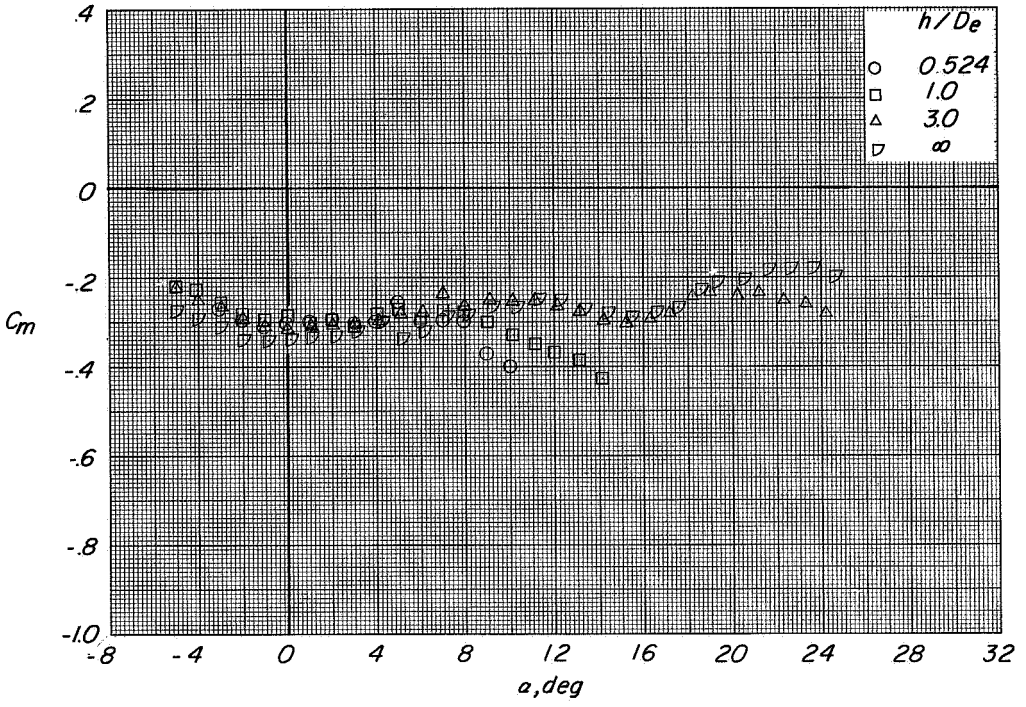

(b) Variation of C_m with α.

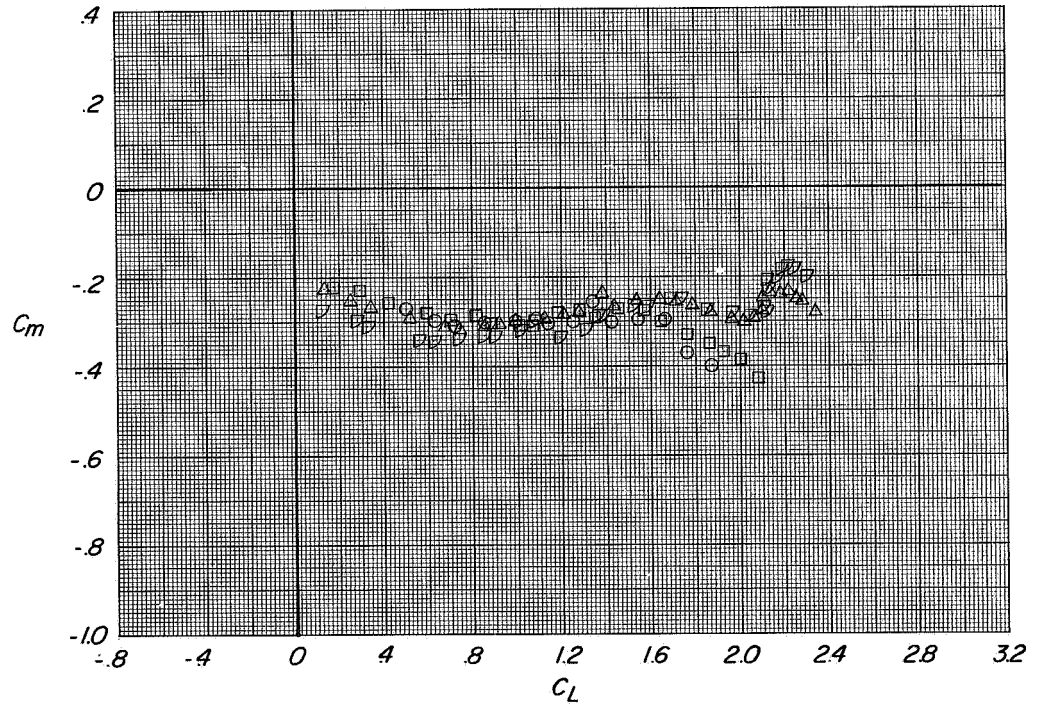

(c) Variation of C_m with C_L.

Figure 36. Concluded.

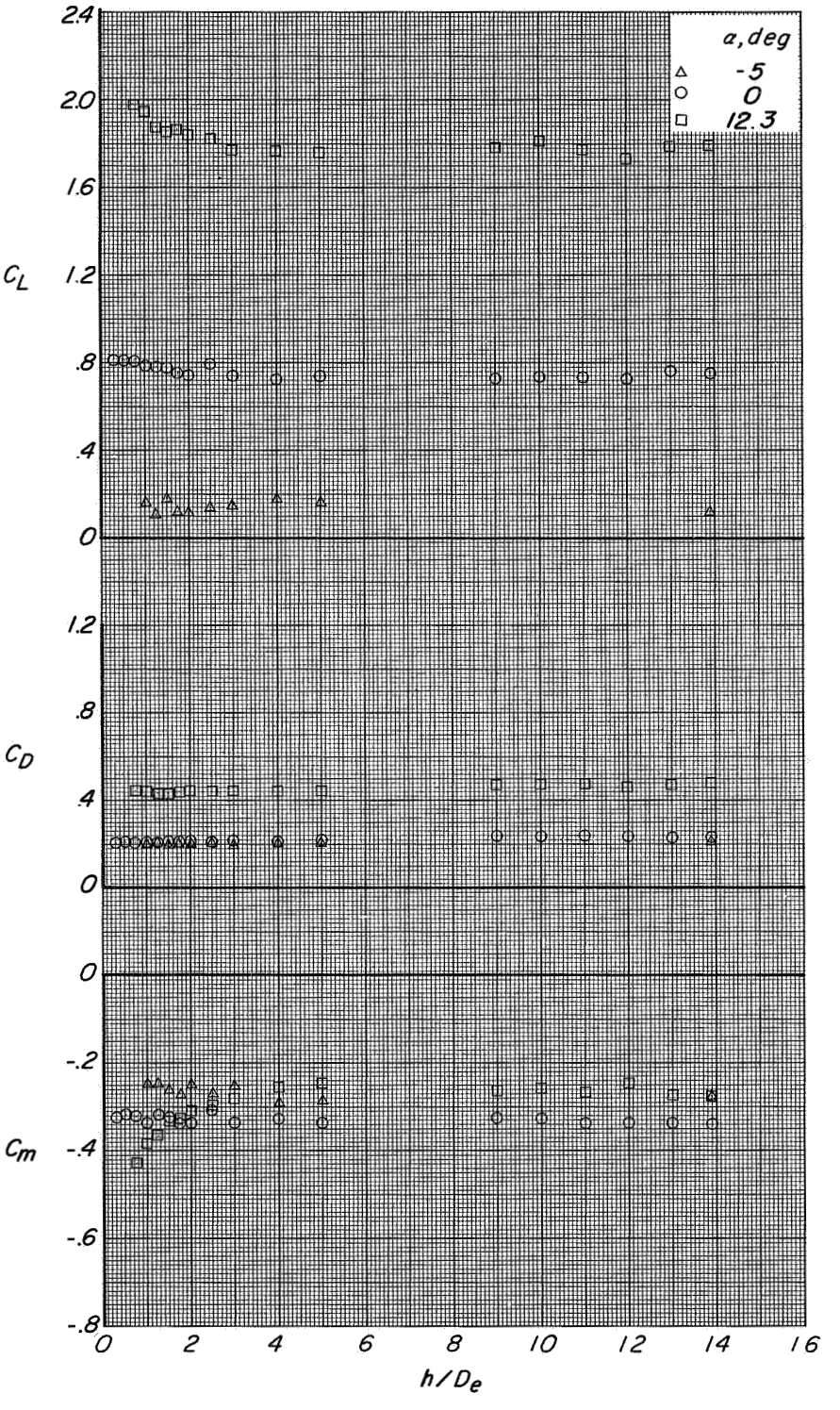

Figure 37.- Effect of height above the moving-belt ground plane on the longitudinal aerodynamic characteristics of configuration A with direct-lift and lift-cruise engines deflected 90°. $i_t = 0°$; $\beta = 0°$; $C_T = 0$.

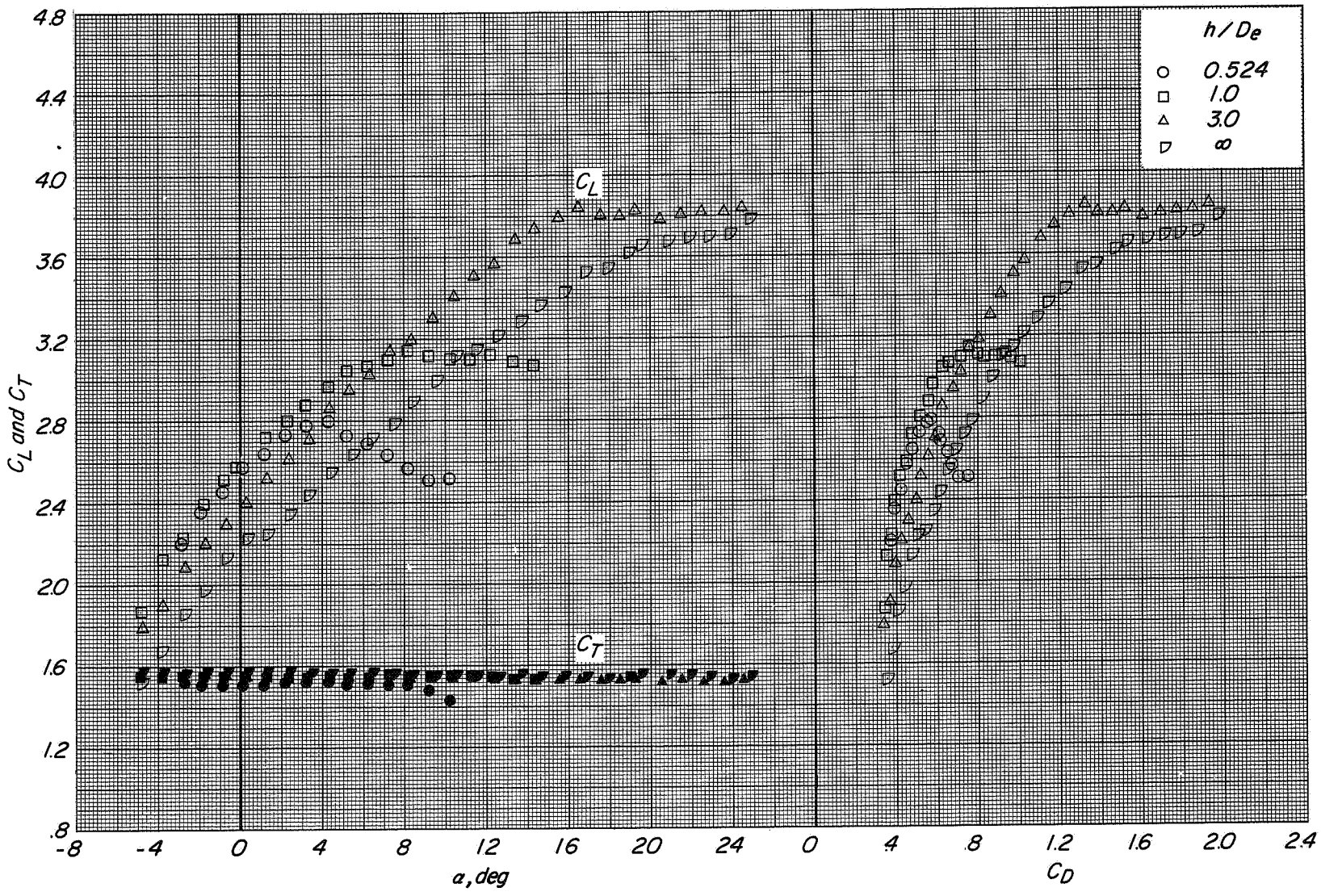

(a) Variation of C_L and C_T with α and C_D with C_L

Figure 38.- Longitudinal aerodynamic characteristics of configuration A with direct-lift and lift-cruise engines deflected 90°. $i_t = 0°$; $\beta = 0°$; $C_T \approx 1.45$.

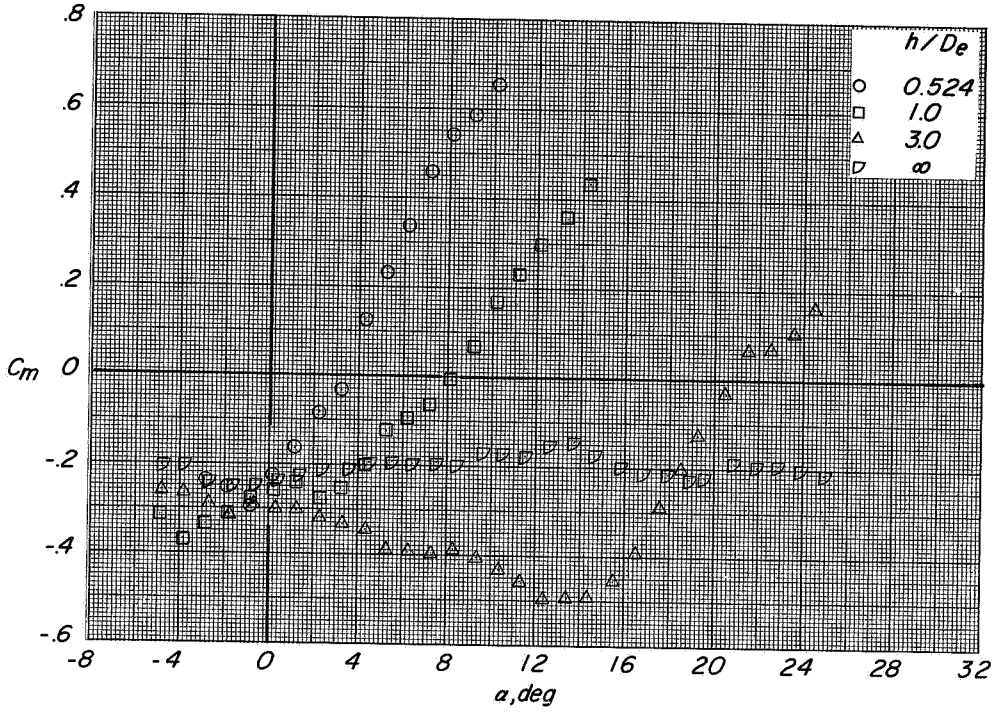

(b) Variation of C_m with α.

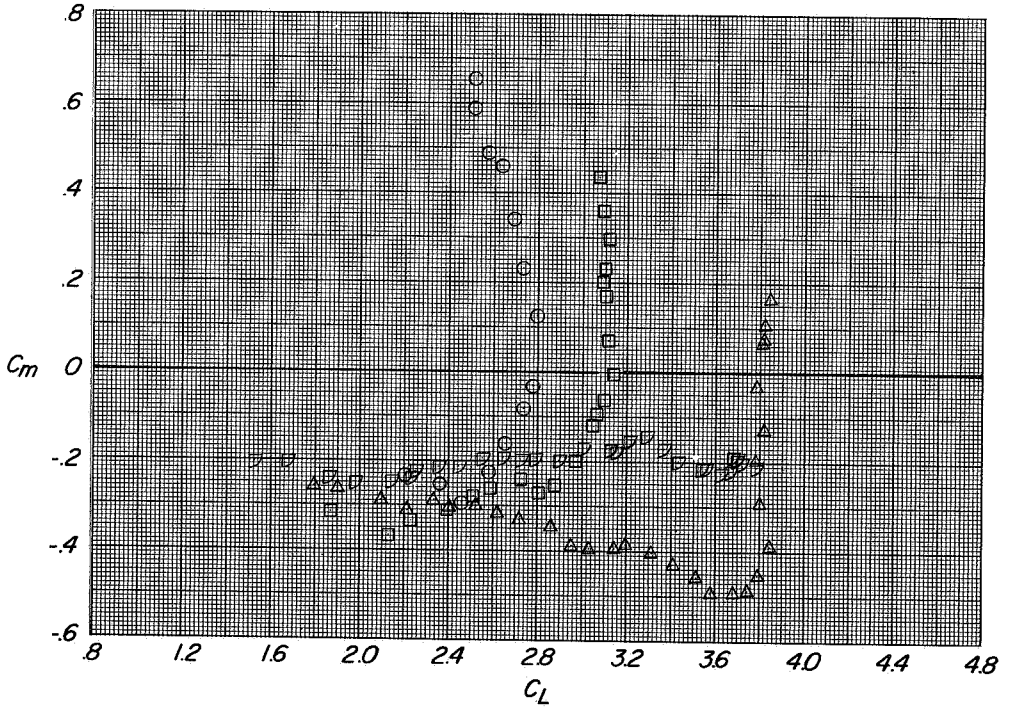

(c) Variation of C_m with C_L

Figure 38.· Continued.

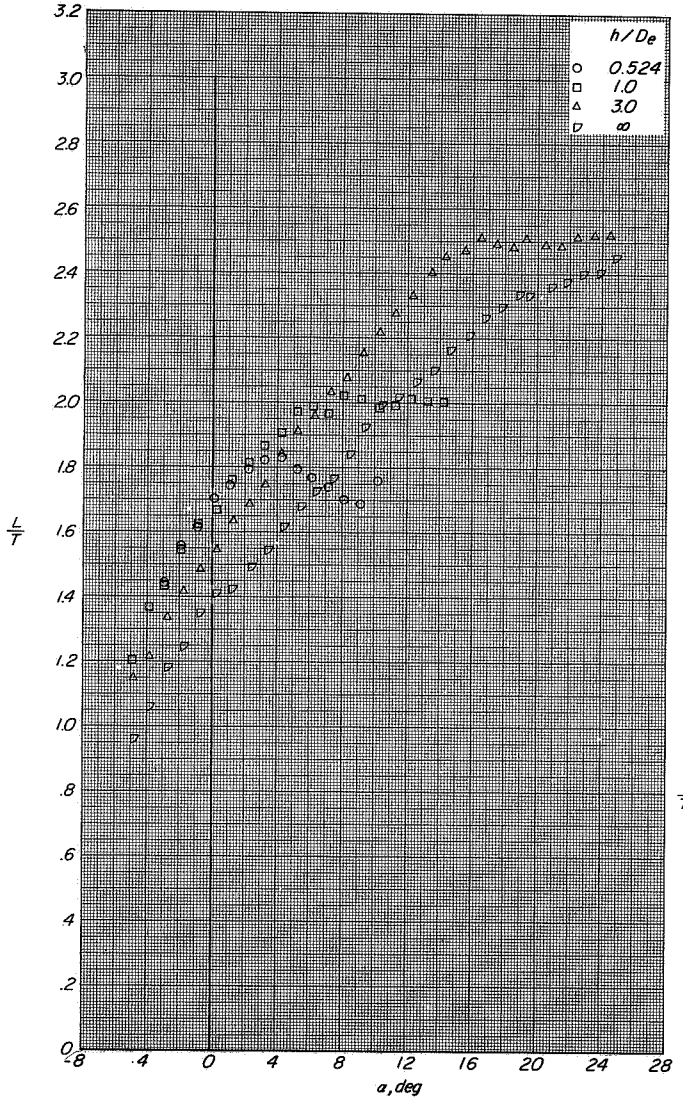

(d) Variation of L/T with α.

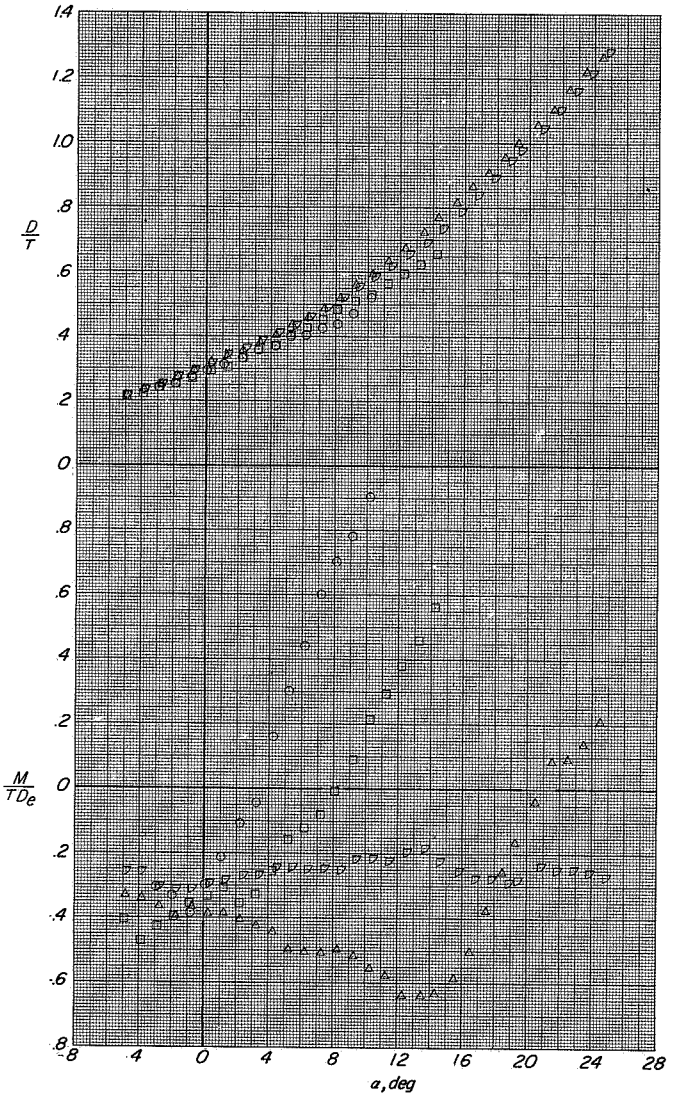

(e) Variation of D/T and M/TD_e with α.

Figure 38. Concluded.

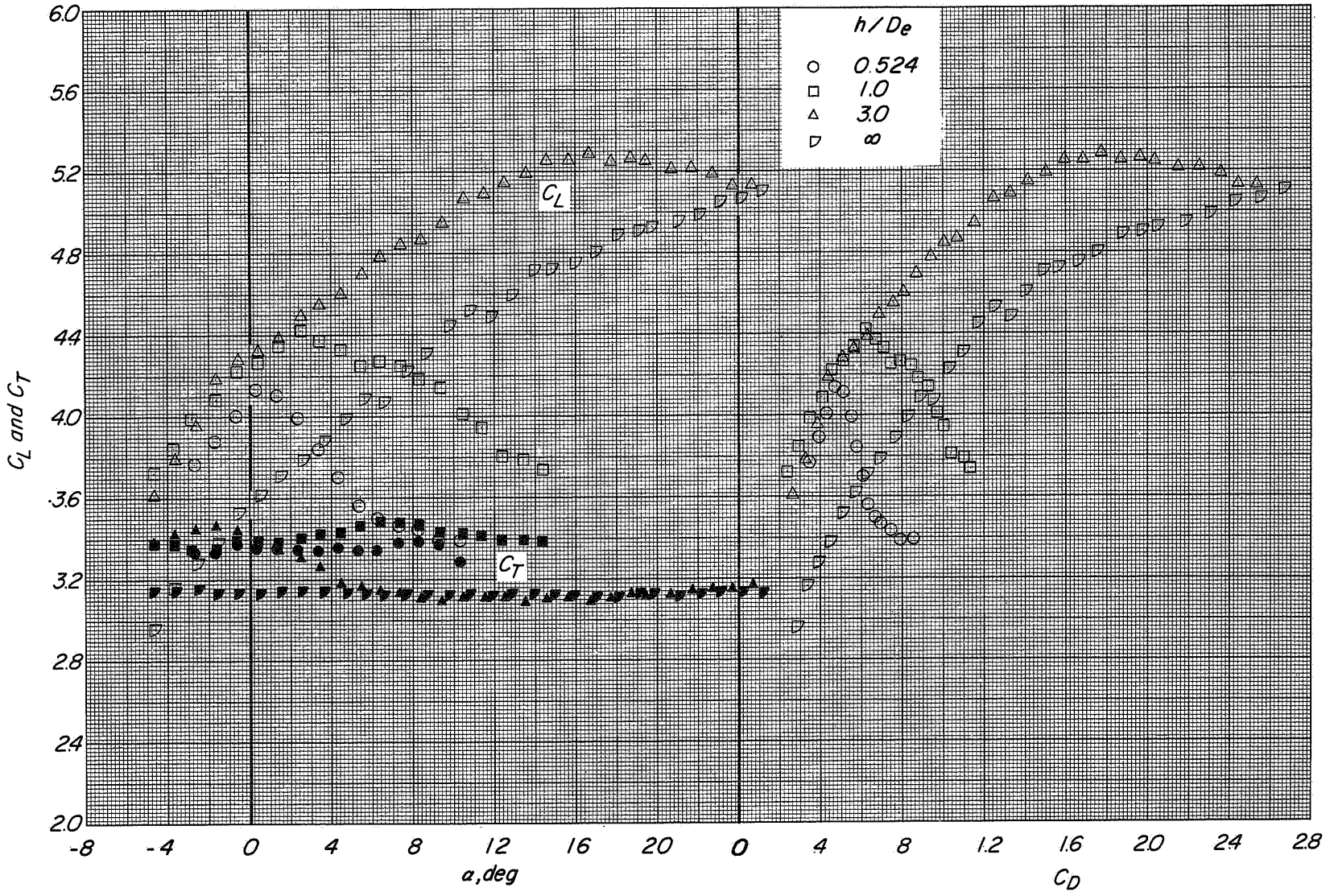

(a) Variation of C_L and C_T with α and C_D with C_L

Figure 39.- Longitudinal aerodynamic characteristics of configuration A with direct-lift and lift-cruise engines deflected 90°. $i_t = 0°$; $\beta = 0°$; $C_T \approx 3.3$.

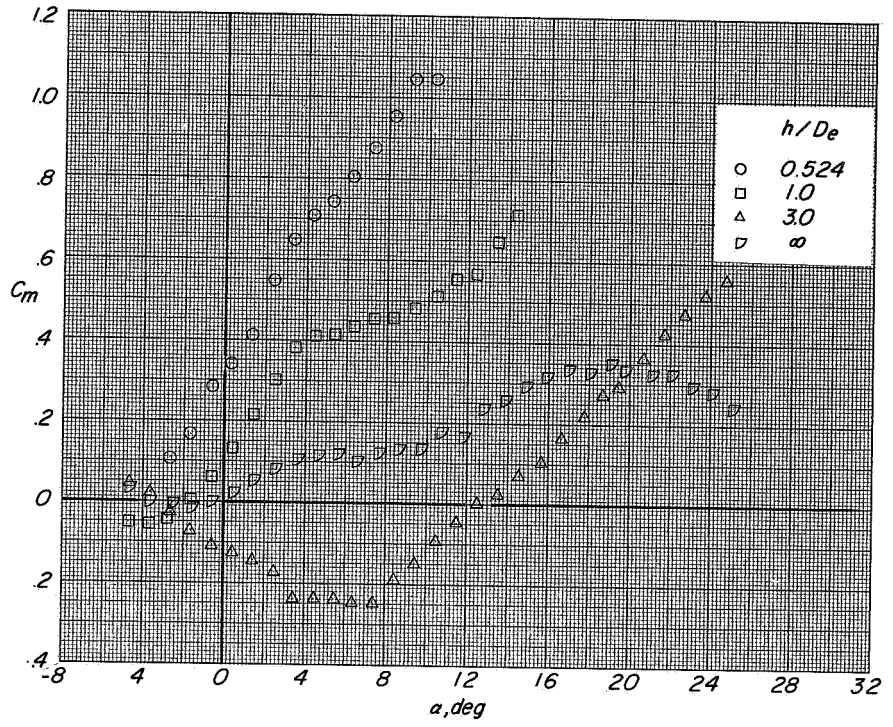

(b) Variation of C_m with α.

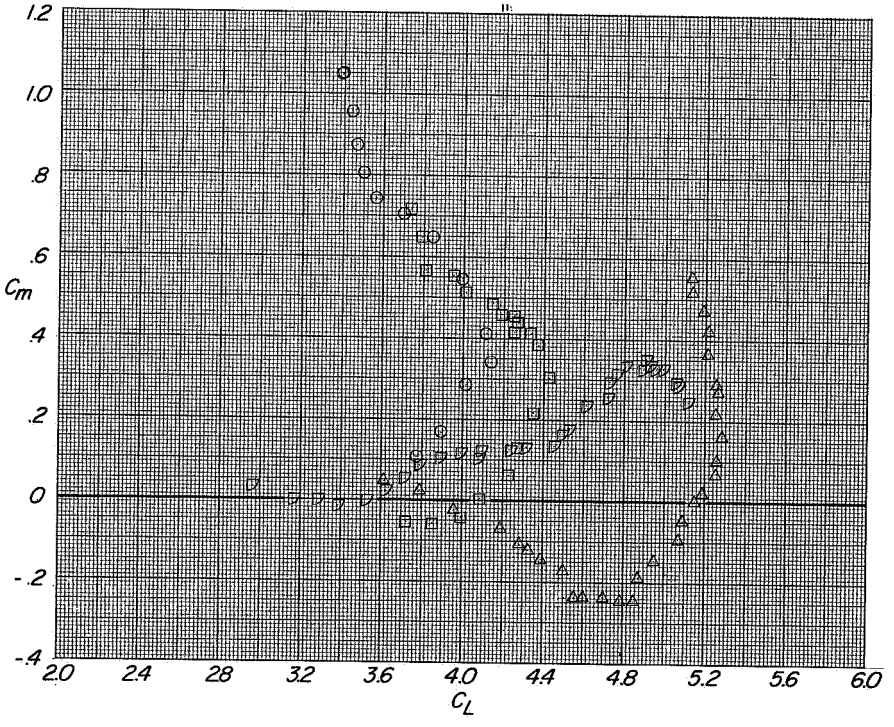

(c) Variation of C_m with C_L

Figure 39.- Continued.

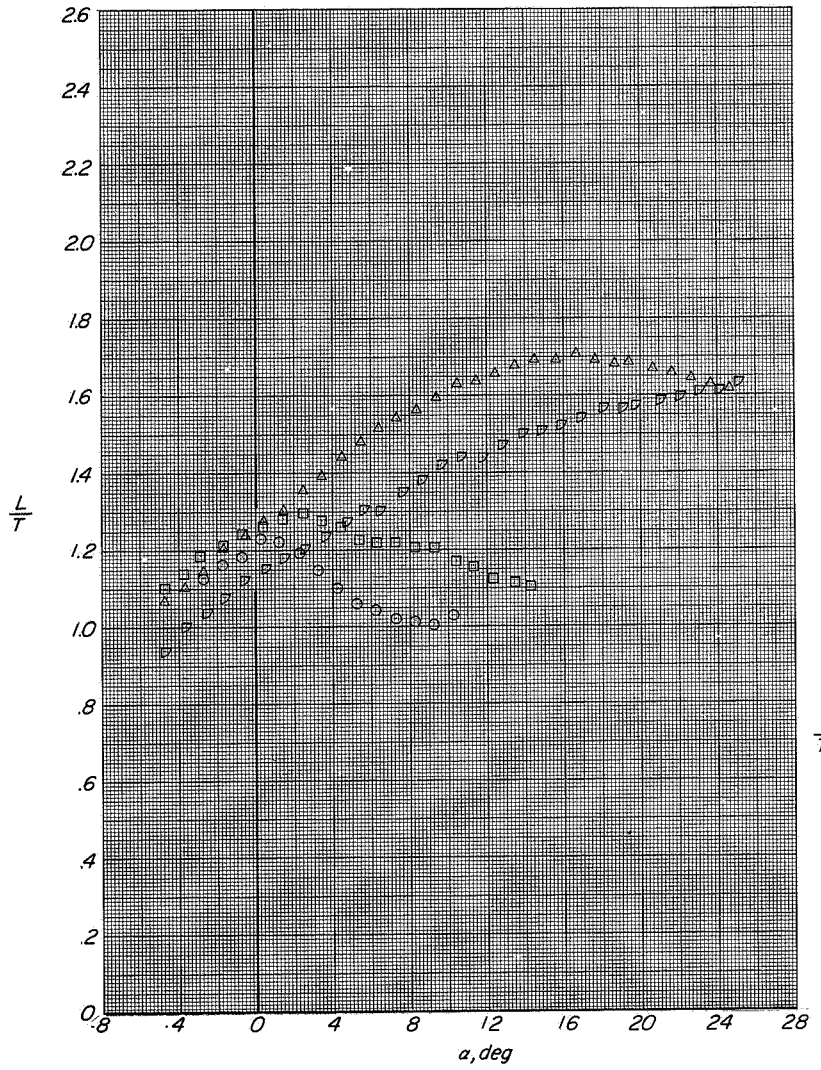

(d) Variation of L/T with α.

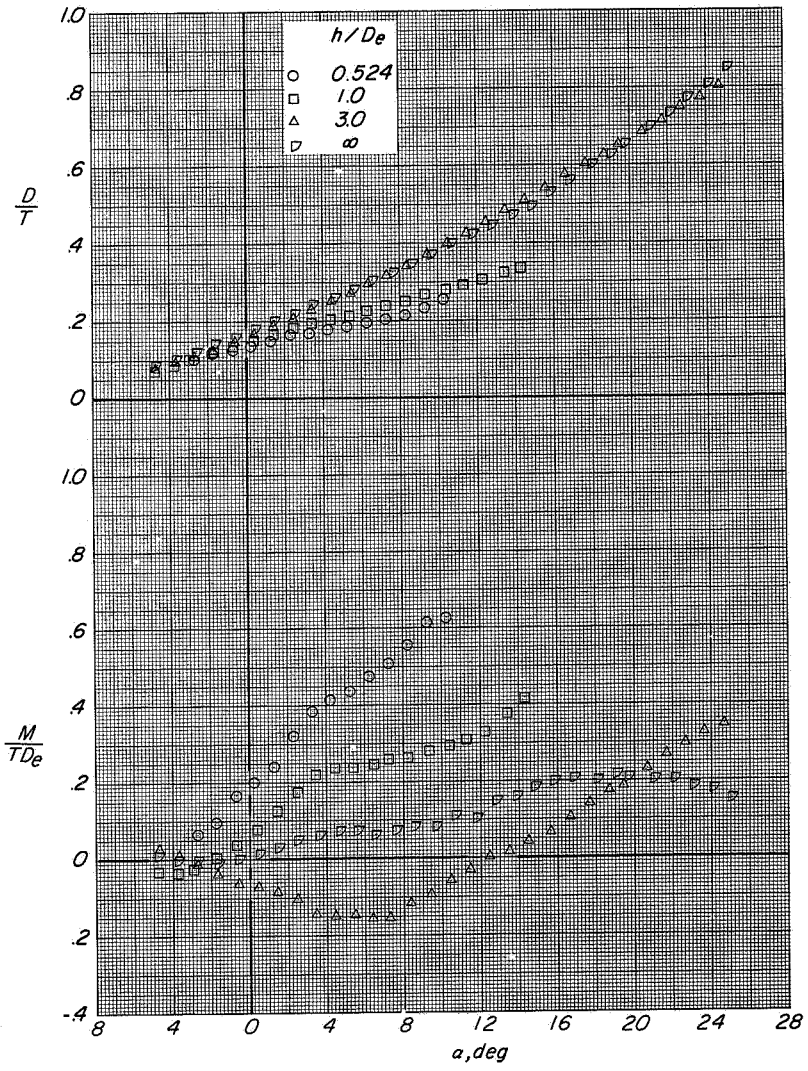

(e) Variation of D/T and M/TD_e with α.

Figure 39. Concluded.

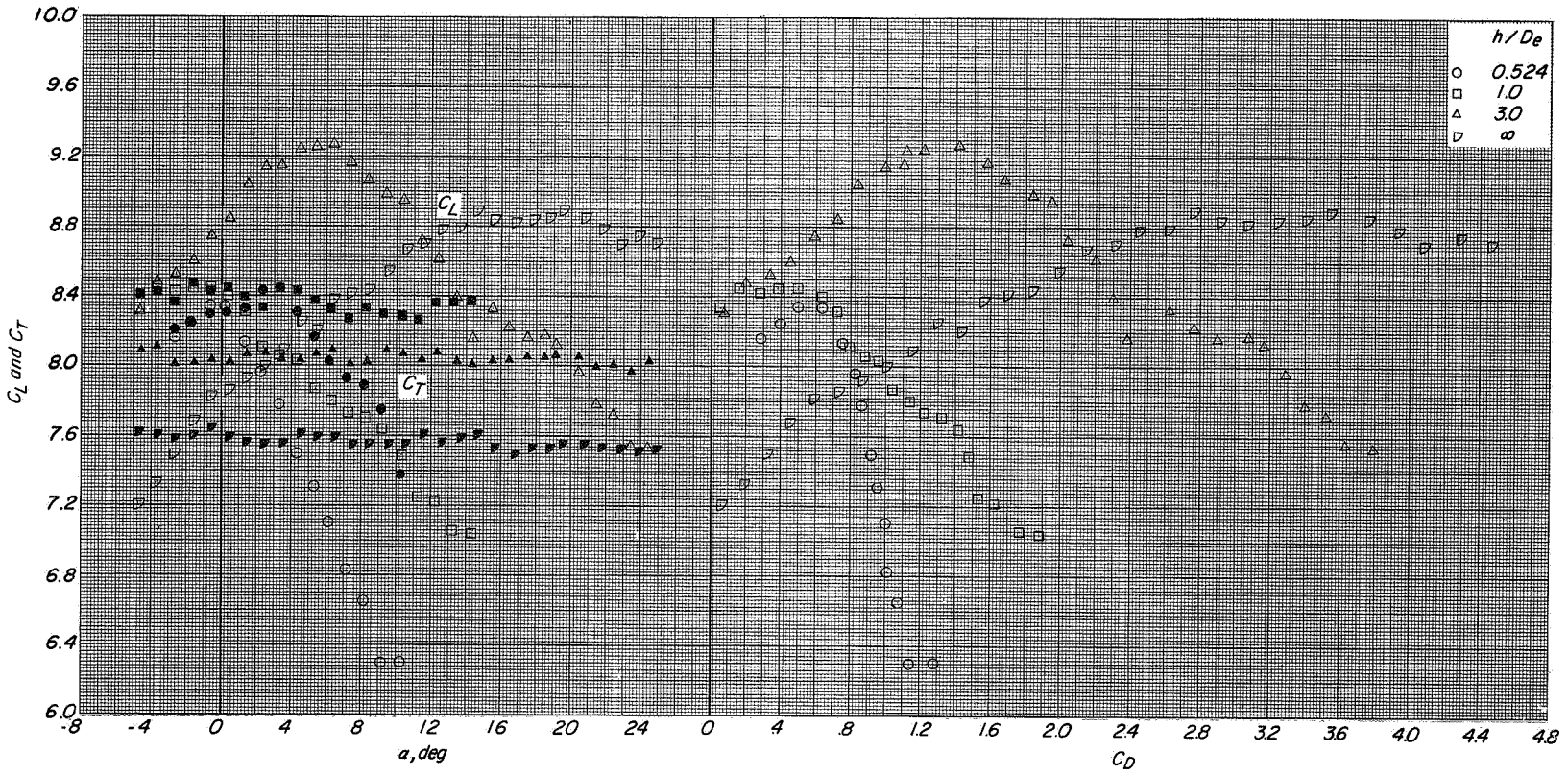

(a) Variation of C_L and C_T with α and C_D with C_L.

Figure 40.- Longitudinal aerodynamic characteristics of configuration A with direct-lift and lift-cruise engines deflected 90°. $i_t = 0°$; $\beta = 0°$; $C_T \approx 8$.

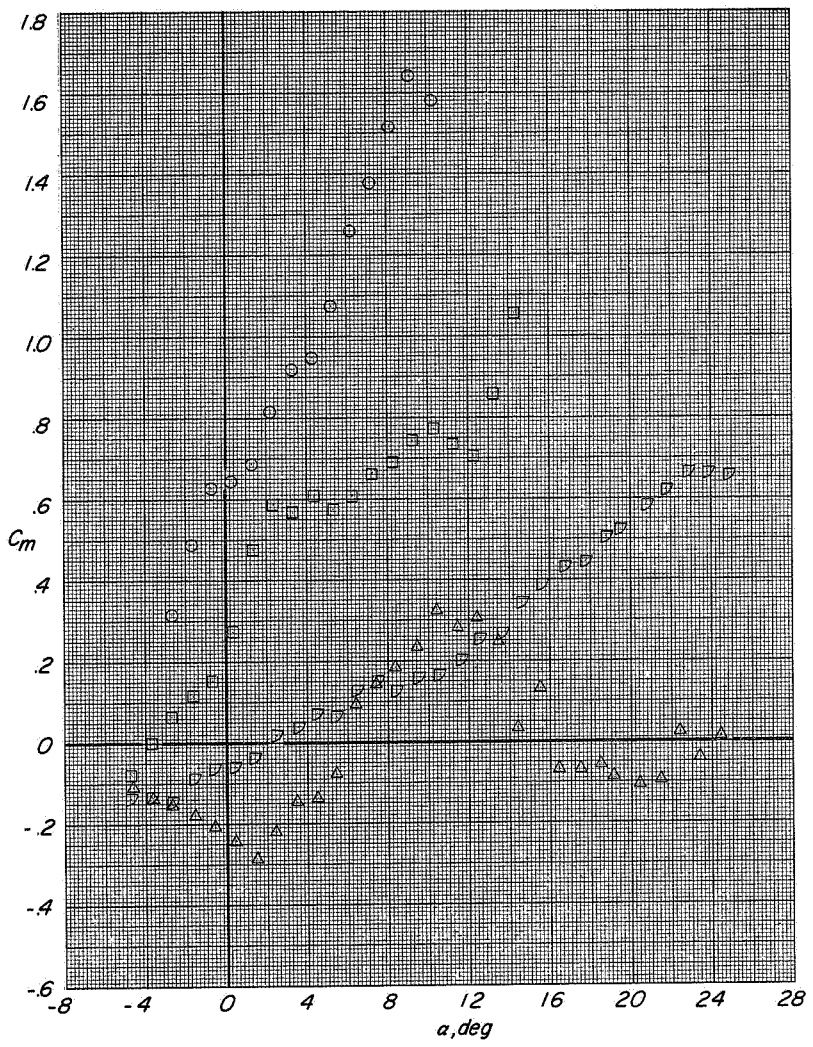

(b) Variation of C_m with α.

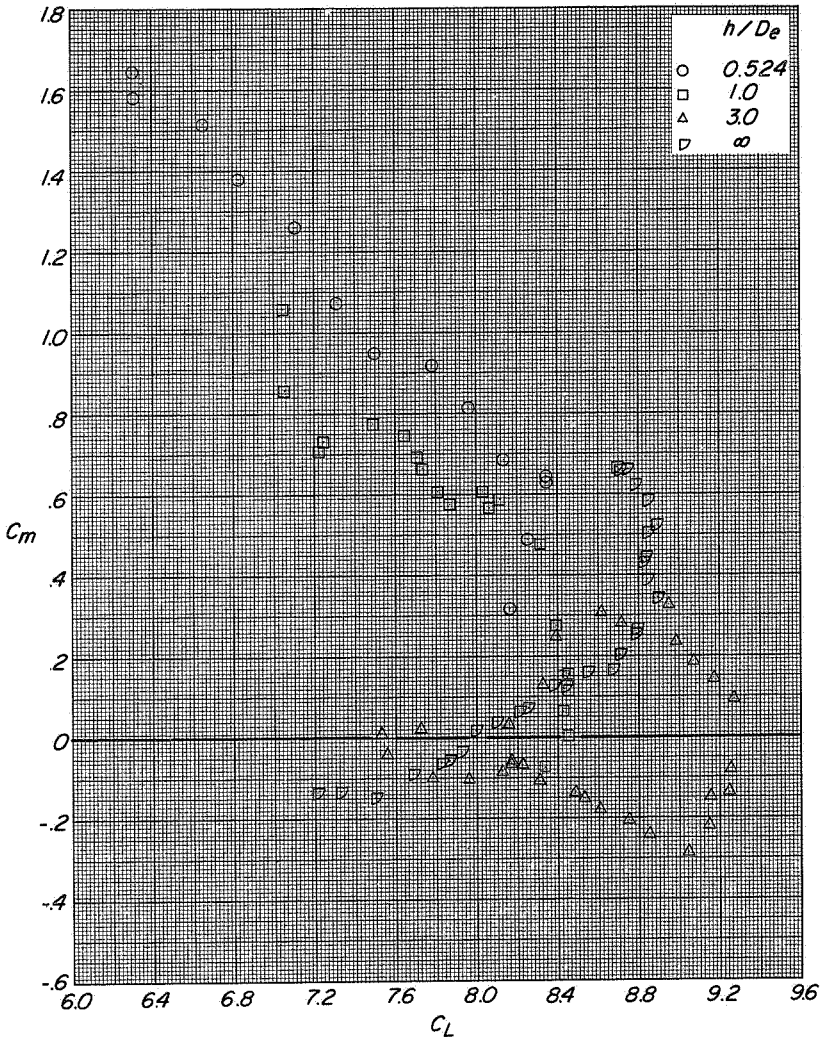

(c) Variation of C_m with C_L

Figure 40.- Continued.

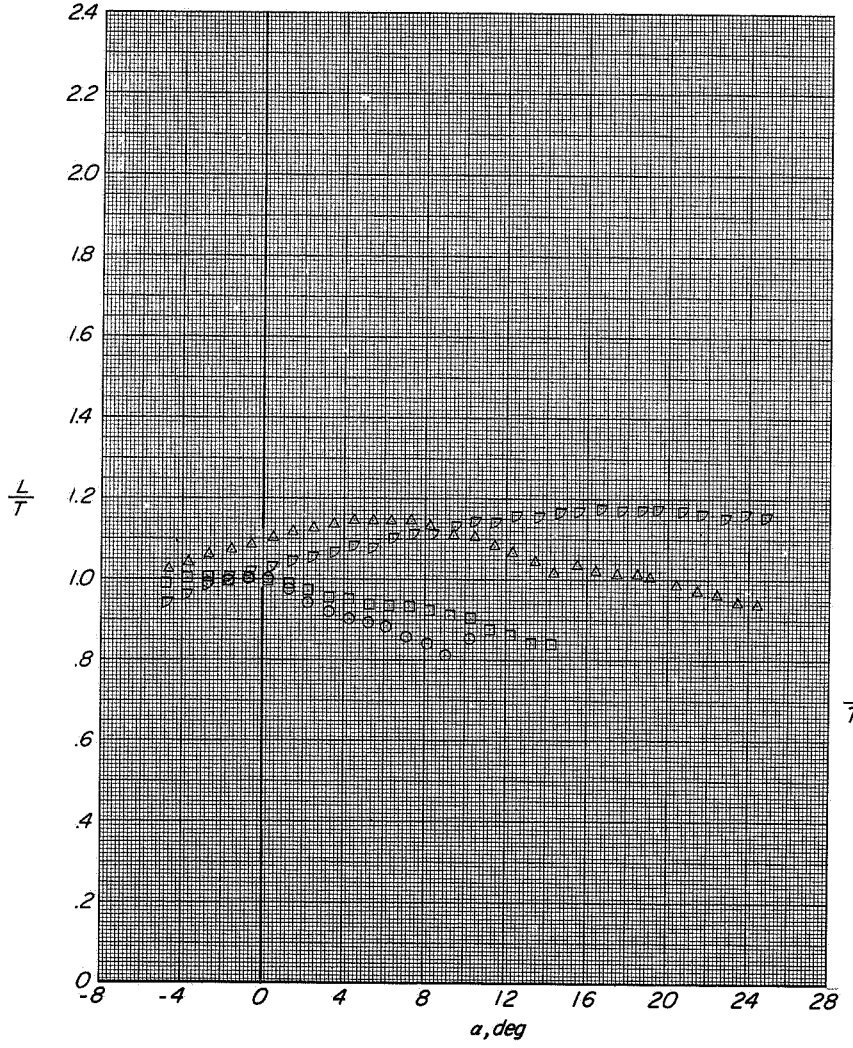

(d) Variation of L/T with α.

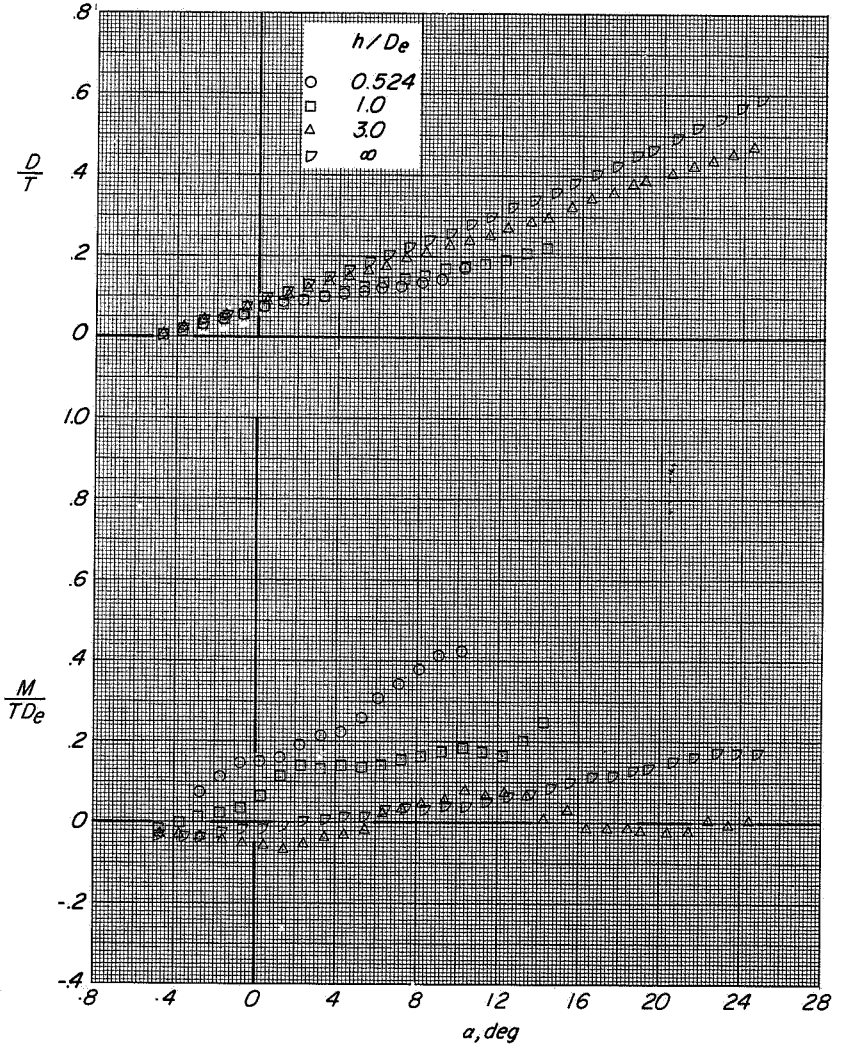

(e) Variation of D/T and M/TD_e with α.

Figure 40.- Concluded.

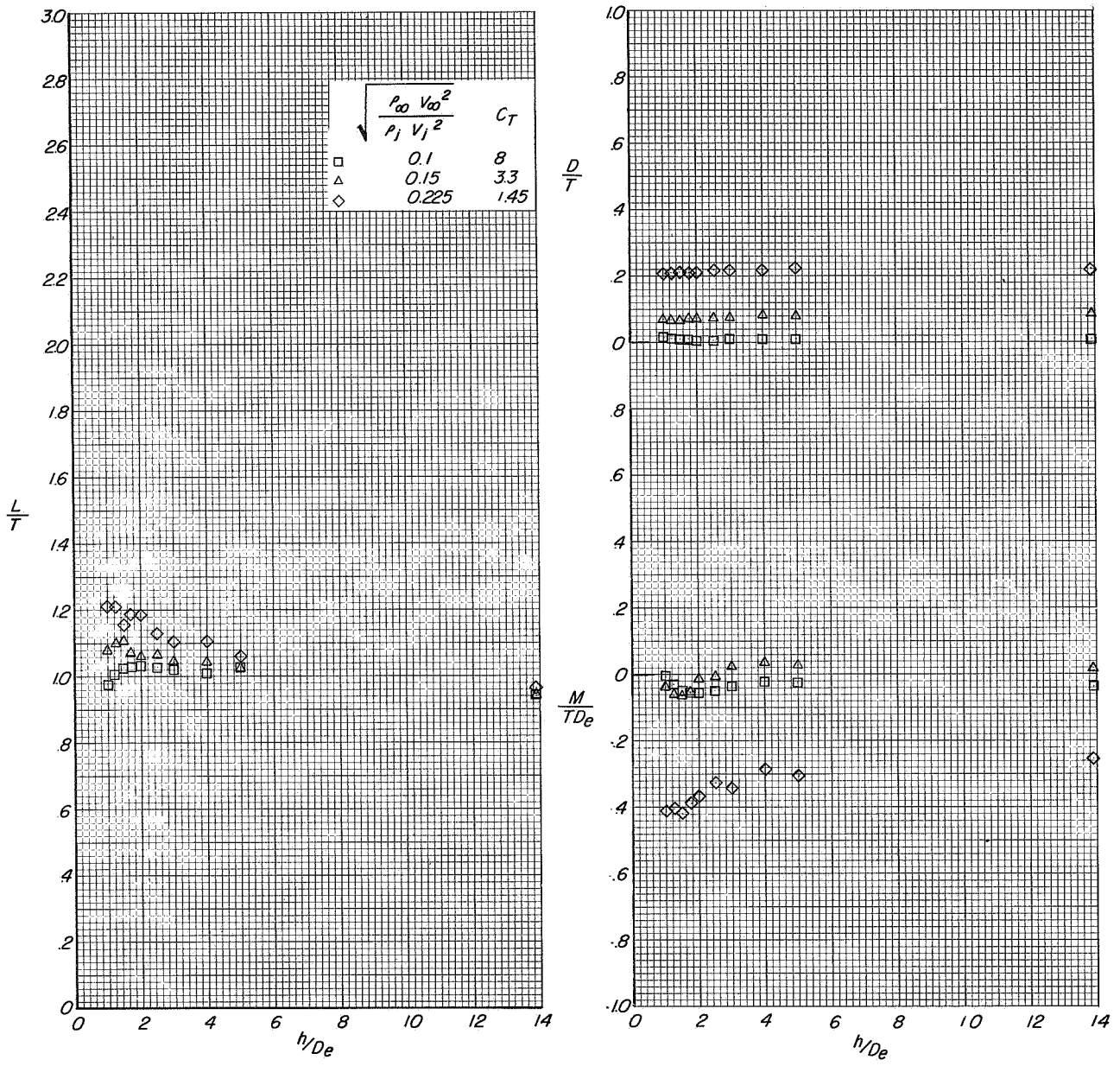

(a) Variation of L/T with h/D_e.

(b) Variation of D/T and M/TD_e with h/D_e.

Figure 41.- Effect of height above the moving-belt ground plane on the longitudinal aerodynamic characteristics of configuration A with direct-lift and lift-cruise engines deflected 90°. $i_t = 0°$; $\beta = 0°$; $\alpha = -4.7°$.

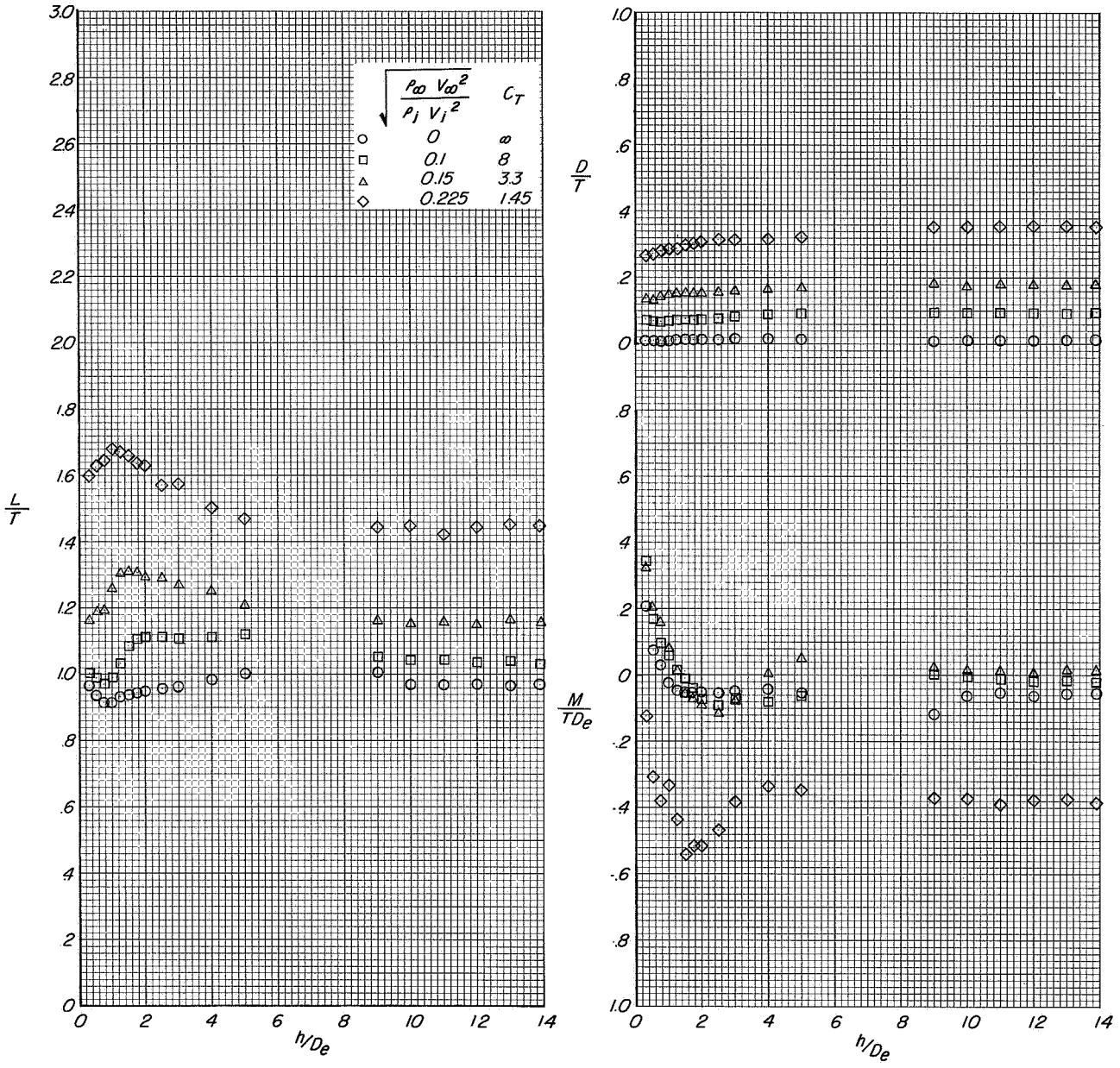

(a) Variation of L/T with h/D_e.

(b) Variation of D/T and M/TD_e with h/D_e.

Figure 42.- Effect of height above the moving-belt ground plane on the longitudinal aerodynamic characteristics of configuration A with direct-lift and lift-cruise engines deflected 90^0. $i_t = 0^0$; $\beta = 0^0$; $\alpha = 0.4^0$.

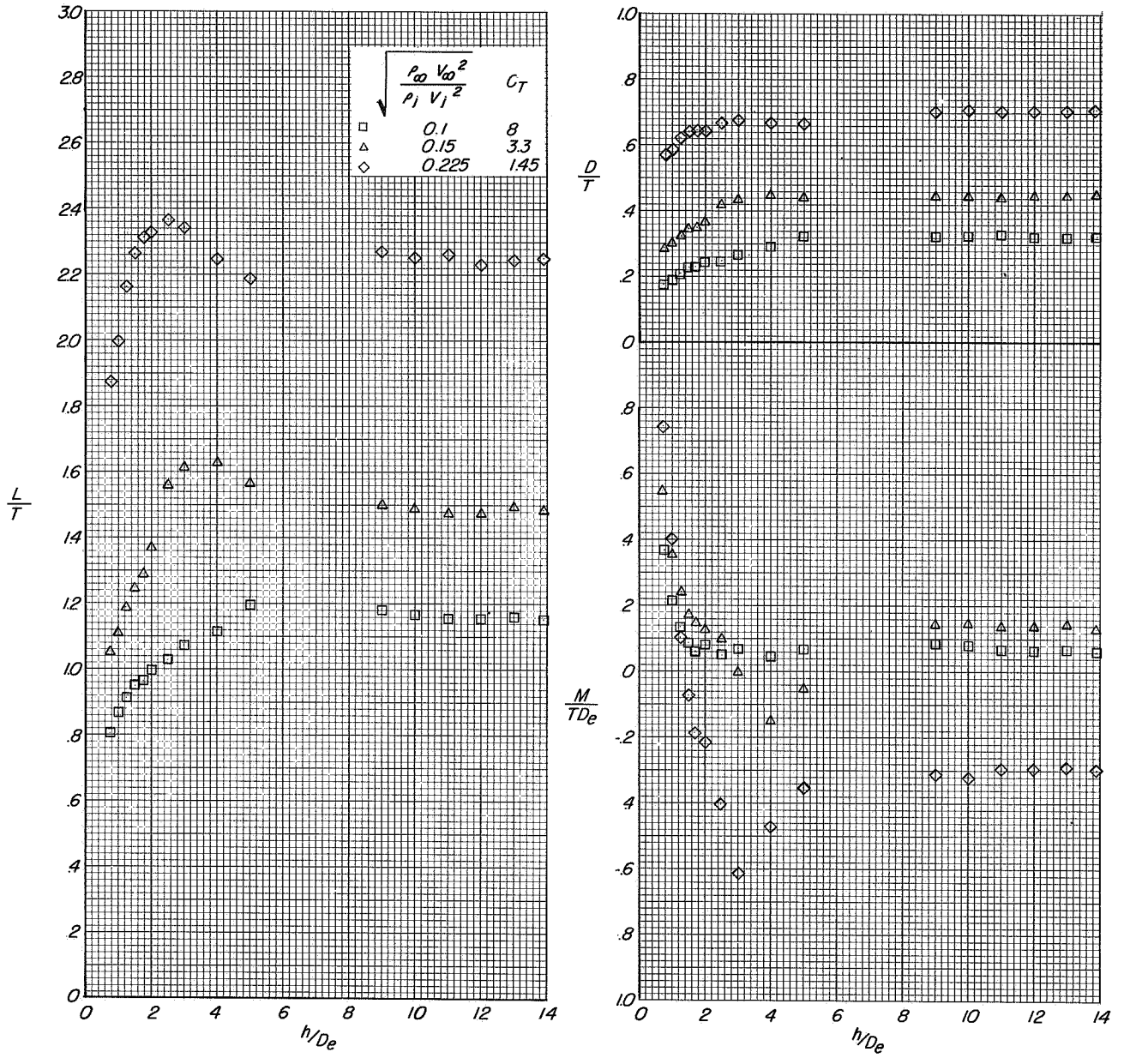

(a) Variation of L/T with h/D_e.

(b) Variation of D/T and M/TD_e with h/D_e.

Figure 43.- Effect of height above the moving-belt ground plane on the longitudinal aerodynamic characteristics of configuration A with direct-lift and lift-cruise engines deflected 90°. $i_t = 0°$; $\beta = 0°$; $\alpha = 12.6°$.

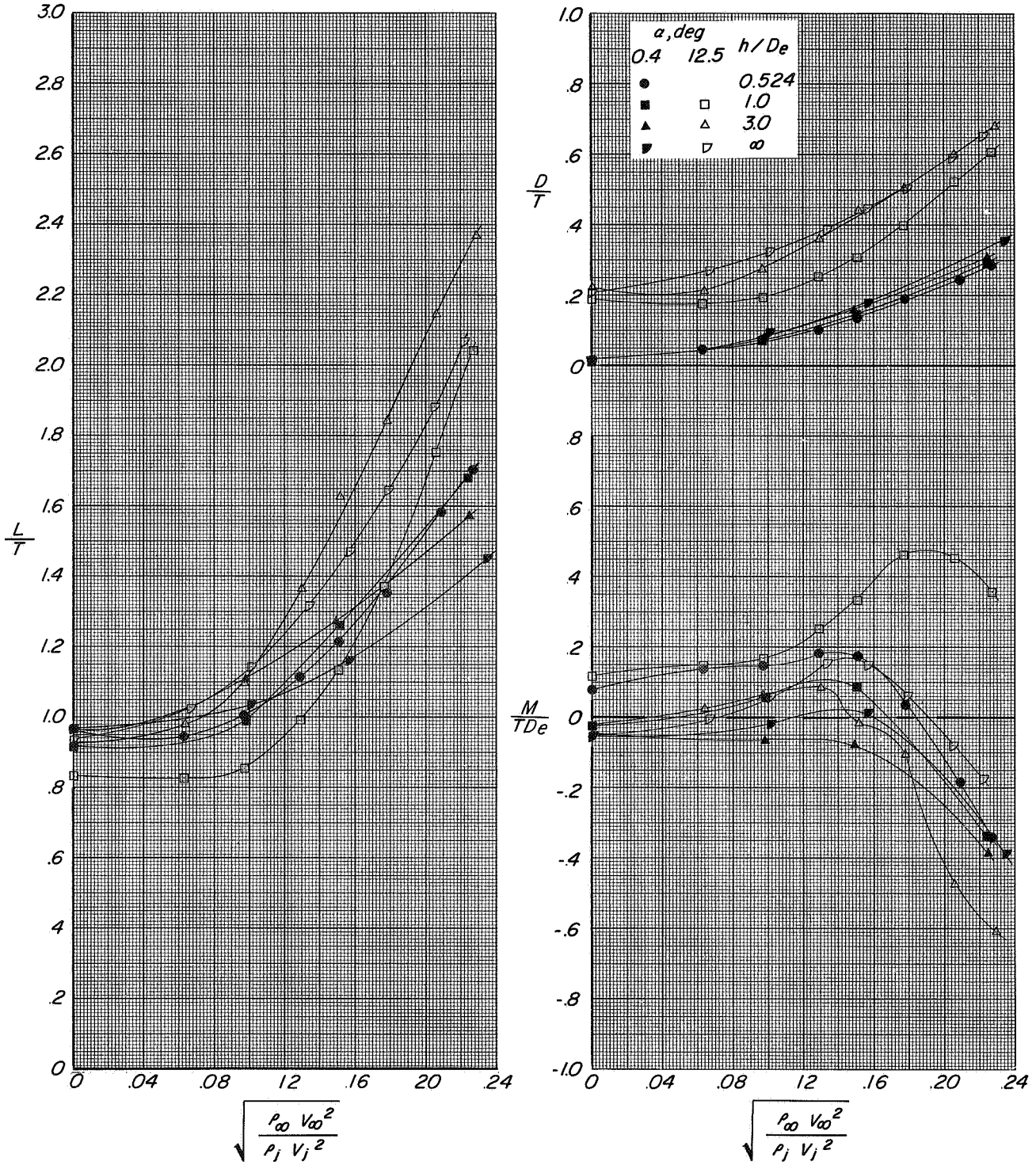

(a) Variation of L/T with effective velocity ratio.

(b) Variation of D/T and M/TD_e with effective velocity ratio.

Figure 44.- Effect of effective velocity ratio on the longitudinal aerodynamic characteristics of configuration A with direct-lift and lift-cruise engines deflected 90^0. $i_t = 0^0$; $\beta = 0^0$

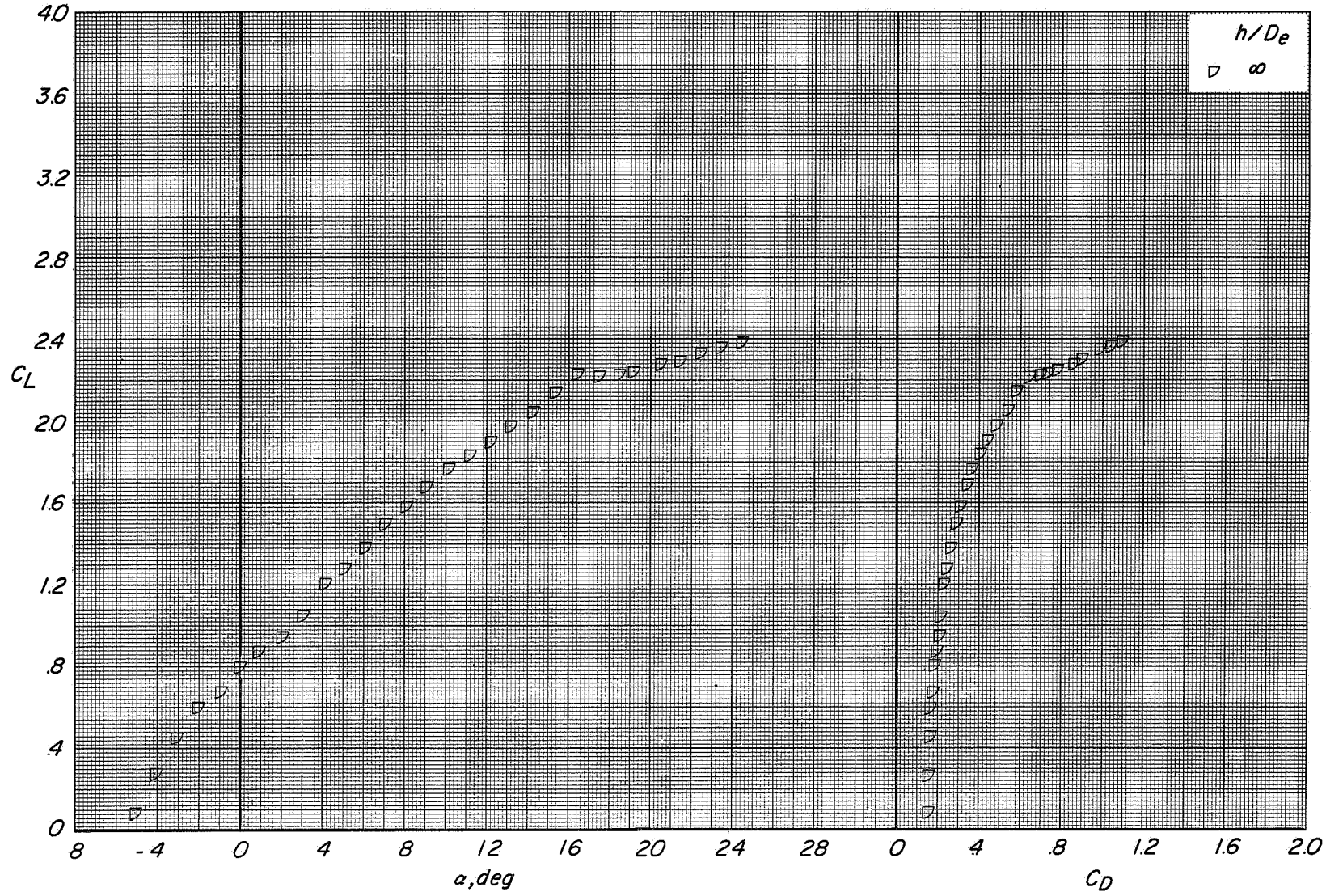

(a) Variation of C_L with α and C_D with C_L

Figure 45.- Longitudinal aerodynamic characteristics of configuration A with direct-lift engines stowed and lift-cruise engines deflected 90^0. $i_t = 0^0$; $\beta = 0^0$; $C_T = 0$.

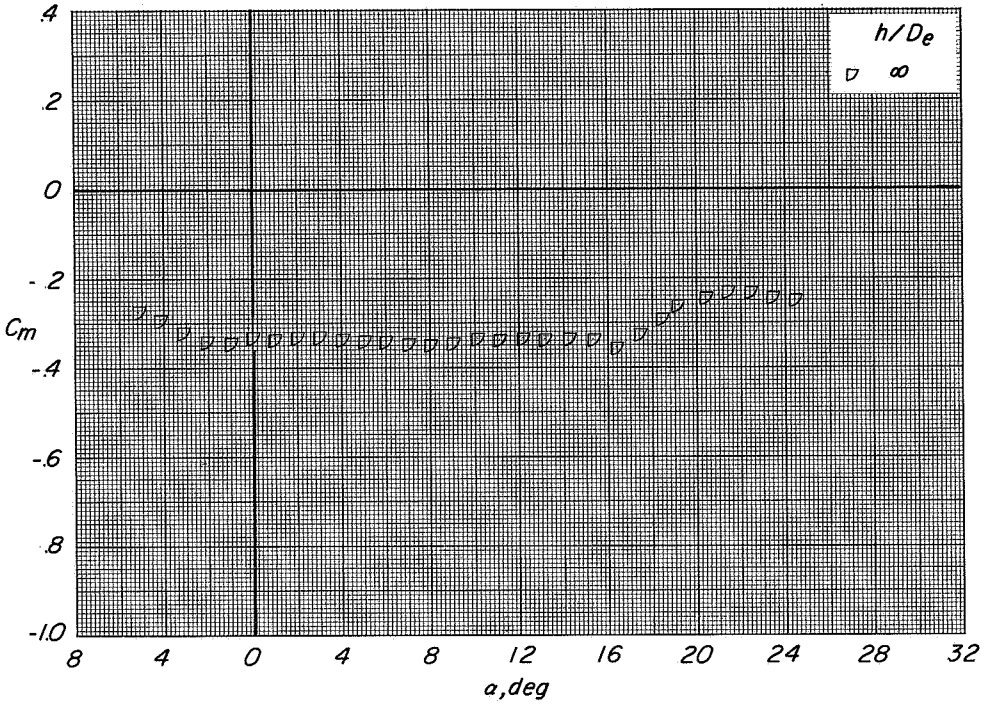

(b) Variation of C_m with α.

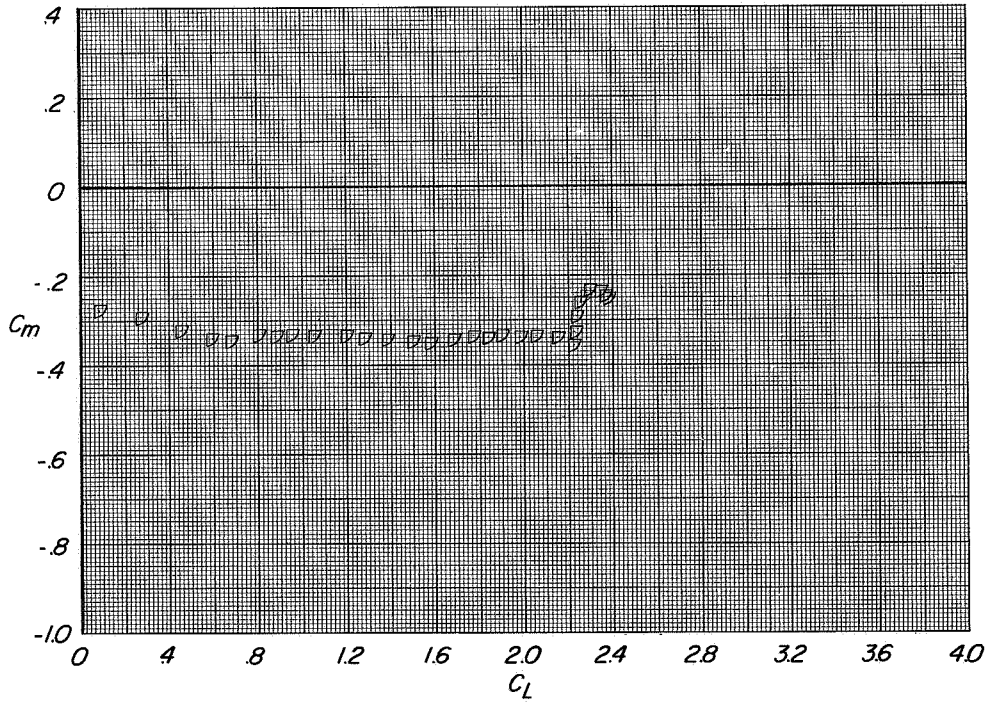

(c) Variation of C_m with C_L.

Figure 45.- Concluded.

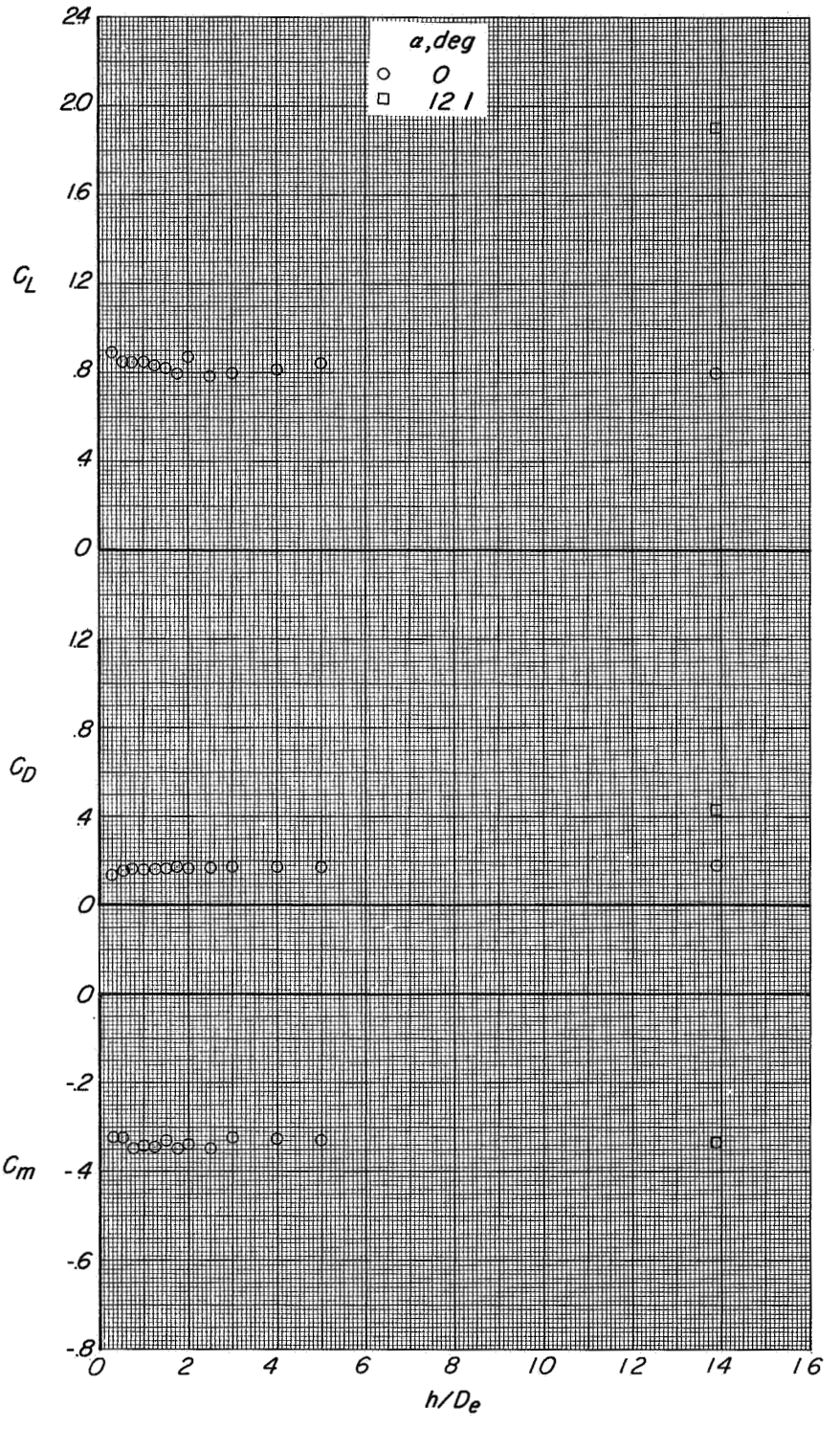

Figure 46.- Effect of height above the moving-belt ground plane on the longitudinal aerodynamic characteristics of configuration A with direct-lift engines stowed and lift-cruise engines deflected 90°. $i_t = 0°$; $\beta = 0°$; $C_T = 0$.

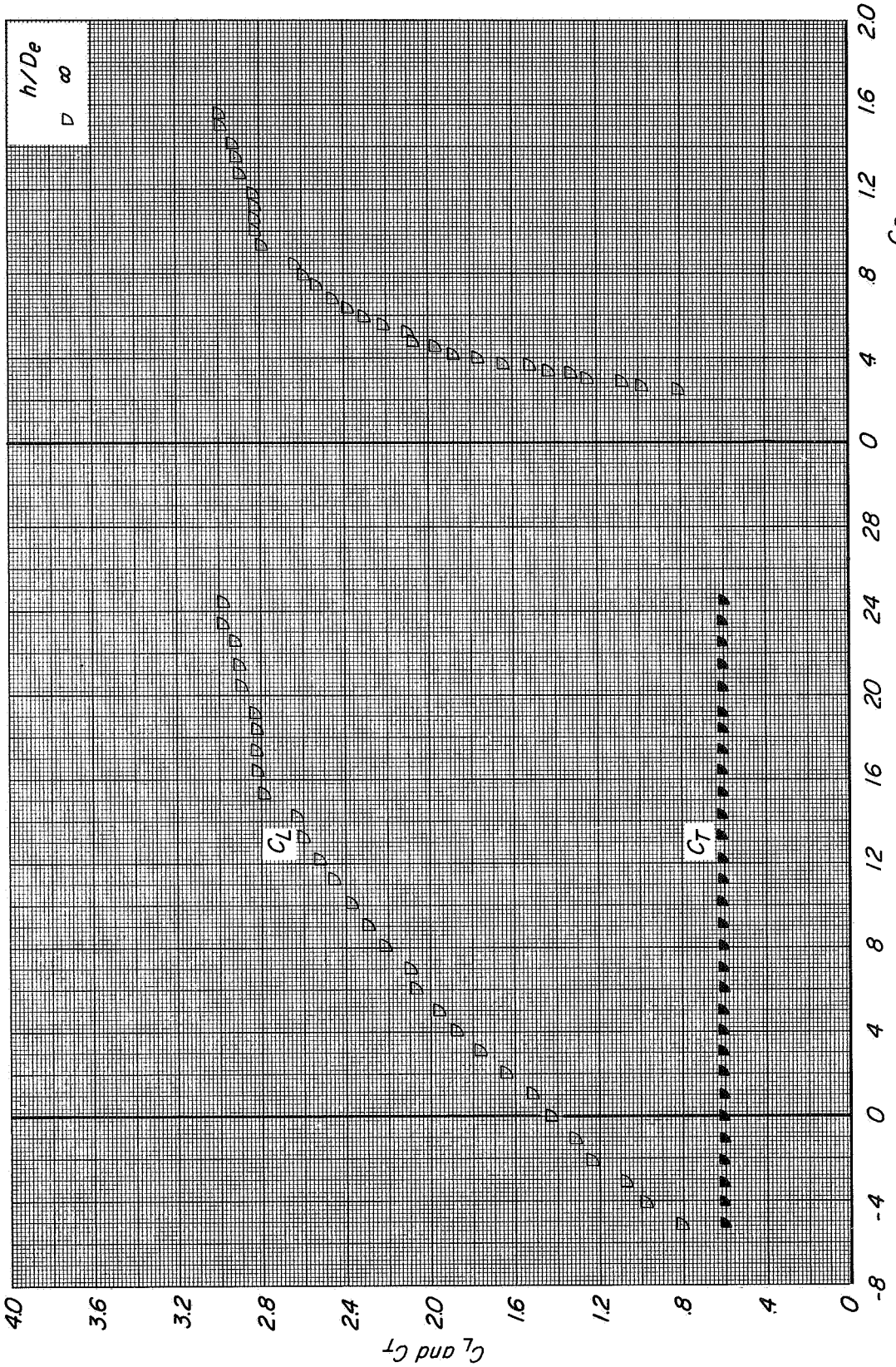

(a) Variation of C_L and C_T with α and C_D with C_L

Figure 47.- Longitudinal aerodynamic characteristics of configuration A with direct-lift engines stowed and lift-cruise engines deflected 90°. $i_t = 0°$; $\beta = 0°$; $C_T \approx 0.6$.

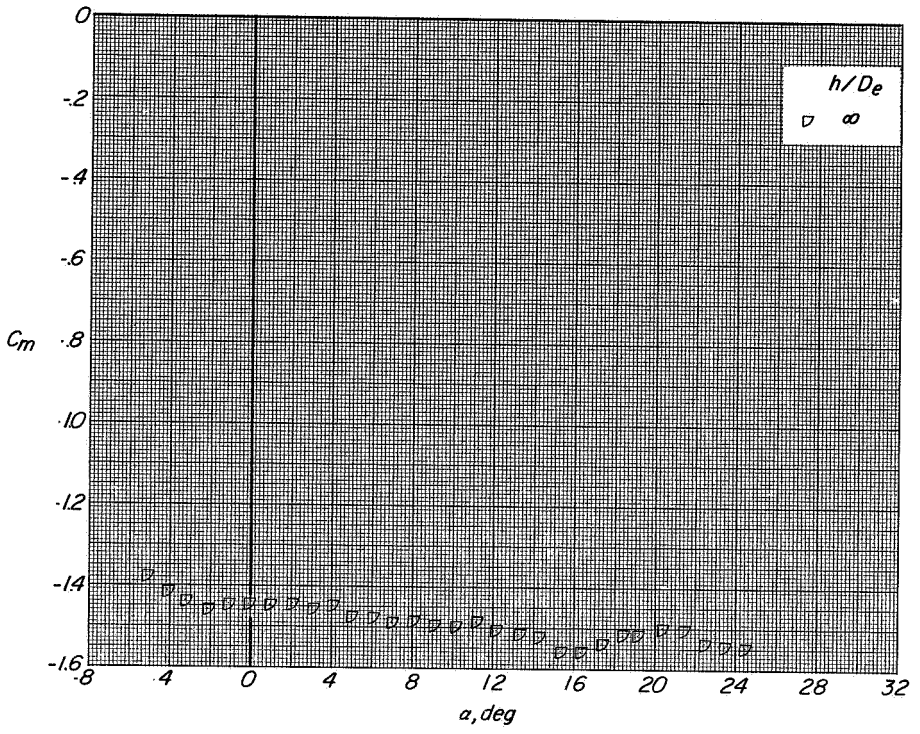

(b) Variation of C_m with α.

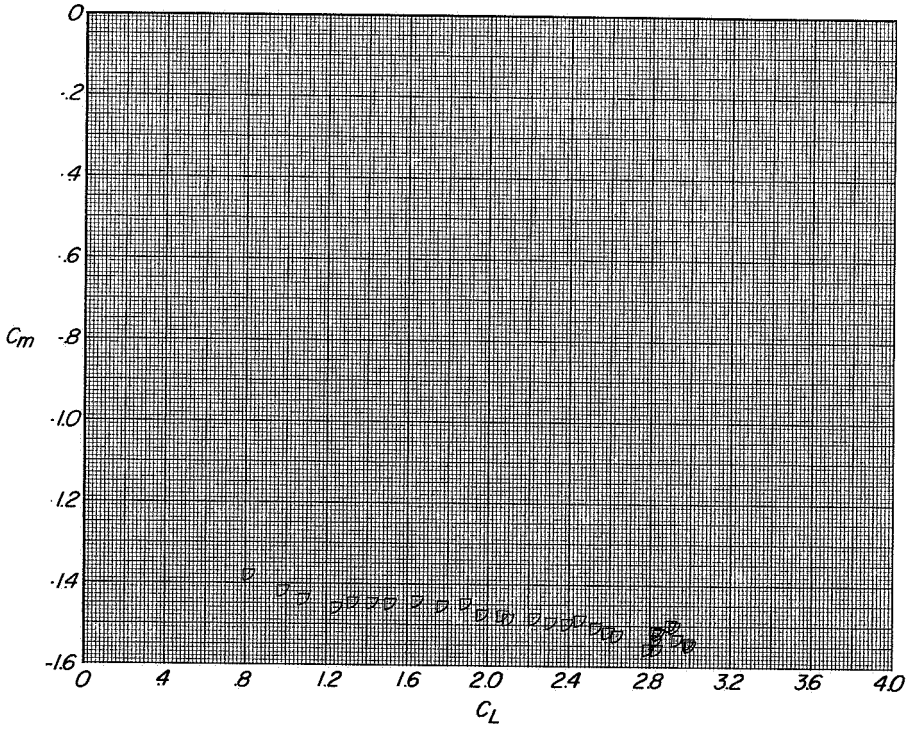

(c) Variation of C_m with C_L

Figure 47.- Continued.

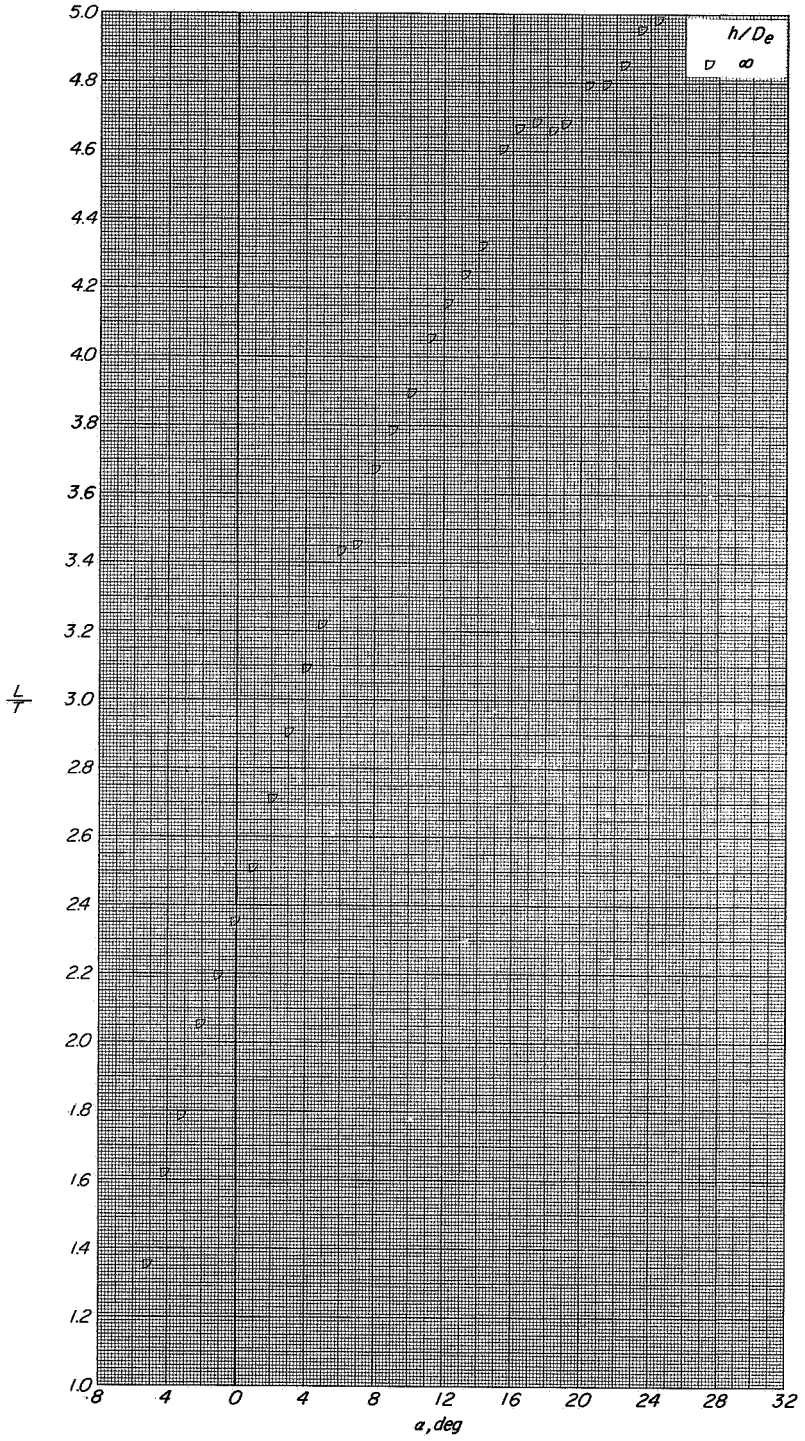

(d) Variation of L/T with α.

Figure 47 - Continued.

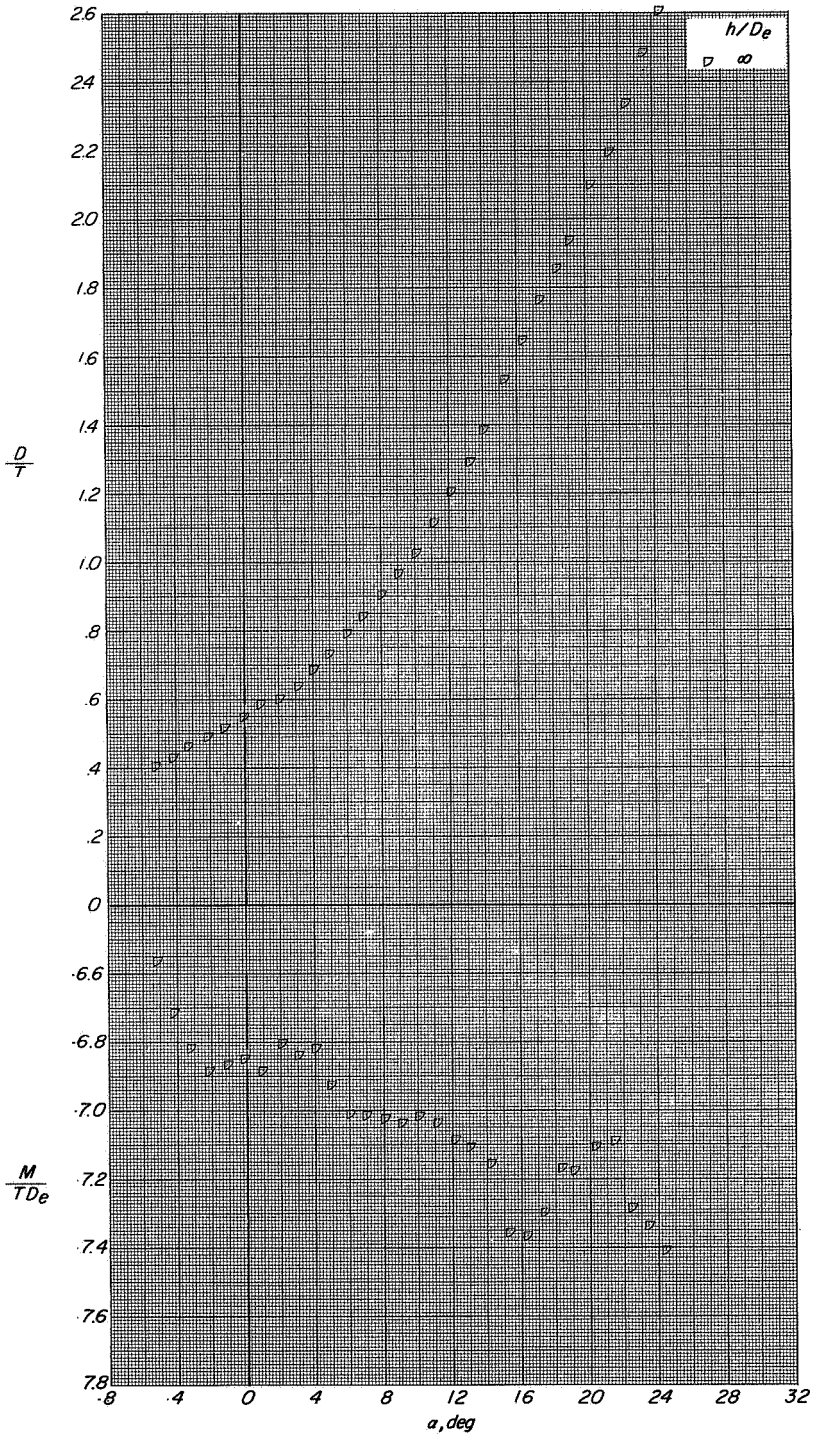

(e) Variation of D/T and M/TD_e with α.

Figure 47.- Concluded.

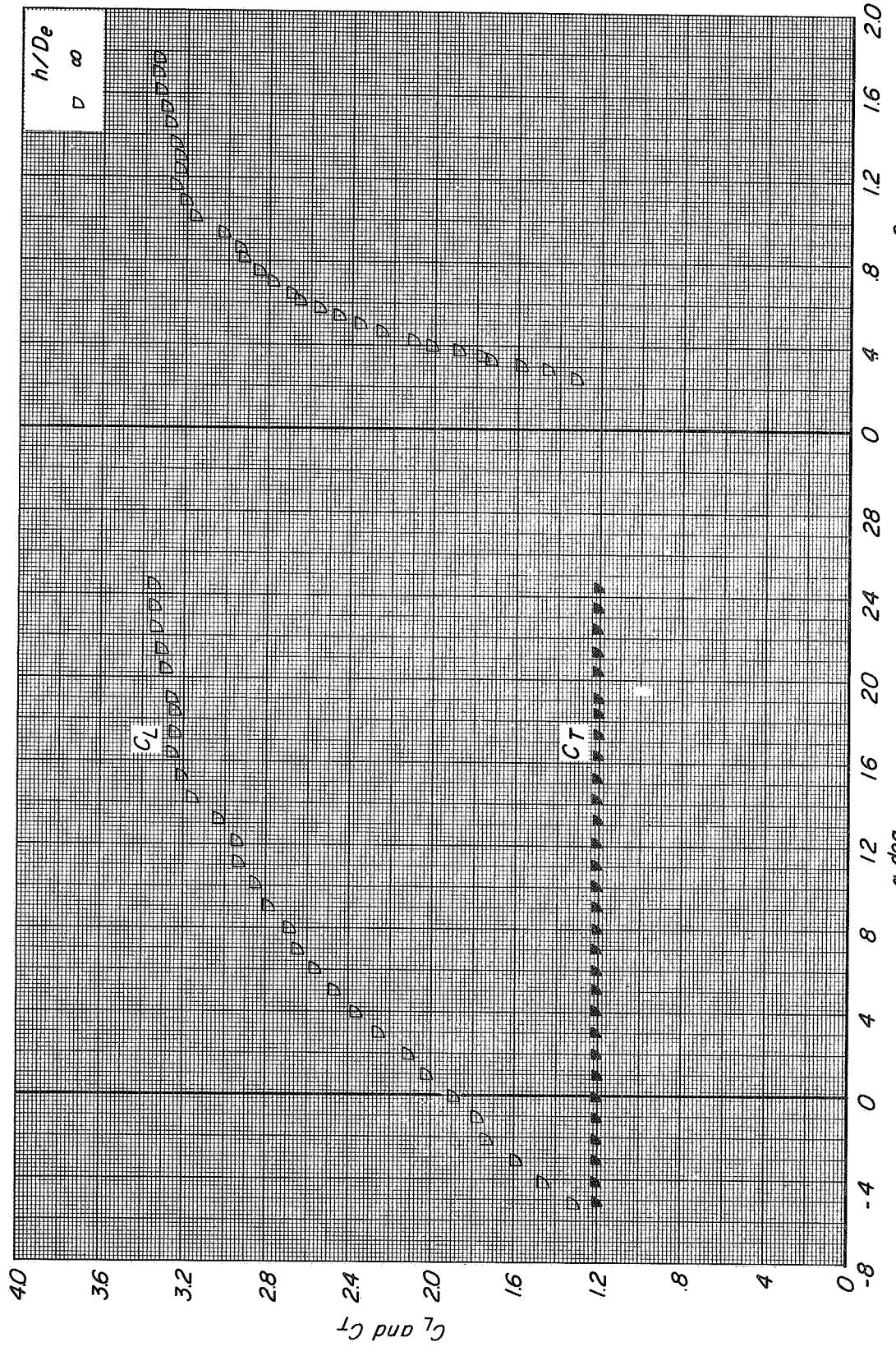

(a) Variation of C_L and C_T with α and C_D with C_L.

Figure 48.- Longitudinal aerodynamic characteristics of configuration A with direct-lift engines stowed and lift-cruise engines deflected 90°. $i_t = 0°$; $\beta = 0°$; $C_T \approx 1.2$.

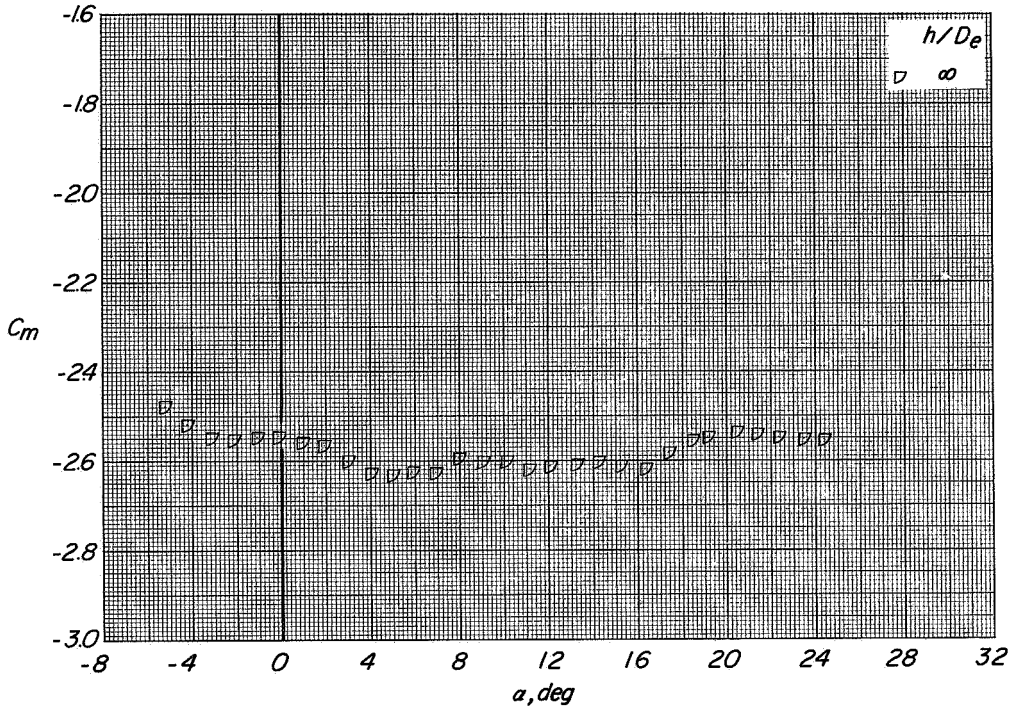

(b) Variation of C_m with α.

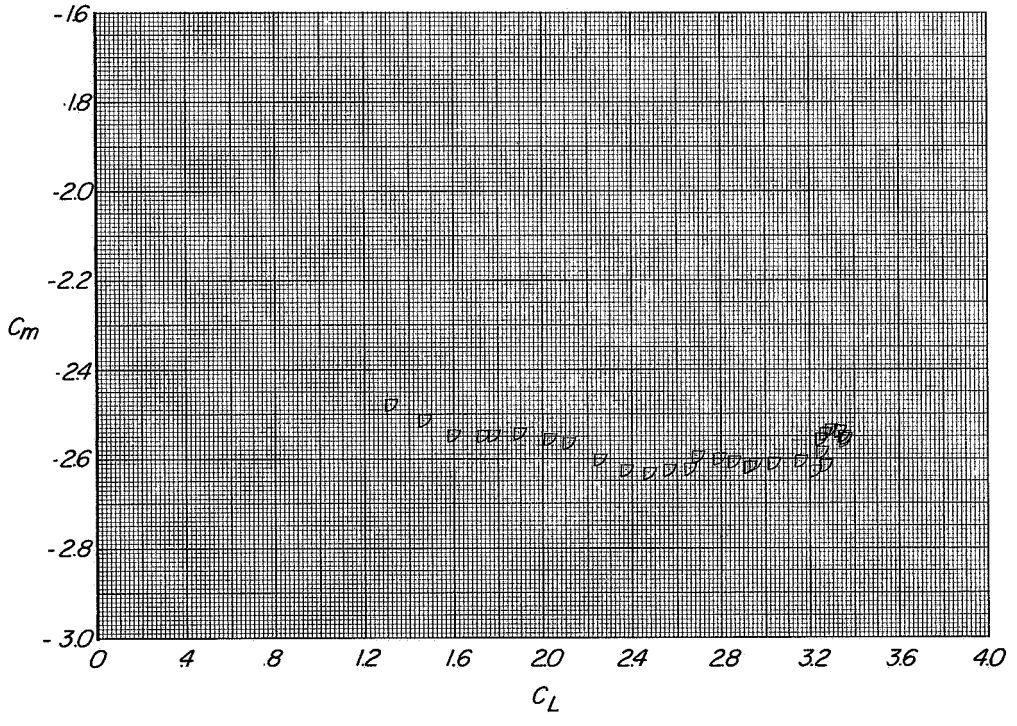

(c) Variation of C_m with C_L.

Figure 48.- Continued

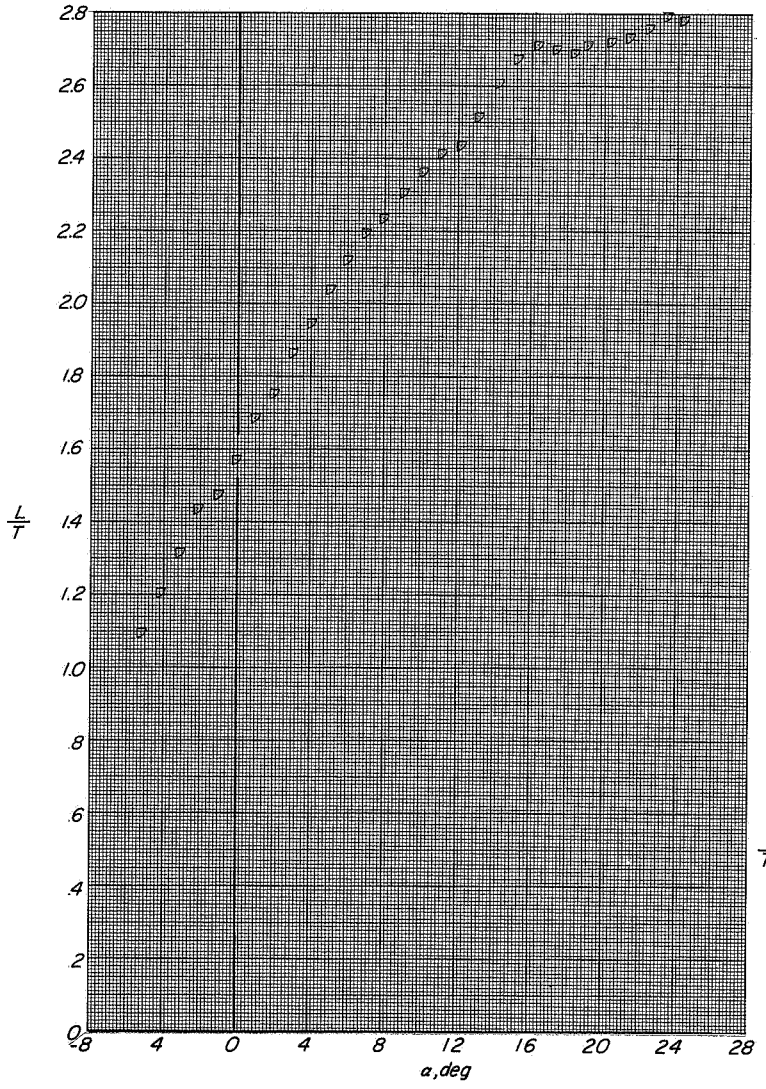

(d) Variation of L/T with α.

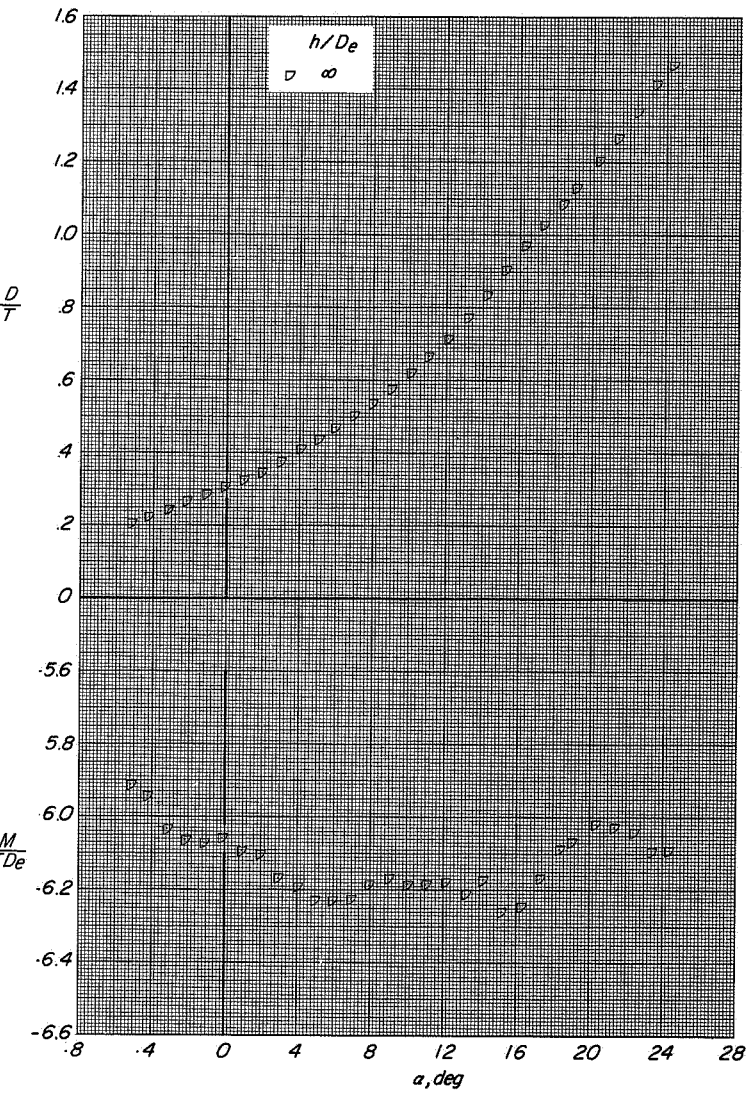

(e) Variation of D/T and M/TD_e with α.

Figure 48. Concluded.

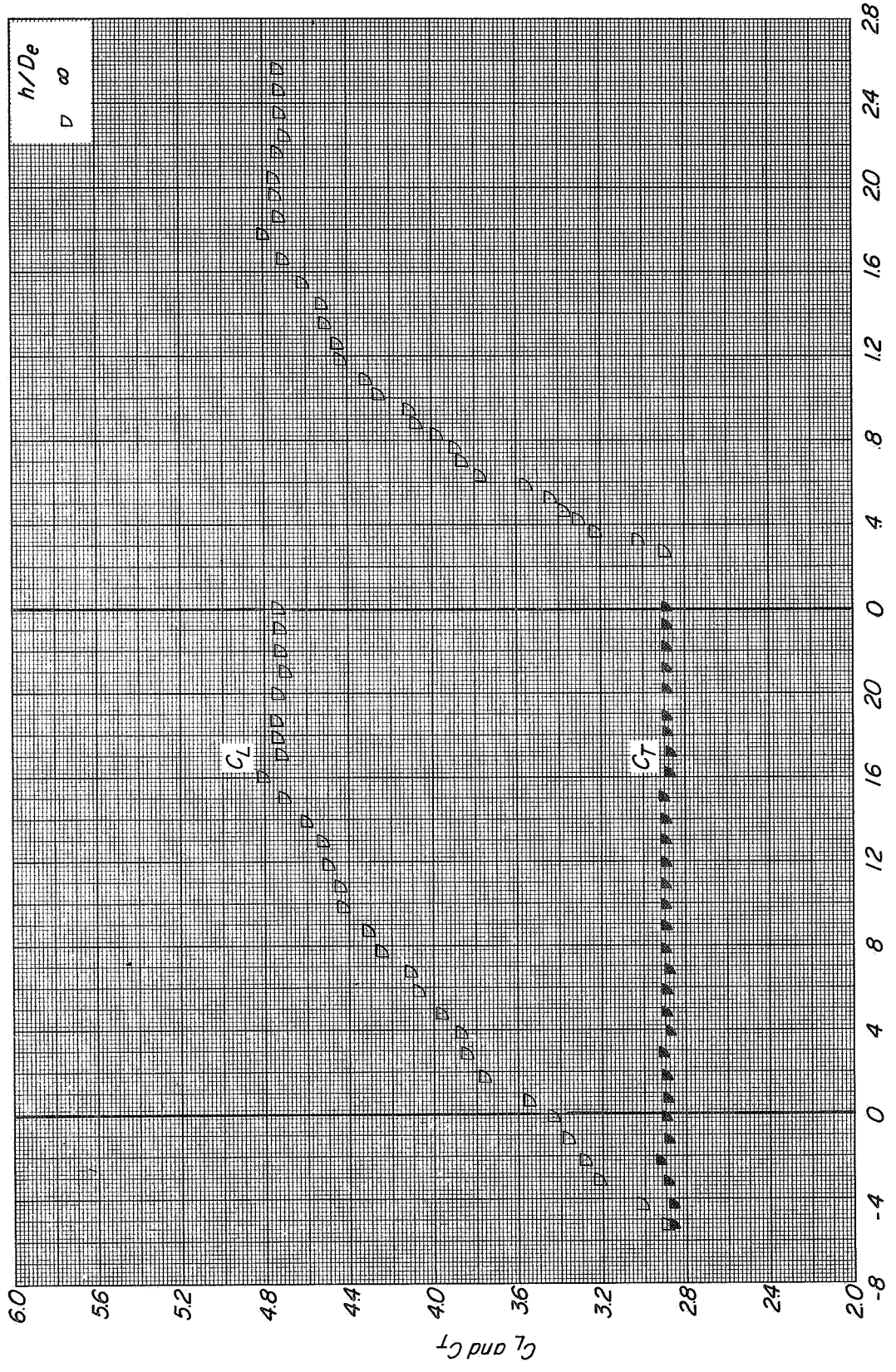

(a) Variation of C_L and C_T with α and C_D with C_L

Figure 49.- Longitudinal aerodynamic characteristics of configuration A with direct-lift engines stowed and lift-cruise engines deflected 90°. $i_t = 0°$; $\beta = 0°$; $C_T \approx 2.9$.

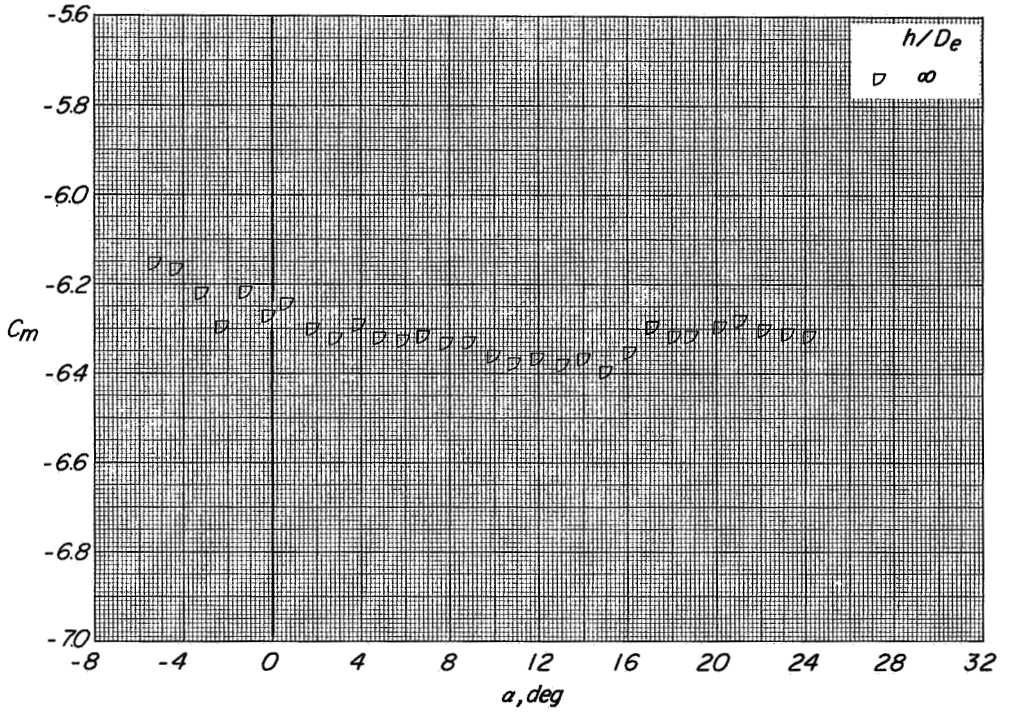

(b) Variation of C_m with α.

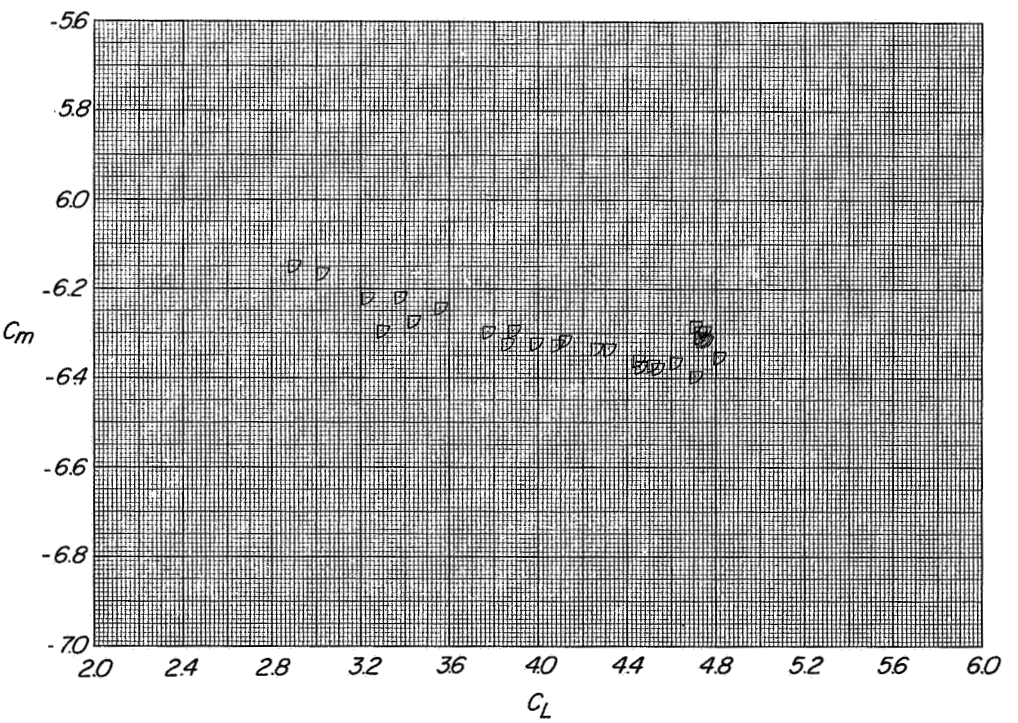

(c) Variation of C_m with C_L.

Figure 49.- Continued.

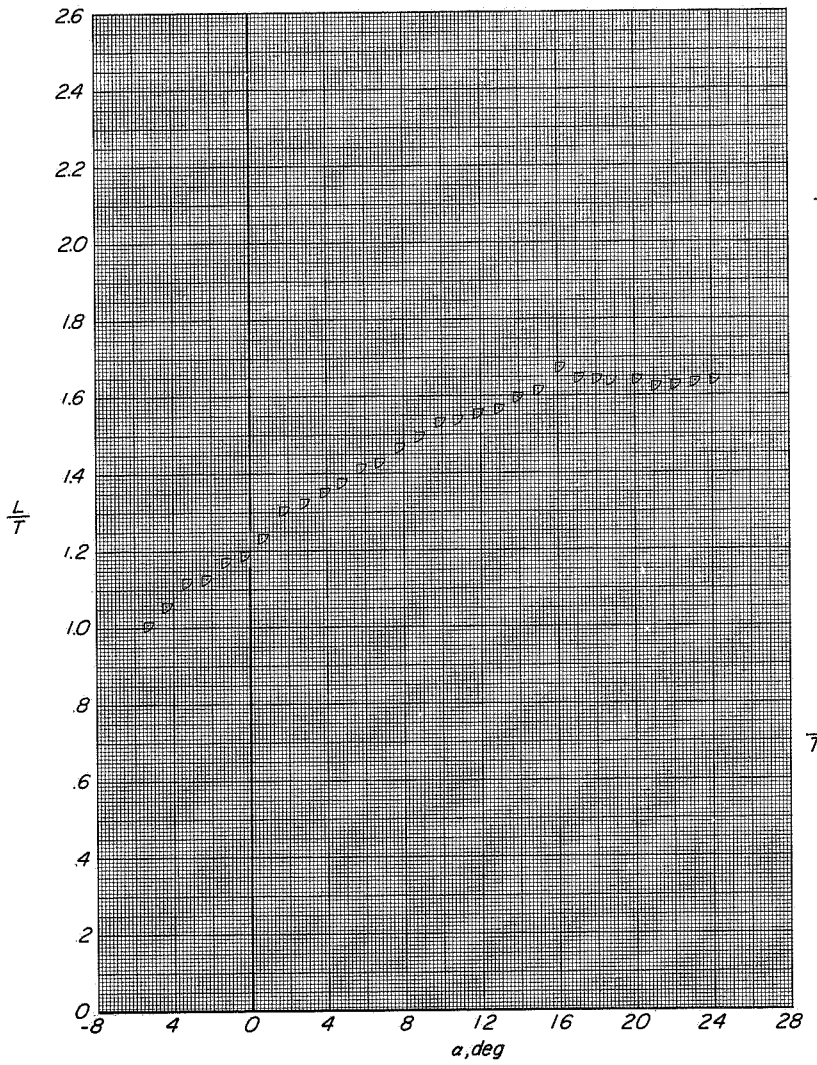

(d) Variation of L/T with α.

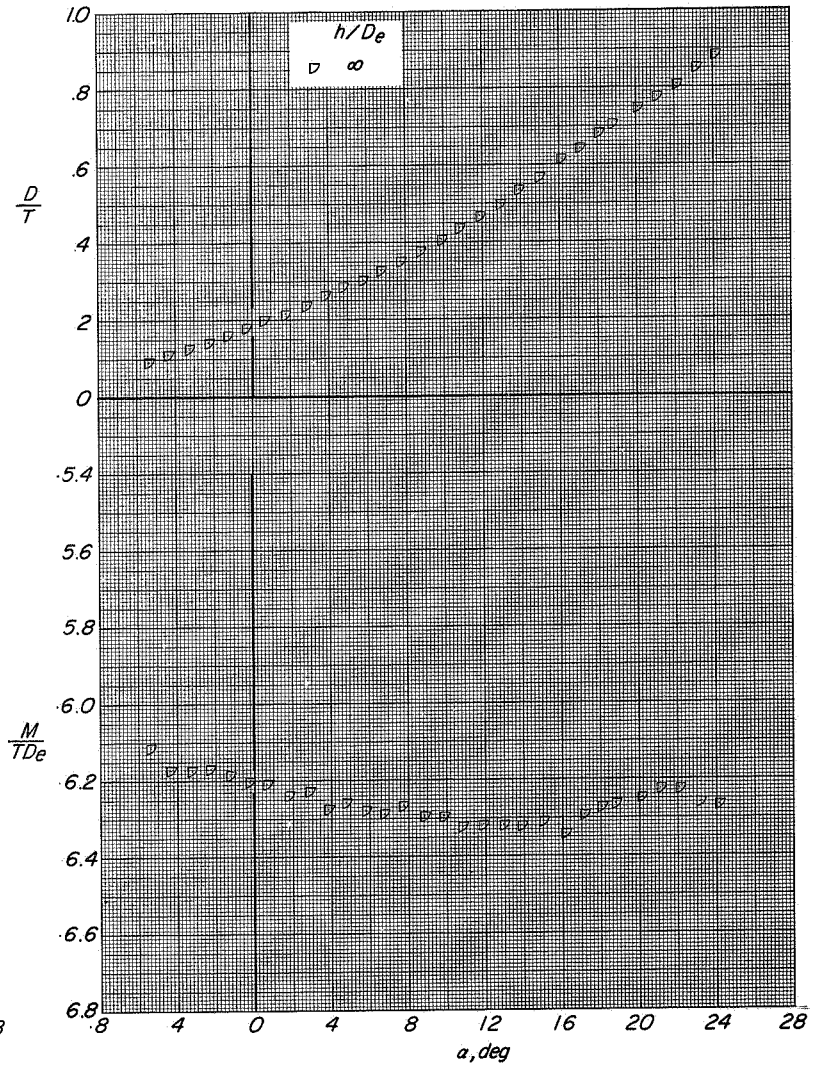

(e) Variation of D/T and M/TDe with α.

Figure 49. Concluded.

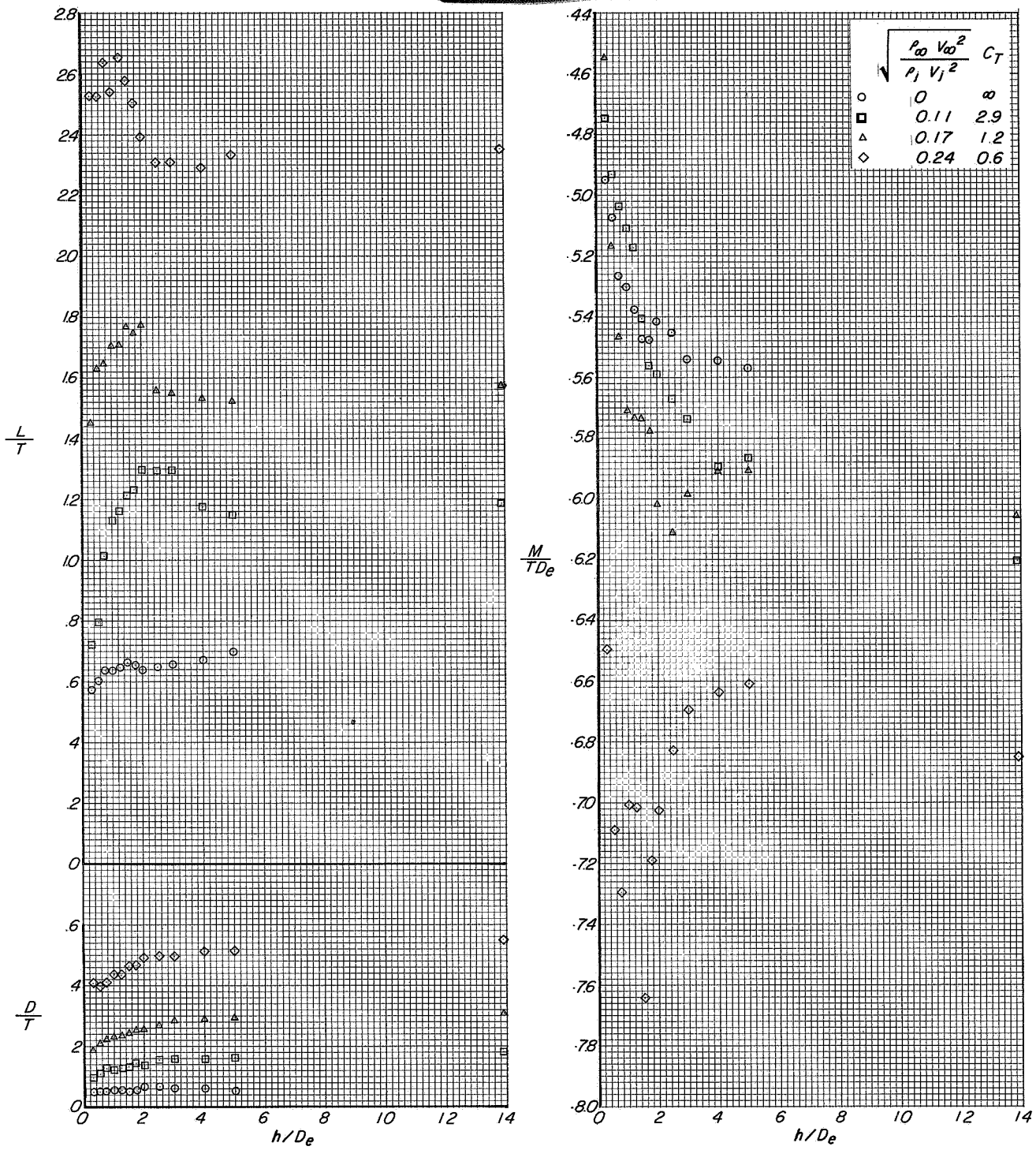

(a) Variation of L/T and D/T with h/D_e.

(b) Variation of M/TD_e with h/D_e.

Figure 50.- Effect of height above the moving-belt ground plane on the longitudinal aerodynamic characteristics of configuration A with direct-lift engines stowed and lift-cruise engines deflected 90°. $i_t = 0^0$; $\beta = 0^0$; $\alpha = 0^0$.

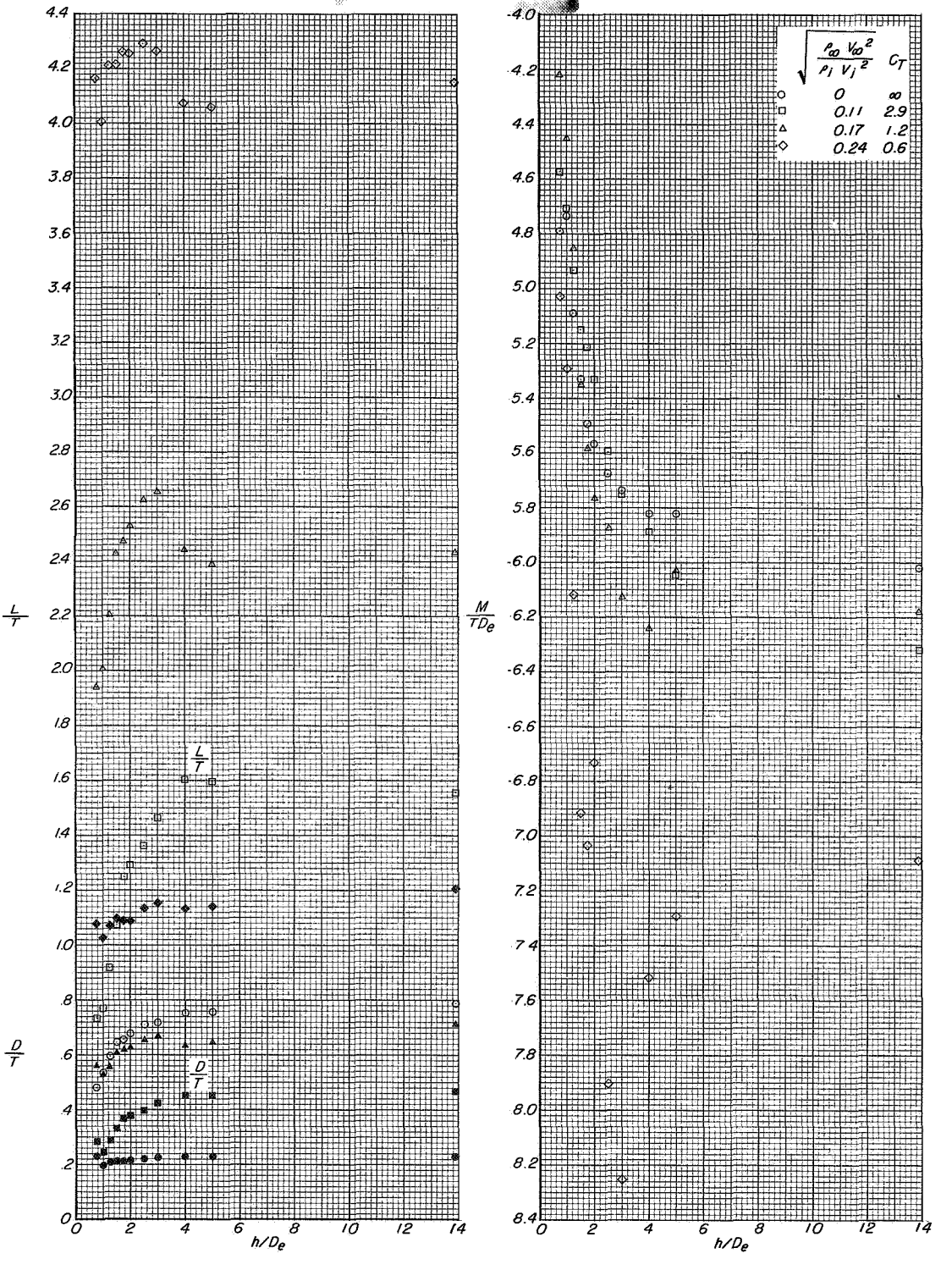

(a) Variation of L/T and D/T with h/D_e.

(b) Variation of M/TD_e with h/D_e.

Figure 51.- Effect of height above the moving-belt ground plane on the longitudinal aerodynamic characteristics of configuration A with direct-lift engines stowed and lift-cruise engines deflected 90°. $i_t = 0°$; $\beta = 0°$; $\alpha = 12°$

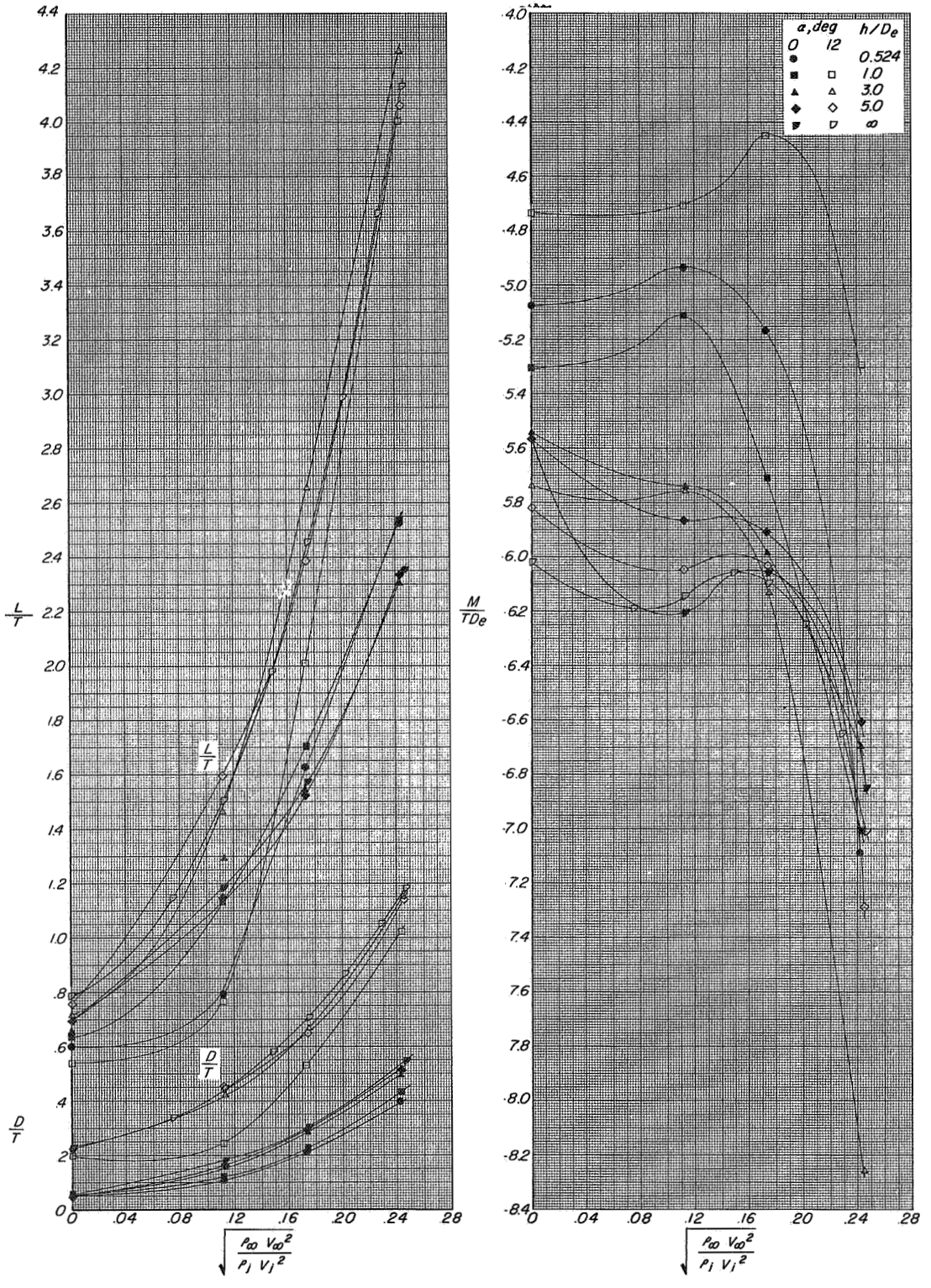

(a) Variation of L/T and D/T with effective velocity ratio.

(b) Variation of M/TD_e with effective velocity ratio.

Figure 52.- Effect of effective velocity ratio on the longitudinal aerodynamic characteristics of configuration A with direct-lift engines stowed and lift-cruise engines deflected 90°. $i_t = 0°$. $\beta = 0°$.

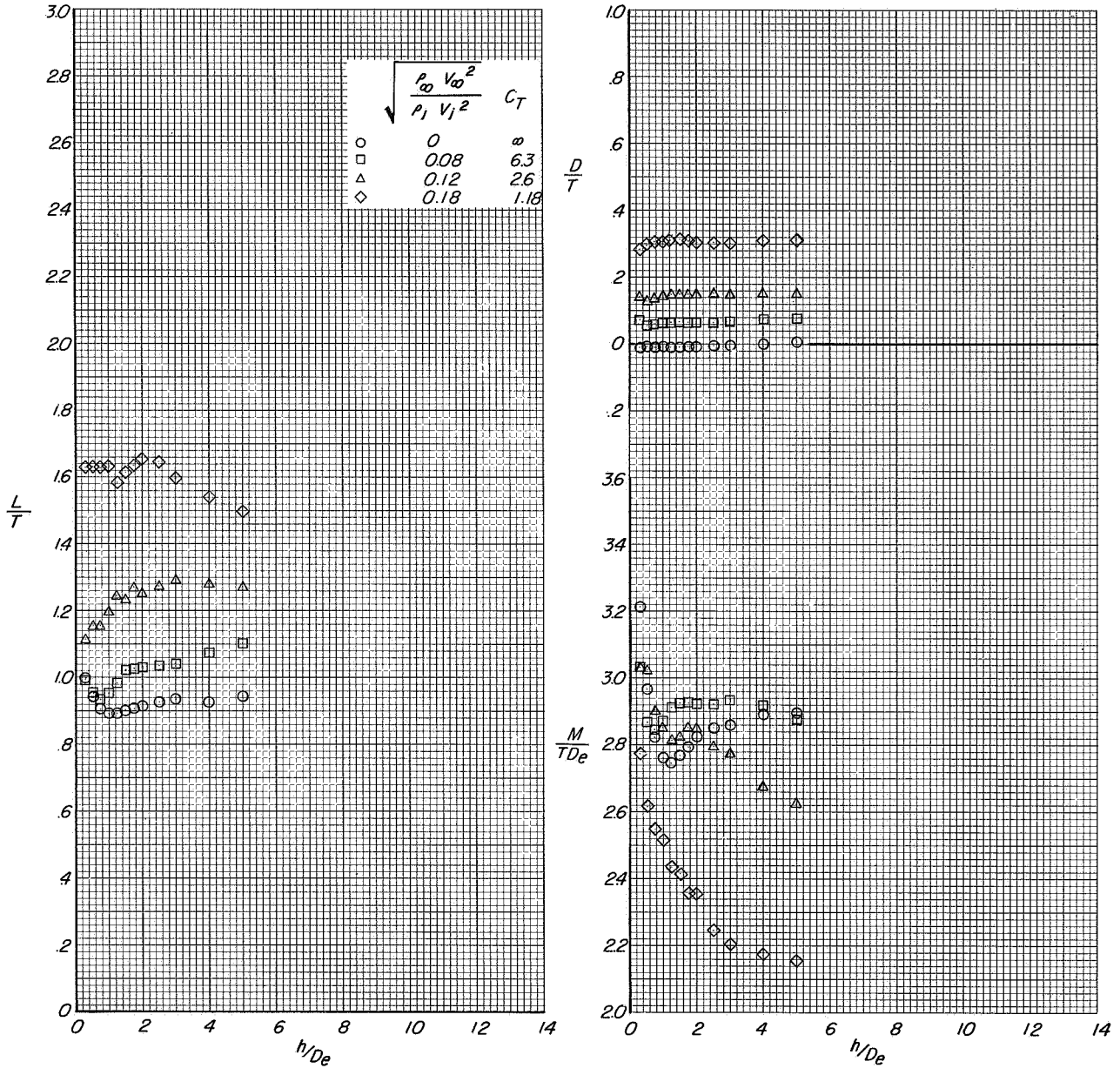

(a) Variation of L/T with h/D_e.

(b) Variation of D/T and M/TD_e with h/D_e.

Figure 53.- Effect of height above the moving-belt ground plane on the longitudinal aerodynamic characteristics of configuration A with direct-lift engines deflected 90° and lift-cruise engines off. $i_t = 0^0$; $\beta = 0^0$; $\alpha = 0^0$

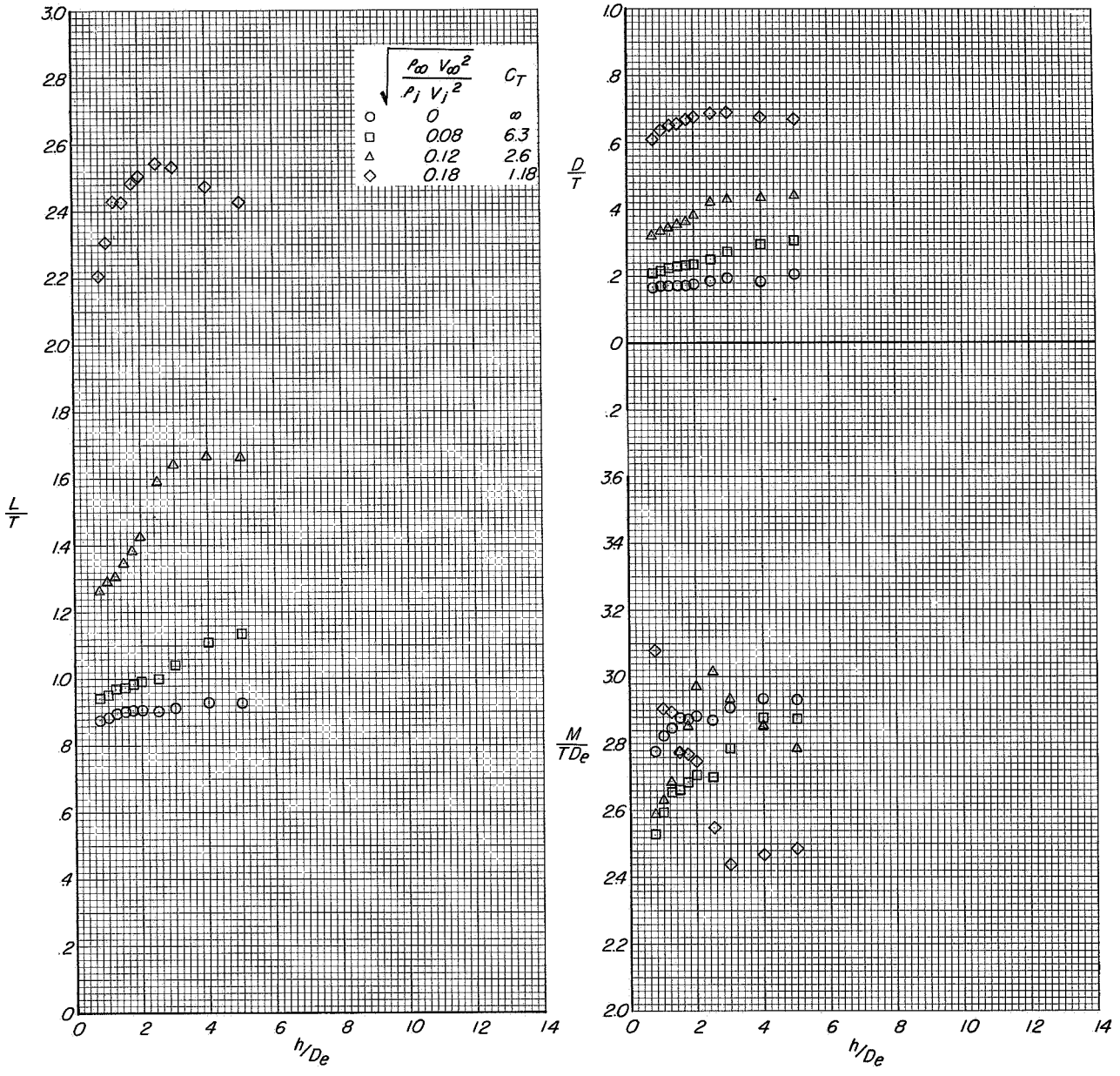

(a) Variation of L/T with h/D_e.

(b) Variation of D/T and M/TD_e with h/D_e.

Figure 54.- Effect of height above the moving-belt ground plane on the longitudinal aerodynamic characteristics of configuration A with direct-lift engines deflected 90° and lift-cruise engines off. $i_t = 0°$; $\beta = 0°$; $\alpha = 12°$.

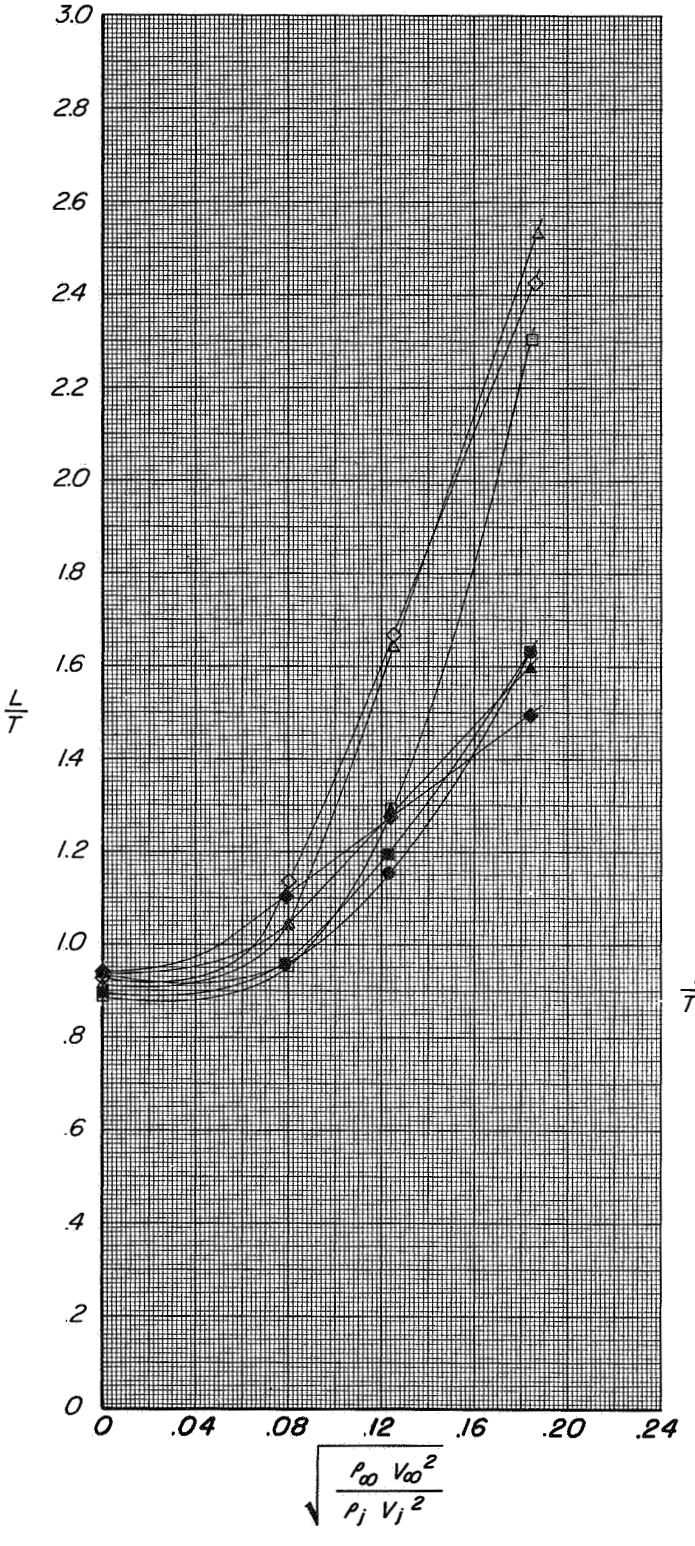

(a) Variation of L/T with effective velocity ratio.

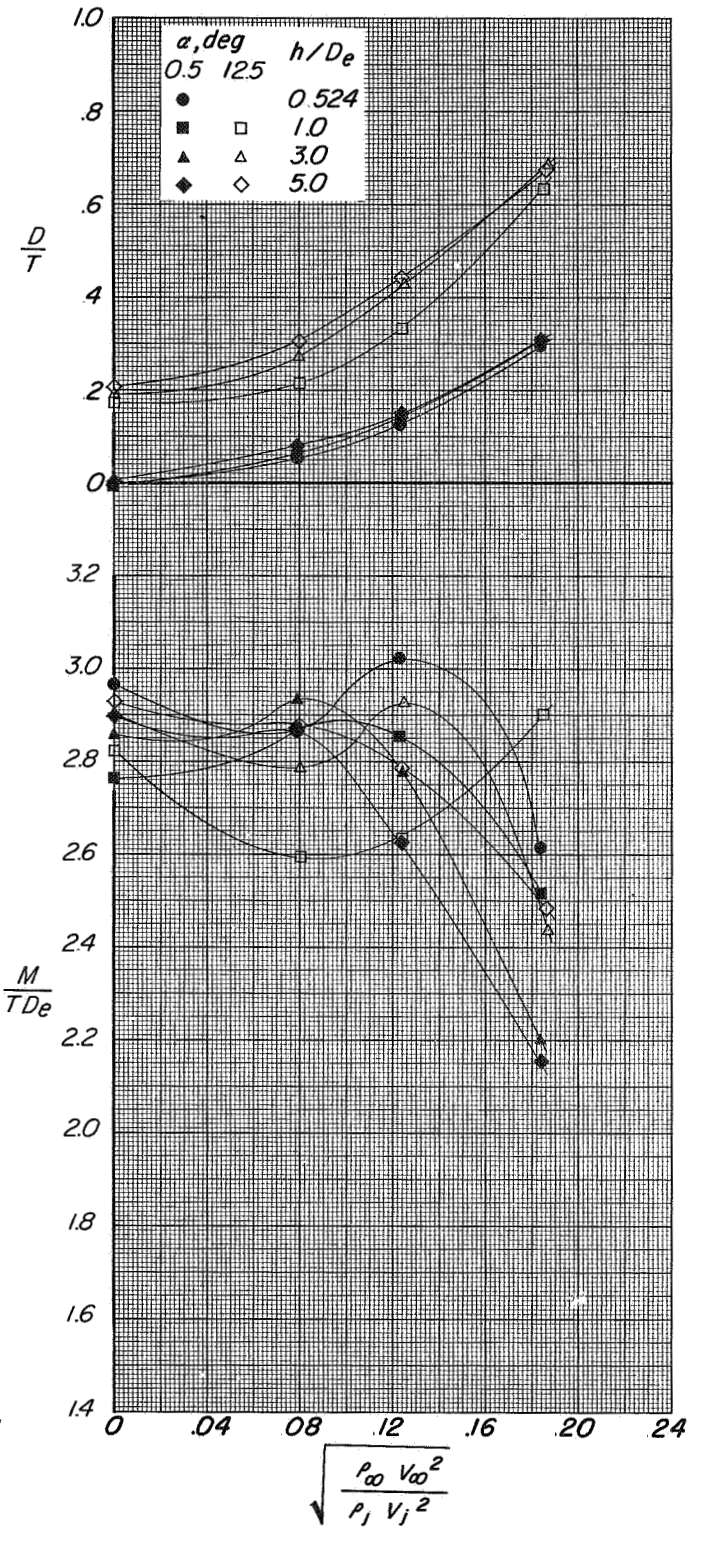

(b) Variation of D/T and M/TD$_e$ with effective velocity ratio.

Figure 55.- Effect of effective velocity ratio on the longitudinal aerodynamic characteristics of configuration A with direct-lift engines deflected 90° and lift-cruise engines off. $i_t = 0°$; $\beta = 0°$

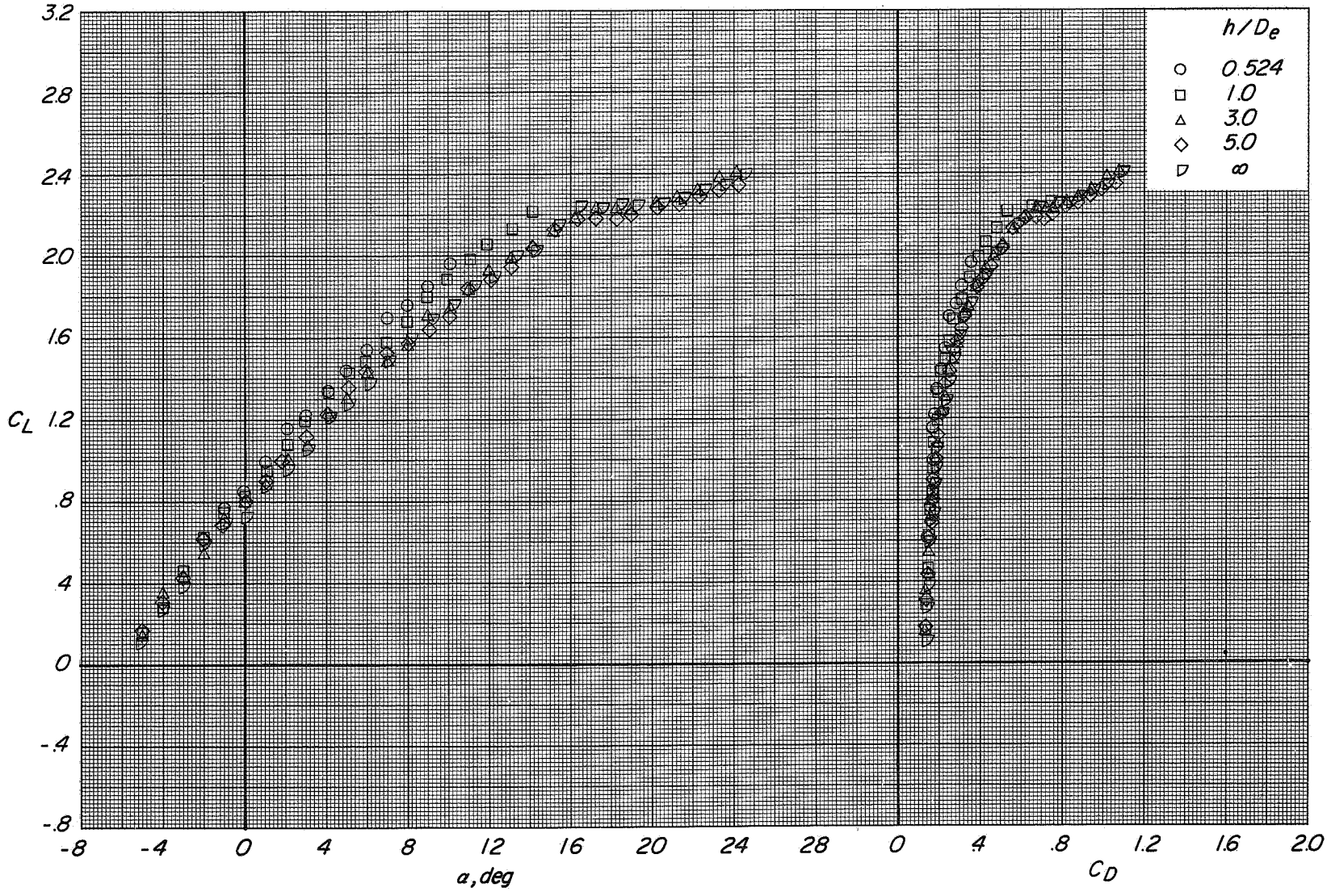

(a) Variation of C_L with α and C_D with C_L.

Figure 56.- Longitudinal aerodynamic characteristics of configuration A with direct-lift engines stowed and lift-cruise engines off. $i_t = 0^o$; $\beta = 0^o$; $C_T = 0$.

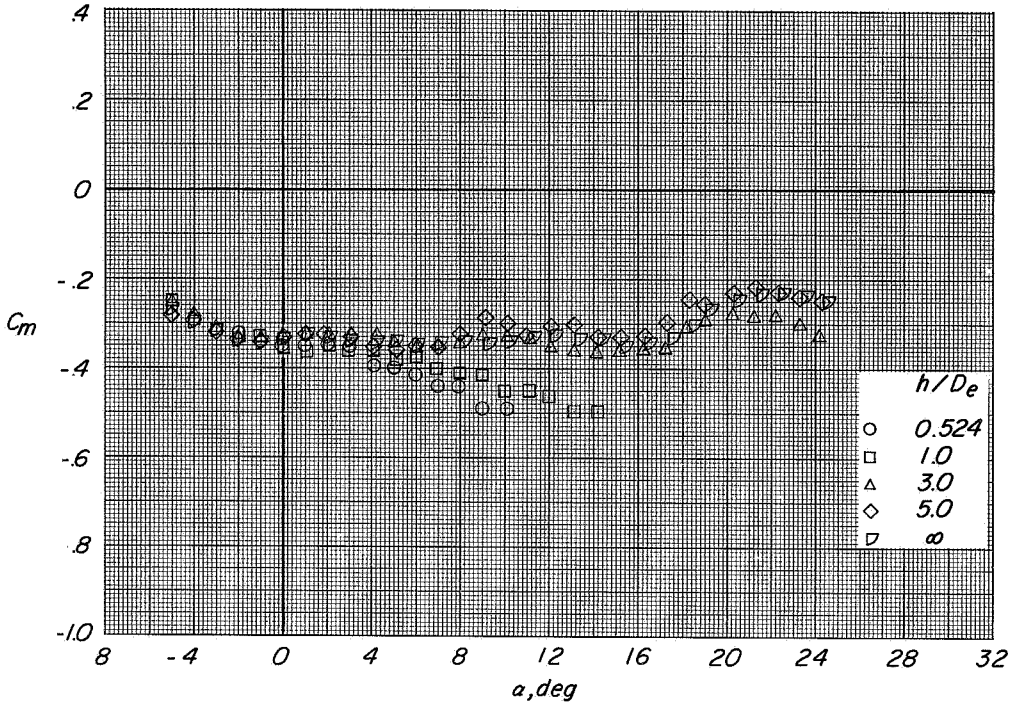

(b) Variation of C_m with α.

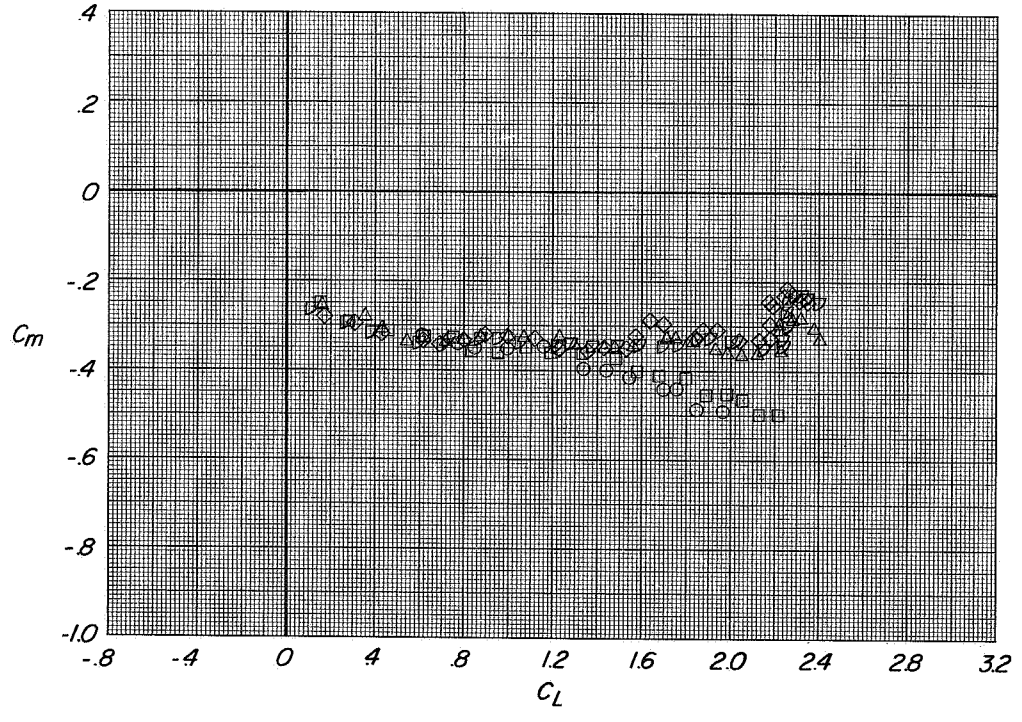

(c) Variation of C_m with C_L.

Figure 56.- Concluded.

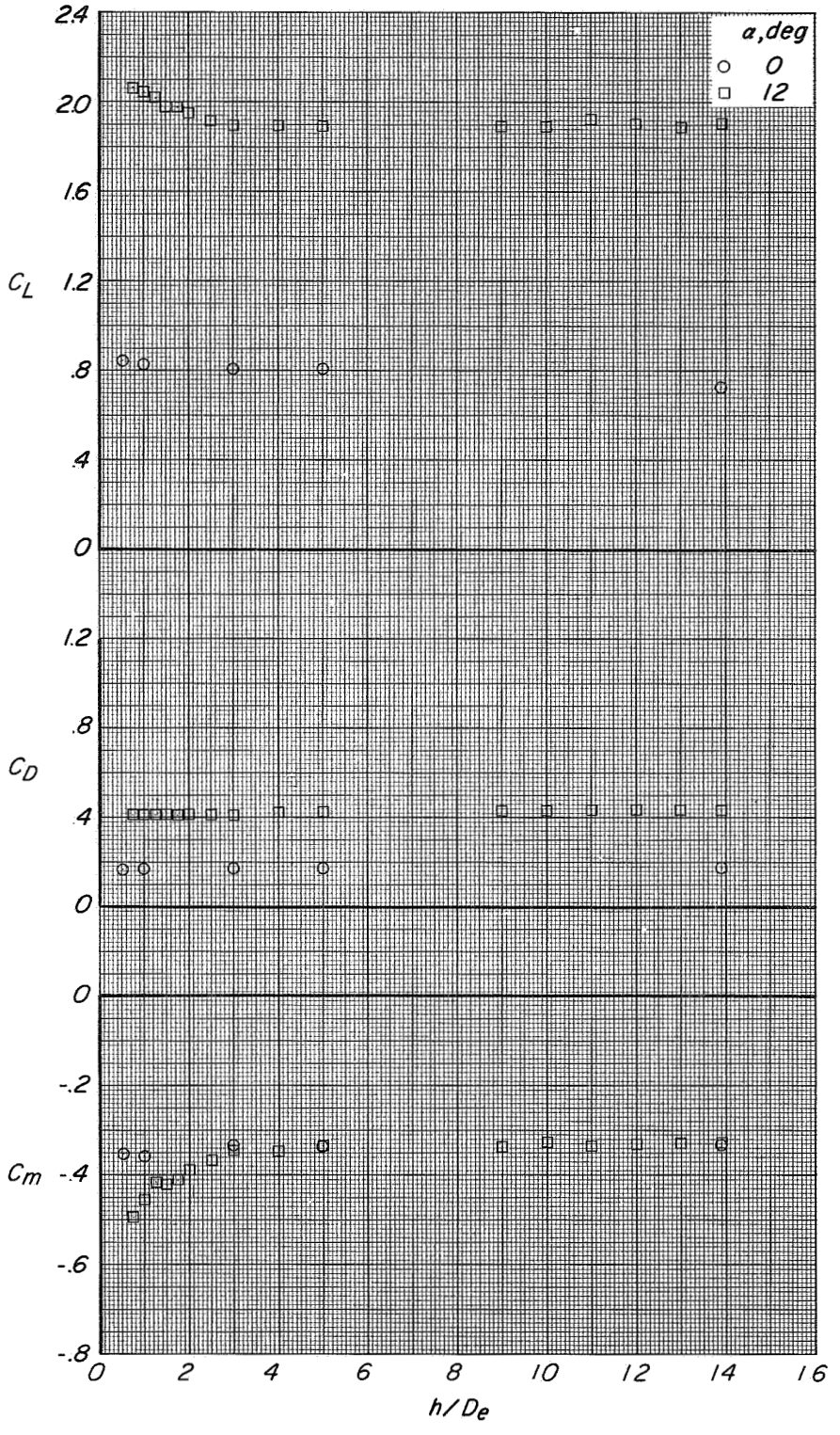

Figure 57.- Effect of height above the moving-belt ground plane on the longitudinal aerodynamic characteristics of configuration A with direct-lift engines stowed and lift-cruise engines off. $i_t = 0^0$; $\beta = 0^0$; $C_T = 0$.

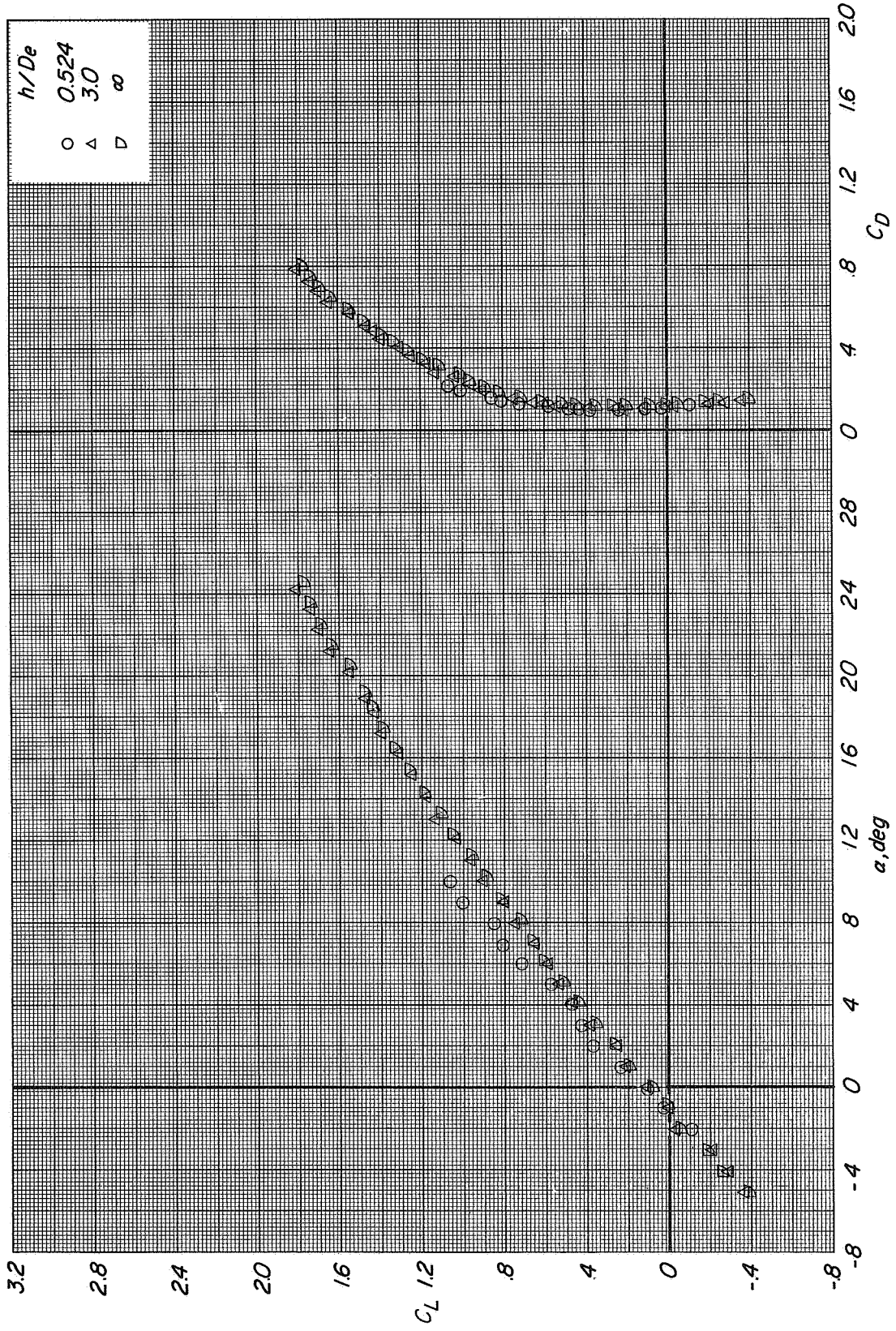

(a) Variation of C_L with α and C_D with C_L.

Figure 58.- Longitudinal aerodynamic characteristics of configuration B with direct-lift and lift-cruise engines deflected 90°. $i_t = 0°$; $\beta = 0°$; $C_T = 0$.

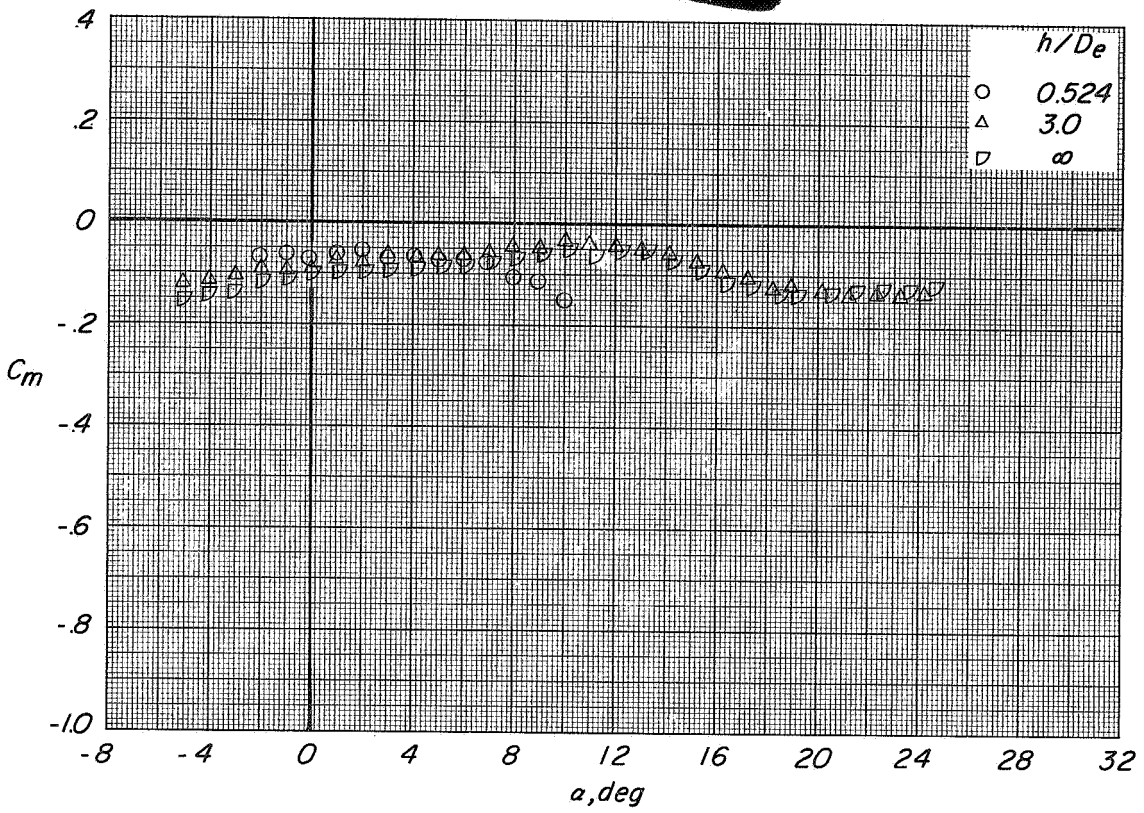

(b) Variation of C_m with α.

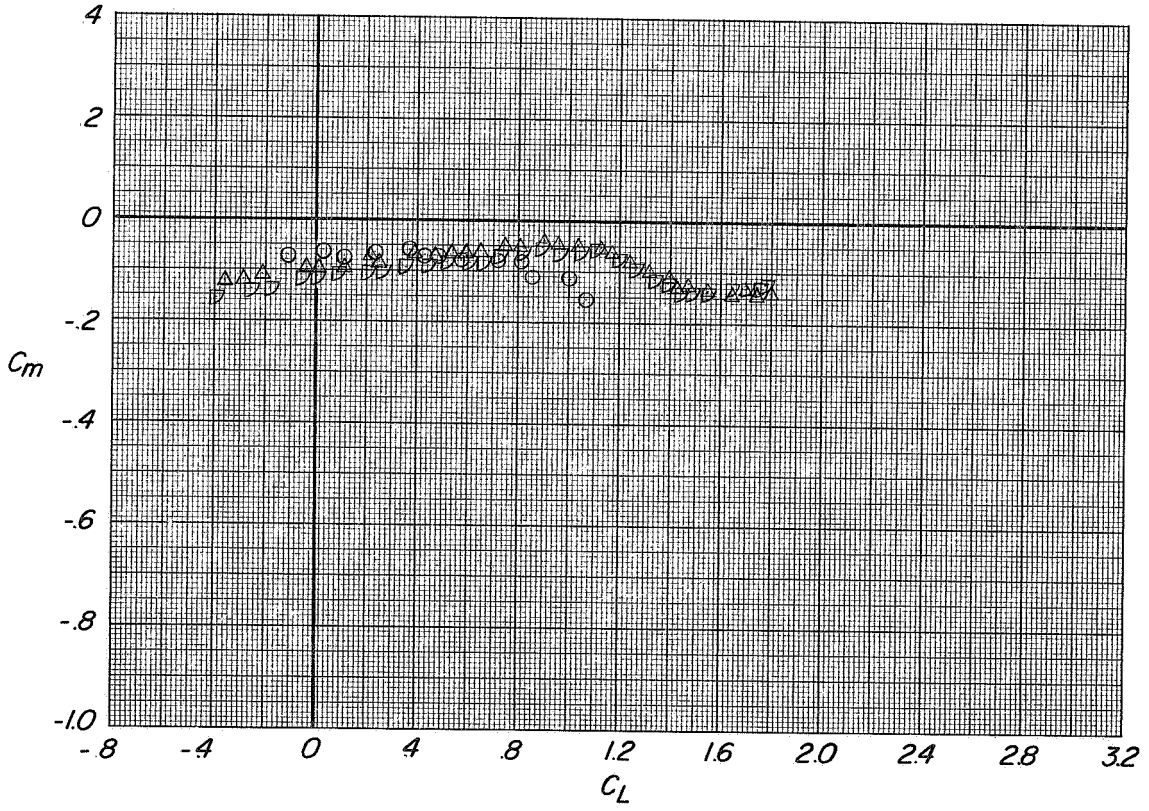

(c) Variation of C_m with C_L

Figure 58.- Concluded.

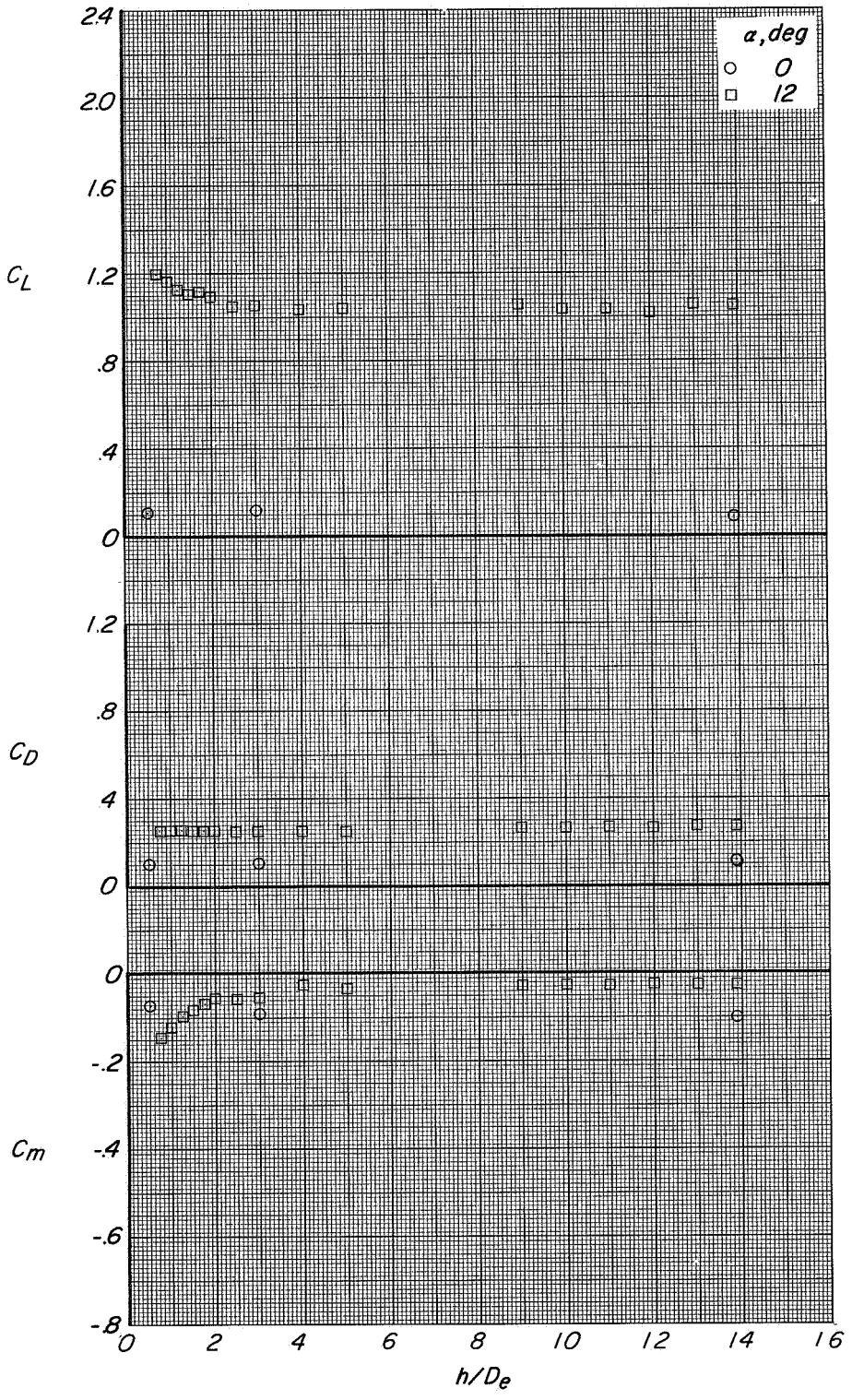

Figure 59.- Effect of height above the moving-belt ground plane on the longitudinal aerodynamic characteristics of configuration B with direct-lift and lift-cruise engines deflected 90^0 $i_t = 0^0$; $\beta = 0^0$; $C_T = 0$.

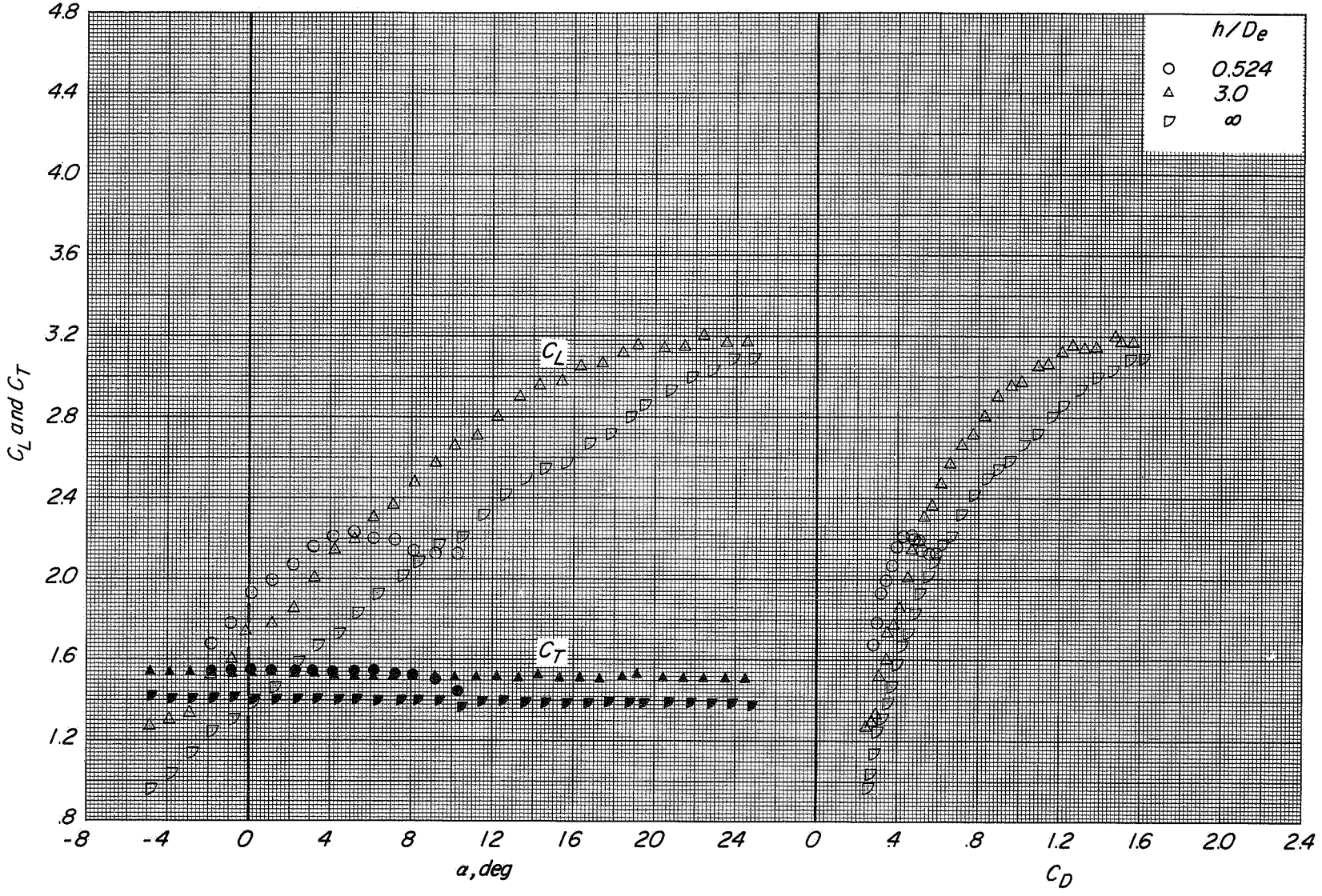

(a) Variation of C_L and C_T with α and C_D with C_L

Figure 60.- Longitudinal aerodynamic characteristics of configuration B with direct-lift and lift-cruise engines deflected 90°. $i_t = 0°$; $\beta = 0°$; $C_T \approx 1.45$.

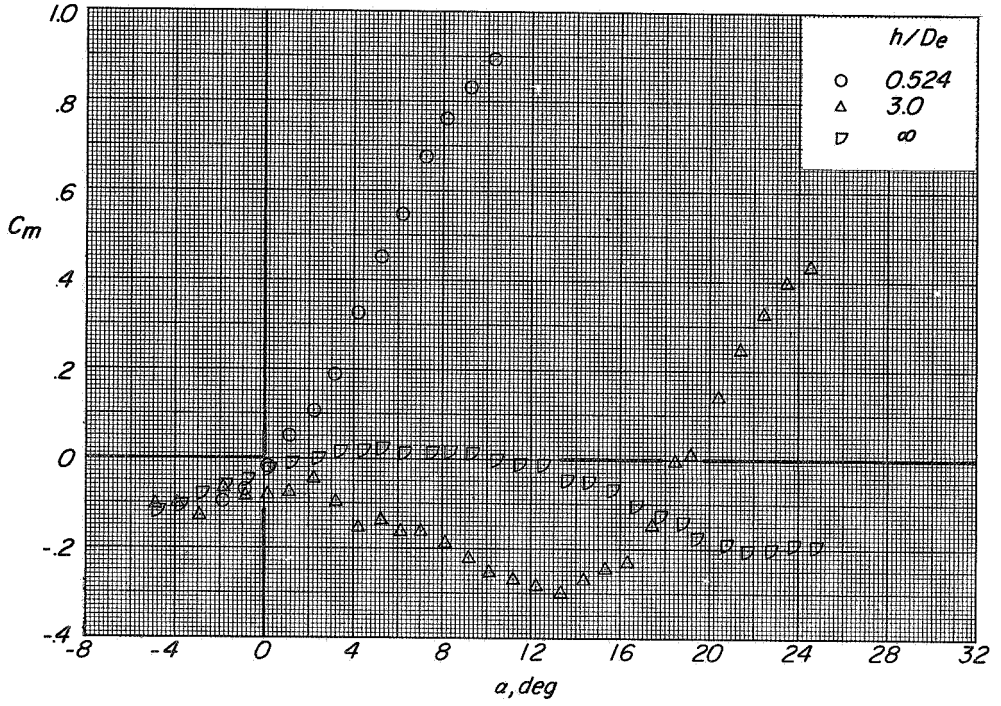

(b) Variation of C_m with α.

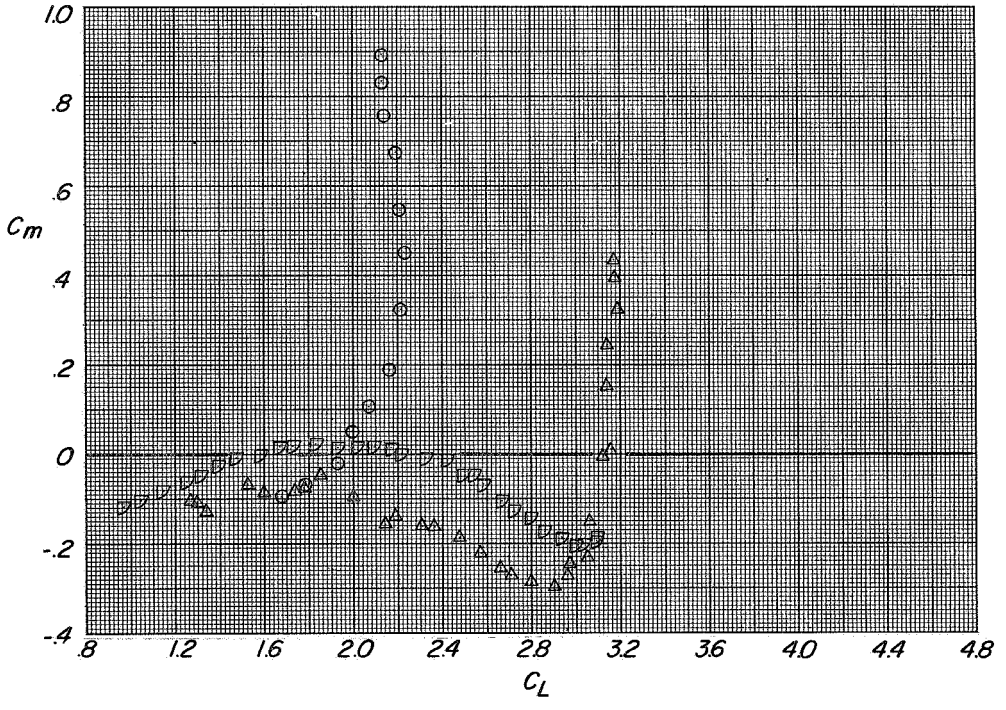

(c) Variation of C_m with C_L

Figure 60.- Continued.

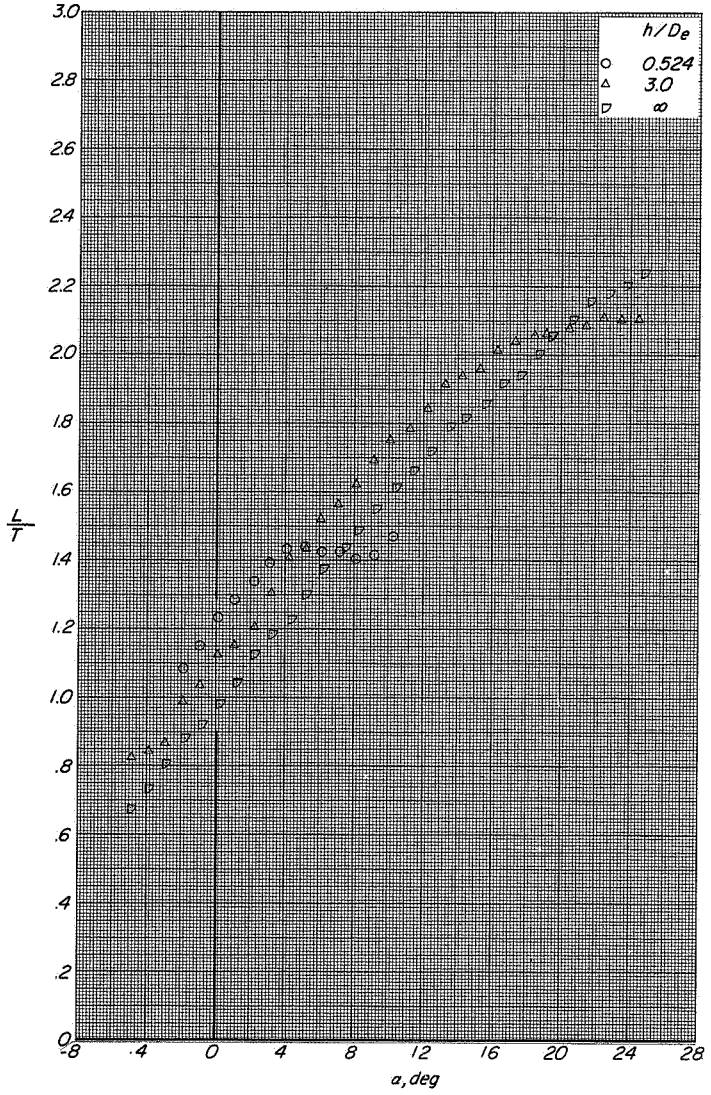

(d) Variation of L/T with α.

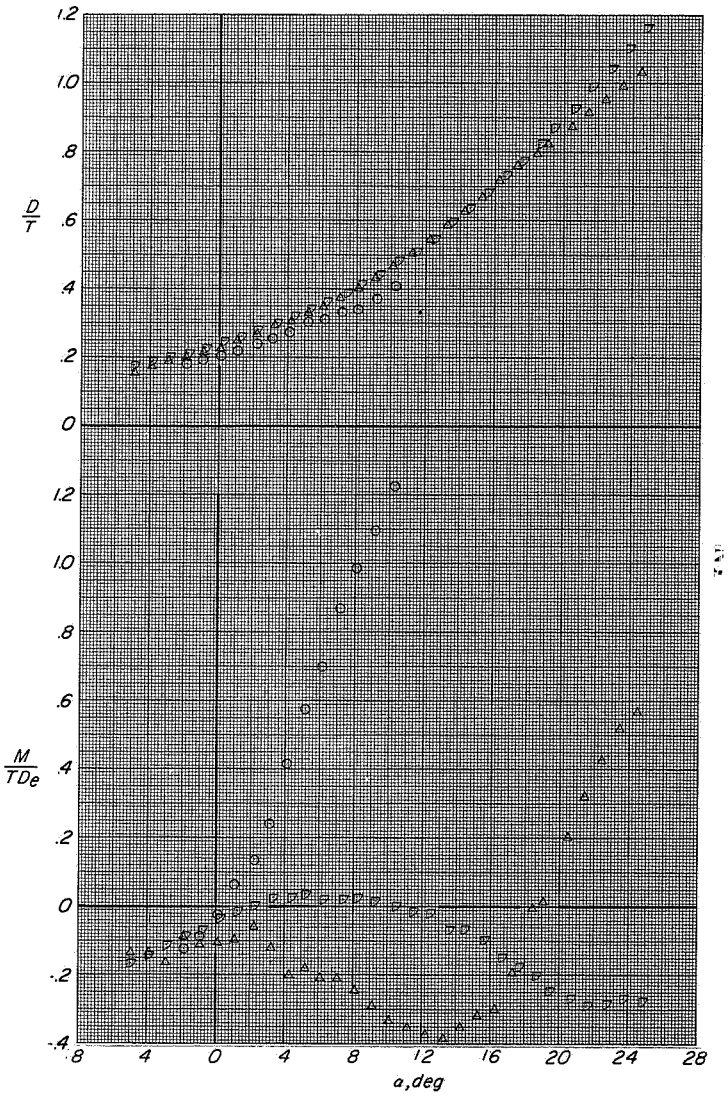

(e) Variation of D/T and M/TDe with α.

Figure 60. Concluded.

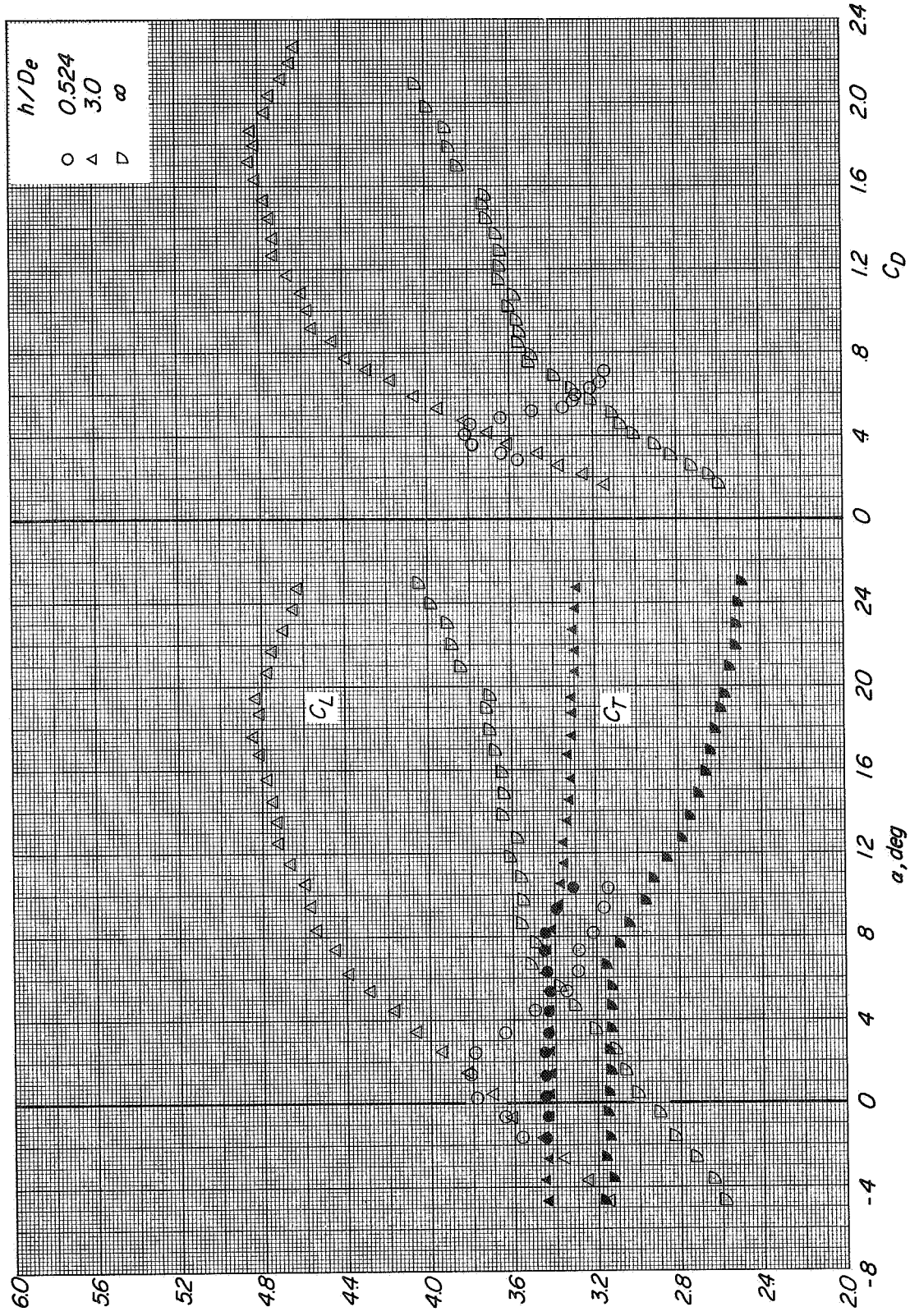

(a) Variation of C_L and C_T with α and C_D with C_L.

Figure 61.- Longitudinal aerodynamic characteristics of configuration B with direct-lift and lift-cruise engines deflected 90°. $i_t = 0°$; $\beta = 0°$; $C_T \approx 3.3$.

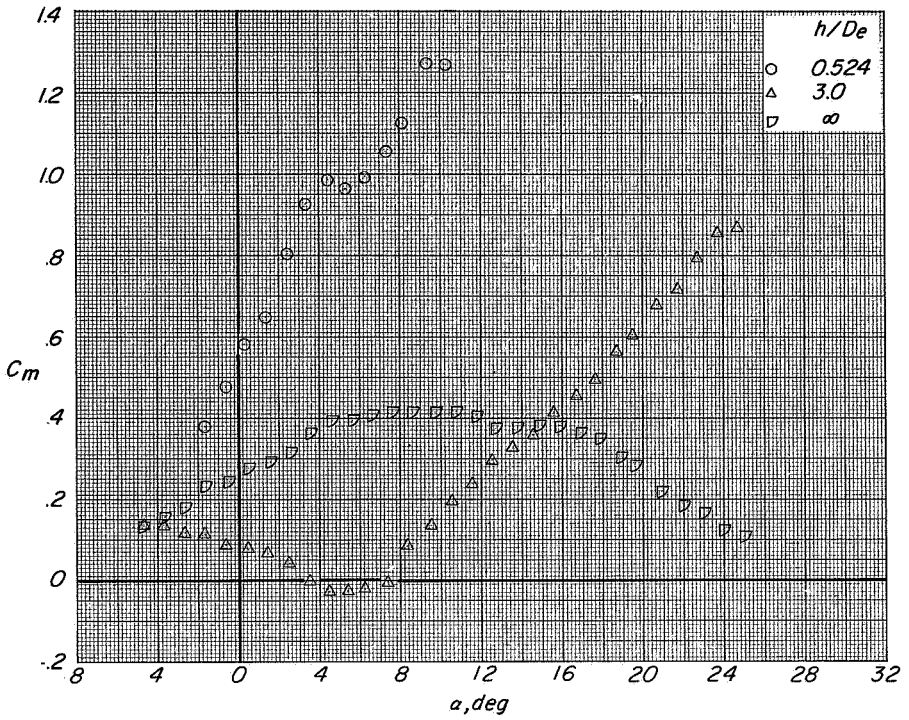

(b) Variation of C_m with α.

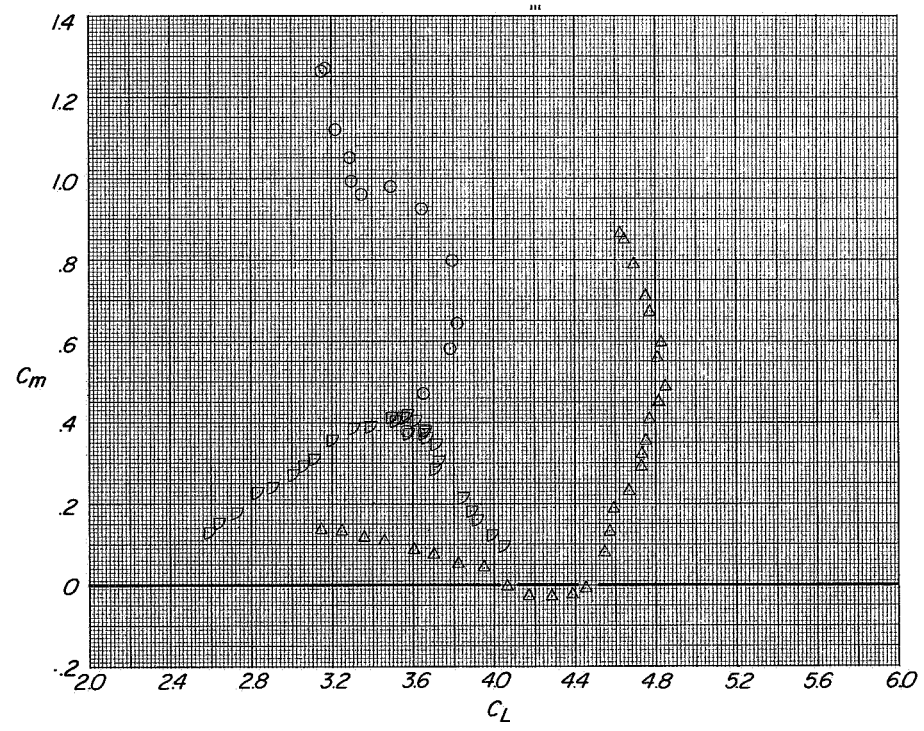

(c) Variation of C_m with C_L.

Figure 61.- Continued.

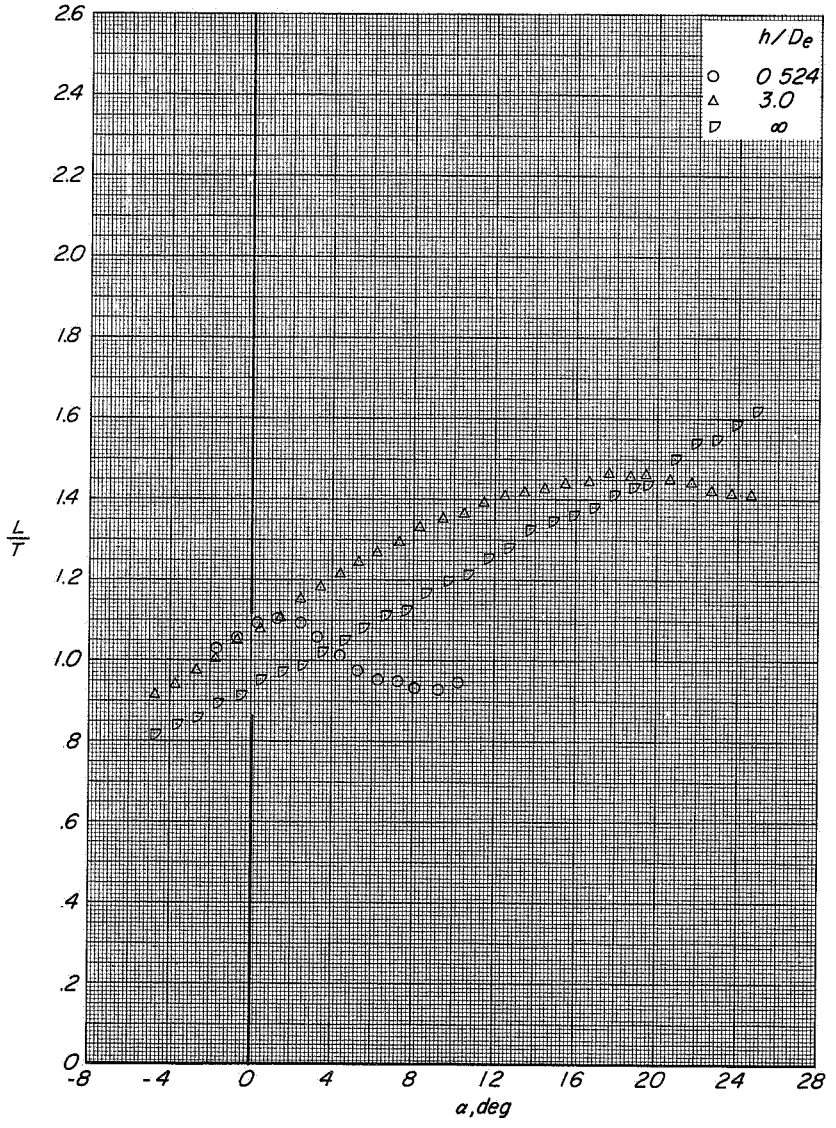

(d) Variation of L/T with α.

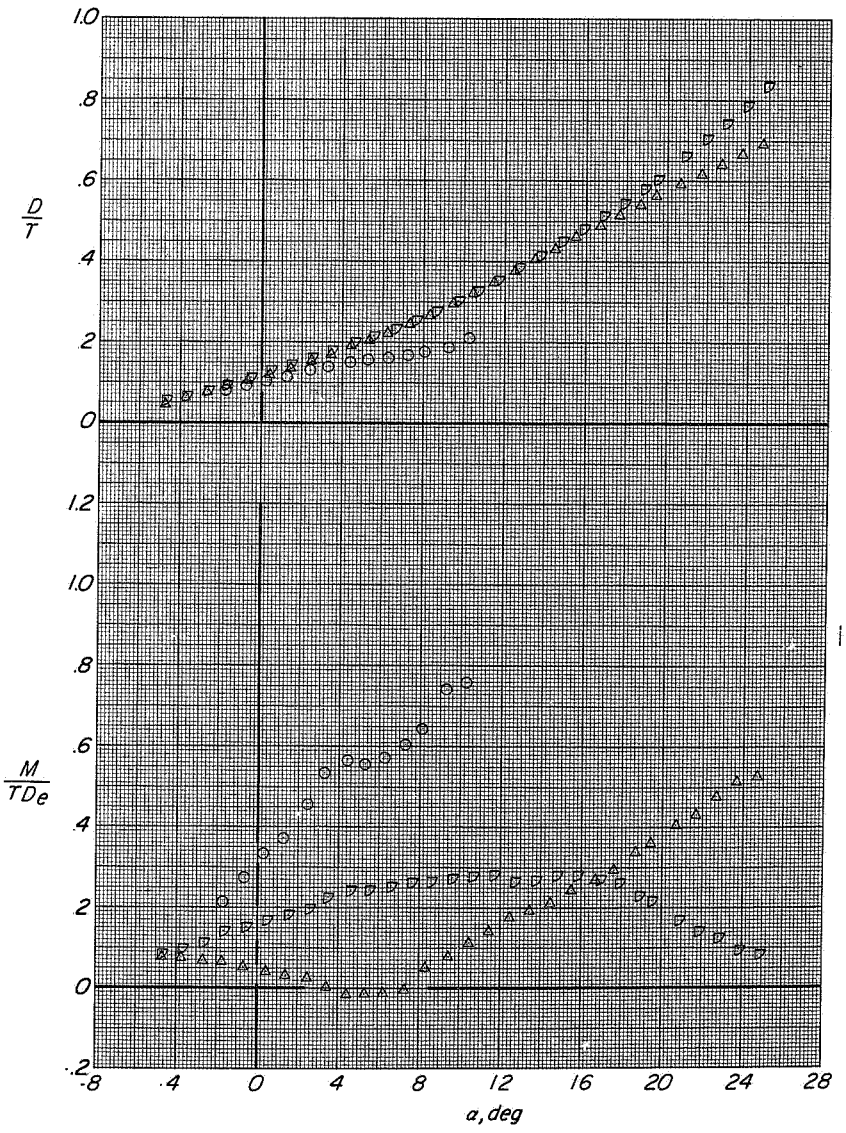

(e) Variation of D/T and M/TD_e with α.

Figure 61.- Concluded.

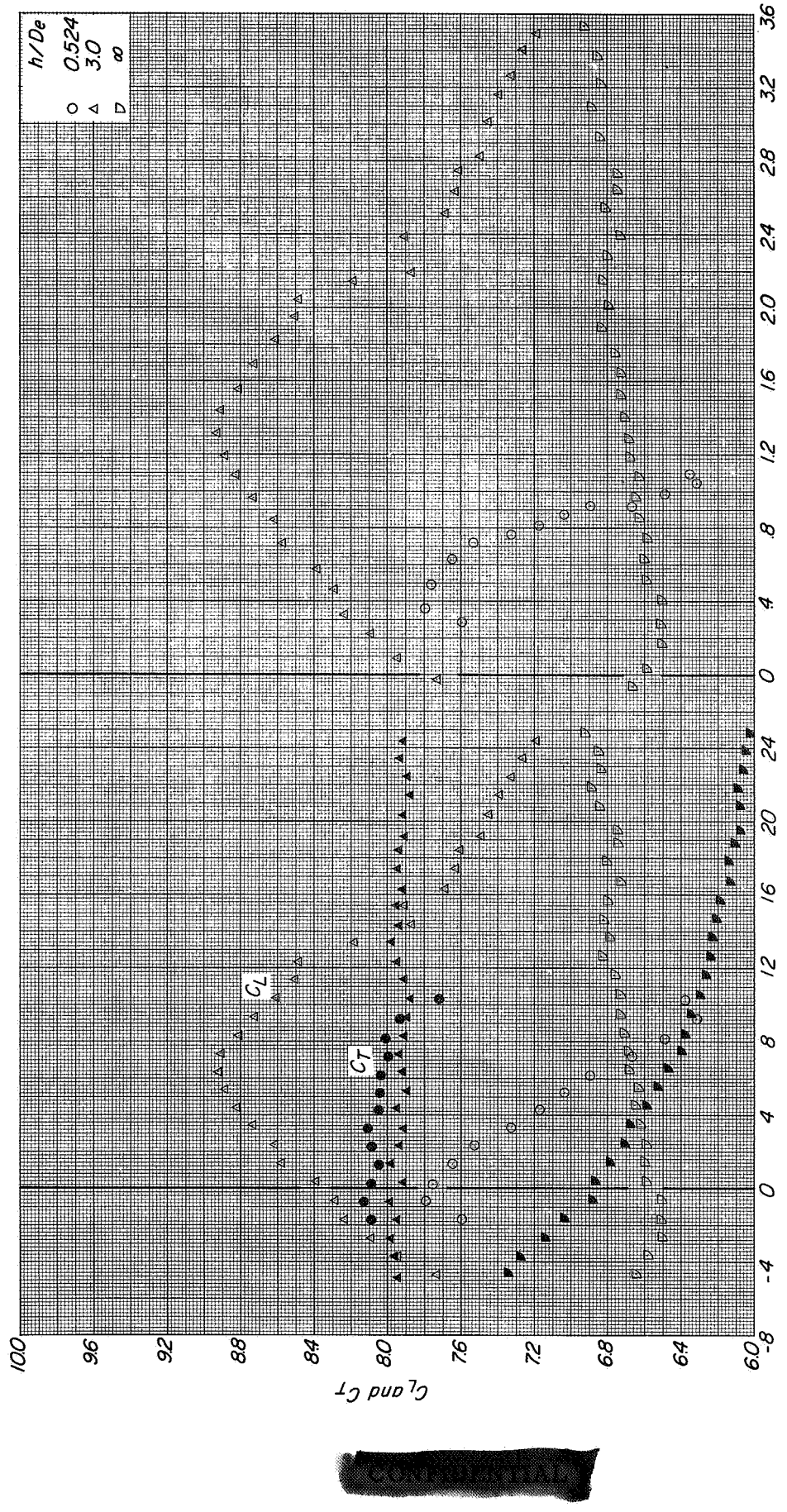

(a) Variation of C_L and C_T with α and C_D with C_L.

Figure 62.- Longitudinal aerodynamic characteristics of configuration B with direct-lift and lift-cruise engines deflected 90°. $i_t = 0°$; $\beta = 0°$; $C_T \approx 8$.

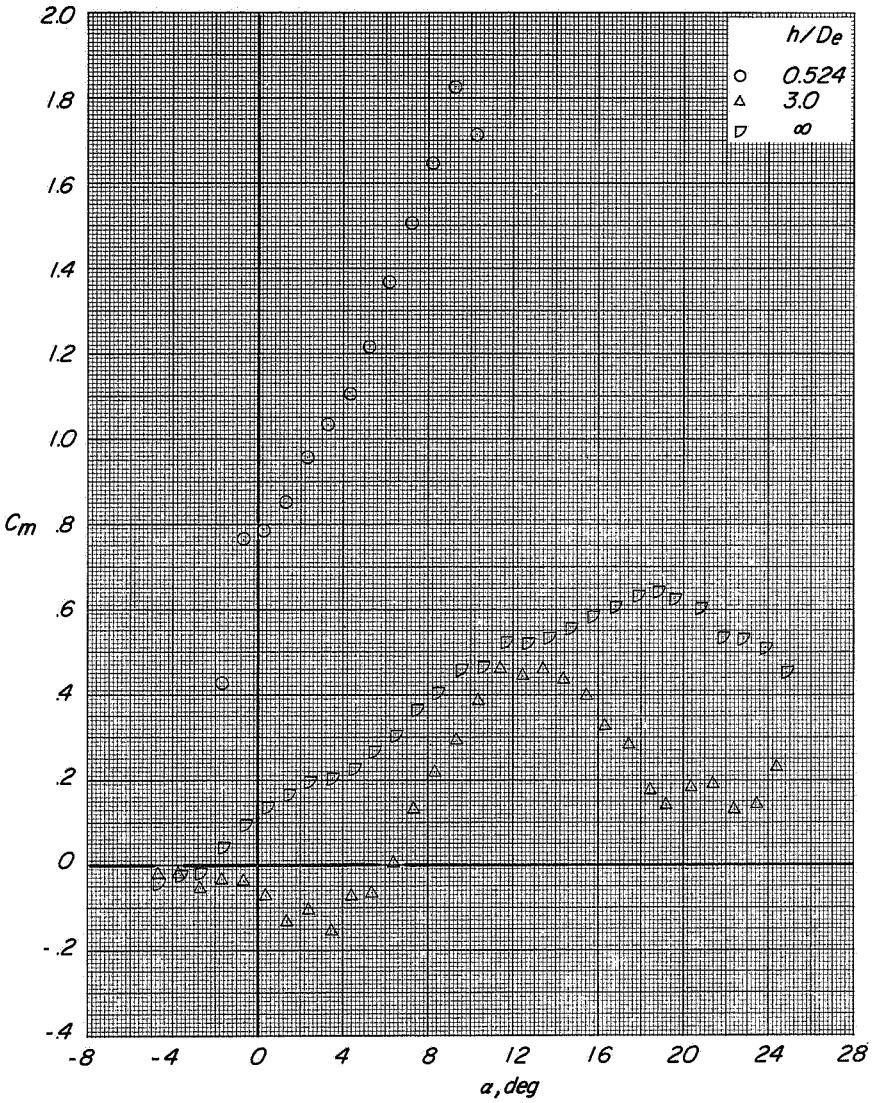

(b) Variation of C_m with α.

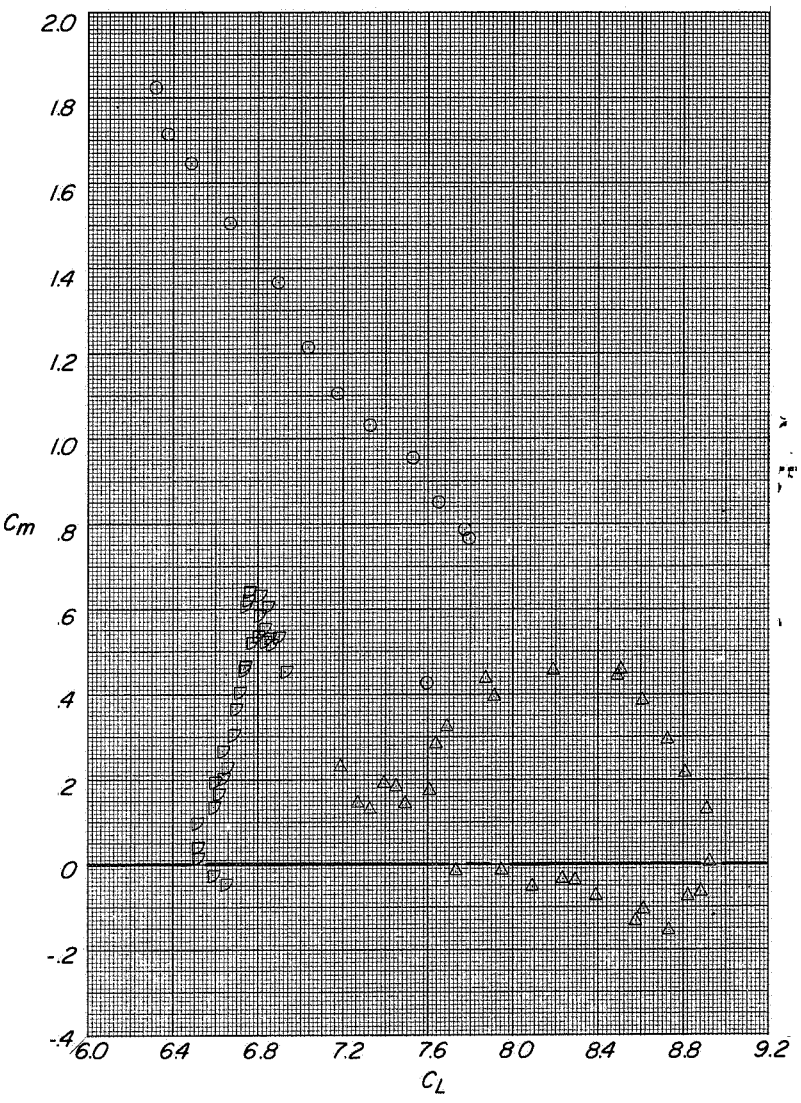

(c) Variation of C_m with C_L.

Figure 62. Continued.

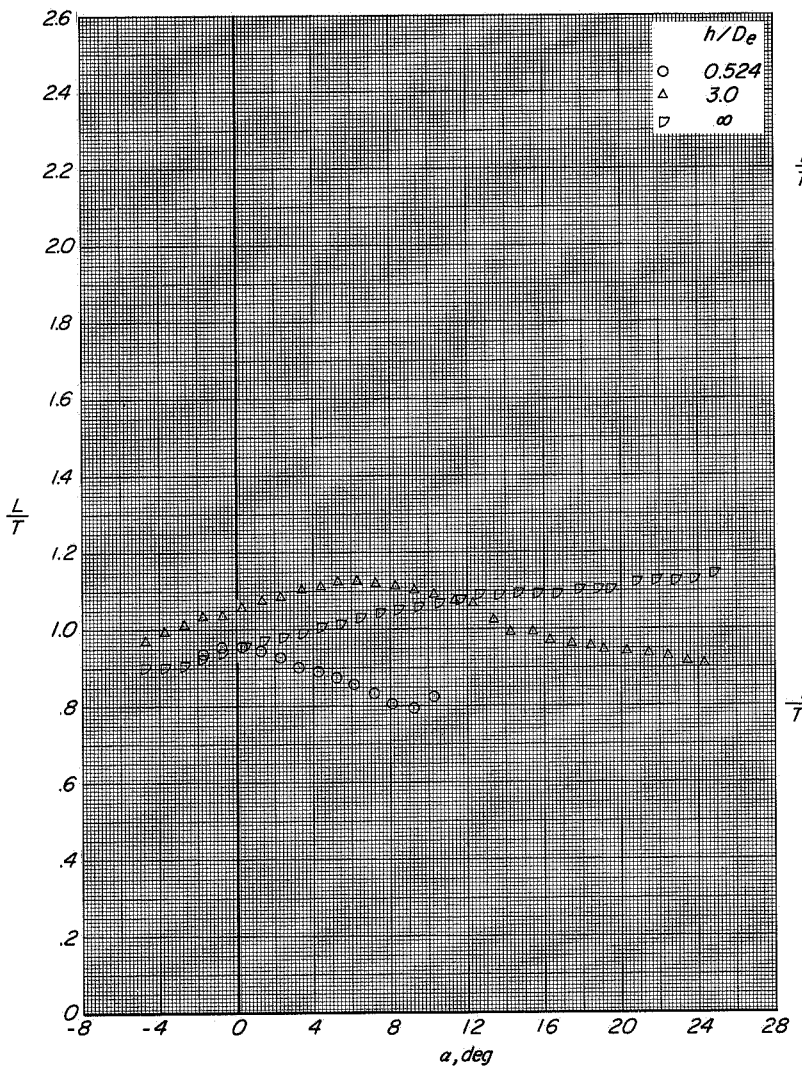

(d) Variation of L/T with α.

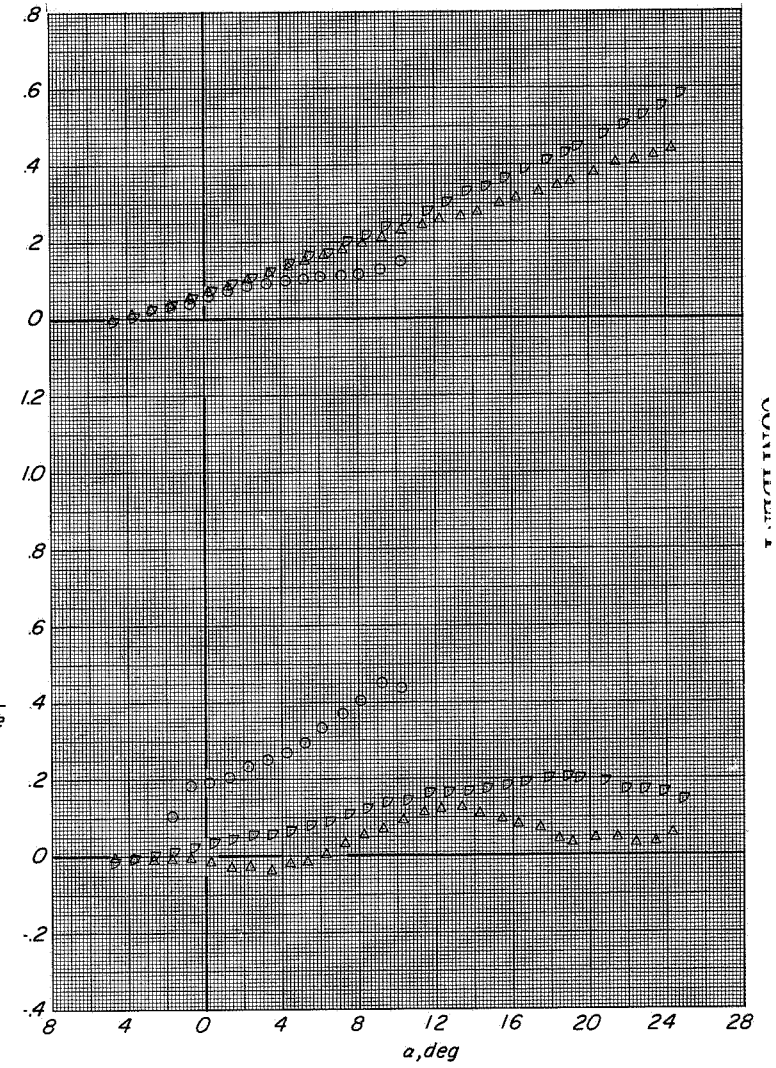

(e) Variation of D/T and M/TDe with α.

Figure 62.- Concluded.

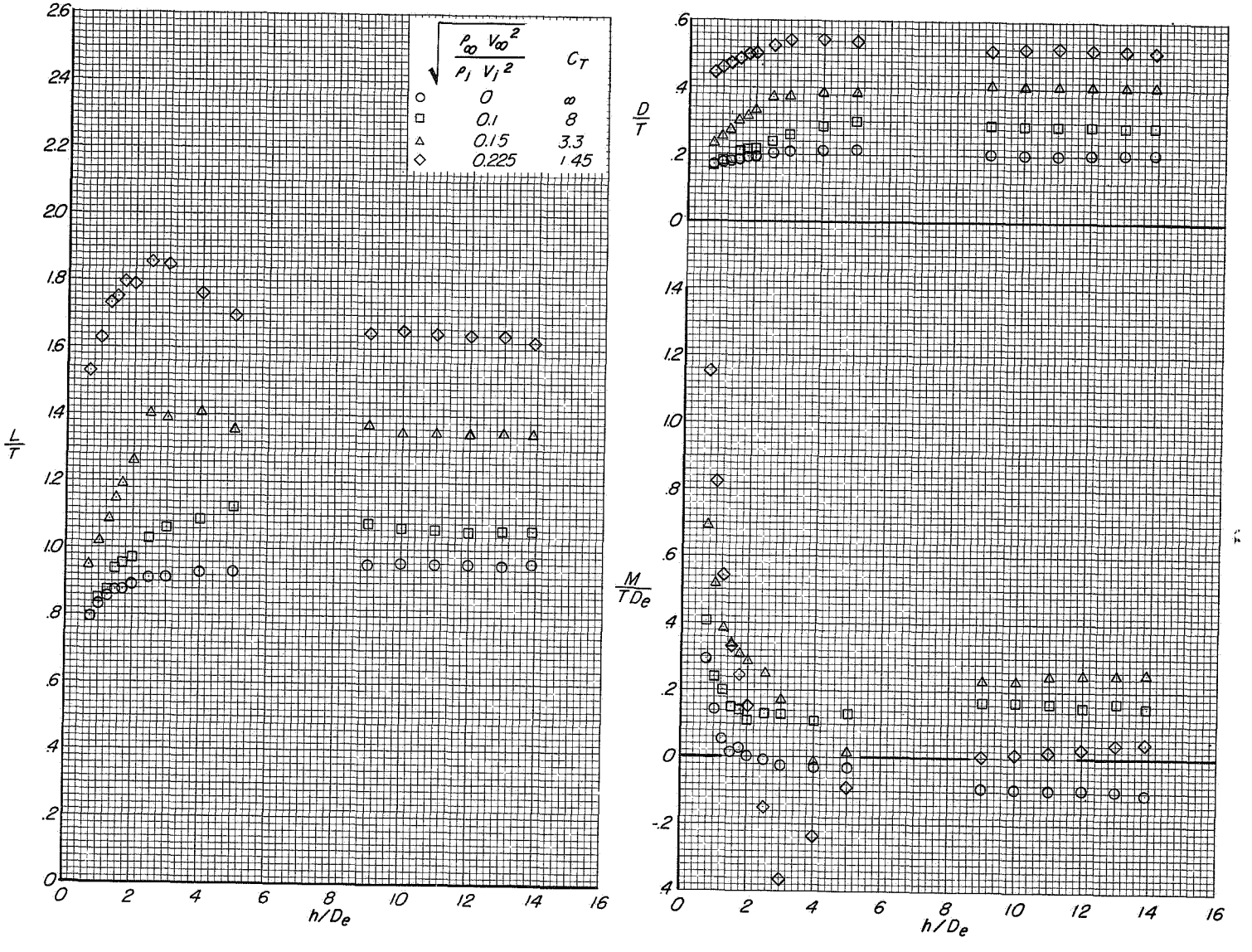

(a) Variation of L/T with h/D_e.

(b) Variation of D/T and M/TD_e with h/D_e.

Figure 63.- Effect of height above the moving-belt ground plane on the longitudinal aerodynamic characteristics of configuration B with direct-lift and lift-cruise engines deflected 90°. $i_t = 0°$; $\beta = 0°$; $\alpha = 12.5°$.

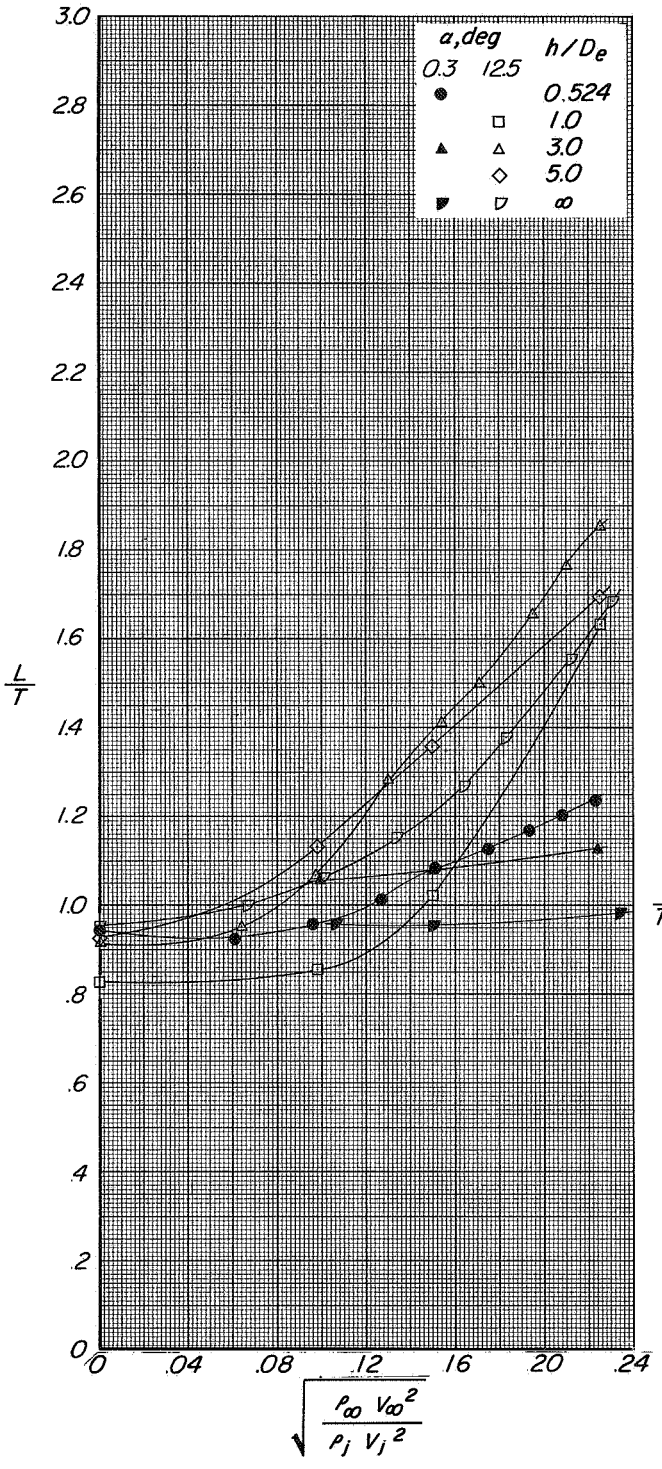

(a) Variation of L/T with effective velocity ratio.

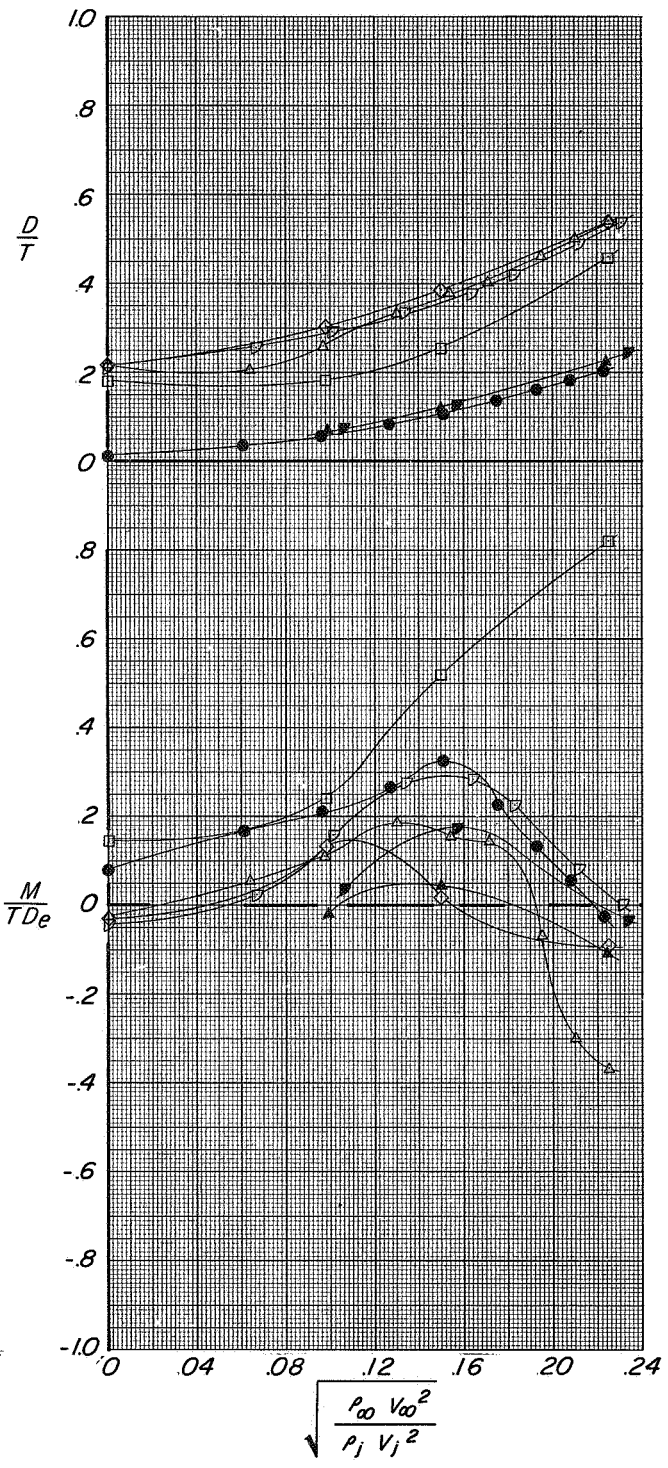

(b) Variation of D/T and M/TD_e with effective velocity ratio.

Figure 64.- Effect of effective velocity ratio on the longitudinal aerodynamic characteristics of configuration B with direct-lift and lift-cruise engines deflected 90^0. $i_t = 0^0$; $\beta = 0^0$

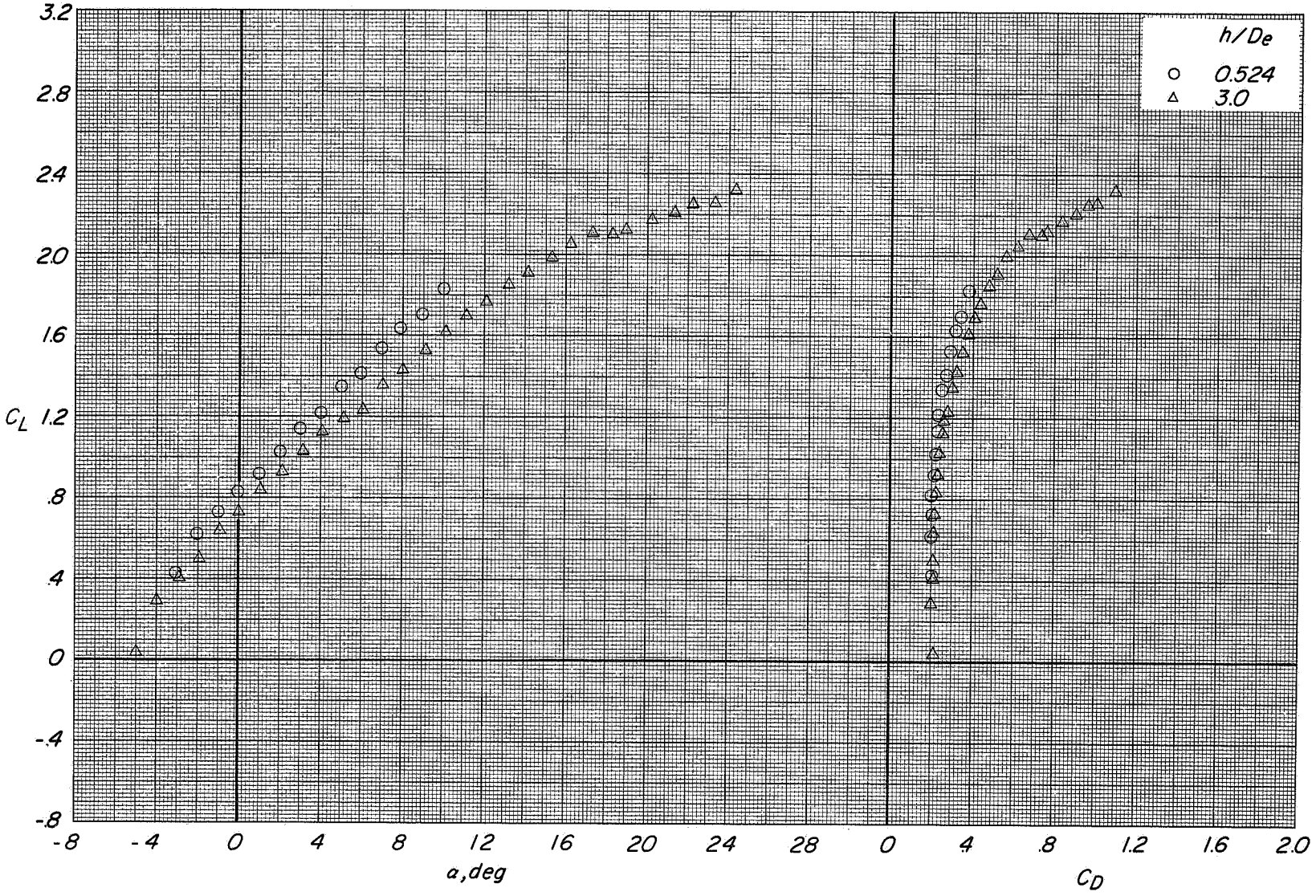

(a) Variation of C_L with α and C_D with C_L

Figure 65.- Longitudinal aerodynamic characteristics of configuration A with direct-lift and lift-cruise engines deflected 90°. $i_t = 0°$; $\beta = 5°$; $C_T = 0$.

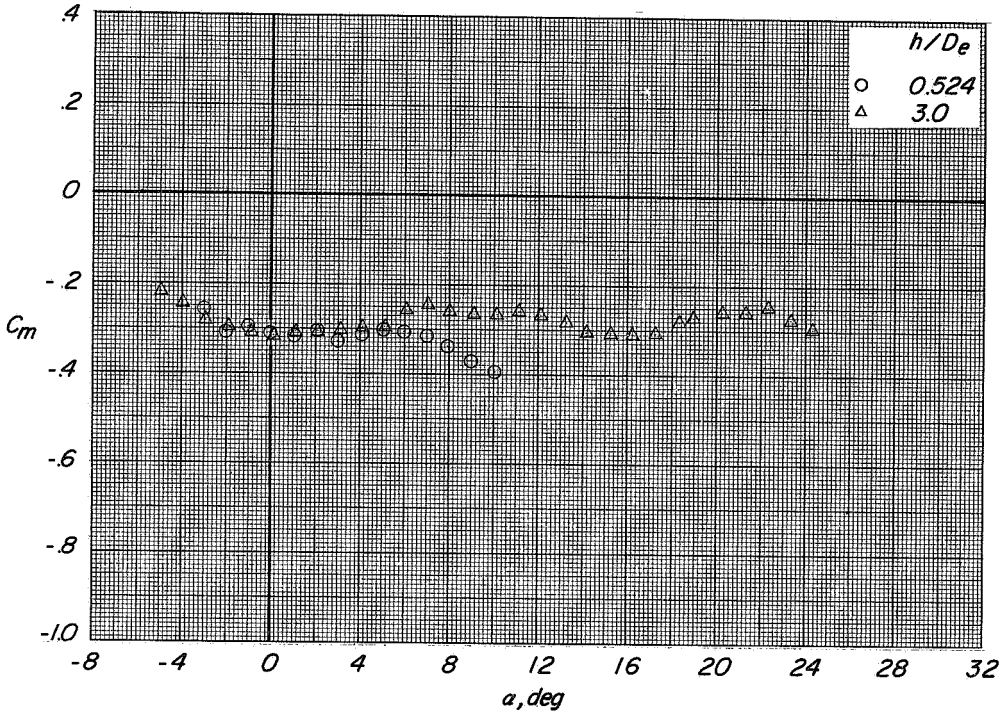

(b) Variation of C_m with α.

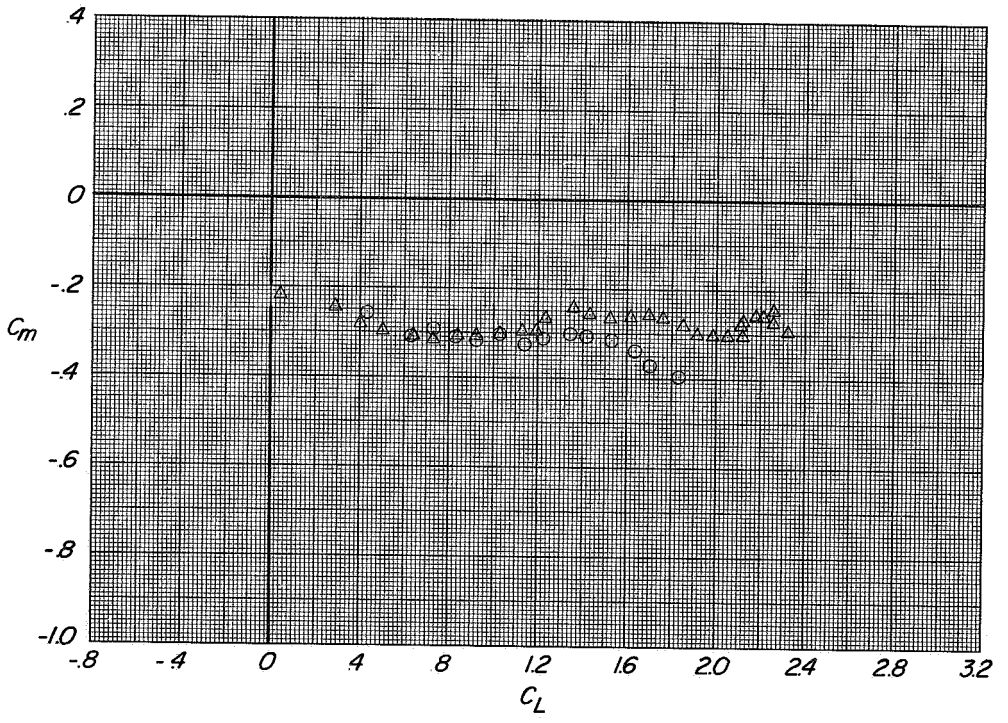

(c) Variation of C_m with C_L.

Figure 65.- Concluded.

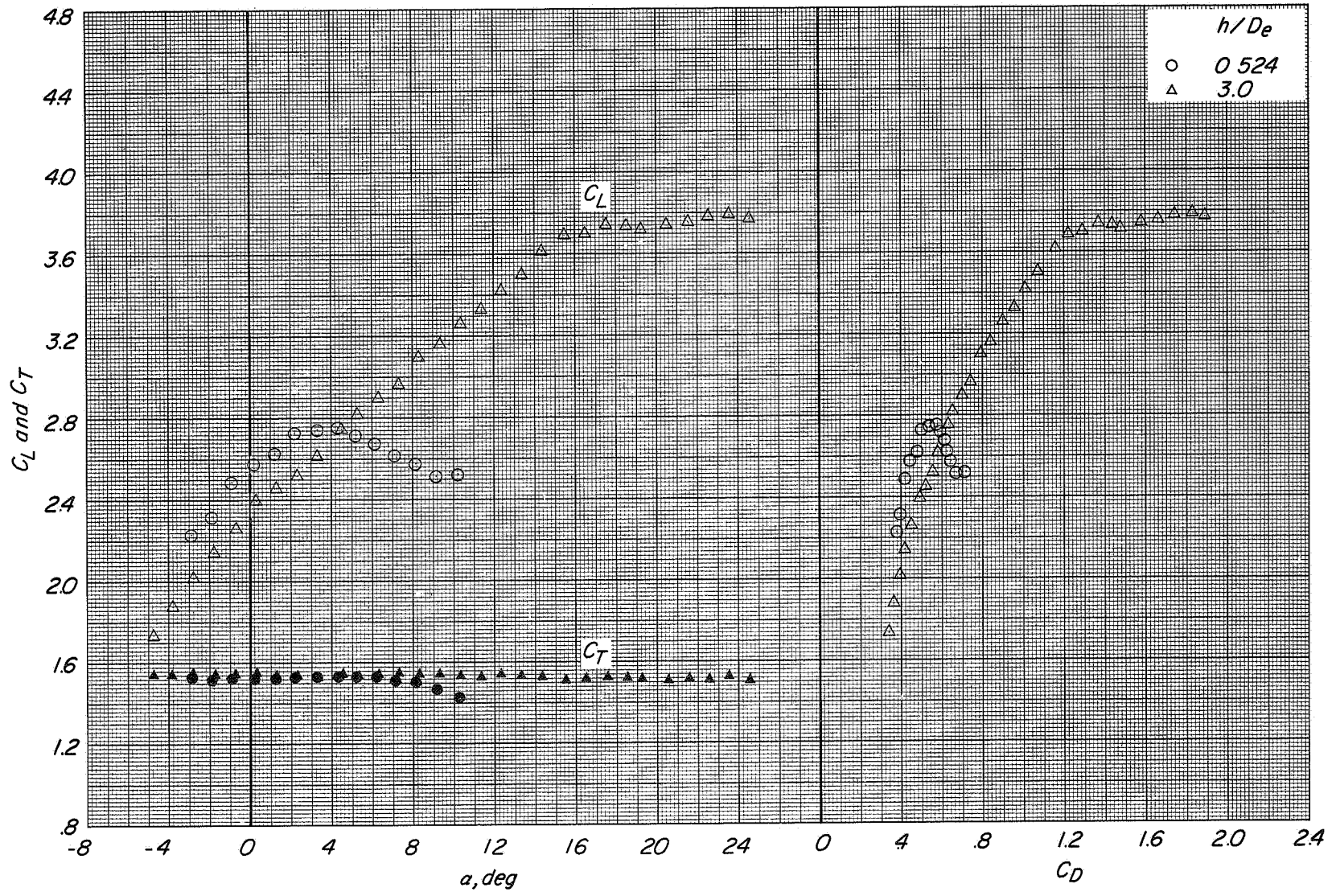

(a) Variation of C_L and C_T with α and C_D with C_L

Figure 66.- Longitudinal aerodynamic characteristics of configuration A with direct-lift and lift-cruise engines deflected 90^0 $i_t = 0^0$: $\beta = 5^0$: $C_T \approx 1.45$.

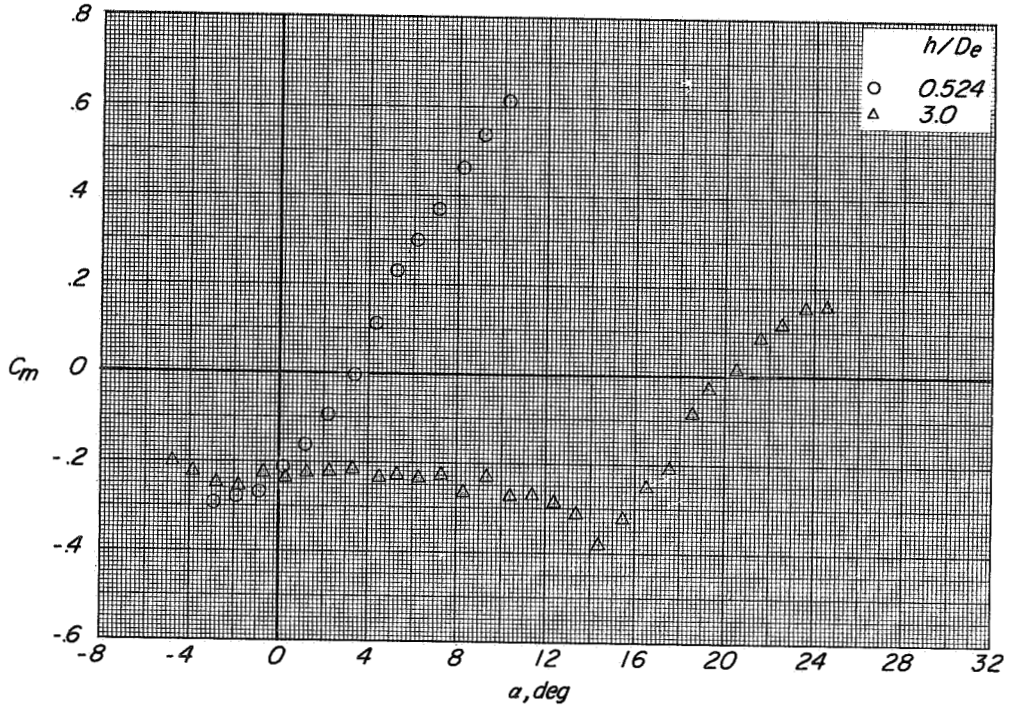

(b) Variation of C_m with α.

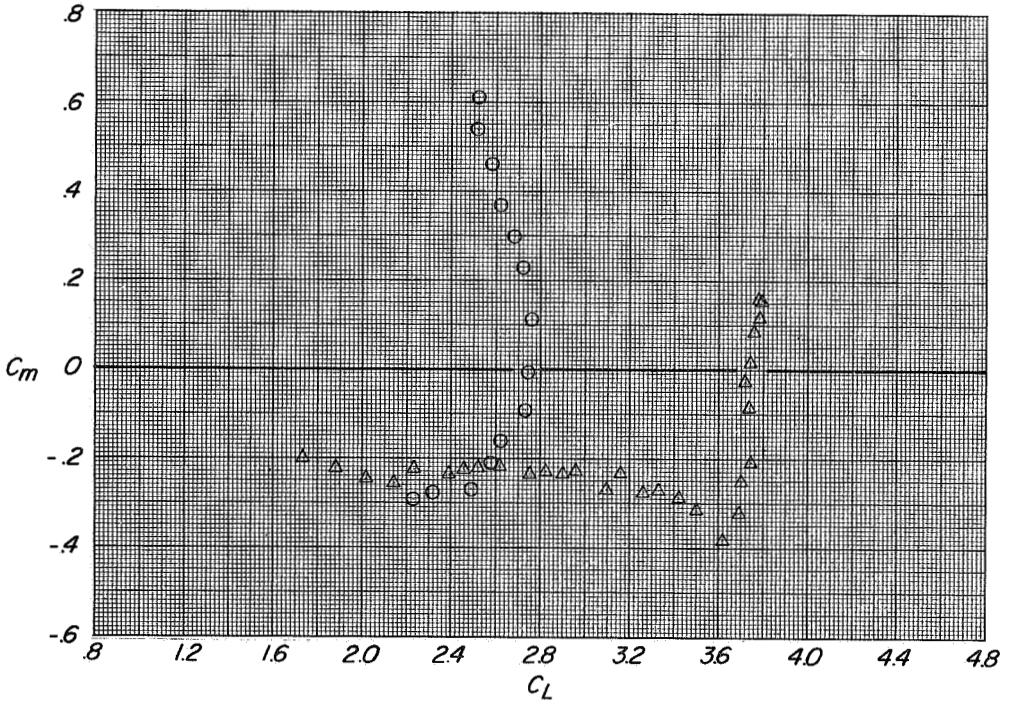

(c) Variation of C_m with C_L.

Figure 66.- Continued.

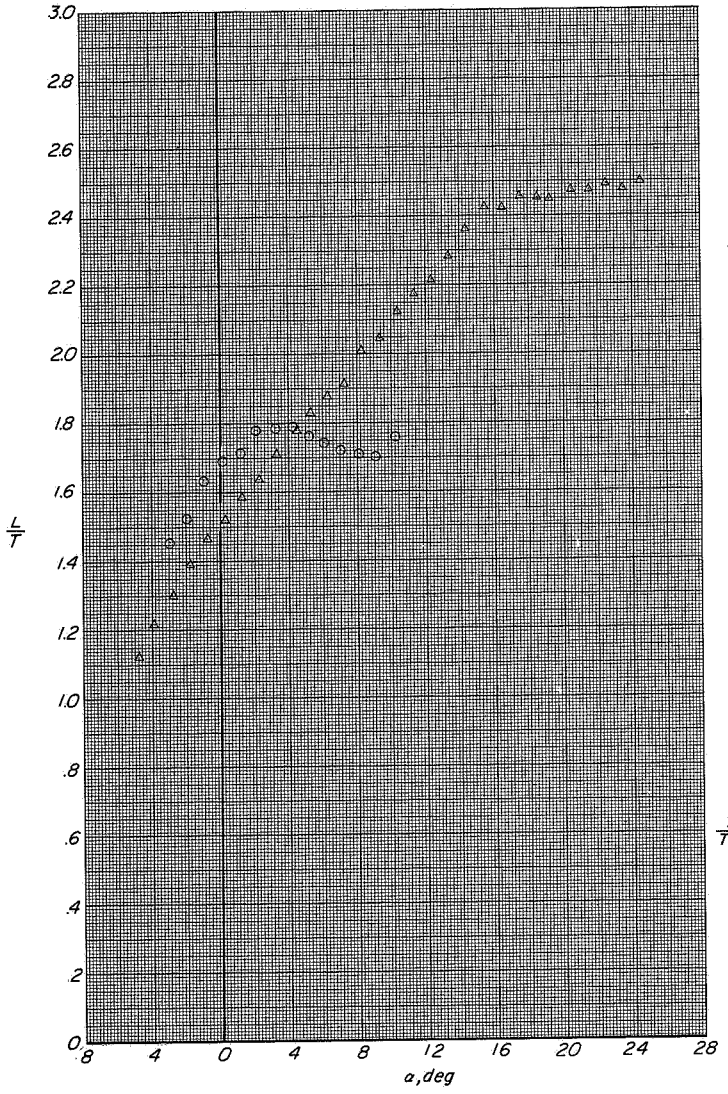

(d) Variation of L/T with α.

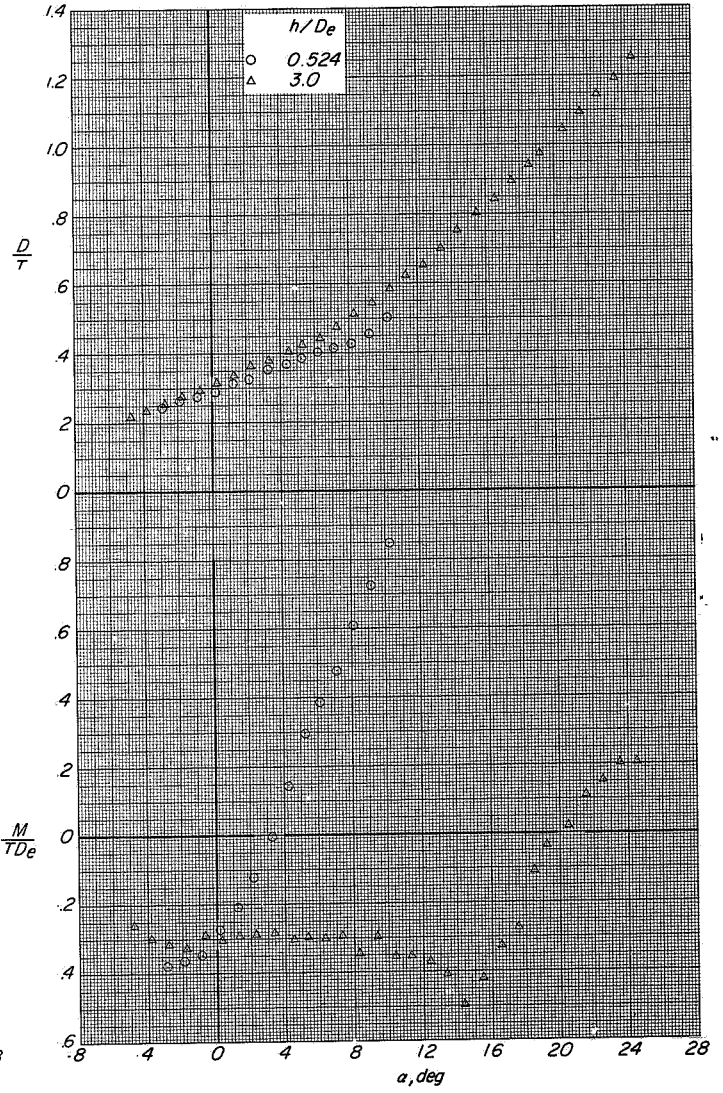

(e) Variation of D/T and M/TDe with α.

Figure 66. Concluded.

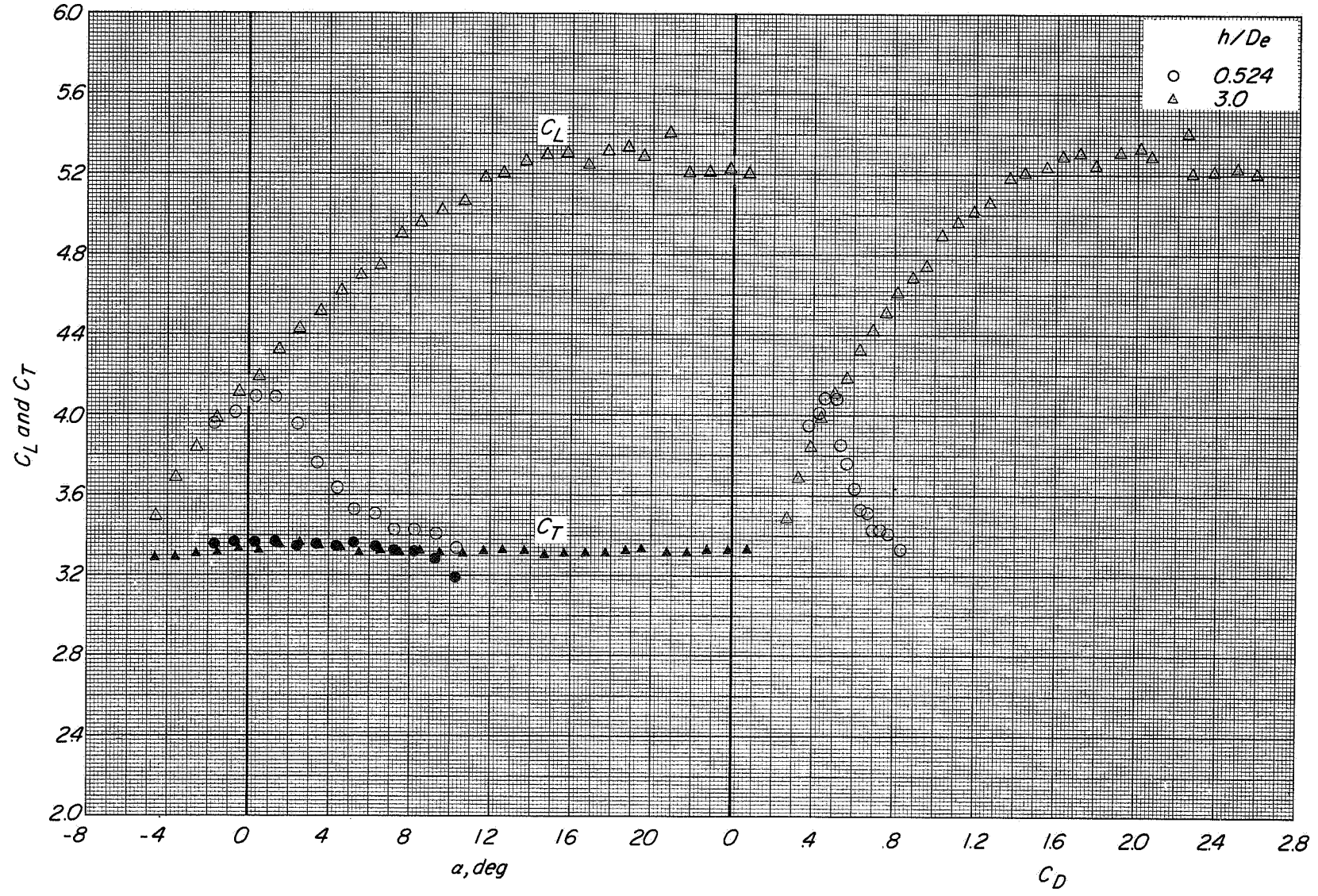

(a) Variation of C_L and C_T with α and C_D with C_L

Figure 67.- Longitudinal aerodynamic characteristics of configuration A with direct-lift and lift-cruise engines deflected 90^0. $i_t = 0^0$; $\beta = 5^0$; $C_T \approx 3.3$.

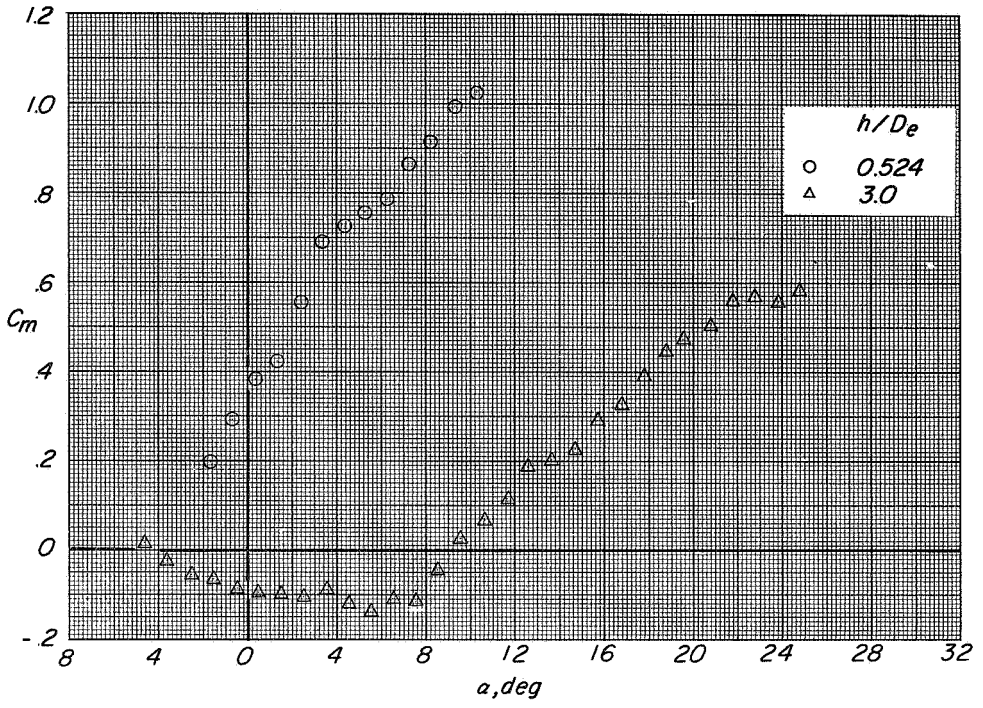

(b) Variation of C_m with α.

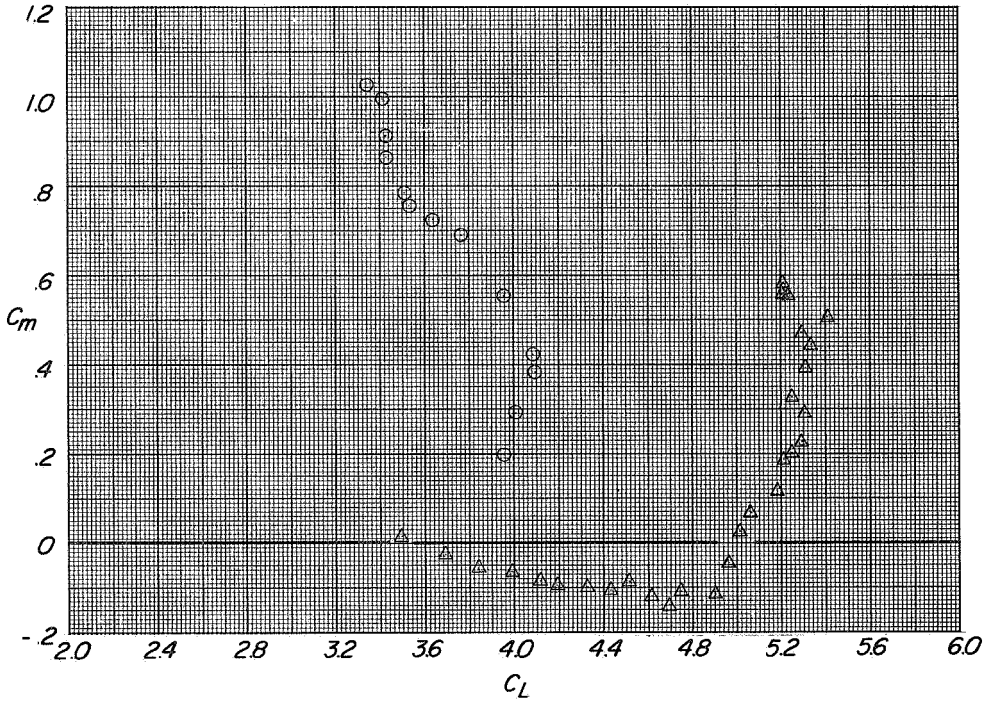

(c) Variation of C_m with C_L.

Figure 67 - Continued.

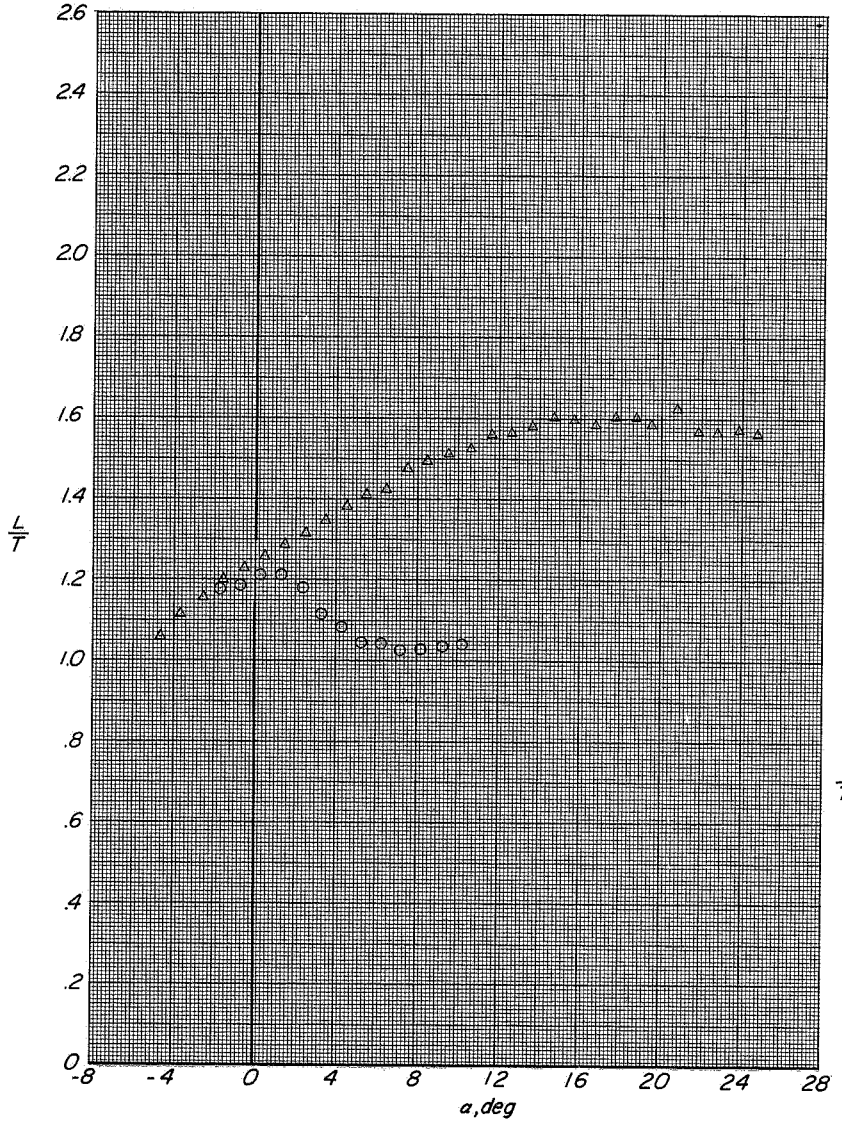

(d) Variation of L/T with α.

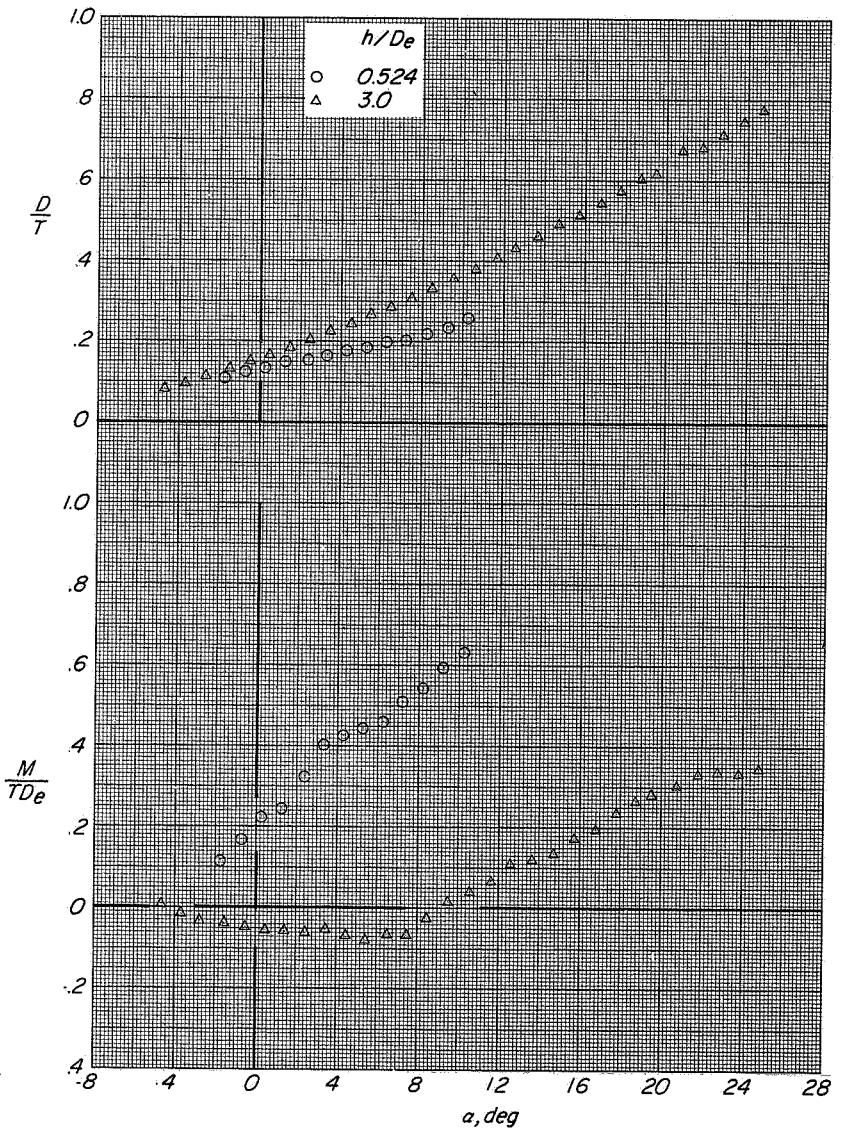

(e) Variation of D/T and M/TD_e with α.

Figure 67.- Concluded.

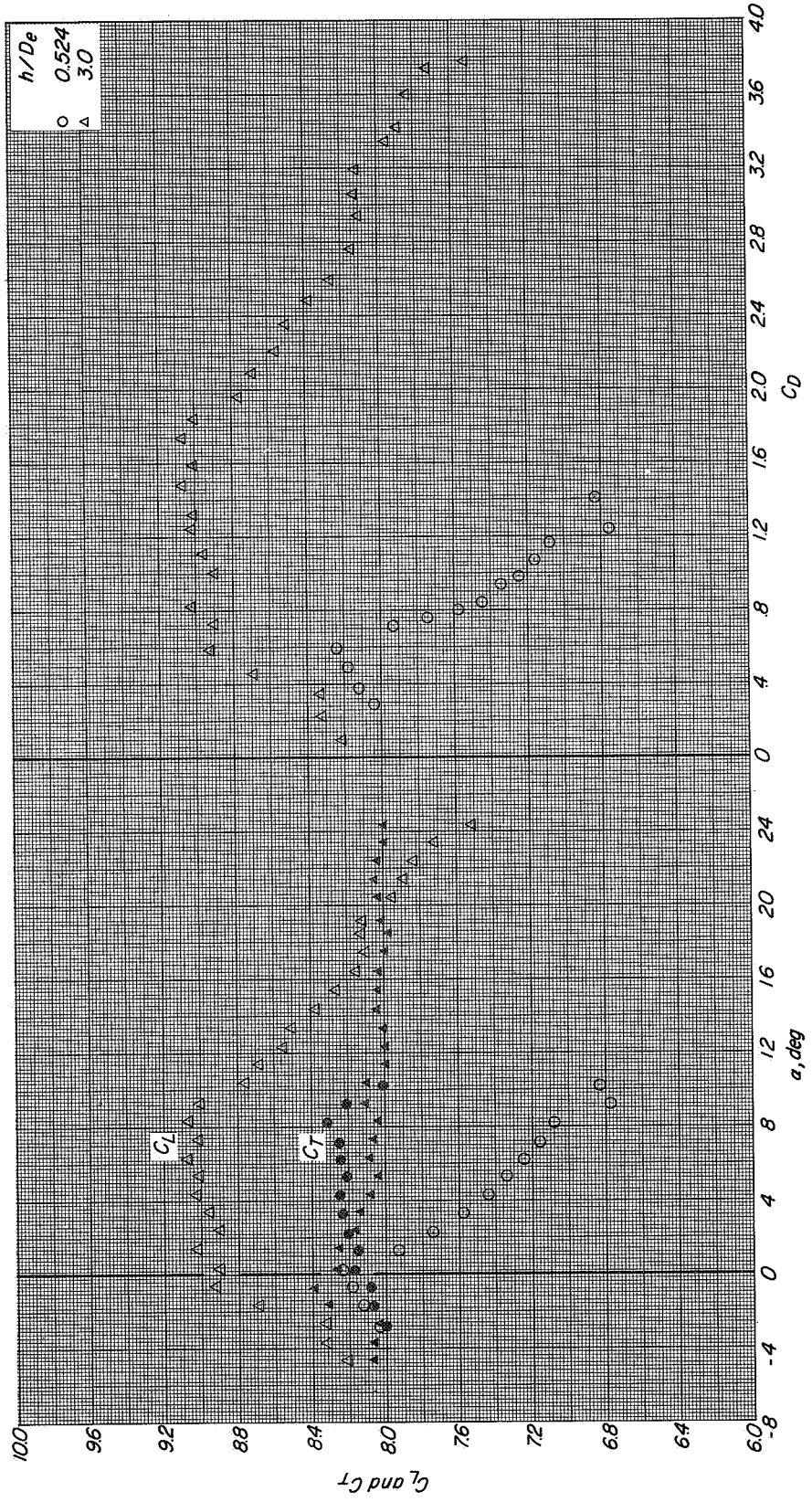

(a) Variation of C_L and C_T with α and C_D with C_L

Figure 68.- Longitudinal aerodynamic characteristics of configuration A with direct-lift and lift-cruise engines deflected 90°. $i_t = 0°$; $\beta = 5°$; $C_T \approx 8$.

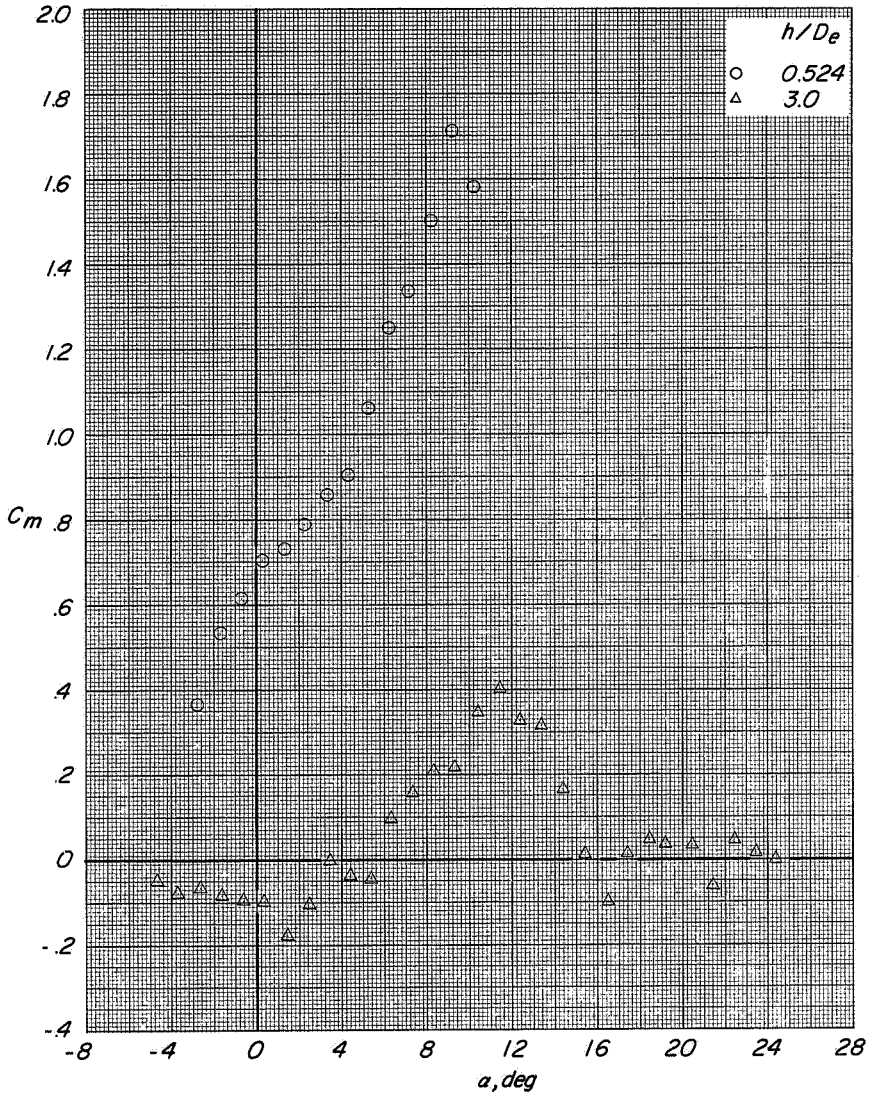

(b) Variation of C_m with α.

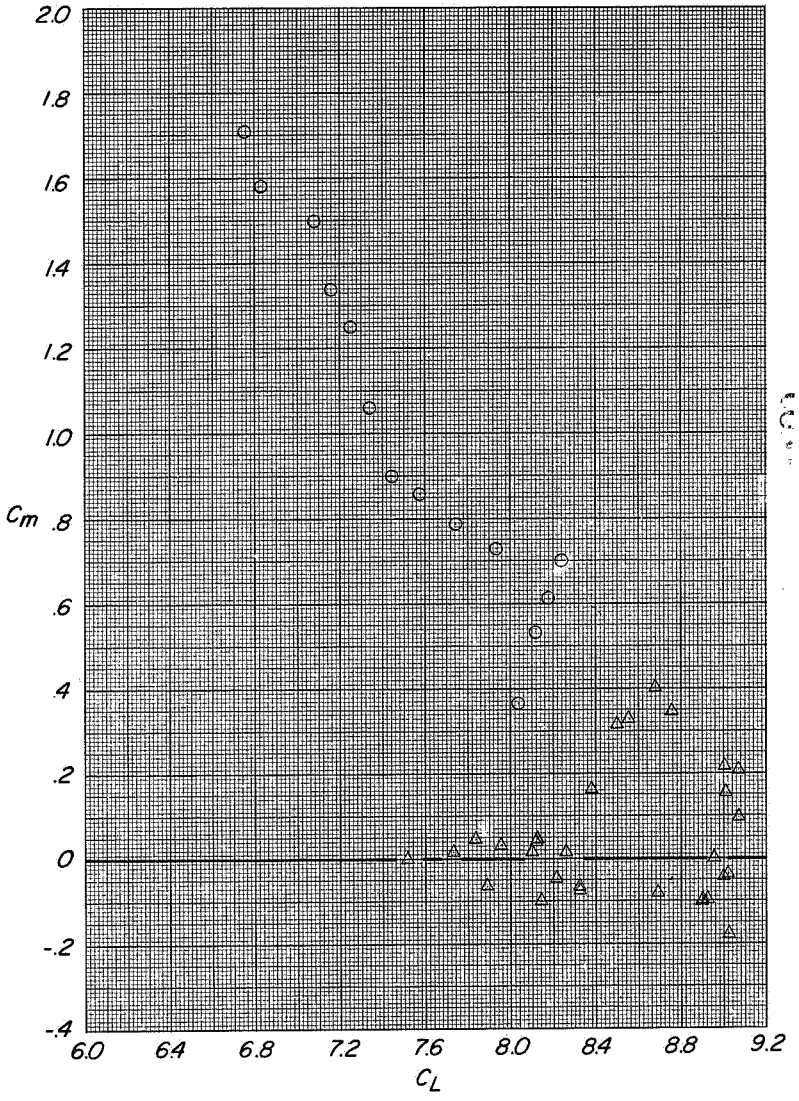

(c) Variation of C_m with C_L.

Figure 68.- Continued.

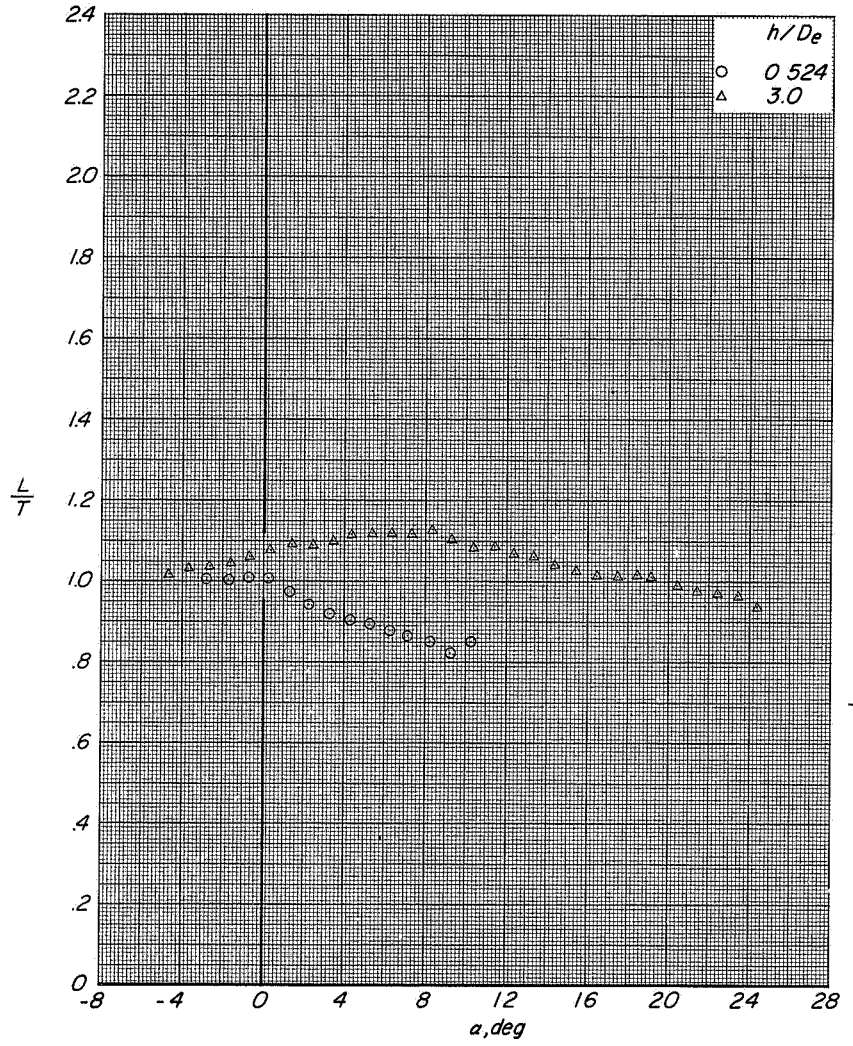

(d) Variation of L/T with α.

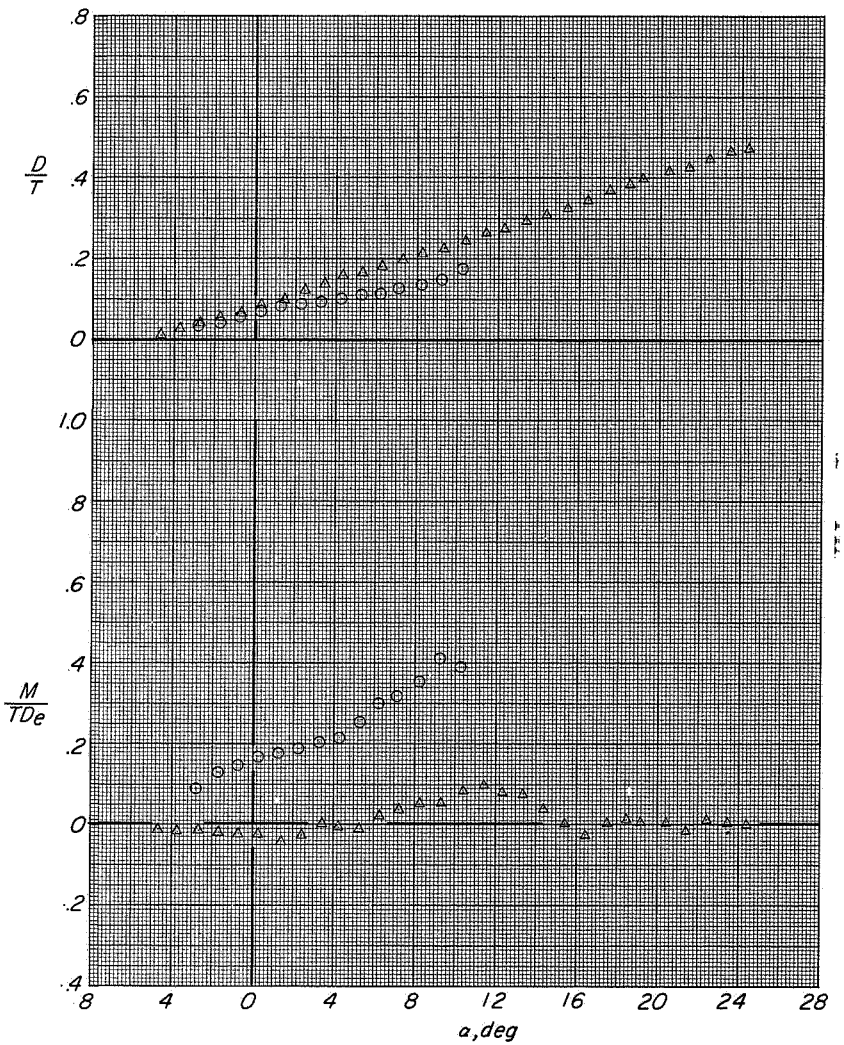

(e) Variation of D/T and M/TD_e with α.

Figure 68. Concluded.

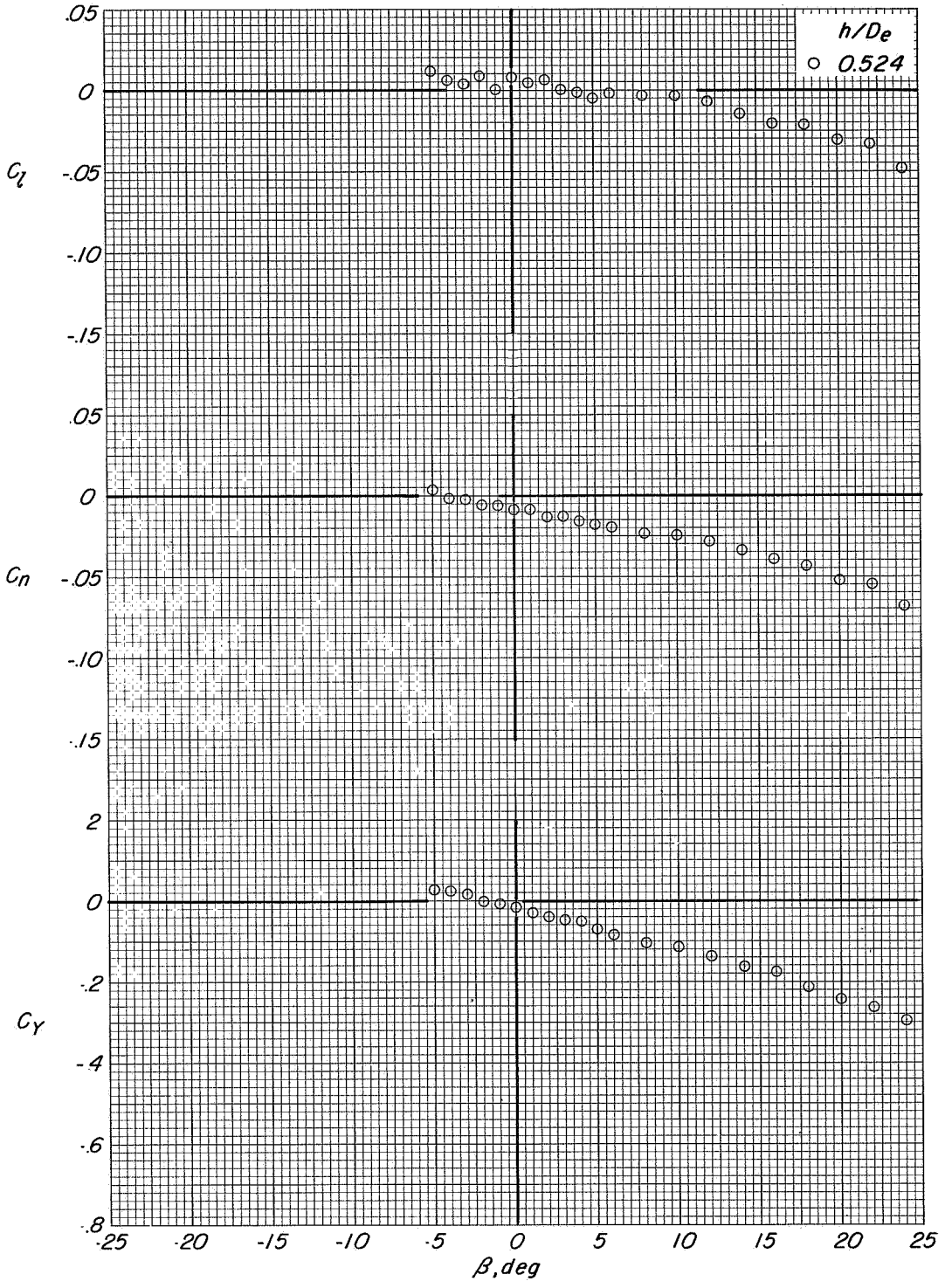

Figure 69.- Lateral aerodynamic characteristics of configuration A with direct-lift and lift-cruise engines deflected 90^0. $i_t = 0^0$: $\alpha = 0^0$: $C_T = 0$.

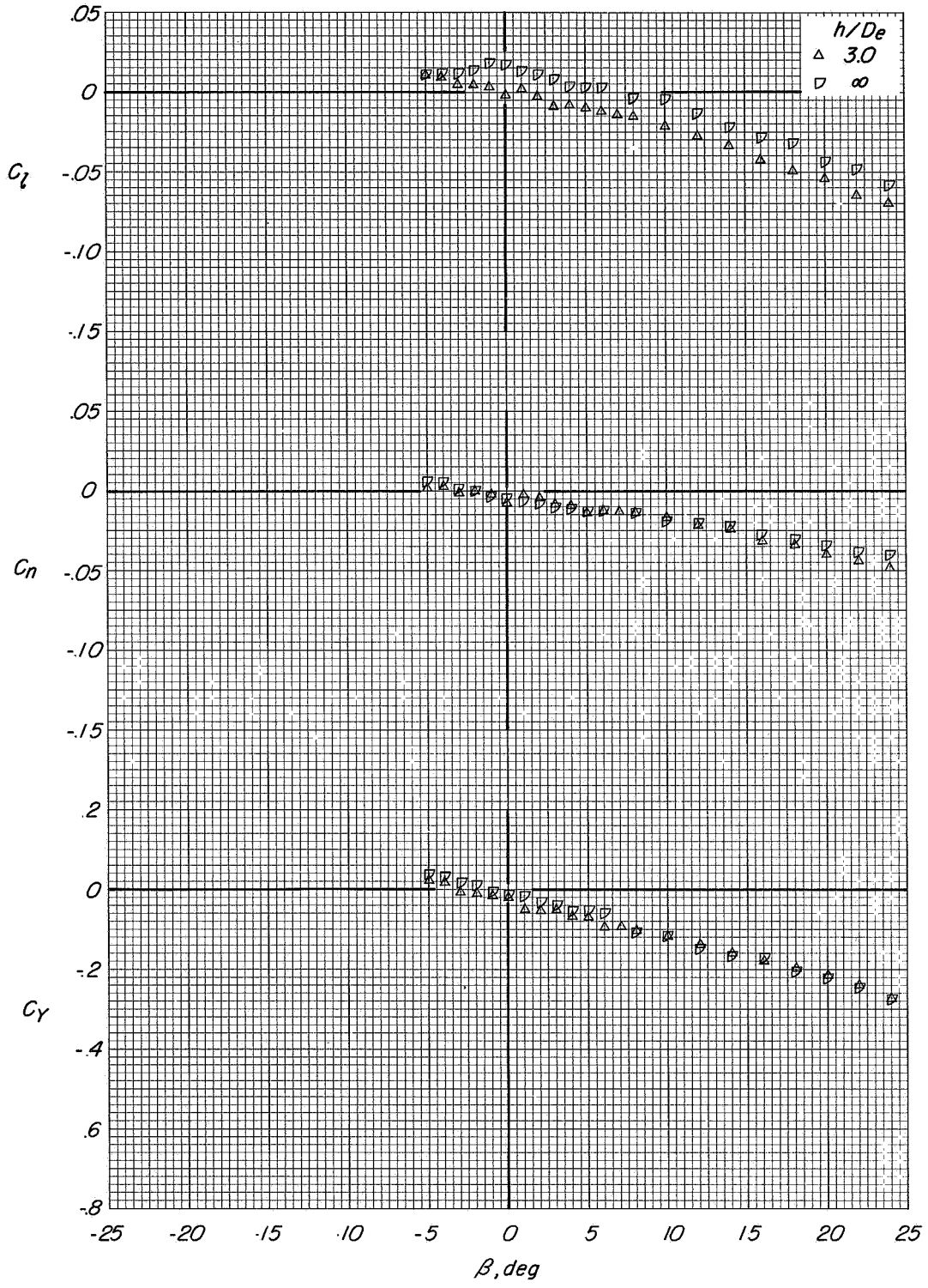

Figure 70.- Lateral aerodynamic characteristics of configuration A with direct-lift and lift-cruise engines deflected 90°. $i_t = 0°$; $\alpha = 12.3°$; $C_T = 0$.

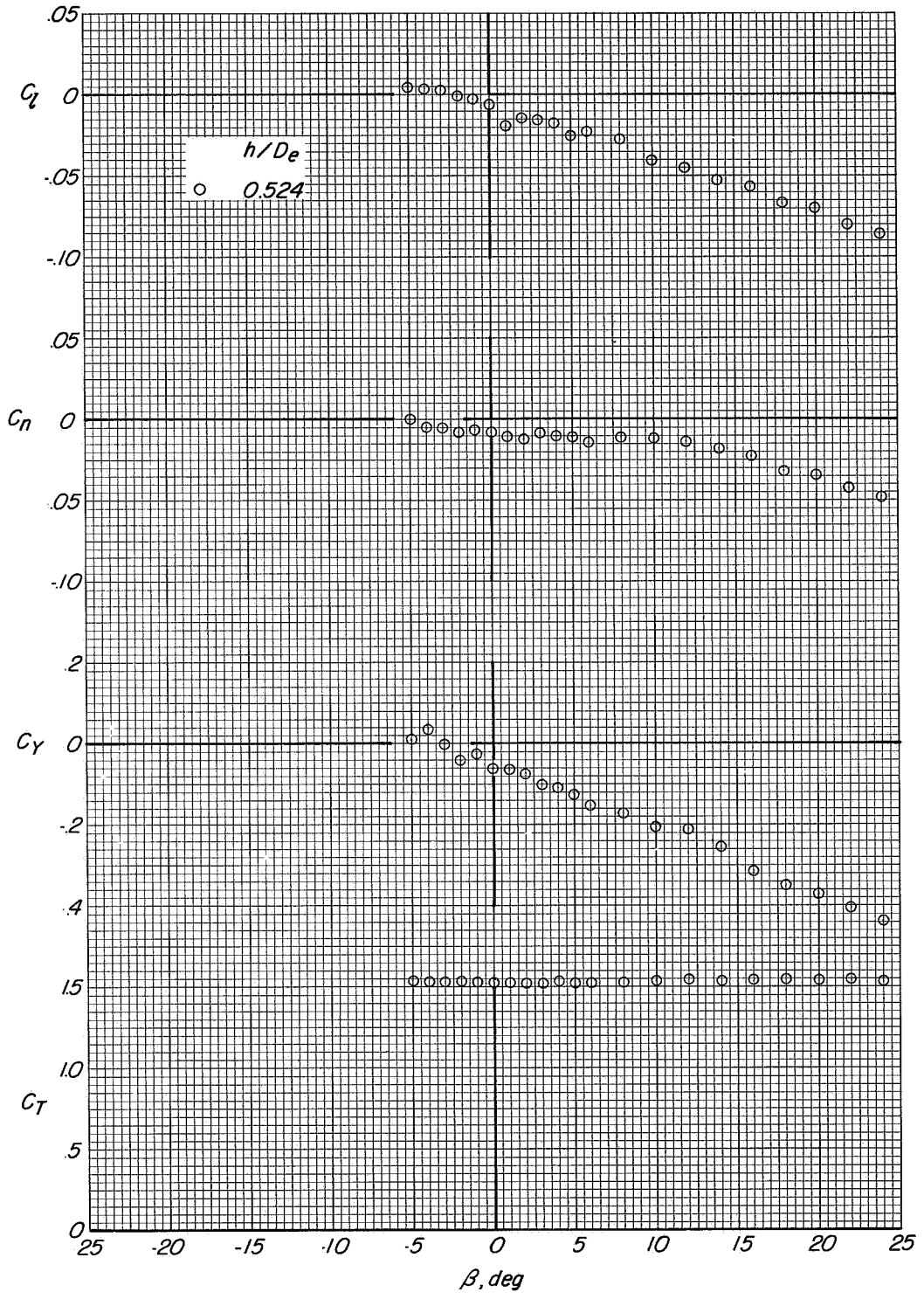

Figure 71.- Lateral aerodynamic characteristics of configuration A with direct-lift and lift-cruise engines deflected 90^0 $i_t = 0^0$: $\alpha = 0.2^0$; $C_T \approx 1.45$.

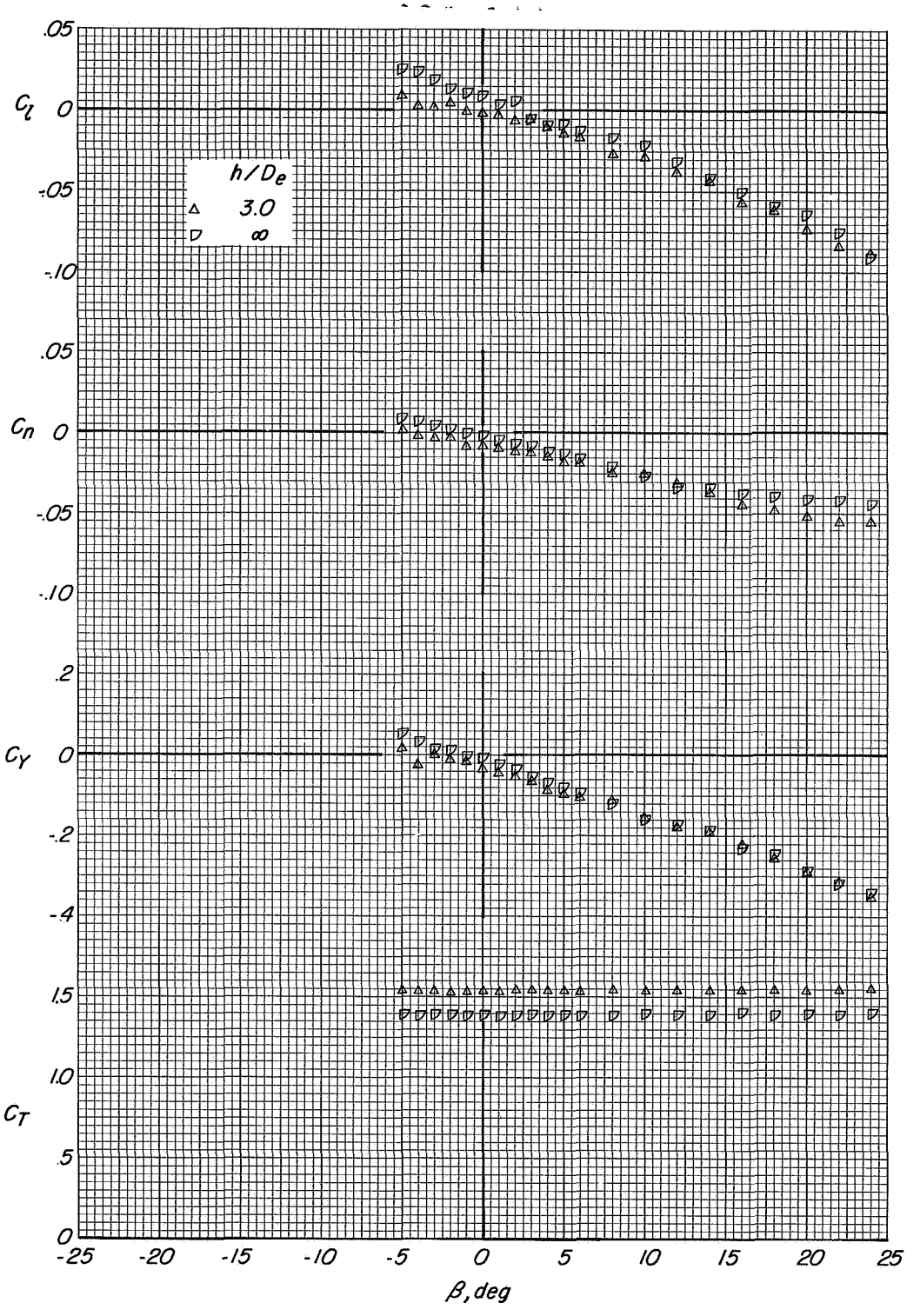

Figure 72.- Lateral aerodynamic characteristics of configuration A with direct-lift and lift-cruise engines deflected 90°. $i_t = 0°$; $\alpha = 12.5°$; $C_T \approx 1.45$.

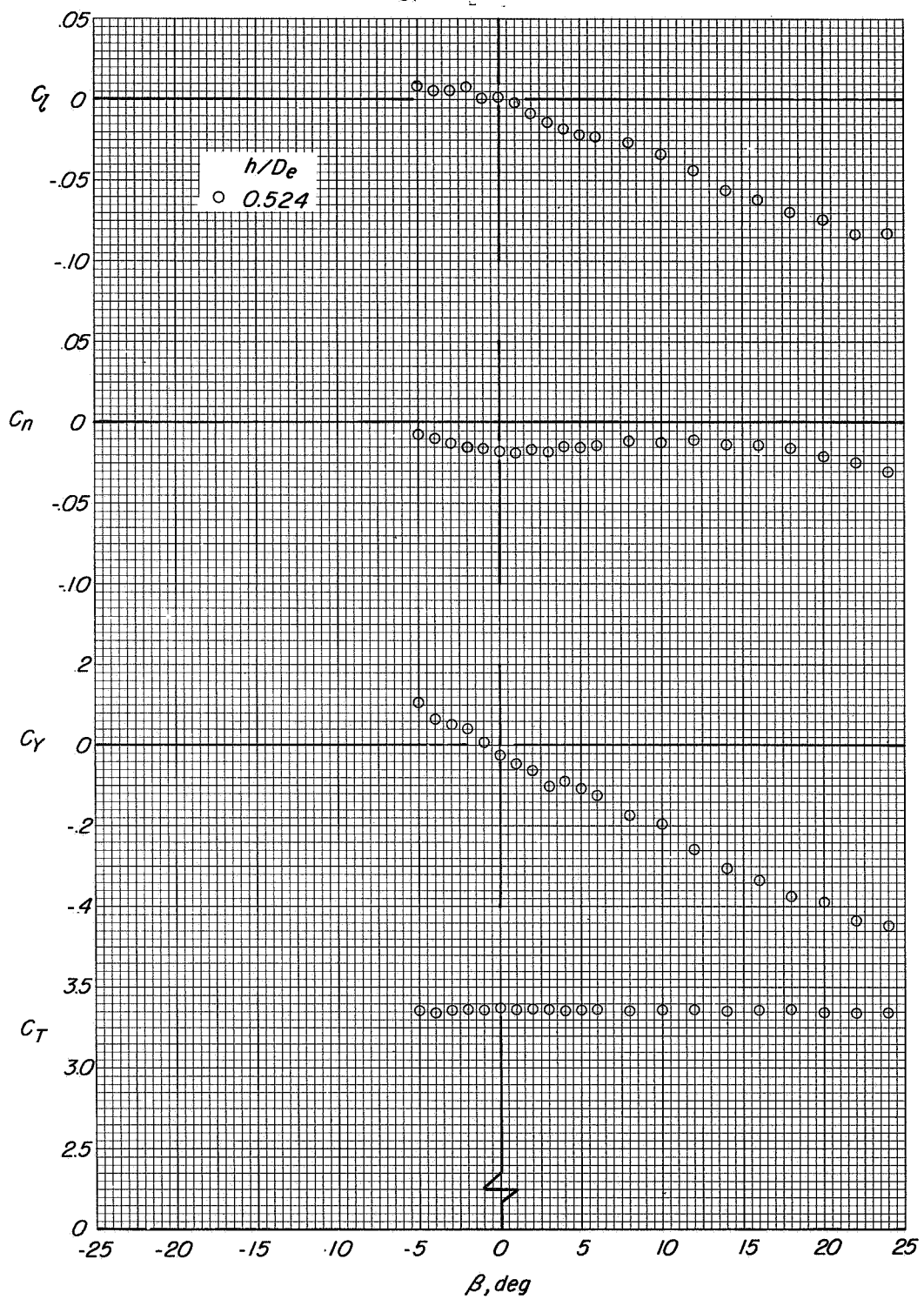

Figure 73.- Lateral aerodynamic characteristics of configuration A with direct-lift and lift-cruise engines deflected 90^0. $i_t = 0^0$; $\alpha = 0.3^0$; $C_T \approx 3.3$.

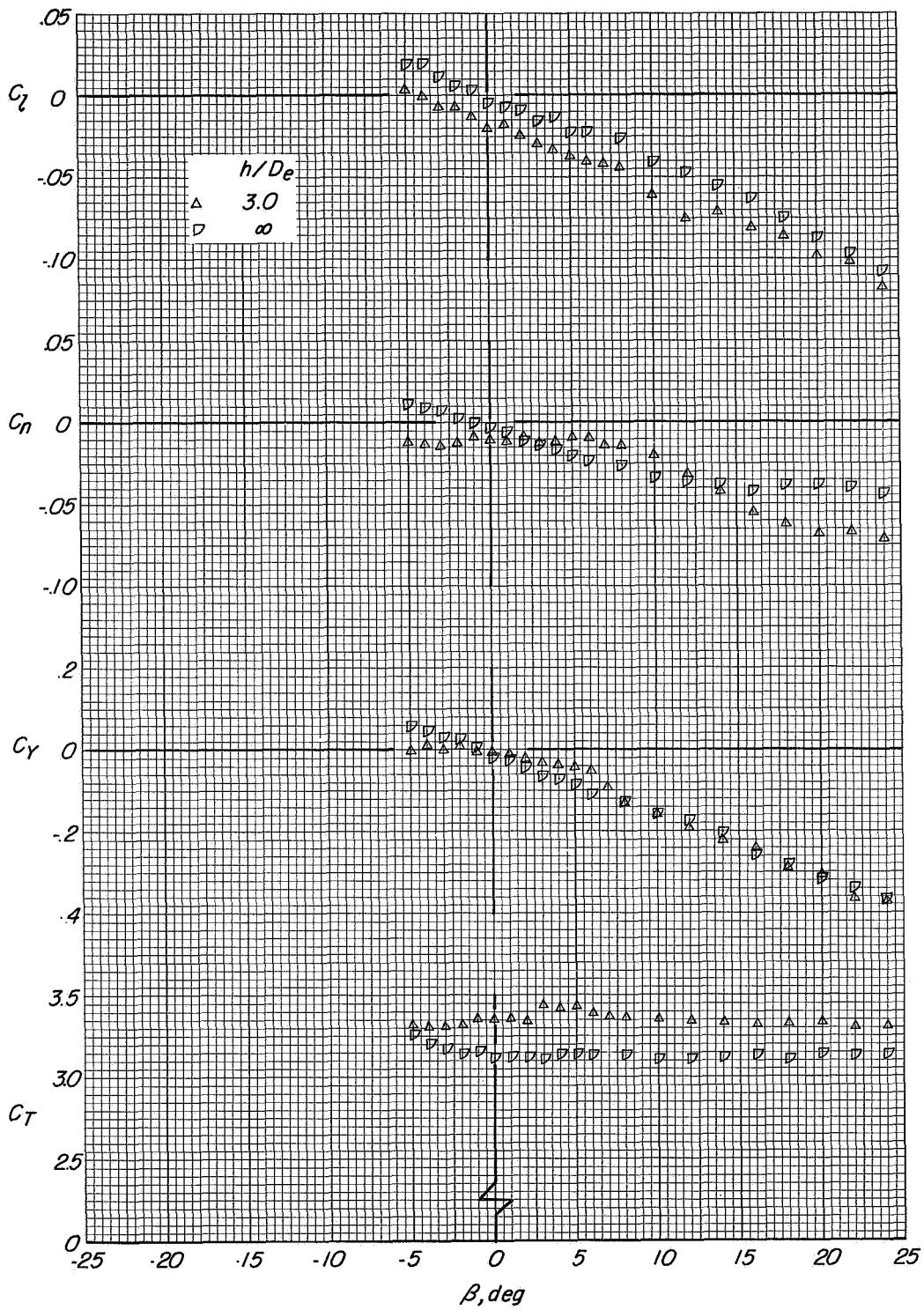

Figure 74.- Lateral aerodynamic characteristics of configuration A with direct-lift and lift-cruise engines deflected 90°. $i_t = 0°$; $\alpha = 12.7°$; $C_T \approx 3.3$.

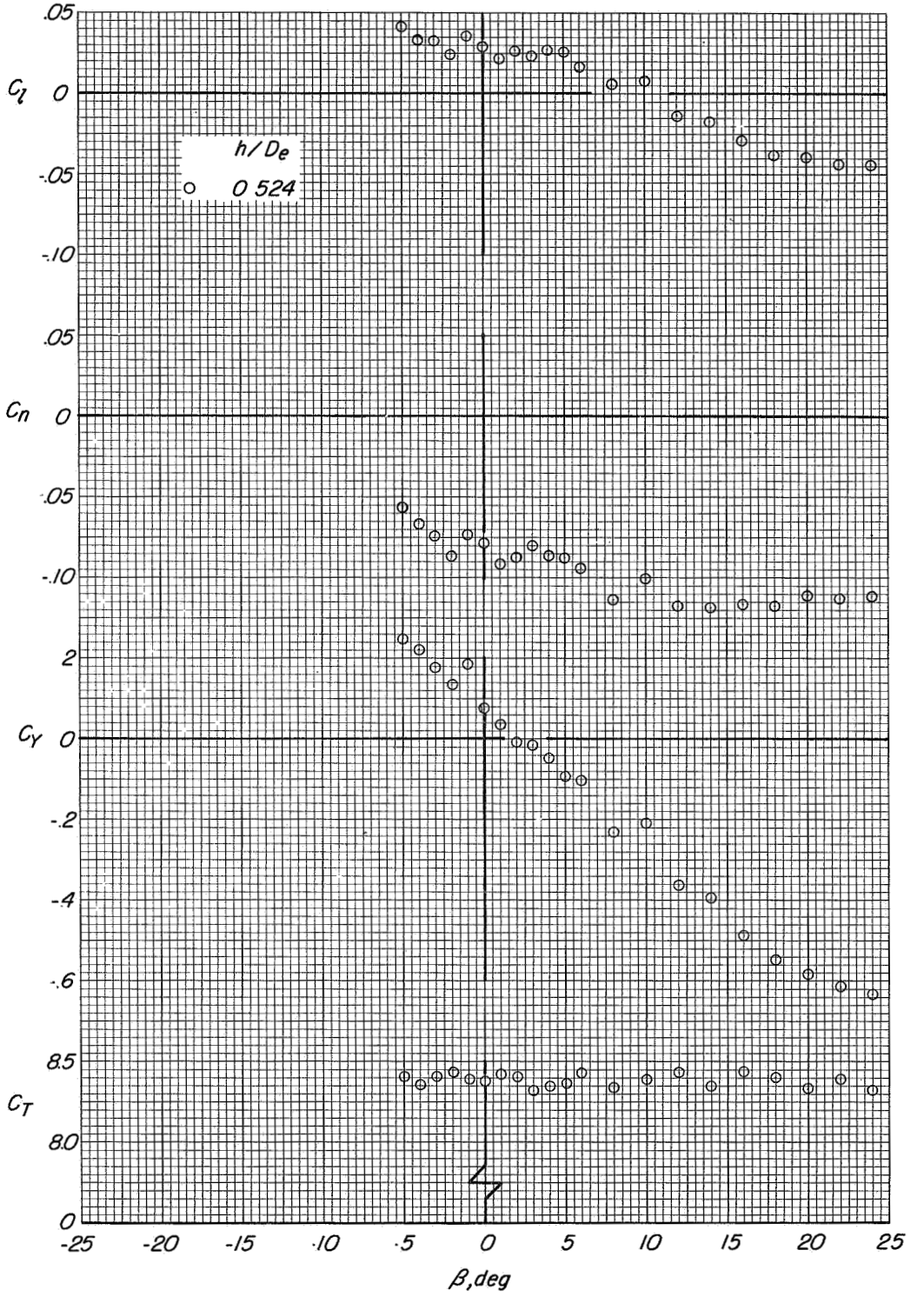

Figure 75.- Lateral aerodynamic characteristics of configuration A with direct-lift and lift-cruise engines deflected 90^0 $i_t = 0^0$; $\alpha = 0.3^0$; $C_T \approx 8$.

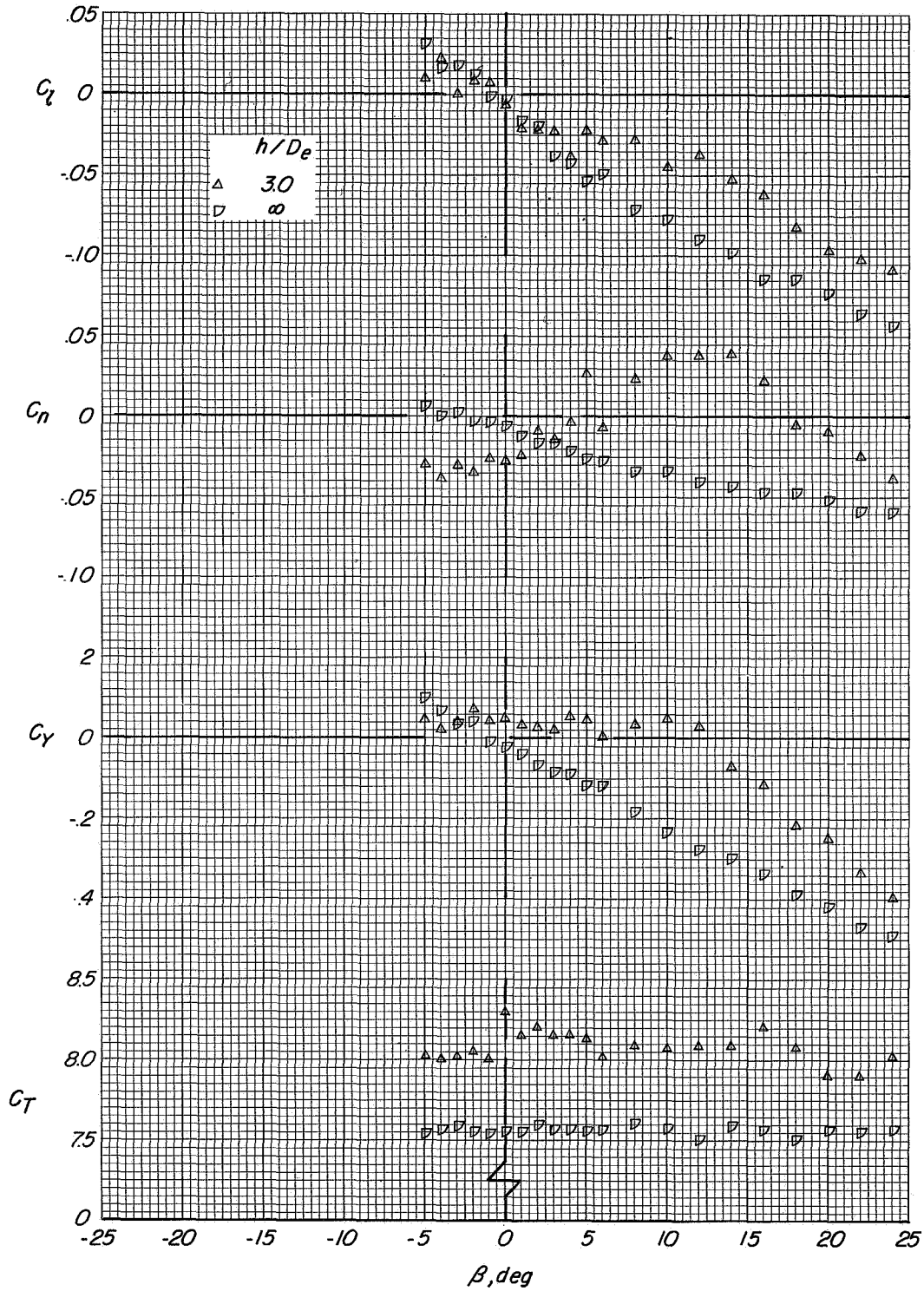

Figure 76.- Lateral aerodynamic characteristics of configuration A with direct-lift and lift-cruise engines deflected 90°. $i_t = 0°$; $\alpha = 12.5°$; $C_T \approx 8$.

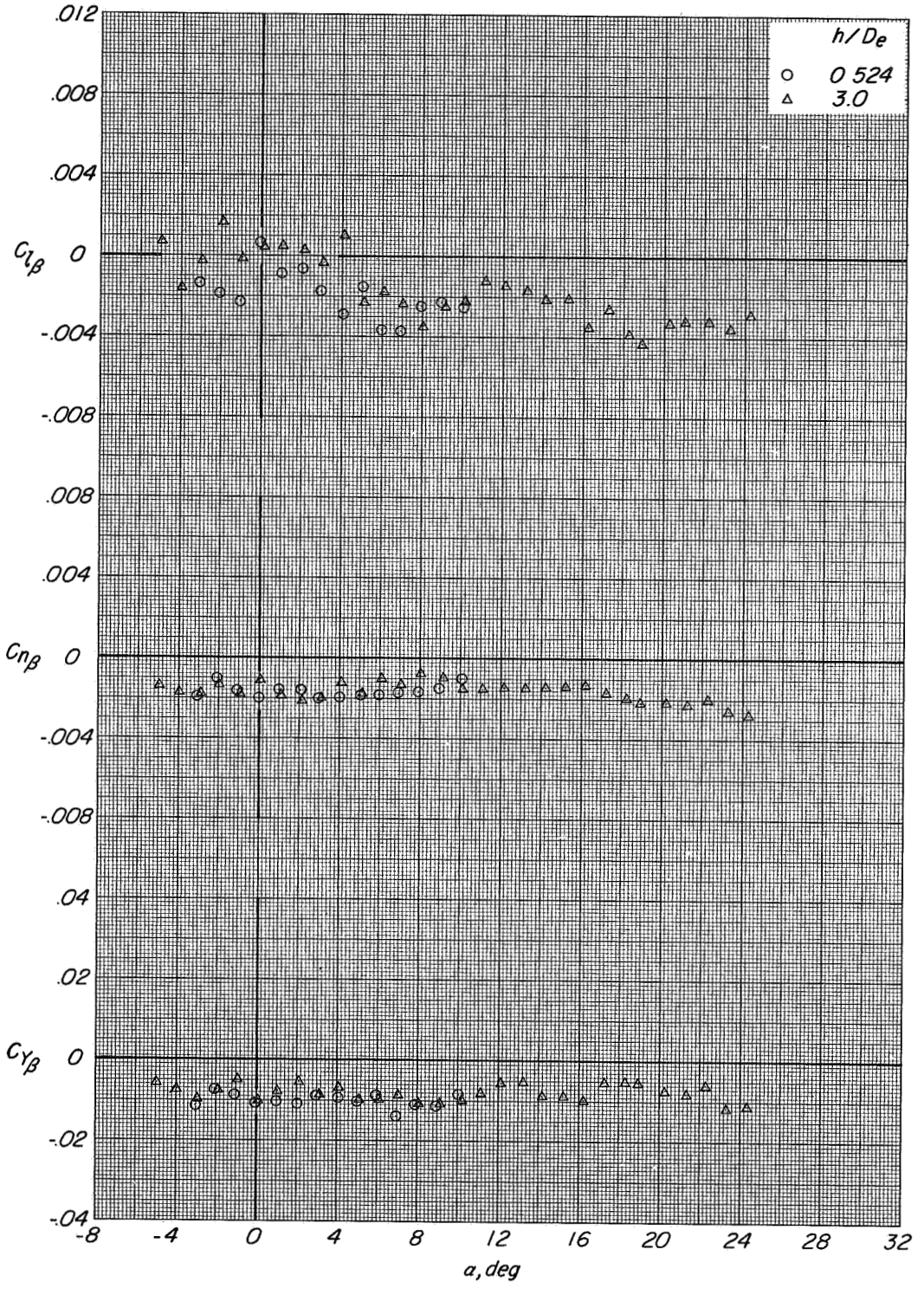

(a) $C_T = 0.$

Figure 77.- Variation of C_{l_β}, C_{n_β}, and C_{Y_β} with angle of attack for configuration A with direct-lift and lift-cruise engines deflected 90°. $i_t = 0°$

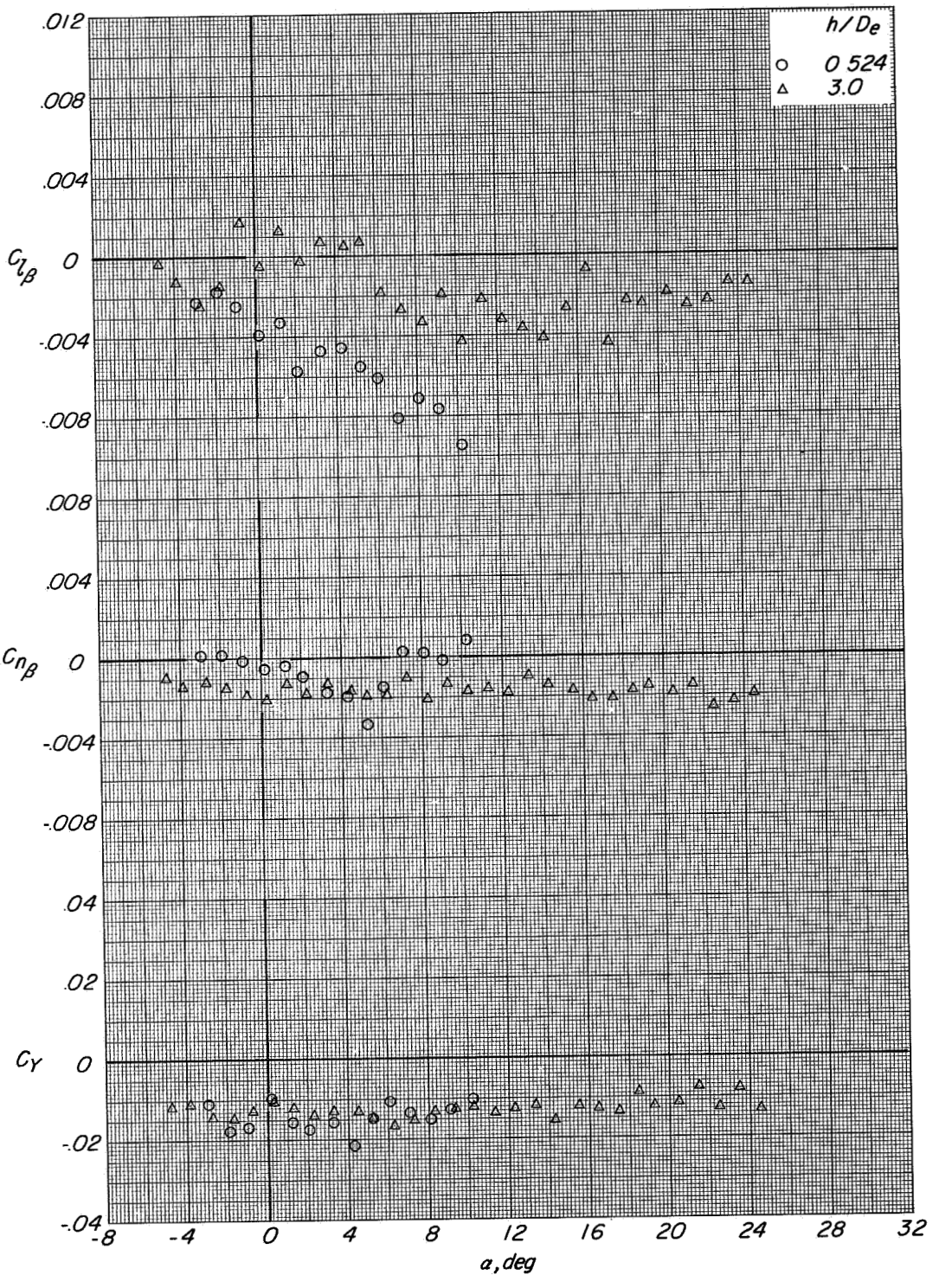

(b) $C_T \approx 1.45$.

Figure 77.- Continued.

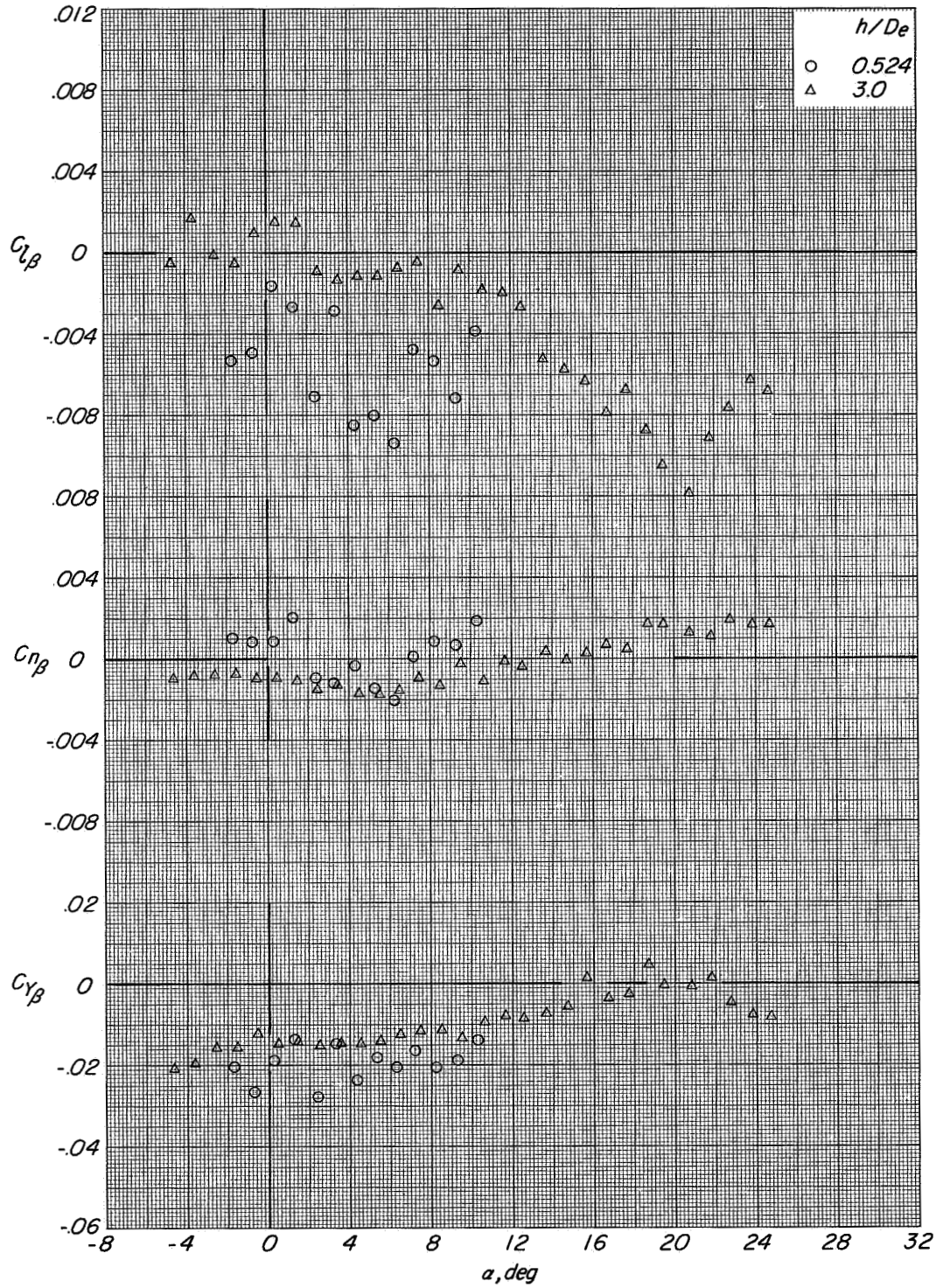

(c) $C_T \approx 3.3$.

Figure 77.- Continued.

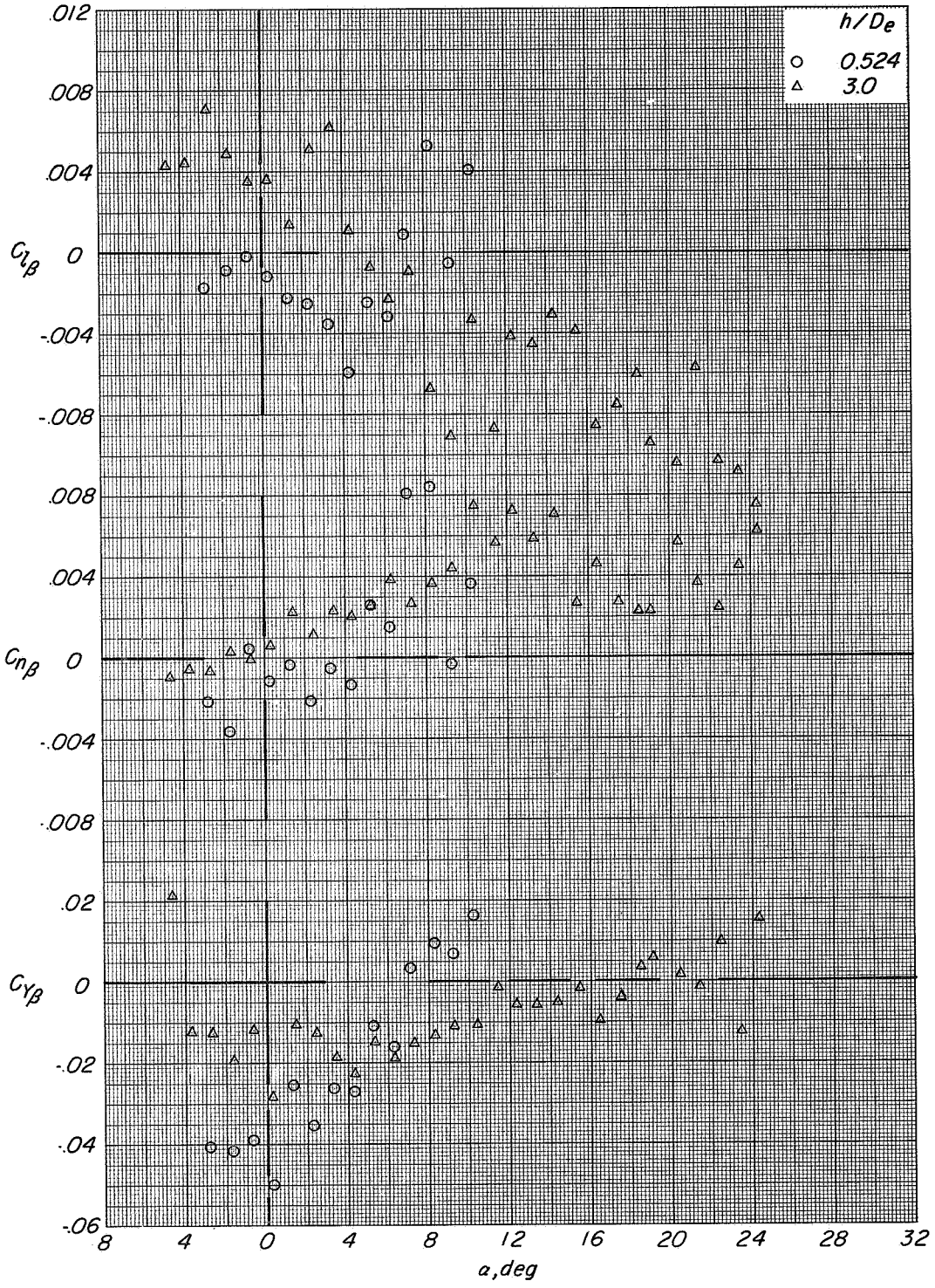

(d) $C_T \approx 8$.

Figure 77.- Concluded.

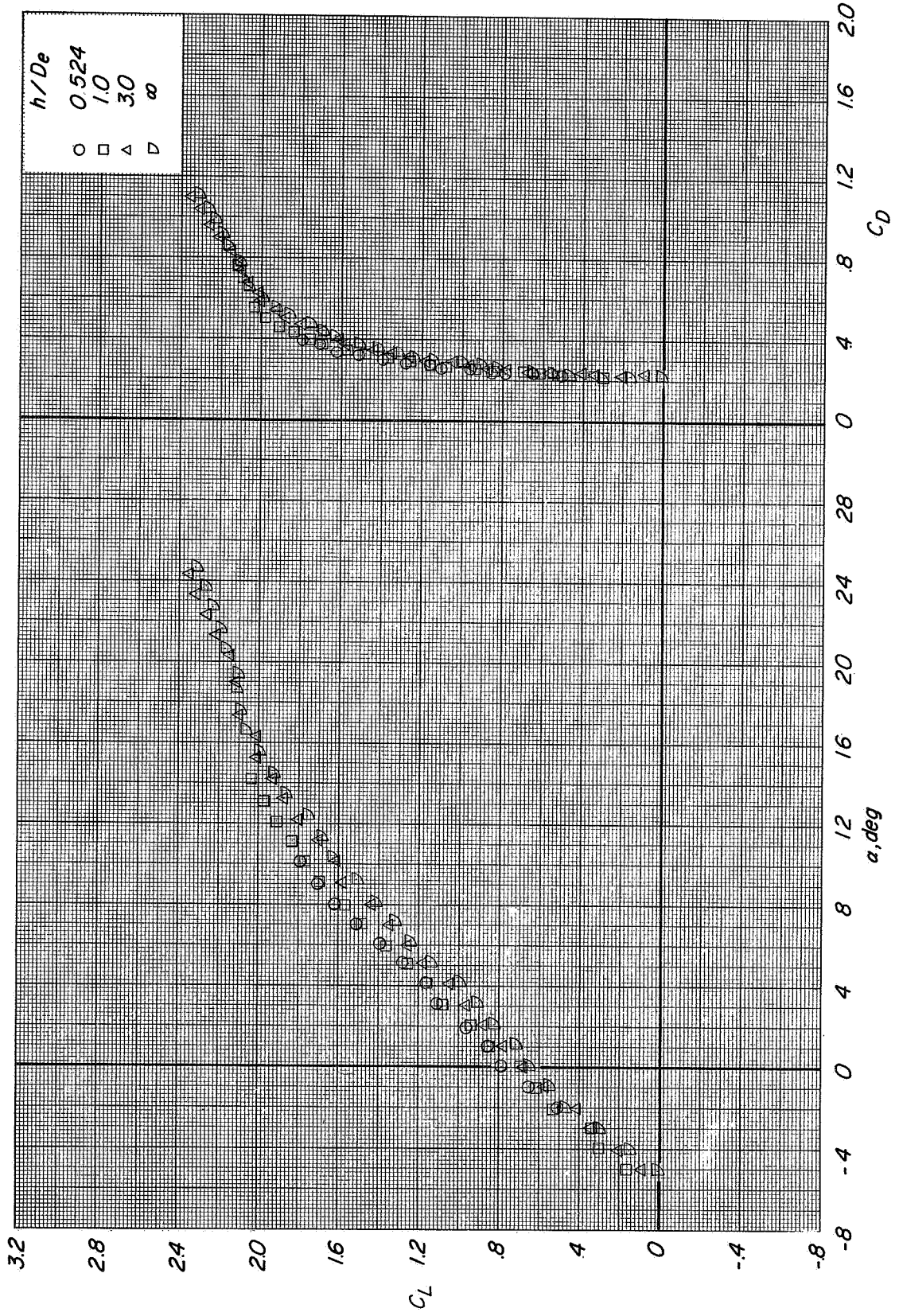

(a) Variation of C_L with α and C_D with C_L

Figure 78.- Longitudinal aerodynamic characteristics of configuration A with direct-lift and lift-cruise engines deflected 25°. $i_t = 0°$; $\beta = 0°$; $C_T = 0$.

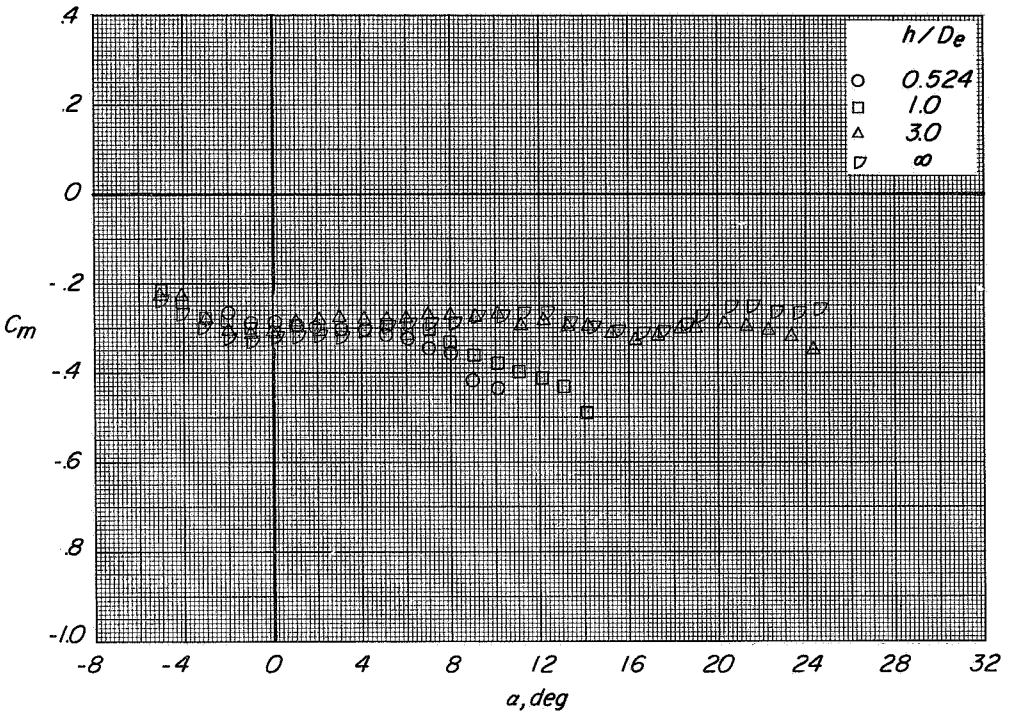

(b) Variation of C_m with α.

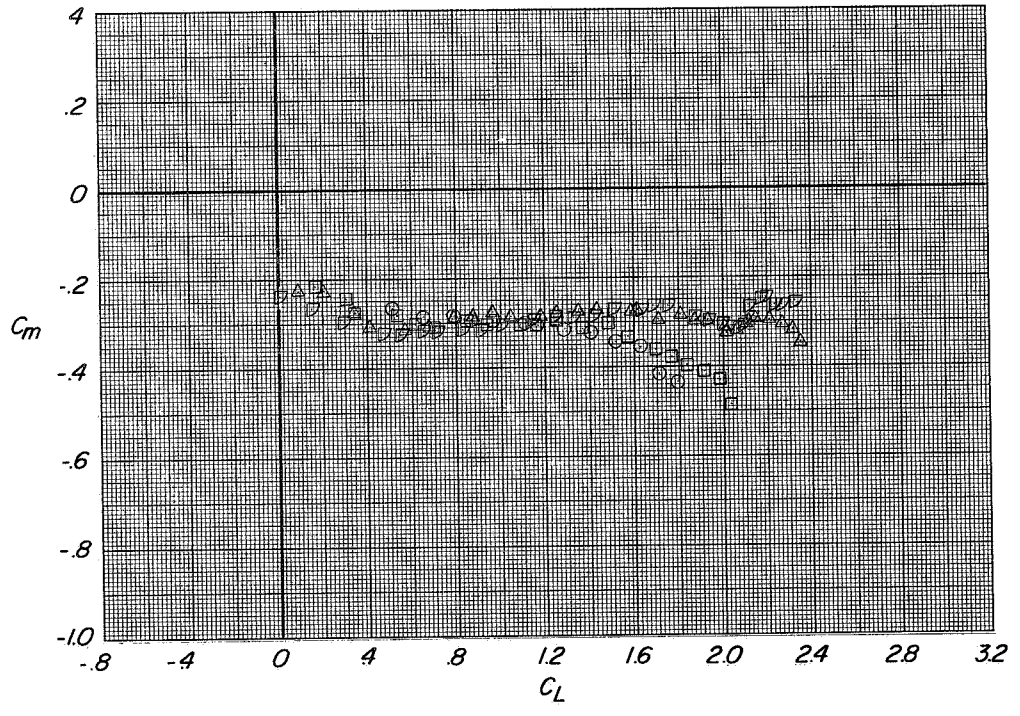

(c) Variation of C_m with C_L.

Figure 78.- Concluded.

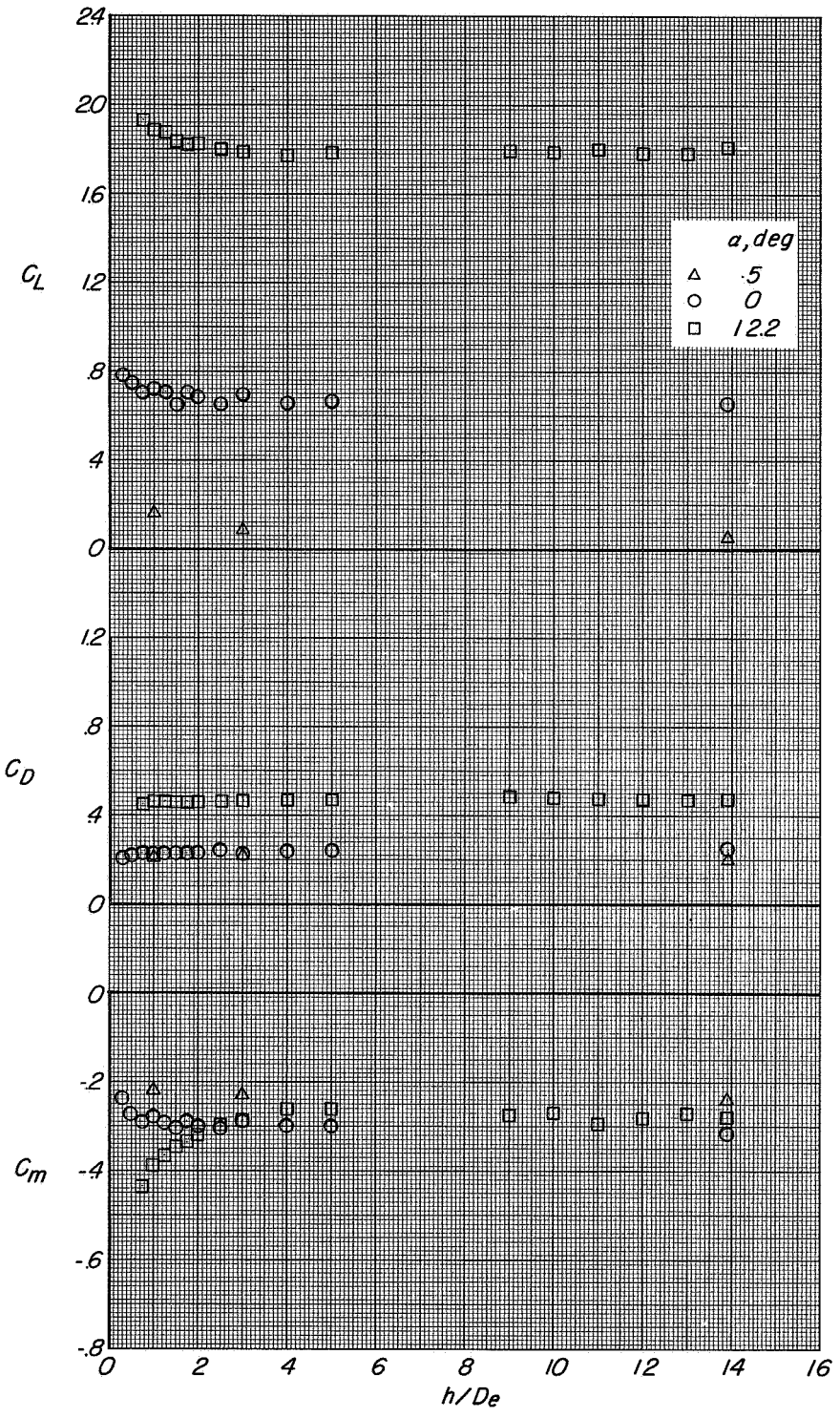

Figure 79.- Effect of height above the moving-belt ground plane on the longitudinal aerodynamic characteristics of configuration A with direct-lift and lift-cruise engines deflected 25°. $i_t = 0°$; $\beta = 0°$; $C_T = 0$.

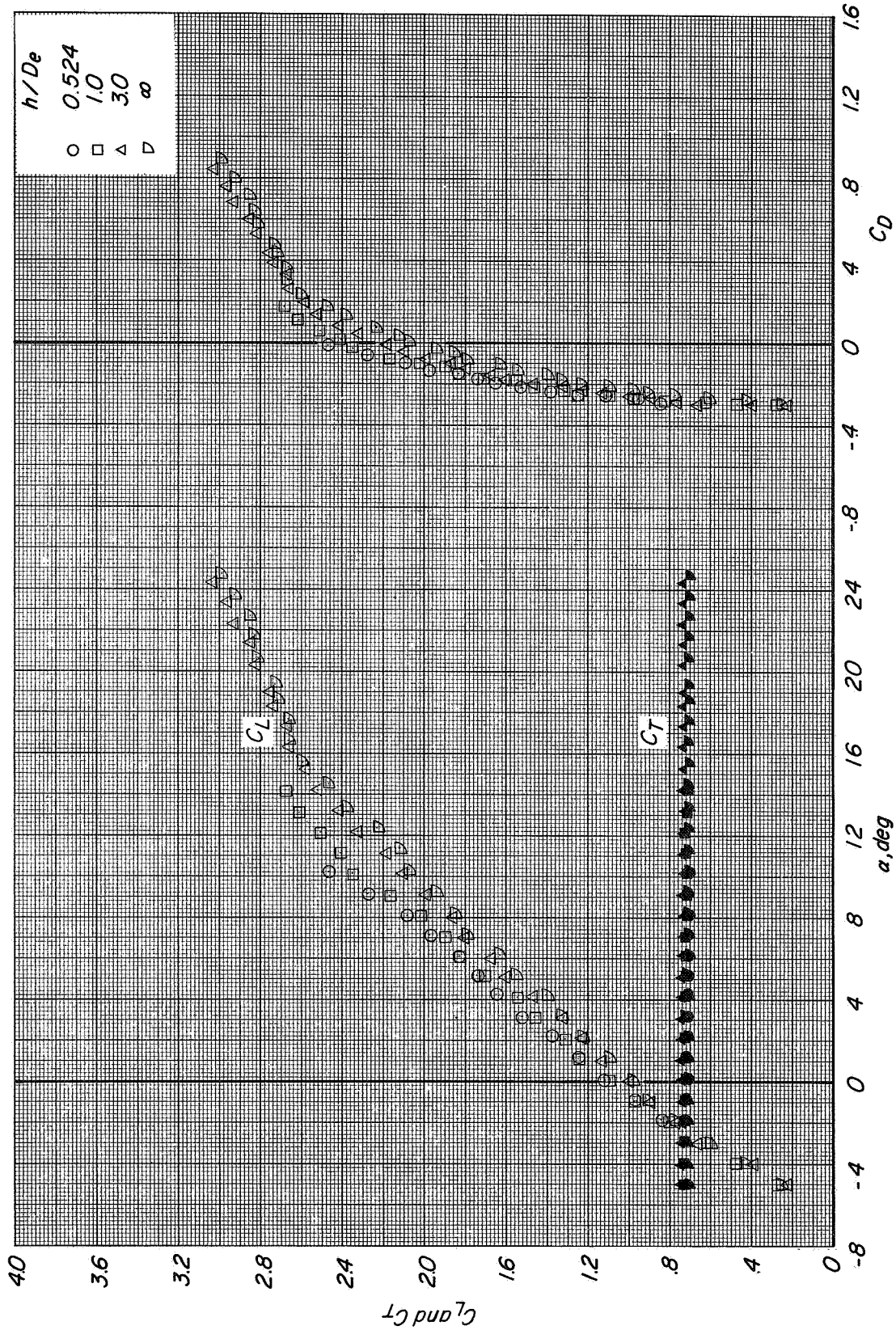

(a) Variation of C_L and C_T with α and C_D with C_L

Figure 80.- Longitudinal aerodynamic characteristics of configuration A with direct-lift and lift-cruise engines deflected 25^0 $i_t = 0^0$; $\beta = 0^0$; $C_T \approx 0.65$.

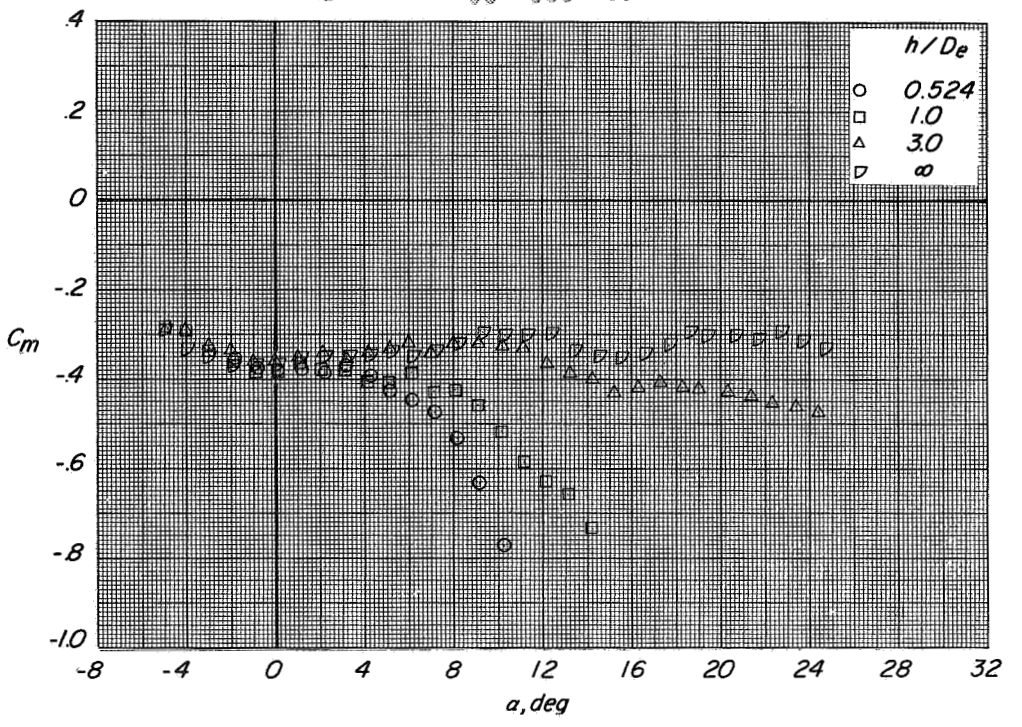

(b) Variation of C_m with α.

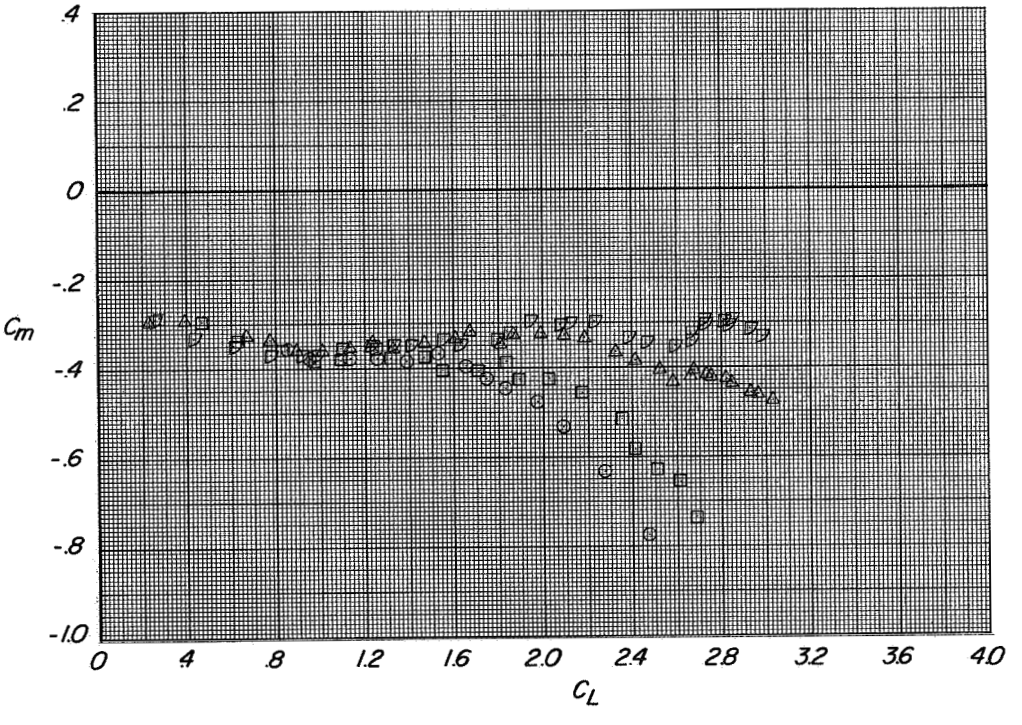

(c) Variation of C_m with C_L

Figure 80.- Continued.

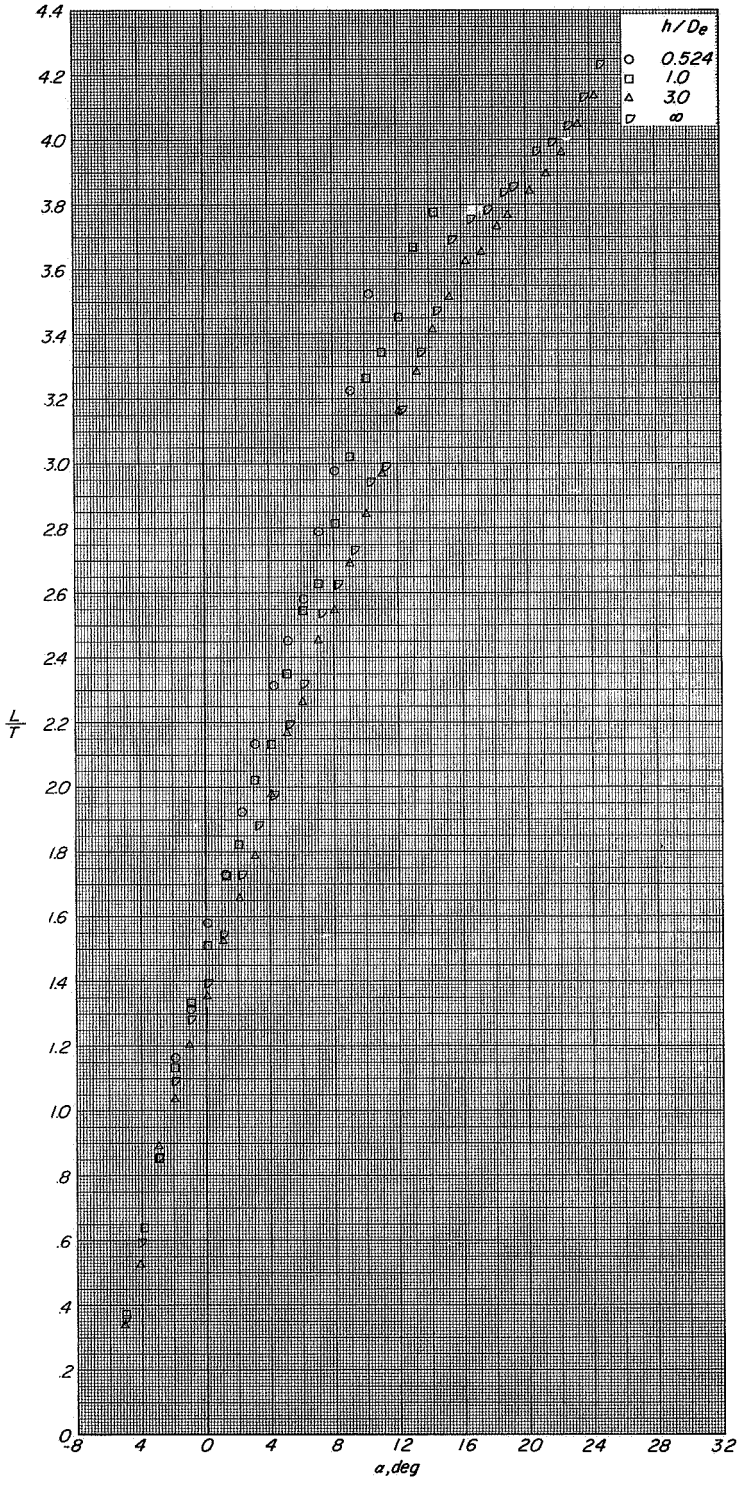

(d) Variation of L/T with α.

Figure 80.- Continued.

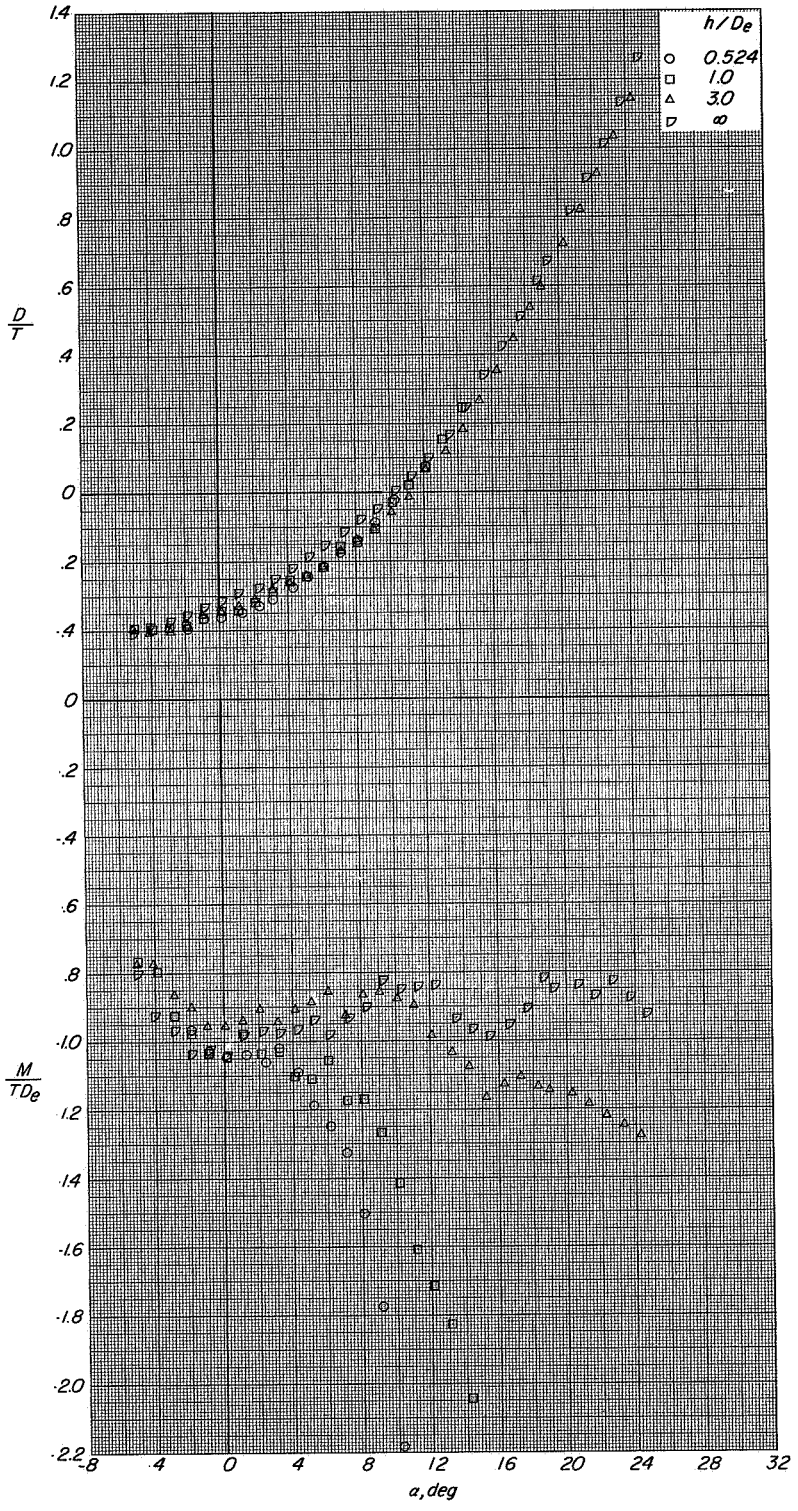

(e) Variation of D/T and M/TD_e with α.

Figure 80.- Concluded.

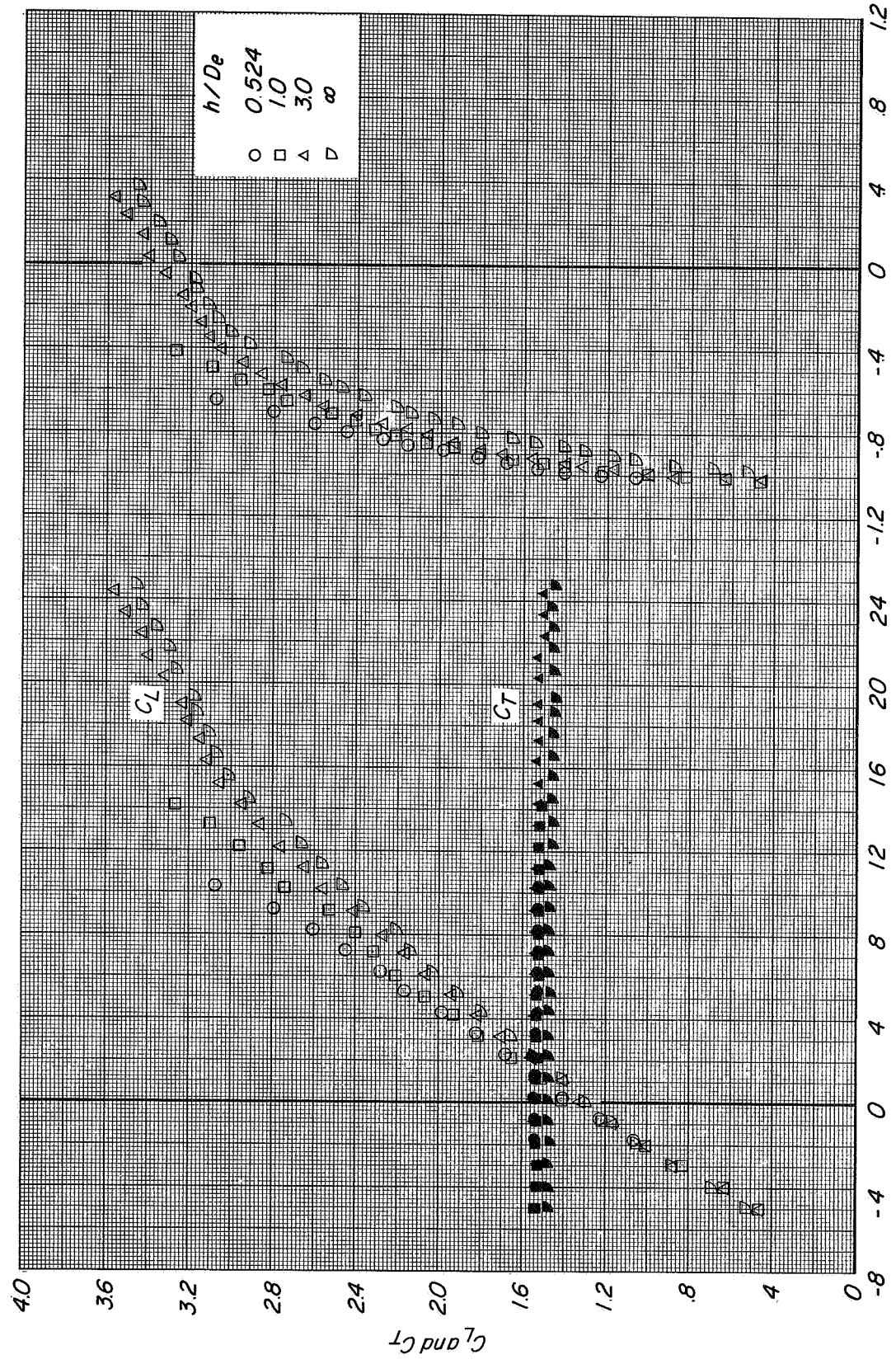

(a) Variation of C_L and C_T with α and C_D with C_L

Figure 81.- Longitudinal aerodynamic characteristics of configuration A with direct-lift and lift-cruise engines deflected 25^0. $i_t = 0^0$; $\beta = 0^0$; $C_T \approx 1.45$.

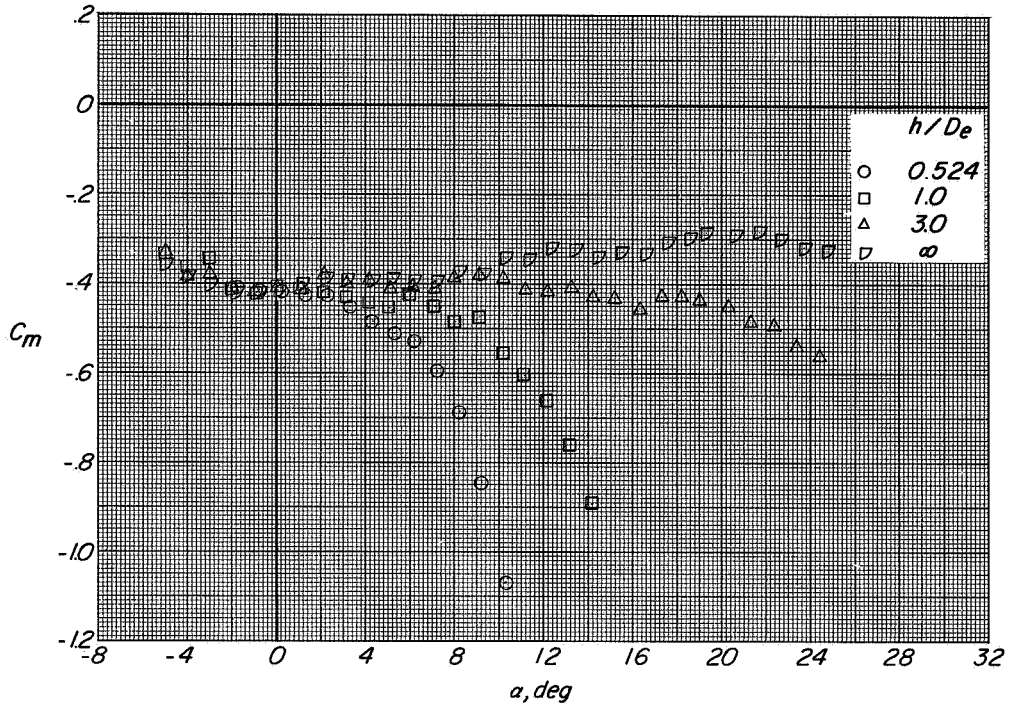

(b) Variation of C_m with α.

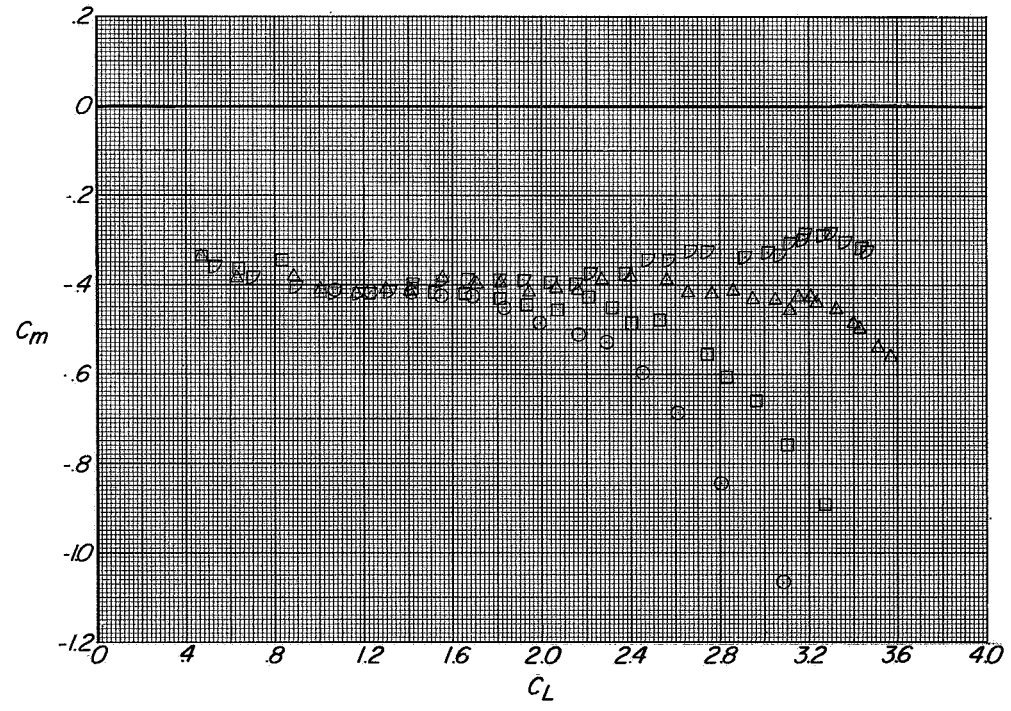

(c) Variation of C_m with C_L

Figure 81.- Continued.

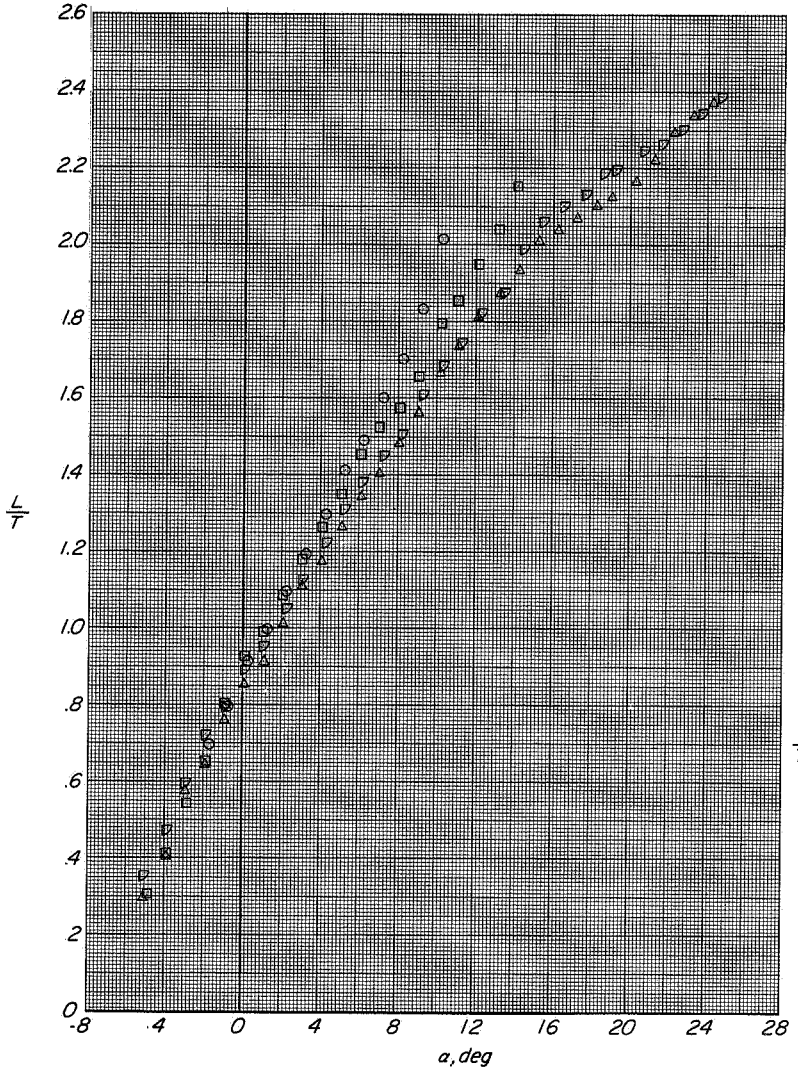

(d) Variation of L/T with α.

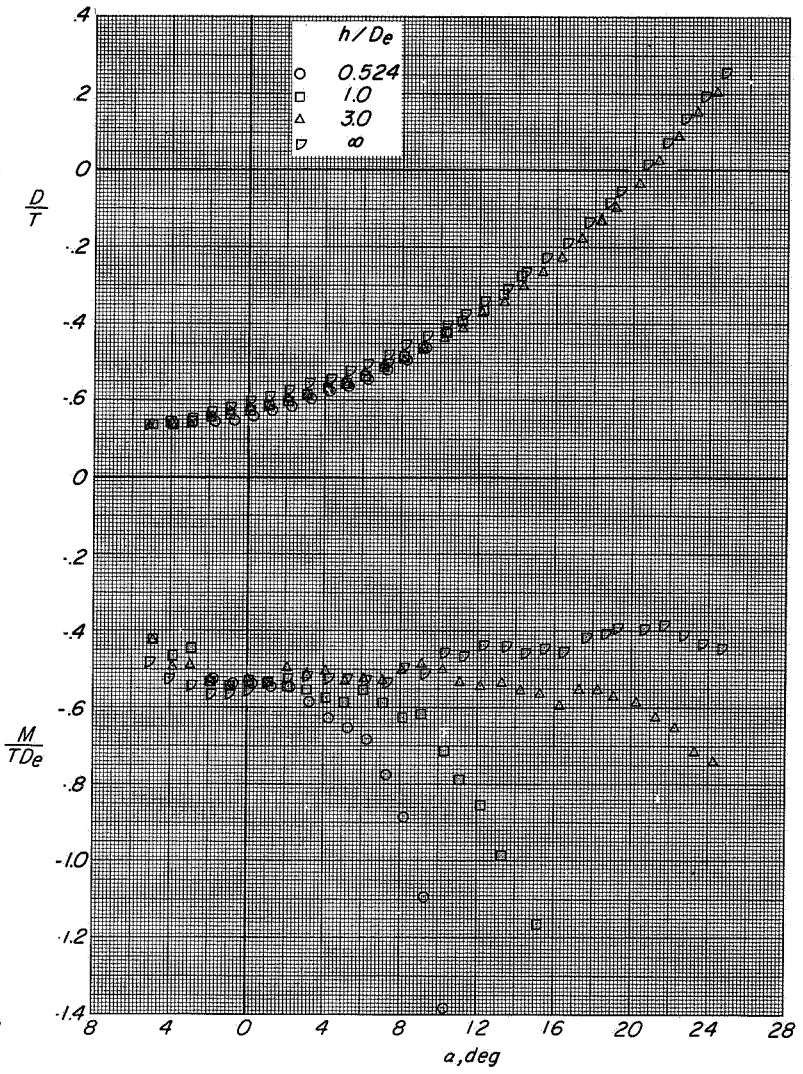

(e) Variation of D/T and M/TDe with α.

Figure 81.- Concluded.

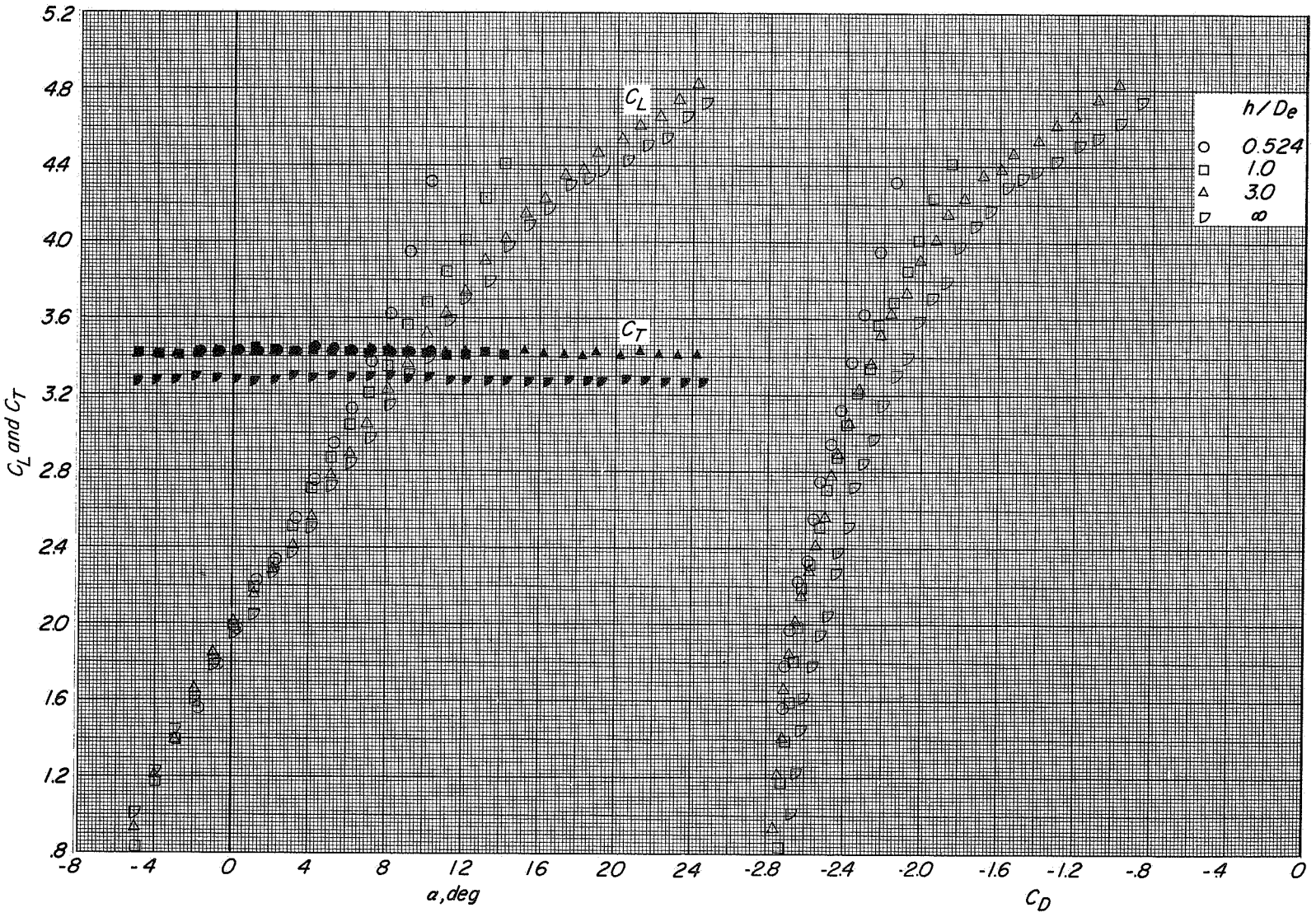

(a) Variation of C_L and C_T with α and C_D with C_L

Figure 82.- Longitudinal aerodynamic characteristics of configuration A with direct-lift and lift-cruise engines deflected 25°. $i_t = 0°$; $\beta = 0°$; $C_T \approx 3.3$.

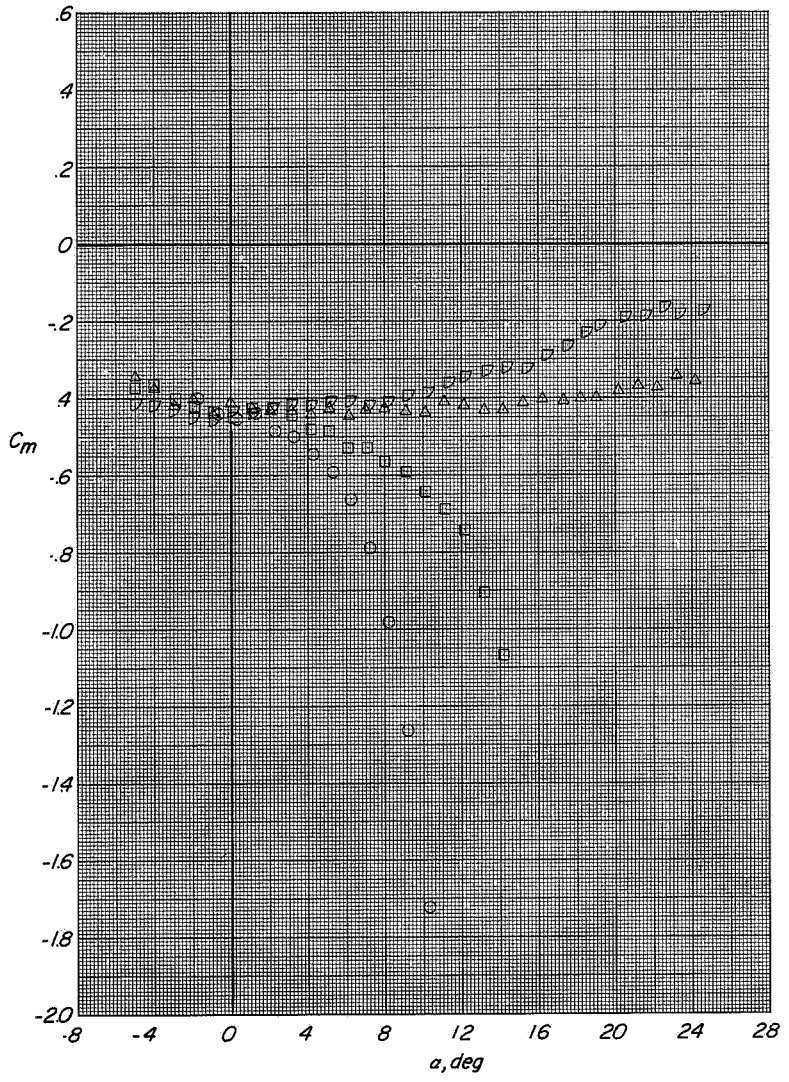

(b) Variation of C_m with α.

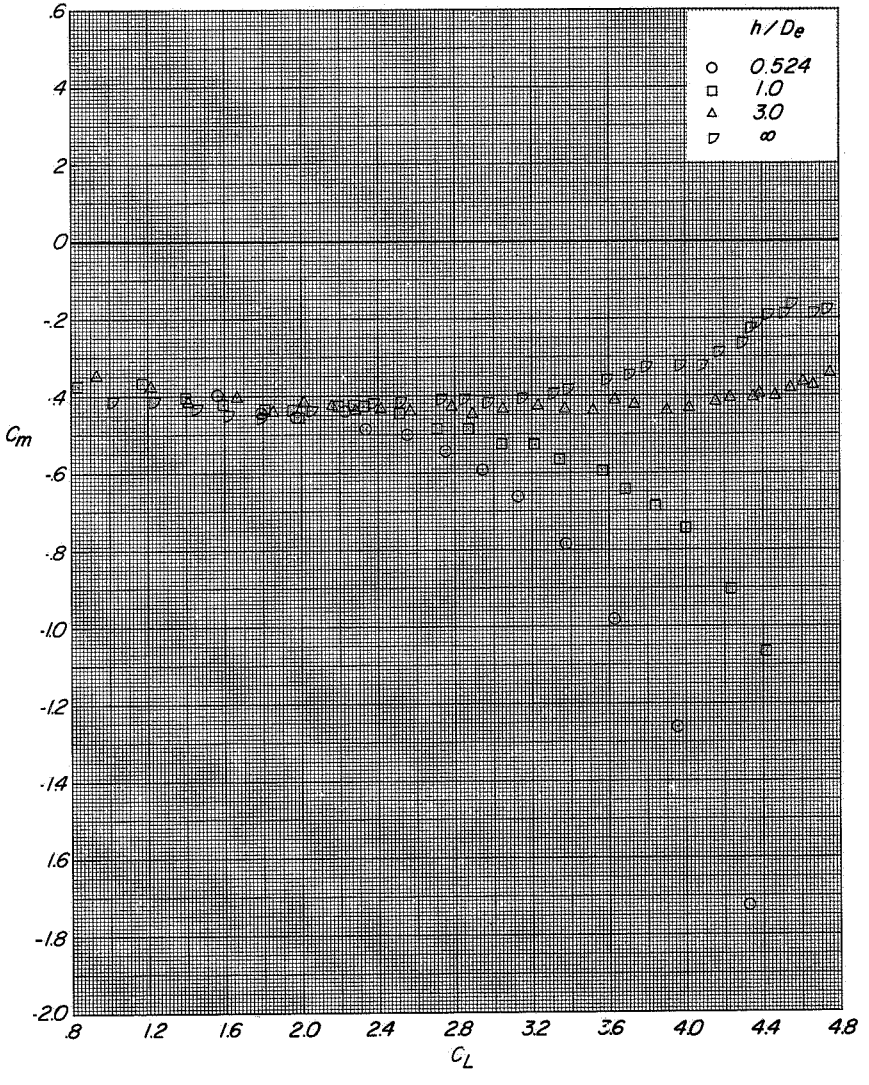

(c) Variation of C_m with C_L.

Figure 82.- Continued.

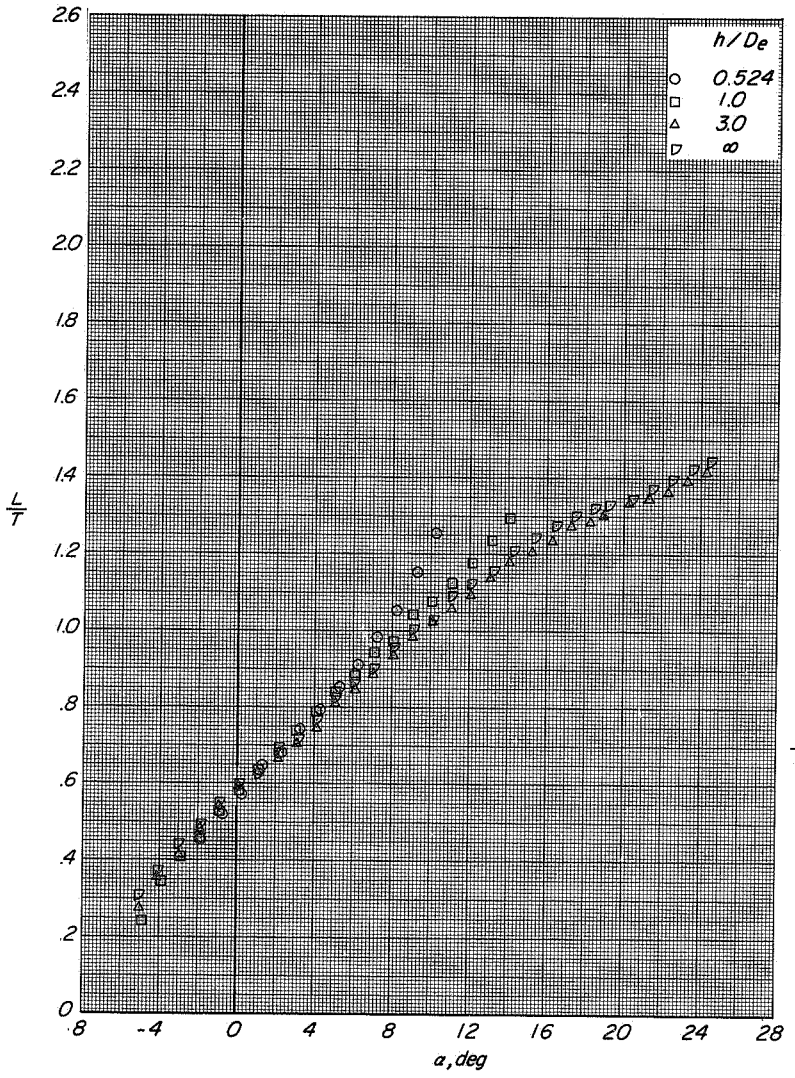

(d) Variation of L/T with α.

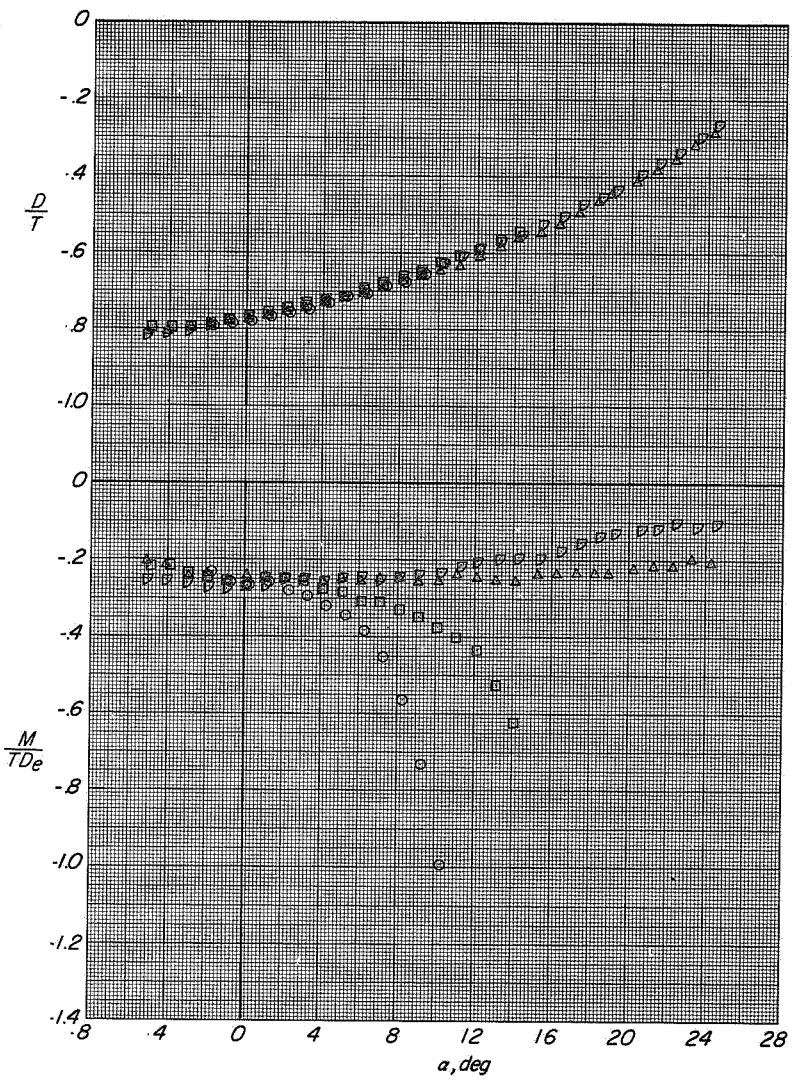

(e) Variation of D/T and M/TDe with α.

Figure 82.- Concluded.

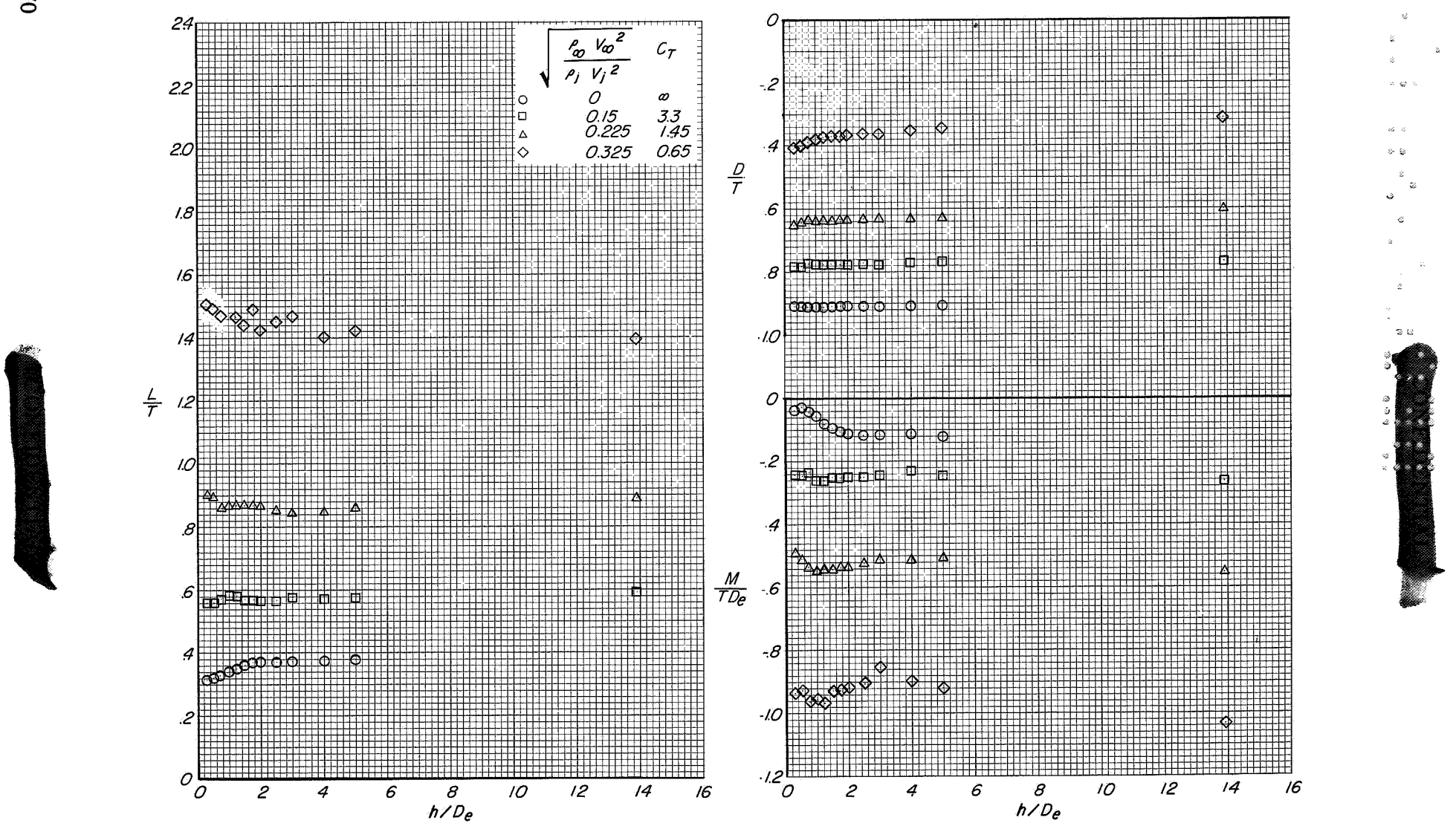

(a) Variation of L/T with h/D_e.

(b) Variation of D/T and M/TD_e with h/D_e.

Figure 83.- Effect of height above the moving-belt ground plane on the longitudinal aerodynamic characteristics of configuration A with direct-lift and lift-cruise engines deflected 25°. $i_t = 0^0$; $\beta = 0^0$; $\alpha = 0^0$

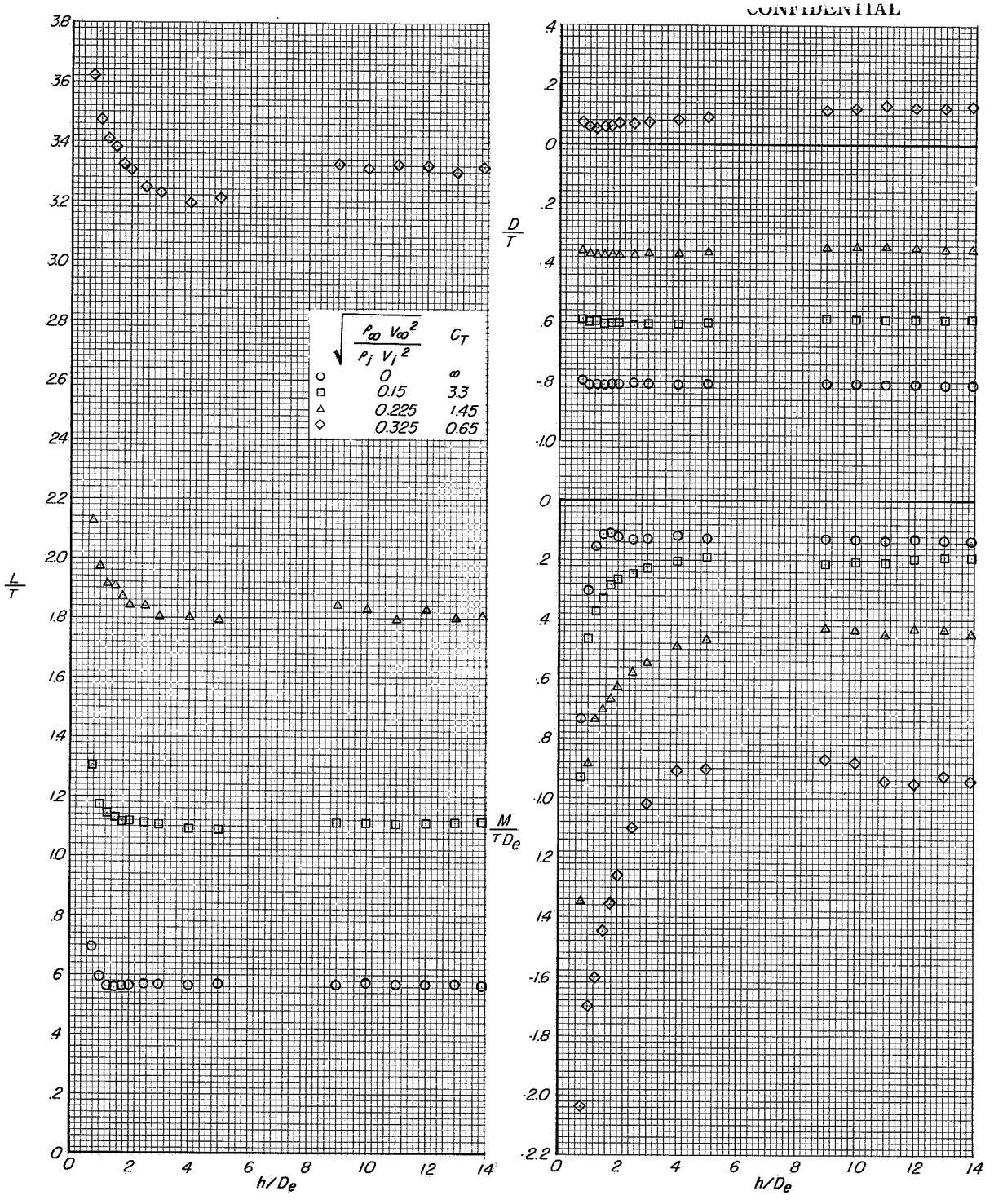

(a) Variation of L/T with h/D_e.

(b) Variation of D/T and M/TD_e with h/D_e.

Figure 84.- Effect of height above the moving-belt ground plane on the longitudinal aerodynamic characteristics of configuration A with direct-lift and lift-cruise engines deflected 25^0. $i_t = 0^0$; $\beta = 0^0$; $\alpha = 12.3^0$.

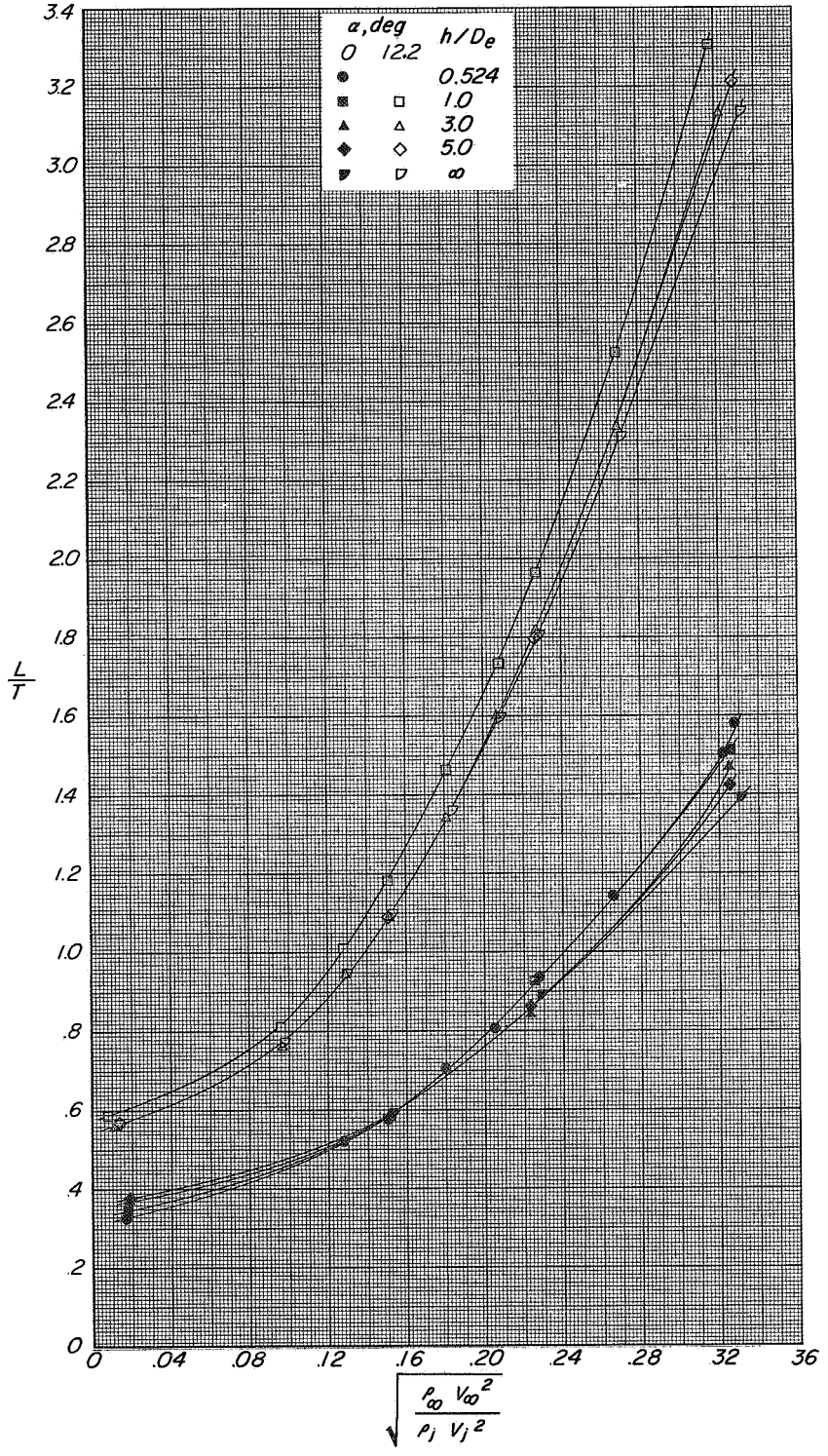

(a) Variation of L/T with effective velocity ratio.

Figure 85.· Effect of effective velocity ratio on the longitudinal aerodynamic characteristics of configuration A with direct-lift and lift-cruise engines deflected 25° $i_t = 0^0$; $\beta = 0^0$

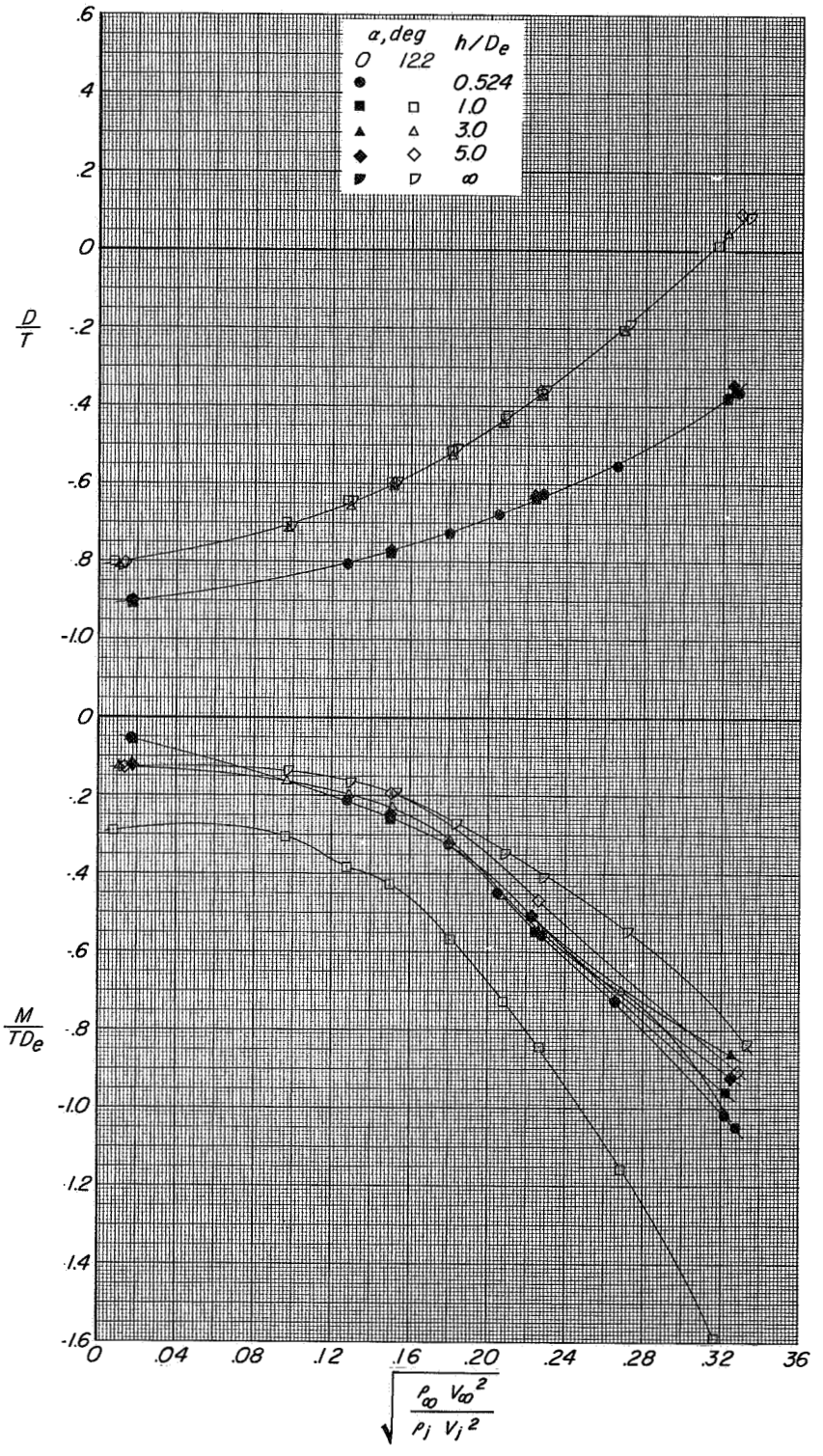

(b) Variation of D/T and M/TD$_e$ with effective velocity ratio.

Figure 85.- Concluded.

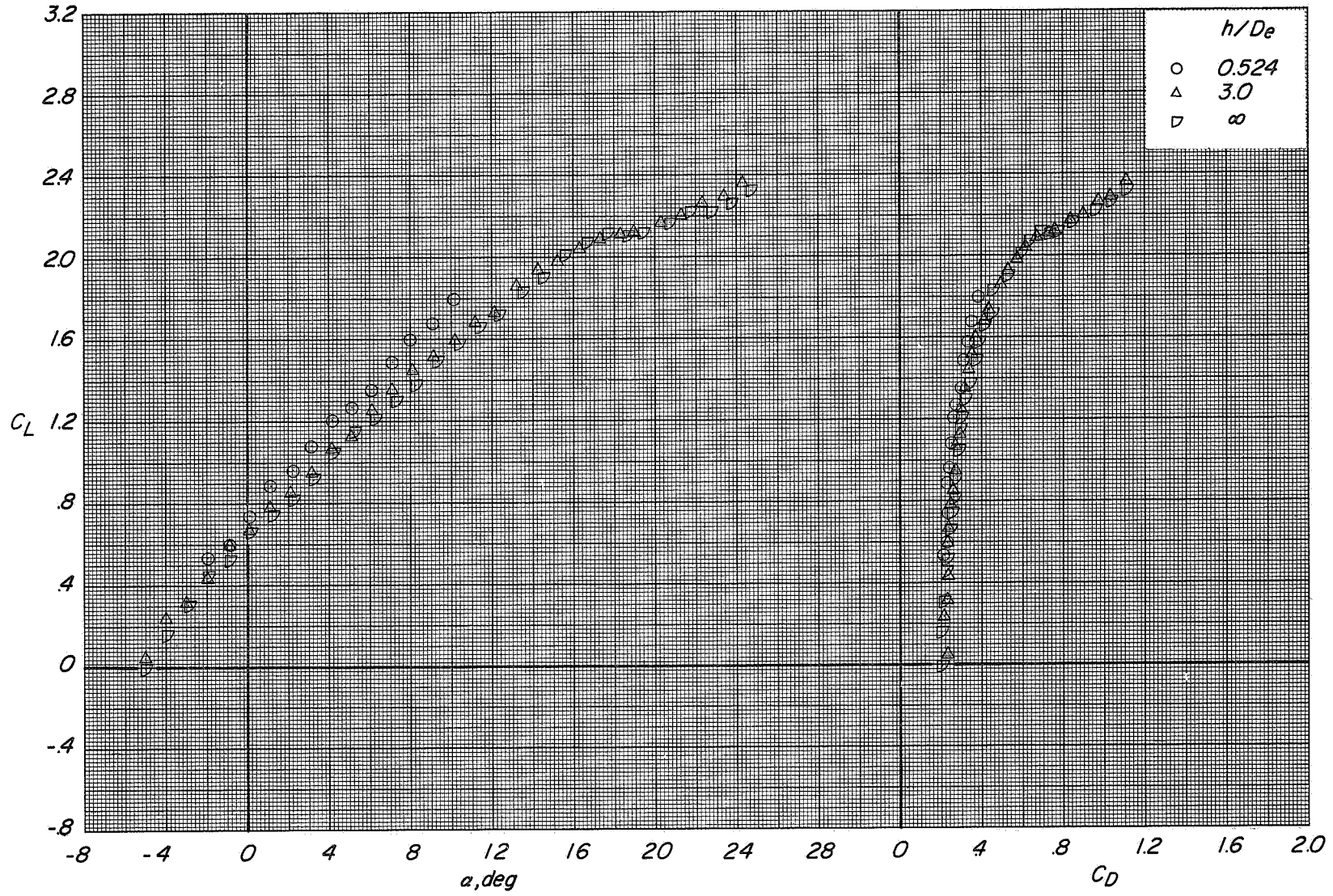

(a) Variation of C_L with α and C_D with C_L

Figure 86.- Longitudinal aerodynamic characteristics of configuration A with direct-lift and lift-cruise engines deflected 25^0. $i_t = 0^0$; $\beta = 5^0$; $C_T = 0$.

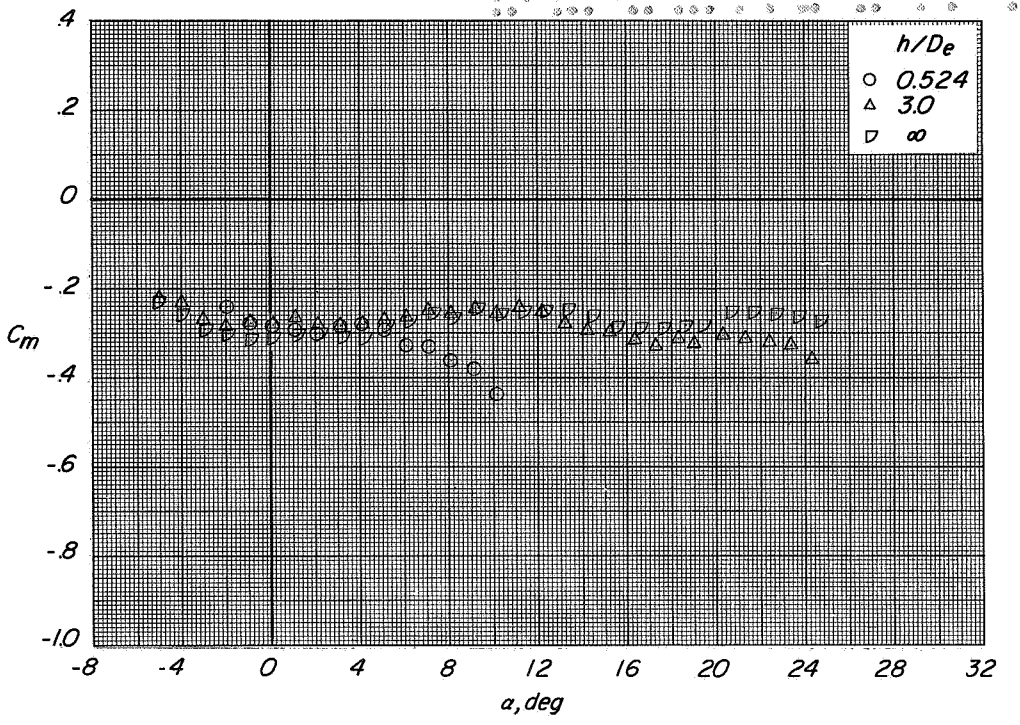

(b) Variation of C_m with α.

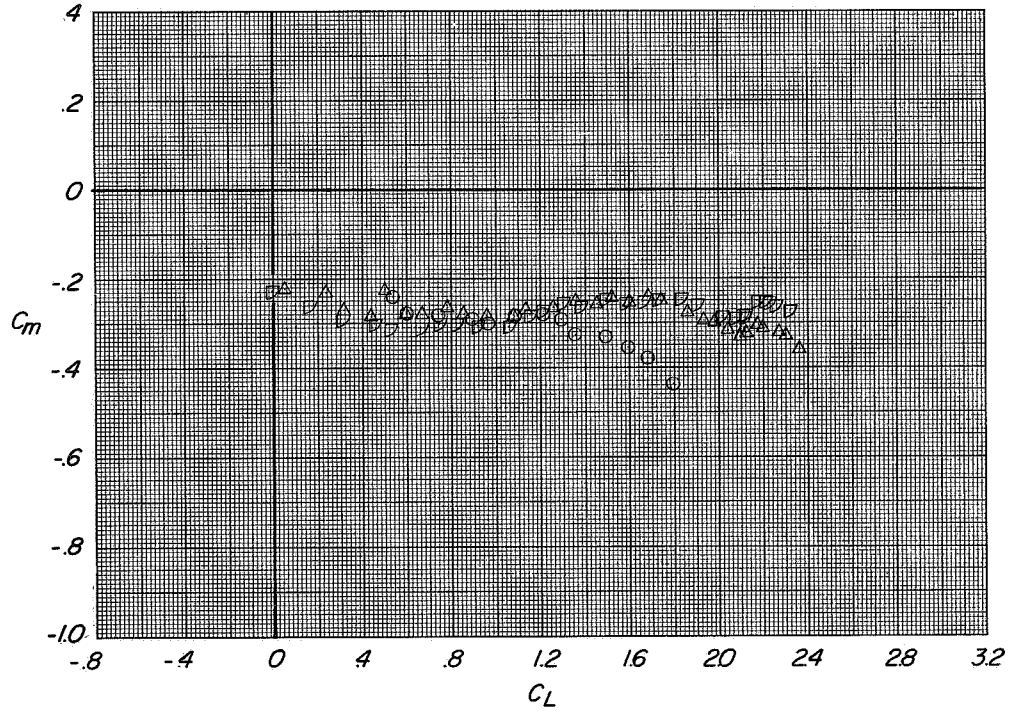

(c) Variation of C_m with C_L.

Figure 86.- Concluded.

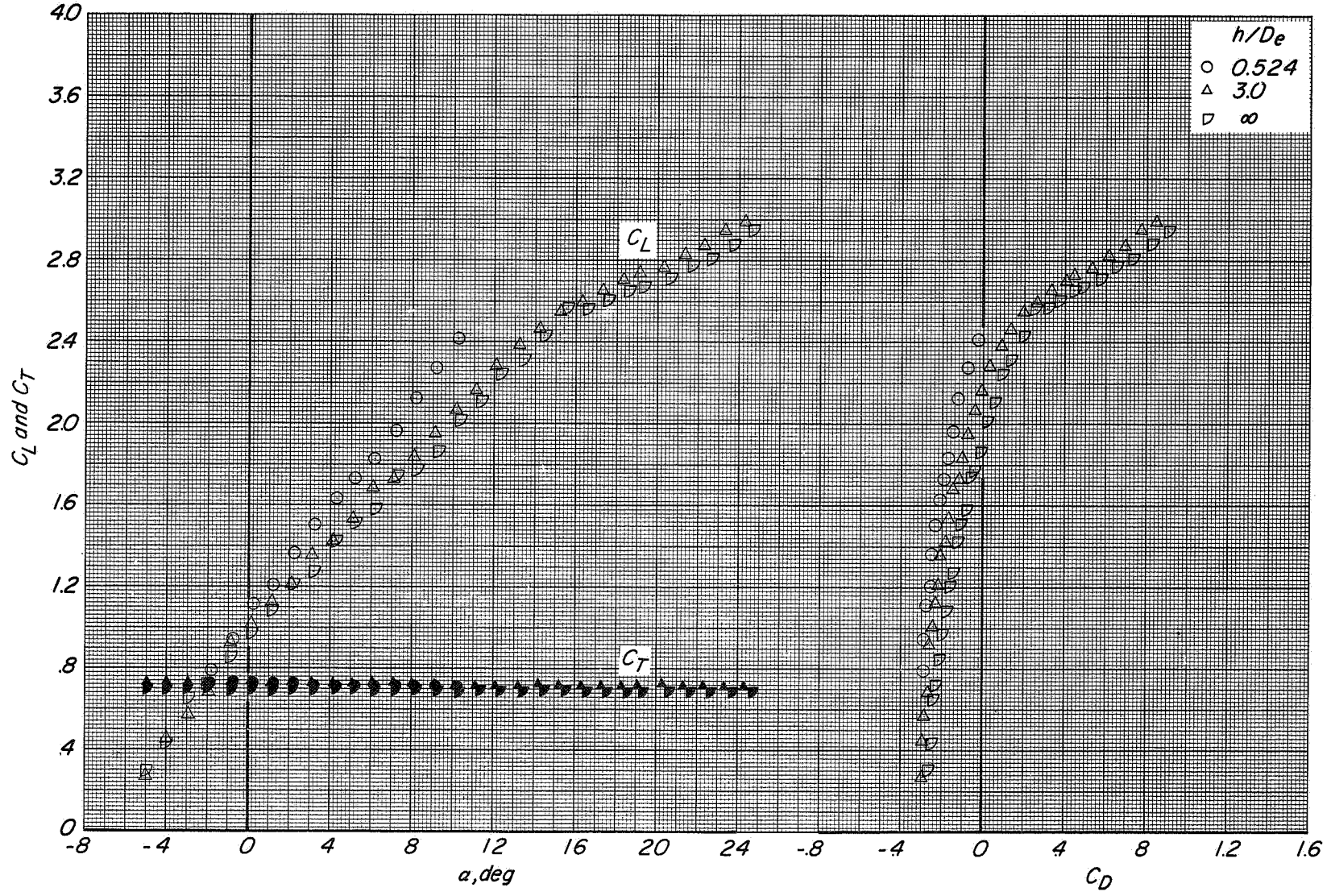

(a) Variation of C_L and C_T with α and C_D with C_L

Figure 87.- Longitudinal aerodynamic characteristics of configuration A with direct-lift and lift-cruise engines deflected 25^0 $i_t = 0^0$; $\beta = 5^0$; $C_T \approx 0.65$.

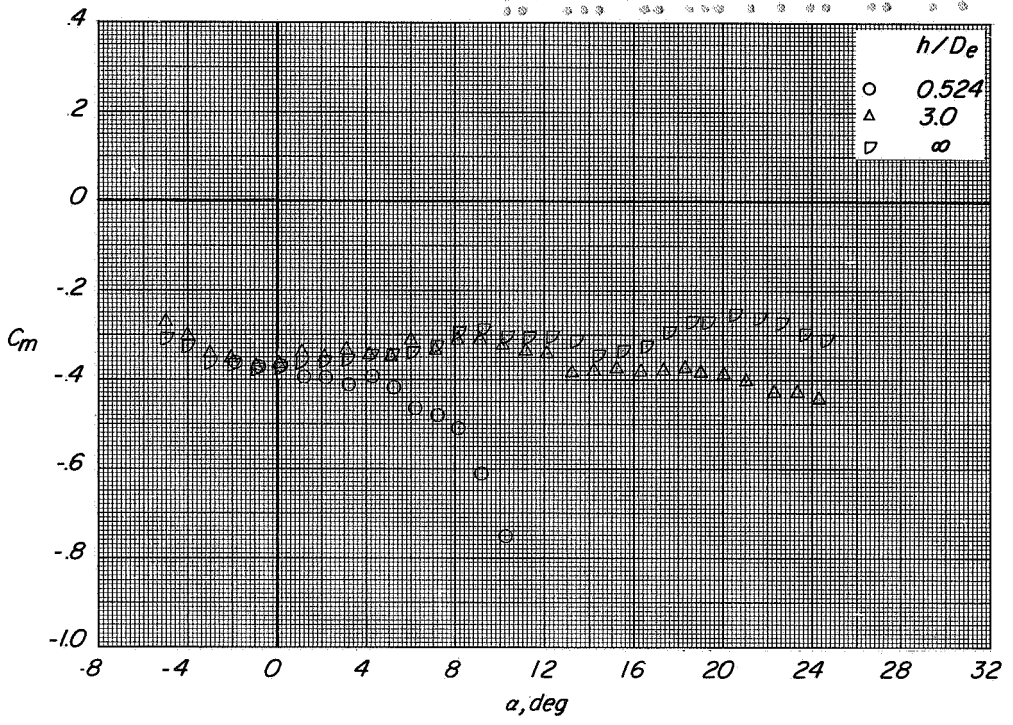

(b) Variation of C_m with α.

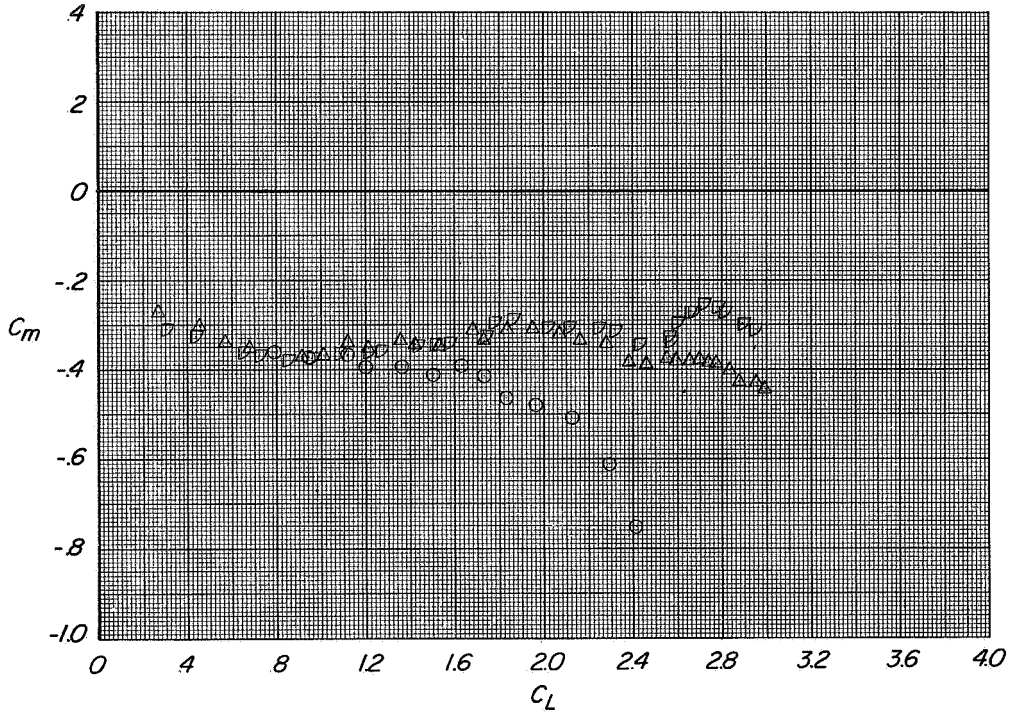

(c) Variation of C_m with C_L.

Figure 87.- Continued.

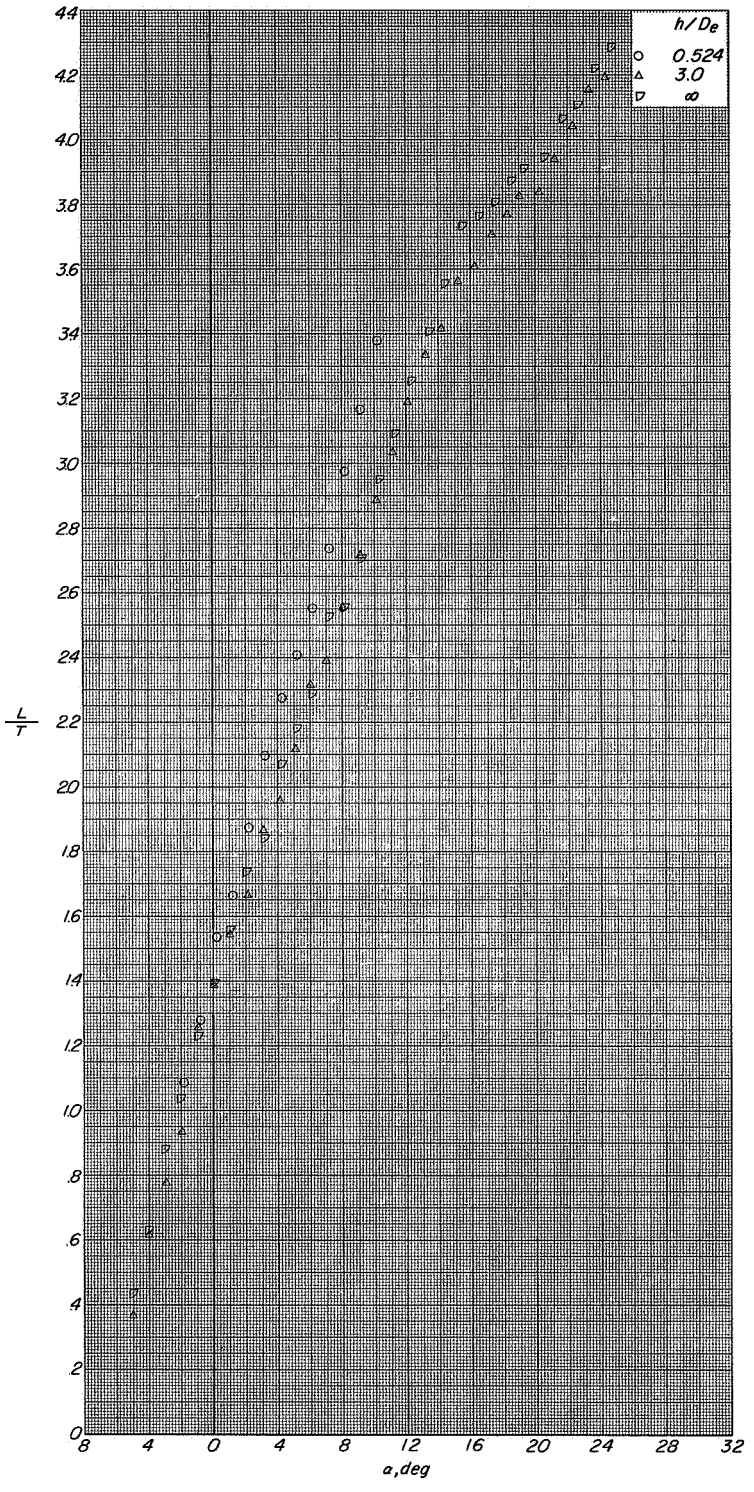

(d) Variation of L/T with α.

Figure 87.- Continued.

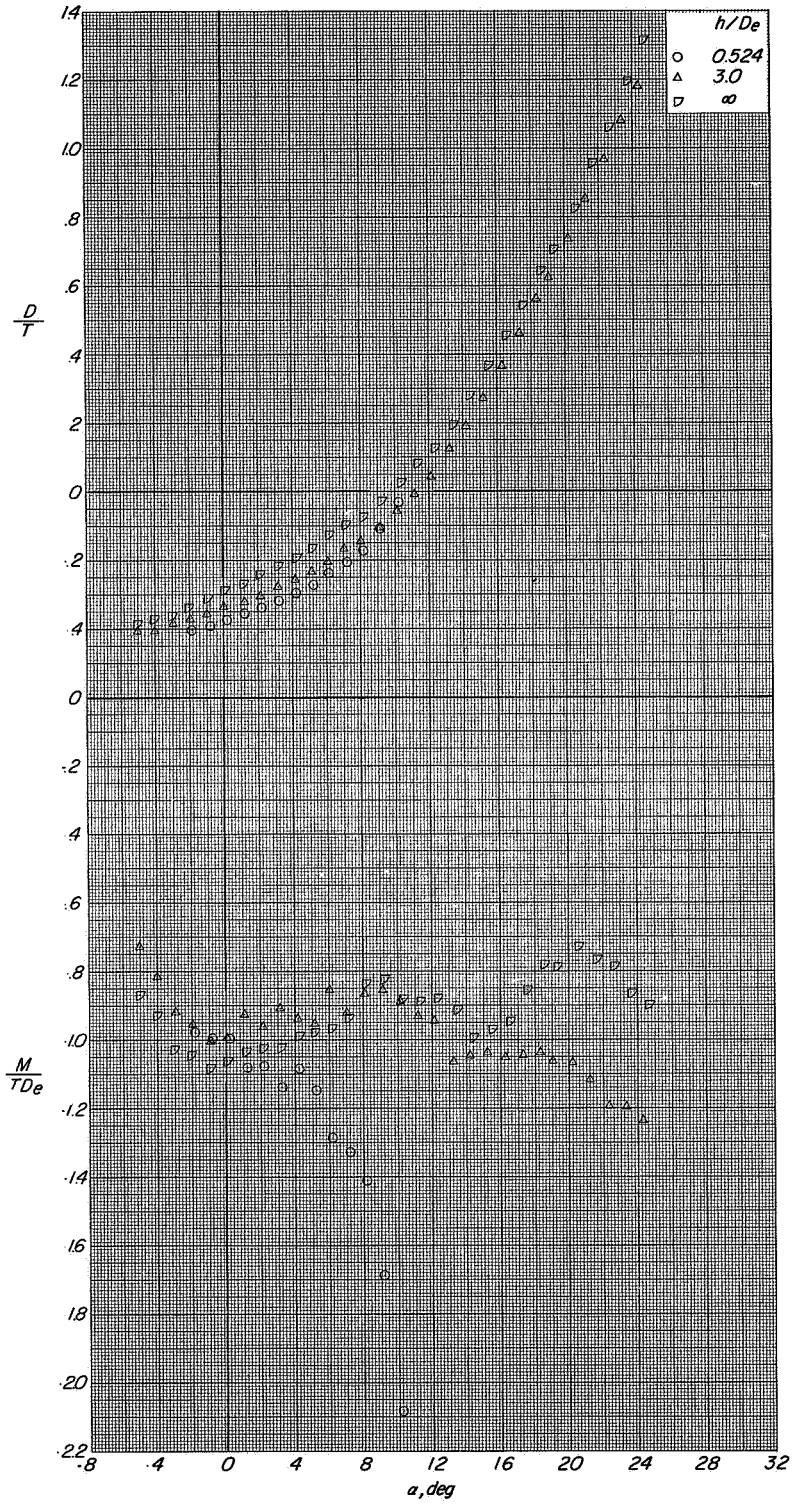

(e) Variation of D/T and M/TD_e with α.

Figure 87.- Concluded.

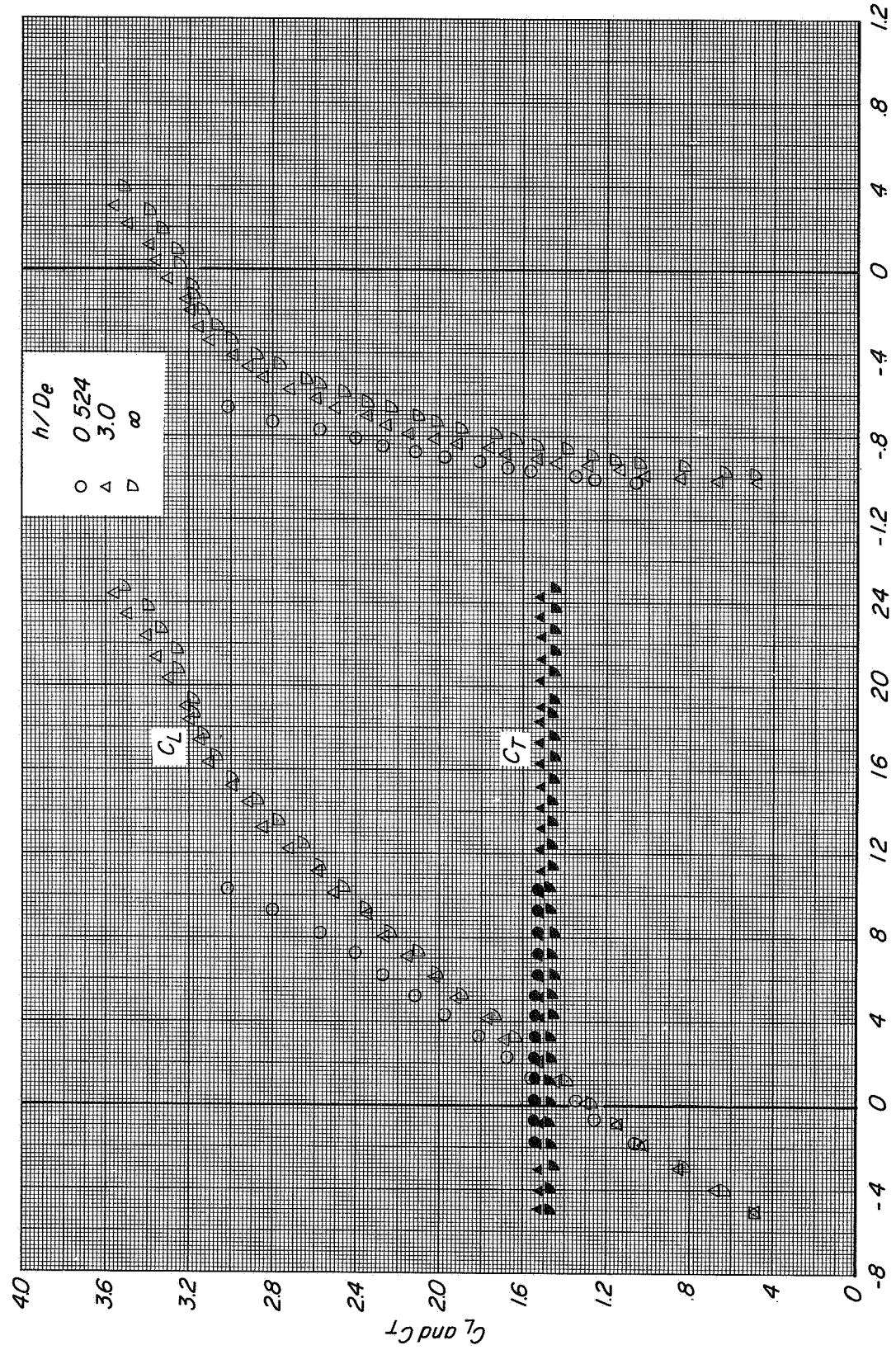

(a) Variation of C_L and C_T with α and C_D with C_L

Figure 88.- Longitudinal aerodynamic characteristics of configuration A with direct-lift and lift-cruise engines deflected 25° $i_t = 0°$; $\beta = 5°$; $C_T \approx 1.45$.

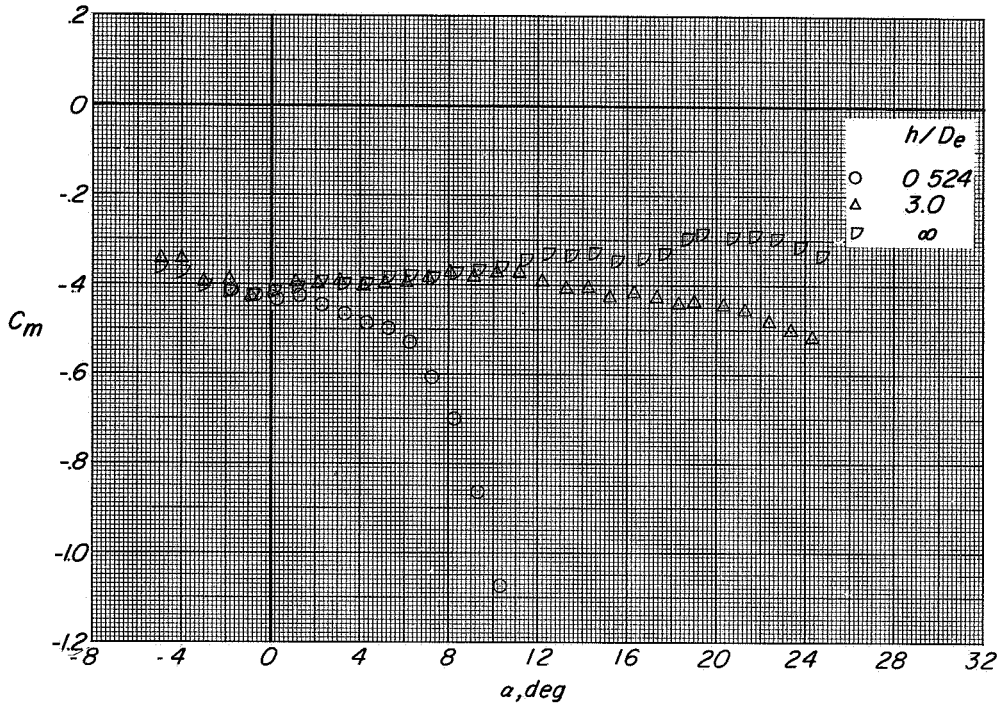

(b) Variation of C_m with α.

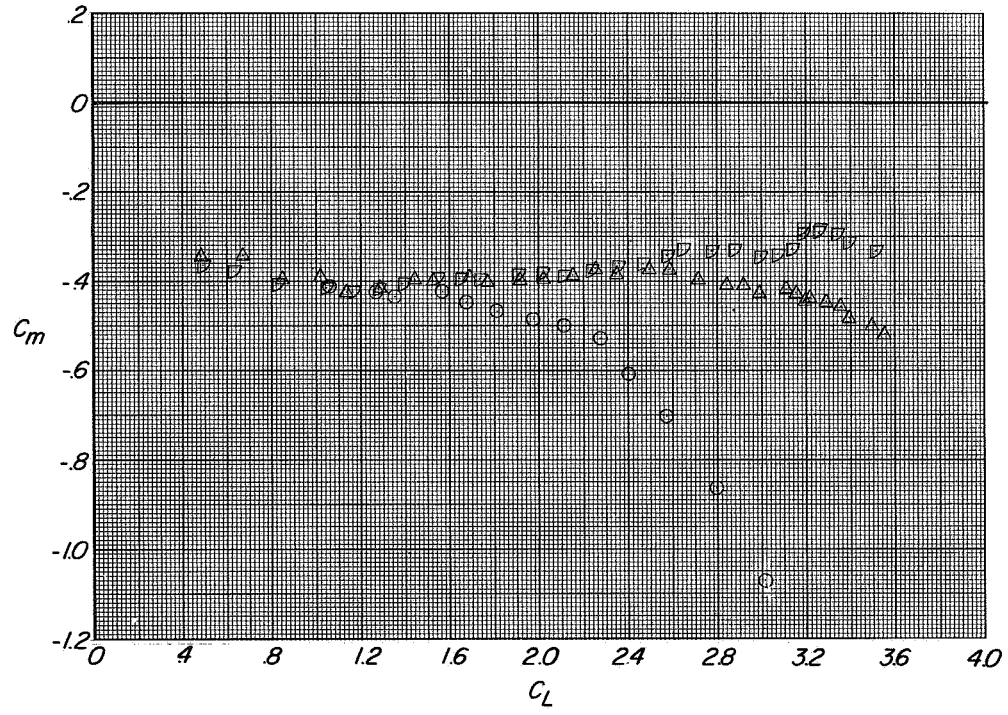

(c) Variation of C_m with C_L

Figure 88.- Continued.

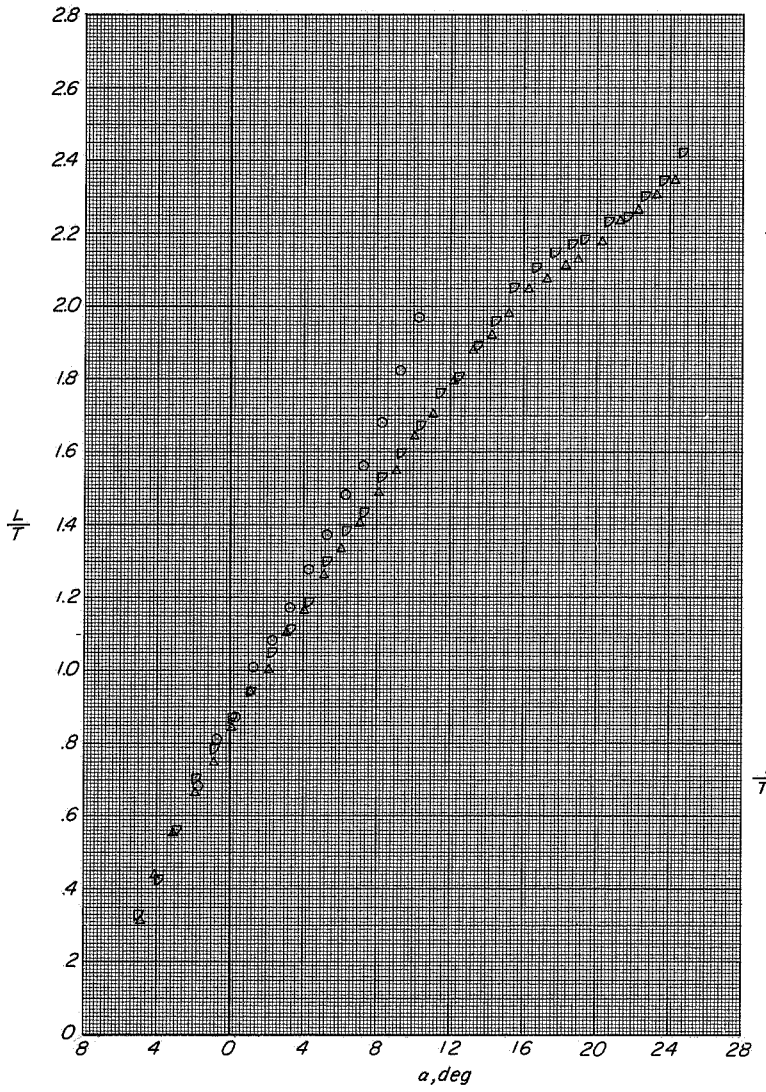

(d) Variation of L/T with α.

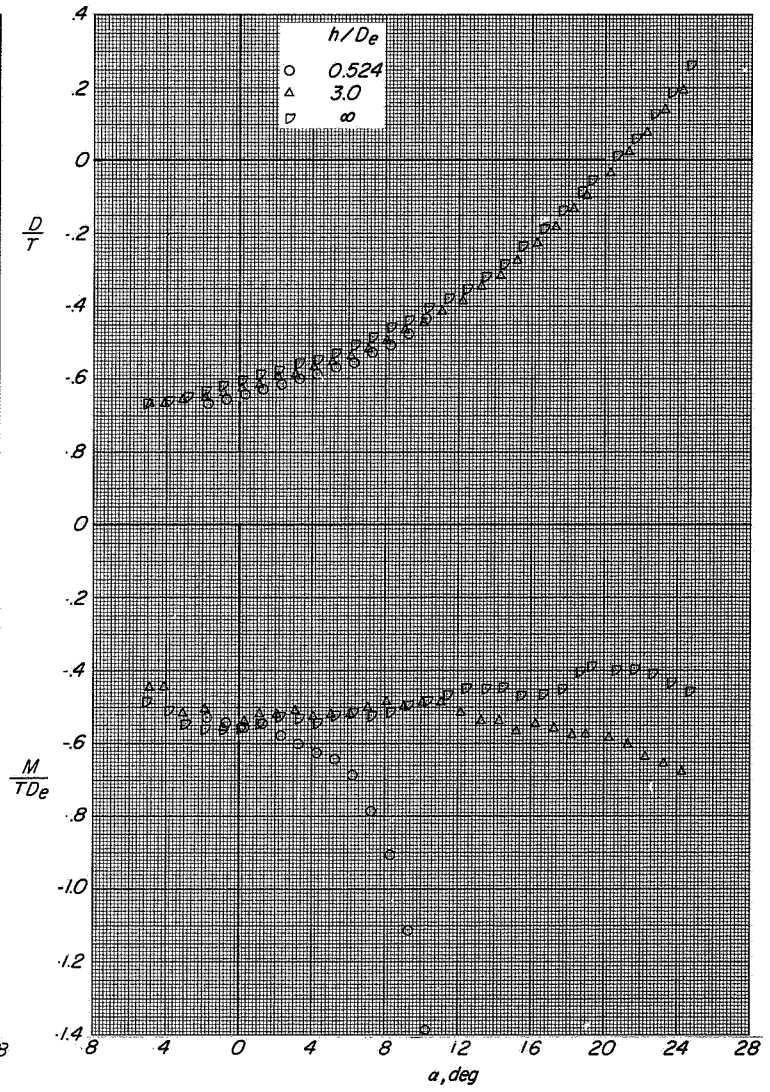

(e) Variation of D/T and M/TD_e with α.

Figure 88.- Concluded.

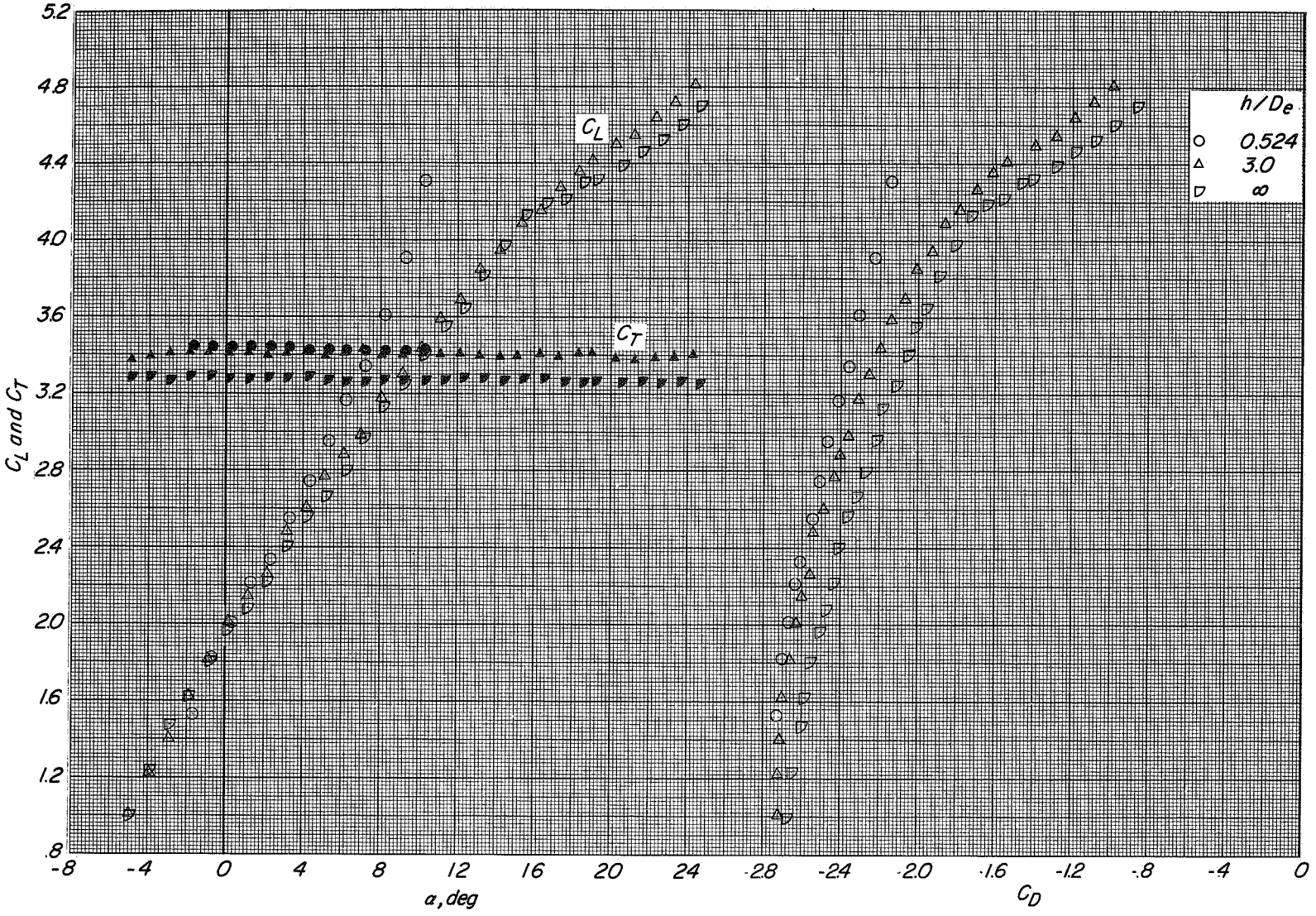

(a) Variation of C_L and C_T with α and C_D with C_L

Figure 89.- Longitudinal aerodynamic characteristics of configuration A with direct-lift and lift-cruise engines deflected 25°. $i_t = 0°$; $\beta = 5°$; $C_T \approx 3.3$.

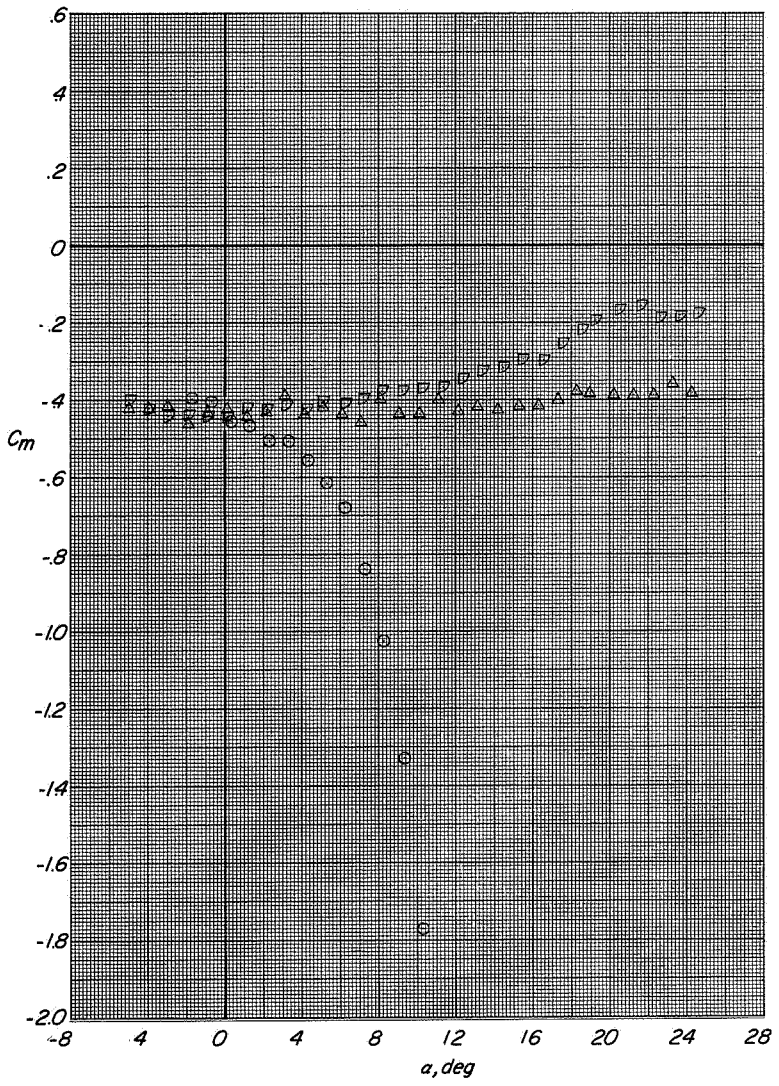

(b) Variation of C_m with α.

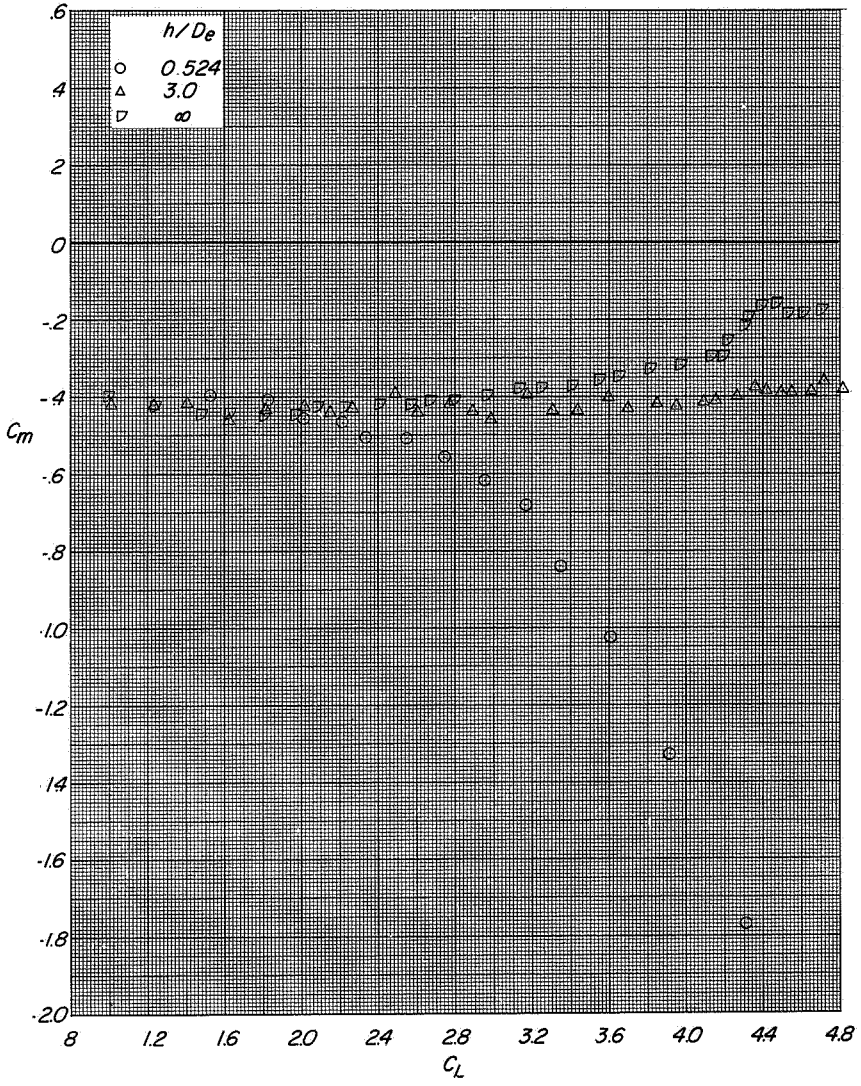

(c) Variation of C_m with C_L.

Figure 89.- Continued.

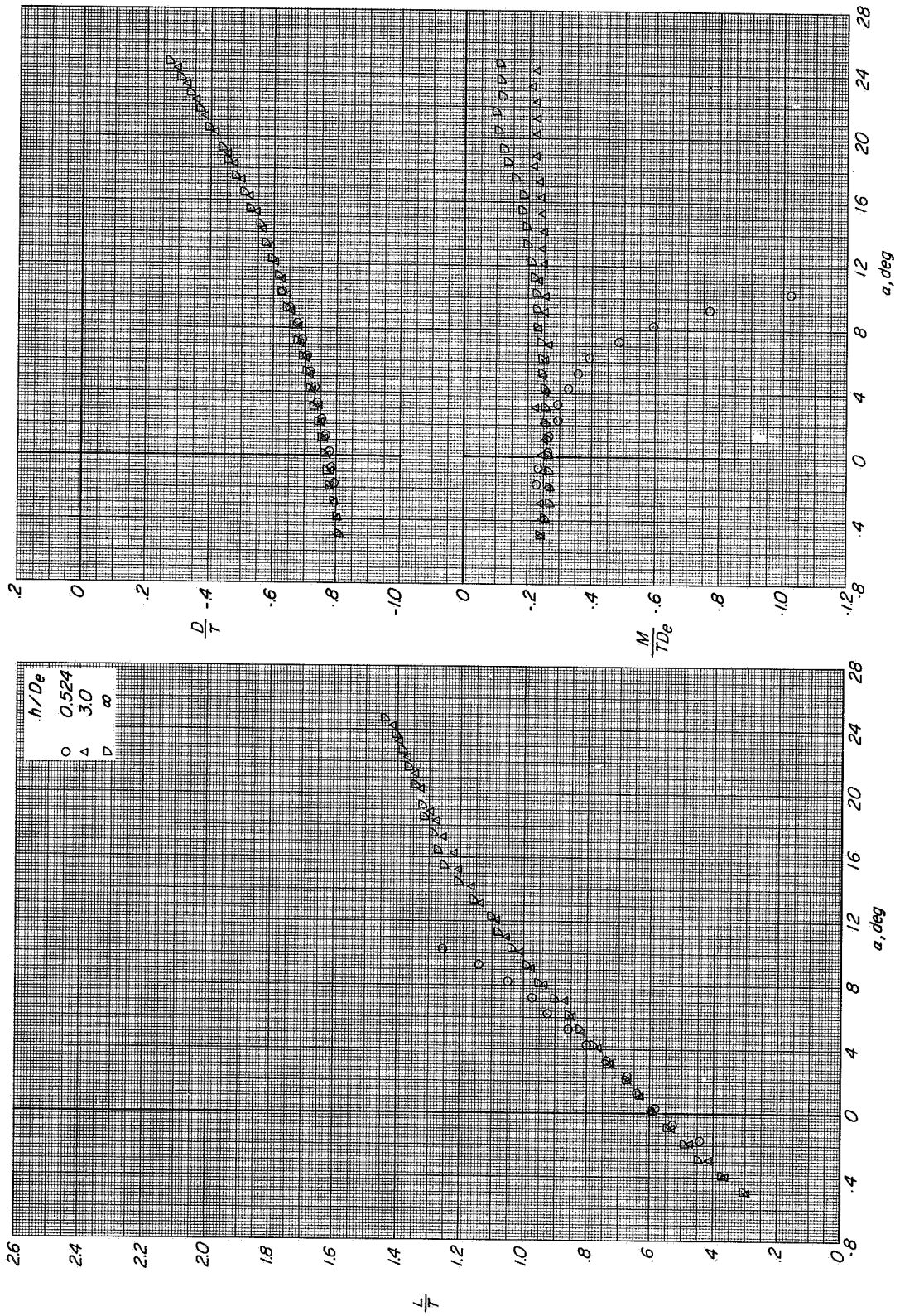

(d) Variation of L/T with α.

(e) Variation of D/T and M/TDe with α.

Figure 89.- Concluded.

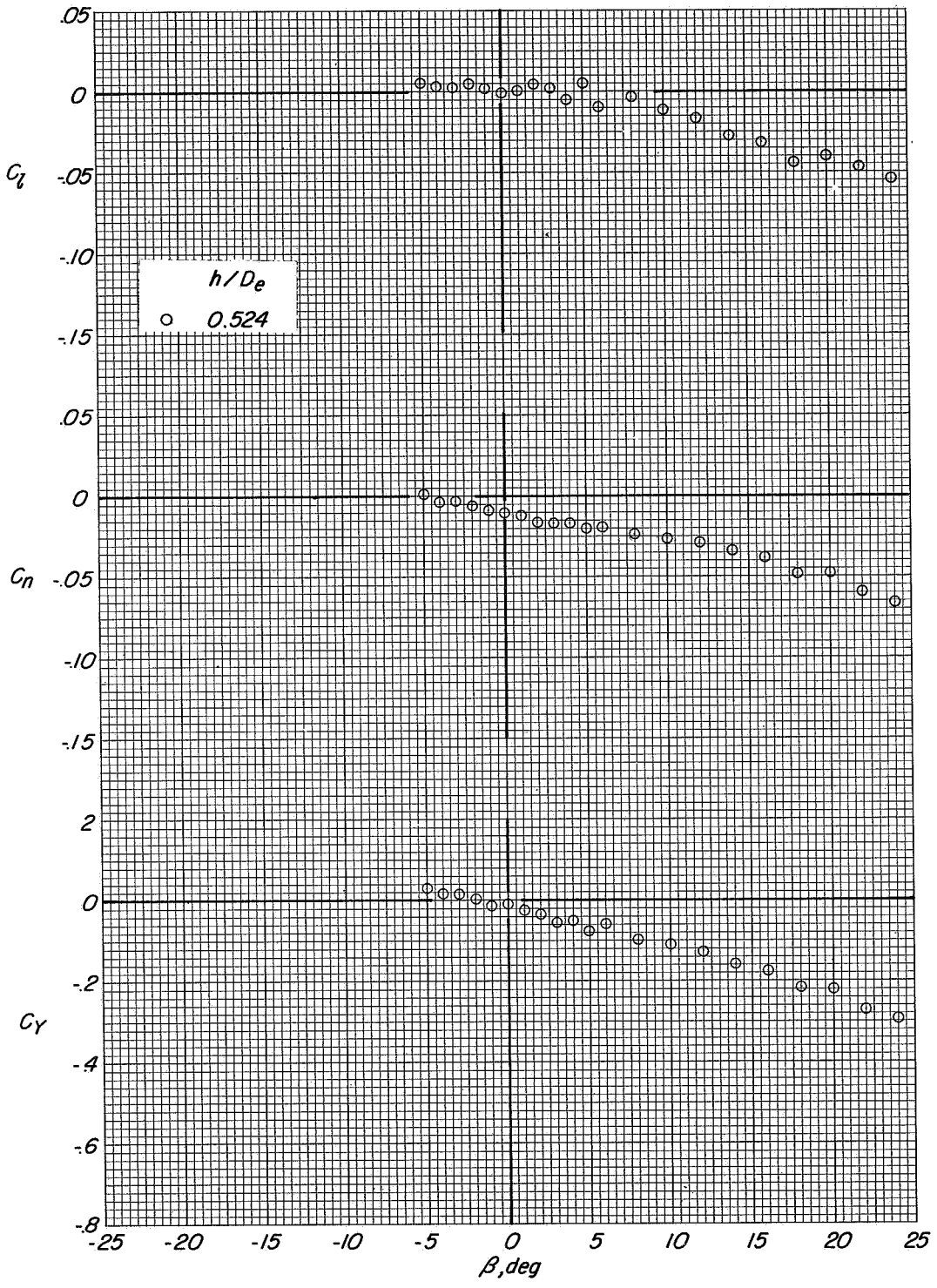

Figure 90.- Lateral aerodynamic characteristics of configuration A with direct-lift and lift-cruise engines deflected 25°. $i_t = 0°$; $\alpha = 0.1°$; $C_T = 0$.

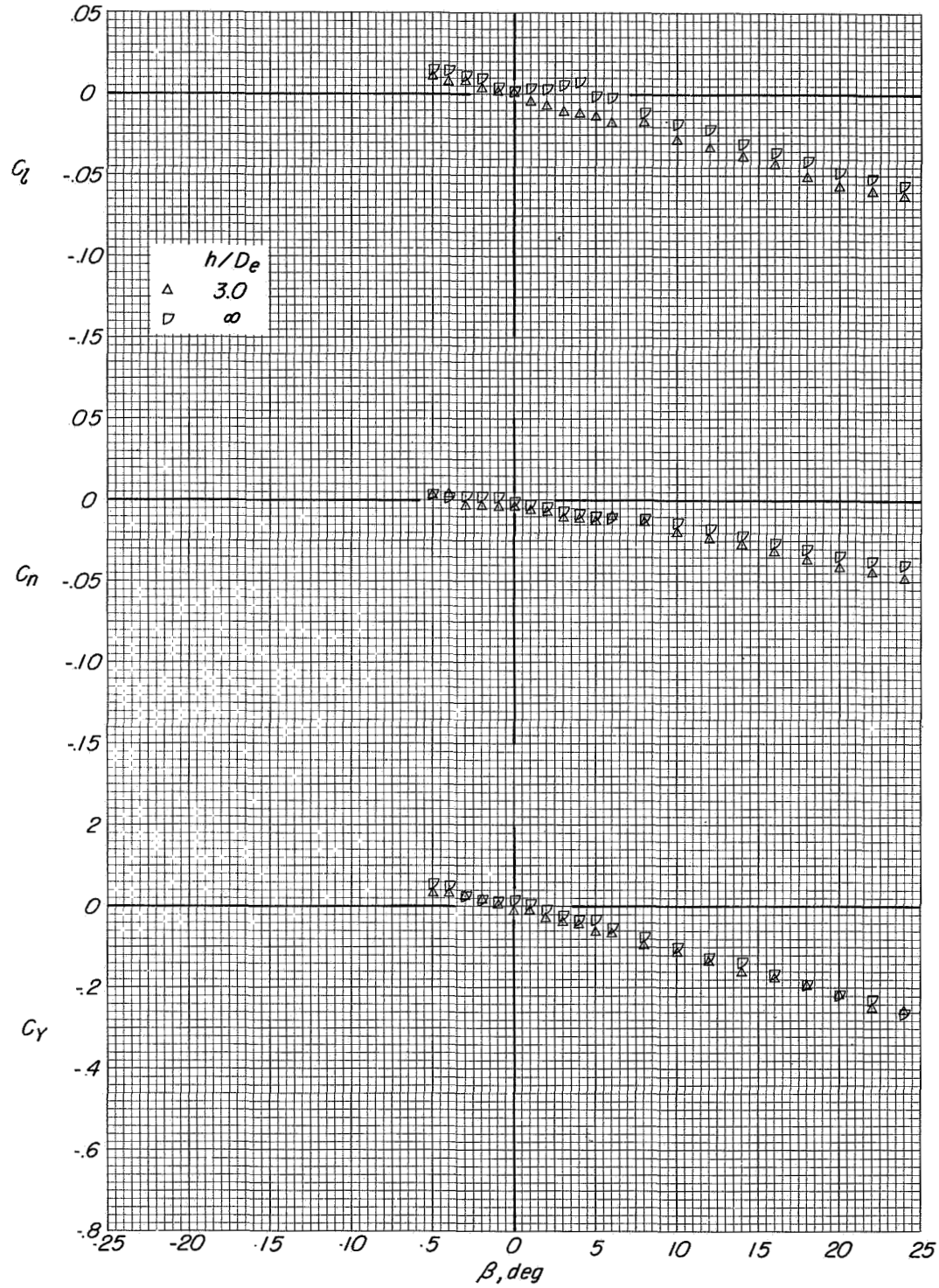

Figure 91.- Lateral aerodynamic characteristics of configuration A with direct-lift and lift-cruise engines deflected 25°. $i_t = 0°$; $\alpha = 12.3°$; $C_T = 0$.

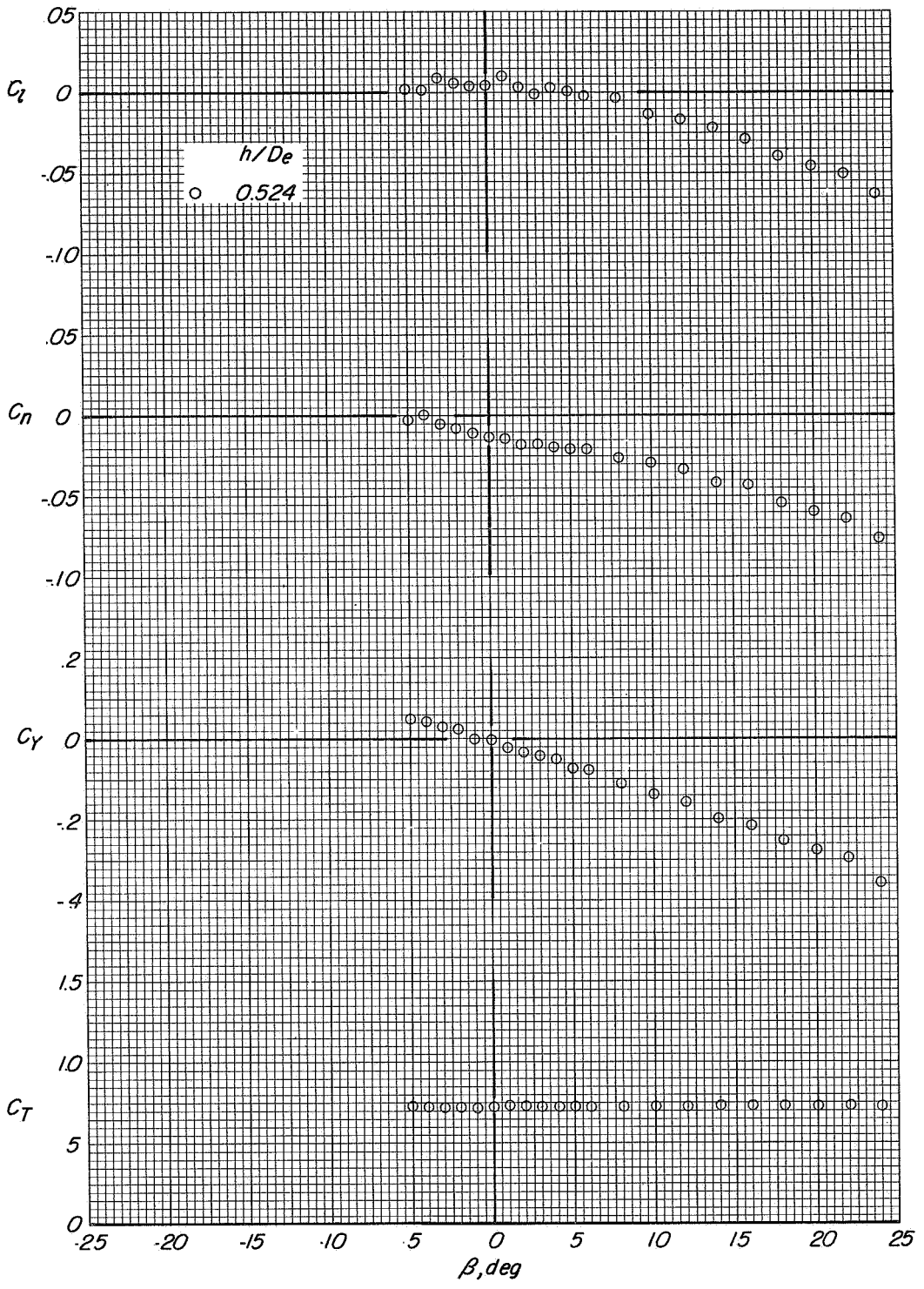

Figure 92.- Lateral aerodynamic characteristics of configuration A with direct-lift and lift-cruise engines deflected 25°. $i_t = 0°$; $\alpha = 0.2°$; $C_T \approx 0.65$.

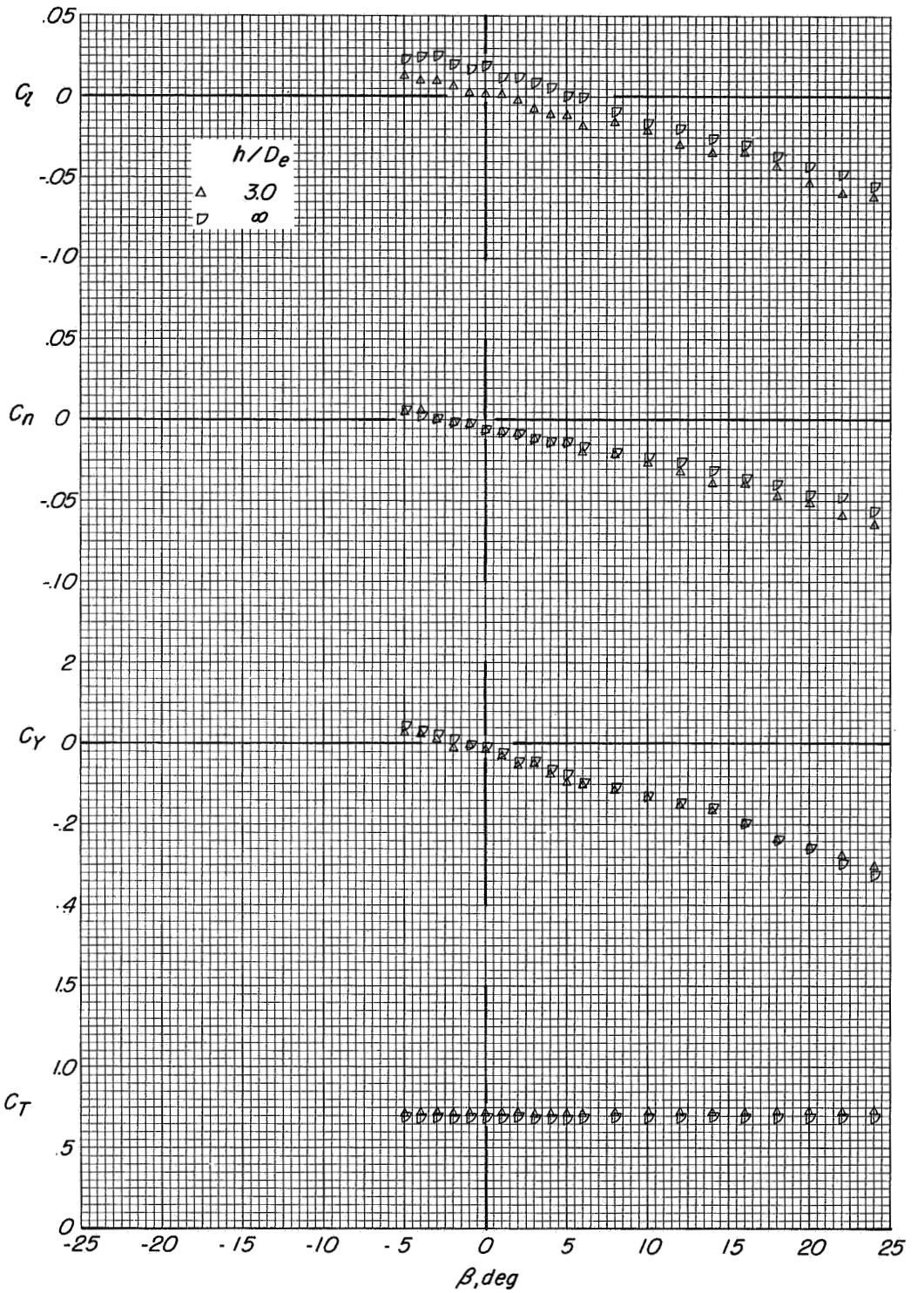

Figure 93.- Lateral aerodynamic characteristics of configuration A with direct-lift and lift-cruise engines deflected 25°, $i_t = 0°$; $\alpha = 12.3°$; $C_T \approx 0.65$.

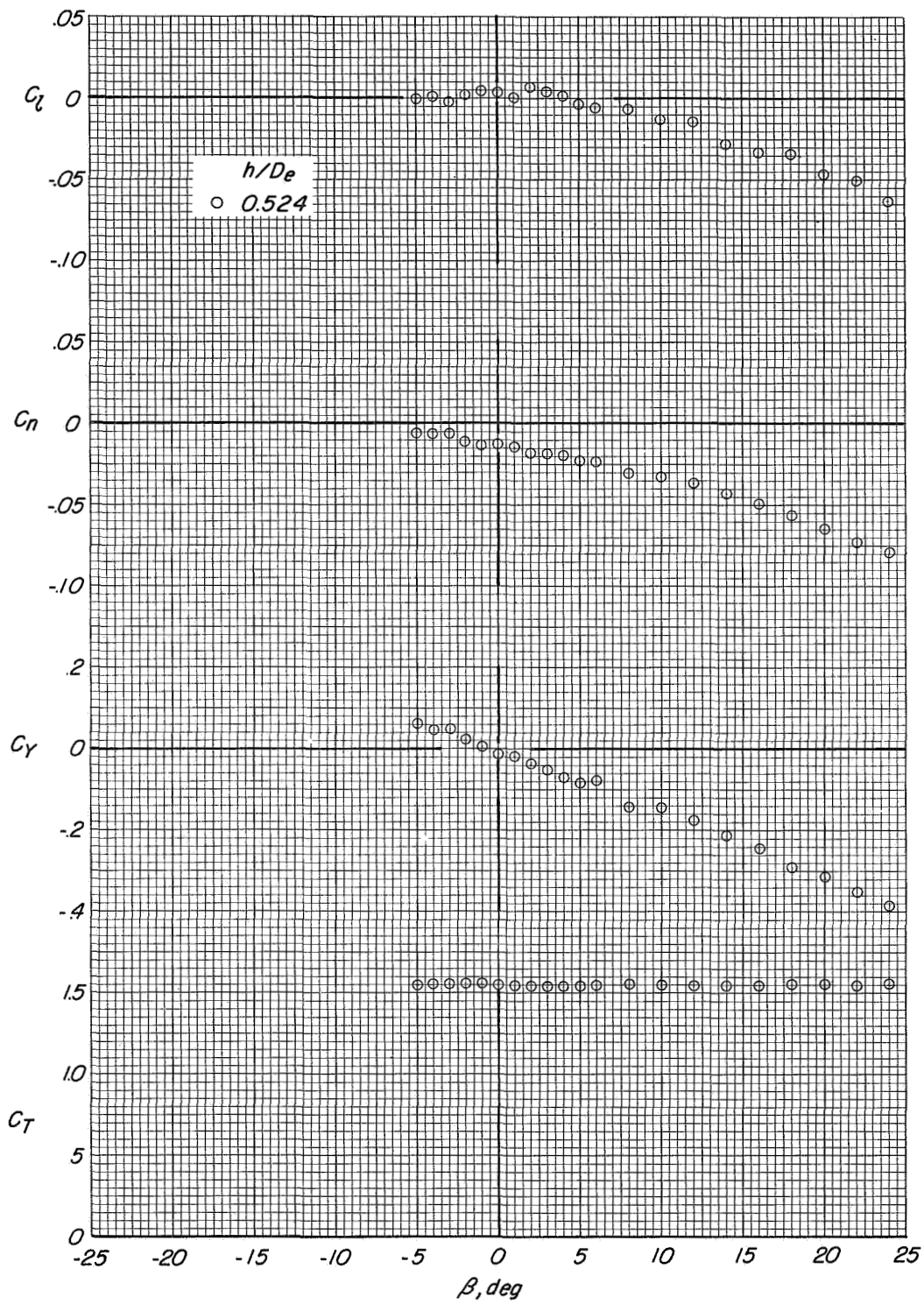

Figure 94.- Lateral aerodynamic characteristics of configuration A with direct-lift and lift-cruise engines deflected 25°. $i_t = 0°$; $\alpha = 0.3°$; $C_T \approx 1.45$.

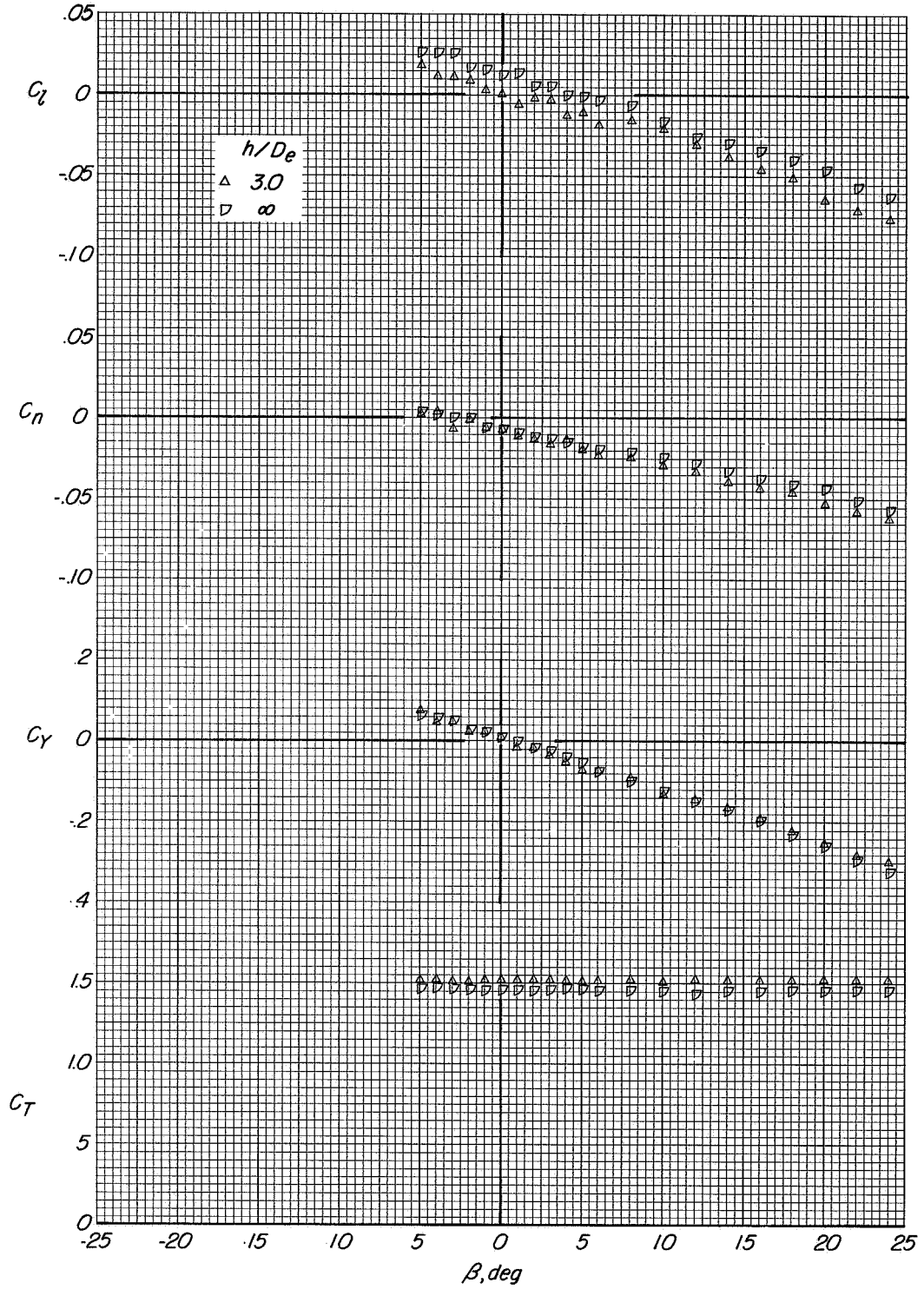

Figure 95.- Lateral aerodynamic characteristics of configuration A with direct-lift and lift-cruise engines deflected 25°. $i_t = 0°$; $\alpha = 12.3°$; $C_T \approx 1.45$.

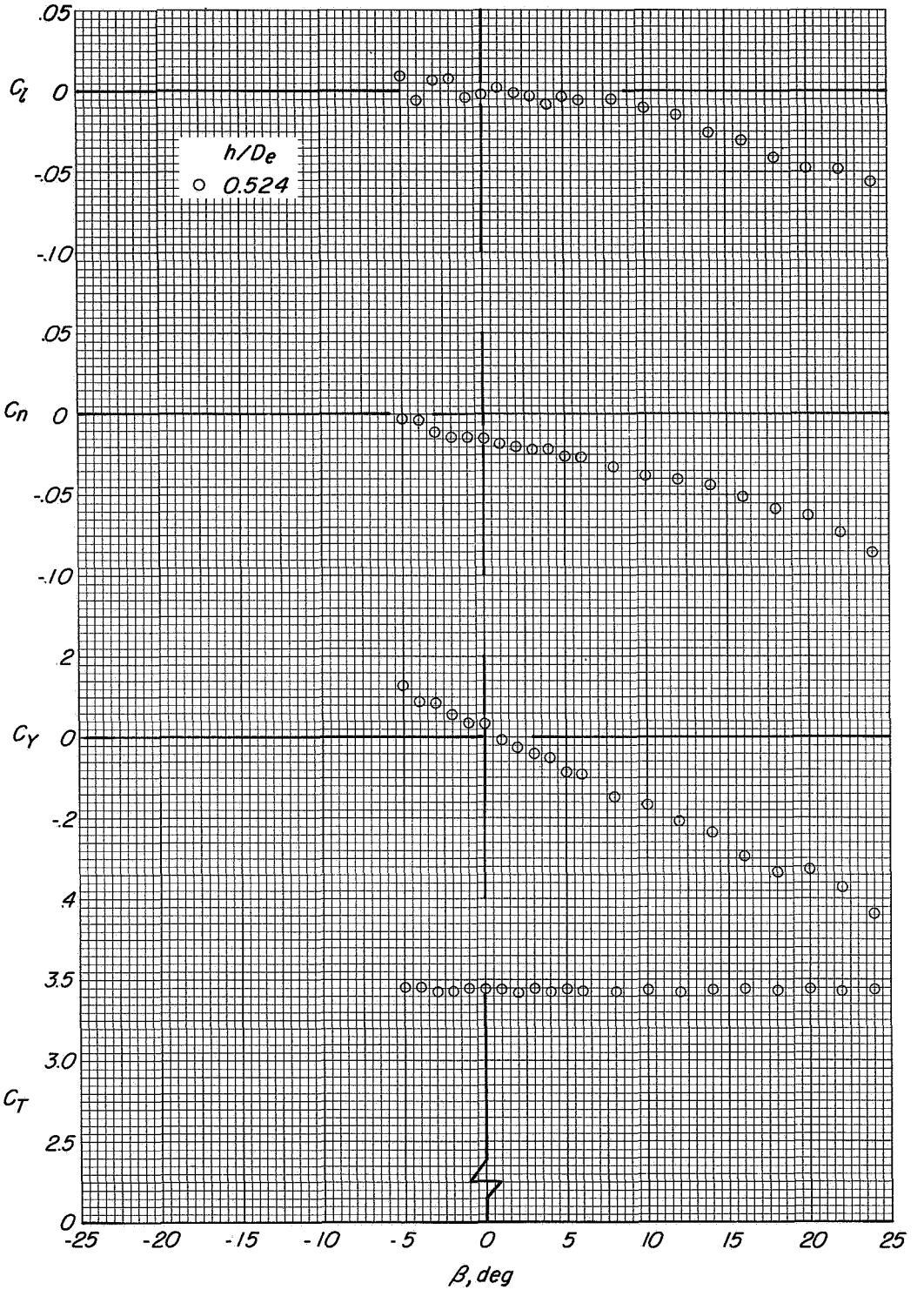

Figure 96.- Lateral aerodynamic characteristics of configuration A with direct-lift and lift-cruise engines deflected 25^0. $i_t = 0^0$; $\alpha = 0.3^0$; $C_T \approx 3.3$.

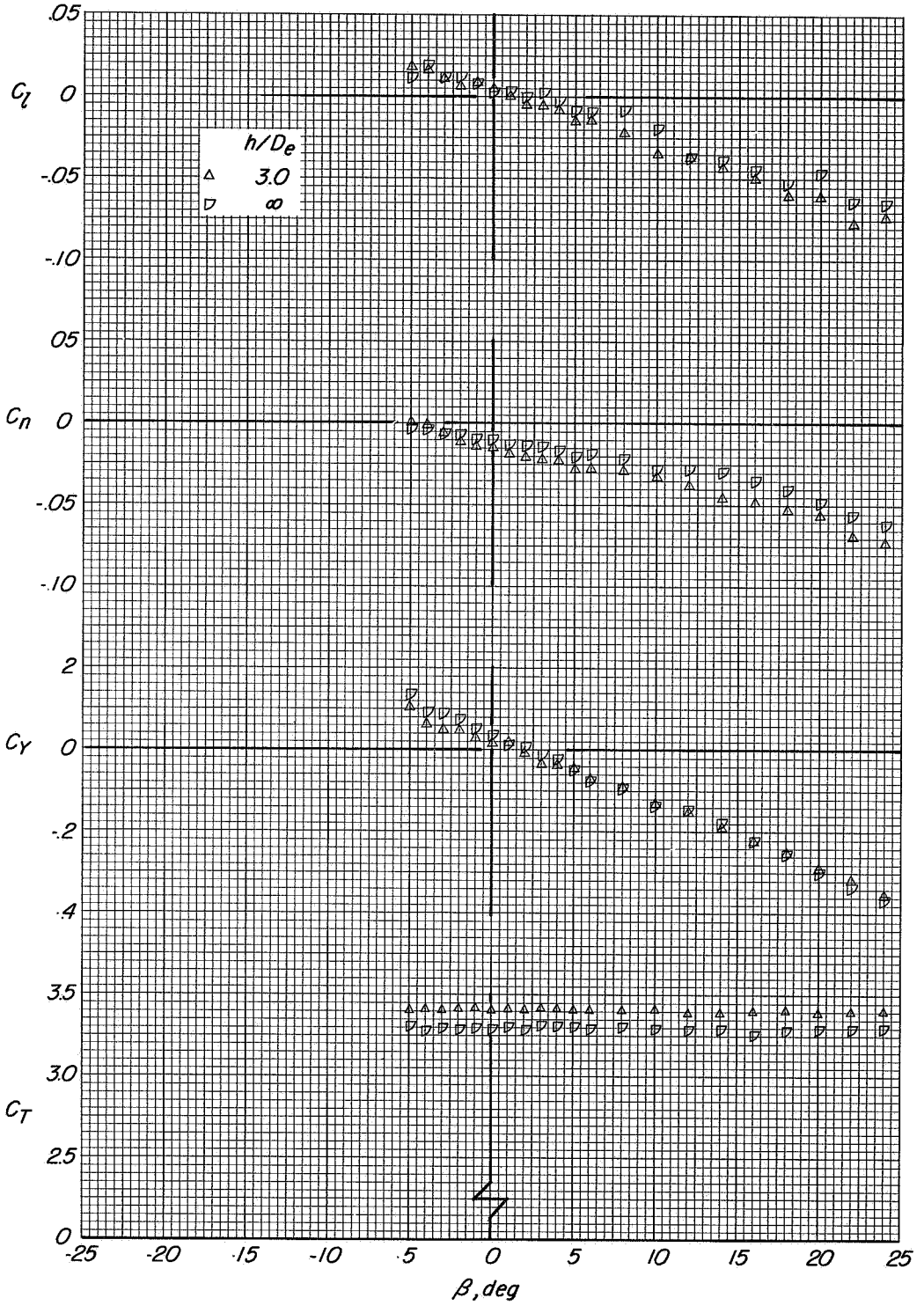

Figure 97.- Lateral aerodynamic characteristics of configuration A with direct-lift and lift-cruise engines deflected 25°. $i_t = 0°$; $\alpha = 12.2°$; $C_T \approx 3.3$.

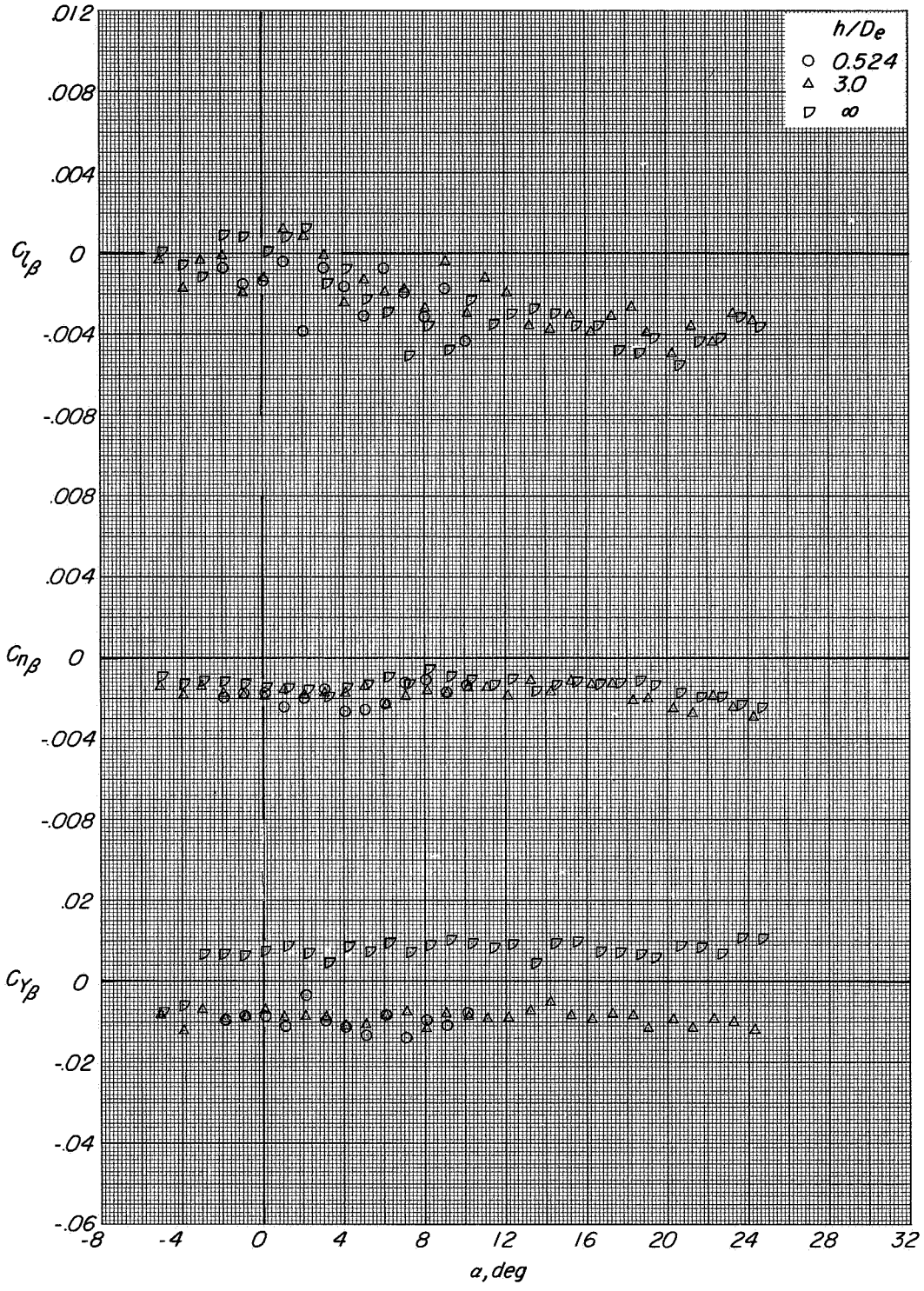

(a) $C_T = 0.$

Figure 98.- Variation of C_{l_β}, C_{n_β}, and C_{Y_β} with angle of attack for configuration A with direct-lift and lift-cruise engines deflected 25°. $i_t = 0°$

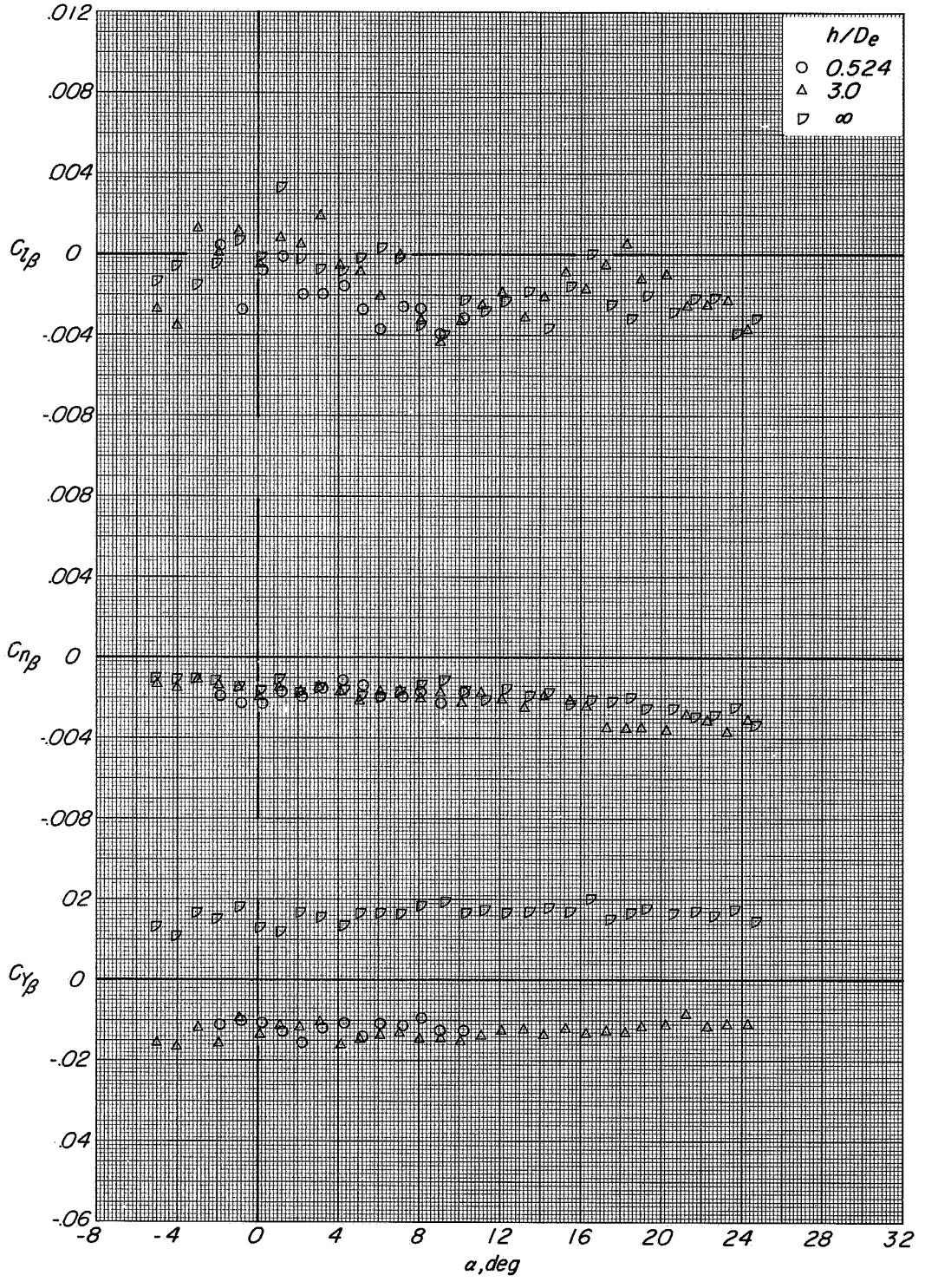

(b) $C_T \approx 0.65$.

Figure 98.- Continued.

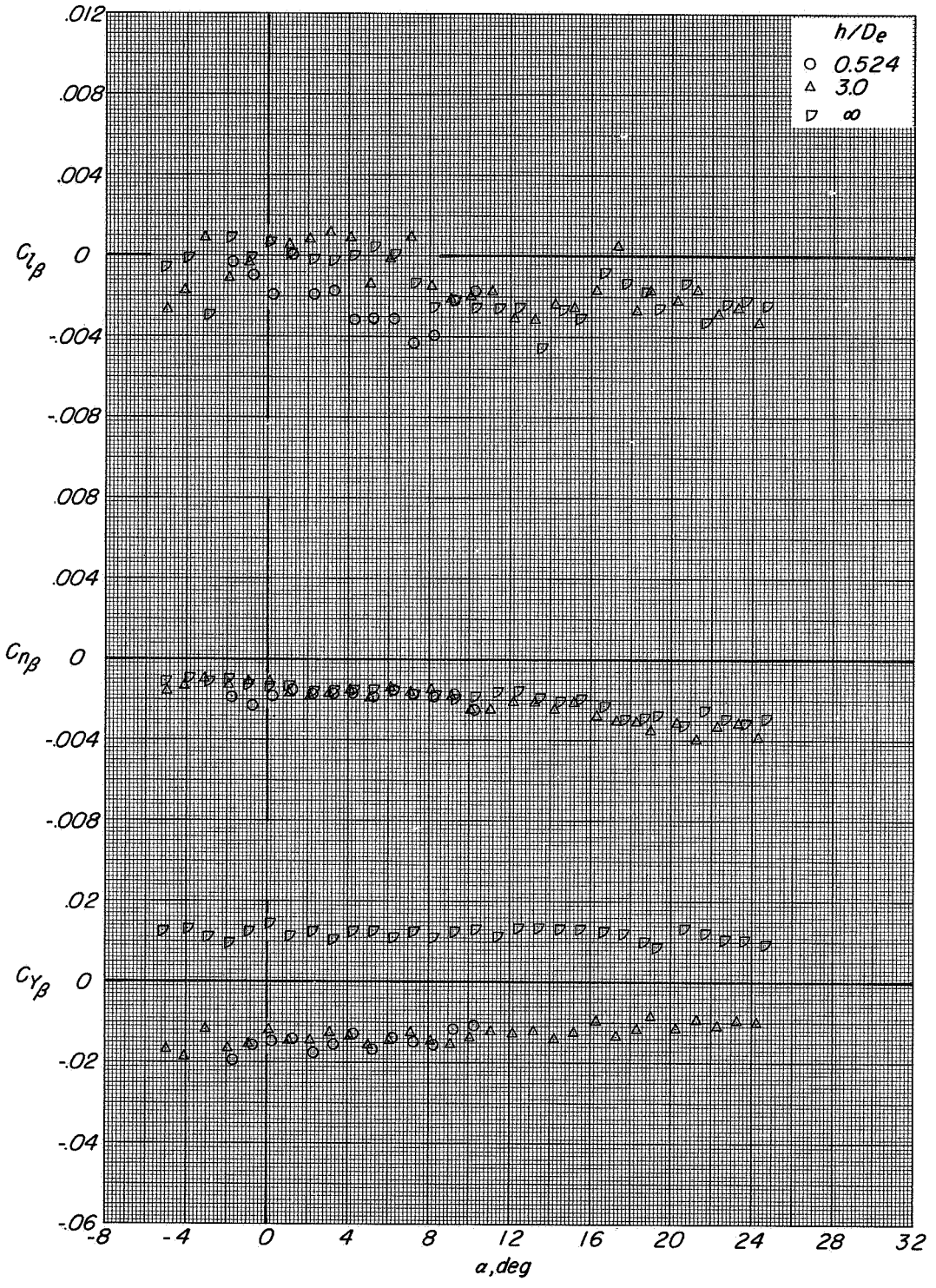

(c) $C_T \approx 1.45$.

Figure 98.- Continued.

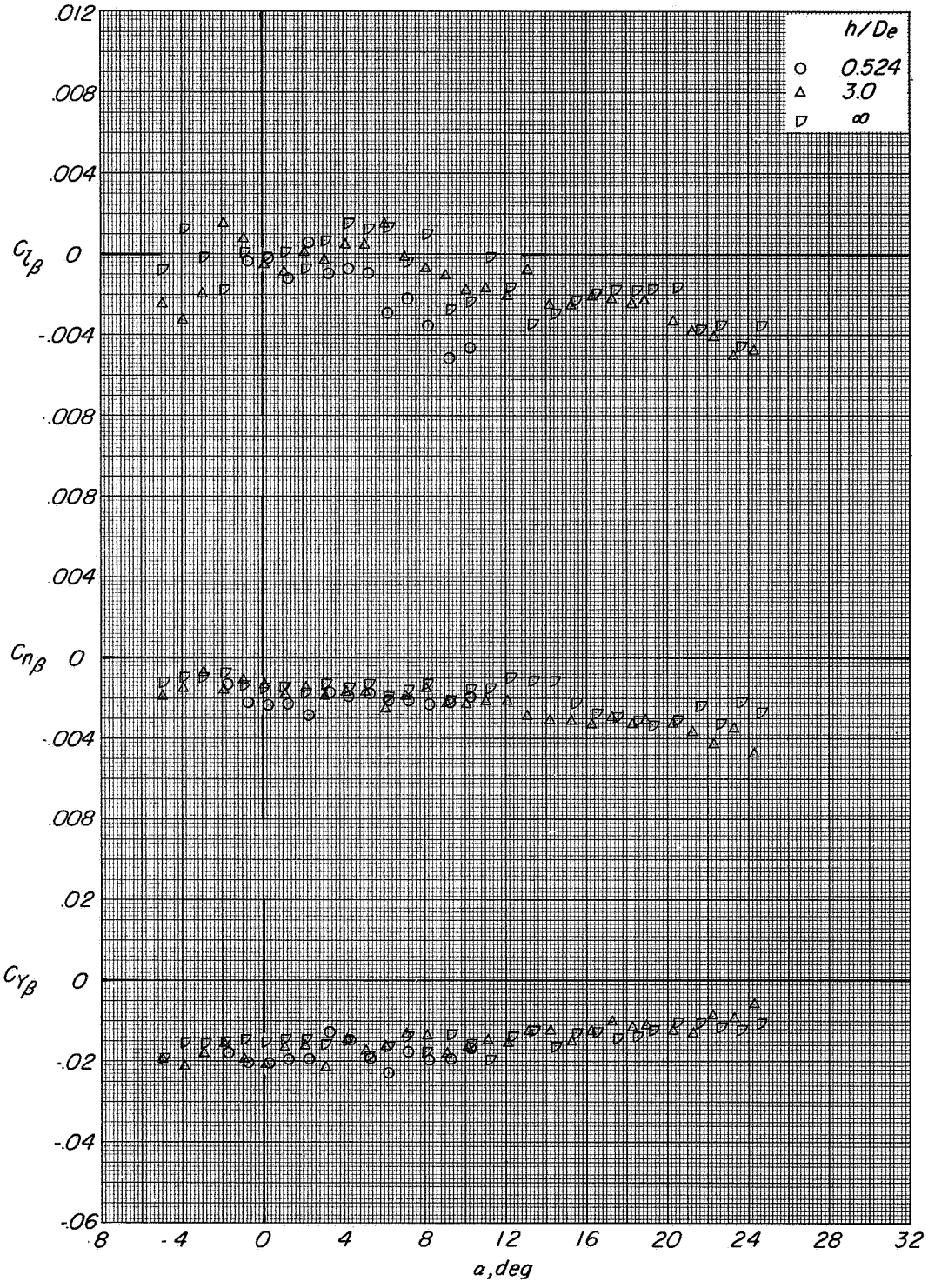

(d) $C_T \approx 3.3$.

Figure 98. Concluded.

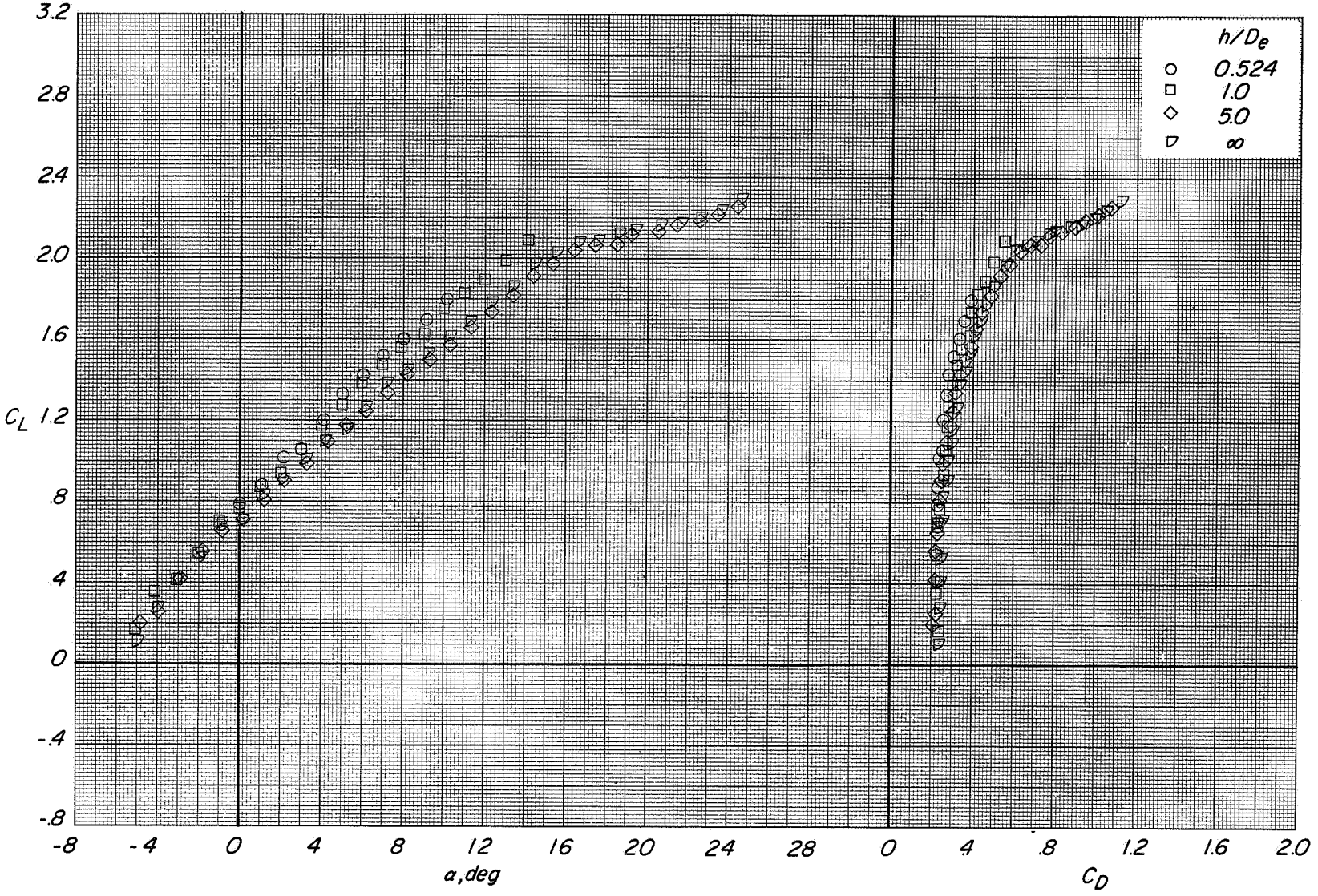

(a) Variation of C_L with α and C_D with C_L

Figure 99.- Longitudinal aerodynamic characteristics of configuration A with left direct-lift engines deflected 70^0, right direct-lift engines deflected 110^0, and lift-cruise engines deflected 90^0. $i_t = 0^0$; $\beta = 5^0$; $C_T = 0$.

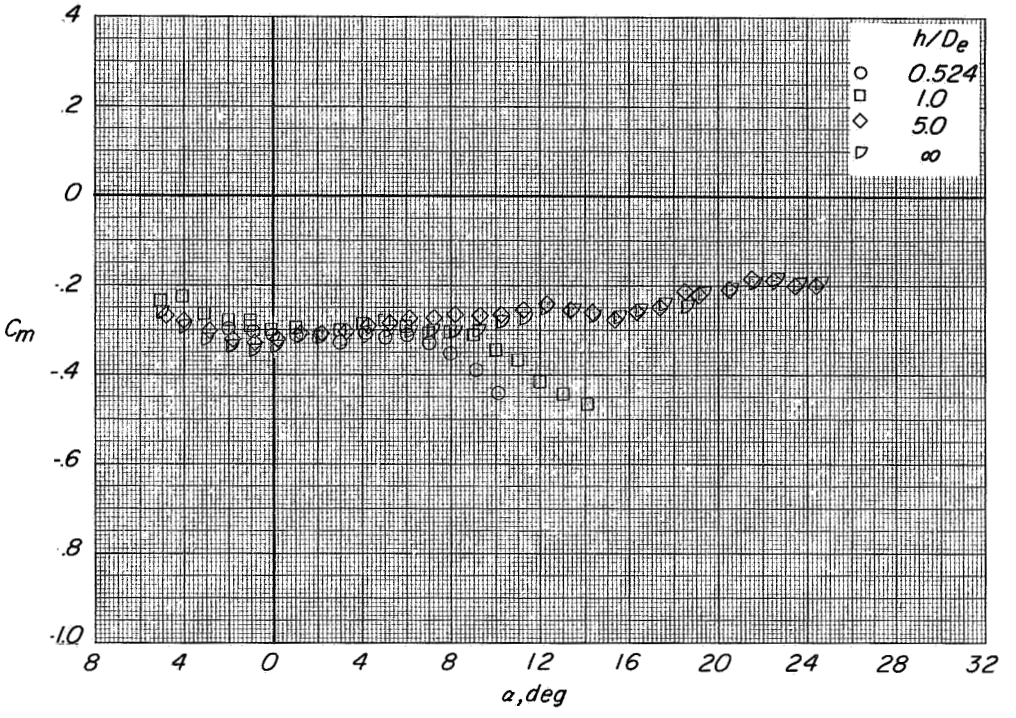

(b) Variation of C_m with α.

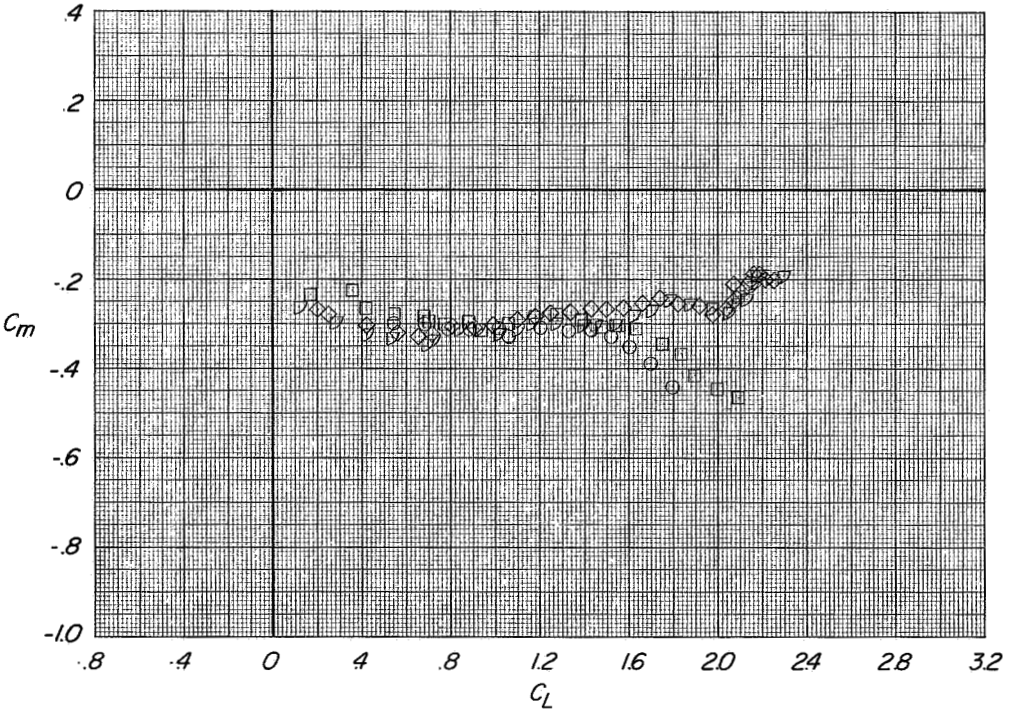

(c) Variation of C_m with C_L

Figure 99.- Concluded.

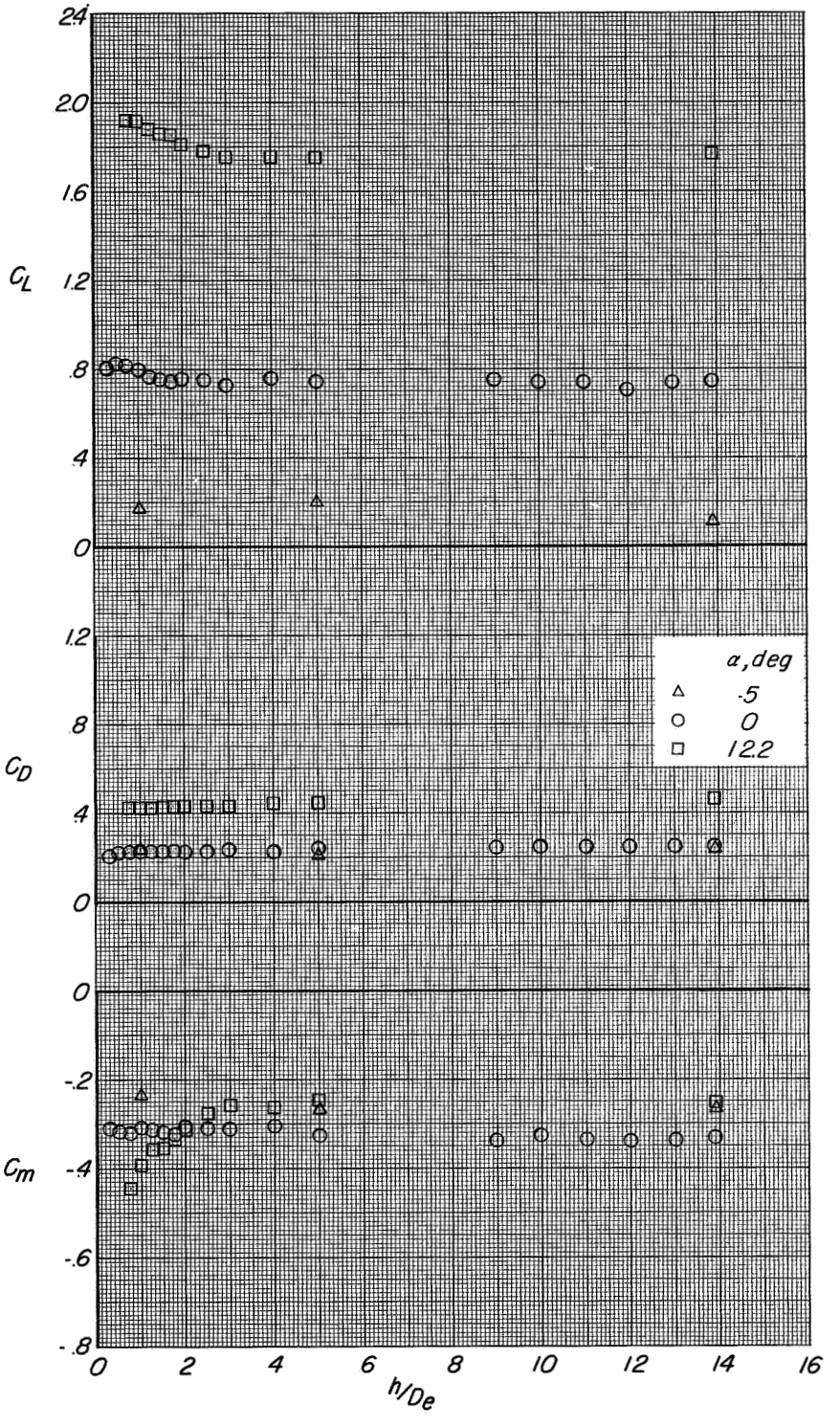

Figure 100.- Effect of height above the moving-belt ground plane on the longitudinal aerodynamic characteristics of configuration A with left direct-lift engines deflected 70°, right direct-lift engines deflected 110°, and lift-cruise engines deflected 90°. $i_t = 0°$; $\beta = 5°$; $C_T = 0$.

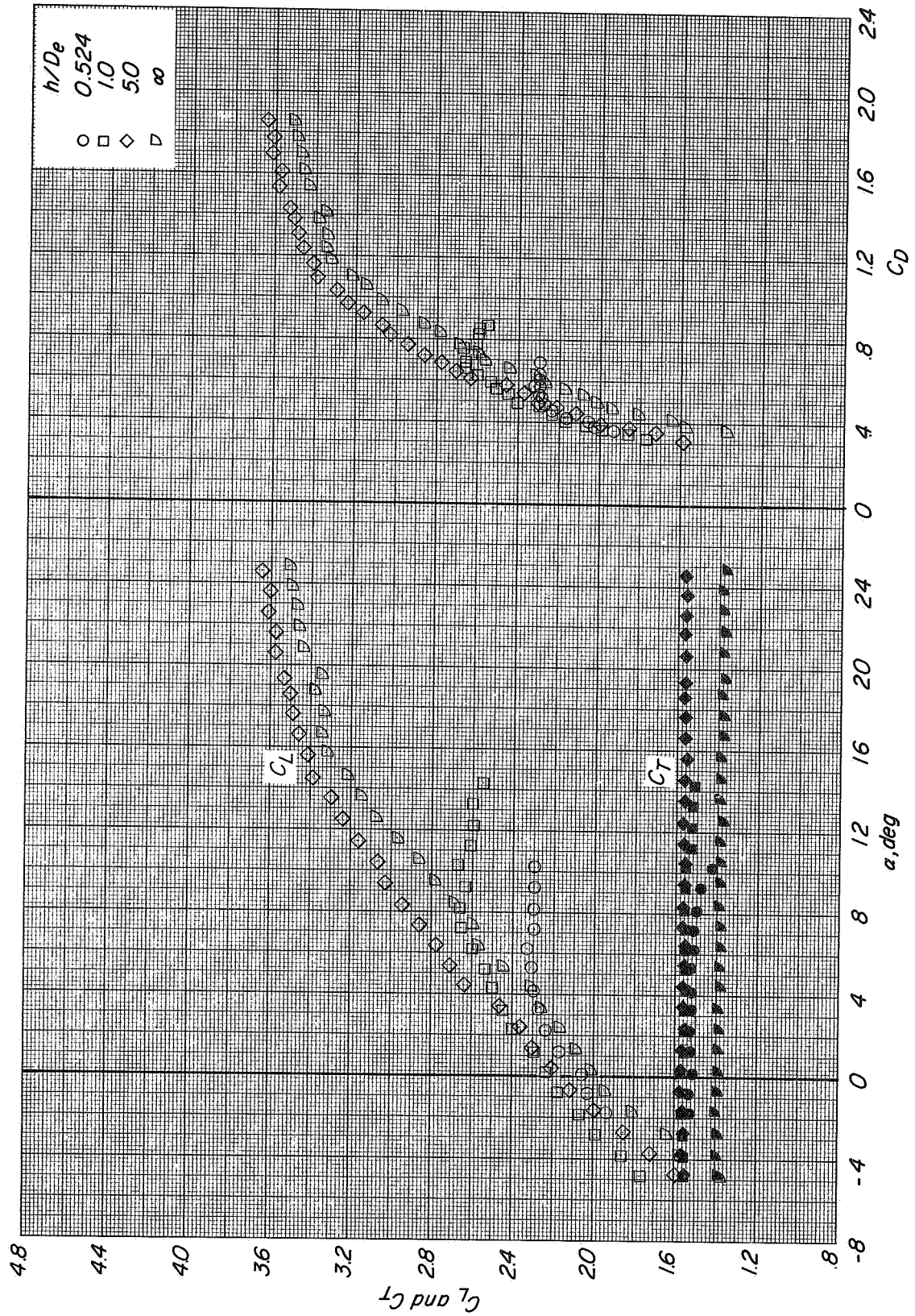

(a) Variation of C_L and C_T with α and C_D with C_L.

Figure 101.- Longitudinal aerodynamic characteristics of configuration A with left direct-lift engines deflected 70°, right direct-lift engines deflected 110°, and lift-cruise engines deflected 90°. $i_t = 0°$; $\beta = 5°$; $C_T \approx 1.45$.

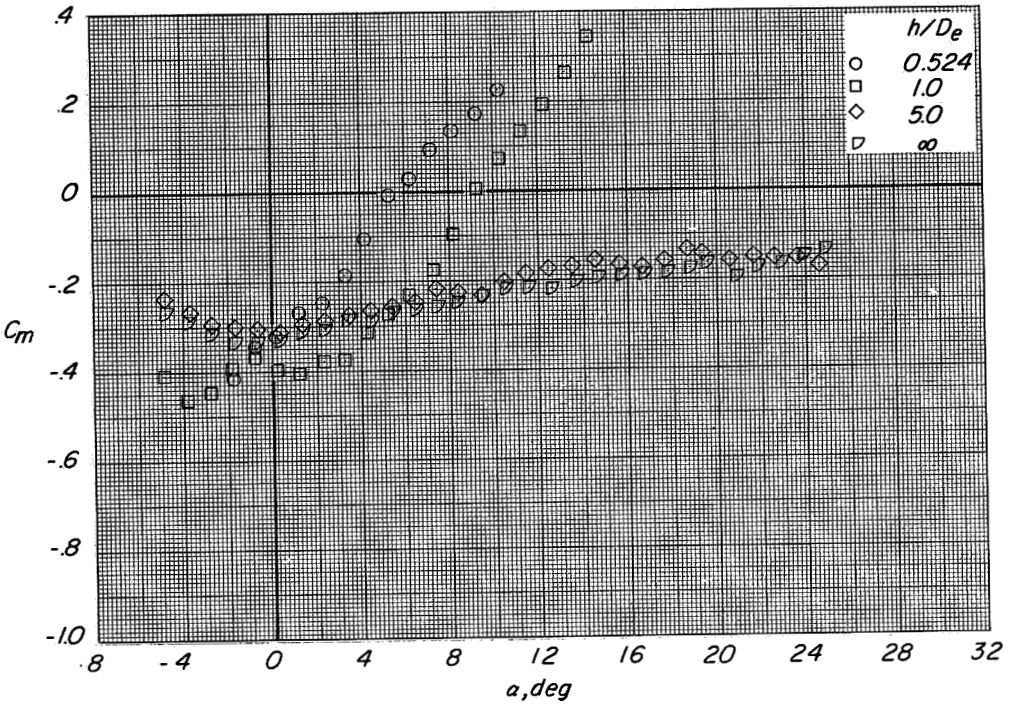

(b) Variation of C_m with α.

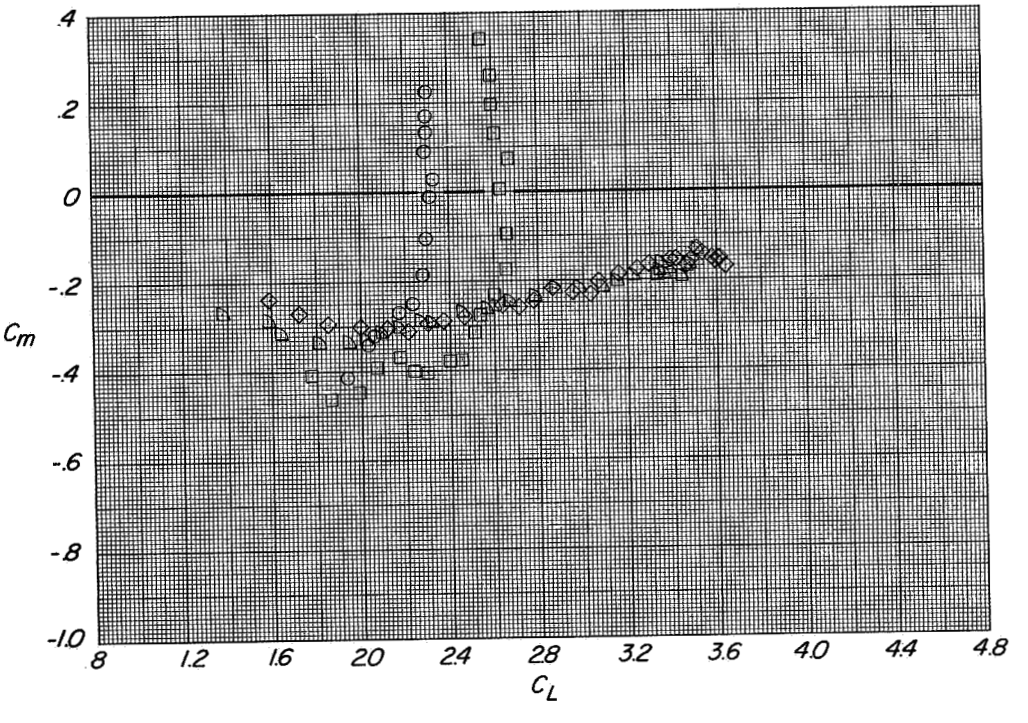

(c) Variation of C_m with C_L

Figure 101. Continued.

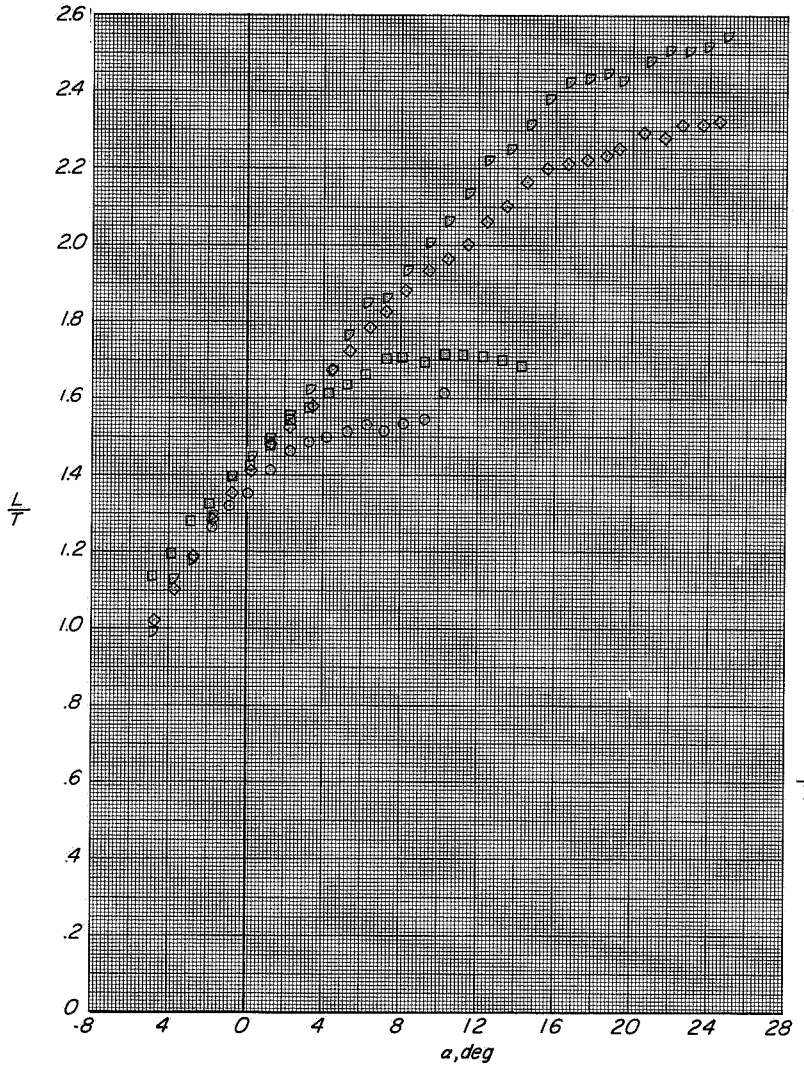

(d) Variation of L/T with α.

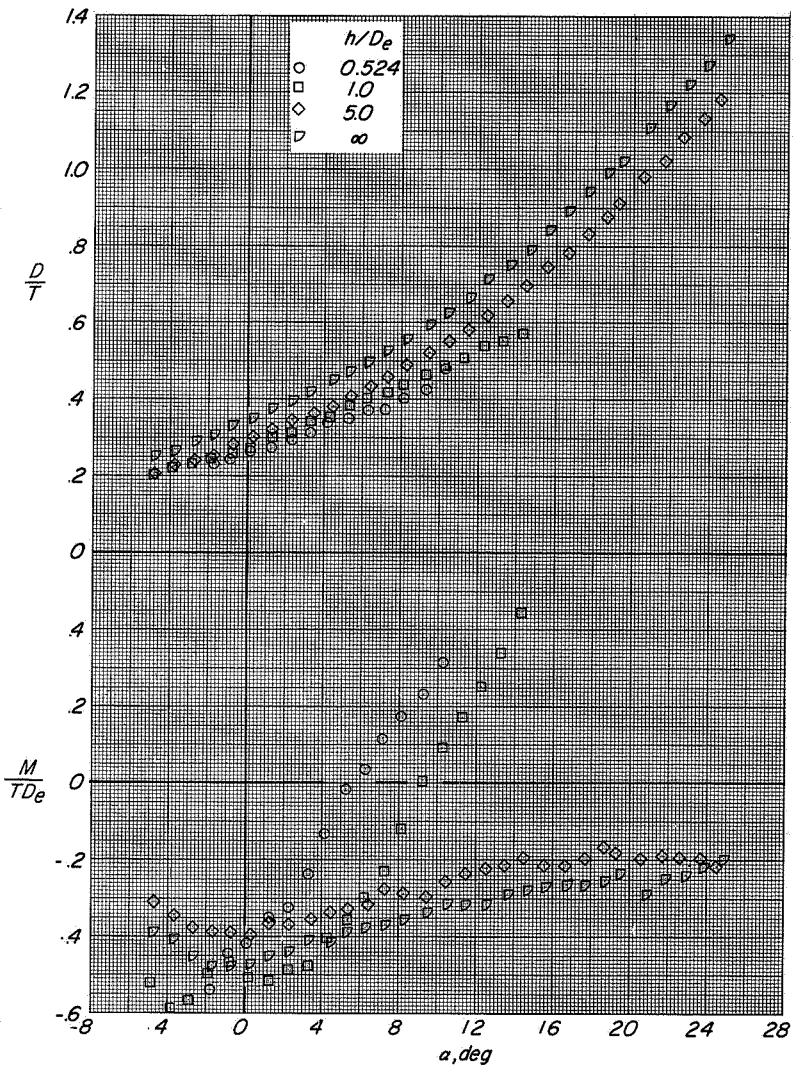

(e) Variation of D/T and M/TDe with α.

Figure 101.- Concluded.

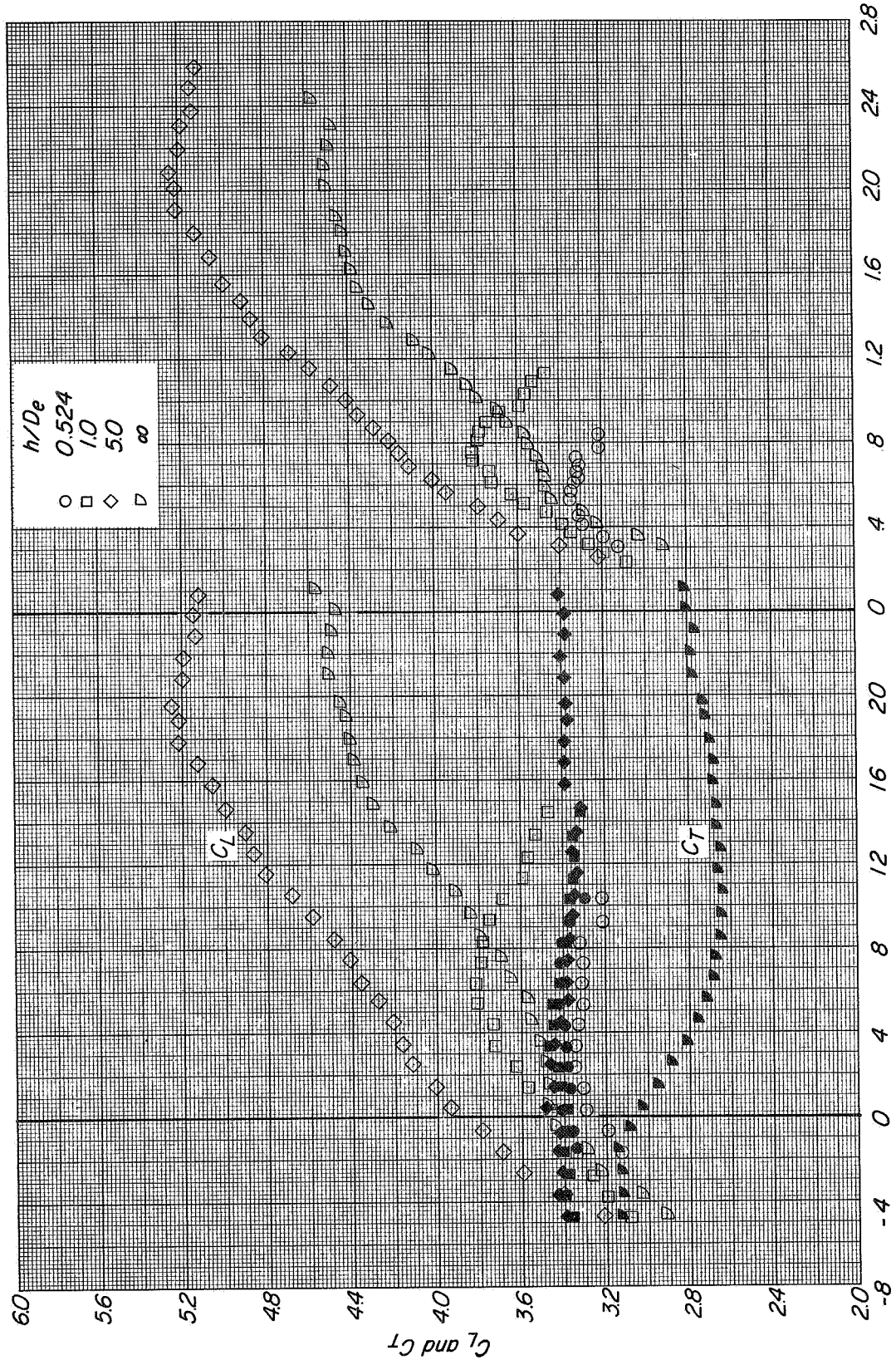

(a) Variation of C_L and C_T with α and C_D with C_L

Figure 102.- Longitudinal aerodynamic characteristics of configuration A with left direct-lift engines deflected 70°, right direct-lift engines deflected 110°, and lift-cruise engines deflected 90°. $i_t = 0°$; $\beta = 5°$; $C_T \approx 3.3$.

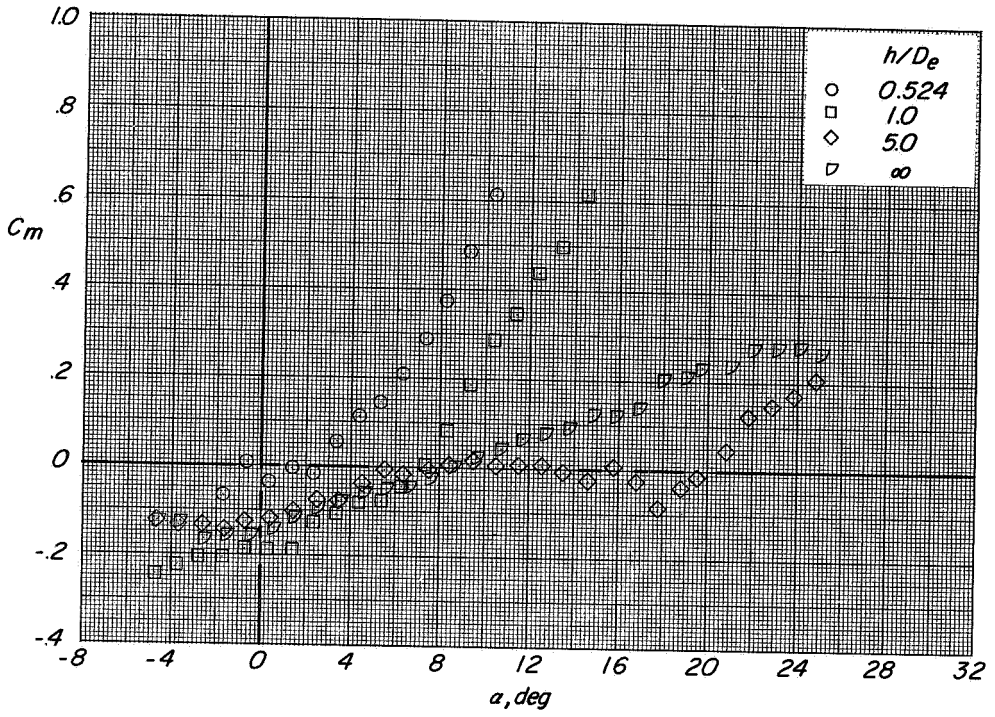

(b) Variation of C_m with α.

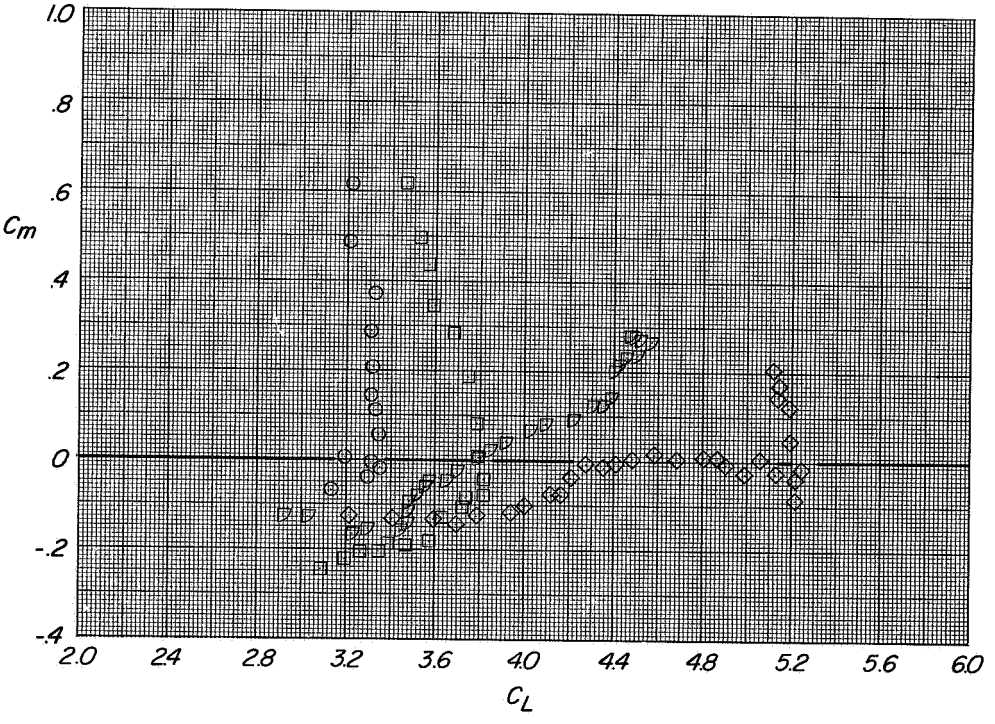

(c) Variation of C_m with C_L

Figure 102.- Continued.

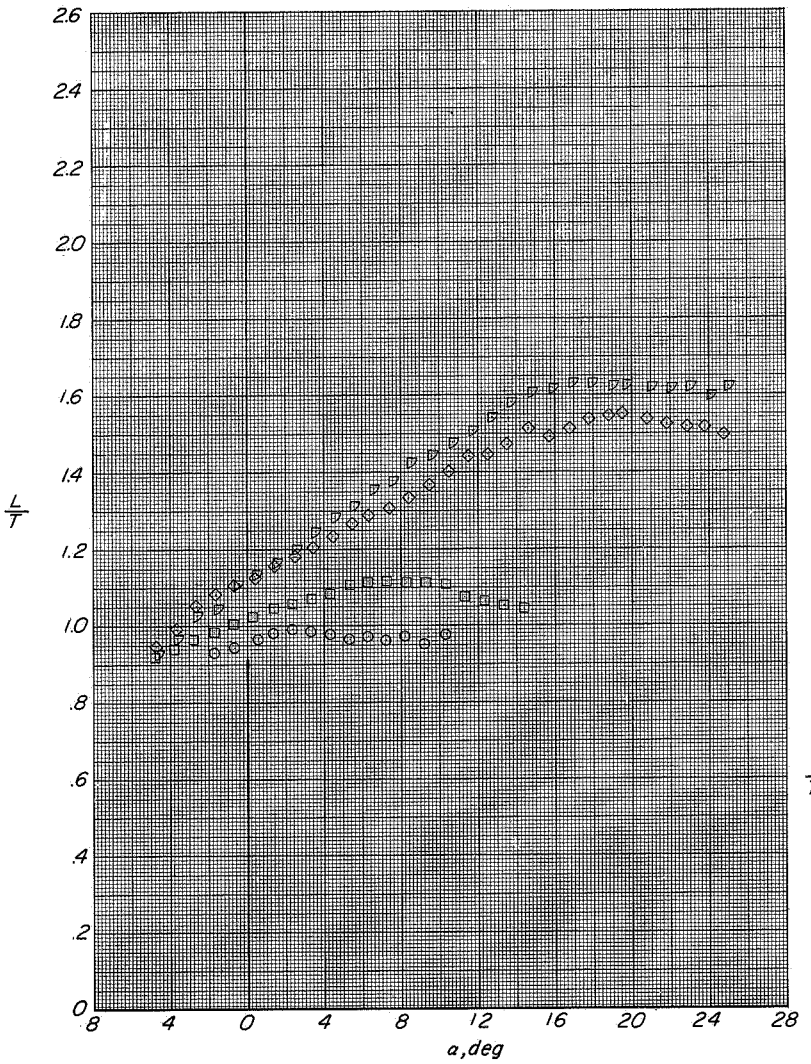

(d) Variation of L/T with α.

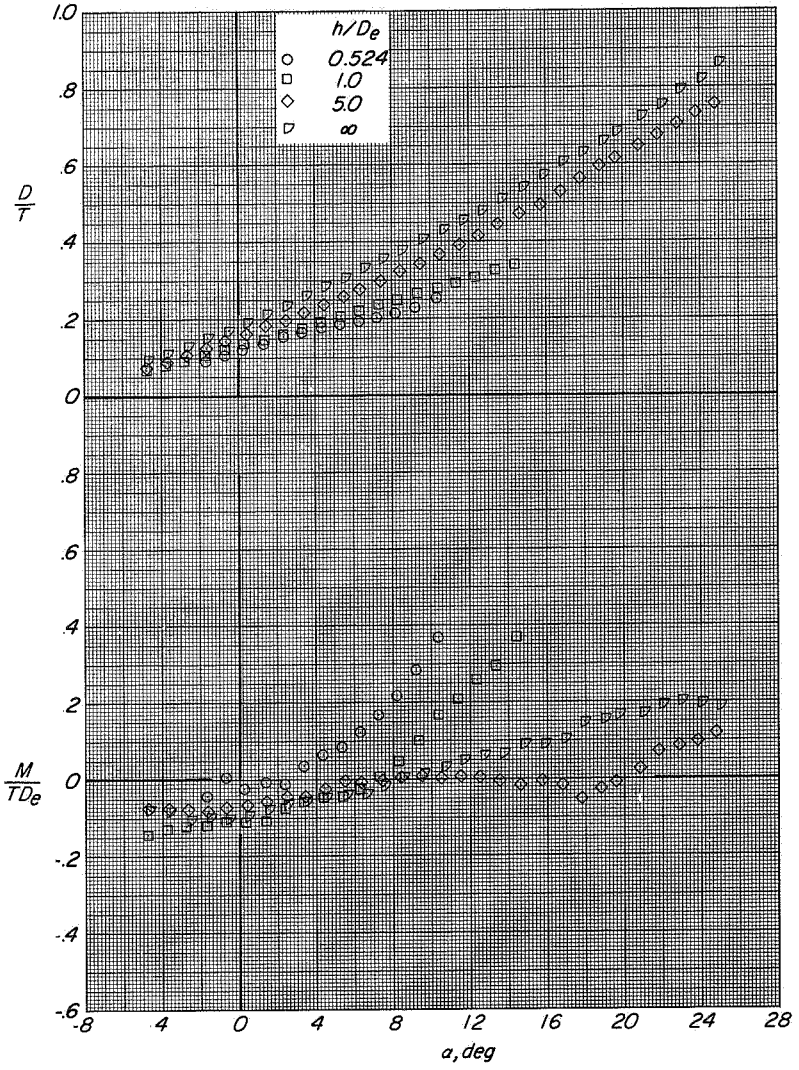

(e) Variation of D/T and M/TD_e with α.

Figure 102.- Concluded.

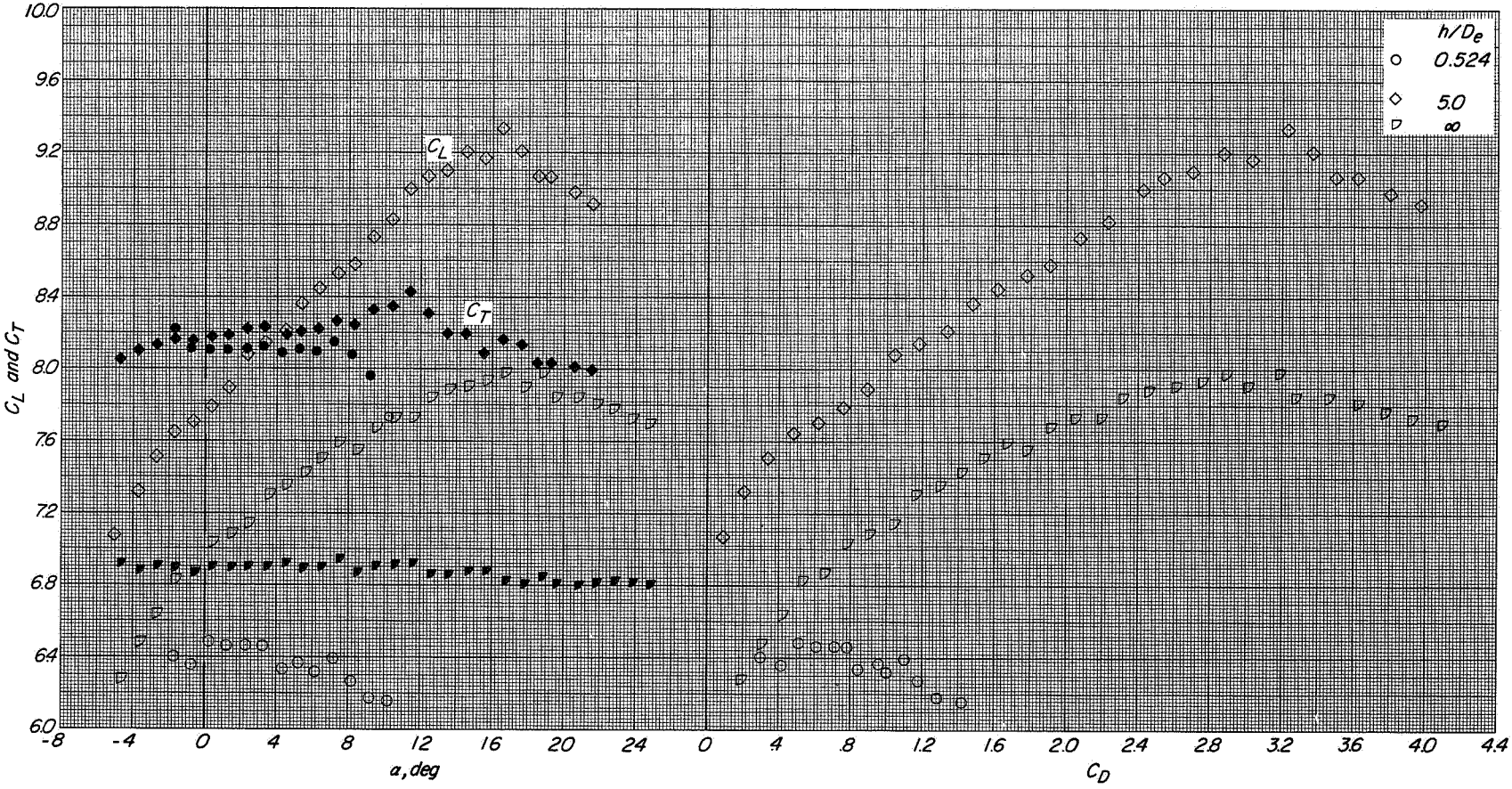

(a) Variation of C_L and C_T with α and C_D with C_L

Figure 103.- Longitudinal aerodynamic characteristics of configuration A with left direct-lift engines deflected 70°, right direct-lift engines deflected 110°, and lift-cruise engines deflected 90°. $i_t = 0°$; $\beta = 5°$; $C_T \approx 8$.

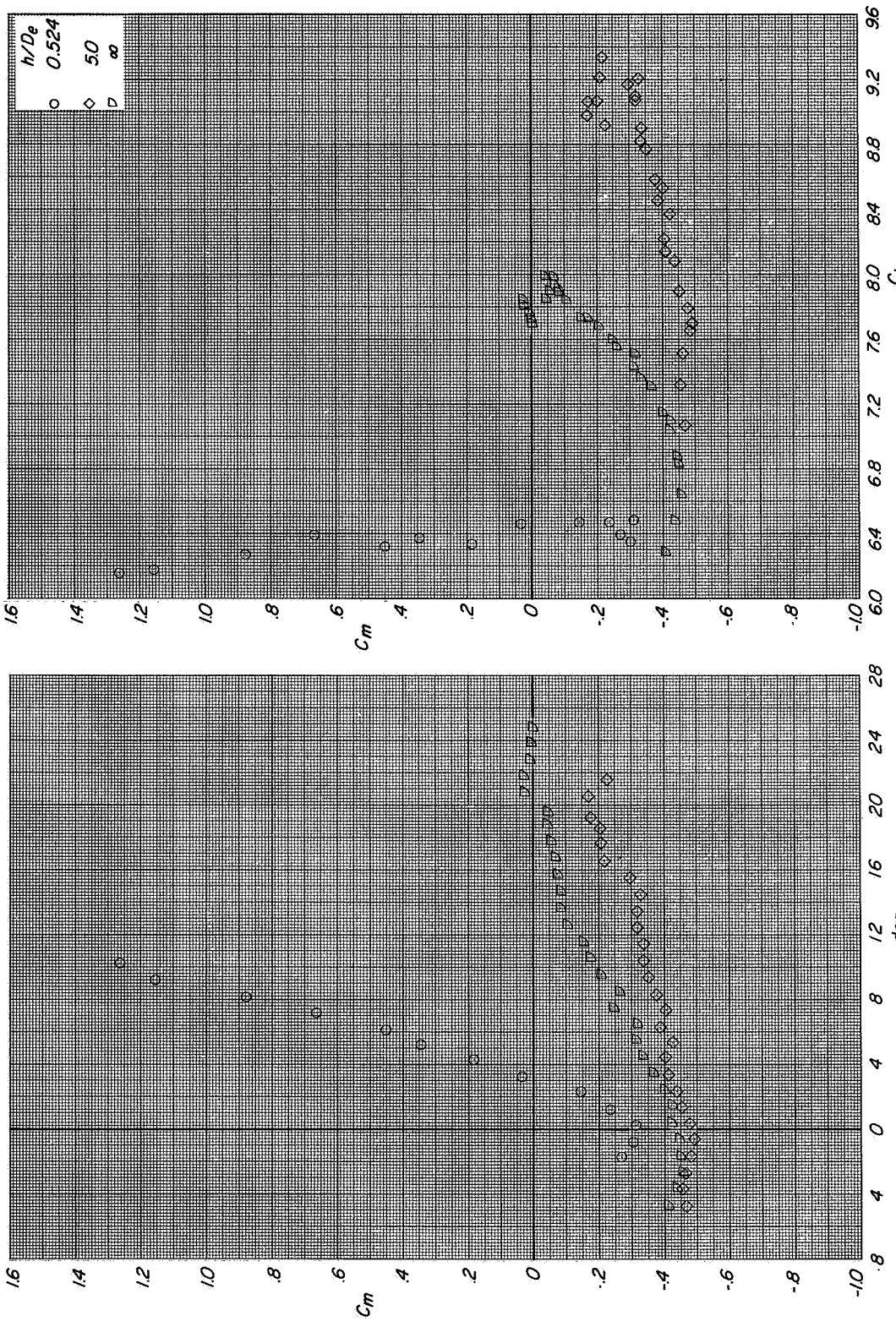

(b) Variation of C_m with α.

(c) Variation of C_m with C_L.

Figure 103.- Continued.

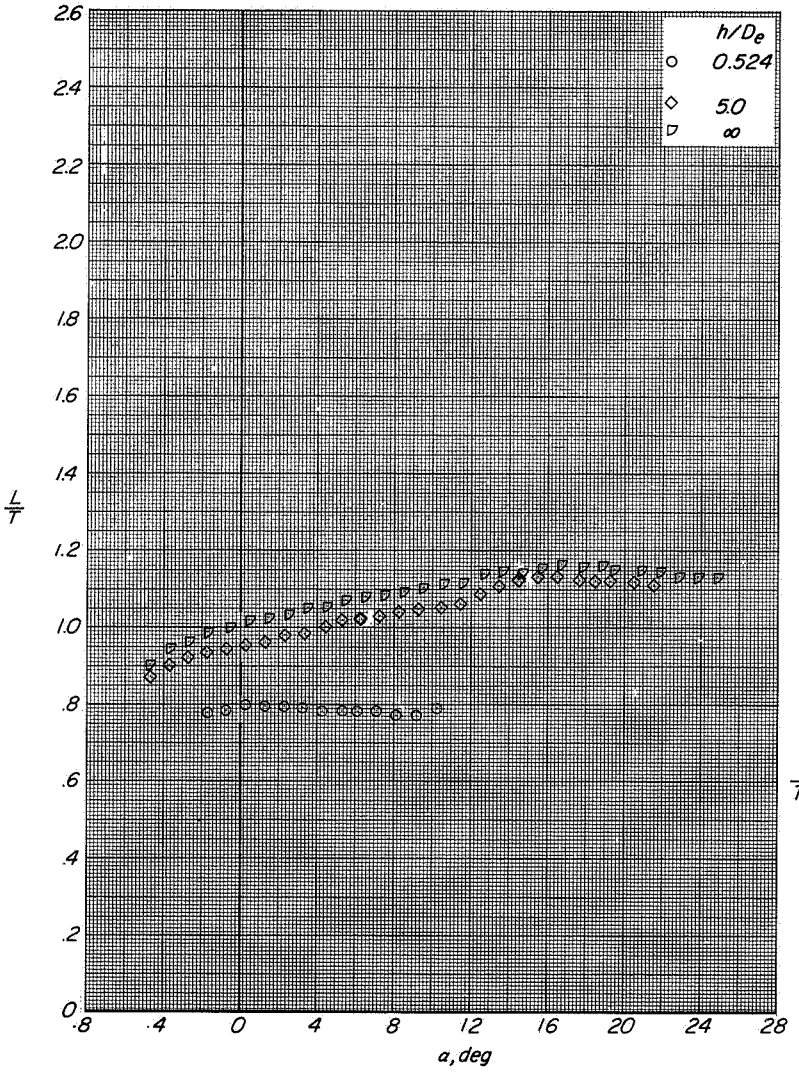

(d) Variation of L/T with α.

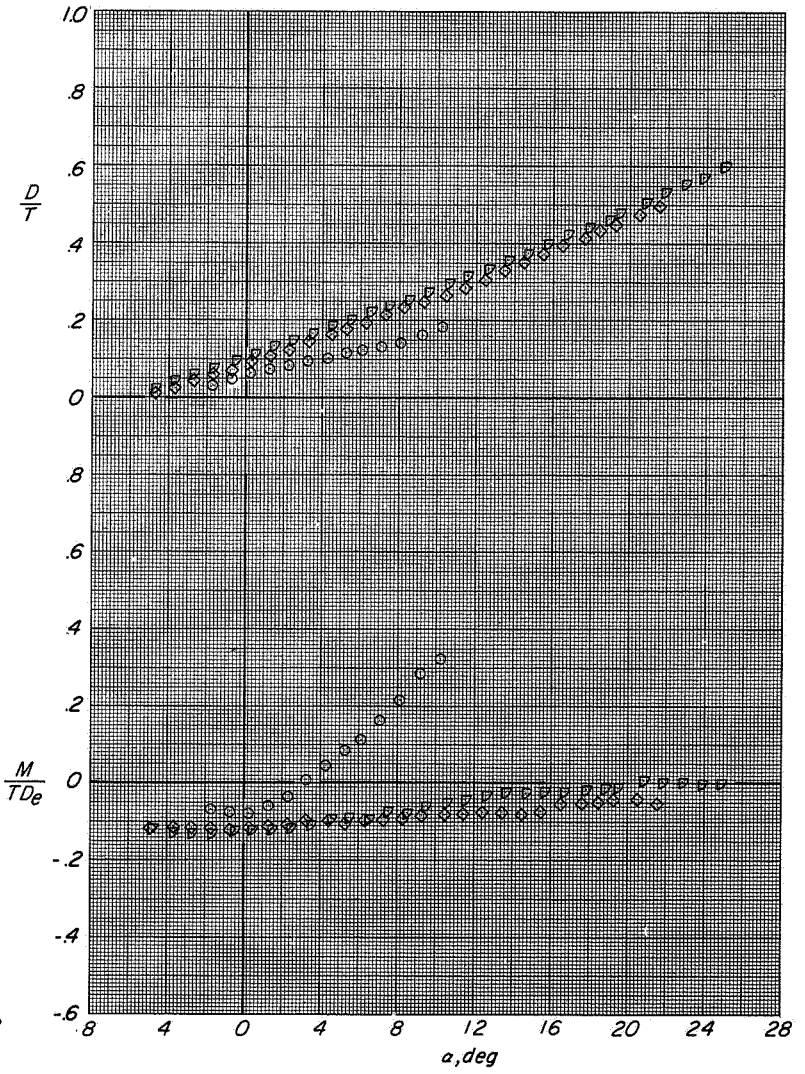

(e) Variation of D/T and M/TD_e with α.

Figure 103.- Concluded.

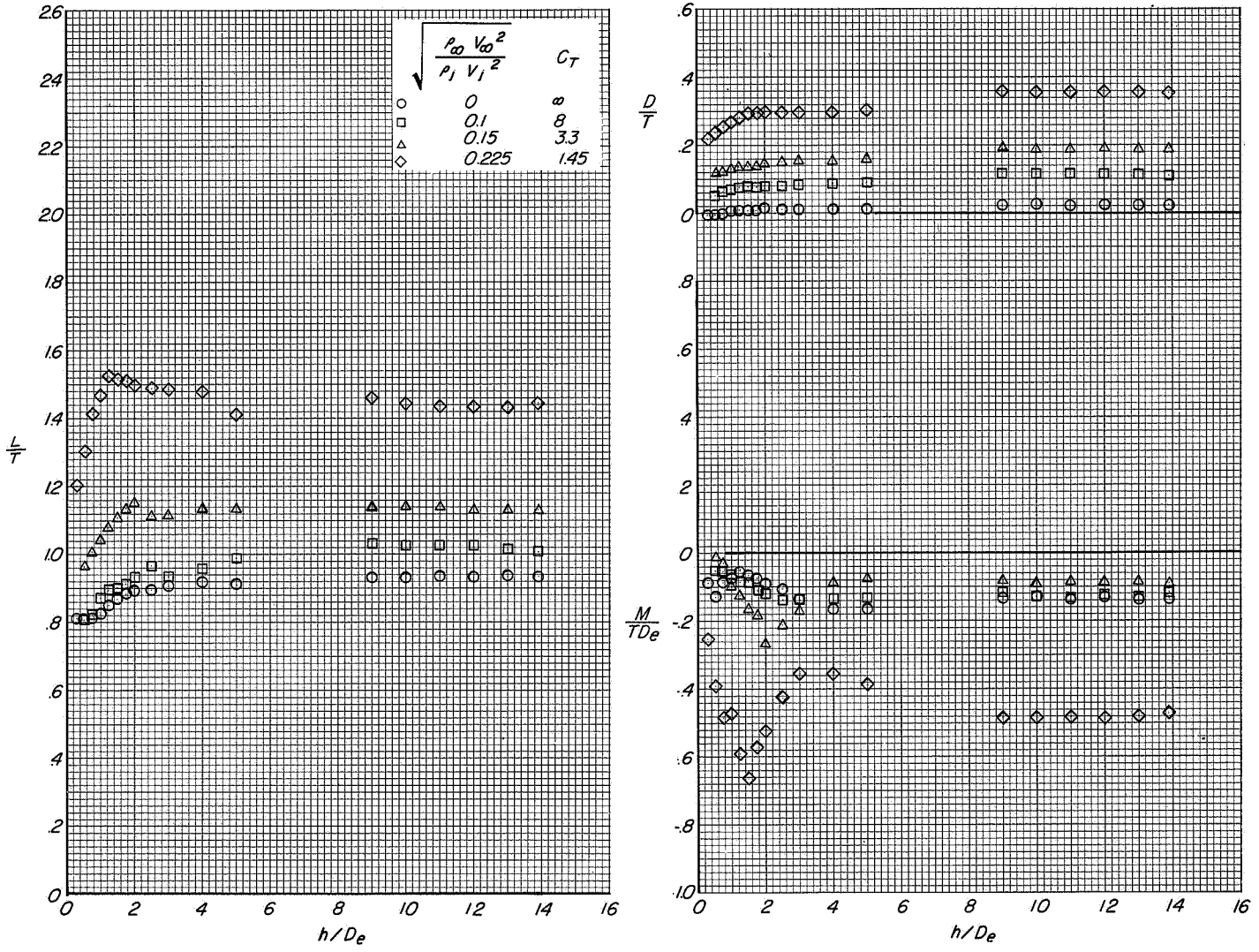

(a) Variation of L/T with h/D_e.

(b) Variation of D/T and M/TD_e with h/D_e.

Figure 104.- Effect of height above the moving-belt ground plane on the longitudinal aerodynamic characteristics of configuration A with left direct-lift engines deflected 70°, right direct-lift engines deflected 110°, and lift-cruise engines deflected 90°. $i_t = 0°$; $\beta = 5°$; $\alpha = 0.3°$.

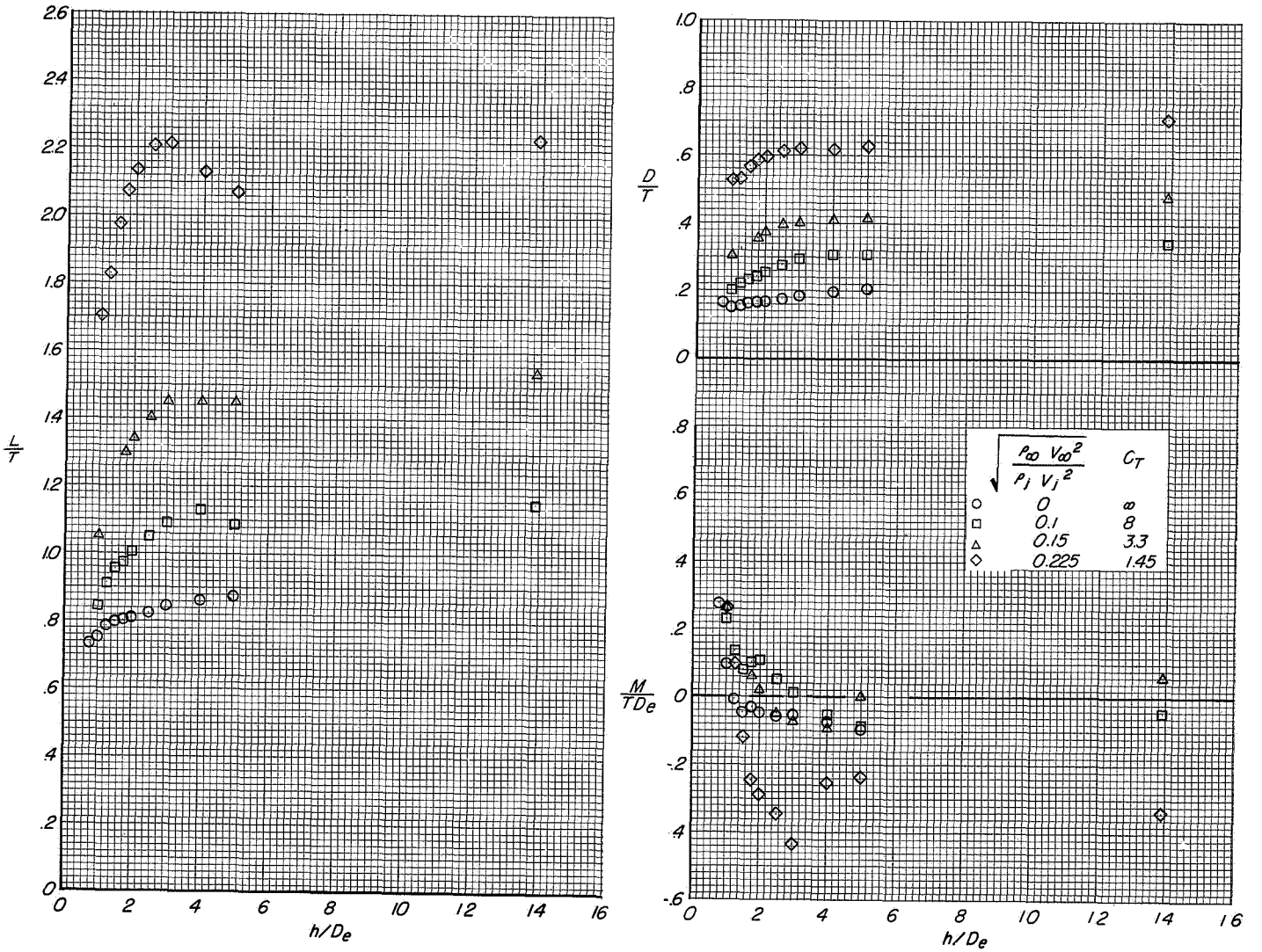

(a) Variation of L/T with h/D_e.

(b) Variation of D/T and M/TD_e with h/D_e.

Figure 105.- Effect of height above the moving-belt ground plane on the longitudinal aerodynamic characteristics of configuration A with left direct-lift engines deflected 70°, right direct-lift engines deflected 110°, and lift-cruise engines deflected 90° $i_t = 0°$; $\beta = 5°$; $\alpha = 12.4°$.

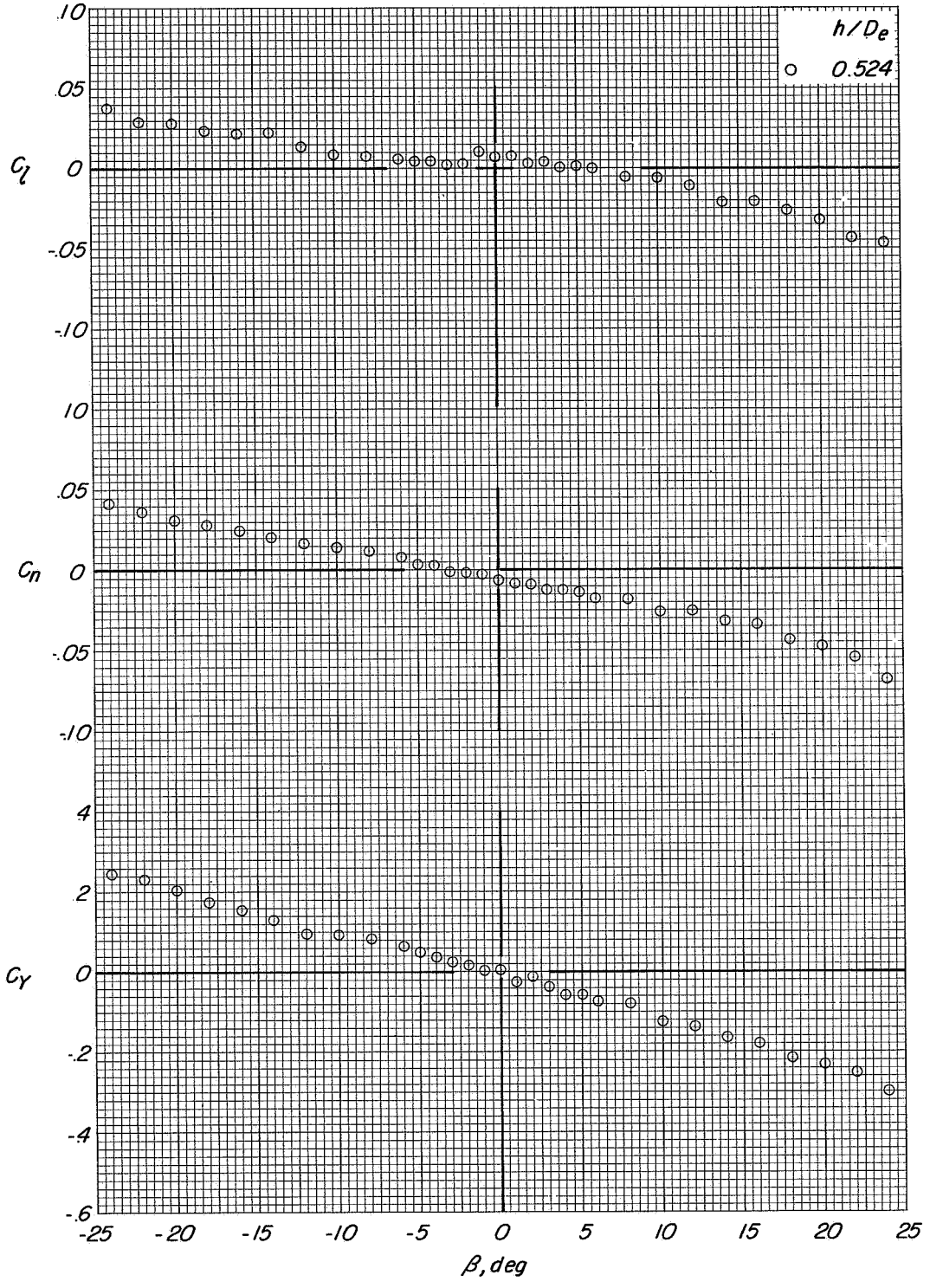

Figure 106.- Lateral aerodynamic characteristics of configuration A with left direct-lift engines deflected 70^0, right direct-lift engines deflected 110^0, and lift-cruise engines deflected 90^0. $i_t = 0^0$; $\alpha = 0.1^0$; $C_T = 0$.

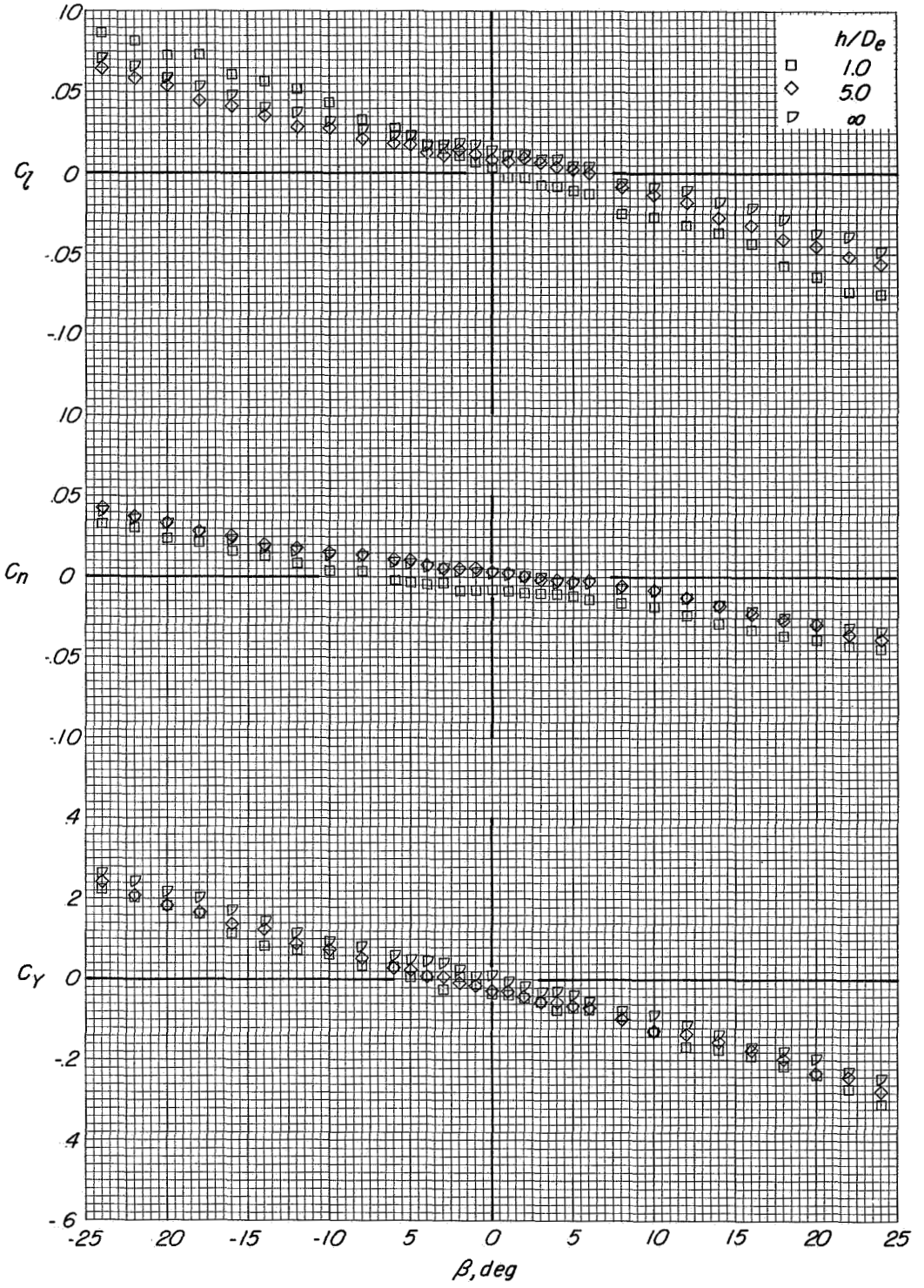

Figure 107.- Lateral aerodynamic characteristics of configuration A with left direct-lift engines deflected 70°, right direct-lift engines deflected 110°, and lift-cruise engines deflected 90° $i_t = 0°$; $\alpha = 12.3°$; $C_T = 0$.

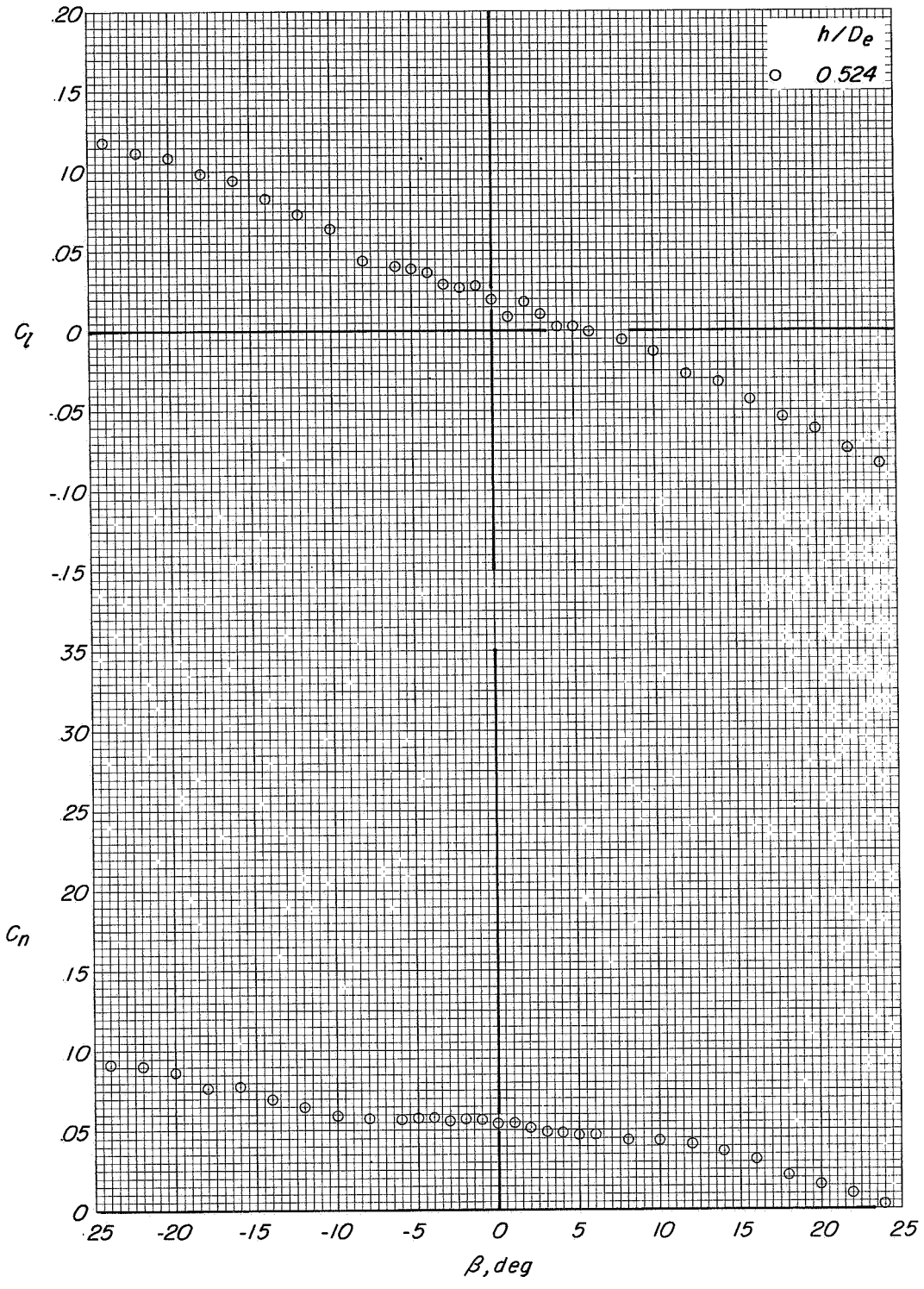

(a) Variation of C_l and C_n with β.

Figure 108.- Lateral aerodynamic characteristics of configuration A with left direct-lift engines deflected 70^0, right direct-lift engines deflected 110^0, and lift-cruise engines deflected 90^0. $i_t = 0^0$; $\alpha = 0.2^0$; $C_T \approx 1.45$.

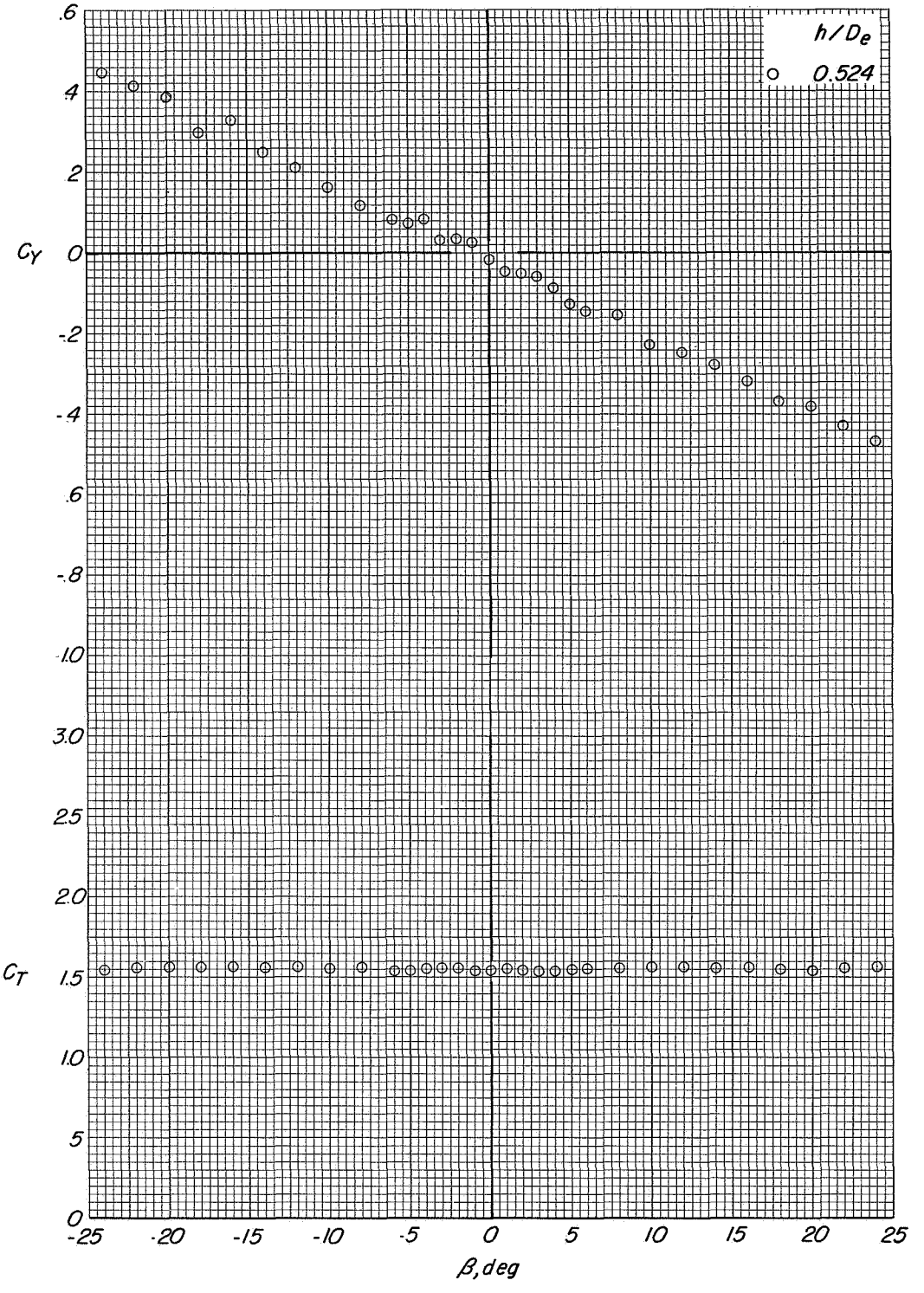

(b) Variation of C_Y and C_T with β.

Figure 108.- Concluded.

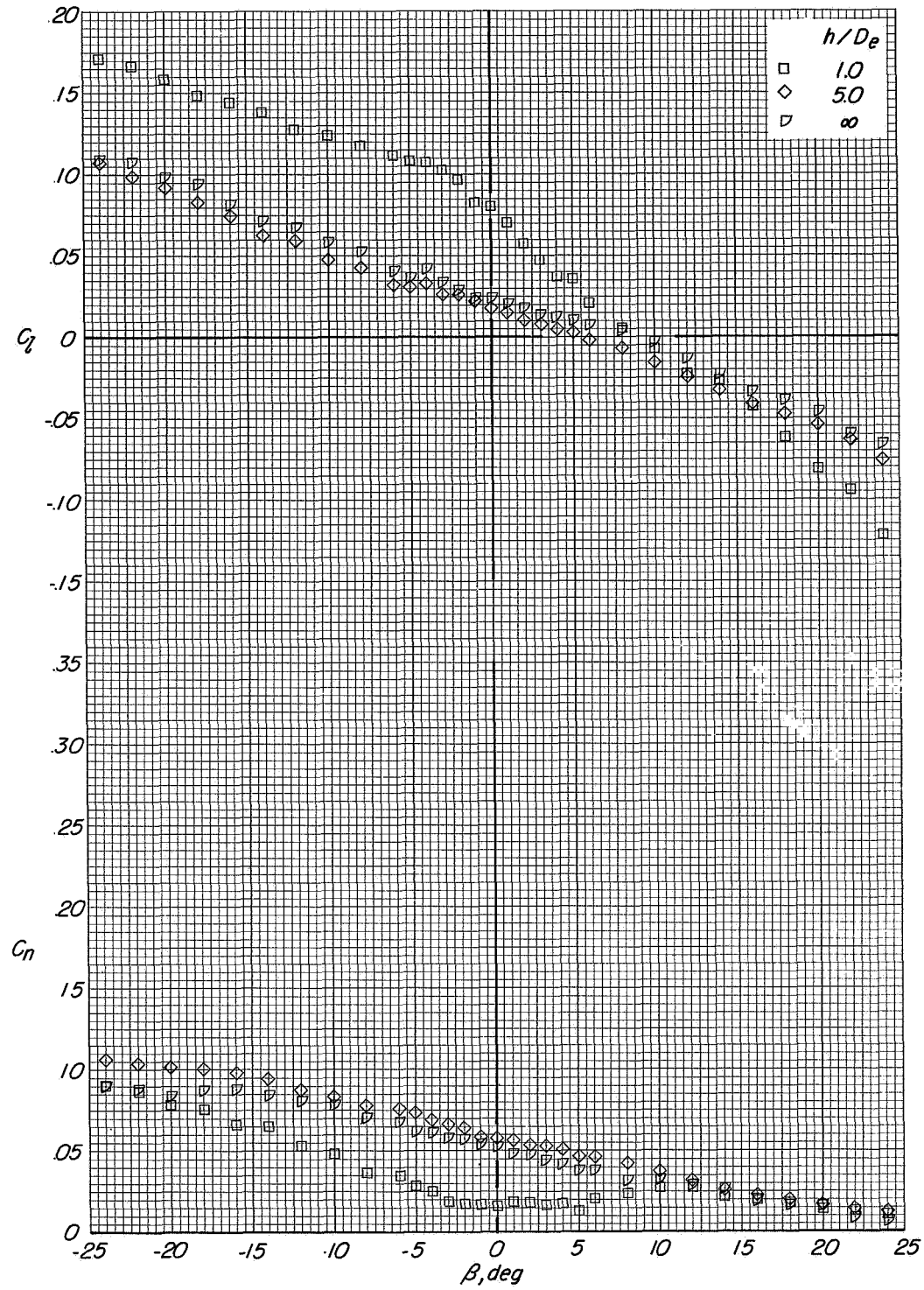

(a) Variation of C_l and C_n with β.

Figure 109.- Lateral aerodynamic characteristics of configuration A with left direct-lift engines deflected 70^0, right direct-lift engines deflected 110^0, and lift-cruise engines deflected 90^0. $i_t = 0^0$; $\alpha = 12.5^0$; $C_T \approx 1.45$.

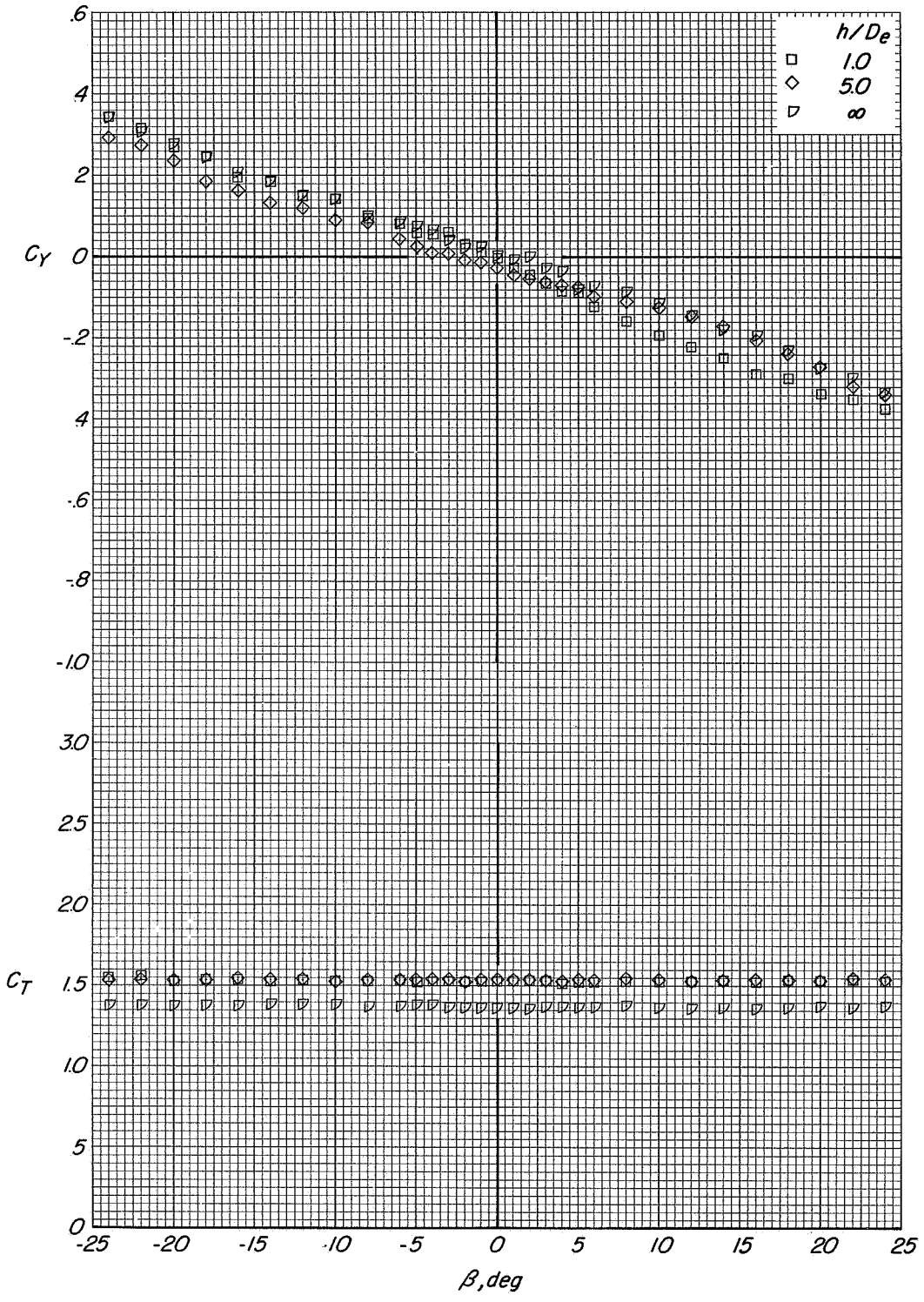

(b) Variation of C_Y and C_T with β.

Figure 109.- Concluded.

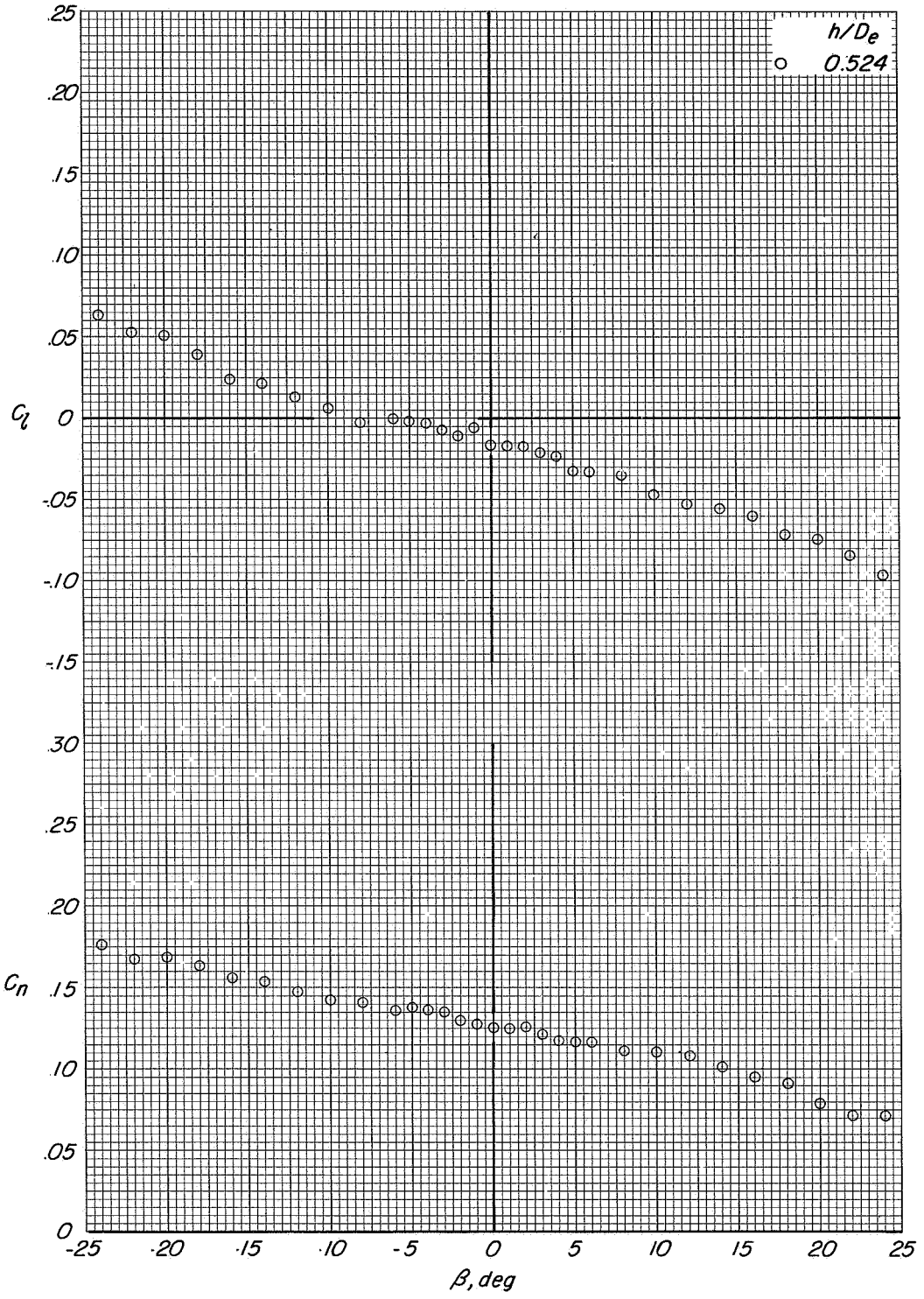

(a) Variation of C_l and C_n with β.

Figure 110.- Lateral aerodynamic characteristics of configuration A with left direct-lift engines deflected 70°, right direct-lift engines deflected 110°, and lift-cruise engines deflected 90°. $i_t = 0°$; $\alpha = 0.3°$; $C_T \approx 3.3$.

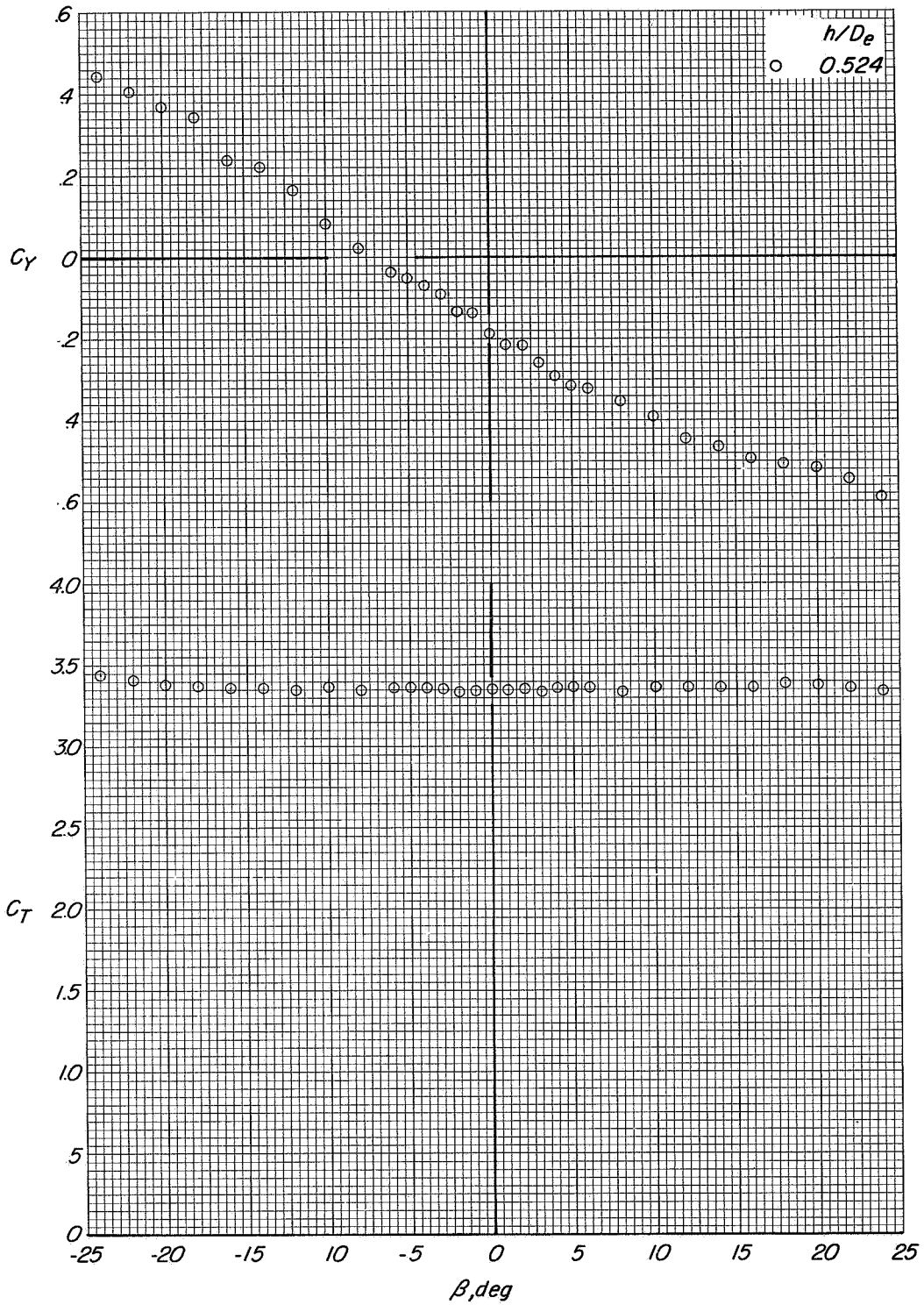

(b) Variation of C_Y and C_T with β.

Figure 110.- Concluded.

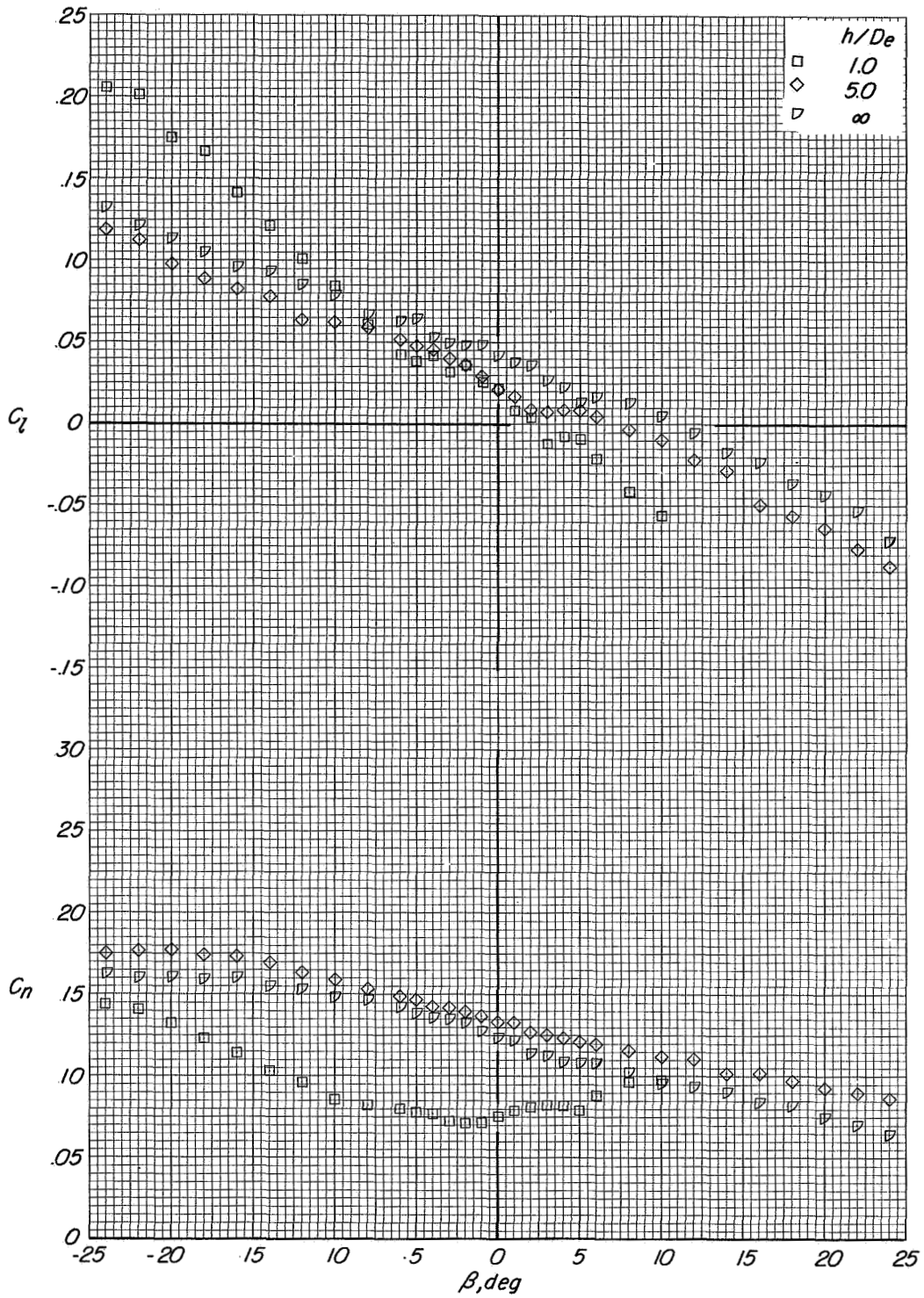

(a) Variation of C_l and C_n with β.

Figure 111.- Lateral aerodynamic characteristics of configuration A with left direct-lift engines deflected 70°, right direct-lift engines deflected 110°, and lift-cruise engines deflected 90°. $i_t = 0°$; $\alpha = 12.6°$; $C_T \approx 3.3$.

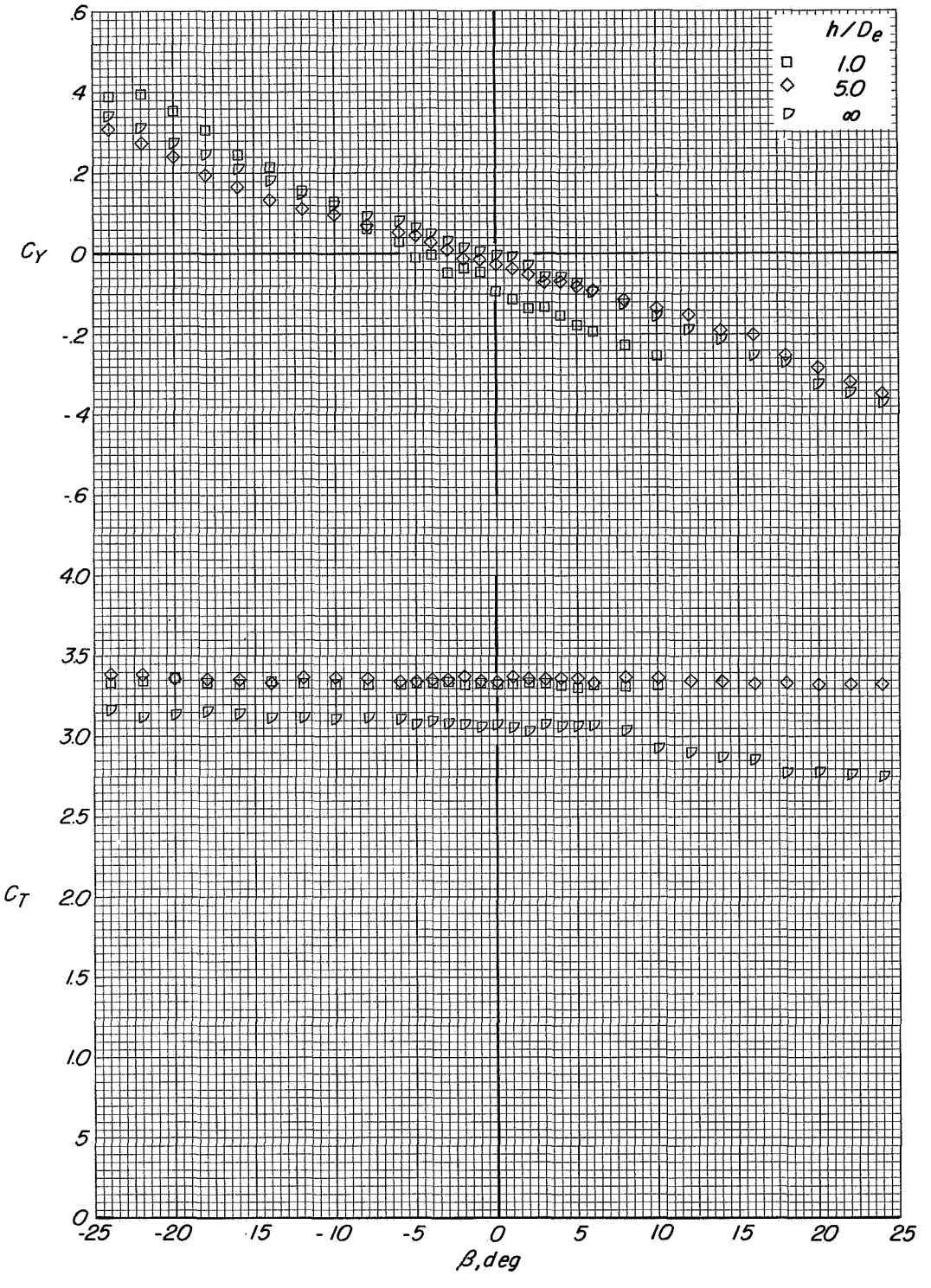

(b) Variation of C_Y and C_T with β.

Figure 111.- Concluded.

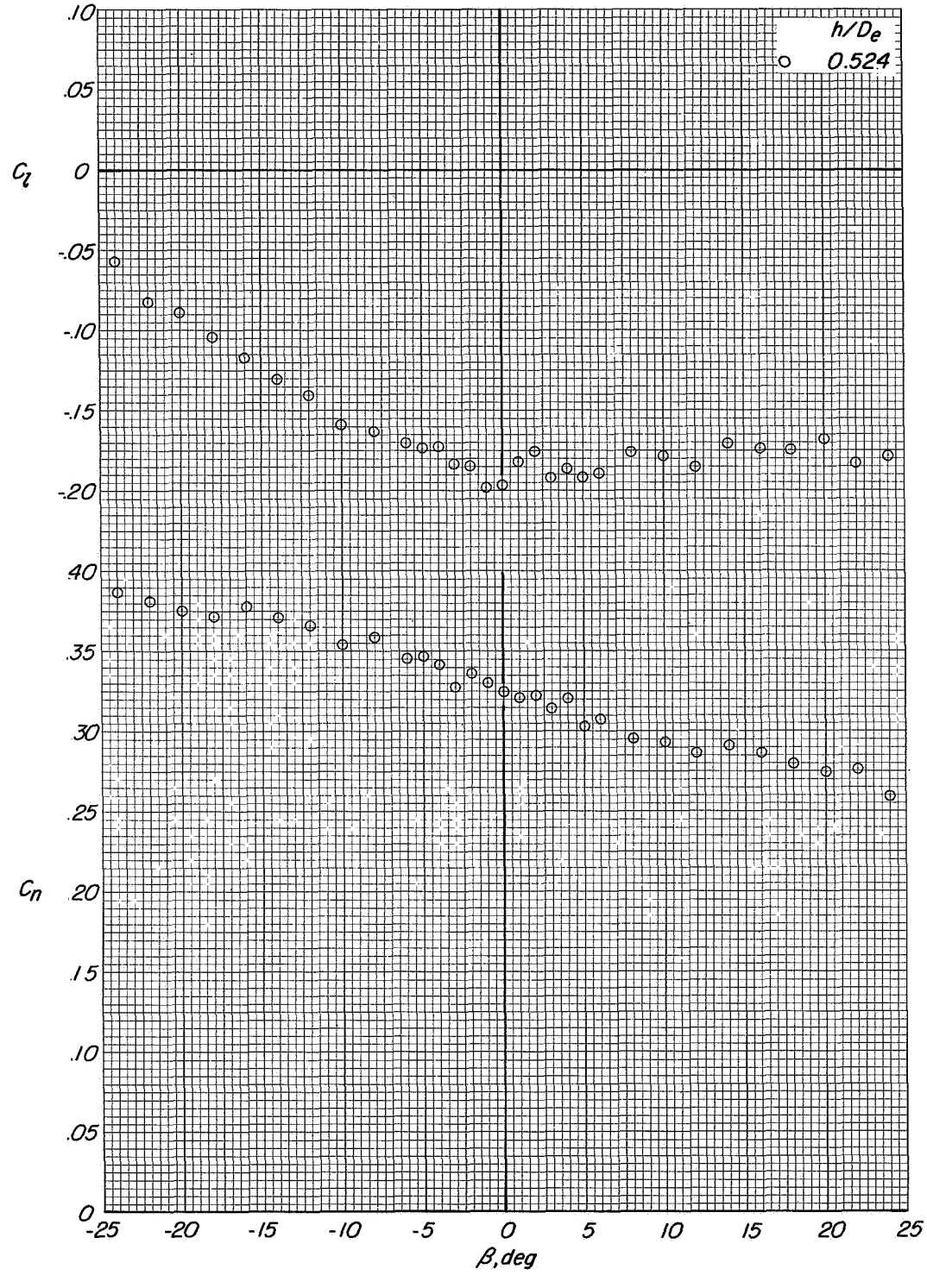

(a) Variation of C_l and C_n with β.

Figure 112.- Lateral aerodynamic characteristics of configuration A with left direct-lift engines deflected 70^0, right direct-lift engines deflected 110^0, and lift-cruise engines deflected 90^0, $i_t = 0^0$; $\alpha = 0.2^0$; $C_T \approx 8.0$.

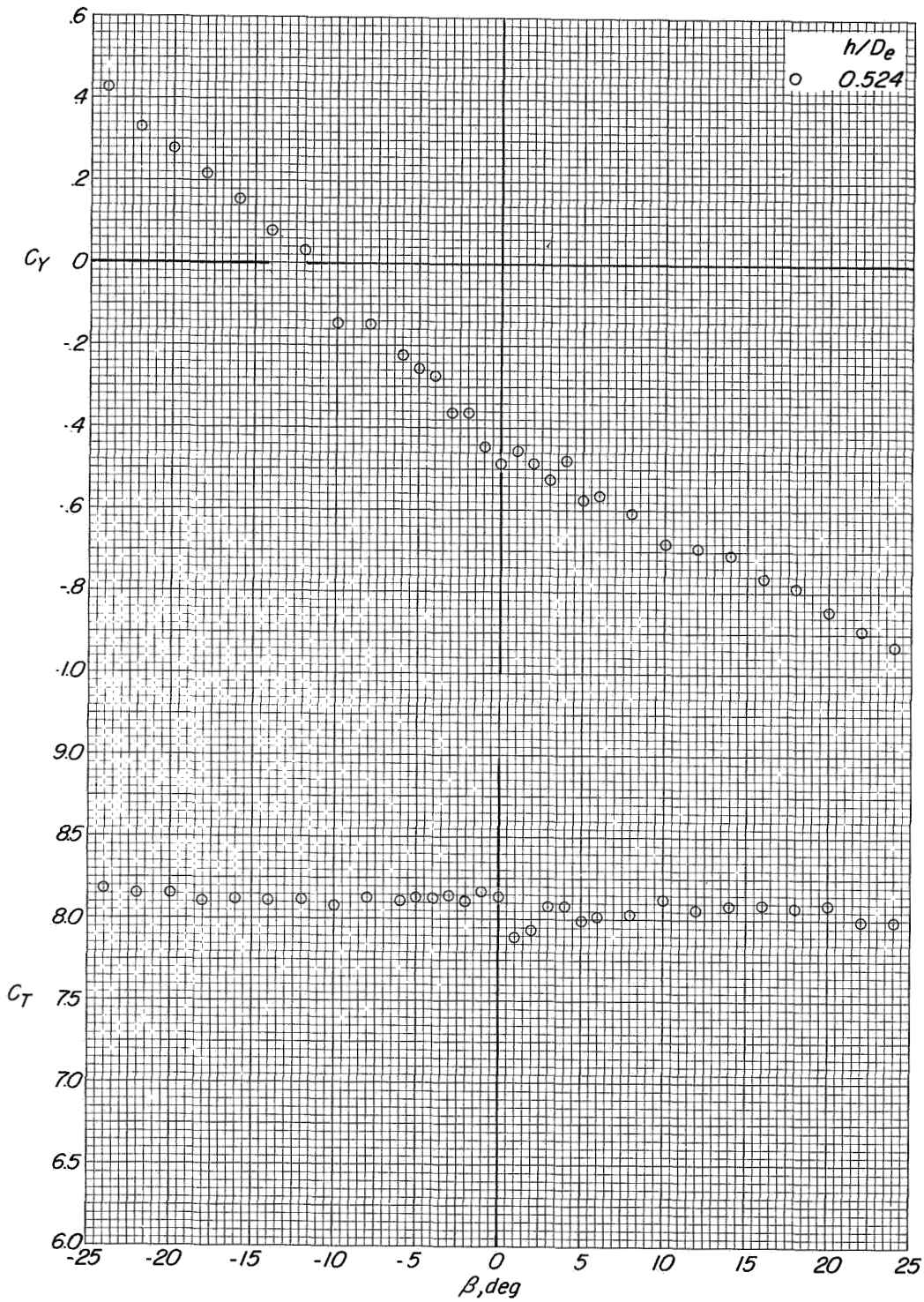

(b) Variation of C_Y and C_T with β.

Figure 112.- Concluded.

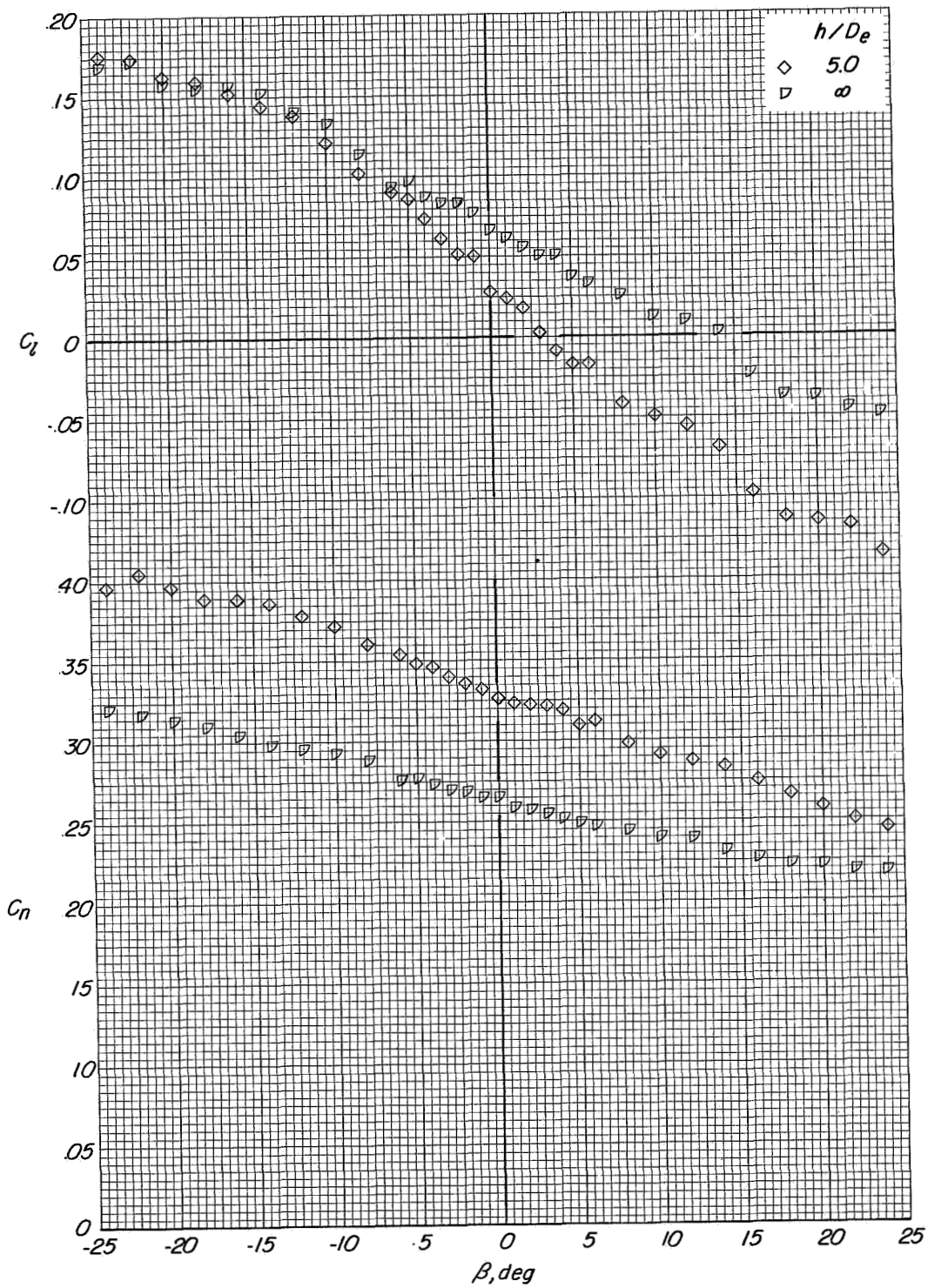

(a) Variation of C_l and C_n with β.

Figure 113.- Lateral aerodynamic characteristics of configuration A with left direct-lift engines deflected 70°, right direct-lift engines deflected 110°, and lift-cruise engines deflected 90°. $i_t = 0°$; $\alpha = 12.5°$; $C_T \approx 8.0$.

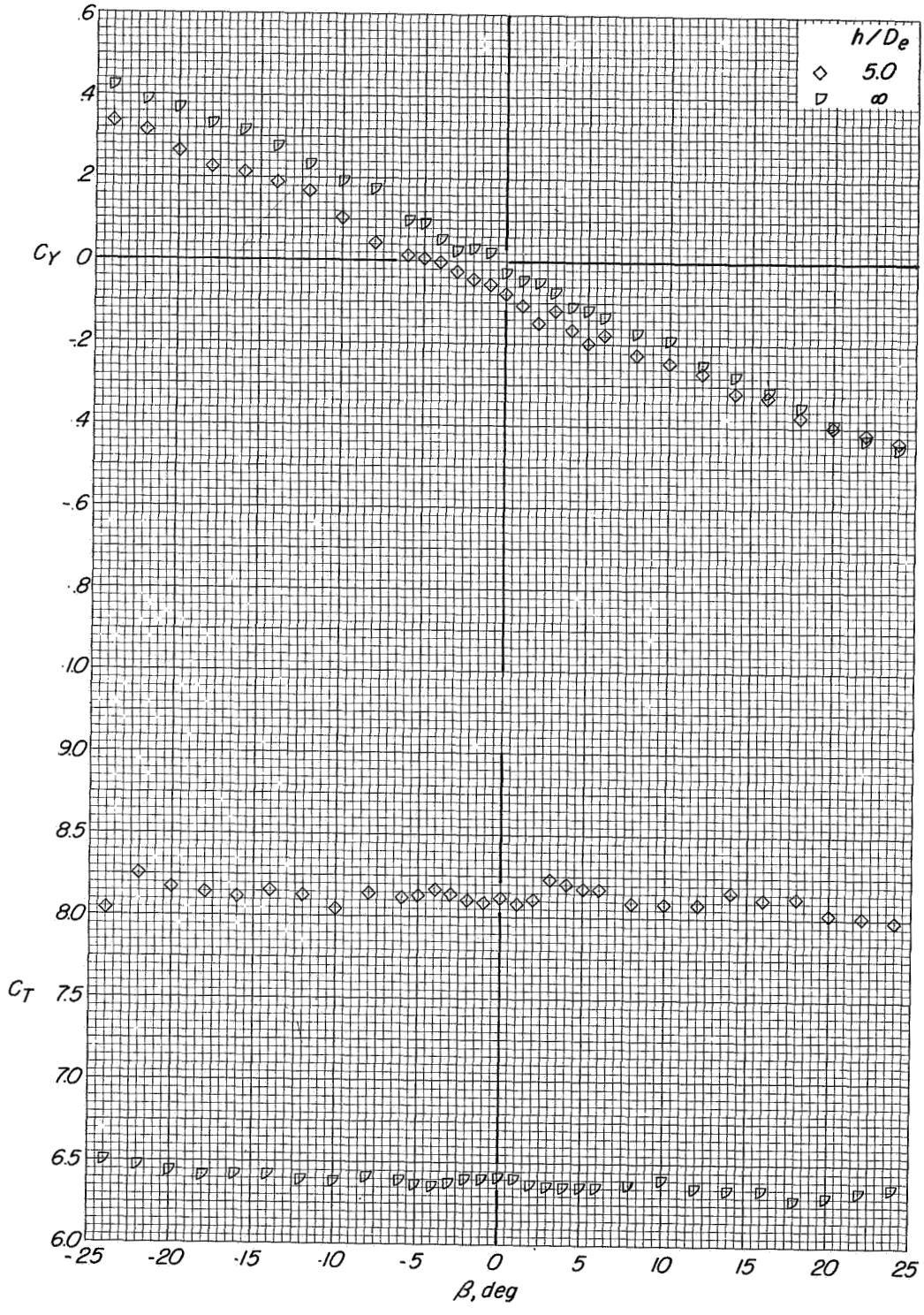

(b) Variation of C_Y and C_T with β.

Figure 113.- Concluded.